



***RADAR***  
***and the***  
***ATMOSPHERE***

## ***The Artech House Radar Library***

David K. Barton, *Series Editor*

*Modern Radar System Analysis* by David K. Barton

*Introduction to Electronic Warfare* by D. Curtis Schleher

*High Resolution Radar* by Donald R. Wehner

*Electronic Intelligence: The Interception of Radar Signals* by R. G. Wiley

*RGCALC: Radar Range Detection Software and User's Manual* by John E. Fielding and Gary D. Reynolds

*Over-The-Horizon Radar* by A.A. Kolosov, *et al.*

*Principles and Applications of Millimeter-Wave Radar*, Charles E. Brown and Nicholas C. Currie, eds.

*Multiple-Target Tracking with Radar Applications* by Samuel S. Blackman

*Radar Propagation at Low Altitudes* by M.L. Meeks

*Radar Cross Section* by Eugene F. Knott, *et al.*

*Radar Anti-Jamming Techniques* by M.V. Maksimov, *et al.*

*Radar System Design and Analysis* by S.A. Hovanessian

*Monopulse Principles and Techniques* by Samuel M. Sherman

*Monopulse Radar* by A.I. Leonov and K.I. Fomichev

*High Resolution Radar Imaging* by Dean L. Mensa

*Radar Detection* by J.V. DiFranco and W.L. Rubin

*Handbook of Radar Measurement* by David K. Barton and Harold R. Ward

*Radar Technology*, Eli Brookner, ed.

*Radar Range-Performance Analysis* by Lamont V. Blake

*Techniques of Radar Reflectivity Measurement* by Nicolas C. Currie

*Radar Reflectivity of Land Sea* by Maurice W. Long

*Aspects of Modern Radar*, by Eli Brookner, *et al.*

*Analog Automatic Control Loops in Radar and EW* by Richard S. Hughes

*VCCALC: Vertical Coverage Plotting Software and User's Manual* by John E. Fielding and Gary D. Reynolds

*Electronic Homing Systems* by M.V. Maksimov and G.I. Gorgonov

*Principles of Modern Radar Systems* by Michel H. Carpentier

*Secondary Surveillance Radar* by Michael C. Stevens

***RADAR***  
***and the***  
***ATMOSPHERE***

***Alfred J. Bogush, Jr.***

***DESE***  
***Research and Engineering, Inc.***

***Artech House***



**Library of Congress Cataloging-in-Publication Data**

Bogush, Alfred J.  
Radar and the atmosphere.  
Bibliography: p.  
Includes index.  
1. Radar. I. Title  
QC973.5.B54 1989 551.6'353 88-35003  
ISBN 0-89006-222-6

Copyright © 1989

**ARTECH HOUSE, INC.**  
**685 Canton Street**  
**Norwood, MA 02062**

All rights reserved. Printed and bound in the United States of America. No part of this book may be reproduced or utilized in any form or by any means, electronic or mechanical, including photocopying, recording, or by any information storage and retrieval system, without permission in writing from the publisher.

**International Standard Book Number: 0-89006-222-6**  
**Library of Congress Catalog Card Number: 88-35003**

10      9      8      7      6      5      4      3      2      1

# ***To Alta***

***An Extraordinary Individual And Companion***



# *Contents*

Preface	xiii
Acknowledgments	xviii
<b>PART I INTRODUCTION</b>	<b>1</b>
Chapter 1 The Radar Environment	3
1.1 Background	3
Considerations	3
A Methodology	4
1.2 The Radar Equation	5
Classical Form	5
A Formal Description	5
Gaussian Form	7
1.3 The Atmospheric Environment	7
Effects	8
System Needs and Models	9
Data Sources	11
1.4 Organization of the Material	12
<b>PART II THE RADAR EQUATION</b>	<b>15</b>
Chapter 2 The Radar Equation—Classical Forms	17
2.1 Initial Derivations	18
Classical	18
Bistatic	22
Search Form	22
Friis' Transmission Formula	24
Radar Equation With Interference	25
2.2 Atmospheric Path Loss	26
2.3 Meteorological Equation	28
2.4 Applications—Methodology for System Analysis	32
Evolution of Radar Requirements	33

---

Radar Parameters	38
Methodology	53
Chapter 3 The Radar Equation—A Formal Treatment	69
3.1 Maxwell's Equations	70
Field Quantities, Units, and Dimensions	70
Integral Forms	72
Differential Forms	77
Boundary Conditions	78
Equation Compilations	80
3.2 Antenna, Scattering, and Radar Equation Formulations	82
Vector Potentials	82
Equivalence Theorem and Kirchhoff's Formula	90
Reciprocity	97
3.3 Derivation of the Radar Equation	100
From a Power Transfer Formulation	101
From Kirchhoff's Formula	104
3.4 Plane Waves	106
Derivations	107
Free Space and Perfect Dielectrics	110
Lossy Dielectrics and Conductors	114
Incidence on Dielectrics	115
Incidence on Perfect Conductors	117
Remarks	119
3.5 Radar Antennas	120
Interpretations and Formulations	120
Properties of an Antenna Pattern	123
Radiation from Current Elements	125
Fourier Transform Methods	138
Hankel Transform Methods	145
Gaussian Field Expansions	147
Introduction to Arrays	169
3.6 Radar Cross Sections	177
Scattering Centers	177
Formulations	180
Long, Thin Bodies of Revolution	180
Target Models	187
3.7 The Radar Signal	188
Basics	189
The Matched Filter	191
Ambiguity Functions	192
Waveforms	192
3.8 Synopsis	195

---

Chapter 4	The Radar Equation—Gaussian Forms	199
4.1	Rationale	199
4.2	Formulations	200
	Power Densities	201
	Power Transfer	203
	Beamwidth, Gain, and Aperture Efficiency	204
4.3	The Square Antenna	206
	Gaussian Equivalents	208
	Radar Equations—Gaussian Equivalents	209
	Radar Equations—General Forms	213
4.4	The Circular Antenna	216
	Gaussian Field Expansions	216
	Gaussian Equivalents	218
	Radar Equations—Gaussian Equivalents	218
	Radar Equations—General Forms	219
4.5	The Meteorological Radar Equation	220
	Derivation	221
	A General Form	223
4.6	Applications	226
	The Radiated Power Density	226
	Pattern Degradations	235
	Two-Term Gaussian Expansion	239
4.7	Formulas	240
PART III	THE ATMOSPHERIC ENVIRONMENT	245
Chapter 5	The Atmosphere	247
5.1	Regions of the Atmosphere	247
	The Troposphere	247
	The Stratosphere	248
	The Mesosphere	250
	The Thermosphere	251
5.2	U.S. Standard Atmosphere	252
	Pressure and Temperature	252
	Air Density	253
	Water Vapor	253
5.3	Clouds	254
	Formation of Clouds	254
	Cloud Families	254
	Precipitation	256
	Cloudiness	258
	Tabulated Cloud Characteristics	260
5.4	Fog	260

---

Chapter 6	Global Rain Regions	265
6.1	Definitions	265
6.2	Climate Regions	266
6.3	Fog Occurrences	268
6.4	Examples	270
PART IV	DATA COMPILATIONS AND MODELS	275
Chapter 7	The Clear Environment	277
7.1	Attenuation	277
	Properties	279
	Altitude Dependence	282
	Zenith Attenuation and Phase Delay	284
7.2	Refractivity	286
	Propagation Constant	286
	Frequency-Independent Refractivity	288
	Frequency-Dependent Refractivity	290
7.3	Additional Formulations and Procedures	290
	Ray Paths	290
	Formulas for Beam Position Errors	293
	Phase Delays	293
	Time Delays	294
7.4	Summary	295
Chapter 8	Rain Data Compilations	297
8.1	Introduction	298
	Types of Rain	298
	Vertical Profiles	300
	Drop Size Distributions	301
	Additional Background	309
8.2	Uniform Rain Model	311
	Attenuation	311
	Backscatter	311
	Use of Model	314
8.3	Path-Dependent Model	316
	Path-Average Attenuation	316
	Backscatter Formulation	318
	A Methodology	318
	Two-Component Dependence	320
8.4	Snow and Hail	325
	Characteristics of Snow	332
	Propagation Effects	335
	Hail	336
	Summary	339

---

8.5	Fractal Formulations	341
	Introduction	342
	Definitions	344
	Fractal Models	346
	Methodology for Analysis and Simulation	358
8.6	Final Remarks	362
Chapter 9	Cloud Environments	365
9.1	Haze	365
9.2	Fog	365
9.3	Clouds	367
9.4	Dusts and Smoke	371
9.5	Data Compilations	373
	Basics	373
	Data	373
9.6	Summary	375
APPENDICES		385
Appendix A	Gaussian Antenna—Scaling Factors and Series Coefficients	385
	Diffraction Integrals	385
	Orthogonal Functions	389
	Hermite-Gaussian Field Expansions	390
	Laguerre-Gaussian Field Expansions	402
Appendix B	Statistical Data	409
	Fractional Differentiation and Integration	410
	The Hyperbolic Distribution	418
	A Random Number Generator	421
	References	428
Appendix C	Bibliography	437
Index		449





## *Preface*

The material contained herein was assembled from more than a decade of involvement in the development of advanced ground-based and missile-borne radars. Activities included a multitude of analysis and simulation investigations, where radar performance was assessed against targets in complex, mostly natural, cluttered environments. Environmental parameters for radar designs were specified and the environmental simulation programs for radar and missile system evaluations were developed.

The activities were conducted in a system environment, where a view of total system design, analysis, test and integration efforts was attained. More importantly, the participation in analysis and simulation efforts occurred at system, radar system, subsystem, and component levels. Each level provided unique considerations from a common framework, but would appear to be compatible. A need to establish guidelines for radar analysis at all levels became apparent. With increased emphasis placed on computer simulation in the development process, further demand is placed upon understanding and modeling of the radar and the operating environment. These observations provided one primary motivation for assembling the material contained in this book. The basis of the analysis is the treatment of the radar equation, which is extensive. A systemic viewpoint is taken.

Many issues were encountered in defining the radar environment. Included were the specification of radar cross sections and attenuations of rain and clouds, definition of the more difficult statistical properties of expected signals, establishment of types of rain and clouds of concern on a global basis, specification of upper and lower bounds of the cloud and rain formations, and definition of other environmental parameters needed for the specification of radar parameters and designs. Although much of the data were available from radar, radar meteorology, communication, remote sensing and atmospheric scientific sources, the necessity for consolidation of data for the radar user became apparent. As a result, environmental data, computer models, and accompanying mathematical formulations were compiled and used in several radar development programs. This resulting data base and its apparent usefulness provided another motivation for writing this book.

There are several factors of importance in compiling the atmospheric data sets in a reasonable way. First, it is necessary to establish a sound theoretical basis from which the data can be used with confidence. Second, it is important to understand some physical properties of the atmospheric environment for a more thorough appreciation of the operating conditions of the radar. In addition, data compilations must contain useful parameters associated with realistic models of the environment. The material provided is structured about these principal considerations.

The material is presented in four separate but related groups: Part I—Introduction; Part II—The Radar Equation; Part III—The Atmospheric Environment; and Part IV—Data Compilations and Models. Each part following the Introduction contains two or more chapters. This format was deemed necessary to establish a reasonable degree of coherence between the differing but related topics. The implications of the quantity of data needed to describe the material in a comprehensive way are also important. To circumvent this problem, theoretical formulations are provided in an applied context while the data compilations are discussed in a handbook format. An annotated bibliography and two appendices containing antenna and statistical data are provided to supplement the material. Background discussions are contained in the Introduction, Chapter 1.

The radar range equation is presented in three ways in Part II. A conventional approach, where antenna principles are directly applied, is provided first in Chapter 2. The classical radar equation is derived and placed in a recognizable form with loss terms separated into external (or atmospheric) and internal (or system) groups. This classical equation is the basis from which many other forms evolve. One form, the search radar equation, is included. Another form sometimes referred to as a one-way or transmission equation, important in the analysis of radar degradations due to interference sources, is described. The classical transmission and radar equations are compared and unified. The radar meteorological equation is derived in a similar manner with the beam representation interpreted as a subset of a general Gaussian form.

The equation derivations serve as a review and introduction to the theoretical treatment of later chapters. Examples of the use of the equations are provided in the context of a methodology for system analysis. A system point of view is emphasized in the context of a total system framework. Topics covering the evolution of the radar requirements include the acquisition process, radar requirements, system specifications, radar, performance, and subsystem parameters. The material is presented in tabular form with concise summary descriptions. The examples, presented in the form of a methodology, relate component through total system viewpoints.

Chapter 3 contains a formal treatment of the radar equation. An applied electromagnetic field theory approach is taken with the equation developed directly from Maxwell's equations, and presented as a generalization of the Friis' trans-

mission formula and as a consequence of Kirchhoff's diffraction formula. In this formulation, a theoretical view of radar is taken which results in a vivid portrayal of signal transmission, propagation, and scattering. Each element of the radar equation is then treated separately with emphasis on theory and applications. Topics include Maxwell's equations, plane wave propagation, Fourier, Hankel, and Gaussian methods of large aperture antennas, an introduction to arrays, radar cross sections, including volume scattering considerations for meteorological applications, and reviews of the radar signal where the ambiguity function is described and interpreted. Special attention is paid to thin wire antennas and scatterers where modal descriptions of the fields yield an insight to the notion of a scattering center.

The general approach taken in the derivation of the radar equation includes near-field considerations, where the use of Gaussian field expansions are convenient for radar system analysis. The review of the field expansions is presented as a generalization of the Gaussian beam approximation that allows antenna patterns to be structured one sidelobe at a time, a feature which is convenient for approximating the near and far fields. A compilation of antenna parameters, including Gaussian forms, supplementing the equation derivations is included in Appendix A.

Following the formal derivations, Gaussian forms of the radar equation are presented in Chapter 4. As in the previous derivations, meteorological forms are included. Near and far fields are treated simultaneously with a generalization of the meteorological equation provided using the Gaussian field expansion approach. A theory of Gaussian equivalence is introduced similar to the known Gaussian beam approximation, but applicable for estimation of the aperture, near, and far fields. The resulting gain computations are simple and convenient for radar range equation calculations. Numerous tables, data compilations, and examples are provided to support this approach.

In Part III, The Atmospheric Environment, a summary description of the radar operational environment is provided. Properties of the atmosphere are summarized in Chapter 5, where descriptions of the regions of the atmosphere and their salient features are given in a reference handbook format. Regions of the atmosphere, including the troposphere, stratosphere, mesosphere and thermosphere, are discussed. Special attention is given to cloud formations where the data compilations include types of clouds, their distinguishing characteristics, microstructure, height, and thickness. These data have been obtained from meteorological sources and are intended to provide basic characteristics and physical properties of the atmosphere useful for radar applications, a basis for more extensive investigations, and a source of data for use in the environmental models that follow.

Global occurrences of rain and cloud environments are described in Chapter 6. Global rain data are emphasized and provided for polar, temperate, subtropical and tropical climate regions in eight categories. Statistics for rain rate occurrences,

expressed as a yearly percentage, are defined for each category. Rain rates in later chapters are expressed first on a point basis and then extended to include cellular and noncellular occurrences. Chapters 5 and 6 describe the radar environment, and the subsequent data sets lead to models of elements of the natural radar environment.

Part IV, Data Compilations and Models, begins with a discussion of the clear environment in Chapter 7. Physical properties, attenuations, indices of refraction, and variations of attenuation with altitude and relative humidity are described. In Chapters 8 and 9, rain and cloud data are also provided in a handbook format, with consideration given to fog, haze, hail, snow, dust, and smoke. The data compilations include backscatter and attenuation coefficients, summary descriptions of the specific environments, model descriptions and methodologies, and numerical examples. The models include attenuation and backscatter parameters within specified volumes.

Emphasis in the data compilations and models is on the rain environment in Chapter 9. Data compilations include statistics for rain rates, backscatter cross sections, and attenuations for a general cellularly-structured rainstorm. Consideration is given to altitude dependence and cell sizes, important in many radar designs. Models are formulated in four levels. At Level 1 a uniform rain rate distribution, most commonly used, is described. The Level 2 model includes a range-dependent formulation, where variations in attenuation along a propagation path, resulting from the cellular structure of storms, are included, with probability distributions for cellular and noncellular or debris regions of a rainstorm.

At Level 3, fractals are introduced into the rain models. Based on recent descriptions of the cellular structure of rain, in a fractal way, a model description for general radar use is given and supported by an appendix containing fractional integration and differentiation summaries, description of a random number generator for use in the models, examples of computations, and a bibliography devoted to fractals. The material is introductory, thought-provoking, and intended to inspire further work in the theory and applications of fractals in radar. In particular, the random number generator is applicable, not only for use in the fractal models, but also in the general area of radar target and clutter modeling.

The author's intent is to provide a collection of material that will serve as an introduction to radar and the atmospheric environment, while providing a useful reference for general radar applications. The formal treatment of the radar equation, the Gaussian field expansions, the electromagnetic scattering derivations, and the fractal formulations are of general applicability. Weather and attenuation models, although more specialized, are useful for many radar applications. An annotated bibliography directing readers to source material for greater depth is included. The chapters devoted to meteorological topics are intended for readers from the radar as well as the communication and microwave communities, because they provide material missing in many electrical engineering curricula. These ele-

ments combined under a single cover should provide a potentially versatile and useful addition to current radar libraries.

ALFRED J. BOGUSH , JR., PHD  
HUNTSVILLE, ALABAMA  
APRIL 1989

## ***Acknowledgments***

The material contained herein has been assembled since 1978 although the Gaussian developments were to some degree applied earlier. Many colleagues were helpful and contributed to the collection of the data. Included were E.J. Chang and D.H. Divis. The development of an approximate theory of large aperture antennas and fractal models and procedures was accomplished in collaboration with Dr. R.E. Elkins, whose efforts and contributions are appreciated. Several government agencies were supportive of the many programs conducted within this decade of activity. Specifically, acknowledgment is extended to M.L. Whitfield and S. Massey for their support and technical contributions. Special acknowledgements are given to Katherine A. Byrd, physicist and daughter, for reviewing the manuscript and making quantitative suggestions, and Alta M. Bogush for typing and editing.

# ***PART I***

## ***INTRODUCTION***

The radar theory and equation derivations, descriptions of elements of the atmosphere, and data compilations and models presented in this volume provide an introduction to the theory of radar and definition of the natural atmospheric environment. An introduction to the theory of radar, independent of applications, follows directly from the radar equation. The equation is provided in the classical form, derived from electromagnetic field theorems, and defined through a Gaussian approximation. Recognizing the formulations as the foundation of radar theory, a field theory view of radar is presented. An introduction to the natural atmospheric environment involves descriptions of elements of the atmosphere, their global distributions, their physical properties, and radar attenuation and scattering parameters. Atmospheric data of these forms are provided and constitute an application of the theoretical formulations.

Technical discussions span fundamental field theory, basic principles of radar, summaries of meteorological principles, system analysis, data compilations, and environmental models. Included are methodologies for application of the material contained within the data descriptions, and an abundance of examples showing the usefulness of the mathematical formulations contained in the theoretical discussions. The introductory context is intended to provide useful and thought-provoking material in the general area of radar and the atmospheric environment.





# *Chapter 1*

## *The Radar Environment*

### **1.1 BACKGROUND**

Radar system design considerations typically involve a complicated man-made and natural operational environment. Interfaces may occur with a higher-level system structure, other radars and system components, various adjuncts, and communication systems of many forms. Inherent in the radar development process are specifications of radar parameters, dictated by the system application and operational scenarios, the man-made operating environment based on global sitings, the static and dynamic target properties and their operational scenarios, the natural atmospheric environment, the radar subsystem and component parameters, and interfaces with other sensors or communication systems.

#### **Considerations**

The subsequent radar design and development process relies predominantly on simulation at many levels. If the radar is an inherent part of a moving platform such as an aircraft, missile, or satellite, system-level simulations may involve sophisticated and extensive three or six degree-of-freedom dynamic considerations, radar and environmental modeling, and other system representations. The simulations at these high system levels assess radar performance subject to the environment, the target scenarios, and the ability of the radar to function in an acceptable way with other systems. The level of detail of the radar simulations may vary between error modeling, where measurement errors are represented, and functional modeling, based on radar equation computations or detailed simulations where signal properties are predominantly taken into account. The system-level simulations, when directed toward the radar, provide performance estimates that may result in changes in the radar specifications and design. Simulations at the lower radar system level also include the primary error, functional, and signal

considerations that are formulated or influenced by the specifics of the radar subsystems and components. Prominent considerations are the radar antenna, the beam properties, the effects of the man-made and the natural environment on the propagation of the signals, the scattering properties of the targets, and the effects of cluttered environments. All are primary constituents of the radar equation.

## **A Methodology**

In the development process, radar basics revert to the radar equation and its effective application at total system, radar system, and component levels. The system development methodology showing applications and interfaces is depicted in Figure 1.1, where each line connecting elements of the diagram represents a two-way flow. Radar specifications evolve from a system configuration defined to meet mission requirements against a defined target scenario within a specified operational environment, and the accented lines show where emphasis is placed with reference to the total radar development process. The operational environments, both natural and man-made, include the targets. The radar development process involves specifications of the radar parameters, the subsystems and components, and interfaces. Radar performance is evaluated through radar and environmental simulation and testing, and total system simulation and testing. Each influence the radar development and the establishment of the operating radar parameters. Although postulated, the methodology is representative of current radar developments influenced by cost, long acquisition times, and recent computer technology and simulation developments. The influence of simulation and analysis on the radar development process is significant.

The use of the range equation in the total system development establishes the framework from which operational systems evolve. We need thorough understanding of the workability of the subsystems that form the radar as well as the properties of the targets, the deployment, the natural environment, and hostile environments that may be encountered. Realistically, radar developments proceed through an iterative approach involving changes in the radar design deemed necessary with evolving definition of the targets and the operational environment. Since modern radar design relies heavily on computer modeling and simulation, many of the uncertainties in the radar design process can be relieved through thorough understanding and combined representation of the radar and its operating environments.

The material presented provides an introduction to the radar and the atmosphere for the specification of the operating environment, the establishment of radar requirements, the development of radar parameters, performance evaluations, and the simulation of radar and the environment. A systemic viewpoint is taken in the diverse discussions, with the intent of unifying the analysis that occurs at the various levels of the system's structure.

---

## 1.2 THE RADAR EQUATION

The radar equation is the foundation of radar theory and applications. When viewed in a functional way, the transmitted power, wavelength, bandwidth, noise temperature, and system losses are the principal parameters of the radar. The fourth-power range dependence, or range-squared dependence for Friis' transmission equations, and the associated atmospheric loss account for the propagation of the signals. The presence of the radar cross section accounts for the target or cluttered background that may be encountered. Each parameter, when examined, is an independent entity associated with the subsystems and components making up the radar, signal propagation, and target cross sections. It is important that we understand the radar equation when it is applied to analysis and simulations at component, radar, and total system levels.

For example, for system analysis applications, we should understand the requirements, the functions of the radar, the target characteristics, and the properties of the environment. The radar parameters need to be understood with an appreciation of atmospheric and system losses. For radar performance analysis, the modeling of the targets and clutter, and the realistic representation of the measurement errors of the radar are critical. Judgments must be made when parameters are selected for analysis to assure realism and confidence in the results. Target cross sections, target models, and clutter parameters are the most troublesome in this respect.

### Classical Form

The radar equation is a prominent subject in many radar references. The early work of Barton, is notable. As a starting point, the classical radar equation is derived from antenna principles following his initial work. The use of the equation within a total system context is delineated where issues of requirements, parameters, and analysis are described from the viewpoint of modern radar development methodology. Our discussions follow the postulated radar development methodology in Figure 1.1.

### A Formal Description

In principle, the radar equation is an application of electromagnetic field theory. Normally, equation derivations follow from a direct application of antenna principles and are applicable when targets are far removed from the radar, which is the normal operating condition. Because antenna theory is a subset of electromagnetic field theory, the derivation of the radar equation follows directly from Maxwell's equations.

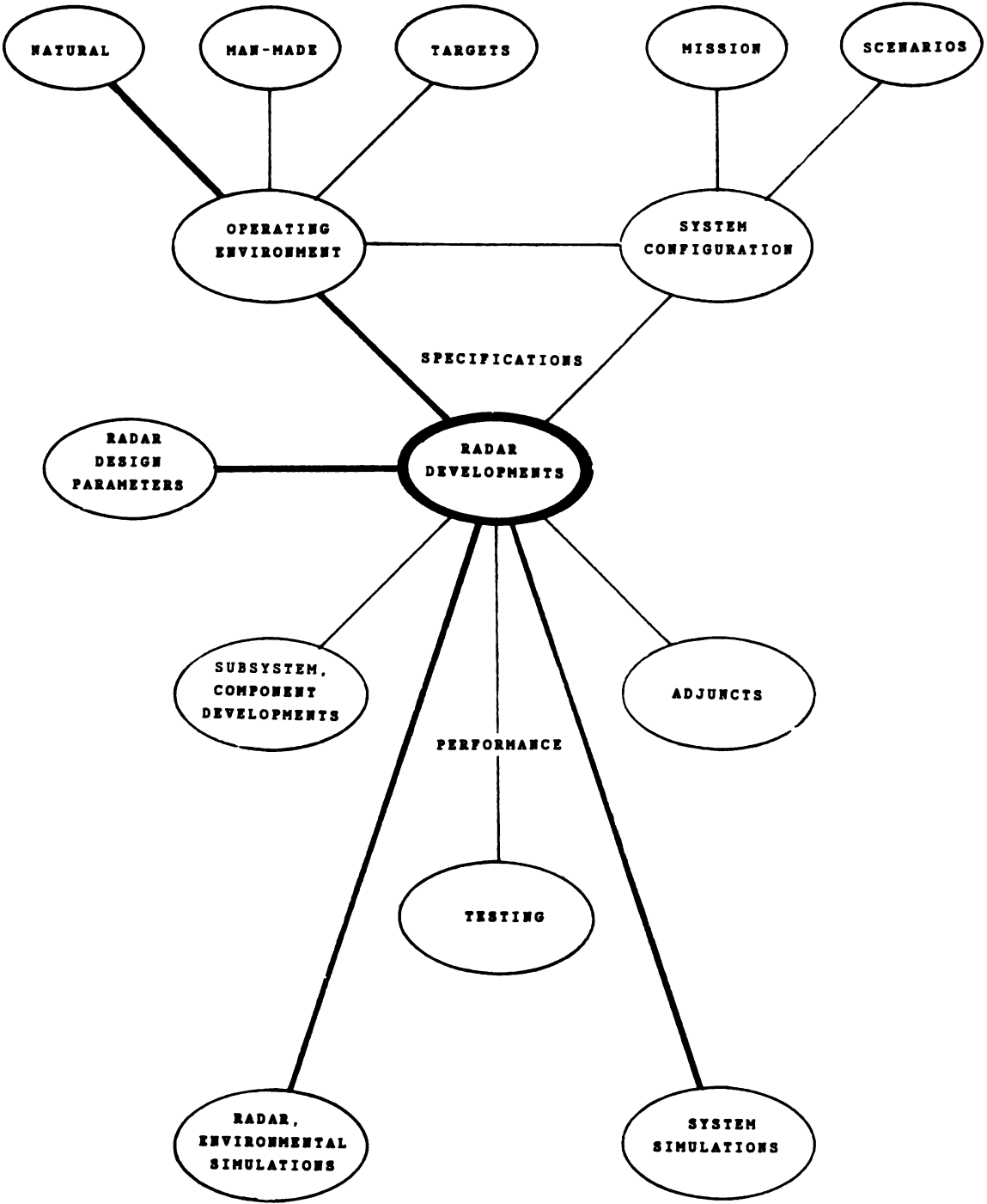


Figure 1.1 A Postulated Radar Development Methodology

The radar equation, like antenna and scattering formulations, can be derived from diffraction theorems. When large aperture antennas are considered, approximations are invoked that exclude edge or diffraction effects about the extremities of the antennas. These restrictions, at first glance, negate their usefulness, but are negligible if aperture sizes are large as compared to a wavelength, which is most often the case in radar applications. Theoretically, complicated field equations are reduced to solvable integral forms. This theory is referred to as Kirchhoff's theory, with the integrals being the diffraction integrals. A similar derivation of scattered fields leads to the physical optics, or Kirchhoff's form of scattering. When the antenna and scattering are combined in a similar formulation, the radar equation evolves, with implicit insight given to antenna and scattering principles. The radar cross section, in particular, is interpreted from a diffraction integral, which gives added meaning to its physical interpretation.

Within this framework, descriptions of elements of the radar equation follow in a correlative way. Consideration is given to antenna formulations—Fourier, Hankel and Gaussian methods, and arrays; propagation—plane waves; and scattering centers—Rayleigh, physical optics, and geometric scattering. Consideration of the radar signal, provided within a similar theoretical and applied context, encompasses all basic parameters of the radar equation.

It is necessary to supplement the equation derivations with a review of field principles. A discussion of Maxwell's equations is included, where attention is given to units and dimensions, sometimes confusing in field theory applications.

## **Gaussian Form**

When targets occur in the near fields, radar equation computations may involve the solution of diffraction integrals in numerical or closed forms, or the computations of field intensities using antenna array formulas. In either case, the computations become unnecessarily complicated. When the Gaussian theory of large aperture antennas is applied, a resulting single form of the radar equation becomes convenient for near-field and far-field computations. The resulting radar equation is an application of the Gaussian theory of large aperture antennas, a generalization of the Gaussian beam approximation commonly used in radar analysis and simulation. When volumetric scattering is of concern, and in particular when rain is considered, the resulting Gaussian form of the radar equation provides a generalization of the current meteorological radar equation, and is also applicable for near-field applications.

## **1.3 THE ATMOSPHERIC ENVIRONMENT**

The radar development process begins with the establishment of target and en-

vironmental specifications. Because the atmosphere is common to most systems and radar frequencies have risen into the millimeter-wave region, important elements of the atmosphere include clear air, rain, and clouds of several forms. Initial considerations include the characterization of the atmospheric environment, and the identification and definition of elements of the atmosphere. It is important in establishing environmental specifications to consider global distributions of the environmental data and their representation in environmental models. A radar system may be degraded in many ways. These initial discussions include an overview of environmental effects on radar, their influence on radar analysis, and the resulting effect on simulation needs.

## **Effects**

Millimeter waves are those radiations having wavelengths between 1 and 10 mm or, equivalently, having frequencies between 30 and 300 GHz. At these wavelengths, high resolution performance may be achieved by systems of modest size. Thus, there is an increasing interest in millimeter waves for use in ground-based and airborne radars of many forms. The physical phenomena that can degrade signal propagation in the atmosphere include attenuation due to molecular absorption in a clear environment; attenuation due to absorption by rain drops; attenuation due to absorption by water droplets (hydrometeors) in fog, haze, and clouds; attenuation due to suspended particles in dust and smoke; scattering from rain drops or other atmospheric constituents that influences radar noise levels; measurement errors due to irregularities in the index of refraction; signal distortions due to irregularities in the index of refraction; propagation effects on signal quality due to atmospheric dispersion; noise emission due to gaseous absorption and absorption by hydrometeors; and depolarization effects.

Absorption occurs when electromagnetic energy is converted to heat by interacting with matter. Absorption by individual molecules and by agglomerations of molecules (particles) is especially important in the design of millimeter-wave systems. Scattering occurs when the propagation direction of electromagnetic energy is altered by interacting matter. Scattering from particles of dust and from hydrometeors (water or ice condensed in the atmosphere (i.e., fog, rain, snow) is of primary concern. On a smaller scale, molecular scattering can be neglected for most millimeter-wave and lower operating frequency systems. Both absorption and scattering from spherical particles are described by Mie scattering theory. Rayleigh scattering, or the Rayleigh approximation, for wavelengths much larger than the particle diameter, is a limiting case of Mie scattering, which occurs at lower operating radar frequencies for rain and other atmospheric environments.

Refraction gives rise to several effects important to atmospheric millimeter-wave propagation, including elevation angle errors, time delay measurement er-

rors, spectral dispersion, and scintillation. These effects are governed by the time and space distribution of the complex atmospheric index of refraction. Elevation angle errors can occur when a radar signal passes through a gradient in the index of refraction. Time delay measurement error, or ranging error, can occur when a radar signal passes through a region of poorly-characterized index of refraction. Spectral dispersion occurs when a signal passes through a medium with a frequency-dependent index of refraction, and can result in varying degrees of signal distortion. Scintillation refers to time variations in amplitude, phase, and angle of arrival of a signal which arise when the signal scatters from turbulence. Scintillation is important primarily for signals propagating over long paths at small elevation angles. Multipath can result when strong gradients in index of refraction and short term instabilities in the atmosphere cause changes in beam path and fluctuations in signal. Multipath is also associated with low elevation angles.

Solid and liquid materials in the air are important to millimeter-wave propagation. When particles are small enough to remain suspended for appreciable periods of time by normal atmospheric processes, an aerosol is said to exist. Suspended particulates are frequently described in terms of a size distribution. This is, by convention, a function of particle radius  $r$ , and equal to the limit (as  $\Delta r$  approaches zero) of the number of particles in the size range between  $r$  and  $r = \Delta r$  found in a unit volume and divided by  $\Delta r$ . It has units of inverse length to the fourth power. Most often, size distribution is given in particles per cubic centimeter of volume per micron of radius. Several empirical models are widely used for fitting observed distributions. Log-normal and power-law distributions are commonly used, but fail to fit some data. Bimodal distributions refer to those in which the size distribution has two maxima. Such distributions are most frequent in dynamic dispersions such as fogs and hygroscopic smokes. Anomalous results can appear to occur if a bimodal distribution is treated with a unimodal model.

Measurement of submicron particles is very difficult and subject to systematic error. Depending on the instrument used, particle agglomeration and preferential fractionation may distort measurements. There is also disagreement about the sensitivity and reliability of some instruments. Older measurements, in general, should be regarded as less reliable than more recent ones.

## **System Needs and Models**

Requirements for radar analysis and modeling depend on the anticipated operating environment and requirements in system robustness. If the system must function in a wide range of adverse environmental conditions, we must understand the existence of atmosphere, the properties, and how likely they are to occur. A system cannot be built to function under every conceivable contingency, but by assessing the likelihoods of adverse conditions, the probability of malfunction can be reduced



to an acceptable level. Robustness describes how well a system must be built to accomplish its mission. Unnecessary robustness and mission failures are prices paid for lacking knowledge of adverse conditions.

The atmosphere has features which change continuously in time and space. Many of those features cannot be predicted deterministically more than a few hours ahead of occurrence. Features such as rain cells may be unpredictable even a few minutes ahead of time. Therefore, statistical models of the atmosphere form an important tool for the designers of systems that must operate in the atmosphere. The accuracy and usability of the models bear directly on the success and cost-effectiveness of the radar systems.

The atmospheric modeling needs for a study of propagation or other atmospheric-related phenomenon involve consideration of operation at a given time of day and year and at a given height and geographic location, operation in specified weather, the possible effects of the atmosphere on the system, and the probability of the occurrence of atmospheric effects. Atmospheric models for radar wave propagation that will meet all of these requirements are not currently available. However, the pieces required to assemble such a model exist. Those pieces fall into three categories: propagation models for millimeter waves in clear air and in aerosols of specified composition; distribution models for constituents and aerosols in given micrometeorological conditions, including man-made events; and distribution models for world wide weather. Many of these data are incomplete and many have large uncertainties. This will be reflected by large uncertainties in any atmospheric model.

The pertinent propagation models describe millimeter-wave transmission for given air pressure, temperature, and humidity, and for given distributions of particulates. Theoretical models and field data which exist for molecular absorption in clear air are in fair agreement. Scattering and absorption by spherical particulates can be described by Mie theory. Scattering and absorption by nonspherical particulates are not well understood, particularly for the complex shapes assumed by ice and dust particles.

A micrometeorological distribution model requires probabilistic data describing air pressure, temperature, and humidity distributions, as well as particulate size, shape, and mass distributions for small-scale weather systems. Existing models are, for the most part, empirical, and are frequently little more than tables of data. Much disagreement can be found among observers, particularly in describing active systems such as clouds and storms. The matter of description is complicated by the fact that even similar systems can exhibit a great deal of variability from one geographic location to the next.

A world wide weather distribution model requires probabilistic data describing micrometeorological events for geographical location and for time of day and year. Existing models primarily comprise tables of data. Some parts of the world are reasonably well characterized, but most parts are very poorly characterized.

---

Therefore, an atmospheric model for propagation that can be assembled from existing data may be subject to large uncertainties. However, the rising interest in millimeter-wave propagation, in particular, can be expected to lead to a continuously improved understanding of pertinent atmospheric phenomena. Thus, any atmospheric model should be reviewed and updated on a regular basis. Emphasis in all the data sets is on attenuation and backscatter. Most of the data provided are rain data, where effects on radar are most pronounced. In all discussions, the material is considered introductory and forms the basis for an understanding of the atmospheric data base with its use in radar analysis and simulation.

### **Data Sources**

The models and data sets described in Parts III and IV are presented in summary form. In some instances, especially when models are described, it is difficult to be thorough while keeping the descriptions within reasonable bounds. The bibliography contains reference material for further detail. Most of the data provided is a result of the work of J.H. Liebe, R.K. Crane, and L.J. Ippolito. Two papers by Liebe covering a number of atmospheric propagation data compilations are used. The most recent contains useful formulations for calculating specific attenuation in four frequency bands for rain, snow, haze, fog, clouds, water vapor and dry air. Two papers by R.K. Crane, which cover the description and modeling of attenuation due to rain are significant. The first paper describes a path-dependent model from which the uniform and path-dependent models are derived. His second paper includes statistical representations of cells and debris, forming the basis for attenuation and drop size estimates included in the third model described. This particular paper may be of more value than indicated in the summary model description provided. Extensive use is also made of the published work of L.J. Ippolito, who compiled most of his material from a NASA handbook. The dust data provided is based on a paper by Seagraves, and fractal formulations are from the work of Mandelbrot and colleagues.

Atmospheric data for radar applications can be found in radar sources and sources in areas including the atmospheric sciences, communications, radar meteorology and, in the most recently expanding technology, the remote sensing sciences. Each of these data sources focuses on a specific area of concern, which although applicable to radar, may require special consideration to bridge the gap between the data sources and the radar user. This consideration is reflected in the discussions covering the data basis and associated models. The approach taken in the model developments emphasizes radar simulation, with an overall applicability to analysis problems involving radar and the natural atmospheric environment.

Data are obtained from the sources stated above. Clear air attenuations and attenuation factors for a number of atmospheric environments are obtained from

the atmospheric sciences. The data obtained from communication sources, which are extensive, are centered about the data base established for satellite communication systems. Not only are useful rain attenuation and scattering parameters available, but the introduction of path dependence in attenuation estimates has origins in the communication work which includes quantitative definitions of heights of storms in reference to the zero-degree isotherm, important in many radar applications. Considerable attenuation and backscatter data of atmospheric constituents for radar use can also be found in remote sensing data compilations. Overall, a special effort is made in the compilations to assure conformity between the varying sources of data.

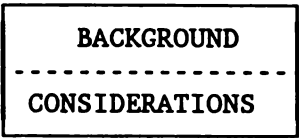
As the level of sophistication of radar technology increases, the importance of modeling is enhanced. The models may be of phenomenological origin, the representation of a subsystem component, or the simulation of a radar subjected to a specific target and clutter environment. Considerations involve representations of complicated cluttered environments by some reasonable means, that will emulate radar performance under known conditions with acceptable interpolations and extrapolations. Generally, this occurs in radar by data collection, reduction, analysis, modeling, and some means of verification. For cluttered environments in particular, the modeling process may follow a mathematical procedure, where theory and measurements are combined to yield models with acceptable levels of accuracy. Emphasis may be placed on mathematical procedures when phenomenology evaluations are inadequate or the data base is incomplete. This system analysis view of model development is reflected in the discussions. The use of environmental models is encouraged where interpolation and extrapolation of data sets provide realism over single-valued representation of complicated occurrences.

The data compilations provided include models for analysis and simulation applications, and methodologies are suggested for use of the data. Rain models of varying fidelity are provided that include a uniform assumption, account for upper altitude bounds, take nonuniformity into account through the use of path dependence, and introduce fractal theory. The fractal formulations, in addition to their use in describing certain rain occurrences, are important in the representation of many radar environments.

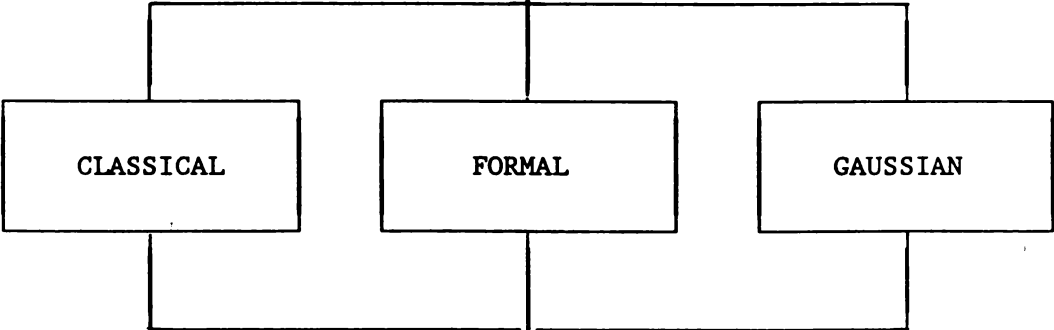
## **1.4 ORGANIZATION OF THE MATERIAL**

The assembly of the material is depicted in the flow diagram in Figure 1.2. The four-part structure is shown with background given in Part I, the radar range equation theory and derivations in Part II, the meteorological discussions and applications in Part III, and the data compilations and models in Part IV. The chapters are numbered consecutively within the three major subdivisions, Parts II to IV, with short summaries provided between each one. The intent of Parts III and IV is to provide the modeling approach and data necessary to include the effects of natural environment in radar performance evaluations.

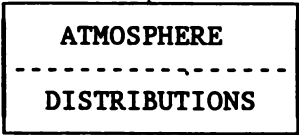
PART I - INTRODUCTION



PART II - THE RADAR EQUATION



PART III - ENVIRONMENT



PART IV - DATA

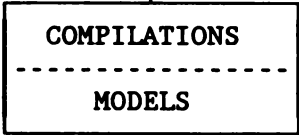


Figure 1.2 Diagram Depicting Interaction between Principal Subject Elements

Classical, formal, and Gaussian treatments of the radar equation are placed in three separate chapters. The material presented is treated independently and may be used directly with the data sets and models. The radar meteorological equation is included in each of the equation derivation groups. An appendix containing properties of antennas in conventional and Gaussian forms supports the equation derivations. The radar equations are derived in classical, conventional, and meteorological forms. They include lossless or idealized environments, the natural atmosphere with propagation path losses, and rain environments. The equations are developed from antenna principles in the classical derivations and Maxwell's equations in a formal treatment. Gaussian forms of the classical equations are derived from the approximate Gaussian theory of large aperture antennas. When combined, the equation derivations serve as an introduction to radar while providing a number of useful formulas.

The two chapters devoted to the meteorological topics in Part III are also structured in an autonomous way, with the environmental data in Chapter 5 and the global distributions in Chapter 6 being part of the models described in the later chapters. These data are intermixed with the reviews of the elements of the atmosphere and are summarized in the model developments. In particular, the global rain distributions in Chapter 6 are an inherent part of a rain model described in Chapter 8.

This independence between parts is continued in Part IV, where data sets and models are described. Each data set is treated separately, with models pertaining to the particular element of the atmosphere being addressed. Methodologies suggesting the use of the data are included in the discussions. Appendix B contains statistical formulations, and it is included to support the data sets and models.

Reference material is provided in Appendix C, which contains an annotated bibliography. We cite the chapters to which references are applicable.

## ***PART II***

### ***THE RADAR EQUATION***

In the three chapters to follow, the classical radar equation is reviewed, placed in several forms, and applied. Then a formal approach is taken, covering Maxwell's equations, the radar equation developed from the Friis' transmission, and Kirchhoff's diffraction formulas. Each element of the equation receives special attention. Gaussian forms of the radar equation are derived, emphasizing near-field applications. The notion of Gaussian equivalents is described, and representations of aperture, near, and far fields are simplified. Volume scattering and meteorological forms of the radar equation are included.

In later chapters, data compilations and models are provided for elements of the atmosphere. The radar equations, given in several forms and described in different ways, may be used separately or together in the application of the environmental data.



## *Chapter 2*

### *The Radar Equation—Classical Forms*

The radar equation provides the means to estimate the sensitivity of a radar for given operational, target, and environmental parameters. The received signal power is proportional to the transmitted power, the transmitting and receiving antenna gains, the target cross section, and the square root of the signal wavelength. The signal power is inversely proportional to the fourth power of the range to the target, is subjected to losses within the operating environment, is dependent on the various subsystems within the radar, and is corrupted by noise.

The *radar equation* is a statement of antenna and scattering principles. It is derived in the normal way, whereby losses within the atmospheric environment are separated from system losses, to allow for convenient representation of multiple degrading effects along a propagation path. Concern is given to path dependence, where attenuation is influenced not only by rain rates or intensity but also the path length. The result is a statement of the classical form of the radar equation from which other forms evolve. The three examples included and applied are the bistatic, search, and interference formulations. Meteorological forms of the classical radar equation are derived, and volume general scattering analysis procedures are included. The use of a Gaussian beam as a convenient analysis tool is demonstrated in the derivation.

Using the radar equation requires an appreciation of the parameters and their system implications, their relationship to higher-level system configurations from which the radar requirements evolve, and to subsystems where radar performance expectations dictate their basic requirements. Introductory material is provided on radar requirements, parameters, performance, and subsystem parameters. As a prelude to the discussions, an evolution of radar requirements is described in the context of modern radar development. Although postulated, the discussions involve actual expected occurrences in the evolution of a radar. The topics, described from a system viewpoint, include the acquisition process, forms and types of specifications, the determination of system requirements, and levels of computer simulation and analysis. The importance of environmental specifications and radar parameters is covered, thereby placing the radar in a realistic development context. Examples provided show how to use the radar equation for analysis at all levels



of the system structure, and how radar applications are derived from the system specifications. The chapter concludes with a quantitative description of an element of the radar and its related performance.

## 2.1 INITIAL DERIVATIONS

The radar equation is presented in the classical form and then placed in useful bistatic and search forms. The equally significant Friis' transmission formula, is commonly used in communication theory, but is also applicable to radar when one-way paths are encountered. These transmissions occur in beacon systems, in radar cross section augmentation configurations, and in normal radar operation subjected to noise interference. The transmission formula is derived, placed in a useful form for interference analysis, and related to the classical radar equation.

### Classical

In this first equation derivation, a monostatic radar deployment is considered as depicted in Figure 2.1 (a). The transmitting and receiving radars are co-located, affected by the atmosphere, and confronted by a single target. The power density at the target can be expressed as the product of the transmitted power uniformly distributed over a spherical surface centered at the radar, and the antenna gain:

$$S_i = \text{Power Density at Target} = \left( \frac{P}{4\pi r^2} \right) (G) \quad (2.1)$$

where  $P$  is the peak power transmitted and  $G$  is the gain of the antenna. The radar cross section is defined as

$$\sigma = \lim_{r \rightarrow \infty} 4\pi r^2 \left( \frac{S_s}{S_i} \right) \quad (2.2)$$

where  $S_s$  is the power density at the radar scattered by the target. Forming the product:

$$S_s = \text{Power Density at Antenna} = \left( \frac{P}{4\pi r^2} \right) (G) \left( \frac{\sigma}{4\pi r^2} \right) \quad (2.3)$$

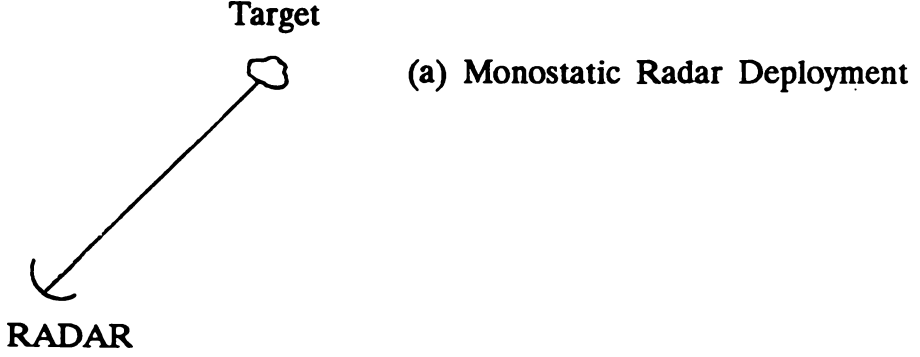


**Figure 2.1** Radar Deployments, (a) Monostatic. (b) Bistatic.

results in the power density at the radar expressed as a function of transmitted power, antenna gain, and radar cross section. The signal power  $S$  at the terminals of the antenna is

$$S = A_e S_s = \left( \frac{P}{4\pi r^2} \right) \left( G \right) \left( \frac{\sigma}{4\pi r^2} \right) \left( A_e \right) \quad (2.4)$$

but the effective area of an antenna is related to the gain:

$$G = \frac{4\pi A_e}{\lambda^2} \quad (2.5)$$

or, equivalently,

$$A_e = \frac{G\lambda^2}{4\pi} \quad (2.6)$$

The signal power at the terminals of the antenna now becomes

$$S = \frac{PG^2\sigma\lambda^2}{(4\pi)^3 r^4} \quad (2.7)$$

which is the classical form of the radar equation. It may appear in the form of Equation (2.4) where, considering Equation (2.6), a difference in transmitting and receiving gains is implied. It is also common in those instances to express the gain as the product  $G_T G_R$ , where  $G_T$  and  $G_R$  are the transmitting and receiving gains,

respectively. The gain is usually the maximum, on-axis gain of the radar, proportional to the radiated power density. Thus, an angular dependence is implied,  $G \rightarrow G(\theta, \phi)$ . The maximum gain of the radar is the directivity, defined as the ratio of the radiated power to an equal power radiated isotropically. The directivity excludes losses in the antenna but includes the aperture efficiency. It is common practice to relate the effective area  $A_e$  to the actual area  $A$  as the product  $\eta A$ , where  $\eta$  is the aperture efficiency. The following gain formula results:

$$G = \frac{4\pi\eta A}{\lambda^2} \quad (2.8)$$

where  $A$  is the area of the antenna and  $\eta$  is the aperture efficiency. Values of  $\eta$  are tabulated for antennas of varying shapes and aperture distributions. Maximum gain occurs when  $\eta = 1$ , achieved with a uniform aperture distribution.

The sensitivity of the radar is corrupted by noise from internal and external sources. By definition and convention, the signal-to-noise output of the receiver is referred to the antenna terminals through a noise temperature  $T_s$ , with the effective noise power defined as

$$N = kT_s B_n \quad (2.9)$$

where  $k$  is Boltzmann's constant,  $T_s$  is the system noise temperature, and  $B_n$  the noise bandwidth of the receiver. The system noise temperature includes external galactic noise sources, thermal noise resulting from antenna and transmission losses, and receiver noise. From Blake, the system noise temperature is expressed in the following way:

$$T_s = T_a + T_r + L_r T_e \quad (2.10)$$

where  $T_a$  is the antenna temperature,

$$T_a = \frac{.876 T_a' - 254}{L_a} + T_0 \quad (2.11)$$

$T_a'$  is the noise temperature of a lossless antenna and  $L_a$  is the loss.  $T_0$  is the ambient temperature, 290K.  $T_r$  is the temperature of the transmission system between the antenna and receiver, related to the actual temperature  $T_{tr}$  and loss  $L_r$  in the following way:

$$T_r = T_{tr} (L_r - 1) \quad (2.12)$$

Returning to Equation (2.10),  $T_e$  is the noise temperature of the receiver given in

terms of the noise figure  $F$  by

$$T_e = T_0(F_n - 1) \quad (2.13)$$

Antenna noise temperatures,  $T_a'$ , have been compiled for varying radar frequencies and elevation angles.

The sensitivity of the radar is also degraded by losses of internal and external origin. When losses resulting from the atmosphere are pronounced, more than one atmospheric effect that is bounded in altitude and horizontal extent may occur. In those instances, it is advantageous to separate the internal and external loss. Let this separation be stated as a total loss of  $L_p L$ , where  $L_p$  is the propagation loss and  $L$  the internal system loss.

Taking the ratio of  $S$  of Equation (2.7) to  $N$  of (2.9), and inserting the loss representations, yields the radar equation:

$$\frac{S}{N} = \frac{PG^2\sigma\lambda^2}{(4\pi)^3 r^4 k T_s B_n L_p L} \quad (2.14)$$

Reviewing and concentrating on units, we have

- $S$  = signal power (watts);
- $N$  = equivalent noise power (watts);
- $P$  = transmitted power (watts);
- $G$  = antenna gain (dimensionless);
- $\sigma$  = radar cross section (square meters);
- $\lambda$  = wavelength (meters);
- $r$  = range to target (meters);
- $k$  = Boltzmann's constant ( $1.38 \times 10^{-23}$  watts per hertz per kelvin);
- $T_s$  = system noise temperature (kelvin);
- $B_n$  = receiver noise bandwidth (hertz);
- $L_p$  = propagation loss (dimensionless);
- $L$  = system loss (dimensionless).

Use of the system temperature to establish the noise level of the radar is common practice. Earlier conventions, based on an assumption of a reference input temperature  $T_0$ , expressed the noise levels as  $kT_0 B_n \bar{N}F$ , where  $\bar{N}F$  is defined as a system noise factor. The system noise temperature convention is preferred because external as well as internal temperatures are taken into account in a well defined way.

## Bistatic

Referring to Figure 2.1(b), two radars are separated, far removed from each other and the target. The bistatic radar equation for this configuration is derived from the product of the power density at the second radar and the effective area:

$$S = S_i \left( \frac{G_2 \lambda^2}{4\pi} \right) = \left[ \left( \frac{PG_1}{4\pi r_1^2} \right) \left( \frac{\sigma_b}{4\pi r_2^2} \right) \right] \left( \frac{G_2 \lambda^2}{4\pi} \right) \quad (2.15)$$

then,

$$\frac{S}{N} = \frac{PG_1 G_2 \sigma_b \lambda^2}{(4\pi)^3 r_1^2 r_2^2 k T_s B_n} \quad (2.16)$$

where  $\sigma_b$  is the bistatic radar cross section.  $G_1, G_2$  and  $r_1, r_2$  designate the respective radar parameters. When bistatic target and clutter data are available, the power density contained in Equation (2.15), and Equations (2.15) and (2.16) are equally useful. Several examples are provided in Chapter 4.

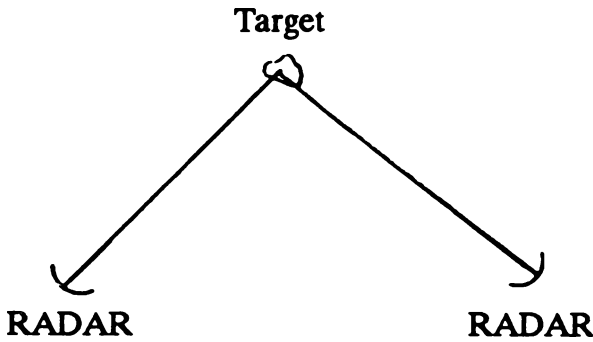


**Figure 2.1** Radar Deployments, (b) Bistatic.

## Search Form

Equations (2.7) and (2.14) have been appropriately referred to as the classical radar equation appearing in very basic forms from which other representations evolve. When radar coverage is large and search functions are performed, it may be convenient, but not necessary, to determine radar sensitivity from average power and aperture area. The principal measure of radar performance then becomes the power aperture product. As we will see, the derivation of the search radar equation is a direct reduction of the classical form.

Let the solid angle searched by  $\Omega$  and the solid angle of the antenna beam be  $\Omega_b$ . In view of Equation (2.8),

$$G = \frac{4\pi}{\Omega_b} \quad (2.17)$$

and

$$\Omega_b = \frac{\lambda^2}{\eta A} \quad (2.18)$$

Now referring to Figure 2.2, assume a matched receiver:

$$\tau B_n = 1.0 \quad (2.19)$$

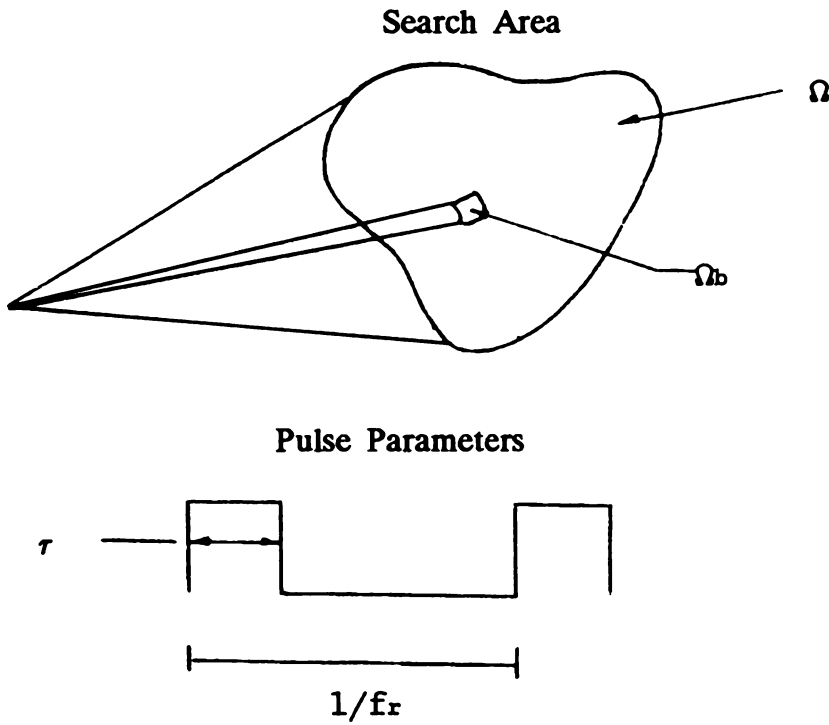


**Figure 2.2** Pulse Formations

and a coherent integration of  $N$  pulses:

$$N = t_0 f_r \quad (2.20)$$

where  $t_0$  and  $f_r$  are the dwell time and pulse repetition frequency depicted in Figure 2.2. When pulses are coherently integrated, the resultant signal to noise is the product of the number of integrated pulses and the single-hit signal-to-noise ratio. Now we have the average power of the radar given by

$$\bar{P} = \tau f_r P \quad (2.21)$$

and

$$\frac{\Omega_b}{\Omega} = \frac{t_0}{t_s} \quad (2.22)$$

where  $t_s$  is the frame time or the total time taken to search the solid angle  $\Omega$ . We then substitute parameters into equation (2.14), and after some manipulation, the following search radar equation is obtained:

$$\frac{S}{N} = \frac{t_s \sigma}{4\pi r^4 \Omega k T_s L} \left[ \bar{P}(\eta A) \right] \quad (2.23)$$

The quantity within the brackets is the power aperture product. The equation relates radar performance to available power. Although not explicit, the wavelength dependence varies with the choice of parameters. This equation is especially useful when dwell times, frame times, and power requirements for a search radar are known.

### Friis' Transmission Formula

Of equal prominence with the classical radar equation is the Friis' transmission formula, which relates the power transfer between two antennas. It is sometimes referred to as a *one-way transmission equation*. The derivation again follows previous ones.

Let the antennas be directed toward each other and be separated by a distance  $r$ . Let the transmitted power of antenna 1 be  $P_1$ , the antenna gain  $G_1$ , and the effective area  $A_{e1}$ . Likewise, let the receiving parameters be  $P_2$ ,  $G_2$ , and  $A_{e2}$ . At antenna 2, the received power is the product of the uniformly-radiated power density, the transmitted power, and the effective area of the receiving antenna. Then,

$$P_2 = \frac{P_1 G_1 A_{e2}}{4\pi r^2} \quad (2.24)$$

This result is applicable for one-way radar transmission occurrences such as beacon interrogations or interference receptions. The ratio of the powers is called the *transmission formula*:

$$\frac{P_2}{P_1} = \frac{GA_{e2}}{4\pi r^2} \quad (2.25)$$

which may also appear in the following form:

$$\frac{P_2}{P_1} = \frac{A_{e1}A_{e2}}{r^2\lambda^2} \quad (2.26)$$

where  $G$  has been replaced by  $4\pi A_{e1}/\lambda^2$ .

The radar equation may be derived from the transmission formula. Let the power received at antenna 2 be transmitted back toward antenna 1; then applying the transmission formula, in two steps, yields the received power  $S$  now at antenna 1 as,

$$S = \left[ \frac{P_1 G_1}{4\pi r^2} \right] \left[ A_{e2} \right] \left[ \frac{G_2}{4\pi r^2} \right] \left[ A_{e1} \right] \quad (2.27)$$

Rearranging terms, we have

$$S = \frac{P_1 G_1 G_2 \lambda^2}{(4\pi)^3 r^4} \left[ A_{e2} G_2 \right] \quad (2.28)$$

In view of Equation (2.20), replacing  $A_{e2} G_2$  with  $\sigma$  and dropping the subscripts yields the classical radar equation, repeated here for convenience,

$$S = \frac{PG^2\lambda^2\sigma}{(4\pi)^3 r^4} \quad (2.29)$$

As we have seen, the Friis' transmission formula applies to radar when one-way paths arise. A prominent example occurs when the radar is subjected to interference, which is covered next.

### Radar Equation With Interference

When a radar is subjected to random noise interference with bandwidth equal to



or greater than the receiver noise bandwidth, the overall effect is an increase in the system noise temperature. Let the receiver noise resulting from the interference be  $I_0$ ; then, applying Equation (2.25) directly, yields the following results:

$$kT_I B_I = \frac{P_I G_I \lambda^2 F}{(4\pi)^2 r_I^2} \quad (2.30)$$

and

$$T_I = \left( \frac{P_I G_I}{B_I} \right) \left[ \frac{G \lambda^2}{(4\pi r)^2 k} \right] (F) \quad (2.31)$$

where the single parameters and groupings are defined as follows:

- $kT_I$  =  $I_0$  = received interference spectral density
- $k$  = Boltzmann's constant
- $T_I$  = noise temperature due to interference
- $B_I$  = interference noise bandwidth
- $P_I G_I$  = effective radiated power (ERP) of the interference source
- $\left( \frac{P_I G_I}{B_I} \right)$  = radiated power density of the interference source
- $G$  = gain of the radar
- $\lambda$  = radar wavelength
- $r_I$  = range to interference source
- $F$  = interference suppression factor

$F$  is usually the radar sidelobe level in the direction of the interference source. Loss terms have been omitted from the formulas, because their effects are usually reflected in the radiated power density levels.

The classical radar equation in the presence of additional noise  $I_0$  can be written as

$$\frac{S}{N} = \frac{P G^2 \sigma \lambda^2}{(4\pi)^3 r^4 k (T_s + T_I) B L_p L} \quad (2.32)$$

which is a useful formula for general radar applications.

## 2.2 ATMOSPHERIC PATH LOSS

Two primary parameters are of concern when atmospheric effects are pro-

nounced—the loss incurred along the propagation path, and the cross section of elements of the atmosphere. Each issue will be treated separately here, beginning with the path loss and concluding with the target and clutter relationships, which are included as part of the development of the meteorological radar equation.

Atmospheric environments that may cause appreciable signal attenuation include clear air, clouds, and rain. Of these, we will assume that the clear air and cloud environments are characterized by uniform attenuations along a propagation path and that cloud environments have specified upper and lower bounds and horizontal extents. When low rain rates of about 1 mm/hr or less are considered, a uniform assumption will also be made, but with a defined upper bound. Higher rain rates will lead to varying attenuations along a path, thus requiring a consideration of path dependence.

Of interest is the development of a convenient representation of the loss term  $L_p$  for radar equation use. Following Crane, let a path-dependent factor  $p_i$  (for the  $i$ th path of concern) be defined in the following way:

$$L_{pi} = 10 \cdot 2a_i p_i D_i \quad (2.33)$$

where  $a_i$  is the specific attenuation per unit length, (i.e., dB/m),  $p_i$  is a dimensionless path length factor, and  $D_i$  is the path length within the atmospheric element. For rain,  $p$  is greater than one when the point attenuation is low to moderate in intensity. When rain rates are high, however, path length factors will be less than one. Both observations are a result of the cellular structure of convective rain, where increases in attenuation can be expected along a path if the radar is situated in areas of low rainfall. If the radar is positioned within a cell, the attenuation along a path can be expected to decrease. For clouds, attention must be given to defining vertical and horizontal extents. In those instances, this formulation remains convenient, with point attenuations used for the given paths  $D$  with the path length factor  $p$  set at unity. Since simulation or analysis programs are usually involved, the problem becomes one of determining the path through the environment for specific target scenarios. Atmospheric environments that fit into this category include clouds of various forms, fog, and light rainfall. Several examples demonstrating the use of this path-dependent formulation will be provided in later chapters when data compilations and atmospheric models are described.

Now let the loss due to elements of the atmosphere be expressed as follows:

$$L_P = \prod_{i=1}^{i=N} L_i \quad (2.34)$$

where  $N$  is the number of path lengths of concern and  $L_i$  is the individual path losses defined by equation (2.33). An example computation is provided below for rain.

### EXAMPLE: ATTENUATION

The specific attenuation of rain is described as a function of the rain rate through the use of two constants. If we let  $a$  be the specific attenuation and  $\alpha$  and  $\beta$  are the constants, then

$$a = \alpha R^\beta$$

Usually  $\alpha$  and  $\beta$  are chosen to allow for computation of the path losses in decibels per kilometer (dB/km). Rain rates are expressed in the customary units of mm/hr. At a frequency of 35 GHz, for rain rates less than 30 mm/hr, the constants are typically stated as  $\alpha = 0.232$  and  $\beta = 1.022$ . For a moderate rain rate of 4 mm/hr, the specific attenuation is estimated to be 0.957, or about 1 dB/km. Data sets are best described in this manner, but if furnished in tabular or graphical form, estimation of the constants ( $\alpha$ ,  $\beta$ ) may be necessary, especially when models for simulation are needed.

### 2.3 METEOROLOGICAL EQUATION

Radar targets appear in several forms. Included here are point targets (such as spheres) observed at high frequencies, extended targets commonly encountered by high-resolution systems, complex targets (such as aircraft) containing many scattering centers, ground and sea surface clutter and volume clutter. Rain environments are characterized as volume clutter, with the resulting radar equation being of meteorological form. The derivation given below follows meteorological procedures and parameter definitions.

Consider the radar resolution cell of Figure 2.3. The radial dimension of the cell is  $c\tau/2$ , where  $c$  is the velocity of light and  $\tau$  is the pulsewidth. The azimuthal ( $\phi$ ) and elevation three dB beamwidths are designated as  $\phi_a$  and  $\theta_e$  respectively.

The cross section of the volume-scattering cell is found from a summation of the scatterers weighted by the antenna pattern. Since most antenna beams are directive and have low sidelobes, the main contribution to the volume cross section results from the vicinity of the peak of the main beam. It is reasonable to assume a uniform distribution of droplets within the cell. Current formulations for general volume scattering include a reflectivity  $\eta$  expressed in units of  $\text{m}^2/\text{m}^3$ , a cell volume estimation based on the 3 dB beamwidths of the antenna, beam shape loss ( $L_b$ ), and a pattern propagation factor ( $F$ ), stated as follows:

$$\sigma_v = \eta V = \eta \left( \frac{c\tau}{2} \right) \left( \frac{r\theta_e}{L_b} \right) \left( \frac{r\phi_a}{L_b} \right) (F^4) \quad (2.35)$$

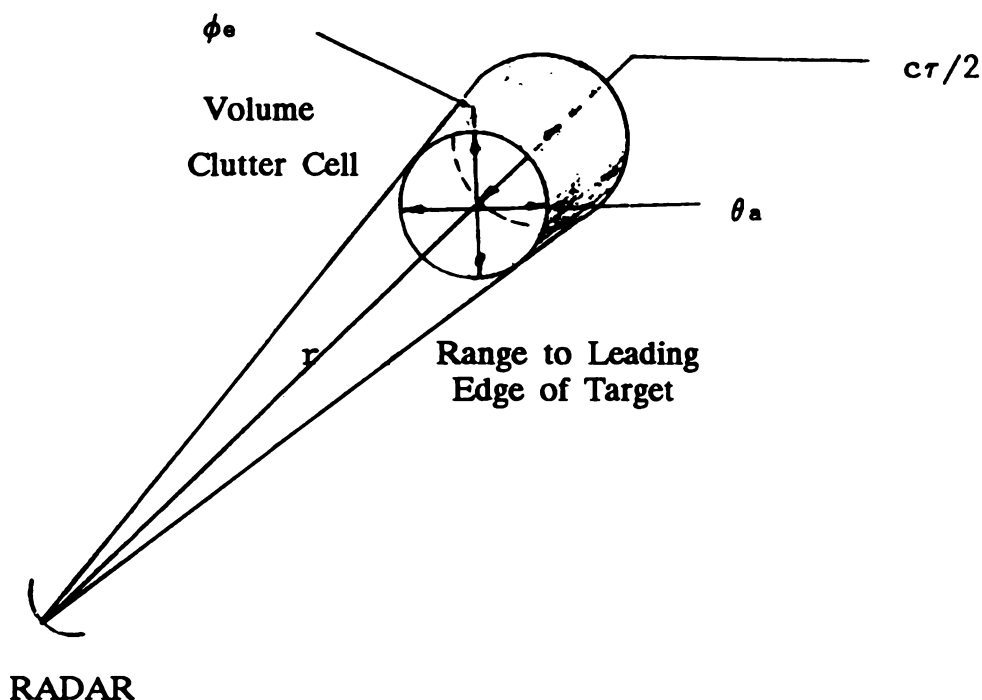


**Figure 2.3** Volume Clutter Cell Referenced to the Elevation and Azimuth Beamwidths, and Range Resolution Element

The fourth-power dependance of  $F$  is a result of a reference to a field pattern expressed in power for a two-way path. Barton provides estimates of  $L_b$  and  $F$  for several beam conditions. In this formulation, the quantity  $(F^2/L_b)^2$  is replaced by an integral of the field pattern expressed in Gaussian form. When the normal Gaussian beam approximation is applied, (i.e., the first term of a general field expansion), the standard form of the meteorological radar equation results. In Chapter 4, we will take advantage of the structured properties of Gaussian field expansions to account for main beam and sidelobe weightings of the scatterers. Equation (2.35) is now expressed in the following way:

$$\sigma_v = \eta \left( \frac{c\tau}{2} \right) r^2 \int_0^{2\pi} \int_0^\pi F^4(\theta, \phi) G^4(\theta, \phi) \sin\theta \, d\theta \, d\phi \quad (2.36)$$

where  $F(\theta, \phi)$  and  $G(\theta, \phi)$  are the antenna patterns.

This general expression, within the uniform scatterer distribution assumption, is now applied to the derivation of the meteorological equation. Let the antenna beam be described as follows:

$$F(\theta) = \exp \left[ -2 \ln 2 \left( \frac{\theta}{\theta_e} \right)^2 \right] \quad (2.37)$$

and

$$G(\phi) = \exp \left[ -2 \ln 2 \left( \frac{\phi}{\phi_a} \right)^2 \right] \quad (2.38)$$

Then, for narrow Gaussian beams,

$$\int_{-\infty}^{+\infty} \int_{-\infty}^{+\infty} \exp \left[ -2 \ln 2 \left( \frac{\phi}{\phi_a} \right)^2 \right] \exp \left[ 2 \ln 2 \left( \frac{\theta}{\theta_e} \right)^2 \right] d\theta d\phi = \frac{\pi \theta_e \phi_a}{8 \ln 2} \quad (2.39)$$

For meteorological applications, the reflectivity  $\eta$  is defined as

$$\eta = \frac{\pi^5}{\lambda^4} \left| \frac{m^2 - 1}{m^2 + 2} \right| \sum_i d_i^6 \quad (2.40)$$

where  $m$  is the complex index of refraction of water and  $d_i$  is the diameter of the  $i$ th raindrop. The quantity within the brackets is defined as

$$\left| \frac{m^2 - 1}{m^2 + 2} \right|^2 = |K|^2 \quad (2.41)$$

where the parameter  $K \approx 0.2$  for ice crystals and snow and  $K \approx 0.93$  for raindrops. A radar reflectivity factor is also defined in the following way:

$$Z = \sum_i d_i^6 \quad (2.42)$$

Replacing appropriate quantities in Equation (2.14) with  $K$  and  $Z$  yields the common form of the reflectivity:

$$\eta = \frac{\pi^5}{\lambda^4} |K|^2 Z \quad (2.43)$$

The radar reflectivity factor is sometimes written as  $Z_e$ , and defined as an effective factor, which designates a resonant scattering state of the raindrops. A further definition of  $Z$ , as we will see, involves rain rates described by a large number of constants, so the  $Z$  designation will be maintained without regard of the scattering formulations.

$Z$  is related to the rain rate  $R$  in the following way (with  $A$  and  $B$  as constants),

$$Z = AR^B \quad (2.44)$$

It is a common practice to express the rain rate in units of mm/hr and the radar reflectivity factor  $Z$  in units of  $\text{mm}^6/\text{m}^3$ . In order to maintain compatibility with these conventions, a multiplying factor of  $10^{-18}$  will accompany the reflectivity parameters in the radar equation, with an exception made, allowing mixed units.

### EXAMPLE: REFLECTIVITY CONSTANT

At frequencies in the vicinity of 35 GHz, with an assumed Marshall-Palmer (M-P) drop size distribution, and for general Mie scattering droplet representations, the reflectivity factors, from the early work of Atlas, are,

$$\begin{aligned} z &= 350R^{1.32}, & 0 &\leq R < 5 \text{ mm/hr} \\ Z &= 450R^{1.15}, & 5 &\leq R < 20 \text{ mm/hr} \\ Z &= 780R^{0.95}, & 20 &\leq R \leq 100 \text{ mm/hr} \end{aligned}$$

Two points are significant—the need for more than one set of constants to accommodate a wide range of rain rates, and the constants are far removed from those used at lower frequencies where typically  $A = 200$  and  $B = 1.6$ . Note the similarity of this scattering representation to the attenuation models of the previous example. As before, the use of these established formulations is advocated for analysis purposes, especially when simulation work is involved.

Now, substituting Equation (2.39) and  $\eta$  into Equation (2.14) (including the conversion factor of  $10^{-18}$ ) yields the standard form of the meteorological radar equation:

$$S_c = \frac{PG^2\lambda^2 c\tau\theta_e\phi_a\eta^{10^{-18}}}{2^{10}\pi^2\ln 2r^2LL_P} \quad (2.45)$$

The ratio of clutter-to-noise power is

$$\frac{S_c}{N} = \frac{PG^2\lambda^2 c\tau\theta_e\phi_a\eta^{10^{-18}}}{2^{10}\pi^2\ln 2r^2kTBT_sL_pL} \quad (2.46)$$

Using Equations (2.14) and (2.45), the target-to-clutter ratio is

$$\frac{S}{S_c} = \frac{2\ln 2\sigma}{\pi r^2 c\tau\theta_e\phi_a\eta^{10^{-18}}} \quad (2.47)$$

Therefore, the radar meteorological equation parameters are

- $S_c$  = clutter power (watts);
- $N$  = noise power (watts);
- $P$  = transmitted power (watts);
- $G$  = antenna gain (dimensionless);
- $\lambda$  = wavelength (meters);
- $\theta_e$  = elevation beamwidth (radians);
- $\theta_a$  = azimuth beamwidth (radians);
- $\eta$  = reflectivity ( $\text{mm}^6/\text{m}^3$ );
- $r$  = range-to-clutter cell (meters);
- $k$  = Boltzmann's constant ( $1.38 \times 10^{-23}$  watts per hertz per kelvin);
- $T_s$  = system noise temperature (kelvins);
- $B$  = receiver noise bandwidth (hertz);
- $L$  = system loss (dimensionless);
- $L_p$  = propagation loss (dimensionless).

Thus, two observations are made. We see that volume scattering is represented by a reflectivity  $\eta$  that includes rain rates and several constants obtained from radar meteorological sources; the second observation concerns the use of the Gaussian beam approximation. When accomplished in the manner described above, the radar beam is represented within the three dB points by a Gaussian function that, according to meteorological reference material, yields acceptable comparisons between measurements and predictions. Formally, these assumptions pertain to the use of the first term of Gaussian field expansions for large-aperture antennas, in the form of Hermite-Gaussian or Laguerre-Gaussian series for rectangular or circular apertures, respectively. Generalization of these formulas involves the use of the Gaussian expansions within the range equation formulations, which is presented in Chapter 4.

## 2.4 APPLICATIONS—METHODOLOGY FOR SYSTEM ANALYSIS

The preceding derivations and resulting formulas are the classical representations of the radar equation in basic target and meteorological forms. Examples in the use of the formulas, and some extensions, are now described in the context of a *methodology for system analysis*. A system point of view is adopted in which the radar is considered part of a larger system structure. The intent is to provide procedures for use of the formulas while considering different levels and intervals of system development. An introduction to radar is provided in a system development framework. Radar requirements, parameters, performance, and subsystem

requirements and parameters are stated and explained in a generic, but quantitative sense. In order to establish the background for these delineations, a review of a modern system development process is provided. A requisite definition is included at a higher-system level, and a summary of a typical methodology is included that typifies modern system development.

Examples of the types of requirements imposed on radar development are given. The radar functions, design, and performance are selected to form the basis for the radar discussions. In this approach, a total view of radar system applications, development, and analysis is provided. Recent changes have occurred that strongly influence radar system development. Perhaps most significant is that the radar has become more a part of a larger structure than a separate entity. The connotation of a basic requirement, therefore, is extended to multiple system levels with more interactions taking place with other equipment, which adds additional complexities and constraints. From an analysis point of view, radar performance is assessed within a larger system framework, from which radar requirements are established and overall system effectiveness is determined.

It is important, therefore, that radar assessments be quantitative and realistic within the operating environment for the targets and scenarios expected, and that the influence of interference sources is considered. A certain minimum depth of radar analysis is needed at these system levels, which will be explained here. In order to achieve this perspective, the discussions first include a postulated system methodology for concept formulation, from which radar specifications will evolve.

## **Evolution of Radar Requirements**

Referring to Figure 1.1, the procedures are of interest and may occur in the establishment of the radar requirements. A system viewpoint is taken in which it is only necessary to establish a system configuration that consists of a number of elements; these elements include radar sensors, with a central element being a  $C^3$ , (i.e., command, control, and communication system). Other system elements may exist, but the emphasis is placed on the radars. They may be treated in a generic way without degrading the quantitative intent of the discussions.

### *The Acquisition Process*

The vast majority of systems, including radars, are purchased by the government for military or commercial applications. Thus, acquisition follows regimented procedures on a time scale with associated funding classifications and levels. System specifications appear in several forms during the acquisition cycle, and are related to the phase of development. In fact, the specifications establish the system requirements as well as the design details.



A *research and exploratory development* phase initiates the acquisition cycle. Ideally, the program is technologically-based, examines system elements and performance under specified conditions, and leads to the definition of a system concept. If positive results are achieved, the acquisition process is continued with a *concept exploration* phase, in which operational requirements are determined, elements of the system are defined, and *system specifications* (the first of several formal specifications) are developed. These specifications serve to define the functional baseline configuration of the system that typically, through brassboard and prototype development, is refined in a *demonstration and validation* phase. Development specifications evolve that are subsystem, design-level specifications, leading to the *full-scale development* phase. Subsystem and component design occurs during this phase, with resulting system prototypes developed following an allocated baseline configuration which evolves from the development specifications.

Three major specifications that result from the full-scale development phase are product specifications, process specifications, and material specifications. These specifications meet requirements for procurement, production and acceptance and establish a *production baseline configuration*. The final *production and deployment* phase follows the evolved specifications in several forms when the system is deployed and an *operation baseline configuration* is established.

Like system development, funding is placed in special categories that are related to the acquisition phases. Currently a 6.1 characterization applies to research and development, 6.2 and 6.3 carry through the concept exploration and demonstration phases, 6.4 covers full scale development, and 6.7 provides funding for production activities. The funding summaries, including extra description of the formal development process, cause additional complexities in an already complex procedure. There are also supplementary major decision efforts that take place within each phase that not only influence the continuation of developments and funding levels but also affect the baseline system configurations, performance, and conduct of the work. The process is long and involved, with time best measured in increments of decades, even for relatively simple systems.

### *Types and Forms of Requirements*

As previously stated, system specifications are assembled during the acquisition process and differ in each phase. As in the acquisition process, specifications follow regimented procedures. They are characterized by type and form, and each one has specific objectives. Types include *system specifications*, *development specifications*, *product specifications*, *process specifications*, and *material specifications*. The forms of specifications are *Specification to Military Standard*, *Commercial Practice Specification with Supplemental Military Requirements*, and *Commercial Practice Specification*, not intended for competitive procurement. Several of the

type and form categories have subjects directed toward special constraints or items.

Formally, system requirements are generated in the system specifications. The system specification (i.e., the type), is intended to provide technical and mission requirements for a system as an entity, an allocation of requirements to functional areas or configuration items, and a definition of interfaces among those functional areas. As the system evolves, the second development specification is intended to provide performance, interface and other technical requirements below the system level in detail sufficient to permit its design. It is these system and development specifications that were implied in the flow diagram of Figure 1.1.

*System Specifications*

In this continuation of the prelude to the discussions of radar parameters, we provide a summary of the contents of a system specification. Aside from the specifics of the summary, it is intended to further show the radar sensor as a part of a larger complex, with its own requirements and performance strongly coupled to the parent system and influenced by companion subsystems.

Radar specifications, when viewed as parts of a system, are described in groups of requirements and quality concerns. The requirements provide results of system evaluations, state functional and mission-related performance requirements, define elements of the system, identify specific functional areas, and describe configuration items or subsystems related to those functional areas. Quality refers to test requirements of several forms and standards, which must be maintained in all phases of testing. Each of the two major groups is further subdivided into special considerations and requirements. These subdivisions are defined and summarized in a concise tabular form as follows.

**REQUIREMENTS**

*System Definition*

<i>Missions</i>	Provides a quantitative statement of the mission of the system, its operation boundaries, and, constraints.
<i>Targets</i>	Identifies targets, target complexities, and models.
<i>Functions</i>	Specifies system functions and associated elements, defines parameters and their relationship to the systems, defines functional modes and operational states of the system, and identifies the functional relationship between the elements of the system.
<i>Subsystem Definition</i>	Identifies elements of systems or subsystems, specifies performance requirements, and relates performance to system functions.
<i>Interface Definition</i>	Specifies requirements for internal and external interfaces for system and subsystem levels, separated into hardware-to-hardware, hardware-to-software, and software-to-software categories.

---

<i>System Characteristics</i>	
<i>Performance</i>	States system level functional and performance requirements in categories established above.
<i>Physical Characteristics</i>	Establishes requirements of size, weight, physical constraints, transportability, durability, safety, security, and other special related requirements.
<i>Processing</i>	Specifies requirements for processing resources in categories of hardware, programming, and utilization.
<i>Environmental Conditions</i>	Defines environmental conditions of the system during manufacture, transportation, and operation, resulting from natural and man-made sources.
<i>Quality Factors</i>	Defines values, allocations, and criteria imposed on the system and its elements for reliability, portability, availability, its ability to be maintained and modified, and other factors.
<i>Logistics</i>	Specifies supply, maintainance, facilities, special equipment, personnel, and special skills and training of personnel.

---

**Quality**

---

<i>Test Definition</i>	Defines tests and standards, responsible organizations and location of testing, verification methods, test requirements, parts and materials testing, and special test procedures.
<i>Qualification Tests</i>	Provides initial tests for design of elements or components.
<i>Acceptance Tests</i>	Defines tests for workability of elements within specifications for expected environmental conditions.
<i>Operational Tests</i>	Provides system tests to verify meeting system requirements, subject to operational conditions.

---

As we view radar in terms of the formality of requirements for a higher system structure, they appear as functional, performance and design, and include internal interfaces (with hardware and computer equipment), and external interfaces (with other subsystems and system elements). Attention must be paid to design considerations that result from operational procedures, the environment, the manning and maintenance of the equipment, logistics, and the many potential influences on the radar design, test requirements and procedures. Each consideration affects the final design, and from a radar point of view, must not degrade the quality of the final product. Many interfaces within the radar are also important in the overall development process, because they will be crucial to the radar operation when it becomes part of a modern system.

*Determination of the Radar Requirements*

In this final topic on the evolution of radar requirements, a summary of a postulated, but realistic procedure is provided that leads to the requirements. Emphasis is placed on analysis procedures that can be expected, occur at various system levels,

vary in depth and complexity, and involve the radar at all levels. Modern radar system analysis extends from the conceptual designs (in a system and hardware context) to a comparable position at a number of higher system levels. Thus, application of radar principles and procedures occur at many levels of a more extensive system development process.

Because analysis implies computer simulation with varying degrees of complexity, initial radar designs are tested in system simulations for performance and cost, radar models for performance within complex target and environmental conditions, and for establishment of subsystem requirements. There are extensive computer-generated radar designs that require analysis procedures identical to those associated with hardware for their development. These occurrences are characteristic of current radar development, and must be taken into account when developing modern radar analysis procedures.

We now summarize a typical procedure that may be encountered in the evolution of radar requirements within a larger system structure. The considerations include analysis procedures, and the overall complexity of the development will become clear in our concise, quantitative discussions. The radar, usually the key element in a larger system, now becomes part of a much larger complex of analysis, requiring careful and realistic representations. The evolution of requirements usually begins with threat assignments and a mission analysis.

---

## AN EVOLUTION OF REQUIREMENTS

---

### *Threat and Mission Analysis*

Of concern are the targets, their deployment and characteristics. Environmental conditions including man-made and natural effects are assessed. Mission analysis based on firm high-level requirements involve characterizations subject to an anticipated system configuration, the targets, and the operating environment.

### *System Analysis*

Analysis occurs at system levels, and through subsystems to component levels. At the highest level, simulations are directed toward missions and effectiveness, concepts and strategies, system performance requirements, and cost. Statistical models that relate modeled system elements to targets, environment, and effectiveness are used. High-level system requirements evolve, and an accompanying preliminary system configuration results.

At a second level of analysis, detailed functional representations of each system element are assembled with appropriate interfaces. The model structure involves a quantitative functional description, a mathematical model including assumptions, reference frames, initiation and suppression, software development and implementation, interfaces module structure and initialization, and operating descriptions. The intent is to provide accurate system simulation based on proper interfacing of high-fidelity subsystem models. Analysis may result in effectiveness assessments, system requirement specifications and subsystem specifications.

Subsystem analysis, most in simulation form, using the radar as an example are *functional*, where radar equation calculations are performed; *signal*, where detailed circuit, antenna and waveform modeling occurs; and *error*, where radar system errors are modeled. Target and clutter representations are usually the limiting factor in the fidelity of the models. Modern systems (radars included), are expensive. System analysis then is intimately connected to the system requirements and effectiveness. Choice of system elements are influenced by cost consideration. The fidelity or realism of cost models follows the same considerations as that of system performance, and is at least equally important.

The principal products of the initial system analysis are the system requirements and initial system configuration.

#### *System Performance Evaluation*

System performance resulting from the optimal use of system elements is evaluated in terms of technical, cost, and fabrication issues associated with its components and the related effectiveness of the system. Specific considerations include projected threats or target characteristics and operating environments, key performance parameters and their influence on the structure of the system, and the rise associated with the development of prominent parts. Overall, analysis relates performance to cost and effectiveness.

#### *Configuring and Testing the System*

Performance, effectiveness and cost analysis leads to a system configuration for evaluation against the threats, in specified missions and realistic operation environments. Element parameters are reassessed, cost considerations are included, and continuing system issues are identified and evaluated. Analysis is parametric at all system levels, within an overall, iterative methodology. Primary concerns within the entire system structure also include an ability to adapt to changing, more severe, targets, operating environments, and mission requirements.

The major product is definitive sets of system and system element or subsystem requirements.

---

Although brief and postulated, this description of the evolution of radar requirements is that which can be expected from modern developments. However, even if the radar development process is centralized, the operability of the radar will have varying degrees of dependence on additional equipment. When reevaluating this information, at least some of the prominent considerations are applicable.

### **Radar Parameters**

In this section, the system point of view of the previous discussions is continued while maintaining a similar format. Radar parameters are described at a higher system level in the form of requirements, at a radar system level in the form of parameters and performance, and at the subsystem level in the form of parameters and requirements. The parameters are identified, defined, and placed in a form

for analysis purposes. In a concluding section, example compilations are provided, where a methodology for the use of the radar equation for system analysis purposes is delineated.

*Requirements*

The specifics of a radar requirement will, of course, vary with the many system functions and applications that are imposed on its design. However, independent of its application, two prominent functions of a radar system are surveillance and tracking. Discussions centering on these two primary functions will also include basic requirements. We allude to a multifunction ground-based system for long-range surveillance and tracking of low to high cross section targets. Later, when an example methodology is detailed, radars of several forms will be described and their expected performance will be determined. Overall, the material provided should be of general applicability.

Radar requirements within a total system context can be expected to include the following principal parameters:

- 1. A definitive statement of missions, with subsequent requirements established for each mission.
- 2. A frequency band (or bands) where expected performance can be expected to be optimal.
- 3. Regions of coverage for surveillance and coverage limits for tracking function.
- 4. Detection ranges for given probability of detection, target type, and target cross section.
- 5. Measurement accuracies including range, angle, and velocity.
- 6. The number of targets the radar is expected to encounter and process within a mission.

Concentration is now placed on those primary parameters and related ones, in tabular form, as follows.

RADAR SYSTEM	
Missions	Although radars are used for a number of purposes, including air traffic control, meteorological measurements, remote sensing marine use, collision avoidance, intrusion monitoring, height finding, altimetry, instrumentation data collection, and many specific military applications, missions usually relate to primary radar functions of surveillance and tracking. A modern radar can be expected to be multifunctional and dedicated to more than one mission. Requirements are established for each mission.  The primary surveillance and tracking functions include additional functions of detection and acquisition. A radar may perform a number

Frequency

of surveillance and tracking functions, each associated with a mode of operation that may also include additional operational-related functions or modes, such as self-testing, training, and other special tasks. Radar states may apply to operation readiness such as idle transporting or disassembly. Functions, modes, and states become part of the top-level radar requirements.

Radar frequencies span from a low value of 3 MHz in the high-frequency (HF) band to 300 GHz, the maximum frequency of the millimeter-wave region. Specific band designations are as follows:

HF:	3–30 MHz
VHF:	30–300 MHz
UHF:	300–1000 MHz
L:	1–2 GHz
S:	2–4 GHz
C:	4–8 GHz
X:	8–12 GHz
Ku:	12–18 GHz
K:	18–27 GHz
Ka:	27–40 GHz
mm:	30–300 GHz

The lower frequency bands are generally used for long-range surveillance. The intermediate and most used frequency bands (L through X) include surveillance and tracking radars for air traffic control, weather observations, marine radars and military radars of many forms. The high-frequency bands, including Ku through Ka, (the lower portion of the millimeter-wave region), are primarily used for high-resolution tracking, surveillance and mapping purposes. Frequency bands are usually stated in a radar specification and may be subdivided into segments for specific functions.

Surveillance Coverage

Surveillance or search is specified as *volumetric*, where azimuth and elevation regions are defined, as *limited search*, where small volumes of space are defined, usually handed over to or from another sensor, or *fence coverage*. Fence coverage is narrow in elevation and wide in azimuth, is formed by one or a small number of beams scanning the prescribed azimuth region, and detects targets passing through the fence. A surveillance radar may include more than one of the coverages cited.

Acquisition

Targets are first detected and then acquired for additional functional operations. Target acquisition is usually expressed as a range for a target of specified cross section within a required detection probability.

Target Cross Section

Target cross sections may be expressed in square meters or decibels per square meter. Modern radar applications may require detection of targets with cross sections as low as .001 meter squared to values exceeding 10 meters squared for a single mission at long target ranges. Radar cross sections result from characteristic locations on the target called *scattering centers*. As a result, targets normally fluctuate rapidly with changes in frequency and aspect angles. A cross section requirement, when specified as a single value, is usually an average over a

band of frequencies or an angular aspect region. Targets rarely appear as point targets, indicative of a single scattering center representation. Exceptions occur with large spherical metallic targets or high-resolution radars, in which case the individual scattering centers are resolved, with each center as a point target with deterministic properties.

### *Target Models*

Considering the statistical nature of typical radar targets, models have been developed that relate detection probability to the number of pulses noncoherently integrated for given signal-to-noise ratios for specified false alarm rates. Commonly-used target models are the Swerling Class I-IV types. Swerling I and II models are governed by Rayleigh statistics, where voltage responses give rise to Rayleigh-distributed signals and intensity or power responses yield exponentially-distributed signals. Physically, the targets represented are characterized by a number of scattering centers that have (more or less) the same scattering amplitudes. In the class I target, signals are correlated on a pulse-to-pulse basis, and are characterized as having *slow target fluctuation*. Class II target responses, independent of pulse-to-pulse, and are classified as having *rapid target fluctuation*. Class III and IV targets are similarly designated as having slow and rapid fluctuations, but differ in the assumption of the occurrence of a dominant scatterer in the target scattering center complex. Statistics follow a chi-square distribution with two degrees of freedom. Other target models include chi-square distributions with degrees of freedom exceeding two, and log-normal distributions, each with special physical interpretations. Because of the complexities of a general dynamic target response, care must be taken in the use of any target model. Because clutter, like targets, is composed of individual scattering elements, statistical models of clutter will contain the same collection of probability distributions.

### *Detection Probabilities*

A detection probability in a total system context is usually related to system effectiveness through a tracking function. When stated, the detection probability refers to the desired tracking or primary function. False alarm probabilities, and the occurrence of false targets, are also system functions that are related to the tracking (handling) capacity of the radar. Typically, detection probabilities are based on multiple coherent or noncoherent target observations, and may approach 1.0 (i.e., 0.99 for certain tracking functions) or less than 0.5 for single-hit observations where cumulative detections occur. False alarm probabilities typically are between  $10^{-4}$  and  $10^{-6}$ . Tabulated data for analysis and design are extensive for Swerling targets, relating the probabilities and signal-to-noise ratios.

### *Tracking*

Tracking specifications can be expected to be similar to acquisition requirements in order and content.

### *Resolution*

Resolution requirements are associated with the expected target deployments, where care must be taken to separate or resolve observables in the primary measurement of azimuth and elevation angles and range. Angular resolution refers to the 3 dB beamwidth of the antenna, while range resolution is dependent on the signal bandwidth.



	<p>For a pulsed transmission, the resolution is approximately one-half of the product of the velocity of light and the pulse width, where allowance is made for a two-way propagation path separating the targets. Specific values depend on waveforms, and will vary greatly between radar functions. Doppler resolutions separating observables in velocity may also be specified.</p>
<i>Accuracies</i>	<p>Sensor accuracies also constitute a primary system requirement that is related to overall system surveillance, tracking missions, and system effectiveness. Principal accuracies include azimuth and elevation angles and range, usually expressed at the outer ranges of the operating region of the radar. Measurement accuracies will generally improve as ranges are reduced, and the sensitivity of the radar is enhanced.</p>
<i>Number of Objects</i>	<p>Modern radars are usually multifunctional, are array systems, and are capable of processing a large number of targets. The requirements usually evolve from a system assessment of the target complex, and thus become important to the timing of the radar in conducting surveillance and tracking functions. Data rates may also be specified, and are likewise related to the timing of the system.</p>
<i>Availability</i>	<p>Availability is expressed as a probability and is the fraction of time the radar can be expected to operate.</p>
<i>Mean Time Between Failure</i>	<p>This important reliability parameter specifies a time between failures of sufficient extent to cease its operability.</p>

Additional requirements can generally be expected, but the ones tabulated here are considered the primary ones. The detection ranges that influence all the radar parameters in varying degrees and the accuracies that dictate the measurement capabilities of the radar are especially important. For analysis purposes, at system levels, where the requirements evolve, radar equation computations should be performed to assure reasonability in the detection requirements, and measurement errors should be within reasonable bounds when compared with the resolution of the radar. They should be described as range-dependent parameters compatible with the radar configurations envisioned and the contemplated resolution.

*Parameters*

A set of radar parameters should at least include the parameters that are necessary to perform radar equation calculations, describe special features of the radar, and indicate basic subsystem parameters. We will now discuss in tabular narrative form, representative system level parameters.

RADAR PARAMETERS	
<i>Frequency</i>	<p>Commonly, a single frequency band is regarded as adequate to describe the operating frequency of the radar. Modern radars may be characterized by multiple smaller frequency bands within a larger</p>

---

<i>Peak Power</i>	<p>frequency band to separate principal functions of the radar.</p> <p>Transmitted power for long-range ground-based systems performing many functions and detecting low-cross-section targets can be expected to exceed a megawatt. Conversely, short-range radars at higher radar frequencies may transmit a few watts of power. Available power depends on tube type or solid-state power sources for single or distributed arrays, and the choice of frequency for both classes of power sources.</p>
<i>Average Power</i>	<p>Most radars are pulsed, with average power being a measure of the time the transmitter is active. Associated with average power is a duty cycle (or factor) which is the ratio of pulsewidth to the interpulse period. Duty factors are limited by the tube type and peak power generated, but are a fundamental measure of power source capability.</p>
<i>PRF</i>	<p>The pulse repetition frequency (PRF) may be a fixed value, dictated by the maximum range of the radar, to avoid ambiguous target responses. It is common to find variable PRFs within an operating radar, with ranges of PRF tabulated.</p>
<i>Pulsewidths</i>	<p>Multifunction radars employ multiple waveforms, each influencing radar sensitivity. Generally, pulsewidths are large for long-range detections and narrow for shorter range special functions. Radar parameters can be expected to include the pulsewidths and their function for each waveform.</p>
<i>Bandwidth</i>	<p><i>Instantaneous bandwidth</i>, a measure of range resolution, is associated with the waveforms. As with many radar parameters, modern systems can employ varying bandwidths, associated with several waveforms, for special purposes that make use of varying range resolutions and measurement accuracies.</p>
<i>Antenna Size</i>	<p>Because of the large number of possible antenna configurations, antenna size may include actual dimensions, shape, and the number of active and passive elements in an array.</p>
<i>Beamwidth</i>	<p>Beamwidths are usually provided for both principal planes (i.e., azimuth and elevation) because radar beams are generally elliptical in cross section. Many radar beams are formed by symmetrical apertures, which yield beams of nearly circular cross section. Then, single beamwidths are listed.</p>
<i>Antenna Gain</i>	<p>Antenna gain is usually a single value indicating equality of transmitting and receiving gains. It is not unusual to have transmitting gains larger than received ones when uniform distributions are used on transmit for maximum gain. Received gains may exceed transmitted ones for multiple, simultaneous beam systems. Associated with gains are effective areas, which may also be tabulated.</p>
<i>Antenna Sidelobes</i>	<p>When listed, sidelobe levels usually pertain to the first sidelobe adjacent to the main lobe. The levels may differ in the principal planes. Also, if the radar is subjected to severe interference, then details of the spatial distribution of the sidelobes may be included.</p>
<i>System Noise Temperature</i>	<p>System noise measures may appear as <i>noise figures</i> or <i>noise temperatures</i>. It has been common practice in radar development to utilize a <i>system noise temperature</i> to establish noise power levels. Values to be expected may range from a few hundred kelvins for low-noise optimal system designs to 400 to 700 K. In long-range high-power</p>

*System Loss*

radars, systems with high hardware losses, and associated receivers with large noise figures, excesses of 1000 K occur. Losses are generally stated as a single value, representative of maximum expected loss and including losses internal to the system resulting from components, and external losses resulting from propagation effects and special beam-forming configurations.

Radar parameters, especially for a multifunction sophisticated radar system, can be more extensive than this listing. However, the primary purpose of establishing a lower bound adequate for radar equation computation has been met.

There are several critical parameters given previously that imply careful system evaluation, and as with all parameters, they influence the radar sensitivity. The first of these are system losses, where good estimates are needed at a component level, through peculiarities in beam forming, and atmospheric attenuations that may include effects of clear air, rain, and clouds. Although separation of internal and external losses is preferred, a definitive statement of total loss is important. From a design point of view, losses should be minimized, with control over internal sources achieved in the design process, and atmospheric losses imposed through mission and radar requirements. Examples of types of losses and expected values in certain instances are given later.

A second major concern is the establishment of a realistic noise figure in the early system analysis stages of radar development. This involves component selection that includes the noise figure of the receiver, the expected losses within the radio frequency (RF) transmission lines and feeding networks, and the losses in antenna elements or structure. Externally, noise is accepted at the antenna, originating within the atmosphere and surrounding ground environments. From a radar design point of view, low system noise temperatures are desired, and strived for in the design process. From a system point of view, we repeat, care must be taken in estimating system temperatures for preliminary performance estimates.

*Performance*

Our discussions, in tabular narrative form, will now be directed toward radar system performance parameters. The basis of discussion will continue to have a long-range search and tracking radar system orientation. The performance parameters bridge the gap between the radar requirements and the establishment of a definite radar configuration, subsystem requirements and parameters. A summary of typical parameters is provided.

**RADAR PERFORMANCE PARAMETERS**

*Frequency*

Specific frequency bands, possibly subdivided into segments for special functions, are normally stated.

---

<i>Boresight</i>	Radar boresight position, expressed in azimuth and elevation angle, is usually stated for fixed radar installations. Otherwise, related radar locations may be included.
<i>Coverage</i>	Specific coverage for search and tracking functions (deployment related), will usually appear in performance parameter listings. As previously stated, the values will be compatible with requirements but may vary because of special siting and target considerations.
<i>Range</i>	Radar range is a direct result of the system requirements imposed on the radar. However, specifics of radar siting, target scenarios, and radar missions may result in a justified range performance that differs from the primary requirements. If multiple missions are of interest, range may be associated with a specific operating mode and included as part of the performance parameters.
<i>Radar Cross Section</i>	Usually, a single value stressing radar cross section is stated. However, if the radar functions in a target environment where cross sections vary greatly from low to high values, then a number of cross section values may be tabulated. Generally, radar cross sections are a result of target assessments conducted at a system level, and may be complicated by a diversity of targets and influenced by the siting of the radar. Special cross section values may occur that are interpreted from initial requirements. Target models may be included in the cross section compilations.
<i>Waveforms</i>	A multifunction radar utilizes a number of waveforms in conducting its mission. Waveform properties are usually contained, in some form, in the performance parameters. Expected, at least, are pulsewidths, compression ratios for coded or <i>linearly frequency modulated</i> (LFM) pulses, and particulars of special waveforms (i.e., a pulse burst).
<i>Duty Factor</i>	Choice of duty factor and accompanying PRF implies a choice of transmitter configuration, and should be included.
<i>Pulse Integrated</i>	The number of pulses that are coherently integrated in the acquisition and tracking modes are usually listed. In many cases, both coherent and noncoherent schemes are employed, and will appear in summaries of radar performance.
<i>Signal-to-Noise Ratios</i>	Tabulations of signal-to-noise ratios for varying acquisition and tracking conditions may appear. When stated, beam positions as well as range considerations for array radars will likely appear.
<i>Accuracies</i>	Accuracies for the primary azimuth and elevation angles and range constitute the principal performance data compilations. Expected here are values for stressing ranges, beam positions, and target sections. Generally, the extremities of the range are of concern where the accuracies are inversely proportional to the square root of the signal-to-noise ratio.
<i>System Noise Temperature</i>	Generally, a system noise temperature is part of system-level radar parameters. However, performance evaluations may be based on special considerations of siting and radar configurations, warranting its inclusion in the performance parameters.

---

When designers concentrate on radar system evaluations, in particular performance estimates involving measurement errors in a total system context, performance parameters are usually focused on limits of operation. Clearly, a radar

operating within a total structure or mission is likely to avoid the stressing situations for most of the deployment. Then, designers must consider error representations or models that are range dependent and include the stressing cases. Realistic error models include, at a minimum, instrumentation and signal-to-noise-dependent errors. Instrumentation error represents the sum of all errors associated with the measurement functions of the radar and, for the most part, is range independent, representing the optimal measurement capability of the radar. The signal-to-noise dependent errors involve radar sensitivity, where all radar parameters effect the measurement errors. For system analysis at radar and total system levels, an accurate assessment of the radar parameters and the establishment of realistic measurement error models are essential. The use of the radar equation also implies the consideration of the waveforms within the analysis that are properly applied to the functioning of the radar.

### *Subsystems*

When viewed as a part of a total system, the radar transmits and receives signals scattered from targets subjected to clutter and propagation effects. In this context, sensitivity, coverage, and measurement accuracy must be considered. Viewed from a radar system point of view, the radar consists of elements or subsystems that dictate its performance. Three major elements of the radar are the transmitter, antenna, and receiver. Additional subsystems, either principal or specific to a design, include indicators and displays, beam-steering or servo control, auxiliary antennas, controllers and other computer elements, signal processors, interface units, peripherals such as printers, tapes, and other related equipment, communications, and facilities that may include prime power, cooling, fire protection, and items peculiar to fixed or mobile installations. Although it is difficult to develop a generic block diagram of a modern radar system because of the specialized functions in any system, a reasonably generic functional flow is shown in Figure 2.4.

Signals are generated within the *transmitter*. Control of the timing or triggering, the waveforms, and the pulse repetition frequency (PRF) is accomplished by a *radar controller*, a separate entity or part of a control computer or processor. The *duplexer*, a part of the radio frequency (RF) transmission system, separates transmitted from received signals sharing a common antenna. The *antenna* radiates directed energy toward selected areas either through mechanical or electronic scanning. A *beam steering unit*, or a *servo system* in mechanically scanned radar (shown as part of the antenna), accepts beam position commands from the central processor and computes specific control commands needed by the antenna to direct the beam. Auxiliary antennas (i.e., in interference suppression systems), may be part of the antenna complex.

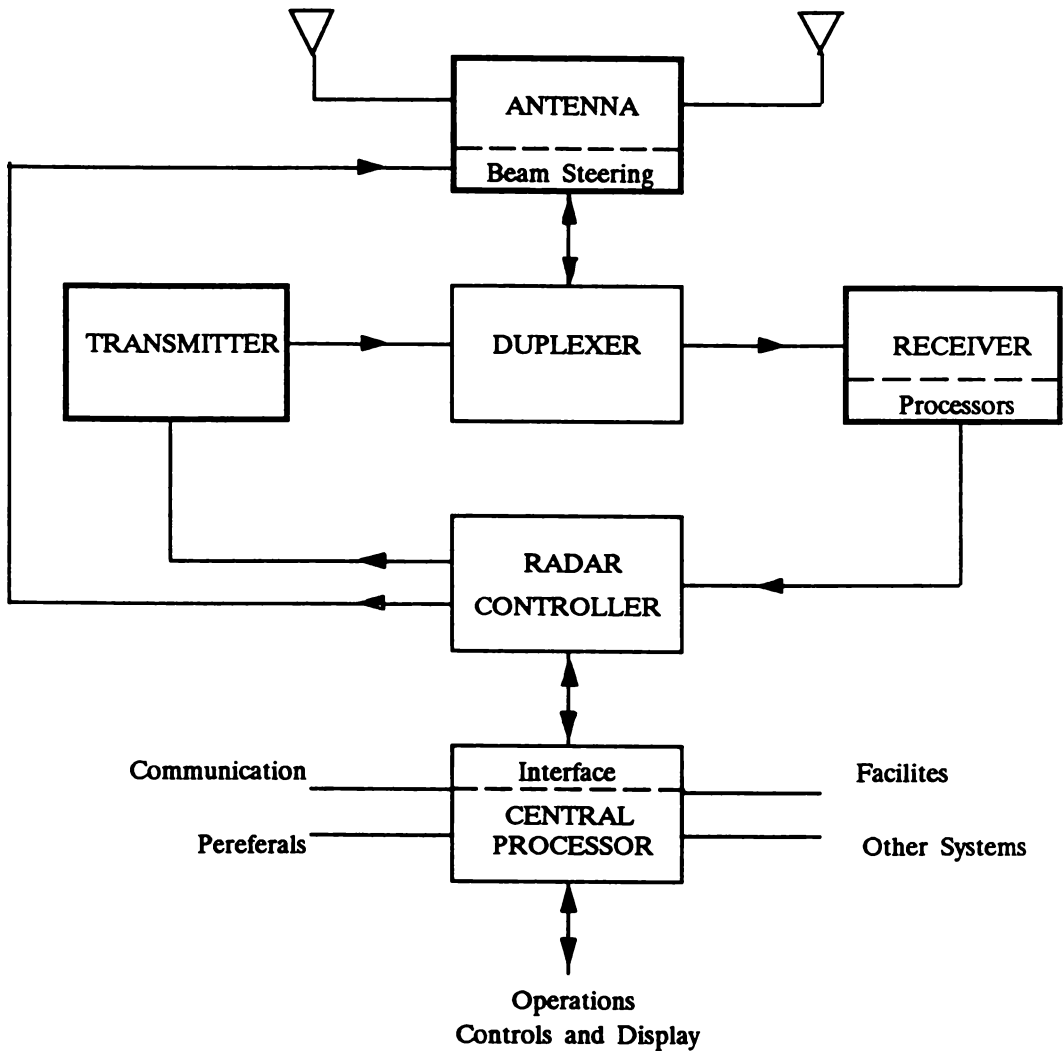


**Figure 2.4** A Simplified Functional Diagram of a Modern Computer Controlled Radar System

Signals from targets, corrupted by background noise and clutter from natural and man-made environments, pass through the duplexer into the *receiver*. Signals are amplified, probably digitized, and directed to the central processor for operational control, data collection, and distribution to other locations, in original or reduced form. Controls from external sources may be observed by the operator and passed into the functioning parts of the radar. The structure of a modern radar is formed about a computer, computer controls and external interfaces. Two-way paths occur throughout the radar for operational monitoring, testing, and training modes of operation. The diagram in Figure 2.4 is simplified and functional, but representative; the implications of complexity of the equipment should be appreciated from this functional view.

In this final review and introductory coverage of radar parameters and performance, proceeding in the same context and following similar formats, the radar parameters of the principal functional parts of the radar will be described. The transmitter, antenna, and receiver will be discussed from a combined requirement and principal parameter point of view. At system and radar levels, and now through subsystem levels, we will attempt to show the relationship of parameters to the placement of the radar within a system development as part of an acquisition process. These relationships and viewpoints are important, as already pointed out, because the final performance of a radar can be influenced at all levels of the system. In this regard, Kahrilas refers to a well designed radar as requiring traceability from target definitions through subsystems. The implication in these discussions is that traceability is important in all phases of radar development, and is required when viewed not only from the radar but also from the system structure.

In this chain, it is common to have radar and performance parameters that meet system requirements dictating the subsystem requirements, from which subsystem design and performance parameters evolve. To avoid unnecessary duplication in the material, subsystem requirements and parameters are unified. Also, particular emphasis is placed within the discussions to maintain a system context. The reader is directed to the references included in the bibliography for further pursuance of any topic. Our intent is to provide a quantitative system view of the many technologies and components that contribute to the performance of a radar. The summaries follow in tabular form.

SUBSYSTEM PARAMETERS	
TRANSMITTER	Transmitters are either tube or solid-state, and may generate high power with a single oscillator or may consist of an amplifier chain. Solid-state sources may be a single low-power source or modular, such as elements in an antenna array. Radars generate pulsed (i.e., noncoherent) or pulsed doppler (i.e., coherent) and continuous wave (CW) signals.
TUBE TYPES	Three primary radar tubes are the <i>magnetron</i> , <i>klystron</i> , and <i>traveling wave tube</i> (TWT). Magnetrons provide high-power RF signals through the interaction of an electron beam and magnetic field coupling energy outward through tuned cavities. Magnetrons provide high-power pulsed signals for noncoherent radars. Klystrons couple RF energy into an electron beam whose passage through one or more cavities results in a bunching in the electron beam and a coupling of energy outward through a tuned cavity. Klystron amplifiers have high gain and peak-power handling capability at moderate to low bandwidths. The TWT couples RF energy into a traveling wave structure of helical geometry, where bunching of an electron beam subjected to an applied magnetic field occurs. Energy is coupled out of the tube through a tuned RF circuit. TWTs have large bandwidths and a high-

power capability. Several additional radar tubes include *tetrodes* and *triodes* of different types and derivatives of the primary ones (i.e., the klystron *extended interaction oscillator* (EIO), the *extended interaction amplifier* (EIA), and *crossed-field amplifier* (CFA)). Each has special applications. A prominent, relatively new tube under development is the *gyrotron*, in which orbital rather than linear beam interactions occur in large cavities. Large peak and average powers are possible for frequencies into the millimeter-wave region.

#### SOLID STATE

Single-unit solid-state transmitters are characterized by low power, requiring multiple sources for high-power applications. Solid-state devices include transistors of several forms and IMPATT diodes applied at higher frequencies.

#### PEAK POWERS

Peak powers, depending on frequency, will range from a few kilowatts to 20 megawatts or more for single tubes. High power tubes may also be combined into groups to yield part of a corporate feeding structure or subarrayed antenna.

#### AVERAGE POWER (DUTY FACTOR)

Most radars are pulsed, characterized by a PRF and *pulse repetition interval* (PRI). The product of the pulse width and peak power is equal to the product of the average power and the PRI. The average power is a fraction of the peak power and is the *duty cycle* or *duty factor*. Typically, duty factors vary from a fraction of a percent to a few percent, nominal for high-power tubes. Duty factors of 10 percent or more may occur for special purpose tubes and solid-state source configurations.

#### PRF

Radar PRFs are usually chosen to yield unambiguous range responses. Given a maximum detection range  $R$ ,  $\text{PRF} \leq c/2R$ . PRFs will vary from tens of Hz to tens of KHz for high-power radars.

#### PULSEWIDTHS

Pulsewidths will vary within the operating structure of a modern radar. Generally, the longest pulsewidth will be used for long-range search or tracking functions. Shorter pulses will be used for closer ranges and may be part of an energy management procedure. Pulses may be compressed through coding or *linear frequency modulation*. The pulse lengths relate to detection and radar sensitivity, and the compressed pulses are measures of bandwidth, resolution, and measurement accuracies.

The PRFs and pulsewidths are usually expressed on a pulse-to-pulse basis. When pulse bursts are transmitted, PRFs and pulsewidths within the burst are of concern. Pulse bursts are usually employed when detection of target in clutter of different and separated spectra content is necessary.

#### BANDWIDTHS

Signal bandwidths are dictated by system resolution requirements, range accuracy, and special function requirements. Long-range detection of small cross section targets usually yields narrow-band signals that are compressed to within desired resolutions. Resolutions of 0.3 (or one foot) enable resolution of scattering centers of many radar targets. Wide-bandwidth signals are generally used for special tasks, such as target identification and discrimination or intrusion detection.

#### RANGE AND DOPPLER SIDELOBES

Matched filter radar responses yield a range and doppler sidelobe structure much like the sidelobes of an antenna pattern when time



and signal spectra are observed. Suppression of sidelobes is necessary for clutter suppression and minimization of masking of target responses by observables of close-in targets, in range or doppler, of high cross section. Its desired waveforms ought to be unambiguous in range and doppler, but in many instances are not, requiring special processing for removal of ambiguous responses. Sidelobes are suppressed through filtration.

#### PHASE COHERENCY

The effectiveness of using coherent waveforms to detect targets in a multitarget or cluttered environment depends on the maintenance of the time and doppler sidelobe levels. Degradation occurs in sidelobe levels and structure when low phase errors are not maintained. Typically, for 40 to 50 dB (Taylor filtered sidelobe levels), a  $1^0$  to  $2^0$  phase coherency limit is needed.

#### ANTENNA

Types of radar antennas are usually large aperture reflector or array types, but exceptions occur. Reflectors are horn-fed and curved, usually parabolic. Configurations may be Cassegrain with horns being of single or multiple excitation, forming monopulse beams. Feeds may nutate, forming a conical scanned beam. High-power tracking radars can be expected to be circular or parabolic, with a precision, mechanically-designed horn, supports, and antenna structure.

Arrays are usually electronically scanned or may have fixed beams, may be stacked, and when combined with a mechanical rotation, provide broad elevation coverage. Usually, phase between elements of the array is controlled, to yield phase scanning in one or two planes. Other scanning methods include *frequency*, *time delay* and *phase velocity* or beams may be switched to a number of positions. Antenna elements are electrically small of wire or slot forms, and are individually- or corporate-fed. Depending on the design of the elements, the array may be fed at the center or ends, may be subarrayed where elements are grouped under a single phase command, and may be thinned where a percentage of the radiating elements are excited. Modern radars usually employ a phased array.

#### SIZE

Rectangular, square, or circular antennas are common. Reflector antennas, in general, are of elliptical shape reaching, in the limit, a circular aperture. Arrays are usually circular or square with irregular edges. Generally, characteristic dimensions and aperture area are cited.

#### NUMBER OF ELEMENTS (ACTIVE)

The total number of elements is stated, or more generally, the number of active radiating elements is given, which may be less than the total number.

#### NUMBER OF ELEMENTS (INACTIVE)

Arrays are sometimes spatially thinned, randomly, with densities following an aperture taper of the same form as an antenna aperture or illumination function. Pattern quality depends on the percentage of active elements. The degree of acceptable pattern degradation depends on the application. A 40 to 50 percent filling of the array is reasonable.

#### ELEMENT SPACING

Radiating elements are commonly spaced at or near a half-wavelength, and arranged in a square or rectangular grid form. When other arrangements are used (i.e., a triangular grid), specifics of the geometry, including dimensions, are given.

---

**COVERAGE (AZIMUTH  
AND ELEVATION)**

Scan limits commonly appear as plus or minus a reference boresight axis for azimuthal plane from near zero (i.e., ground plane), to a maximum elevation angle. Total coverage evolves from system specifications, with actual ones possibly restricted at the limits of the coverage. When search fences are employed, the number of beams in the elevation plane and the azimuthal limits are provided. Special, but common, coverage listings may pertain to handover coverage from other sensors, and when wide-bandwidth signals are employed, restrictions on scanning.

**APERTURE DISTRIBUTION**

Aperture distribution or illumination functions are common listings. In many instances, in order to achieve optimal sensitivity for low-cross-section targets at long ranges, uniform distribution is employed on transmit. For clutter and interference suppression, tapered illuminations, commonly optimal Taylor distributions, are used. Both constitute part of the parameters.

**BEAMWIDTHS**

Beamwidths are listed for elevation and azimuth planes and transmitting and receiving tapers. Since the beamwidth is proportional to the ratio of wavelength and aperture characteristic dimensions, the beamwidths, sidelobe levels, and gain must be compatible. For pencil beam radars, a single value can be expected. If the radar employs special beams, then their basic parameters may be stated.

**SIDELOBES**

Sidelobes may be tabulated as near-in, far-out, and intercardinal space in peak, average, or rms values for each illumination function. Peak sidelobe refers to the first sidelobe adjacent to the main beam, and is the critical design sidelobe level used for comparing beamwidth and sidelobe parameters dictated by the aperture distribution. Single sidelobe values are usually given, including peculiar sidelobe properties or special system demands.

**GAIN**

Gains provided are almost always maximum, which, for arrays, represent the broadside condition. Since antenna gain is proportional to the effective area of the antenna, which is the product of the actual area and the aperture efficiency, losses within the antenna may also be included in the gain tabulations. Ideally, gain, effective area, aperture efficiency and loss definition should be cited and should be compatible with the beamwidth and sidelobe levels.

**POLARIZATION**

Polarization may be linear, usually vertical, horizontal or circular. Circular polarization is the special case of an elliptical one, and when listed, may include a measure of degree of ellipticity. Circular polarization may be characterized as right or left, depending on the direction of rotation of the electric field vector.

**RECEIVER**

Unless otherwise specified, receivers are superheterodyned. Signals may be amplified at RF frequencies, down-converted to a lower intermediate frequency (i.e., IF), then amplified, detected, filtered and processed in a number of ways. The primary function of the receiver is to detect target signals in the presence of interference, due to internal, external, man-made or naturally occurring sources. In a benign external environment, thermal noise from galactic sources, and losses in the antenna and receiver circuits, and the receiver combine to yield a noise level. Generally, radar receiver parameters emphasize noise figure or noise temperatures and minimize tabulation

---

<i>NUMBER OF CHANNELS</i>	of receiver component parameters. More than one receiver channel is common. For monopulse systems, azimuth and elevation sum and difference channels may be provided, with special receiver channels for auxiliary functions (i.e., sidelobe cancellers), for example.
<i>NOISE FIGURE</i>	Receiver noise figures are expressed in dB and will vary from 1 or 2 to values in excess of 10. Generally, noise figures are frequency-dependent, with the higher frequency having the highest values.
<i>BANDWIDTH</i>	Receiver bandwidths may be a part of summary receiver parameters. When provided, they refer to an instantaneous bandwidth.
<i>PULSEWIDTHS</i>	Receiver pulsewidths may also be tabulated, and should conform to the waveforms used by the radar.
<i>INTERMEDIATE FREQUENCIES</i>	If channels may utilize more than one IF channel, down converting more than once, frequencies will be tabulated for each and may depend on the particular waveforms (i.e., narrow or wide bandwidth).
<i>DYNAMIC RANGE</i>	The dynamic range of the receiver is a measure of its ability to process a wide range of signal amplitudes without occurrence of saturation or general signal degradation. Value is expressed in dB.
<i>STABILITIES</i>	Phase or amplitude stability parameters may appear. Phase stability influences (enhances or degrades) spectral properties of coherent signals, thus degrading radar sensitivities. Amplitude stability influences signature measurement accuracies in instrumentation-deployed, special-purpose radars.

---

Additional transmitter characteristics, related more to the specifics of the transmitter design and signal quality, include noise levels of interpulse and intrapulse forms, stability in amplitude, pulse jitter, and harmonic content related to the shape of the pulse. Characteristics related to implementation and influencing deployment include tube or power source efficiencies, the total transmitter efficiency, tube power requirements, power supply requirements, size, and weight. The transmitter, the basic power source of the radar, receives attention in reliability and ease of maintenance for long-life capability. Associated with high-power tube transmitters are modulators and power supplies.

Radar reflector antenna systems are driven by servo systems, which in a modern system complex, would be automated and under computer control. The mechanical system interfaces remain, however, and have traditionally been dependable and of eloquent design. Beam positions of arrays are computer-controlled and driven by a beam steering computer. Servo systems are basically analog devices, while beam positioning in arrays is done by digital mechanisms. Array elements radiate broadside to the surface, thus scanning of the beam will result in losses; and depending on the design, the beam will be limited in total scan coverage. Ground-based systems, employing the lower radar frequency bands, radiate broadside or nearly so, with coverage that implies meeting scanning requirements with acceptable losses. Airborne systems, occupying the higher-frequency bands, lead to requirements of beam positioning off normal approaching end-fire, where special

array elements and array structures are necessary. Array radars, by virtue of fast beam-switching times, are characterized as high traffic-handling multifunctional systems. Reflector systems are generally precise and specialized, with limited traffic-handling capabilities. Fixed beam arrays lead to or tend to be mechanical scanning systems from the array technologies, while stacked-beam systems relate to array performance; in both cases an overlapping of performance capabilities is achieved with subarray characteristics, including size, number of elements, grids employed, and differing forms. Aperture illuminations are commonly optimal Taylor, but after the antenna design process, result in nonoptimal distributions. For analysis purposes, measured and modeled aperture and radiated fields should be compatible and based on the design goals. When transmitting and receiving modules (usually solid-state) are employed, parameters associated with the transmitter and receiver may be included in the antenna listings. It is not common to list phase shifter types, or switching times dictating minimal achievable beam positioning times. Mechanical properties of the antenna may also be tabulated, and may include surface tolerances, reliability, and maintenance parameters as well as special considerations related to the structure and operating environment.

Special components or functions of the receiver may also be part of subsystem summaries. Analog to digital converters may be summarized by their number bits and rate. *Sensitivity time control* STC circuits may be employed to adjust receiver gains, to prevent saturation or suppression of unwanted returns where attenuation values and their range dependence are specified in dB. Tunable frequency bands may also be stated.

Additional subsystem parameters may be tabulated for special-purpose processors, the beam steering computer, the displays or radar indicators, and communication systems, including the specifics of the indicator and facilities. The subsystem parameters given above pertain mainly to higher-level system designations. If the parameters are expanded, including additional ones, then the resultant tabulations apply more to lower-level or component descriptions. In our discussions here, the system level view is being maintained.

## Methodology

A methodology for radar system analysis is provided within the framework of a total system. A view of varying system levels of analysis is taken, where the flavor of a development process is established. A cohesiveness is established between, for example, a requirement and a subsystem concern. The analysis procedure focuses on the radar equation with its inputs from target, environmental, and performance requirements and its outputs for total system and radar system analysis, cost, reviews, projections, and subsystem definitions. Special concern is given to a thorough understanding of the target and environment, the functioning of the

radar, the losses encountered internal and external to the radar, and a modeling of measurement errors. When viewed as a segment of a system, radar system analysis is concerned primarily with the functioning of the radar (which may be described by the radar equation), and its capability of performing measurements to an acceptable degree of accuracy, but the analysis may require realistic error models. The use of the radar equation and associated error models is the very minimal of resources advocated for use in all levels of analysis.

Areas of concern are discussed first in the form of a methodology for system analysis. An example follows that is representative of the procedures indicated.

### *Framework*

The framework of an analysis methodology is shown in the flow chart of Figure 2.5. The target specifications, system performance, requirements, and environmental specifications contribute to the assembly of radar parameters in different ways, each being worthy of separate discussion.

The development of the target or threat specifications may indeed be involved. Two analysis concerns are paramount; any single value cross section used in computations must conform to reasonable expectations for the size and shape of the target and the radar frequencies. In addition, the radar cross sections may evolve from theory or measurements, all of which may vary from one circumstance to another with complicated dramatic cross section variations occurring, and depending on radar viewing angle. It is advantageous to construct flight paths or target motions with a high enough degree of accuracy to characterize a realistic description of target orientation. From these data, realism of cross section values can be assessed and inadequacies of the data base may be understood. It is also advantageous, for relatively simple targets, to appreciate the target signatures displayed by the radar observable. The resulting target scattering center description will be a first indication of the choice of a target cross section model and will be an indication of further analysis to modify one of the standard Swerling models to accommodate the targets or derive (or utilize) special models. An understanding of the target signature is essential if target identification or target discrimination functions are involved. Target cross section values lead to radar sensitivities, while the target models provide the sensitivities required to meet detection requirements. Considering the expected variations in radar cross sections and the uncertainties in the models, careful evaluation of the specifications of targets and models is essential in any analysis methodology.

Environmental specifications also have pronounced effects on radar sensitivity. Three prominent parameters include attenuations, backscatter and spatial boundaries for a number of atmospheric environments that may include rain, fog, and clouds. Several analysis procedures are essential, with an evaluation of the

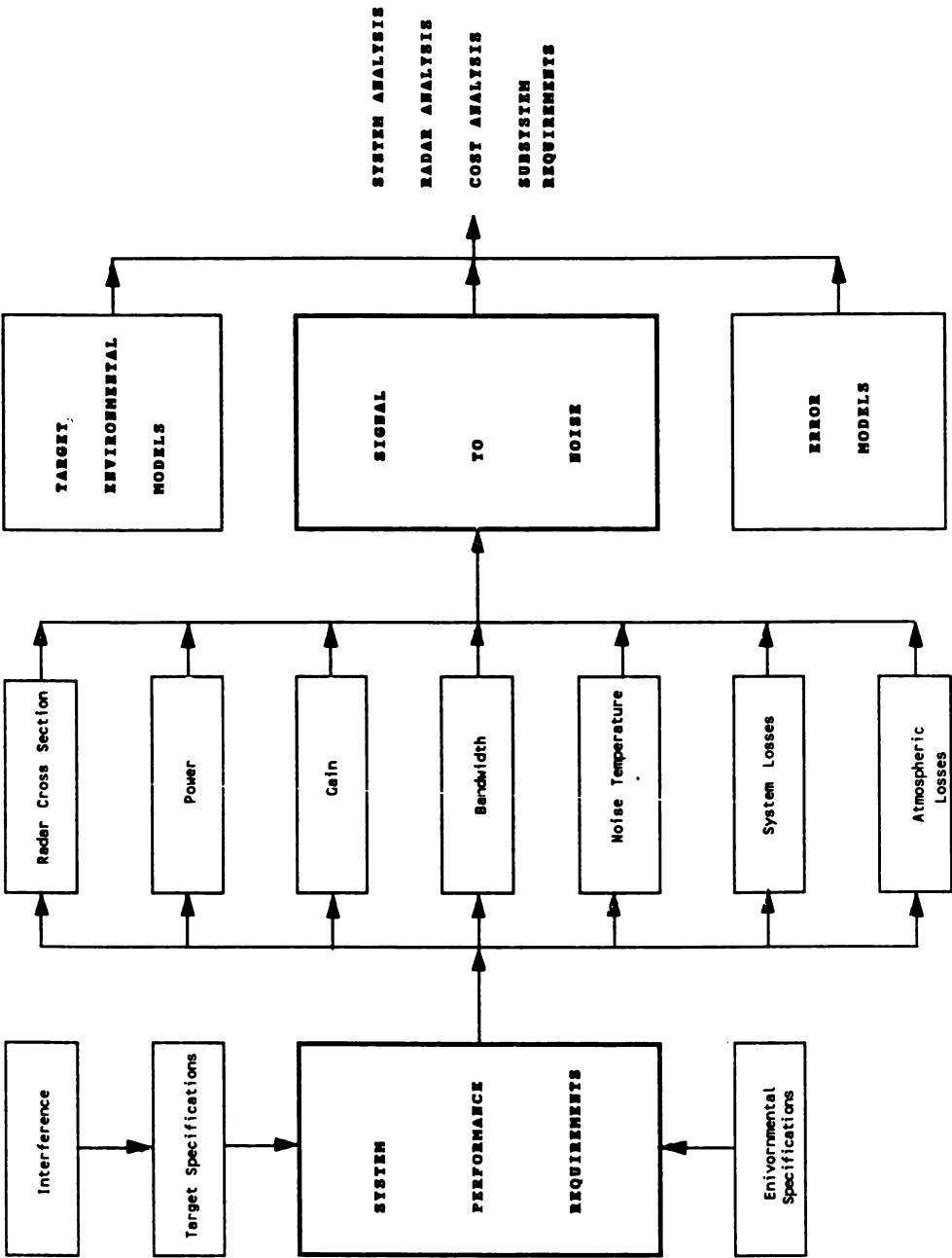


Figure 2.5 Framework of a Radar Analysis Methodology

specifications (their types and forms), global occurrences (and their realism), and the radar's capability in the deployment all studied. All natural occurrences of atmospheric conditions have spatial limits or boundaries, which should also become part of any analysis formulation. Rain, for example, especially of low to moderate intensities, has an upper boundary coincident with the zero-degree isotherm, which may effect path lengths and resultant attenuations to a noticeable degree. Environmental parameters such as attenuation and backscatter have been assembled from many sources, and usually appear in specifications and references as tabulated or plotted values. A single data base has not been established, with the exception of the U. S. Standard Atmosphere. The results are differences between data sources of the same type that may occur in relation to differing theoretical procedures, coupled with the usual measurement instrumentation uncertainties.

Considerable data, however, have been analyzed to develop models dependent on one or more constants that show quantitative trends of the data. We advocate the use of such models, with parameter adjustments made to account for anomalies in data bases (if they occur) and also to allow for excursions to higher or lower environmental parameters. It is generally a good analysis practice to establish a nominal parameter with upper boundaries to stress the system, and lower boundaries to assess the system's reaction to its return to a normal (or benign) state. Since atmospheric effects, and in particular losses, may result from several independent environments simultaneously, each with separate boundaries, separation of atmospheric losses from system ones is advocated, for both general analysis convenience and for use in the radar equation. Considering the target and deployment specifications, cross sections, and other environmental parameters that form parts of a radar, requirements must be critically reviewed, placed in the context of the anticipated radar performance, and then presented in a useful form for analysis purposes.

Sources of interference are associated with the target and environmental specifications. If signals are present that degrade system performance, then analysis procedures must be established for performance estimates that include clear or benign environments where concentration, from an environmental point of view, focuses on 1.) the complexities of the target, 2.) environmental effects and their resultant degradation of radar performance, and 3.) the establishment of levels of interference and their impact on system performances. Interference sources in particular, like the targets, have a profound effect on the radar design with parameters established within the hierarchy of the system structure. A realistic radar analysis approach is to establish nominal levels with defined lower and upper boundaries, and to determine the physical constraints of the radar design that limit suppression of the radar signals. The effectiveness of the radar is then viewed from a total system performance standpoint to determine its usefulness. In its most simplified form, interference degradation results from noise sources that raise the system noise temperature of the radar. Radar system analysis involves performance

estimates with this increased system noise temperature.

The system requirements that include primary functions of coverage for search radars, detection ranges, errors, and the number of targets to be encountered, directly effect the radar design parameters of power, antenna gains, and bandwidth. *Transmitted power* involves sensitivity that is paramount in target detection at prescribed ranges, and through the PRFs, establishes the basis for target handling capability and resultant data rates. *Signal bandwidth* relates to choice of waveforms intimately associated with the primary functions of the radar, the transmitted power, and the sensitivity. The *antenna gains* infer an antenna design and with the transmitted power, directly affect radar sensitivity. The choice of radar parameters, as it continues in this system vein, then relates radar sensitivity to requirements subjected to specified targets, their deployment, and subjected to natural operating environment and interference sources. The underlying choice of parameters is subjected to physical constraints, such as an antenna gain and antenna size relationship, the current technology and availability of the components, and the judgment, skill and ingenuity portrayed in the assembly of the components into a workable system.

The system noise temperature and system losses, two parameters contained in Figure 2.5, need special attention, since both are indicative of the quality of the design. The system noise temperature involves antenna losses, losses between the antenna and receiver, and the receiver noise figure. A measure of the quality of antenna design is first the loss which, if excessive, reduces the gain, increases the noise temperature, and overall, degrades the radar sensitivity. The signal loss incurred between the antenna and receiver includes the feeding system. The feed network design must be compact and efficient with minimal radio frequency networks, especially when arrays are utilized. Long waveguide runs, also associated with compactness, are avoided in good antenna designs. Receiver noise figures, likewise, are always kept at the lowest possible value in radar designs. The combination of the three considerations, therefore, appears first as a low system noise temperature, accounts for at least one of the system losses, and is significant in establishing overall radar sensitivity.

System losses also require special concern. Like the noise temperature, the total system loss is, to a large degree, controlled by the specifics of the radar design. In addition to external propagation losses, losses arise internally from components that may include the antenna, transmission lines and feeding system, duplexers, isolators, filters, and phase shifter quantization and insertion loss. Losses also arise from antenna beam formations that include aperture edge effects or spillover, radomes, beam shape loss (taking into account average deviations of signal returns during a search scan for off-peak occurrences of target positions), cross over of beams within a search beam pattern, and losses due to beam scanning. Processing losses occur within filtration or special circuits, with additional losses relating to integration circuits, and fluctuation losses associated with the detection of fluc-



tuating targets. Of practical origin, losses may occur from mismatches or high *voltage standing wave ratios* (VSWR) within the radio frequency portions of the radar. In general, the system losses originate within the specifics of the radar design and appear in the form of a *loss budget*, are influenced by all parts of the radar, and are a primary measure of the quality of the radar. Radar specifications may establish an upper boundary on the total system losses ( $L_p L$  in the range equation formulation) resulting from system performance evaluations, but usually, as stated, is a result of the particulars of the design of the radar that evolve in the initial process of meeting the requirements.

From a total system viewpoint, the radar (as a sensor within a hierarchical structure), performs a number of assigned functions that include target position measurements that are some combination of range, angle (including elevation and azimuth), and velocity. Associated with the measurements are errors, such as losses and noise temperatures, that are intimately related to the components and design. Primary considerations in performance analysis constitute another measure of quality of the radar, and are a principal quantity used in higher-level system performance analysis. Two concerns are significant; one is the sources of error and the other is a replacement in a form usable for analysis. Sources of error, extensive from a system point of view, may be characterized as range-dependent or range-independent. Range-independent errors, sometimes constituting the total instrumentation errors, are the best that can be achieved by the radar. At far-out ranges, where the radar sensitivity is stressed, the errors are dependent on the signal-to-noise levels. At near-in ranges, target glint errors, that are range-dependent, will predominate. Therefore, errors are a sum of contributions from glint, instrumentation, and signal-to-noise sources or effects. Instrumentation errors, such as system losses, may appear in the form of a budget, from which they are appropriately summed to yield a single value. When radar error models are assembled, they are treated separately and related to operational sequences of the radar. Possible error sources within a modern radar are listed in Table 2.1 without description, but show typical rms values and vividly demonstrate their relation to the species of the radar design. This compilation, from a radar design handbook by Kahrilas, is representative and rather complete, with further specific evaluations and formulas referred to this original source. Another measure of the quality of the radar is its error budget, sometimes viewed as a fraction of the related resolutions.

For radar and system analysis purposes, error representations assembled from error budgets are most conveniently expressed in the following form:

$$\sigma = \left( \sigma_G^2 + \sigma_I^2 + \sigma_S^2 \right)^2 \quad (2.48)$$

**Table 2.1 Radar Error Sources\***

<i>Angle</i>	<i>Range</i>	<i>Velocity</i>
Pointing .001 to .003 bw	Data Quantization .01 to 0.1m	Quantization .01 to .1 m/s
Phase Shifter Quantization .001 to .005 bw	Pulse Jitter .09 to .43 m	Pulse Jitter .06 to .3 m/s
Data Quantization .001 to .03 mils	Range clock .05 to .5 m	Doppler Discrimination + Aid Conversion .15 to .7 m/s
Aid conversion .01 to .05 mils	FM waveform .15 to 15 m	<i>Thermal</i> .5 to 50 m/s
<i>Thermal Noise</i> 1/5 to 1/200 bw	Aid Conversion .1 to .5 m	<i>Thermal – Noncoherent</i> 1.5 to 15 m/s
<i>Instrumentation</i> 1/100 to 1/400 bw	<i>Thermal Noise</i> 1/5 to 1/200 $\Delta r$	Dynamic Lag .15 to 15 m/s
Dynamic Lag .1 to .5 mils	Dynamic Lag .1 to 10 m	Multipath .005 to .06 m/s
Scan 1/25 to 1/50 bw	Multipath 1/200 to 1/1000 $\Delta r$	<i>Glint</i> .5 to 15 m/s
Multipath 1/200 to 1/1000	<i>Glint</i> .1 to 10 m	Propagation 0 – .01 m/s
<i>Glint</i> 1.0 <sup>2</sup> to .5 mils		
Propagation 0 – 300 $\mu$ rad		

\*From Kahrilas.

bw = beamwidth

 $\Delta r$  = range resolution

(Values given are typical rms.)

where

- $\sigma$  = total rms measurement error;
- $\sigma_G$  = rms glint error;
- $\sigma_I$  = rms instrumentation or total range-independent error;
- $\sigma_S$  = rms signal to noise-dependent error.

Usually measurement errors stated within radar requirements are stressing values occurring at a maximum range for the lowest specified radar cross section. Performance analysis should consider range dependence, and the formulation of Equation (2.48) is considered as minimal. Referring to Table 2.1 for angle, range and velocity error sources, the loss model is assembled from the root summed squared values of the thermal, glint, and remaining terms, with each also summed to form the range-independent error estimates in each category.

The use of the radar equation, then, pertains to radar performance, system analysis, costing, and subsystem requirements and specification. Considerations involve the targets, the environment, sources of interference and system specifications. Performance measures are obtained from radar parameters with consideration of target models, environmental models, and error representations.

*Procedures*

Following the format of the tabulation of brief summaries used in the previous sections, procedures constituting the ingredients of a methodology for system analysis are described. The flavor is one of analysis, based on system requirements and the availability of at least a partial radar design. The intent is to demonstrate the use of the radar equation and related considerations, while establishing a reasonable methodology for general analysis purposes. Also, the level of detail should be adequate for preliminary concept designs or radar system sizing. However, we refer the reader to additional source material, with this introductory material serving as the basis for additional study.

---

**RADAR PERFORMANCE ANALYSIS — AN EXAMPLE**

---

<i>Requirements</i>	<i>Performance</i>
<i>Functions</i>	
Long range search, Tracking	
Instrumentation and Data Gathering,	
Wideband	

<i>Type</i>	Multifunction Phased array, Mechanically positioned	
<i>Frequency</i>	S-Band	Compromise between long-range tracking at <i>C</i> band or above, and low-frequency search at <i>L</i> band or below. Center frequency = $f = 3$ GHz wavelength = $\lambda = 0.1$ m.
<i>Coverage</i>	One beam fence $\pm 30^\circ$	Coverages may occur simultaneously.
<i>Volumetric</i>	900 square degrees Tracking Azimuth, $\pm 30^\circ$ Elevation, $10^\circ - 70^\circ$	Positioned above fence.
<i>Detection</i>	1 m <sup>2</sup> target at 275 km ( $\approx 150$ nmi) Swerling I Target Detection Probability = 0.98  False alarm Probability = $10^{-4}$ 0.1 m <sup>2</sup> target at 185 km ( $\approx 100$ nmi) Swerling III Target	Instrumental range of radar is 300 km.  The PRFs for unambiguous range at 275 and 150 km are $f_r = c/2r = 550$ Hz and $f_r = 820$ Hz.  Given (or postulated), a $N_C$ pulse coherent integration per search dwell, with three sweeps past target, noncoherently integrated. The cumulative probability of detection is set at 0.98, the required detection probability is found from,  $P_C = 1 (1 - P_D)^3 = 0.98$  $P_D = 0.73$ (Single hit detection probability requirement)  Detection probabilities for Swerling targets, from Meyer and Mayer are as follow:  $S/N = \text{Requirements} = 13 \text{ dB, Swerling III}$ $S/N = \text{Requirements} = 16 \text{ dB, Swerling I}$  Compressed pulsewidth,  $\tau = 2\Delta r/c = 6.6\mu\text{s}$
<i>Resolution</i>	Range—1 km Angle— $3^\circ$	

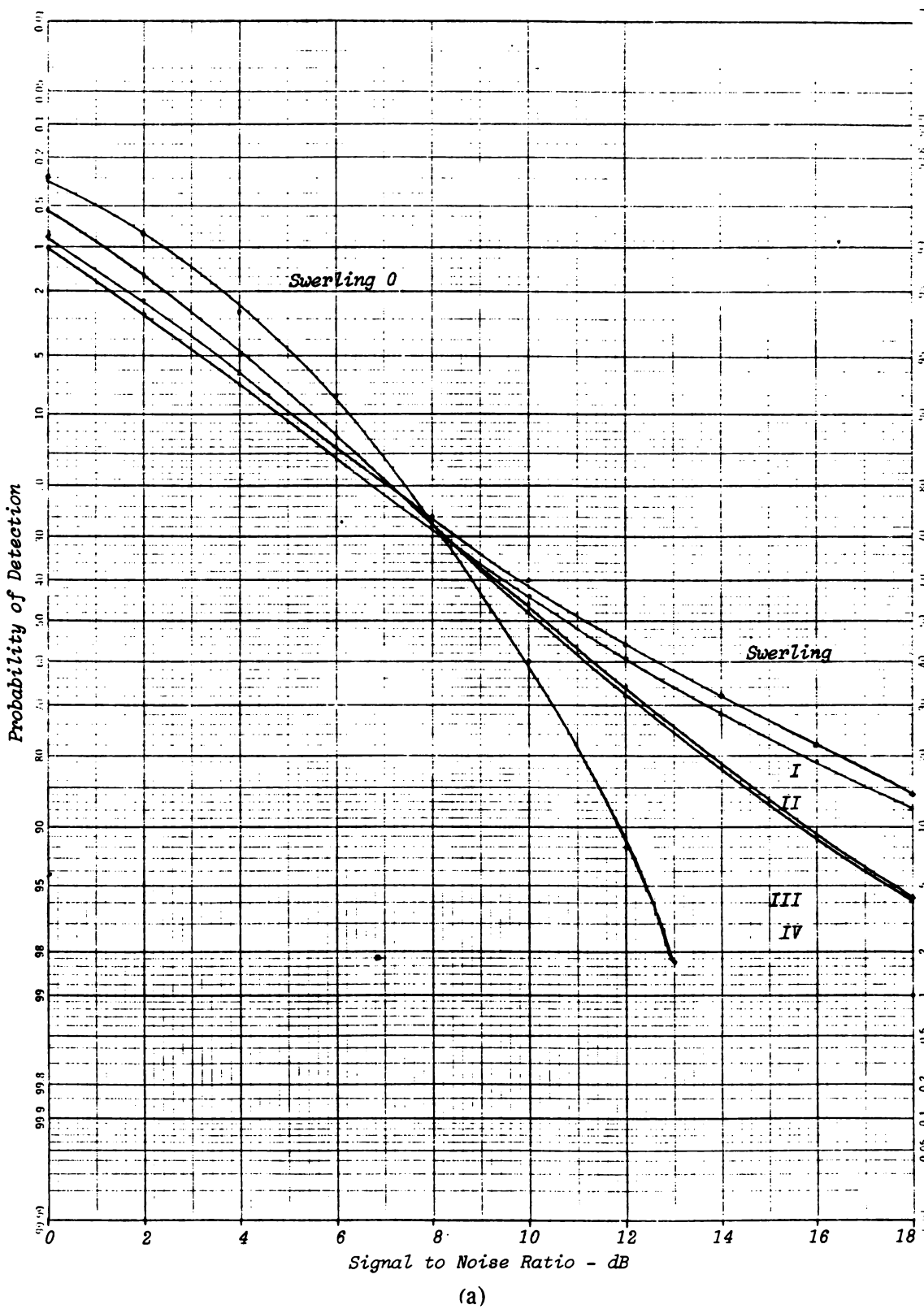


Figure 2.6(a) Detection Probabilities, Swerling 0, I, II, III, and IV

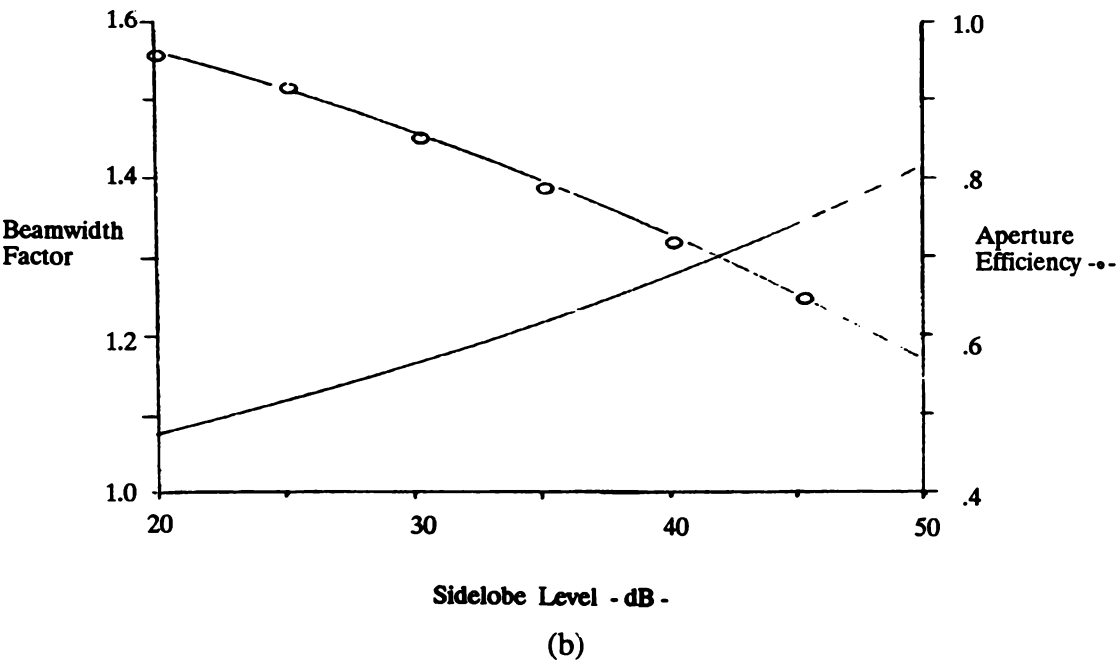


Figure 2.6(b) Properties of Optimal, Circular, Taylor Antennas. (From Barton and Ward)

Wideband—Range	Assume initial waveforms $\tau_s = 66.67 \mu s$ , compressed to $66 \mu s$ (pulse compression ratio of 10); $\tau_s = 6.67 \mu s$ uncompressed.
Wideband—Range—10 m	For a wideband measurement of target signatures, $\tau_s = 6.67 \mu s$ compressed to $67 ns$ , pulse compression ratio of 100.
Antenna	Assume circular antenna, $d =$
Beamwidth— $\leq 3.0$	diameter = 3 m
Sidelobe level - $\leq -50$ dB	For maximum gain, let transmitted aperture distribution be uniform, then
Polarization - Linear	
Maximum Aperture Dimension - 3 m	$G = \pi^2 d^2 / \lambda^2 = 39.5$ dB
	Transmitting sidelobe level = 17.6 dB.
	Assume 50 dB, optimum Taylor distribution on reception.

Aperture efficiency = 0.6.

$G_R = \eta \pi^2 d^2 / \lambda^2 = 37.3 \text{ dB}$

Beamwidth, Transmit = 1.9°.

Beamwidth, Receive = 2.5°

For System noise temperature estimate, given

Antenna loss =  $L_a = 0.5 \text{ dB}$ .

Transmission loss =  $L_r = 1 \text{ dB}$ .

Antenna noise temperature = 20°K  
(For lowest beam position about 20°,  
from Blake)

then,

$T_s = T_a + T_r + L_r T_e$

Tabulating (Equations (2.10) to (2.13))

$T_a = 79.3 \text{ K}$

$T_r = 75.0 \text{ K}$

$T_e = 288.6 \text{ K}$

$T_s = 516.6 \text{ K}$

Assume  $L_p = \text{propagation loss} = 0 \text{ dB}$ .

Given  $S = \text{System loss} = 8 \text{ dB}$ .

Given power source of 500 kw, duty factor, 3.5%  
at 550 Hz and 0.5 to 5% at 820 Hz.

Radar Parameters, in Blake chart,  
Equation (2.14), dB form are as  
follows:

(+) dB	(-) dB
--------	--------

Peak Power (500 kw)	57	
Pulsewidth (6.67 to 66.7 μs)		Variable
Transmitting Gain	39.5	
Receiving Gain	37.3	
Wavelength Squared (0.1) <sup>2</sup>		- 20

Radar Cross Section	Variable	
$(4\pi)^3$		- 33
Boltzmann's Constant	228.6	
System Noise Temperature (516.6 K)		- 27.1
Propagation Loss		0
System Loss		- 8
Range		Variable
Signal-to-Noise Ratio	Variable	
TOTALS	+ 365.4 dB	88.1 dB

The signal to noise ratio is

$$\frac{S}{N} = 274.3 + 10 \log \tau + 10 \log \sigma - 40 \log r$$

For two pulses coherently integrated per dwell, de-  
tection range for

$$\begin{aligned}\tau &= 66.6 \mu s \\ \sigma &= 0.1 \text{ m}^2\end{aligned}$$

$$S/N = 13 \text{ dB}$$

is  $R = 205.8 \text{ km}$ . Detection range for

$$\begin{aligned}\tau &= 6 \mu s \\ \sigma &= 0.1\end{aligned}$$

$$S/N = 13 \text{ dB}$$

Detection range for

$$\begin{aligned}\tau &= 66.6 \mu s \\ \sigma &= 1.0 \text{ m}^2\end{aligned}$$

$$S/N = 16$$

is  $R = 308 \text{ km}$ . Detection range for

$$\begin{aligned}\tau &= 66.6 \mu s \\ \sigma &= 1 \text{ m}^2\end{aligned}$$

$$S/N = 16$$



Interference Noise Power  
Density: 100 W/MHz

$P_I G_I / B_I$  (100 W/MHz)

Antenna Gain

Wavelength Squared  $(0.1)^2$

Interference Suppression

Range to Interference Source  
(300 km)

$(4\pi)^2$

Boltzmann's Constant

TOTALS

is  $R = 172.78$  km.

Interference noise temperature in  
Blake (Equation 2.31) form is as follows:

	(+) dB	(-) dB
		- 40
	37.3	
		- 20
		- 50
		- 109.5
		- 21.9
	228.6	
	265.9	241.4

$T_s = 10^{2.45} = 281.8$  K  
System noise temperature with interference is 788.4 K.

Detection range with interference is

$$R_I = R \left( \frac{T_s}{T_s + T_I} \right)^{1/4}$$

For detection ranges given above,  
subjected to interference,

205.8 km → 184.6 km  
11.5 km → 103.6 km  
308.0 km → 276.2 km  
172.8 km → 154.9 km

Measurement Accuracies

(Angle example is provided with range accuracies  
treated the same way.)

Angle—3.0 mr  
Range—100 m

Wideband range—0.1 m

Thermal noise dependent error component is

$$\sigma_{\theta} = \frac{\theta_3}{k_m \sqrt{2n \left( \frac{S}{N} \right)}}$$

$n$  = number of hits, assumed 1 for coherent integration,  $K_m$  = normalized monopulse slope set at 1.9.

Assume 6 pulses dedicated to track, at the maximum range for  $\sigma = 0.1\text{m}^2$ , angle error estimate is

$$\sigma_{\theta r} = 2.0 \text{ } mr$$

Given an angular instrumentation error of 1 *mr*, then the range dependent angular error is estimated, ignoring glint, as

$$\sigma_{\theta} = (1 + \theta_3^2/3.8(S/N))^{1/2}$$

where the beamwidth is expressed in *mr*.

The example, although not complete, is introductory in context, demonstrates procedures, indicates scope of analysis, and contains useful formulas in the form of models for simulation work. This performance analysis appears at many levels in the hierarchical system structure influencing system effectiveness at high levels and component design at the lower levels. This example, in addition to the discussions of the classical form of the radar equation and discussion of parameters from several points of view, should be both introductory and stimulate interest in further work.

This system perspective covers the use of the radar equation. Later at the end of Chapter 9, a similar discussion of environmental requirements is described with a similar point of view. Both examples are intended to be quantitative and representative of typical radar and system developments.



## *Chapter 3*

### *The Radar Equation—A Formal Treatment*

The radar equation follows directly from Maxwell's equations. This approach will be taken in the discussions to follow. We will begin the equation development with a review of field quantities, units and dimensions, and the assembly of the field equations into differential and integral forms. Through the use of vector potentials and application of several field theorems, Kirchhoff's diffraction formula is derived to develop a general power transfer formula. The formulas provide the basis of antenna and scattering theory and the derivation of the radar equation, first by a power transfer formulation, then by a direct interpretation of the diffraction formulas. The equation derivations are provided in a concise way, and are directly related to fundamental physical principles. The resulting radar equation provides radiated fields and intensities resulting from antenna and scatterers. Thus, the equations are equivalent to the classical ones, but include accompanying theoretical interpretations.

We continue this approach with a discussion of plane waves, which are important in radar applications for consideration of signal propagation within the operating environment. Topics include propagation in free space, lossless and lossy dielectrics, and conducting media. Explicit definitions cover propagation constants, impedances, and signal velocities. Plane waves incident on dielectrics and conductors are covered, and are applicable to the scattering discussions that follow.

Most radar antennas are characterized by dimensions much larger than the signal wavelengths. As a result, the theory we present concentrates on large aperture antennas. Formulations that we summarize include Kirchhoff's theory and transform methods, the geometric theory of diffraction, and the plane wave spectrum method of analysis. Emphasis is placed on Kirchhoff's theory, transform methods, and Gaussian forms, which are a generalization of the Gaussian beam approximation used in many radar analyses. Definitions of antenna beam characteristics, directivity and gain, near-field and far-field regions, and aperture distribution functions are provided. Because modern radar antennas are usually scanning arrays, we also cover fundamentals of array theory.

Radar cross sections, when viewed from a physical point of view, fall into the categories of *geometric optics*, where the characteristic dimensions of the scatterer are much larger than a wavelength, *physical optics*, where the dimensions are larger than a wavelength, *resonant scattering*, with dimension and wavelength nearly equivalent, and *Rayleigh scattering*, where the wavelength is much smaller than the target maximum dimension. Each is reviewed from a theoretical point of view and interpreted in terms of common radar targets. Scattering center formulations are prominent in the discussions of cross sections. A summary of target models is contained within the cross section delineations.

Properties of the radar signal conclude our radar equation discussions. Topics include basic signal properties, waveforms, and ambiguity functions.

Examples will be provided to supplement the discussions. An appendix is also included, for the same purpose, with compilations of diffraction integrals, orthogonal functions, Gaussian field expansions, and tables of Gaussian series scaling factors and coefficients.

### 3.1 MAXWELL'S EQUATIONS

Electric charges produce forces on other charges, with the forces measured as fields. A stationary charge yields an electric or electrostatic field, charges in motion at constant velocity produce magnetic or magnetostatic fields, and when charges are accelerated, electromagnetic fields consisting of electric and magnetic fields are excited. The physical law governing fields is combined into a set of classical field equations developed by Maxwell.

An abundance of reference materials is available covering Maxwell's equations and electromagnetic fields. The material provided here was selected from the works of Schelkunoff, Kraus, Skitek and Marshall, and Stratton, with additional reference material included in the bibliography.

#### Field Quantities, Units, and Dimensions

Electromagnetic fields are described by four vector quantities:

$E$  = electric field intensity

$H$  = magnetic field intensity

$D$  = electric flux density or electric displacement

$B$  = magnetic flux density or magnetic induction

A current density is

$J$  = current density

and, like the field quantities, is a vector quantity.

The electric field intensities are related to the electric flux densities in the following way:

$$\mathbf{D} = \epsilon \mathbf{E} = \epsilon_r \epsilon_0 \mathbf{E} \quad (3.1)$$

where

$\epsilon$  = permittivity of dielectric

$\epsilon_0$  = permittivity of a vacuum

and

$\epsilon_r$  = relative permittivity or dielectric constant

For the magnetic fields and flux densities,

$$\mathbf{B} = \mu \mathbf{H} = \mu_r \mu_0 \mathbf{H} \quad (3.2)$$

where

$\mu$  = permeability of material

$\mu_0$  = permeability of vacuum

and

$\mu_r$  = relative permeability

The current density is defined as

$$\mathbf{J} = \sigma \mathbf{E} \quad (3.3)$$

where  $\sigma$  is the conductivity of material. This equation is a formal statement of Ohm's law, and is sometimes referred to *Ohm's law at a point*.

In general, the establishment of dimensions is somewhat arbitrary, being selected (for convenience) in the specification of the units. In field theory, the velocity of light is a physical constant that must be maintained, independent of the choice of the other physical parameters. With dimensions of  $M$ –mass,  $L$ –length,

and  $T$ —time, the constant  $c$ , the velocity of light, will have dimensions of  $LT^{-1}$ . The field equations, by virtue of the relationships between the field intensities and flux densities, yield the constant  $c$  as  $1/\sqrt{\epsilon_0\mu_0}$ . The choice of either the permittivity or permeability as unity, for example, in specifying the field units, constrains the remaining quantity.

In the development of the MKS or Giorgi system of units, a transition from an early absolute CGS system with c—centimeter, g—gram, s—second, to a practical system occurred in order to place the field quantities in a more convenient form for computational and measurement purposes. Since the need for a fourth unit was recognized, the practical system would then contain the dimensions of  $M$ ,  $L$ ,  $T$ , with the fourth being the coulomb, ampere, or ohm. Considering the required practicability of the units and resulting dimensions of field quantities where fractional exponents occurred when the ohm was used as the primary measure, the coulomb was established as the fourth unit. From these early considerations, the Giorgi MKS system of units was established with the units being meter-kilogram-second-coulomb. This commonly used system had been referred to as MKSC, and most recently was adopted as the *SI (System Internationale)* or International System of Units.

The MKS system of units is commonly used, although CGS units may appear in theoretical works. Generally, a rationalized system of units is applied where a factor of  $4\pi$  is included in the force equations to avoid a continual appearance of the factor in the field equations.

Adding a power density quantity  $S$  and a commonly occurring charge density parameter  $\rho$  to the field quantities given above, while adding basic circuit parameters and the primary units, results in the compilation of the units and dimensions given in Table 3.1. The quantities, units, and dimensions are grouped in the primary, field, and circuit characterizations. The convenience of this established MKS system of units becomes apparent when applied in the solution of field problems. Similarly, radar problems, for consistency and convenience, should maintain this basic rationalized MKS system of units.

## Integral Forms

Maxwell's equations are best developed in integral form, where physical laws of electromagnetism are directly applied. Differential forms of the equations follow directly from the integral ones and are provided later.

### *From Faraday*

Given a time-varying electromagnetic field described by the vector quantities

Table 3.1 Units and Dimensions

Quantity		Units	Dimensions
<i>L</i>	Length	meter	<i>L</i>
<i>M</i>	Mass	kilogram	<i>M</i>
<i>T</i>	Time	second	<i>T</i>
<i>Q</i>	Charge	coulomb	<i>Q</i>
<i>E</i>	Field intensity	volts/meter	<i>ML/T<sup>2</sup>Q</i>
<i>H</i>	Field intensity	ampere/meter	<i>Q/TL</i>
<i>D</i>	Flux density	coulomb/meter <sup>2</sup>	<i>Q/L<sup>2</sup></i>
<i>B</i>	Flux density	weber/meter <sup>2</sup>	<i>M/TO</i>
<i>S</i>	Power density	watts/meter <sup>2</sup>	<i>M/T<sup>3</sup></i>
<i>J</i>	Current density	ampere/meter <sup>2</sup>	<i>Q/TL<sup>2</sup></i>
$\rho$	Charge density	coulomb/meter <sup>2</sup>	<i>Q/L<sup>3</sup></i>
$\sigma$	Conductivity	mho/meter	<i>TO<sup>2</sup>/ML<sup>3</sup></i>
$\epsilon$	Permittivity	farad/meter	<i>T<sup>2</sup>Q<sup>2</sup>/ML<sup>3</sup></i>
$\mu$	Permeability	henry/meter	<i>ML/Q<sup>2</sup></i>
<i>V</i>	Potential	volts	<i>ML<sup>2</sup>/T<sup>2</sup>Q</i>
<i>I</i>	Current	ampere	<i>Q/T</i>
<i>P</i>	Power	watts	<i>ML<sup>2</sup>/T<sup>3</sup></i>
<i>R</i>	Resistance	ohms	<i>ML<sup>2</sup>/TO<sup>2</sup></i>
<i>L</i>	Inductance	henry	<i>ML<sup>2</sup>/Q<sup>2</sup></i>
<i>C</i>	Capacitance	farad	<i>T<sup>2</sup>Q<sup>2</sup>/ML<sup>2</sup></i>

$\epsilon_0 = 8.854 \times 10^{-12}$  farad/meter

$\epsilon_0 \approx 1/36\pi \times 10^{-9}$  farad/meter

$\mu_0 = 4\pi \times 10^{-7}$  henry/meter

**E, D, H, and B**, consider first a closed path *l* with a differential element of length **dl** and surface area **ds**, confined as shown in Figure 3.1(a). From Faraday, the electromotive force (emf) generated is equal to the time rate of change of magnetic flux linked by the loop, and the current flowing in the direction of the induced emf. The induced voltage at the terminal of the loop is

$$V = \frac{d\Psi}{dt}$$
(3.4)

but

$$\Psi = \int \mathbf{B} \cdot \mathbf{ds}$$
(3.5)

Because



$$V = \oint \mathbf{E} \cdot d\mathbf{l} \quad (3.6)$$

Then, combining Equations (3.4), (3.5), and (3.6), we have

$$\oint \mathbf{E} \cdot d\mathbf{l} = \int \frac{\delta \mathbf{B}}{\delta t} \cdot d\mathbf{s} \quad (3.7)$$

which is a statement of Faraday's law relating magnetic flux linkages to a line integral of an electric field. It is the first of Maxwell's equations in integral form.

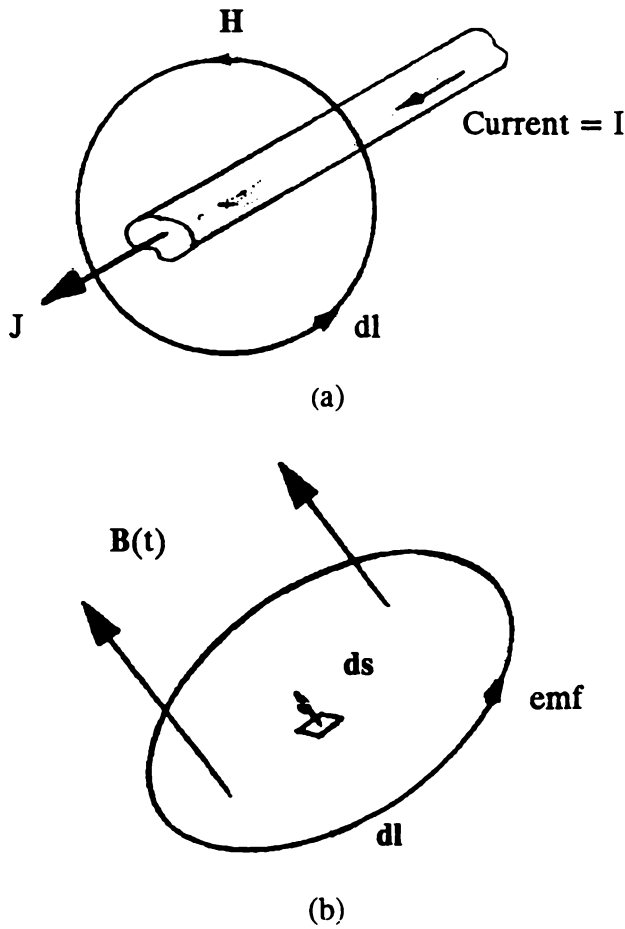


**Figure 3.1** Depiction of Faraday's and Ampere's Law: (a) From Faraday (b) From Ampere

### *From Ampere and Maxwell*

Ampere's *circuital law* states that a line integral of the magnetic field about a closed path, enclosing a current-carrying conductor, as shown in Figure 3.1(b), is

$$\oint \mathbf{H} \cdot d\mathbf{l} = I \quad (3.8)$$

Because the current can be expressed as an integration of the current density over a cross-sectional area of the conductor, then

$$I = \int \mathbf{J} \cdot d\mathbf{s} \quad (3.9)$$

Because  $\mathbf{J} = \sigma \mathbf{E}$ , setting Equation (3.8) equal to (3.9) yields

$$\oint \mathbf{H} \cdot d\mathbf{l} = \int \mathbf{J} \cdot d\mathbf{s} \quad (3.10)$$

which relates the magnetic field to a steady current. Referring to Figure 3.2(a), a line integration about a closed path enclosing a time-varying electric field is equal to a surface integration of the time-varying flux density. This result, from Maxwell, defines the displacement current. Thus, we have an equation which is equivalent to Equation (3.8) for time-varying fields:

$$\oint \mathbf{H} \cdot d\mathbf{l} = \int \frac{\partial \mathbf{D}}{\partial t} \cdot d\mathbf{s} \quad (3.11)$$

Combining Equations (3.8) through (3.11) yields the second of Maxwell's equations:

$$\oint \mathbf{H} \cdot d\mathbf{l} = \int \left( \mathbf{J} + \frac{\partial \mathbf{D}}{\partial t} \right) \cdot d\mathbf{s} \quad (3.12)$$

### *From Gauss, Electric Flux Density*

Referring to Figure 3.2(b), *Gauss law* states that an integration of the electric flux density, over a closed surface enclosing a volume, yields the charge enclosed. Thus,

$$\oint \mathbf{D} \cdot d\mathbf{s} = Q \quad (3.13)$$

or, given a charge density  $\rho$  within the enclosed volume, we have

$$\oint \mathbf{D} \cdot d\mathbf{s} = \int \rho \, dv \quad (3.14)$$

By definition, the divergence of the flux density  $\mathbf{D}$  is the total flux emanating from an enclosed volume (in the limit) as the volume approaches zero. Because one

flux line emanates from a unit of charge, then

$$\nabla \cdot \mathbf{D} = \rho \tag{3.15}$$

Equation (3.14) can also be written in the form:

$$\oint \mathbf{D} \cdot d\mathbf{s} = \int \nabla \cdot \mathbf{D} \, dv \tag{3.16}$$

Equation (3.14) is the third of Maxwell's equations, which may also appear in the form of Equation (3.16). The divergence relationship (Equation (3.15)) is the differential counterpart.

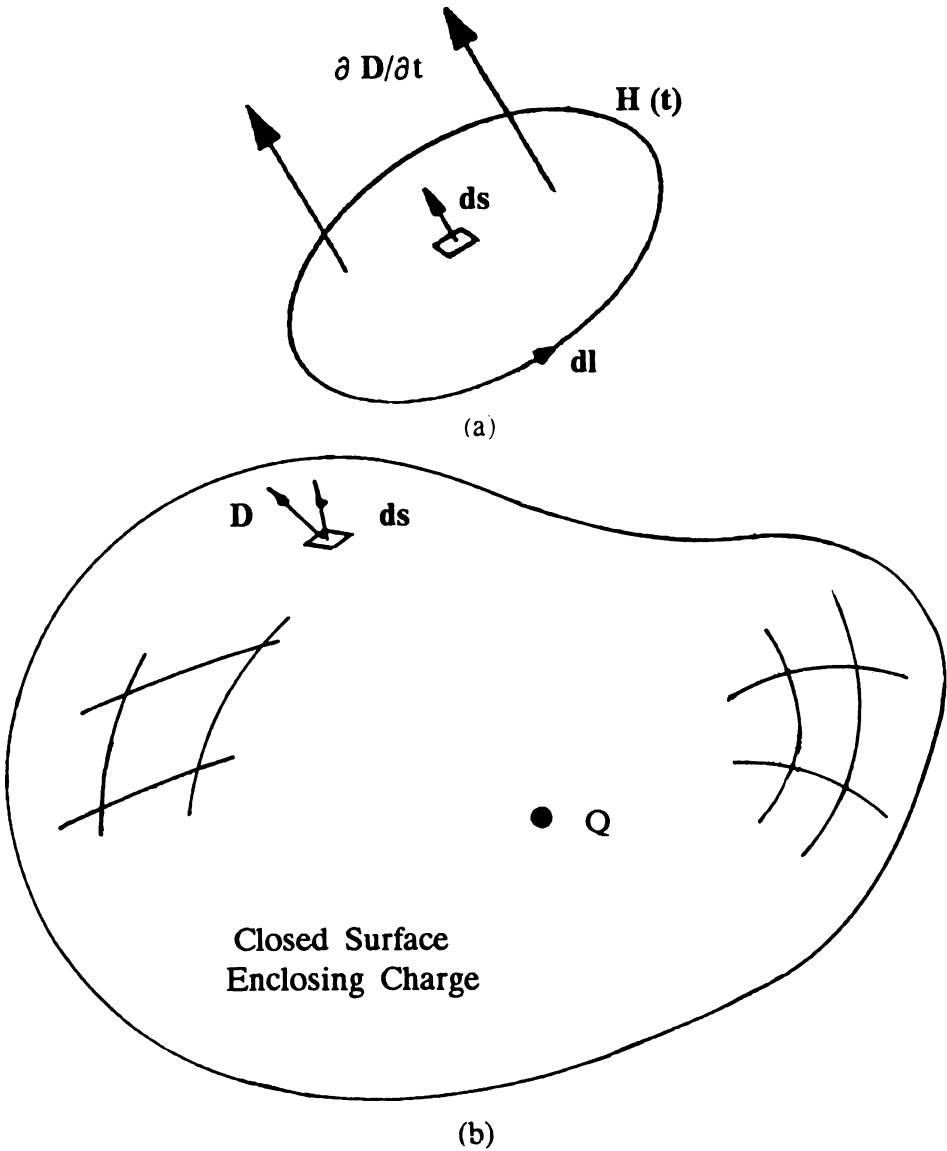


**Figure 3.2** Depiction of Maxwell's Displacement Current and Gauss's Law: (a) From Maxwell (b) From Gauss

### *From Gauss, Magnetic Flux Density*

Unlike electric fields that emanate or terminate on charges, magnetic flux lines are closed. Therefore, an integration of the magnetic flux density over a closed surface is identically zero, so

$$\oint \mathbf{B} \cdot d\mathbf{s} = 0 \quad (3.17)$$

which is the fourth of Maxwell's equations in integral form.

### **Differential Forms**

Differential forms of Maxwell's equations follow directly from the integral forms. A vector identity which relates a line integral to a surface integral is needed. According to Stoke's law, given a vector  $\mathbf{A}$

$$\oint \mathbf{A} \cdot d\mathbf{l} = \int \nabla \times \mathbf{A} \cdot d\mathbf{s} \quad (3.18)$$

By applying Equation (3.18) and the divergence theorem stated above, Equations (3.7), (3.12), (3.14), and (3.15) will yield Maxwell's equations in differential form. The results, provided with the integral forms of the equations, are as follows:

$$\oint \mathbf{E} \cdot d\mathbf{l} = - \int \frac{\partial \mathbf{B}}{\partial t} \cdot d\mathbf{l} \quad \nabla \times \mathbf{E} = - \frac{\partial \mathbf{B}}{\partial t} \quad (3.19)$$

$$\oint \mathbf{H} \cdot d\mathbf{l} = \int \left( \mathbf{J} + \frac{\partial \mathbf{D}}{\partial t} \right) \cdot d\mathbf{s} \quad \nabla \times \mathbf{H} = \mathbf{J} + \frac{\partial \mathbf{D}}{\partial t} \quad (3.20)$$

$$\oint \mathbf{D} \cdot d\mathbf{s} = \int \rho \, dv \quad \nabla \cdot \mathbf{D} = \rho \quad (3.21)$$

$$\oint \mathbf{B} \cdot d\mathbf{s} = 0 \quad \nabla \cdot \mathbf{B} = 0 \quad (3.22)$$

Associated with Maxwell's equations is a continuity relationship that is a statement of conservation of charge. An integration of the current density in the following way:

$$\oint \mathbf{J} \cdot d\mathbf{s} = \frac{\partial q}{\partial t} = \int \frac{\partial \rho}{\partial t} \, dv \quad (3.23)$$

yields

$$\nabla \cdot \mathbf{J} = \frac{\partial \rho}{\partial t} \quad (3.24)$$

which is the continuity equation. The interpretation of this result as a conservation of charge is an appropriate and expected one.

### Boundary Conditions

The presence of the material parameters  $\epsilon$ ,  $\mu$ , and  $\sigma$  in Maxwell's equations imply explicit conditions imposed on the fields at a boundary between dissimilar materials. The boundary conditions, much like the integral forms of the equations, besides being of mathematical significance, are useful in the physical interpretation of the fields.

The boundary conditions are derived directly from Maxwell's equations, and are summarized below. Referring to Figure 3.3, the field quantities are designated by the subscripts 1 and 2, corresponding to the two materials. A unit vector  $\mathbf{n}$  normal to the planer surface at the interface is defined, with the boundary conditions provided in vector form.

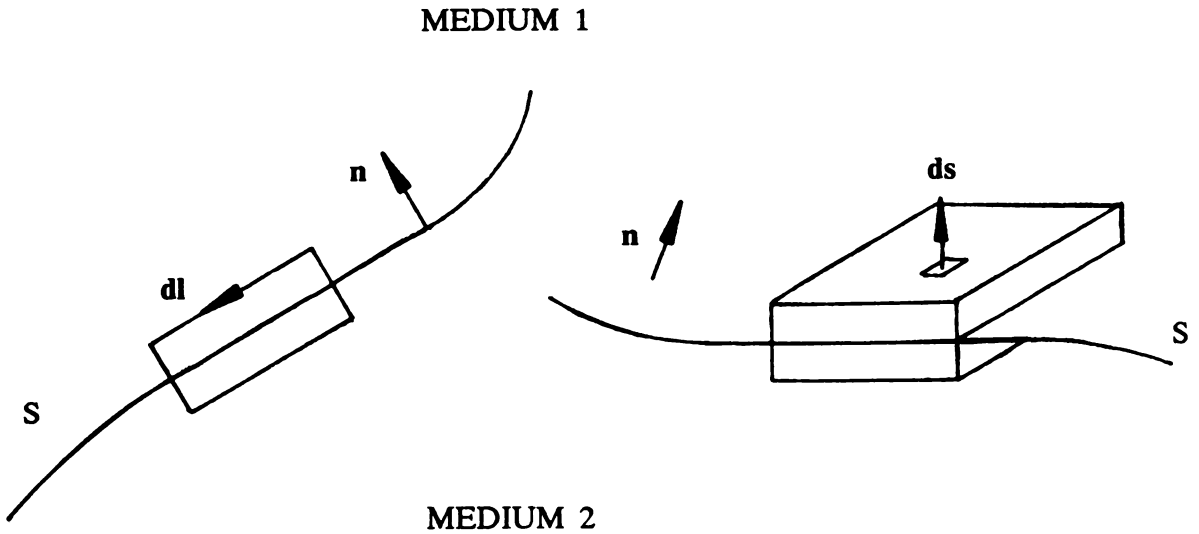


**Figure 3.3** Field Components at a Boundary

At the boundary between two media, with material constants  $\epsilon$ ,  $\mu$ , and  $\sigma$ :

$$\text{Tangential } \mathbf{E} \quad \mathbf{n} \times (\mathbf{E}_2 - \mathbf{E}_1) = 0 \quad (3.25)$$

$$\text{Normal } \mathbf{D} \quad \mathbf{n} \cdot (\mathbf{D}_2 - \mathbf{D}_1) = \rho_s \quad (3.26)$$

$$\text{Tangential } \mathbf{H} \quad \mathbf{n} \times (\mathbf{H}_2 - \mathbf{H}_1) = \mathbf{K} \quad (3.27)$$

$$\text{Normal } \mathbf{B} \quad \mathbf{n} \cdot (\mathbf{B}_2 - \mathbf{B}_1) = 0 \quad (3.28)$$

Equation (3.25) states that the tangential component of the electric field is continuous at the boundary, while the normal component of the flux density in (3.26) is equal to the surface charge density  $\rho_s$ . The tangential component of the magnetic field in (3.27) equals the surface current density  $\mathbf{K}$ . The normal component of the magnetic flux density  $\mathbf{B}$  in (3.28) is, as expected, continuous at the boundary.

The general boundary conditions given above include charge and current densities at the interface which do not always occur. The occurrence of boundaries separating two dielectric media, one of which is usually air, and the occurrence of air and perfect conductor boundaries are common in radar applications. At an interface between two dielectric materials (i.e.,  $\sigma = 0$ ,  $\mu = \mu_0$ ), we have

$$\text{Tangential } \mathbf{E} \quad \mathbf{n} \times (\mathbf{E}_2 - \mathbf{E}_1) = 0 \quad (3.29)$$

$$\text{Normal } \mathbf{D} \quad \mathbf{n} \cdot (\mathbf{D}_2 - \mathbf{D}_1) = 0 \quad (3.30)$$

$$\text{Tangential } \mathbf{H} \quad \mathbf{n} \times (\mathbf{H}_2 - \mathbf{H}_1) = 0 \quad (3.31)$$

$$\text{Normal } \mathbf{B} \quad \mathbf{n} \cdot (\mathbf{B}_2 - \mathbf{B}_1) = 0 \quad (3.32)$$

At the boundary between a dielectric and a perfect conductor, we have

$$\text{Tangential } \mathbf{E} \quad \mathbf{n} \times \mathbf{E}_1 = 0 \quad (3.33)$$

$$\text{Normal } \mathbf{D} \quad \mathbf{n} \cdot \mathbf{D}_1 = \rho_s \quad (3.34)$$

$$\text{Tangential } \mathbf{H} \quad \mathbf{n} \times \mathbf{H}_1 = \mathbf{K} \quad (3.35)$$

$$\text{Normal } \mathbf{B} \quad \mathbf{n} \cdot \mathbf{B}_1 = 0 \quad (3.36)$$

The tangential component of the electric field is zero at a dielectric and conductor boundary, while the normal component of the electric flux density gives rise to a charge density at the boundary. The normal component of the magnetic field is zero at the interface, with the current density equal in magnitude to the magnetic field.

### *Summary*

In summation, the tangential component of the electric field is continuous at the boundary between two media with the differing parameters  $\epsilon$ ,  $\mu$ , and  $\sigma$ . When one medium is a perfect conductor ( $\sigma \rightarrow \infty$ ), the tangential component of the

electric field in the other medium is zero. Likewise, the tangential component of the magnetic field is continuous at the boundary between any two media. When a current sheet occurs at a boundary, the difference in the tangential components of the magnetic fields is equal to the current density. If one medium is a perfect conductor, a current sheet occurs at the boundary, with the current density equal to the amplitude of the tangential component of the magnetic field at the boundary surface. If one medium is characterized by infinite permeability, the tangential magnetic field in the other media is zero. The normal components of the electric flux densities are continuous at a boundary free of charge, with their difference equal to a charge density. At a boundary containing charge on the surface of a perfect conductor, the electric flux density in the other media is equal to the charge density. Finally, the normal component of the magnetic flux density is always continuous at a boundary separating two media.

### Equation Compilations

The important phasor forms of the general set of Maxwell's equations are now presented. The more applicable and simple equations for free space are tabulated, with steady-current and static forms included.

#### Phasor Form

Equations (3.19) through (3.22) are statements of Maxwell's equations in a general form. When harmonic time variations (i.e., *exp(jωt)*) are assumed, the integral and differential formulas are readily placed in the harmonic variation or *phasor form* given as follows:

$$\oint \mathbf{E} \cdot d\mathbf{l} = j\omega\mu \oint \mathbf{H} \cdot d\mathbf{s} \quad \nabla \times \mathbf{E} = -j\omega\mu\mathbf{H} \quad (3.37)$$

$$\oint \mathbf{H} \cdot d\mathbf{l} = (\sigma + j\omega\epsilon) \oint \mathbf{E} \cdot d\mathbf{s} \quad \nabla \times \mathbf{H} = (\sigma + j\omega\epsilon)\mathbf{E} \quad (3.38)$$

$$\oint \mathbf{D} \cdot d\mathbf{s} = \int \rho \, dv \quad \nabla \cdot \mathbf{D} = \rho \quad (3.39)$$

$$\oint \mathbf{B} \cdot d\mathbf{s} = 0 \quad \nabla \cdot \mathbf{B} = 0 \quad (3.40)$$

The flux density  $\mathbf{D}$  in the curl equations has been replaced by  $j\omega\epsilon \mathbf{E}$ ,  $\mathbf{J}$  by  $\sigma\mathbf{E}$ , and  $\mathbf{B}$  by  $j\omega\mu\mathbf{H}$ . Phasor forms of Maxwell's equations are prevalent in all but theoretical field theory developments, where general forms are usually maintained. Later, magnetic current sources, avoided thus far, will be inserted into the equations.

### *Free Space*

In free space, the current density  $\mathbf{J}$  and charge density  $\rho$  are zero. Maxwell's equations are then expressed in the following phasor form:

$$\oint \mathbf{E} \cdot d\mathbf{l} = j\omega\mu \oint \mathbf{H} \cdot d\mathbf{s} \quad \nabla \times \mathbf{E} = -j\omega\mu\mathbf{H} \quad (3.41)$$

$$\oint \mathbf{H} \cdot d\mathbf{l} = j\omega\epsilon \oint \mathbf{E} \cdot d\mathbf{s} \quad \nabla \times \mathbf{H} = j\omega\epsilon\mathbf{E} \quad (3.42)$$

$$\oint \mathbf{E} \cdot d\mathbf{s} = 0 \quad \nabla \cdot \mathbf{E} = 0 \quad (3.43)$$

$$\oint \mathbf{H} \cdot d\mathbf{s} = 0 \quad \nabla \cdot \mathbf{H} = 0 \quad (3.44)$$

Later, when the waves are discussed, this set of equations and the general forms will be applied, with  $\mathbf{J} \neq 0$ , but with the charge density  $\rho$  maintained at zero. Lossless conditions are described by the free space conditions, with lossy plane-wave propagations requiring use of the general forms of the equations.

### *Steady-Current and Static Forms*

For steady currents,  $\mathbf{J} \neq 0$ , but time-varying electric and magnetic fields are zero. In those instances, Maxwell's equations become

$$\oint \mathbf{E} \cdot d\mathbf{l} = 0 \quad \nabla \times \mathbf{E} = 0 \quad (3.45)$$

$$\oint \mathbf{H} \cdot d\mathbf{l} = \oint \mathbf{J} \cdot d\mathbf{s} \quad \nabla \times \mathbf{H} = \mathbf{J} \quad (3.46)$$

$$\oint \mathbf{D} \cdot d\mathbf{s} = \int \rho \, dv \quad \nabla \cdot \mathbf{D} = \rho \quad (3.47)$$

$$\oint \mathbf{B} \cdot d\mathbf{s} = 0 \quad \nabla \cdot \mathbf{B} = 0 \quad (3.48)$$

When  $\mathbf{J} = 0$ , the equations describe the behavior of static electric and magnetic fields. The equations are

$$\oint \mathbf{E} \cdot d\mathbf{l} = 0 \quad \nabla \times \mathbf{E} = 0 \quad (3.49)$$

$$\oint \mathbf{H} \cdot d\mathbf{l} = 0 \quad \nabla \times \mathbf{H} = 0 \quad (3.50)$$



$$\oint \mathbf{D} \cdot d\mathbf{s} = \int \rho \, dv \quad \nabla \cdot \mathbf{D} = \rho \quad (3.51)$$

$$\oint \mathbf{B} \cdot d\mathbf{s} = 0 \quad \nabla \cdot \mathbf{B} = 0 \quad (3.52)$$

The general and free space forms of Maxwell's equations will be used in the following sections. The steady and static equations will not be directly applied, but will be of some value in the interpretation of the results. Overall, further pursuance of the theory and use of the field equations is encouraged, with reference material included in the bibliography serving as a starting point toward that end.

### 3.2 ANTENNA, SCATTERING, AND RADAR EQUATION FORMULATIONS

A formal approach to diffraction theory is taken here. Vector potentials are reviewed, and solutions to Maxwell's equations provided. The fundamental Stratton-Chu diffraction formula is developed and discussed, with a general power transfer formula described. The equation derivations form the basis and introduction to the radar equation, plane waves, antennas, and cross sections of the paragraphs to follow.

#### Vector Potentials

In general, a lossy medium is one with material parameters  $(\epsilon, \mu, \sigma)$  with  $\mu = \mu_0$ . Electric and magnetic current sources are assumed, which give rise to radiated fields. The sources consist of an impressed current density  $\mathbf{J}$  (i.e., A/m<sup>2</sup>), and magnetic current density  $\mathbf{M}$ . Postponing the interpretation of both current densities temporarily, we will let the *total radiated fields* be the sum of the fields due to applied current densities. Then, we have

$$\mathbf{E} = \mathbf{E}_e + \mathbf{E}_h \quad (3.53)$$

and

$$\mathbf{H} = \mathbf{H}_e + \mathbf{H}_h \quad (3.54)$$

where, as before, the subscripts  $e$  and  $h$  denote quantities resulting from electric and magnetic sources, respectively. Since the sources radiate independently, Maxwell's equations may be solved for each current source independently, with the resulting solutions summed. This problem is formulated in Figure 3.4.

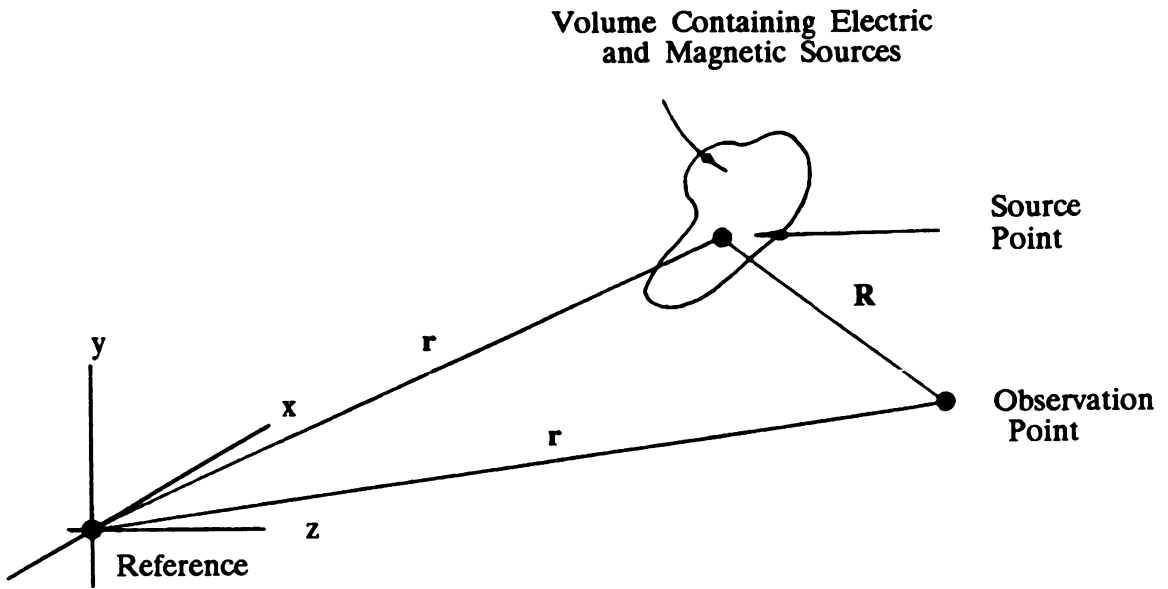


**Figure 3.4** Formulation of the Radiation Problem

From the general form of Maxwell's equations, (3.19) and (3.20), the addition of the current sources  $\mathbf{J}$  and  $\mathbf{M}$  separately yields

$$\nabla \times \mathbf{E}_e = - \frac{\partial \mathbf{B}_e}{\partial t} \quad (3.55)$$

$$\nabla \times \mathbf{H}_e = \sigma \mathbf{E} + \frac{\partial \mathbf{D}_e}{\partial t} + \mathbf{J} \quad (3.56)$$

and

$$\nabla \times \mathbf{E}_m = - \frac{\partial \mathbf{B}_m}{\partial t} - \mathbf{M} \quad (3.57)$$

$$\nabla \times \mathbf{H}_m = \sigma \mathbf{E}_m + \frac{\partial \mathbf{D}_m}{\partial t} \quad (3.58)$$

In phasor form, the above equations become

$$\nabla \times \mathbf{E}_e = -j\omega\mu\mathbf{H}_e \quad (3.59)$$

$$\nabla \times \mathbf{H}_e = j\omega\tilde{\epsilon}\mathbf{E}_e + \mathbf{J} \quad (3.60)$$

$$\nabla \times \mathbf{E}_m = -j\omega\mu\mathbf{H}_m + \mathbf{M} \quad (3.61)$$

$$\nabla \times \mathbf{H}_m = j\omega\tilde{\epsilon}\mathbf{E}_m \quad (3.62)$$

where a complex permittivity is defined as

$$\tilde{\epsilon} = \epsilon \left( 1 + \frac{\sigma}{j\omega\epsilon} \right) \quad (3.63)$$

### EXAMPLE: INTERPRETATION OF CURRENT DENSITIES

As we concentrate on the magnetic current density, and take the divergence of equations (3.61) and (3.62), we have

$$\nabla \cdot \mathbf{H}_m = - \frac{\nabla \cdot \mathbf{M}}{j\omega\mu}$$

or

$$\nabla \cdot \left( \mathbf{H}_m + \frac{\mathbf{M}}{j\omega\mu} \right) = 0$$

where

$$\mathbf{M} = -j\omega\mu\mathbf{H}_m = - \frac{\partial \mathbf{B}_m}{\partial t}$$

which is a time-varying magnetic flux density. Magnetic conduction currents, unlike electric currents, do not exist. When used in the field equations,  $\mathbf{M}$  pertains to the representation of time-varying flux densities resulting from complicated electric current distributions by time-varying magnetic flux densities. Use of a similar procedure for the electric current density yields the expected result:

$$\mathbf{J} = \frac{\partial \mathbf{D}_e}{\partial t}$$

which is Maxwell's displacement current.

We will consider the electric current density first. Solutions of Equations (3.59) and (3.60) are needed. Because  $\nabla \cdot \beta = 0$ ,  $\mathbf{H}$  is a vector solenoidal field, and can be expressed as the curl of a vector. If we let this vector be  $\mathbf{A}$ , a magnetic potential with units of amperes, then

$$\mathbf{H}_e = \nabla \times \mathbf{A} \quad (3.64)$$

Substituting  $\mathbf{H}_e$  into equation (3.59) yields

$$\nabla \times \mathbf{E}_e = -j\omega\mu (\nabla \times \mathbf{A}) \quad (3.65)$$

or

$$\nabla \times (\mathbf{E}_e + j\omega\mu\mathbf{A}) = 0 \quad (3.66)$$

Because the curl of the vector field  $\mathbf{E}_e$  is zero, it may be represented by the gradient of a scalar potential. If we let this potential be  $\Phi_e$ , then

$$\mathbf{E}_e = -j\omega\mu\mathbf{A} - \nabla\Phi_e \quad (3.67)$$

Given  $\mathbf{E}_e$  and  $\Phi_e$ , the electric field can be found from (3.67). Equations for both potentials can be derived directly from Maxwell's equations (as we will demonstrate), but this will lead to a pair of coupled equations. The solution is readily obtained when the vector and scalar potentials are related. This is accomplished by specifying the divergence of  $\mathbf{A}$ , and imposing the Lorentze condition, with the resulting relationship being the *Lorentze gauge*. This procedure is demonstrated by first substituting Equation (3.64) into Equation (3.60):

$$\nabla \times \nabla \times \mathbf{A} = j\omega\epsilon\mathbf{E}_e + \mathbf{J} \quad (3.68)$$

but

$$\nabla \times \nabla \times \mathbf{A} = \nabla(\nabla \cdot \mathbf{A}) - \nabla^2\mathbf{A} \quad (3.69)$$

Equation (3.68) now becomes

$$\nabla^2\mathbf{A} + \omega^2\mu\epsilon\mathbf{A} - \nabla(j\omega\epsilon\Phi + \nabla \cdot \mathbf{A}) = -\mathbf{J}_e \quad (3.70)$$

The Lorentze gauge specifies the divergence of  $\mathbf{A}$  as,

$$\nabla \cdot \mathbf{A} = -j\omega\epsilon\Phi \quad (3.71)$$

with the parameter  $\omega^2\mu\tilde{\epsilon} = \tilde{k}$  defined as a complex wave number. If we apply both defining quantities to Equation (3.70), we have the final result

$$\nabla^2 \mathbf{A} + \tilde{k}^2 \mathbf{A} = -\mathbf{J} \quad (3.72)$$

which is a vector wave equation relating the magnetic potential  $\mathbf{A}$  to the electric current source  $\mathbf{J}$ .

A solution of Equation (3.72) and formulas for the field quantities will be provided. However, we will first let electric vector potential be defined as

$$\mathbf{E}_m = \nabla \times \mathbf{F} \quad (3.73)$$

then, proceeding as before, using the gauge transformation:

$$\nabla \cdot \mathbf{F} = -j\omega\mu\Phi_m \quad (3.74)$$

leads to the vector differential equation:

$$\nabla^2 \mathbf{F} + \tilde{k}^2 \mathbf{F} = -\mathbf{M} \quad (3.75)$$

The solutions of Equations (3.72) and (3.75) are

$$\mathbf{A} = \frac{1}{4\pi} \iiint \frac{\mathbf{J}(\mathbf{x}', y', z') \exp(-j\tilde{k}R)}{R} d\mathbf{v}' \quad (3.76)$$

and

$$\mathbf{F} = \frac{1}{4\pi} \iiint \frac{\mathbf{M}(\mathbf{x}', y', z') \exp(-j\tilde{k}R)}{R} d\mathbf{v}' \quad (3.77)$$

The radiated fields resulting from the electric and magnetic currents can be obtained from

$$\mathbf{E} = -j\omega\mu\mathbf{A} + \frac{1}{j\omega\tilde{\epsilon}} \nabla(\nabla \cdot \mathbf{A}) - \nabla \times \mathbf{F} \quad (3.78)$$

and

$$\mathbf{H} = -j\omega\tilde{\epsilon}\mathbf{F} + \frac{1}{j\omega\mu} \nabla(\nabla \cdot \mathbf{F}) + \nabla \times \mathbf{A} \quad (3.79)$$

### EXAMPLE: GREEN'S FUNCTION SOLUTION OF THE VECTOR WAVE EQUATION

Using the geometry of Figure 3.5, and for convenience considering a potential  $\psi = \Psi(\mathbf{r} - \mathbf{r}') = \Psi(\mathbf{R})$  and current source  $\mathbf{J} = \mathbf{J}(\mathbf{r} - \mathbf{r}') = \mathbf{J}(\mathbf{R})$ , the Helmholtz equation becomes,

$$(\nabla^2 + k^2)\Psi = -\mathbf{J}$$

A Green's function solution involves a solution for a point source, and then a solution for a distributed current is found by integration. Consider the function  $G = G(\mathbf{r} - \mathbf{r}') = G(\mathbf{r}|\mathbf{r}')$  a solution of

$$(\nabla^2 + k^2)G = -\delta(\mathbf{r} - \mathbf{r}')$$

where  $\delta(\mathbf{r} - \mathbf{r}')$  is the delta function.  $G$  is the Green's function

$$G = \frac{\exp(-jkR)}{4\pi R}$$

Constructing the equations, we have

$$G\nabla^2\Psi + k^2G\Psi = -\mathbf{J}G$$

and

$$\Psi\nabla^2G + k^2G\Psi = -\mathbf{J}G$$

Adding and integrating, we obtain

$$\iiint [G\nabla^2\Psi - \Psi\nabla^2G] dv + \iiint \mathbf{J}G dv = \Psi$$

The first volume integral can be expressed as the surface integral:

$$\iint \left[ G \frac{\partial \Psi}{\partial n} - \Psi \frac{\partial G}{\partial n} \right] ds$$

where  $n$  is an outward unit vector, normal to a closed surface containing the current sources  $\mathbf{J}$ . The Green's function,  $G$ , a solution to the second Helmholtz equation, is given above. Then,

$$\frac{\partial G}{\partial R} = -j \frac{k \exp(-jkR)}{4\pi R} + \frac{\exp(-jkR)}{4\pi R^2}$$

When  $R \rightarrow \infty$ , the surface integral becomes

$$\iint \frac{\exp(-jkR)}{R} \left[ \frac{\partial \Psi}{\partial R} - jk\Psi \right] ds$$

The expression within the brackets is the radiation condition. The integral vanishes when  $R \rightarrow \infty$ . The Green's function solution now becomes

$$\Psi = \iiint \mathbf{J} G \, dv$$

which justifies the results of Equations (3.76) and 3.77).

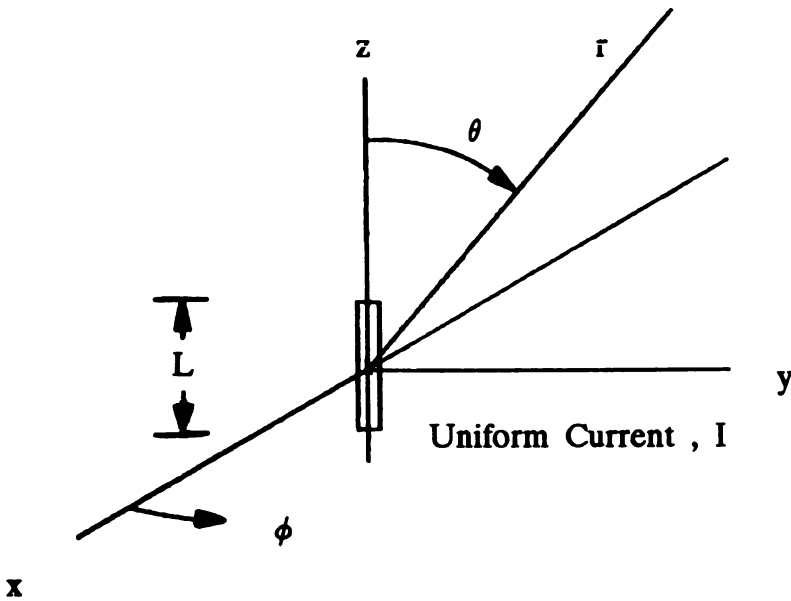


**Figure 3.5** The Infinitesimal Electric Radiating Element

These equations, credited to Schelkunoff (as stated by Hu) form a vector generalization of Kirchhoff's formula. They represent a theory of antennas describing the radiation from time-varying current sources. These are the fundamental equations for describing the radiated field of wire antennas, including dipoles and loops. Procedurally, the fields emanating from an infinitesimal dipole are determined. The total fields of an antenna with a given current distribution are found

by integration of the current element fields over the surface or volume of the antenna. The fields of the infinitesimal dipole, of fundamental importance in antenna formulations, are given in the following example.

**EXAMPLE: THE RADIATED FIELDS OF AN INFINITESIMAL DIPOLE**

Consider an electric current element of length  $l \rightarrow 0$  positioned along the  $z$ -axis, as shown in Figure 3.4. The current is uniformly distributed with intensity  $I$ . The vector potential is

$$A_z = \int_{-l/4}^{+l/4} IG \, dz$$

with the solution:

$$A_z = \mathbf{k} \frac{I l}{4\pi r} \exp(-jkr)$$

Because

$$\mathbf{k} = \cos\theta \, \mathbf{r} - \sin\theta \, \boldsymbol{\theta}$$

and with  $\mathbf{M} = 0$ , we have

$$\mathbf{E} = -j\omega\mu\mathbf{A} + \frac{1}{j\omega\epsilon} \nabla(\nabla \cdot \mathbf{A})$$

and

$$\mathbf{H} = \nabla \times \mathbf{A}$$

It follows that

$$\begin{aligned} \nabla(\nabla \cdot \mathbf{A}) &= \mathbf{r} \frac{Il}{4\pi} \cos\theta \exp(-jkr) \left[ \frac{2jk}{r^2} - \frac{k}{r} + \frac{2}{r^3} \right] \\ &\quad + \boldsymbol{\theta} \frac{Il}{4\pi} \sin\theta \exp(-jkr) \left[ \frac{1}{r^3} + \frac{jk}{k^2} \right] \end{aligned}$$

and



$$\nabla \times \mathbf{A} = \Phi \frac{Il}{4\pi} \exp(-jkr) \left[ \frac{jk}{r} + \frac{1}{r^2} \right]$$

From which the following field quantities are derived:

$$E_r = \frac{Il}{2\pi r^2} \exp(-jkr) \sqrt{\mu/\epsilon} \left[ 1 + \frac{1}{jkr} \right]$$

$$E_\theta = \frac{jk\mu Il}{4\pi r} \exp(-jkr) \sin\theta \left[ 1 + \frac{1}{jkr} - \frac{1}{kr^2} \right]$$

$$H_\phi = \frac{jkIl}{4\pi r} \exp(-jkr) \sin\theta \left[ 1 + \frac{1}{jkr} \right]$$

The field quantities with  $1/r$  dependence are the *radiated fields* of the antenna element. The remaining fields are confined close to the current element and are the *near fields*. Later, when large aperture antennas are of concern, the radiating fields will be defined as near and far fields, pertaining only to the radiated fields with  $1/r$  dependence. Although awkward, this designation is preferred over the Fresnel and Fraunhofer designations.

### Equivalence Theorem and Kirchhoff's Formula

Equivalence theorems relate the radiated fields of current sources within a volume  $V$  to fields emanating from equivalent sources on a closed surface enclosing the volume  $V$ . Referring to Figure 3.6, let  $\mathbf{E}$  and  $\mathbf{H}$  be the fields on the surface  $S$  due to the antenna enclosed by  $S$ ; then, quoting from Schelkunoff, in the source-free region, this field (i.e., the field radiated by the antenna), equals that produced by an electric sheet of density  $\mathbf{n} \times \mathbf{H}$  and a magnetic current sheet of density  $\mathbf{E} \times \mathbf{n}$ , both on  $S$ . In the remaining region (i.e., inside  $S$ ), the field produced by these sources vanishes. Integrating over  $S_\infty$  and imposing the radiation conditions in a manner similar to the examples given above yields negligible fields from the surface  $S_\infty$ .

Inserting the current densities  $\mathbf{n} \times \mathbf{H}$  and  $\mathbf{E} \times \mathbf{n}$  into Equations (3.76) and (3.77) with the integrations now taken over a surface, yields

$$\mathbf{A} = \iint \mathbf{n} \times \mathbf{H} \mathbf{G} \, ds \quad (3.80)$$

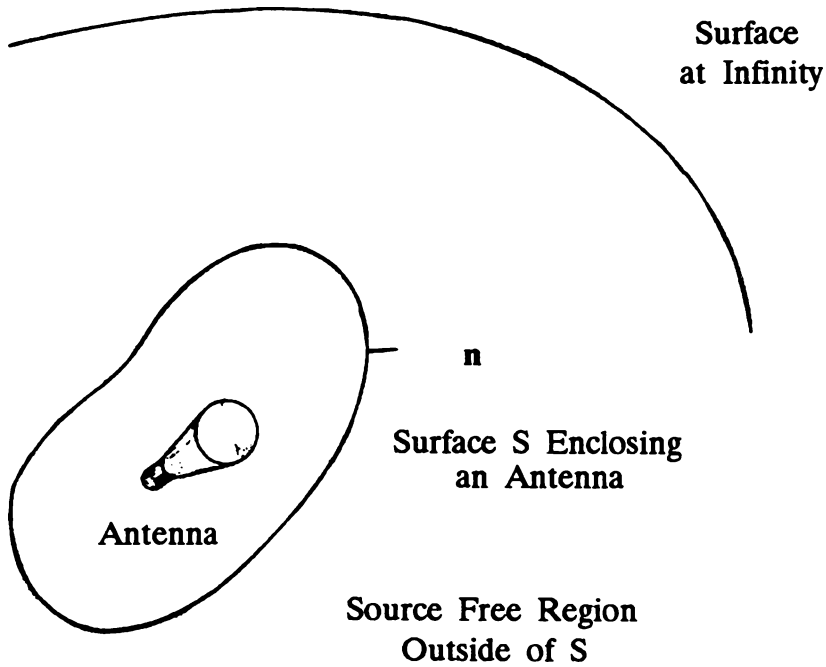


Figure 3.6 A Closed Surface Enclosing an Antenna

and

$$\mathbf{F} = \iint \mathbf{E} \times \mathbf{n} G \, ds \quad (3.81)$$

Substituting Equations (3.80) and (3.81) into (3.78) and (3.79), and interchanging integration and differentiation operations yields the *Stratton-Chu diffraction formulas*:

$$\mathbf{E} = - \iint [j\omega\mu \mathbf{n} \times \mathbf{H} G + (\mathbf{n} \times \mathbf{E}) \times \nabla G + \mathbf{n} \cdot \mathbf{E} \nabla G] \, ds \quad (3.82)$$

$$\mathbf{H} = \iint [j\omega\epsilon \mathbf{n} \times \mathbf{E} G - \mathbf{n} \times \mathbf{H} \times \nabla G - (\mathbf{n} \cdot \mathbf{H}) \nabla G] \, ds \quad (3.83)$$

These equations, like (3.78) and (3.79), as pointed out by Hu, are vector generalizations of Kirchhoff's formula. When applied directly, the radiated fields of an antenna evolve from a vector diffraction theory. In those instances, the electric and magnetic fields are coupled. In the scalar theory, widely used for estimating the radiated fields of large-aperture antennas, each field component gives rise to a separate radiated field, where the aperture and radiated fields

maintain the same polarization. In the vector theory, polarizations of radiated fields will differ.

In the scalar theory of diffraction, widely used for solution of diffraction and radiation problems, a scalar function  $U$  is a solution of the Helmholtz equation:

$$(\nabla^2 + k^2)U = 0 \quad (3.84)$$

In the source-free region shown in Figure 3.7, a large-aperture antenna is depicted, with the source-free region bounded by  $A$ , the aperture of the antenna,  $S_a$ , the surface of the antenna adjacent to the aperture  $A$ , and  $S_\infty$ , the surface at infinity. Kirchhoff's theorem states that the fields at a point  $P$  within the closed surface  $S$  consisting of  $A$ ,  $S_a$ ,  $S_\infty$  is

$$U(P) = \iint \left[ U \frac{\partial G}{\partial n} - G \frac{\partial U}{\partial n} \right] ds \quad (3.85)$$

Kirchhoff diffraction formulas (or integrals) are reductions of Equation (3.85), subject to the boundary conditions:

$$U = U_a, \frac{\partial U}{\partial n} = \frac{\partial U_a}{\partial n} \text{ on } A \quad (3.86)$$

$$U = 0, \frac{\partial U}{\partial n} = 0 \text{ on } A \quad (3.87)$$

with a vanishing contribution from the integration over  $S_\infty$ . Equation (3.85), subject to these boundary conditions, leads to the diffraction integral:

$$U(P) = -\frac{j}{2\lambda} (1 + \cos\theta) \iint \frac{U_a \exp(-jkr)}{r} ds \quad (3.88)$$

This important result constitutes the basis of the scalar theory of large-aperture antennas, which is used extensively in radar applications. It is an approximate formulation because of the boundary conditions imposed.

Maintaining this general connotation, with applications of the formulas provided later, the complexity of the solution of the diffraction integrals depends on the choice of  $r_o$ , the distance between the source and observation point. The general approach taken is to expand  $r$  in a power series of  $r_o$ , the aperture coordinates.

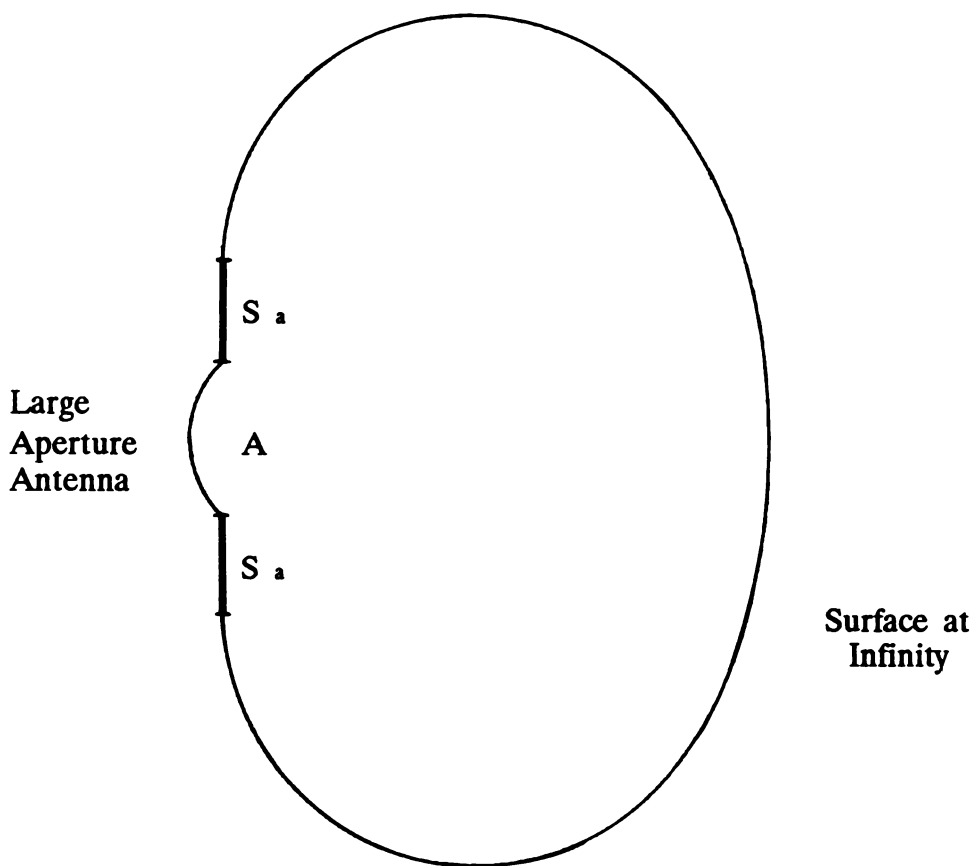


**Figure 3.7** Interpretation of Kirchhoff's Diffraction Integrals for a Large-Aperture Antenna

Referring to Figure 3.8, consider a planar aperture with coordinates  $(\xi, \eta)$  and the aperture distribution  $f(\xi, \eta)$ ; the radiated electric field  $E$  can then be expressed in the following way:

$$E = \frac{jk}{4\pi r} (1 + \cos\theta) \iint f(\xi, \eta) \exp[-jkq(\xi, \eta)] ds \quad (3.89)$$

where

$$r = r_o + q(\xi, \eta) \quad (3.90)$$

and where it is assumed that changes in the amplitude of the radiated field resulting from differences in  $1/r$  and  $1/r_o$  can be neglected. Starting with

$$R^2 = (x - \xi)^2 + (y - \eta)^2 + z^2 \quad (3.91)$$

then,

$$\begin{aligned} R^2 &= x^2 + y^2 + z^2 - 2(x\xi + y\eta) + \xi^2 + \eta^2 \\ &= r^2 \left[ 1 - 2 \frac{(x\xi + y\eta)}{r^2} + \frac{(\xi^2 + \eta^2)}{r^2} \right] \end{aligned} \quad (3.92)$$

By expanding this, we have:

$$R = r - \frac{x\xi + y\eta}{r} + \frac{\xi^2 + \eta^2}{r} - \dots \quad (3.93)$$

When all terms above the linear ones are ignored, the diffraction integral yields the far or *Fraunhofer fields*. When quadratic terms are maintained with higher-order ones neglected, then *Fresnel fields* occur. For the far fields,

$$q(\xi, \eta) = - \frac{x\xi + y\eta}{r} \quad (3.94)$$

When the quadratic terms are included, we have

$$q(\xi, \eta) = - \frac{x\xi + y\eta}{r} + \frac{\xi^2 + \eta^2}{r} \quad (3.95)$$

Referring to Figure 3.9, it is customary to subdivide the radiating fields into near- and far-regions, corresponding to the quadratic and linear approximations used in representing  $R$ . This avoids the Fraunhofer or Fresnel designations, and prevents possible confusion with the near fields of small antennas with  $1/r^n$  dependence when  $n > 1$ . The far fields traditionally occur when

$$r \geq \frac{2D^2}{\lambda} \quad (3.96)$$

where an arbitrary choice is made based on an assumption of a maximum allowable phase error of  $\lambda/16$  in the approximation of  $R$ .

Equation (3.89) is a statement of Kirchhoff's scalar diffraction theory, in Fresnel-Kirchhoff form, that is applicable for near- and far-field use. Because both field regions are important in many radar applications, special topics are provided in a later section covering antenna regions, and Appendix A contains a compilation

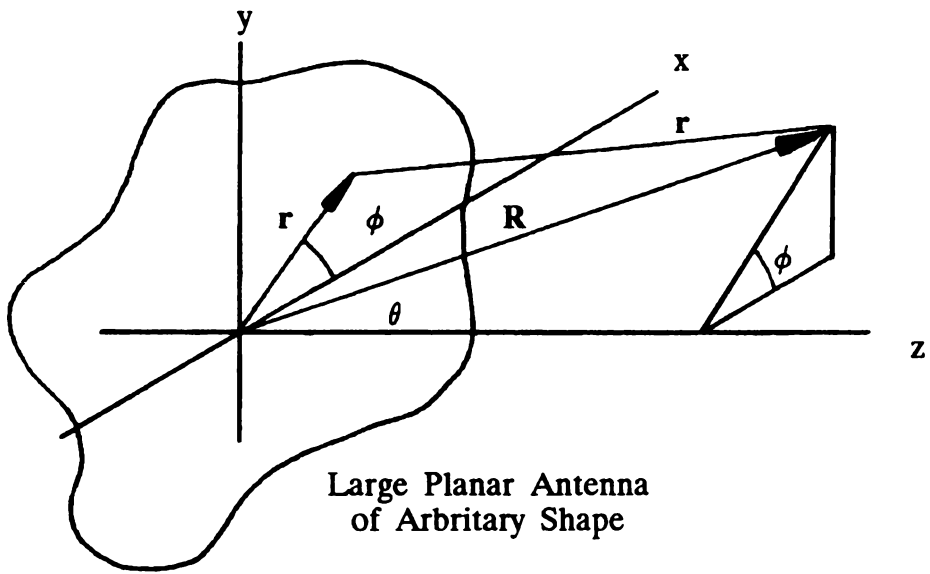


**Figure 3.8** Planar Aperture and Coordinates

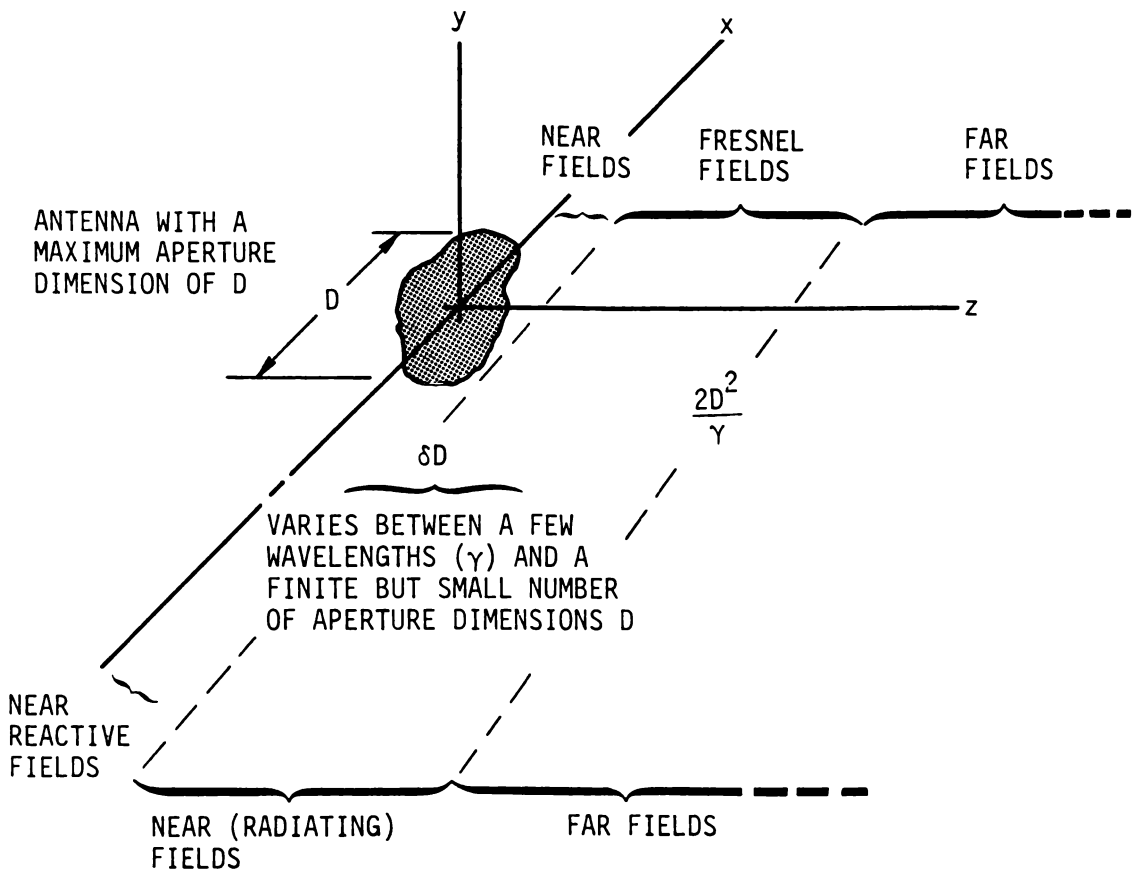


**Figure 3.9** Aperture, Near and Far Field Regions

of diffraction integrals. However, for generality and convenience, Equation (3.89) will be used in the radar equation derivations.

### EXAMPLE: POYNTING'S THEOREM

The energy flow in a radiated field is the product of  $\mathbf{E} \times \mathbf{H}$ , designated as  $\mathbf{S}$ , in the units of  $\text{W}/\text{m}^2$ , and is a statement of Poynting's theorem. The derivation follows directly from Maxwell's equations. From (3.19) and (3.20), we form the equations:

$$\mathbf{E} \cdot \nabla \times \mathbf{H} - \mathbf{E} \cdot \frac{\partial \mathbf{D}}{\partial t} = \mathbf{E} \cdot \mathbf{J}$$

and

$$\mathbf{H} \cdot \nabla \times \mathbf{E} + \mathbf{H} \cdot \frac{\partial \mathbf{B}}{\partial t} = 0$$

If we subtract and note that

$$\nabla \cdot (\mathbf{E} \times \mathbf{H}) = \mathbf{H} \cdot \nabla \times \mathbf{E} - \mathbf{E} \cdot \nabla \times \mathbf{H}$$

then,

$$\nabla \cdot (\mathbf{E} \times \mathbf{H}) + \mathbf{E} \cdot \frac{\partial \mathbf{D}}{\partial t} + \mathbf{H} \cdot \frac{\partial \mathbf{B}}{\partial t} = \mathbf{E} \cdot \mathbf{J}$$

Integrating, we obtain

$$\iint (\mathbf{E} \times \mathbf{H}) \cdot \mathbf{n} \, ds + \iiint \left[ \left( \mathbf{E} \cdot \frac{\partial \mathbf{D}}{\partial t} \right) + \left( \mathbf{H} \cdot \frac{\partial \mathbf{B}}{\partial t} \right) \right] dv = \iiint \mathbf{E} \cdot \mathbf{J} \, dv$$

The first term is the radiated energy, and the second term represents stored energies in the fields close to the sources. When  $\mathbf{E}$  is separated into two components, one being an applied field, the term on the right-hand side of the equation represents losses and the applied energy.

The mean energy flow for time varying fields is

$$\mathbf{S}^* = \frac{1}{2} \mathbf{E} \times \mathbf{H}^*$$

where  $\mathbf{H}^*$  is the conjugate of  $\mathbf{H}$ . These results are of fundamental importance, because they relate radiated power or intensity to field quantities. Radar equation calculations involve power estimates, while antenna and scattering formulations usually evolve from field quantities. The Poynting vectors  $\mathbf{S}$ , and  $\mathbf{S}^*$  relate the differing basic quantities. The ratio of radiated fields (assumed to be planar at a point in space) is equal to an intrinsic impedance of the medium  $\sqrt{\nu/\epsilon}$ , which for free space is  $\sqrt{\mu_0/\epsilon_0} = 377 \Omega$ .

### Reciprocity

Although the reciprocity theorem of antennas may be readily derived directly from Maxwell's equations, its derivation is omitted here because it is included in several references listed in the bibliography. Referring to Figure 3.10 (and following the derivations and explanations of Hu), given that the current sources  $\mathbf{J}$  and  $\mathbf{M}$  are within volumes 1 and 2, and each radiates fields  $\mathbf{E}$  and  $\mathbf{H}$ , the reciprocity theorem states that

$$\iiint (\mathbf{J}_1 \cdot \mathbf{E}_2 - \mathbf{M}_1 \cdot \mathbf{H}_2) dv = \iiint (\mathbf{J}_2 \cdot \mathbf{E}_1 - \mathbf{M}_2 \cdot \mathbf{H}_1) dv \quad (3.97)$$

which can also be expressed as

$$\iiint (\mathbf{J}_1 \cdot \mathbf{E}_2 - \mathbf{M}_1 \cdot \mathbf{H}_2) dv = \iiint (\mathbf{H}_2 \times \mathbf{E}_1 + \mathbf{E}_2 \times \mathbf{H}_1) dv \quad (3.98)$$

These fundamental statements show the fields and sources within (or on) the surface of volumes containing the electric and magnetic sources.

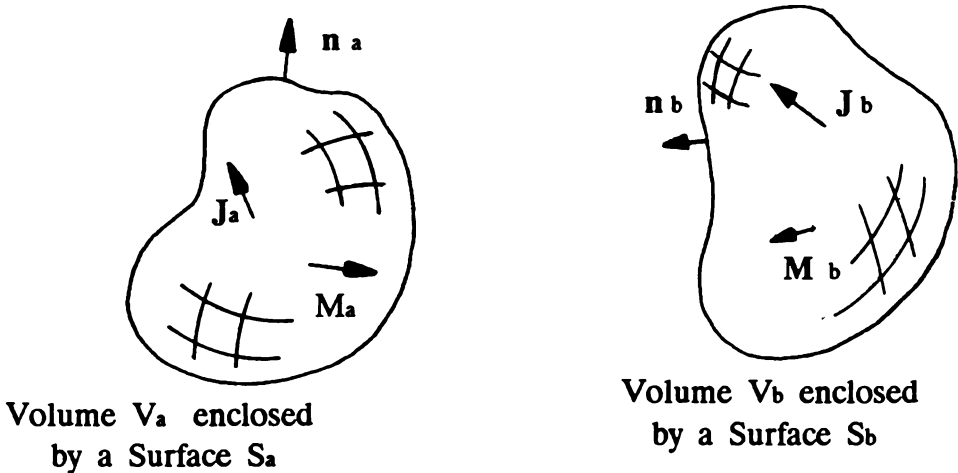


**Figure 3.10** Reciprocity Theorem, Formulation



For radar applications, reciprocity is more usefully expressed in power rather than voltage terms. When accomplished, as we will show, a generalization of the Friis' transmission formula results, from which radar equations evolve. As we continue the summary of Hu's equation derivations, and refer to Figure 3.11, let the terminals of the antenna within  $V_1$  be 1-1 and  $V_2$  be 2-2. The following parameters are defined:

- $S$  = surface surrounding either antenna
- $S_1$  = surface surrounding antenna 1
- $A_1$  = aperture surface of antenna 1
- $S_2$  = surface surrounding antenna 2
- $A_2$  = aperture surface of antenna 2
- $N_1$  = outward, normal, unit vector on  $S_1$
- $N_2$  = outward, normal, unit vector on  $S_2$
- $P_{11}$  = power transmitted by antenna 1
- $P_{12}$  = power received by antenna 2
- $P_{21}$  = power received by antenna 1
- $P_{22}$  = power transmitted by antenna 2
- $\left. \begin{matrix} E_1, H_1 \\ E_2, H_2 \end{matrix} \right\}$  = fields of antennas 1 and 2

The power reciprocity theorem states that the ratio of transmitted to absorbed powers is equal when the transmitting and receiving antennas are interchanged. Thus,

$$\frac{P_{11}}{P_{12}} = \frac{P_{22}}{P_{21}} \quad (3.99)$$

In field form, of general applicability, and analogous to the reciprocity relationships of (3.91) and (3.92), Equation (3.93) can be expressed as follows:

$$\frac{P_{12}}{P_{11}} = \frac{\left| \iint (\mathbf{H}_2 \times \mathbf{E}_1 + \mathbf{E}_2 \times \mathbf{H}_1) \cdot \mathbf{n} \, ds \right|^2}{4 \left[ R_e \int_{s_1} \mathbf{E}_1 \times \mathbf{H}_1^* \cdot \mathbf{n}_1 \, ds \right] \left[ r_e \int_{s_2} \mathbf{E}_2 \times \mathbf{H}_2^* \cdot \mathbf{n}_2 \, ds \right]} \quad (3.100)$$

For large aperture antennas, with the impedance  $Z_0 = \sqrt{\mu_0/\epsilon_0}$ , we have

$$Z_0 \mathbf{H}_1 = \mathbf{n}_1 \times \mathbf{E}_1 \quad (3.101)$$

The quantities within the brackets are the near-field or far-field gains, depending on the choice of  $q(\xi, \eta)$ . The result is a statement of a general form of the Friis' transmission formula. When applied in the far field, the use of a spherical coordinate system is common, whereas, in the near field, the use of a rectangular system of units is convenient. In general, the gain function relates the power radiated in a given direction to the average power radiated per unit (far-field) solid angle. Some definitions are now in order. Antenna gain is defined by

$$\tilde{G} = \left\{ \frac{4\pi}{\lambda^2} \frac{|\iint f(\xi, \eta) \exp[-jkq(\xi, \eta)] ds|^2}{\iint |f(\xi, \eta)|^2 ds} \right\} \quad (3.107)$$

where  $\tilde{G}$  represents a general form of the gain  $G$ . The effective area of any antenna and its gain are related by

$$G = \frac{4\pi}{\lambda^2} A_e \quad (3.108)$$

and

$$Z_0 \mathbf{H}_2 = \mathbf{n}_2 \times \mathbf{E}_2 \quad (3.102)$$

With  $\mathbf{n}_1 = -\mathbf{n}_2$ , Equation (3.94) becomes

$$\frac{P_{12}}{P_{11}} = \frac{\left| \iint [(\mathbf{n}_2 \cdot \mathbf{E}_1) \mathbf{E}_2 - (\mathbf{E}_2 \cdot \mathbf{E}_1) \mathbf{n}_2 + (\mathbf{E}_2 \cdot \mathbf{E}_1) \mathbf{n}_1 - (\mathbf{E}_2 \cdot \mathbf{n}_1) \mathbf{E}_1] \cdot \mathbf{n}_2 ds \right|^2}{4 \left[ \int_{A_1} \int |\mathbf{E}_1|^2 ds \right] \left[ \int_{A_2} \int |\mathbf{E}_2|^2 ds \right]} \quad (3.103)$$

which reduces to the following useful power reciprocity formula for near- and far-field applications

$$\frac{P_{12}}{P_{11}} = \frac{\left| \iint (\mathbf{E}_1 \cdot \mathbf{E}_2) ds \right|^2}{4 \left[ \int_{A_1} \int |\mathbf{E}_1|^2 ds \right] \left[ \int_{A_2} \int |\mathbf{E}_2|^2 ds \right]} \quad (3.104)$$

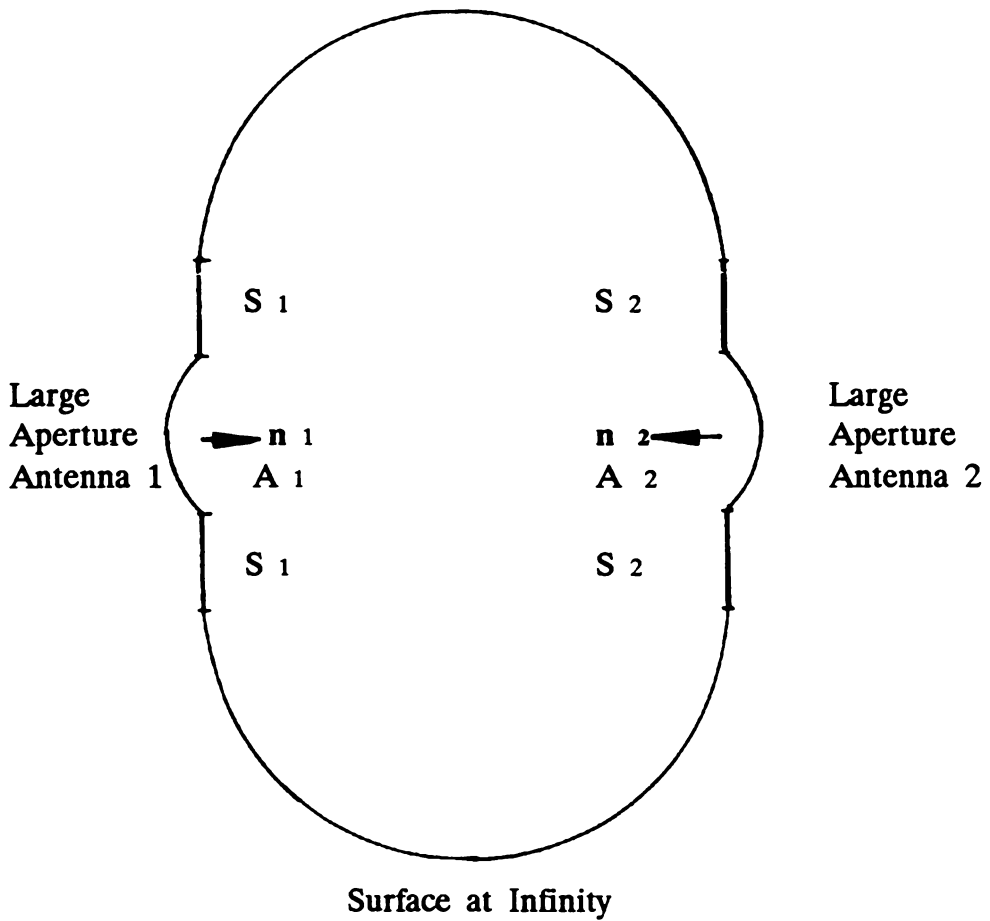


**Figure 3.11** Antenna Placement for Derivation of a General Friis' Transmission Formula

Equation (3.98), like previous formulas, is provided in a general form. When applied in the remainder of this chapter and in subsequent ones, it will be reduced to simpler forms. The equations derived from fundamental electromagnetic field equations constitute the basis for antenna, scattering, and radar equation developments and serve, at least in part, as an introduction to the theory of radar.

### 3.3 DERIVATION OF THE RADAR EQUATION

Several interesting and informative derivations follow. Starting with a power reciprocity theorem applied within Kirchhoff approximations, a generalized Friis' transmission formula is derived. Within defined limits, the results are used for the near and far radiated fields. By itself, the generalized Friis' formula is a radar equation which may be applied for analysis of problems in which one-way paths occur. Following the procedure used for the derivation of the classical radar equation from the transmission formula, we obtain the radar equation. The equation,

in this general form, shows, in an explicit way, the radar antenna in transmitting and receiving modes, with diffraction integral representation.

The discussions provide a derivation of the radar equation from a vector diffraction formulation. A Kirchhoff representation is applied again, but in a scattering way, so that a clear depiction of the radar, viewed from field theory formulations, is provided. The results give a further insight into the definition of the radar cross section and how it is applied in radar theory. When combined and compared to the Friis' formula and the field theorems used in the derivations are taken into account, the results can be interpreted as a Kirchhoff formulation of the radar equation.

### From a General Power Transfer Formulation

To review briefly, we refer to Equations (3.102), (3.103), and (3.104); the function  $q(\xi, \eta)$  within the diffraction formulas specifies the near or far fields. Using (3.104), we let the antennas be linearly polarized and similarly oriented, which gives us

$$\frac{P_{12}}{P_{11}} = \frac{\left| \int_{A_1} \int E_1 \, ds \right|^2 \left| \int_{A_2} \int E_2 \, ds \right|^2}{\left| \int_{A_1} \int |f(\xi, \eta)|^2 ds \right| \left| \int_{A_2} \int |f(\xi, \eta)|^2 ds \right|} \quad (3.105)$$

Substituting for  $E_1$  and  $E_2$ , (from Equation (3.89)), we obtain

$$P_{12} = \frac{P_{11} \lambda^2}{(4\pi r)^2} \left\{ \frac{4\pi}{\lambda^2} \frac{\left| \int_{A_1} \int f_1(\xi, \eta) \exp[jkq_1(\xi, \eta)] \, ds \right|^2}{\int_{A_1} \int |f(\xi, \eta)|^2 ds} \right\} \\ \left\{ \frac{4\pi}{\lambda^2} \frac{\left| \int_{A_2} \int f_2(\xi, \eta) \exp[-jkq_2(\xi, \eta)] \, ds \right|^2}{\iint |f(\xi, \eta)|^2 ds} \right\} \quad (3.106)$$

From Equation (3.107), by definition, the effective area is

$$\tilde{A}_e = \frac{\int_A \int f(\xi, \eta) \exp[-jkq(\xi, \eta)] ds}{\iint |f(\xi, \eta)|^2 ds} \quad (3.109)$$

The *directivity* of an antenna is defined as the maximum value of the gain. Directivity usually appears in the following way, with  $\theta = \phi = \theta$ , and far-field considerations, then,

$$D = \frac{4\pi |\iint f(\xi, \eta) ds|^2}{\lambda^2 \iint |f(\xi, \eta)|^2 ds} \quad (3.110)$$

It is common to refer to directivity simply as the antenna gain with its value usually used in the radar equation. Antennas, dish or array, may be subjected to losses other than those from the feeding networks. In such instances, the gain is degraded, with losses usually being accounted as part of the total system loss.

Several radar equations can now be written directly from the transmission formula. Two applications are prominent, as sketched in Figure 3.12. The transponder (or beacon) equation yields, in Figure 3.12(a), the power density at an aircraft due to the power transmitted by the radar. The transmitting antenna normally is large, the receiving antenna is small, and both antennas are in each other's far field. When interference sources occur, as sketched in Figure 3.12(b), the transmitting antenna is small, the receiving antenna is large, and the antennas are usually in each other's far field.

### General Transmission Formulas

The radar equations are first compiled with the recognizable far-field forms. They are the result of the generalization of the Friis' transmission formula, but are sometimes referred to as a *one-way transmission formula* in contrast to the two-way radar equation. The equation compilation is as follows:

---

#### TRANSMISSION FORMULA EQUATIONS

---

Far-field Transmission Formula—Gain	$P_{12} = \frac{P_{11} \lambda^2 G_1 G_2}{(4\pi r)^2}$	(3.111)
-------------------------------------	--	---------

Far-field Friis' Transmission Formula—Effective Aperture	$P_{12} = \frac{P_{11} A_1 A_2}{\lambda^2 r^2}$	(3.112)
--	---	---------

General Transmission Formula	$P_{12} = \frac{P_{11} \lambda^2 \tilde{G}_1 \tilde{G}_2}{(4\pi r)^2}$	(3.113)
------------------------------	--	---------

Transmission Formula for Near-field and Far-field Gains	$P_{12} = \frac{P_{11} \lambda^2}{(4\pi r)^2} \tilde{G}(\theta, \phi) \tilde{G}(x, y, z)$	(3.114)
---	---	---------

In these general formulations, the diffraction integrals require a numerical solution, because of the complexity of closed-form solutions. Gaussian beam approximations, which relieve this situation somewhat, are described in later chapters.

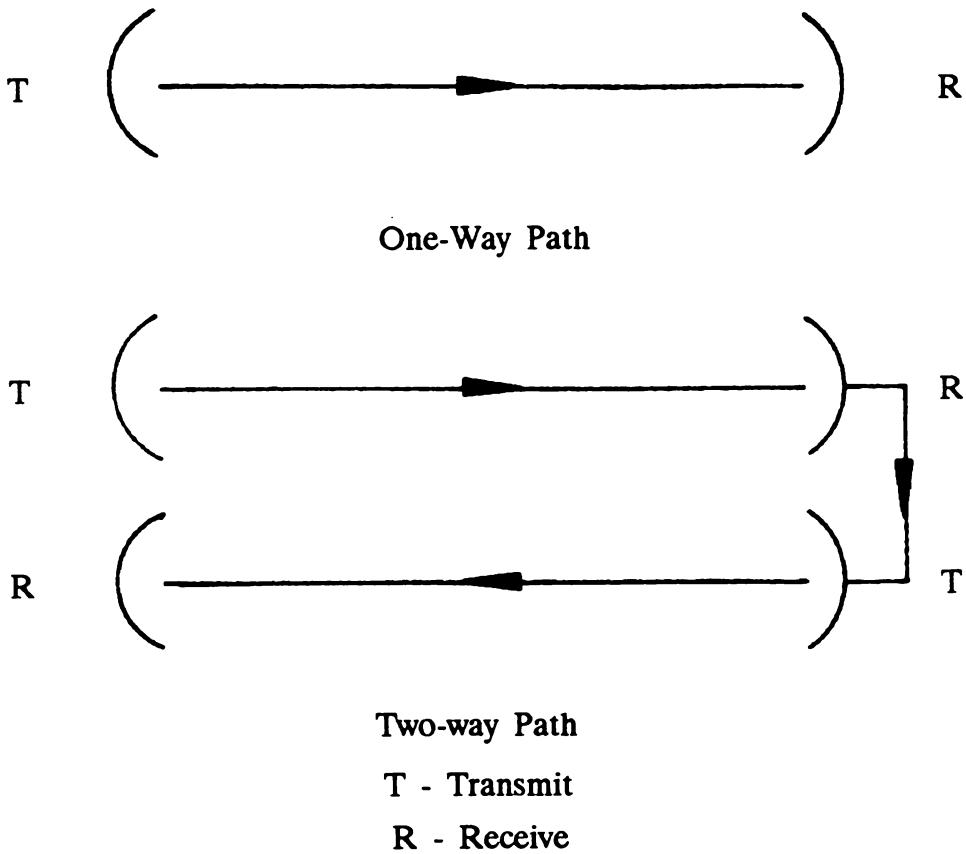


**Figure 3.12** Application of Generalized Friis' Transmission Formula to Radar (From Kraus): (a) One-way Path (b) Two-way Path

This formulation is an approximation, derived from Kirchhoff's theory, for antennas with similar linear polarization, where interaction between the antennas is neglected. When applied, one antenna is usually small and phase errors inferred in the derivations are minimal; thus, the formulas can be used with confidence. If both antennas are large, in close proximity and not facing each other, validation of estimates is advisable by experimentation or numerical integration of the more general formulas.

### *The Radar Equation*

Following the procedures of Chapter 2, applying the one-way formulation of the Friis' transmission formula twice, and using the general form of Equation (3.106) with the radar cross section ( $\sigma A_{e2} G_2$ ) yields

$$S = \frac{P \lambda^2 \sigma}{(4\pi)^3 r^4} \bar{G}^2 \quad (3.115)$$

where  $\tilde{G}$  is given by Equation (3.107), which is a statement of the classical radar equation in field form and an application of a general power reciprocity theorem.

### From Kirchhoff's Diffraction Formula

In this derivation, the radar and scattering problem is formulated in a general way, subjected to Kirchhoff's approximation, and developed using the reciprocity theorems. A further insight into the definition of a radar cross section is provided, with an additional perspective of the theoretical basis of the radar equation given.

Consider the radar and scatterer bounded with surfaces  $S_r$  and  $S_s$ , respectively, with both bounded at infinity by the surface  $S_\infty$ . In the vector theory of diffraction, Equation (3.82) is applicable, with integrations performed over  $S_r$ ,  $S_s$ , and  $S_\infty$ . In the previous transmission formulation, only the radars were considered. The surface at infinity was included, with the radiation condition imposed, and a Kirchhoff solution of the vector diffraction formula was applied. Maintaining this approach, but including the scatterer or target, what remains is an integration over the surface  $S_s$  with the other results applicable.

When applied to scattering theory, Kirchhoff's formulations are usually referred to as a *physical optics approximation* of the general diffraction formula of Equation (3.82). The physical optics solution for a large, perfectly-conducting scatterer requires the application of the boundary conditions of Equations (3.33) through (3.36), and the following assumptions:

$$\mathbf{n} \times \mathbf{H} = 2 \mathbf{n} \times \mathbf{H}_i \quad (3.116)$$

on the illuminated conducting surface, and

$$\mathbf{n} \times \mathbf{H} = 0 \quad (3.117)$$

on the shadow boundary. Imposing these conditions, the magnetic field scattered from a conducting body in the direction of the incident wave is

$$\mathbf{H}_s = \frac{1}{j\lambda r} \left[ \iint \mathbf{n} \times \mathbf{H}_i \exp(-jkr) ds \right] \exp(-jkr) \quad (3.118)$$

where  $\mathbf{H}_s$  and  $\mathbf{H}_i$  are the scattered and incident magnetic fields. The geometry of the radar and scatterer positions is shown in Figure 3.13. From Equation (3.115), the magnitude of the scattered power density at a distance  $r$  from the scatterer is

$$\mathbf{S} = \frac{S_i}{\lambda^2 r^2 H_i^2} \left| \iint \mathbf{n} \times \mathbf{H}_i \exp(-jkr) ds \right|^2 \quad (3.119)$$

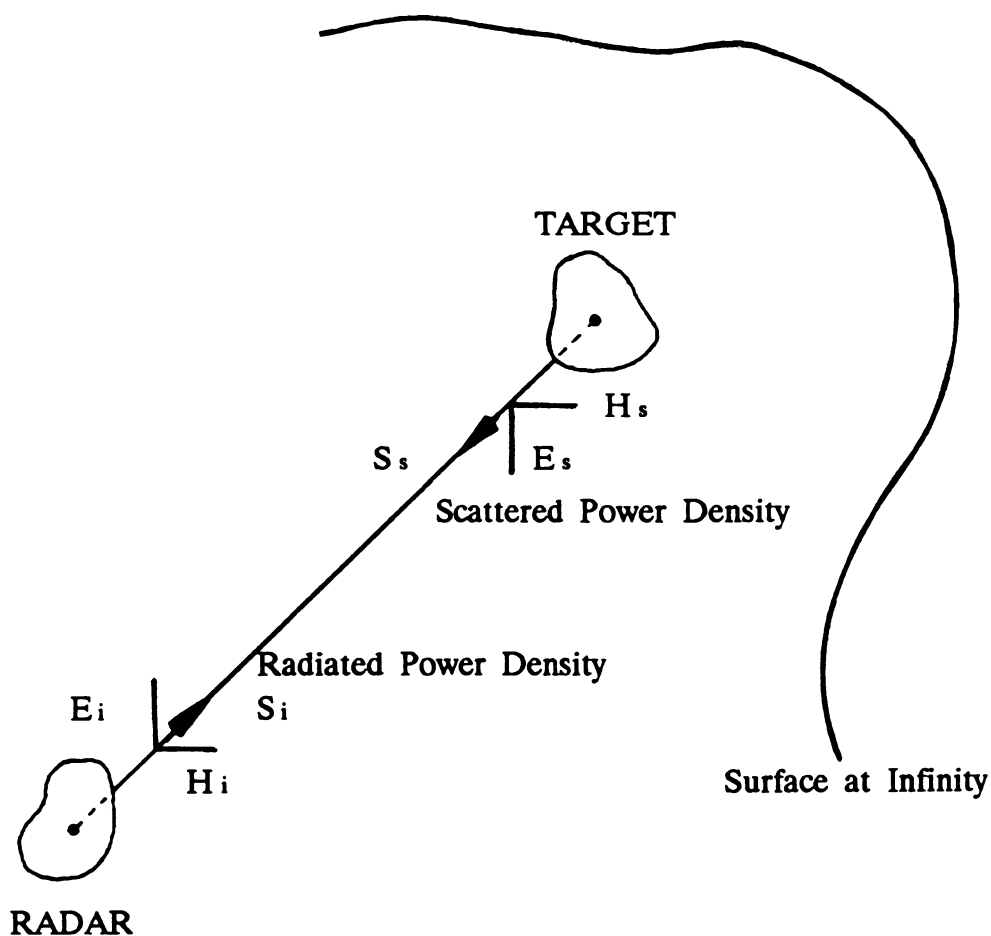


**Figure 3.13** Formulation of the Radar Equation Derivation from Kirchhoff's Diffraction Principles

or

$$\mathbf{S} = \frac{1}{4\pi r^2} \left[ \frac{4\pi}{\lambda^2} \left| \iint \mathbf{n} \times \mathbf{h} \exp(-jkr) ds \right|^2 \right] \quad (3.120)$$

where we have assumed that the incident magnetic field is uniformly distributed over the surface of the scatterer and  $\mathbf{h}$  is a unit vector in the direction of the incident magnetic field. The quantity within the brackets is the radar cross section  $\sigma$  relating the scattered and incident power densities in the following way:

$$S_s = \left( \frac{S_i}{4\pi r^2} \right) \sigma \quad (3.121)$$

then, for large  $r$ , we obtain



$$\sigma = \lim_{r \rightarrow \infty} 4\pi r^2 \left( \frac{S_s}{S_i} \right) \quad (3.122)$$

By definition, the *radar cross section* is proportional to the power scattered into a unit solid angle, divided by the incident power per unit area. Because the power densities are proportioned to the square of the electric or magnetic field,

$$\sigma = \lim_{r \rightarrow \infty} 4\pi r^2 \left| \frac{E_s}{E_i} \right|^2 = \lim_{r \rightarrow \infty} 4\pi r^2 \left| \frac{H_s}{H_i} \right|^2 \quad (3.123)$$

Scattered magnetic fields are usually determined with the cross section definition appearing as a ratio of the magnetic field quantities. The ratio of power densities is more meaningful when radar cross sections are interpreted in a radar equation context where power, not voltage or current quantities, are applied.

Specifying  $\sigma$  as the radar cross section obtained in the Kirchhoff or physical optics sense, then following the procedure in Chapter 2, Equations (2.1) and (2.3) lead to the classical radar equation ((2.4)), which in field form, yields

$$s = \left\{ \frac{P}{4\pi r^2} \right\} \left\{ \tilde{G} \right\} \left\{ \frac{1}{4\pi r^2} \right\} \left\{ \sigma \right\} \left\{ \tilde{A}_e \right\} \quad (3.124)$$

The gain, cross section, and effective area are given by Equations (3.107), (3.108) and (3.109), respectively, with  $\tilde{A}_e$  related to  $\tilde{G}_e$  by (3.108). These equations are derived by an integration over the surfaces  $S_r$  and  $S_s$ , which contain the radar and targets, and limit to zero over the surface  $S_\infty$  at infinity. The result is a direct application of Kirchhoff's diffraction theory. Extensions to different and more general antenna and scattering formulations appear likely.

Equations (3.124), (3.115), and (2.4) are equivalent, with quantities derived in the formal treatments placed in more general terms. Both near- and far-field situations are covered in the formulas. Likewise, the transmission formulation is generally applicable. From a theoretical point of view, the radar equation has been presented as an application of field theorems derived from Maxwell's equations.

### 3.4 PLANE WAVES

We now introduce the first of three topics covering plane waves, antennas, and scattering. The theoretical formulations are applied to the propagating medium of the radar. We have shown that radiated fields at large distances from the radar exhibit a  $1/r$  dependence, in the form of spherical waves. At these large distances, the propagation of the signals is near planar and can be represented as such. Thus,

atmospheric effects on radar are, in many cases, determined from plane-wave representations. An introduction to this subject is provided here. Our discussions will include a general derivation of a wave equation, and properties of plane waves will be described. Attention is given to lossy environments and plane waves incident on dielectric and conducting media.

## Derivations

The general derivation of Maxwell's equations in differential form, Equations (3.19) to (3.22), is applied in a source-free region. Then, the divergence equations are zero. Recall that  $\mathbf{B} = \mu\mathbf{H}$ ,  $\mathbf{D} = \epsilon\mathbf{E}$ , and  $\mathbf{J} = \sigma\mathbf{E}$ , all quantities already defined and summarized in Table 3.1.

Taking the curl of Equations (3.19) and (3.20), substituting (3.20) into the curl of (3.19), and *vice versa*, results in

$$\nabla \times \nabla \times \mathbf{E} = -\sigma\mu \frac{\partial \mathbf{E}}{\partial t} - \epsilon\mu \frac{\partial^2 \mathbf{E}}{\partial t^2} \quad (3.125)$$

and

$$\nabla \times \nabla \times \mathbf{H} = -\sigma\mu \frac{\partial \mathbf{H}}{\partial t} - \epsilon\mu \frac{\partial^2 \mathbf{H}}{\partial t^2} \quad (3.126)$$

For an arbitrary vector  $\mathbf{A}$ , we have

$$\nabla \times \nabla \times \mathbf{A} = \nabla(\nabla \cdot \mathbf{A}) - \nabla^2 \mathbf{A} \quad (3.127)$$

Now, with  $\nabla \cdot \mathbf{E} = \nabla \cdot \mathbf{H} = 0$ , the following equations are obtained:

$$\nabla^2 \mathbf{E} = \sigma\mu \frac{\partial \mathbf{E}}{\partial t} + \epsilon\mu \frac{\partial^2 \mathbf{E}}{\partial t^2} \quad (3.128)$$

and

$$\nabla^2 \mathbf{H} = \sigma\mu \frac{\partial \mathbf{H}}{\partial t} + \epsilon\mu \frac{\partial^2 \mathbf{H}}{\partial t^2} \quad (3.129)$$

which are vector wave equations. Each component of the electric and magnetic field satisfies a scalar wave equation. Plane wave solutions are of particular interest. Without loss in generality, and for convenience in introducing the basic concepts,

we will consider a single component of the electric fields  $\mathbf{E} = \mathbf{i}E_x$  with an assumed propagation in the  $z$  direction. Let the field be independent of the  $x$  and  $y$  coordinates and dependent on  $z$ . Ignoring the magnetic field components and power flow designations momentarily, Figure 3.14 shows the coordinate system and field position. As postulated, the field component is positioned in a specific direction and is linearly polarized. If the  $(x, z)$  plane is the ground reference, this choice of direction represents a horizontally polarized wave. If  $E_y$  was chosen, then a vertically polarized wave occurs.

Expanding the curl equation (3.19) in rectangular coordinates, we have

$$\mathbf{i} \left( \frac{\partial E_z}{\partial y} - \frac{\partial E_y}{\partial z} \right) + \mathbf{j} \left( \frac{\partial E_x}{\partial z} - \frac{\partial E_z}{\partial x} \right) + \mathbf{k} \left( \frac{\partial E_y}{\partial x} - \frac{\partial E_x}{\partial y} \right) - \mu \frac{\partial}{\partial t} (\mathbf{i}H_x + \mathbf{j}H_y + \mathbf{k}H_z) \quad (3.130)$$

For an assumed  $\mathbf{i}E_x$  field component, subject to the conditions stated above,

$$\mathbf{j} \frac{\partial E_x}{\partial t} = -\mathbf{j}\mu \frac{\partial H_y}{\partial t} \quad (3.131)$$

Because power flow is the cross product  $\mathbf{E} \times \mathbf{H}$  and  $E_x$  and  $H_y$  components of the field are present, then wave propagation is in the positive  $z$  direction as indicated in Figure 3.14. The wave equations now become

$$\frac{\partial^2 E_x}{\partial z^2} = \sigma\epsilon \frac{\partial E_x}{\partial t} - \frac{\partial^2 E_x}{\partial t^2} \quad (3.132)$$

and

$$\frac{\partial^2 H_y}{\partial z^2} = \sigma\epsilon \frac{\partial H_y}{\partial t} + \frac{\partial^2 H_y}{\partial t^2} \quad (3.133)$$

Assuming time variations of the form  $\exp(j\omega t)$ , let the solution to the scalar wave equations be of the form:

$$E_x = E_0 \exp(j\omega t - \gamma z) \quad (3.134)$$

where  $\gamma$  is a complex constant given by

$$\gamma = \pm j\omega \sqrt{\epsilon + \frac{j\sigma}{\omega}} \quad (3.135)$$

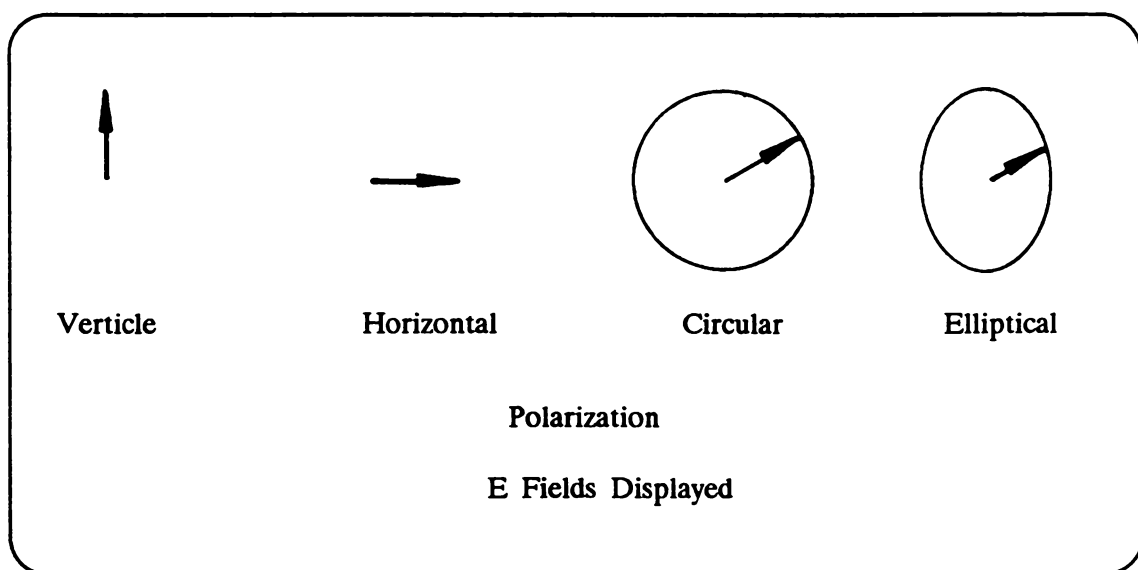
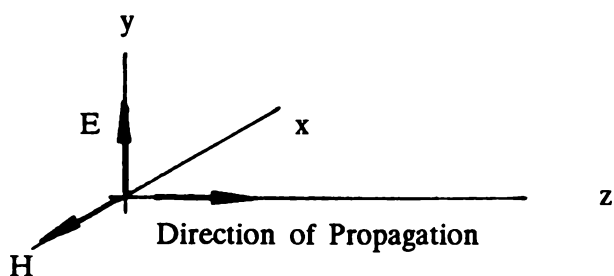


**Figure 3.14** Field Quantities in a Plane Wave

and is usually expressed as the sum of real and imaginary parts:

$$\gamma = \alpha + j\beta \quad (3.136)$$

The parameters are defined as follows:

$\gamma$  = propagation constant

$\alpha$  = attenuation constant

$\beta$  = phase constant

Phase constant designations of  $\beta$  and  $k$  are used interchangeably in antenna and propagation work. Common notation also includes the following:

$\epsilon_c$  = complex permittivity

$$= \epsilon - j\sigma/\omega$$

$$= \epsilon' - j\epsilon'' \quad (3.137)$$

$$\epsilon' = \text{Re}\epsilon_c = \epsilon \quad (3.138)$$

$$\epsilon'' = \text{Im}\epsilon_c = \sigma/\omega \quad (3.139)$$

with  $\gamma$ ,  $\alpha$ , and  $\beta$  expressed in terms of  $\epsilon'$  and  $\epsilon''$ . The general solution of the wave equation now becomes

$$E_x = E_0 \exp(\mp \gamma z) \exp[j(\omega t \mp \beta z)] \quad (3.140)$$

Special cases are discussed next, with compilations of some useful formulas for the physical constants included.

### Free Space and Perfect Dielectrics

For free space conditions,  $\sigma = 0$ ,  $\mu = \mu_0$ , and  $\epsilon = \epsilon_0$ . For perfect dielectrics, losses are negligible and  $\epsilon = \epsilon_r \epsilon_0$ . The wave Equations ((3.128) and (3.129)) now become

$$\frac{\partial^2 E_x}{\partial t^2} = \epsilon \mu \frac{\partial^2 E_x}{\partial t^2} \quad (3.141)$$

and

$$\frac{\partial^2 H_y}{\partial t^2} = \epsilon \mu \frac{\partial^2 H_y}{\partial t^2} \quad (3.142)$$

In addition,

$$-j \frac{\partial H_y}{\partial z} = j \epsilon \frac{\partial E_x}{\partial t} \quad (3.143)$$

The solution for the electric field for wave propagation in the positive  $z$  direction is

$$E_x = E_0 \exp[j(\omega t - \beta z)] \quad (3.144)$$

For the magnetic field component, the solution is

$$H_y = H_0 \exp[j(\omega t - \beta z)] \quad (3.145)$$

Substituting (3.143) into (3.140), we show that,

$$\beta = \omega \sqrt{\mu\epsilon} = \frac{\omega}{v} = \frac{2\pi}{\lambda} \quad (3.146)$$

where some definitions are as follows:

$$v = \text{velocity of the propagation wave} = 1/\sqrt{\mu\epsilon} \quad (3.147)$$

$$v = 1/\sqrt{\mu_0\epsilon_0} = c = \text{the velocity of light} \quad (3.148)$$

$$\lambda = \text{wavelength} = 1/f\sqrt{\mu\epsilon} = c/f\sqrt{\epsilon_r} \quad (3.149)$$

$$\lambda = c/f = \text{free-space wavelength} \quad (3.150)$$

$$\eta = \text{index of refraction} = \sqrt{\epsilon_r} = 1.0 = \text{free space} \quad (3.151)$$

Forming the ratio of the electric and magnetic fields yields an additional definition:

$$\eta = \sqrt{\frac{\mu}{\epsilon}} \quad (3.152)$$

which is the intrinsic impedance of the medium. In free space  $\eta = \eta_0 \approx 120\pi \approx 377$  ohms. In Equations (3.160) and (3.161),  $H_0 = E_0/\eta$ .

By setting the argument of Equation (3.144) or (3.145) equal to a constant, we obtain:

$$z - vt = \text{constant} \quad (3.153)$$

then differentiating, we have

$$v = \frac{dz}{dt} \quad (3.154)$$

Here,  $v$  is the phase velocity of the propagating wave. With propagation directed in the positive  $z$  direction, with transverse field components  $E_x$  and  $H_y$ , a *transverse electromagnetic wave* (TEM) is said to occur.

### EXAMPLE: SINUSOIDAL FIELD VARIATIONS

As we consider the real part of the electric field component of Equation (3.142),

for a positive propagating wave, we observe

$$E_x = E_0 \cos[\omega(t - \beta z/\omega)] \quad (3.155)$$

and

$$H_y = \frac{H_0}{\eta} \cos[\omega(t - \beta z/\omega)] \quad (3.156)$$

The fields, plotted in Figure 3.15 are characterized by a sinusoidal variation in the  $z$  and  $y$  directions (as a function of  $z$ ), as shown. At each point along  $z$ , the fields will oscillate at a frequency  $f$ , taking on positive and negative values. The power density propagating in the  $z$  direction is

$$\mathbf{S} = \mathbf{E} \times \mathbf{H} = \frac{E_0^2}{\eta} = \eta H_0^2 \quad (3.157)$$

Wave equation solutions are of the general form:

$$f\left(t \pm \frac{z}{v}\right) \quad (3.158)$$

Then a pulse of arbitrary shape, length, and spectral composition will propagate. This situation is depicted in Figure 3.15 for a Gaussian-shaped pulse. Pulse positions along the  $z$  axis (or distances separating pulses reflected at varying points along  $z$ ), are found by using the free-space distance traveled in a time  $t$  of  $z = ct$ . Examples of this are also contained in Figure 3.15.

The first example qualitatively explains CW radar signal propagation; the second example depicts pulsed transmissions.

In the discussions thus far, linearly polarized waves have been considered. If two field vectors,  $\mathbf{i}E_x$  and  $\mathbf{j}E_y$ , are combined with a controlled phase difference, the wave is elliptically polarized. Therefore, we let

$$E_x = E_0 \cos\omega\left(t - \frac{z}{v}\right) \quad (3.159)$$

and

$$E_y = E_0 \cos\left[\omega\left(t - \frac{z}{v}\right) + \delta\right] \quad (3.160)$$

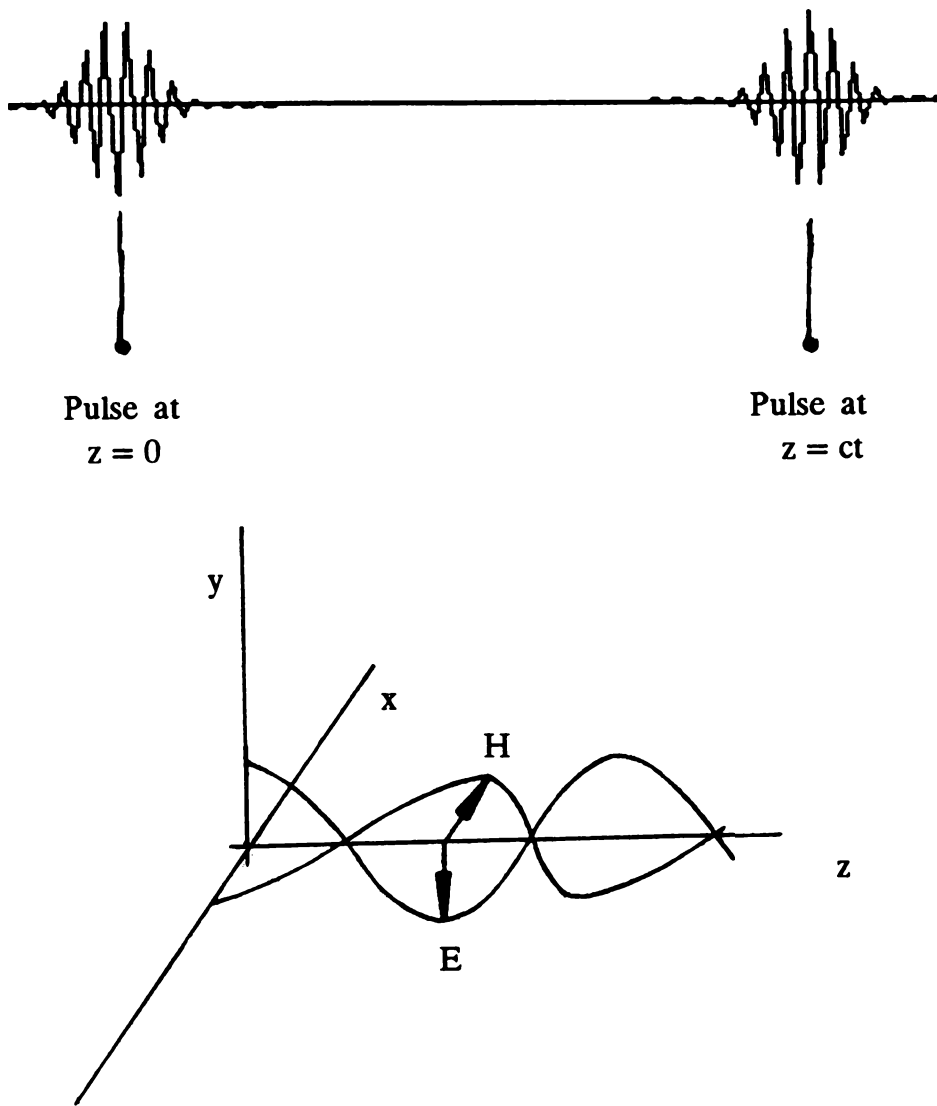


**Figure 3.15** Traveling Wave with Sinusoidal Field Distribution

If  $z = 0$ , then the values represented are the field component variations in any plane normal to  $z$ . Thus,

$$E_x = E_0 \cos \omega t \quad (3.161)$$

and

$$E_y = E_0 \cos(\omega t + \delta) \quad (3.162)$$



which are parametric equations of an ellipse. When  $\delta = \pm \pi/2$ , the wave is circularly polarized. When  $\delta = -\pi/2$ , the wave is right-hand circularly polarized, and when  $\delta = +\pi/2$ , a left-hand circularly polarized wave occurs. This convention has been adopted by viewing the rotating field vector with angular velocity  $\omega$ , in the direction of propagation.

### Lossy Dielectrics and Conductors

This material, assembled from Skitek and Marshall, covers special cases of the general formulation and is considered subject to the following definitions and conventions:

$$\text{Free Space:} \quad \sigma = 0, \quad \mu = \mu_0, \quad \epsilon = \epsilon_0 \quad (3.163)$$

$$\text{Lossless Dielectric:} \quad \sigma = 0, \quad \mu = \mu_0 \quad (3.164)$$

$$\text{Lossy Dielectric:} \quad \epsilon_0 = \epsilon' - j\sigma/\omega \quad (3.165)$$

$$\text{Slightly Lossy Dielectric:} \quad \sigma/\omega\epsilon \ll 1 \quad (3.166)$$

$$\text{Good Conductor:} \quad \sigma/\omega\epsilon \gg 1 \quad (3.167)$$

Formulas for the propagation constant  $\gamma$ , phase velocity  $v$ , and intrinsic impedance  $\eta$  are compiled for all the conditions listed above. The results can be obtained from the derivations and definition of the previous sections, subjected to these conditions. The formulas are as follows:

#### *FREE SPACE*

$$\gamma = j\omega\sqrt{\mu_0\epsilon_0}, \quad v = \frac{1}{\sqrt{\mu_0\epsilon_0}} = c, \quad \eta = \sqrt{\frac{\mu_0}{\epsilon_0}} \quad (3.168)$$

#### *LOSSLESS DIELECTRIC*

$$\gamma = j\omega\sqrt{\mu\epsilon}, \quad v = \frac{1}{\sqrt{\mu\epsilon}}, \quad \eta = \sqrt{\frac{\mu}{\epsilon}} \quad (3.169)$$

#### *LOSSY DIELECTRIC*

$$\gamma = j\omega\sqrt{\mu\epsilon} \sqrt{1 - j\frac{\sigma}{\omega\epsilon}}, \quad v = \frac{\omega}{\beta}, \quad \eta = \frac{\sqrt{\frac{\mu}{\epsilon}}}{\sqrt{1 - j\frac{\sigma}{\omega\epsilon}}} \quad (3.170)$$

### SLIGHTLY LOSSY DIELECTRIC

$$\gamma = j\omega\sqrt{\mu\epsilon} \left(1 - j\frac{\sigma}{2\omega\epsilon}\right), \quad v = \frac{\omega}{\beta}, \quad \eta \approx \sqrt{\frac{\mu}{\epsilon}} \left(1 + j\frac{\sigma}{2\omega\epsilon}\right) \quad (3.171)$$

### GOOD CONDUCTOR

$$\gamma \approx \sqrt{\pi f \mu \sigma} (1 - j), \quad v = \frac{\omega}{\beta}, \quad \eta \approx \sqrt{\frac{\omega \mu}{\sigma}} \quad (3.172)$$

The velocities, when expressed as the ratio  $\omega/\beta$ , are obtained from the propagation constants, because  $\gamma = \alpha + j\beta$ . Propagation in lossy media will be subject to a loss of  $\exp(-\gamma z)$  (defined in Equation (3.135)), with the attenuation constant deduced from the tabulated propagation constants. When good conductors are encountered, it is common practice to refer to the depth a plane wave propagates into the media, reaching a level  $e^{-1}$  of its original value, as the *skin depth*.

### Incidence on Dielectrics

Perfect or *lossless dielectrics* are now considered, with the case of normal incidence covered first. Reflections occur at boundaries because of the boundary conditions. In this instance, the boundary conditions of Equations (3.29) through (3.32) apply where all field components are continuous across the boundary.

Referring to Figure 3.16, we will let the electric component of the incident wave in Region 1 be  $E_0 e^{-jkz}$ , then define the reflected field as  $\rho E_0 e^{jkz}$  where  $\rho$  is a reflection coefficient. Now, we will define the comparable field component in Region 2 as  $\tau E_0 e^{-jkz}$ , where  $\tau$  is a transmission coefficient. At the boundary, where  $z = 0$ :

$$E_0 + \rho E_0 = \tau E_0 \quad (3.173)$$

$$H_0 - \rho H_0 = \tau H_0 \quad (3.174)$$

$$\frac{E_0}{\eta_1} - \frac{\rho E_0}{\eta_1} = \frac{\tau E_0}{\eta_1} \quad (3.175)$$

Taking the ratio of Equation (3.174) to (3.175) yields

$$\left( \frac{1 + \rho}{1 - \rho} \right) \eta_1 = \eta_2 \quad (3.176)$$

or

$$\rho = \frac{\eta_2 - \eta_1}{\eta_2 + \eta_1} \quad (3.177)$$

The transmission coefficient is

$$\tau = \frac{2\eta_2}{\eta_2 + \eta_1} \quad (3.178)$$

The composition of both the transmitted and reflected waves is shown in Figure 3.16.

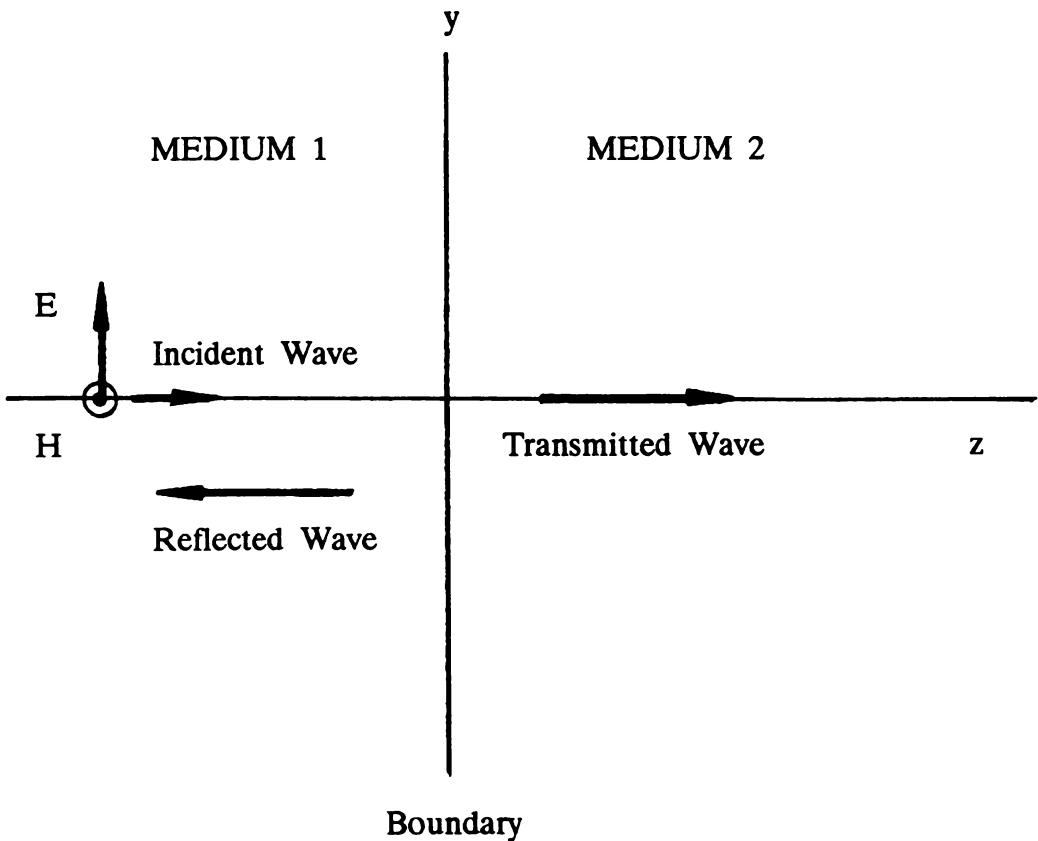


**Figure 3.16** Plane Wave Incident on Dielectric Boundary

At oblique angles of incidence, polarization of the incident wave must be considered. Standard procedure is to determine wave impedances from the field components, as demonstrated, with propagation referenced to the normal of the boundary. Because oblique incidence is involved, a coordinate transformation is inferred. Details of these derivations for further study can be found in several of the references contained in the bibliography. However, we mention three important physical properties of plane wave propagation at a dielectric interface. Referring to Figure 3.17, we see

$$\theta'_i = \theta_i \quad (3.179)$$

or the angle of reflection,  $\theta'_i$ , is equal to the angle of incidence,  $\theta_i$ . Within the second medium, with  $\eta_2 < \eta_1$ , the wave is refracted toward the normal. The angle of incidence and the angle of refraction are related by

$$\theta_i = \frac{\sin \theta_i}{\sin \theta_r} \quad (3.180)$$

which is *Snell's law of refraction*. For a parallel polarized incident wave, the reflection coefficient vanishes at an angle  $\theta_b$ , related to the dielectric constant by

$$\sin \theta_b = \sqrt{\frac{\epsilon_2}{\epsilon_1 + \epsilon_2}} \quad (3.181)$$

This is a definition of the *Brewster angle*. When all the conditions are met, all energy is propagated into the second medium.

These three properties pertain to plane-wave propagation at oblique angles of incidence at a boundary, and are useful in many radar applications. Plane waves are reflected and refracted at a boundary where infinite interfaces are implied. In many instances, propagation through curved layers of differing materials are assumed to be infinite in extent, at a point where plane-wave conditions are applied. Radome models that yield acceptable performance predictions have been structured in this manner.

### **Incidence on Perfect Conductors**

At the conducting boundary sketched in Figure 3.18, the boundary conditions of Equations (3.33) through (3.36) state, in the absence of a surface-charge density, that the normal components of the electric and magnetic fields are zero. The tangential component of the electric field is zero, and the tangential component of the magnetic field is equal to the surface-current density. The electric field components are

$$E_x = E_0 [\exp(-j\beta z) - \exp(j\beta z)] = -2jE_0 \sin\beta z \quad (3.182)$$

with a corresponding magnetic field

$$H_y = \frac{2E_0}{\eta} \cos\beta z \quad (3.183)$$

Equations (3.182) and (3.183) describe a standing-wave pattern. The tangential component of the electric field is always zero at the boundary, with the magnetic field at a maximum. Because of the presence of  $j$  in Equation (3.182), the electric and magnetic fields are  $90^\circ$  out of phase.

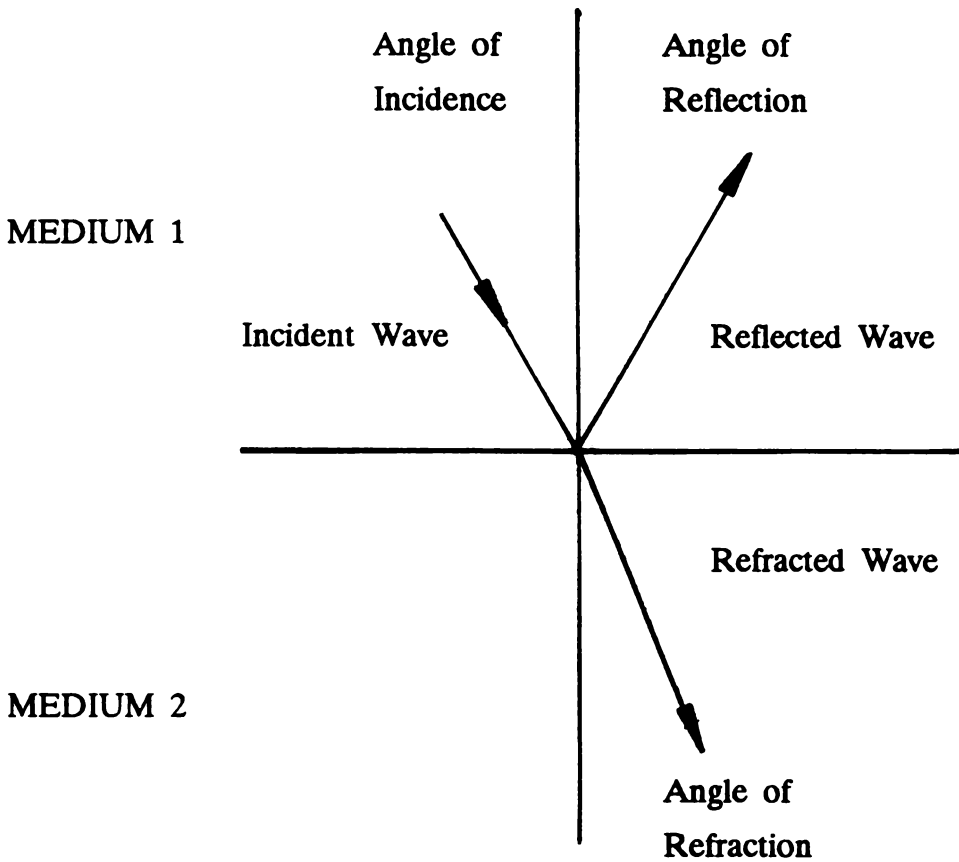


**Figure 3.17** Angle of Incidence and Reflected Wave

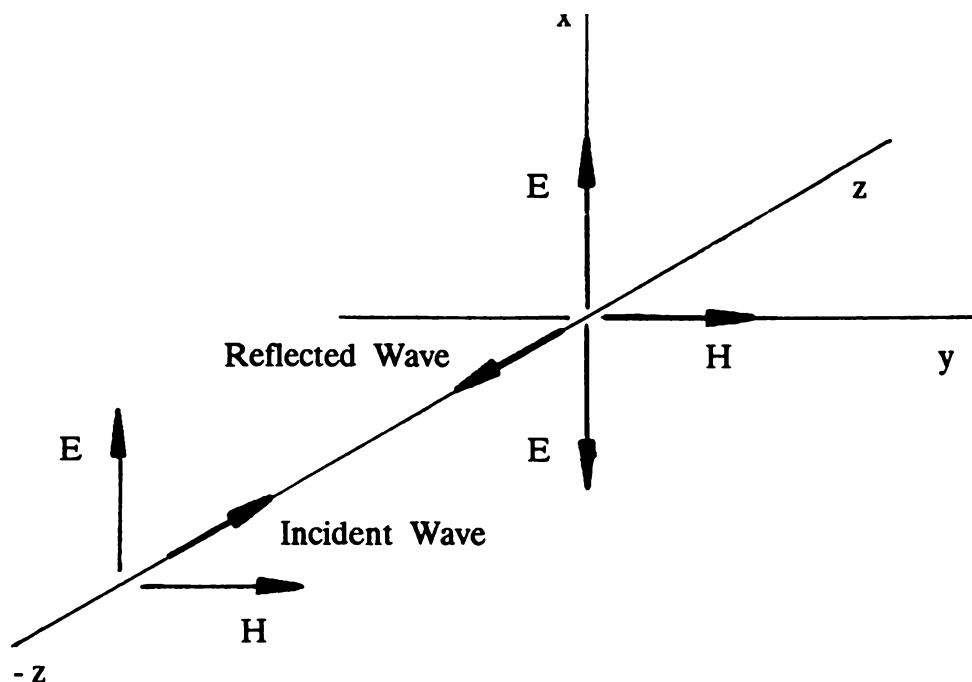


Figure 3.18 Plane Wave Incident on a Conducting Boundary

### Remarks

The plane wave topics covered here constitute introductory material. The reader is encouraged to do further theoretical work for general radar propagation applications, and also to become familiar with RF transmission systems and lines. The important concepts of propagation constant, phase velocity, reflection and transmission coefficients, and standing waves resulting from a wave equation occur, and thus form the basis of the theory. The collection of formulas and accompanying discussions should be of value in each of these technological areas.

We have described reflection and transmission at boundaries that are physically large. When objects are of finite extent, a propagating electromagnetic wave illuminates the surface, and energy is generally scattered in all directions. A measure of this scattered energy is the radar cross section. For plane-wave propagation, the reflection and transmission coefficients are comparable.

### 3.5 RADAR ANTENNAS

Radar antennas, for the most part, are characterized by large radiating apertures. Earlier radars employed reflector or dish antennas with specially-designed single or multiple horn-type feeds. Modern radars are likely to use array antennas, with a variety of radiating elements, feeding structures or networks, and transmitter or power distribution systems. We provide introduction to radar antennas, emphasizing principles and methods of analysis. Topics covered include a review of theoretical formulations, descriptions of antenna parameters, radiation from current elements, transform methods of analysis (including Gaussian formulations), and an introduction to the theory of arrays.

#### Interpretations and Formulations

In our derivation of the radar equation from Maxwell's equations, radiation and diffraction principles were approached from an analysis of current elements, with radiated fields conveniently obtained using vector potentials, the application of field equivalence theorems that relate current sources (within bounded volumes) to field quantities on the surfaces enclosing the sources, and the derivation of a general vector theory of diffraction. Although somewhat complex, the theory has definite and apparent physical interpretations. As we pursue this point and interpret the theoretical observations first, we see that in the infinitesimal current element, radiated fields result from time-varying current elements, and are justified within Maxwell's field equations, by the presence of the displacement currents. Radiated fields are inversely proportional to the distance from the antenna, with power densities proportional to the square of the distance. Spherical waves are excited, propagate at the speed of light in free space, and are composed of an electric and magnetic field at right angles to each other. The radiated fields of an antenna can conceptually be found by an integration of the current sources over the surface or volume of the antenna. The radiated fields can also be found by an integration of the electromagnetic fields on the surface enclosing the antenna. Theoretically, the solutions are exact, but the derivations show (from strictly a theoretical point of view), that the solution of the integrations of the fields in the Stratton-Chu formulation is difficult; they also imply that the determination of the currents in the Schelkunoff vector potential formulation is difficult. Solutions are readily obtained when approximations are imposed, such as the Kirchhoff boundary conditions, that neglect the effects of currents or diffracted fields at the edges of the antenna.

The radiated fields of an antenna or an antenna pattern are composed of a principal or main lobe, and a sidelobe structure. The sidelobes are usually highest adjacent to the main lobe, and diminish at outer positions. Ideally then, the antenna pattern consists of a principal lobe, and secondary lobes with clearly-defined nulls

or positions of zero intensity. A direct application of Kirchhoff's theory yields these idealized results. Because radar beams are directive, with narrow beamwidths and low sidelobes (implying large apertures), the approximation is very good for predicting basic antenna pattern parameters of beamwidth, gain, and at least the first few sidelobes. Compilations of antenna pattern properties used for radar analysis are usually based on these assumptions. In practice, however, idealized patterns are not realized for two main reasons. It is always desirable to achieve the highest resolution (or narrowest beamwidth), with the smallest possible aperture. As a result, aperture distributions yield finite (but small) currents or fields at the edges of an aperture. The resultant radiated fields, not accounted for in the Kirchhoff theory, emanate from the edges, disrupt the sidelobe structure of the antenna, and, for most antenna designs, appear in the outer sidelobes and backlobes, raising and disrupting the field intensities and distributions. Circumvention of these effects involves increasing the size of the aperture, in an attempt to reduce the current distributions at the edges, or changing the structure of the other edge in material and shape in a way that reduces edge effects on the antenna patterns. From a system viewpoint, excessive sidelobes and back lobes increase the system noise temperature by accepting increased external noise, and increase the reception of interference noise sources.

A second disruption of the idealized antenna patterns results from phase errors that arise in the fabrication process of the antenna and feeding structure. Random phase errors within the aperture plane resulting from, for example, the surface imperfections in a parabolic dish antenna, give rise to radiated fields that are the sum of coherent and noncoherent parts. The coherent part, the perturbed idealized pattern assuming small errors, is recognized by the decrease in antenna gain and the increase in relative sidelobe level. The noncoherent radiated fields appear as a filling of the nulls of the antenna pattern.

Real-world antenna patterns, when interpreted on a physical basis, consist of a principal lobe and near-in sidelobe structure, resulting from the aperture distribution or illuminations, a description of the sidelobe structure due to edge effects, and the filling in of the walls, resulting from fabrication imperfections. The extent of these observables is a measure of the quality of the antenna design. From a design point of view, edge effects apply to the choice of aperture illumination and the design of the ground plane, and for phase error consideration, apply to the electrical and mechanical design of the antenna. These two considerations are of paramount importance in the design of a radar antenna. From an analysis point of view, all models of antennas should have phase error algorithms, to at least yield a more real-world appearance of computed antenna patterns with nonzero wall depths. Finally, from a system point of view, edge effects and phase errors have physical limits that influence the performance of the radar whenever sidelobe levels are important. These limits should be known for system-level assessments,



to provide a quantitative description of the ultimate performance than can be expected from a given radar design.

Antenna analysis follows (to a large extent) from Kirchhoff's theory in several forms. The diffraction integrals can be solved for the near and far fields in closed form. Many simple solutions, suitable for system analysis and design purposes, occur. When solutions are inconvenient, especially when near fields are encountered, the diffraction integrals may be solved numerically. Direct numerical solutions of the diffraction integrals may be useful to validate other approximate methods of analysis. The diffraction integrals and resulting antenna patterns can be represented as a Fourier transform of the aperture distribution. Then, Fourier transform theory development, using rigorous mathematical principles with an abundance of applications in many technical disciplines (including circuit theory), is applicable to the antenna problem. Numerically, the development of fast Fourier transforms in recent years enhances the use of numerical methods of antenna pattern computations and is a welcome addition to available antenna analysis resources.

Recent theoretical extensions to Kirchhoff's theory have been developed. One procedure, the *plane-wave spectrum field representation*, is based on a plane-wave supposition of the aperture field. Near-and far-field distributions are obtained from the transform of the plane-wave spectrum, which is calculated from the aperture fields. Transform methods are applied, with fast Fourier transform numerical methods particularly advantageous to the computations. The spectral field method of analysis has proven to be useful in relating far-field patterns to near-field measurements.

Another recent extension to Kirchhoff's theory has been the use of Gaussian functions in the form of Hermite-Gaussian and Laguerre-Gaussian field expansions. In this approach, the Gaussian beam approximation is extended to include near-and far-field descriptions in a structured way, where the number of sidelobes in a radiated field corresponds to the number of terms in the series. The theory is useful in representing near and far fields with simple mathematical expressions, suitable for antenna and radar analysis purposes, and particularly useful when near fields are of interest.

The edge effects of antennas and many scattering objects have been determined using the geometrical theory of diffraction. In this theory, the bending of ray paths in the vicinity of a discontinuity placed in the presence of a magnetic field is computed, using an asymptotic (i.e., high frequency), short-wavelength form of the general Stratton-Chu diffraction formula. In this approach, the physical interpretation of diffraction phenomena is one of a ray path giving rise to diffracted rays about the point of discontinuity. Total fields, in this optical sense, arise from incident, reflected, and perhaps refracted and diffracted rays, which may be described using an asymptotic form of the general diffraction formula. The radiated fields of several special antenna configurations have been successfully described using this theory.

Final remarks on antenna principles, with this concentration on theory, belong to experiments and measurements. It is rare to implement an antenna into a radar system without extensive measurements. Actually, it is not uncommon for antenna designs to be, or perhaps thought to be, a result of excessive experimentation without a full advantageous use of the theoretical procedures and numerical methods that are available. From a theoretical point of view, an appropriate mixture of theory and experiment is needed in any antenna design. From the experimental point of view, the edge effects, phase errors, and overall measurement quality of patterns require careful consideration in instrumentation, measurement techniques and physical interpretation of results. All are important parts of the development of a radar antenna.

Properties of an Antenna Pattern

Large antennas imply large characteristic dimensions, expressed in wavelengths, narrow beamwidths and high gain, and a well-defined sidelobe structure. An antenna or radiation pattern is a description, usually a graphic one, of the radiated fields of an antenna. When an electric field is plotted, patterns are referred to as voltage amplitude or field, and in most cases, are normalized to unity at the peak value. When intensities, proportional to the square of the field, are described, power patterns occur. The plots may be expressed as linear in voltage or power, or in decibels. When dB units are used, the scales are  $20 \log E$  or  $20 \log E^2$ , where  $E$  is a normalized field component. It is common to graph broadbeam antenna patterns on a linear scale and directive antenna patterns in dB, using polar and rectangular descriptions, respectively.

A sketch of a directive antenna pattern is provided in Figure 3.19. A summary description of the characteristics follows.

PATTERN PARAMETERS	
Types	Antenna patterns, in most cases, are expressed vertical and horizontal planes which are referred to as <i>principal plane patterns</i> . For linearly-polarized antennas, the patterns in the plane of electric field, either vertical or horizontal, may be called <i>E-plane patterns</i> . Similarly, <i>H-plane patterns</i> are described. Three-dimensional patterns of many forms are common, including field contours plotted over surfaces enclosing the antenna.
Antenna Beam	The antenna pattern is described in two principal segments: the antenna beam (i.e., major lobe or main beam) and sidelobes. The peak of the main beam corresponds to the maximum gain of the antenna.
Beamwidth	The beamwidth of an antenna is the width between the angles, where the intensity of the beam is at a power level of one-half of the peak, or at the $-3$ dB points. Beamwidths are proportional to wavelength, and inversely proportional to the maximum dimension of the antenna

in the plane of the antenna pattern. The constant of proportionality is dependent on the aperture distribution (or illumination function) and will vary from a value of 0.88 for uniform apertures to over 1.5 for tapered aperture distribution, with patterns characterized by low sidelobes.

Exceptions may occur with antenna beamwidths expressed at different intensity levels. For example, in those instances, the levels are specified (i.e.,  $-6$  dB).

*Main-Lobe Width*

The width of the main lobe is measured in angular units, to the first wall position. An anomaly occurs when the radiated fields arise from an out-of-focus aperture; then the first walls fill in and the first sidelobe appears as an extension to the mainbeam. In those instances, lobe widths may refer to the second wall of the pattern.

*Nulls* The occurrence of nulls is characteristic of antenna patterns, with positions related to the aperture distribution and size of the antenna, the presence of diffraction or edge effects, and fabrication imperfections. Null depths are similarly influenced.

*Sidelobes* Sidelobes are characterized by the first and minor (or far) lobes. A sidelobe reference usually applies to the first lobe, with all minor ones being of equal or less intensity. Exceptions will occur, especially for scanning arrays. The sidelobe level and beamwidths are related to the aperture distribution when an optimal narrow beamwidth and low sidelobe relationship is desired for a given antenna size. Real-world antenna patterns are usually degraded replicas of ideal optimal ones.

Sidelobe levels, as recently characterized, are as follows:

*Normal*  $> -25$  dB

*Low*  $-25$  to  $-35$  dB

*Very Low*  $-35$  to  $-45$  dB

*Ultra low*  $< -45$  dB

Special design considerations are necessary for sidelobe levels at the low (or lower) characterizations.

*Minor Lobes* Minor lobes, for some optimal aperture distributions, will maintain a level equal to the first lobe for a given design number of lobes, then decrease. Generally, sidelobe levels should be minimal, and they should decrease rapidly and be close to the first sidelobe. The secondary lobes, because of their low intensities, are subjected to degradation due to diffraction effects from the edges of the aperture and objects in close proximity to the radar antenna. These will appear as back lobes in the vicinity of the  $180^\circ$  angular position, and as minor lobes in the intermediate region bounded by the first sidelobe.

---

Antenna patterns are generally complicated if viewed theoretically, where accuracy in their prediction is desired, or experimentally, where definitive interpretations of observations are attempted. Overall, the antenna pattern is a quantitative description of the performance of the antenna, and the standard reference for all radar equation applications if antenna parameters are involved.

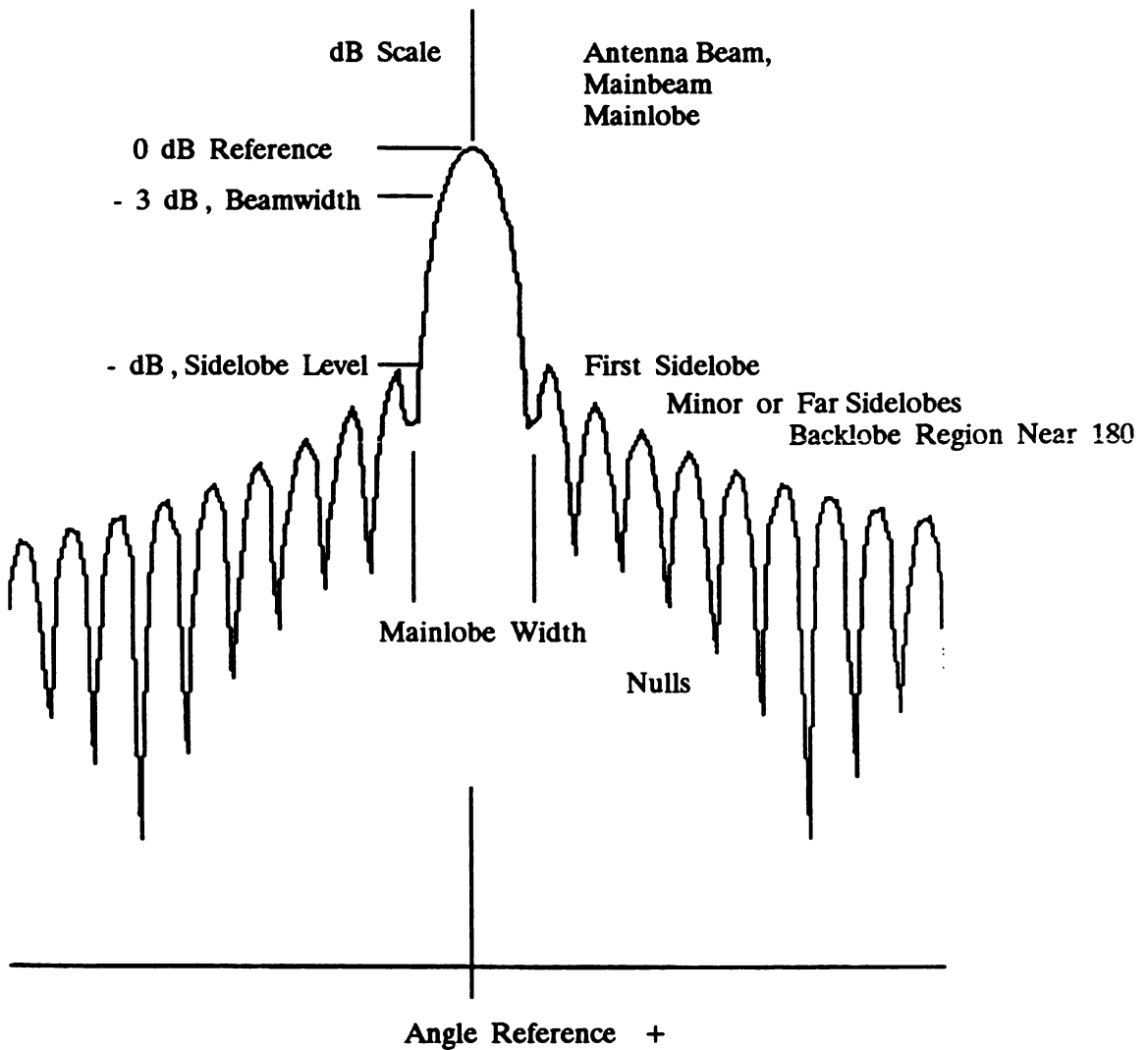


**Figure 3.19** Sketch of a Narrow-Beam Antenna Pattern Showing Principal Parameters

### Radiation from Current Elements

Radar antennas are large, with characteristic dimensions much larger than a wavelength. Arrays are formed by individual radiating elements that can be further subdivided into two main categories: (I) small-wire, dipole, or monopole antennas, and (II) small slot radiators.

In these initial antenna reviews, the radiated fields of several wire antennas, a resonant slot, and a finite current are described. The antennas of concern, their primary features, and applications are included in the following summary.

---

*ANTENNA TYPES*

---

<i>Dipole</i>	The radiated fields of a thin wire, center-fed dipole are computed using integrations of current elements. The aperture distribution is sinusoidal, zero at the extremities and maximum at the feed. Dipole antennas may be the radiating elements in array antennas.
<i>Slot</i>	Because of the symmetrical form of Maxwell's equations, a duality principle shows the radiated fields of a resonant slot to be equal to the dipole fields, with the electric and magnetic fields interchanged. Slots are common elements in radar array antennas and frequently occur as cuts in the broad or narrow wall of a waveguide, an open-ended rectangular or circular waveguide, or a cavity-backed slot.
<i>Line Source</i>	A line source antenna is an assumed current source of finite but large extent $L \gg \lambda$ , with specified current distribution, and of infinitesimal cross section dimensions. Line sources are convenient for evaluating antenna patterns with specified illumination functions, and a convenient tool for estimating radiated fields of more complex two- and three-dimensional current distributions.
<i>Traveling Wave, Thin-Wire Antenna</i>	A traveling wave thin-wire antenna is excited at one end, electrically long, and assumed to be terminated (i.e., no reflections at the end). This antenna is a principal segment of many low-frequency antennas, demonstrates the principles of traveling-wave antennas in general, and structures the radiated fields in a way that is useful in describing and interpreting the scattering from many long and thin radar targets.

---

Whenever applied, the radiated fields from current sources are exact, provided that the current distributions are known. Normally, current distributions are estimated, with the resulting antenna patterns being approximate.

*The Dipole Antenna*

The radiated field of an infinitesimal dipole or current element, from the example of Section 3.2, is

$$E_{\theta} = j \frac{\omega \mu I l}{4 \pi r} \sin \theta \exp(-jkr) \quad (3.184)$$

with the magnetic field given by

$$H_{\phi} = \frac{E_{\theta}}{\eta} \quad (3.185)$$

The current element is positioned along the  $z$  axis of a rectangular coordinate system, with fields expressed in spherical coordinates; each one is shown in Figure 3.20.

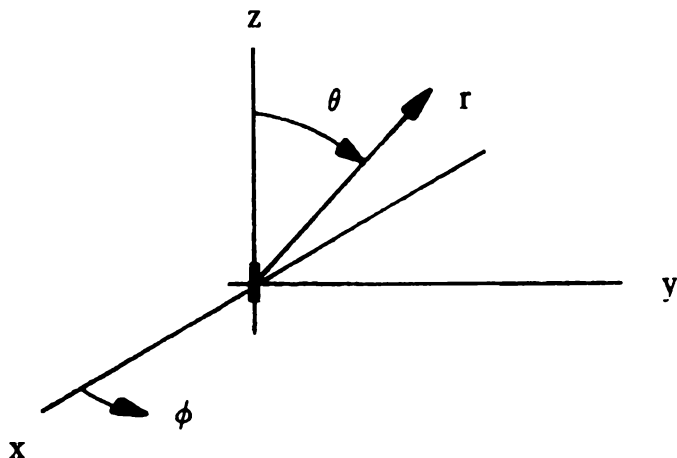


**Figure 3.20** Current Element and Coordinates

The normalized antenna pattern, a function of  $\theta$  and independent of  $\phi$ , is

$$F(\theta) = \sin\theta \quad (3.186)$$

A polar plot of the antenna pattern is contained in Figure 3.21. In three dimensions, the patterns are of doughnut shape with maximum fields occurring in the  $(x,y)$  plane and with a null along the  $z$  axis. In this plot, the amplitude of the fields is given. The electric field is in the direction of the current element; with  $(x,y)$  being a plane containing the ground, the small antenna is vertically polarized.

The radiated fields of center-fed wire antennas of arbitrary length can be found by an integration of the current distribution with the radiated field of a current element. A resonant dipole is a wire antenna, one-half wavelength in length and fed at the center. The current is zero at the ends and assumes a sinusoidal distribution. A sketch of the wire antenna is contained in Figure 3.22.

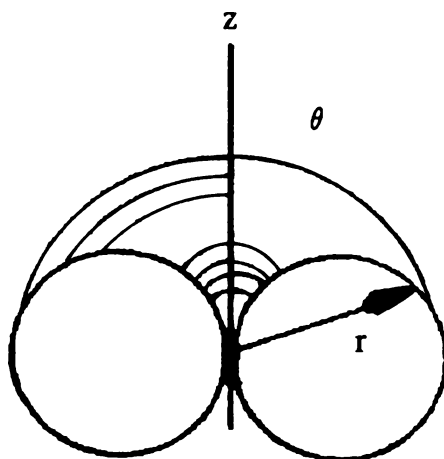


**Figure 3.21** Polar Pattern of a Current Element

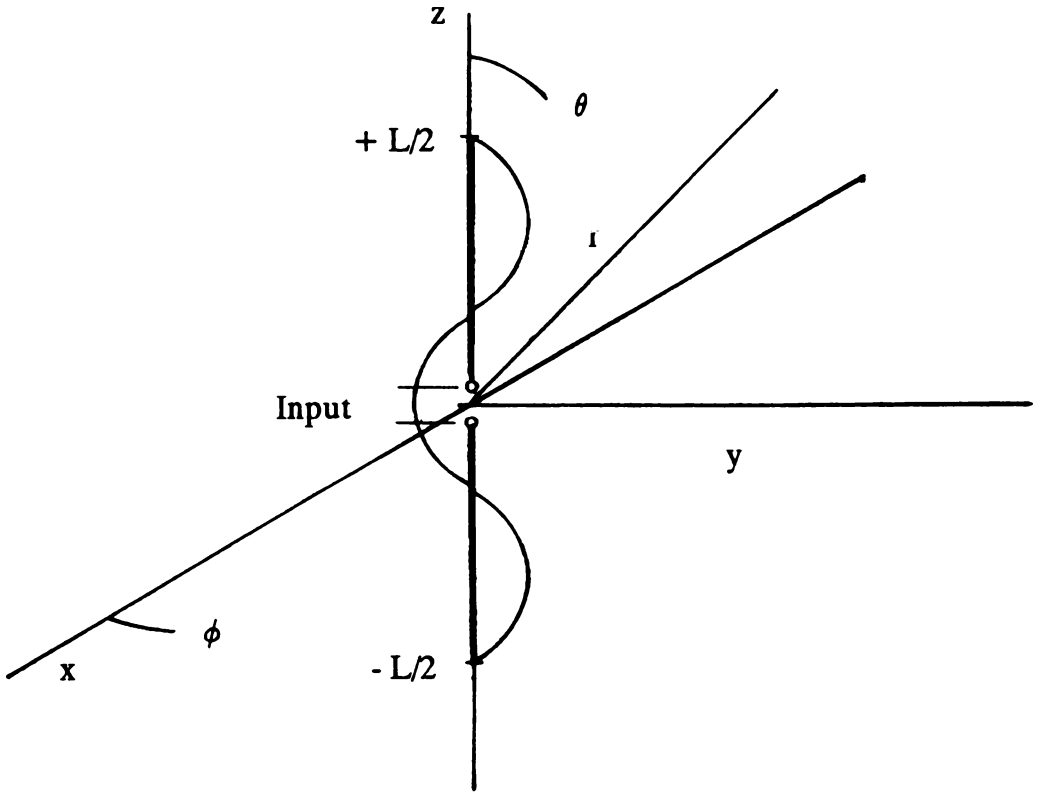


**Figure 3.22** A Thin-wire Symmetrical, Center-fed Antenna

The current distribution for the antenna is

$$I = I_0 \sin \left[ k \left( \frac{L}{2} - |z| \right) \right] \quad (3.187)$$

and, in the far field is

$$R = r - z \cos \theta \quad (3.188)$$

The radiated far-field is

$$EE_\theta = j \frac{\omega \mu I_0}{4\pi r} \sin \theta \exp(-jkr) \int_{-L/2}^{+L/2} \sin \left[ k \left( \frac{\lambda}{2} - |z| \right) \right] \exp(-jkz \cos \theta) dz \quad (3.189)$$

with solutions

$$E_\theta = j \frac{\eta I_0}{2\pi r} \left[ \frac{\cos(1/2 kL \cos \theta) - \cos(1/2 kL)}{\sin \theta} \right] \exp(-jkr) \quad (3.190)$$

and

$$H_\phi = E_\theta/\eta$$

When  $L = \lambda/2$ , Equation (3.190) reduces to

$$E_\theta = j \frac{\eta I_0}{2\pi r} \left[ \frac{\cos(\pi/2 \cos\theta)}{\sin\theta} \right] \exp(-jkr) \quad (3.191)$$

The antenna patterns are contained within the brackets of Equations (3.190) and (3.191), with the half-wave antenna pattern plotted in Figure 3.23. The pattern maintains the same doughnut characteristic of the infinitesimal dipole, but with a different angular functional relationship. The beamwidth of the half-wavelength antenna is  $78^\circ$ .

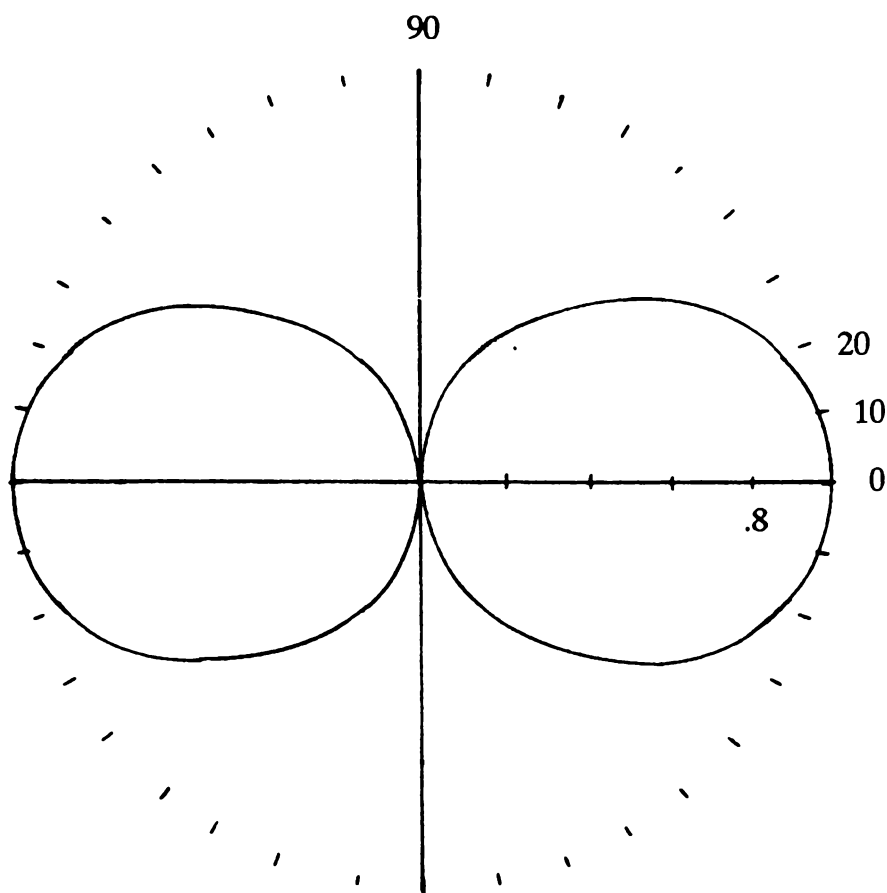


**Figure 3.23** The Pattern of a Half-wave Resonant Dipole



These fundamental results provide an antenna pattern for a half-wave, thin-wire antenna. The patterns are useful for first estimates of fields radiated by wire antennas with diameters small in comparison to a wavelength. Analysis of certain arrays containing dipole elements serves as an example of such application. When dipole elements become thick, a common occurrence in radar applications, formal treatments of antenna patterns involve the determination of the current distribution and an integration, similar to the one performed here, to obtain the radiated fields. The impedance properties of the antenna are more important in the design of an array feeding system, which depends on the length and thickness of the antenna. When implemented in an array, consideration must be given to self-impedances (or admittances) of the antenna and mutual impedances resulting from coupling between closely spaced antennas. Mutual coupling affects input impedances, and therefore the excitation current,  $I_0$  in the above derivation. Several references are included in the bibliography for further pursuance of this topic, which is also addressed when arrays are discussed.

### Slot Antenna

Figure 3.24 shows a thin resonant slot in an infinite, perfectly-conducting ground plane. The radiated fields of the slot are the same as the fields of thin dipole, with the electric and magnetic fields interchanged. The radiated electric field is

$$E_{\phi} = j \frac{\eta I_0}{2\pi r} \left[ \frac{\cos(\pi/2 \cos\theta)}{\sin\theta} \right] \exp(-jkr) \quad (3.192)$$

and the magnetic field is  $H_{\theta} = E_{\phi}/\eta$ .

The radiated electric field, which was vertically polarized for dipole orientation, is now horizontally polarized. The field is now best related to the electric field across the slot, the boundary conditions of which must be zero at the extremities. With the ground plane contained in the  $(x, z)$  plane, the normal component of the electric field when  $\theta = 0$  and  $180^\circ$  is nonzero, an acceptable condition, and is independent of the angle  $\phi$  varying with  $\theta$ . The antenna pattern is, of course, identical to that of the dipole, but is an  $H$ -plane rather than  $E$ -plane pattern.

The interchange of electric and magnetic fields results from the symmetrical properties of Maxwell's equations. For example, referring to Equations (3.41) and (3.42), describing plane wave propagation, we have the fields:

$$\mathbf{E} = \sqrt{\frac{\mu}{\epsilon}} \mathbf{H} \quad (3.193)$$

and

$$\mathbf{H} = \sqrt{\frac{\epsilon}{\mu}} \mathbf{E} \quad (3.194)$$

which also satisfy Maxwell's equations. The property of Maxwell's equations is referred to as *duality*, which, in general, relates dual fields and sources.

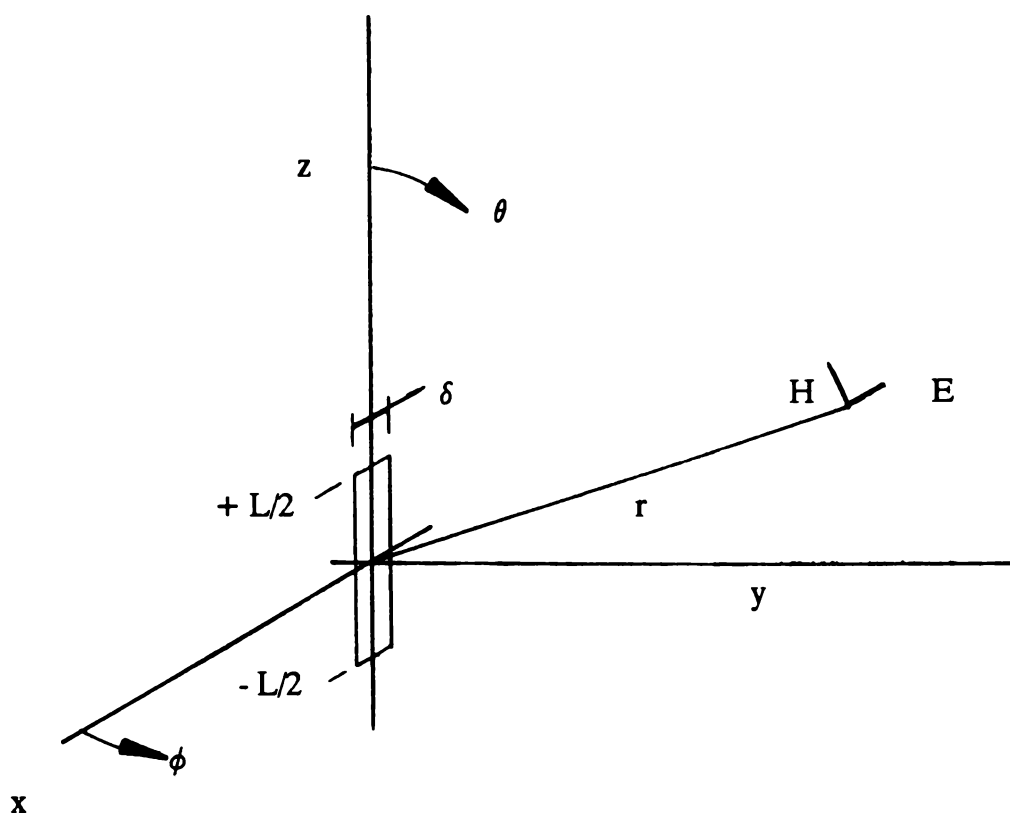


**Figure 3.24** The Slot Antenna and Coordinates

Slot antennas, if implemented, are very sensitive to ground plane conditions or cuts within and in the vicinity of the slots. When implemented in an array, mutual effects occur, as with the wire elements. For radar analysis purposes, whether antenna patterns are computed for system evaluations or component designs, care must be taken in the estimation of the slot antenna pattern. Measurements are usually advisable, with the formulas given here serving as first estimates while providing realistic field orientations and regions where low radiated fields can be expected to occur.

### Line Source

We will now describe a uniform line source antenna. The antenna is positioned as shown in Figure 3.25 and is characterized by a current  $I_0$ , uniform throughout its length. The radiated fields are found by an integration of current elements, as demonstrated for the dipole. Using the same far-field approximation as before, we have

$$E_\theta = j \frac{\omega \mu I_0}{4\pi r} \sin\theta \exp(-jkr) \int_{-L/2}^{+L/2} \exp(jkz \cos\theta) dz \quad (3.195)$$

with its solution:

$$E_\theta = j \frac{\omega \mu I_0 L}{4\pi r} \sin\theta \exp(-jkr) \left\{ \frac{\sin[(kL/2) \cos\theta]}{(kL/2) \cos\theta} \right\} \quad (3.196)$$

The normalized field pattern for the line source is

$$F(\theta) = \sin\theta \left\{ \frac{\sin[(kL/2) \cos\theta]}{(kL/2) \cos\theta} \right\} \quad (3.197)$$

Several fundamental antenna properties are demonstrated by this result. Within the braces, the function is in the form of  $(\sin x)/x$ , a commonly-occurring function in antenna field descriptions. The total pattern is the product of  $\sin\theta$  and the  $(\sin x)/x$  function. Demonstrated here is pattern multiplication, an antenna principle occurring in array theory.

As we have pointed out, current line sources are useful as segments of a more complex current distribution for computations of fields. They are also useful in estimating the effects of aperture distribution on patterns in a convenient way.

### Thin-wire Traveling Wave Antenna

The radiated field of the antenna will be determined from an integration of current sources, which is a relatively simple procedure. The results will then be interpreted as a summation of spherical waves, originating at the ends of the wire, and explained as principal waves in Schelkunoff's mode theory of antennas. Using these results, formulas will be provided that relate the near and far fields of thin-wire antennas to summations of spherical waves with origins at the ends (or excitation regions) of the antenna. In this way, the radiated fields are given a very simple physical interpretation and, theoretically, are solutions of Maxwell's equations. In antenna theory the phenomenology is related, at least conceptually, to radiation from long

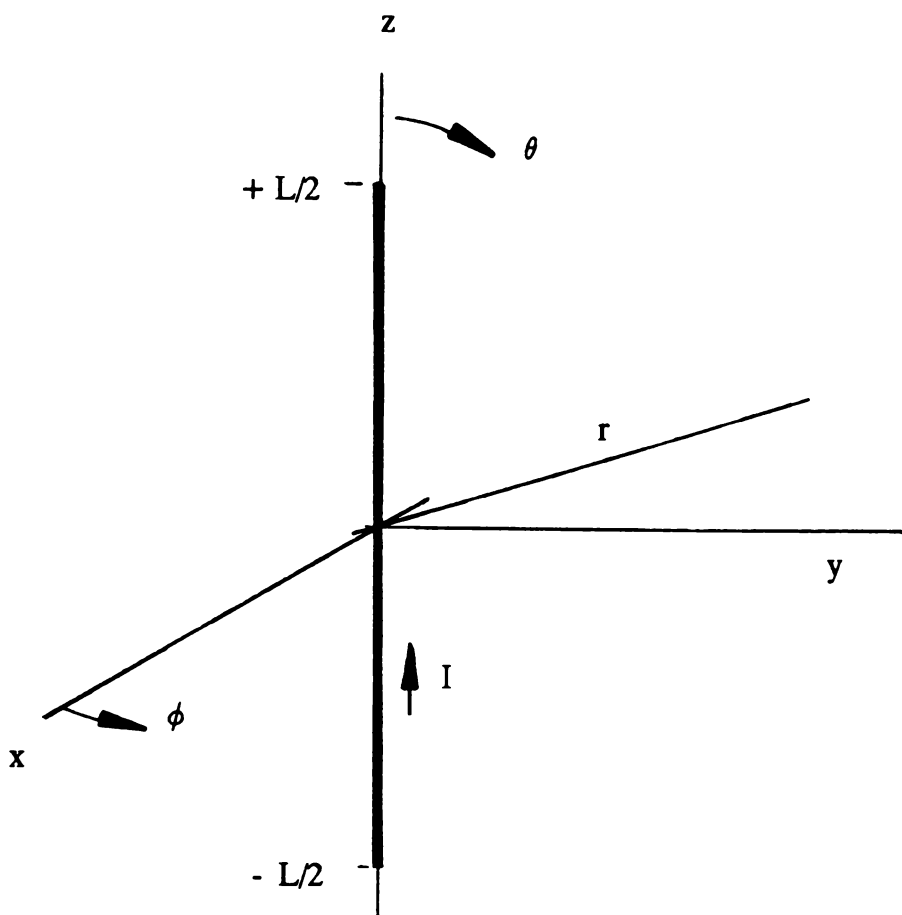


**Figure 3.25** The Line Source Antenna

thin objects of arbitrary shape, and clearly shows the formation of the fields. In scattering theory, long thin objects give rise to fields of the same form as the antennas, resulting from spherical waves excited at the ends of the scatterer. When we examine a thin wire antenna in a later section, the spherical waves will be shown to be of the same form, with their points of origin being the scattering centers.

This interesting antenna is shown in Figure 3.26. A thin wire antenna of length  $L$  is positioned along the  $z$  coordinate axis and excited at the base. A traveling wave current distribution such as

$$I = I_0 \exp(-jkz) \quad (3.198)$$

is assumed. A free-space phase velocity is postulated, with an assumed perfect termination at the end of the wire. A transmission system with a termination equal to the characteristic impedance, and an absence of reflection at the termination is

implied. Proceeding as before, the radiated field of the antenna is

$$E_{\theta} = j \frac{\omega \mu I_0}{4\pi r} \sin\theta \exp(-jkr) \int_0^L \exp(-jkz) \exp(jk \cos\theta) dz \quad (3.199)$$

with solution:

$$E_{\theta} = \frac{\eta I_0}{4\pi r} \left( \frac{\sin\theta}{1 - \cos\theta} \right) [1 - \exp(-jkL) \exp(jkL \cos\theta)] \exp(-jkr) \quad (3.200)$$

Let the radiated electric field be written in the following way:

$$E_{\theta} = \frac{\eta I_0}{4\pi r} \left( \frac{1 + \cos\theta}{\sin\theta} \right) \exp(-jkr) \\ + \frac{\eta I_0}{4\pi r} \left( \frac{1 + \cos\theta}{\sin\theta} \right) \exp(-jkL) \exp(jkL \cos\theta) \exp(-jkr) \quad (3.201)$$

The first term is a spherical wave at its origin. The angular dependence of the field will vary in intensity from unity at  $\theta = 130^\circ$  to infinity at  $\theta = 0$ . For a finite thickness wire antenna, the field component at the surface of the conductor will be large but not infinite.

The fields, which are solutions of Maxwell's equations, were originally derived by Mannaback to explain radiation from transmission lines. Schelkunoff described radiation from thin wires in this manner and also showed their occurrence in the mode theory of antennas, where the total radiated fields of conical and perturbed conical antennas of arbitrary shape are described by a model structure of expanding spherical waves. These waves may be most appropriately described as *principal waves* in Schelkunoff's mode theory of antennas.

A spherical wave with the same angular dependence is excited at the opposite end of the antenna. The second term shows a phase retardation of  $kL$  and a spherical wave centered at  $z = L$  with a phase advance of  $kL \cos\theta$ . The field originating at  $z = L$  is

$$E_{\tilde{\theta}} = \frac{\eta I_0}{4\pi \tilde{r}} \left( \frac{1 + \cos\tilde{\theta}}{\sin\tilde{\theta}} \right) \exp(-jkL) \exp(-jk\tilde{r}) \quad (3.202)$$

which reduces to the result of Equation (3.192), when the far-field approximation is applied. The coordinates  $(\tilde{r}, \tilde{\theta})$  are referenced to  $z = L$ . If we let

$$m_+(r, \theta) = \frac{1 + \cos\theta}{\sin\theta} \left[ \frac{\exp(-jkr)}{4\pi r} \right] \quad (3.203)$$

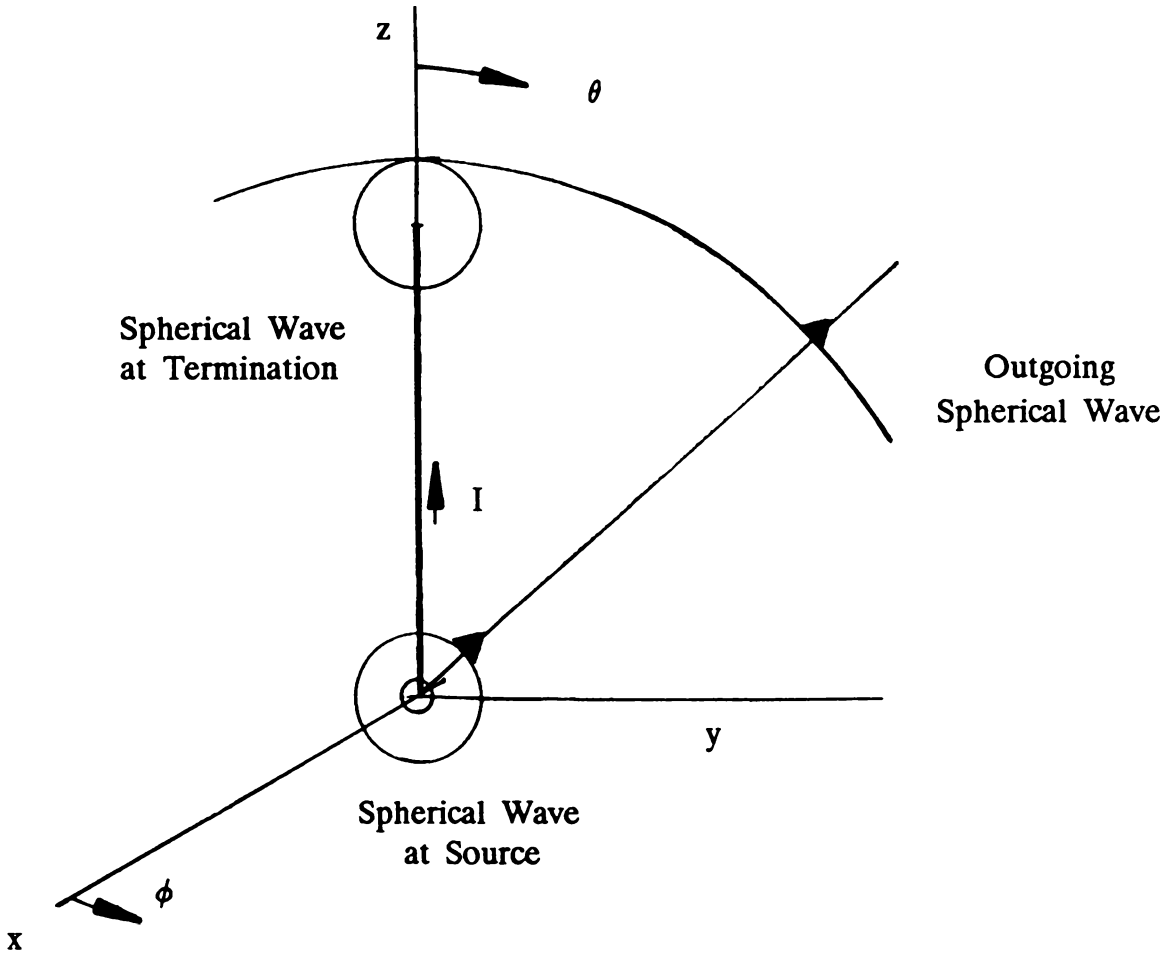


**Figure 3.26** A Thin-wire, Traveling Wave Antenna

then the fields of the antenna can be written in shorter notation:

$$E(r, \theta) = \eta I_0 [m_+(r, \theta) + m_+(\tilde{r}, \tilde{\theta})] \quad (3.204)$$

This notation applies to near and far fields. In the far field using this shortened notation,

$$E_\theta = \eta I_0 m_+(r, \theta) [1 - \exp(-jkL) \exp(jkL \cos \theta)] \quad (3.205)$$

The far-field antenna pattern obtained is

$$F(\theta) = \frac{1 + \cos \theta}{\sin \theta} \{\sin[kL(1 - \cos \theta)]\} \quad (3.206)$$

The pattern is plotted in Figure 3.27 for  $L = 10\lambda$ . The beam is positioned as shown, at an angle  $\theta_0$  from the wire. When the phase velocity of the spherical wave is less than the velocity of light, the beam will be directed at angles greater than  $\theta_0$ . Scanning the end-fire or leaky antenna beams has been demonstrated where beam positions are related to the phase velocity in a controlled manner. These characteristics represent general properties of traveling wave antennas.

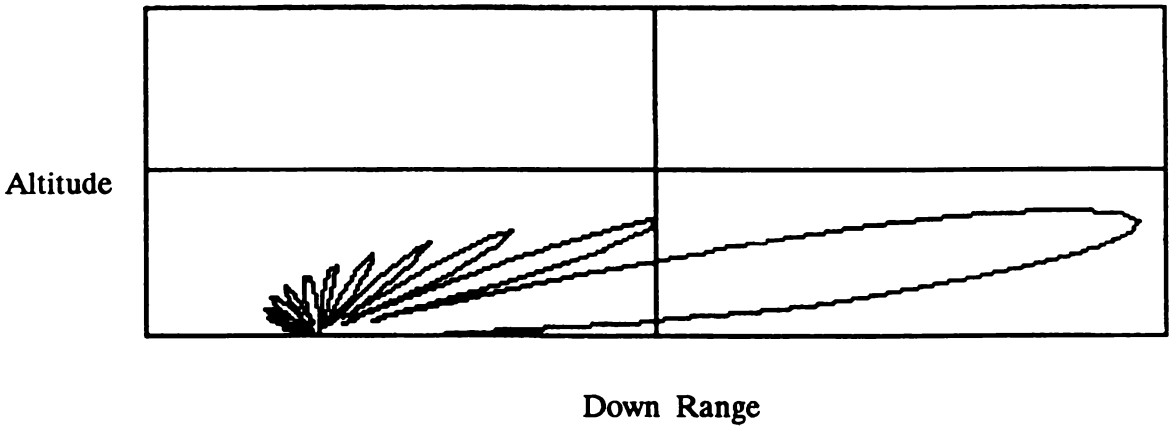


**Figure 3.27** Antenna Pattern for a Long, Thin Traveling Wave Antenna

For pulsed excitation, let a signal of length  $\tau$  with  $c\tau < L$ , the length of the antenna, be applied at  $z = 0$ . The radiated fields are now written as principal waves originating at the extremities of the wire:

$$E(r, \theta; \tilde{r}, \tilde{\theta}) = \eta [m_+(r, \theta) I(t - r/c) - m_-(\tilde{r}, \tilde{\theta}) I(t - L/c - r/c)] \quad (3.207)$$

The antenna subjected to excitation by a short pulse is sketched in Figure 3.28 for  $c\tau \ll L$ . The structuring of the antenna pattern by an expanding spherical wave excited at the extremities of the wire is clearly demonstrated. When interpreted in the context of mode theory of antennas, radiation originates at the ends of the antenna in the form of expanding spherical waves, with the shape of the antenna determining the characteristic impedance of the spherical wave. The phase velocity and losses along the wire may occur, depending on the physical constants associated with the antenna element and the surrounding medium. Also implied in this description is the design of thin-wire antennas of arbitrary shape, which, as we will show in the discussion that follows, depends on the minute details of the ends and excitation regions of the antenna. This observation is also supported by experiment.

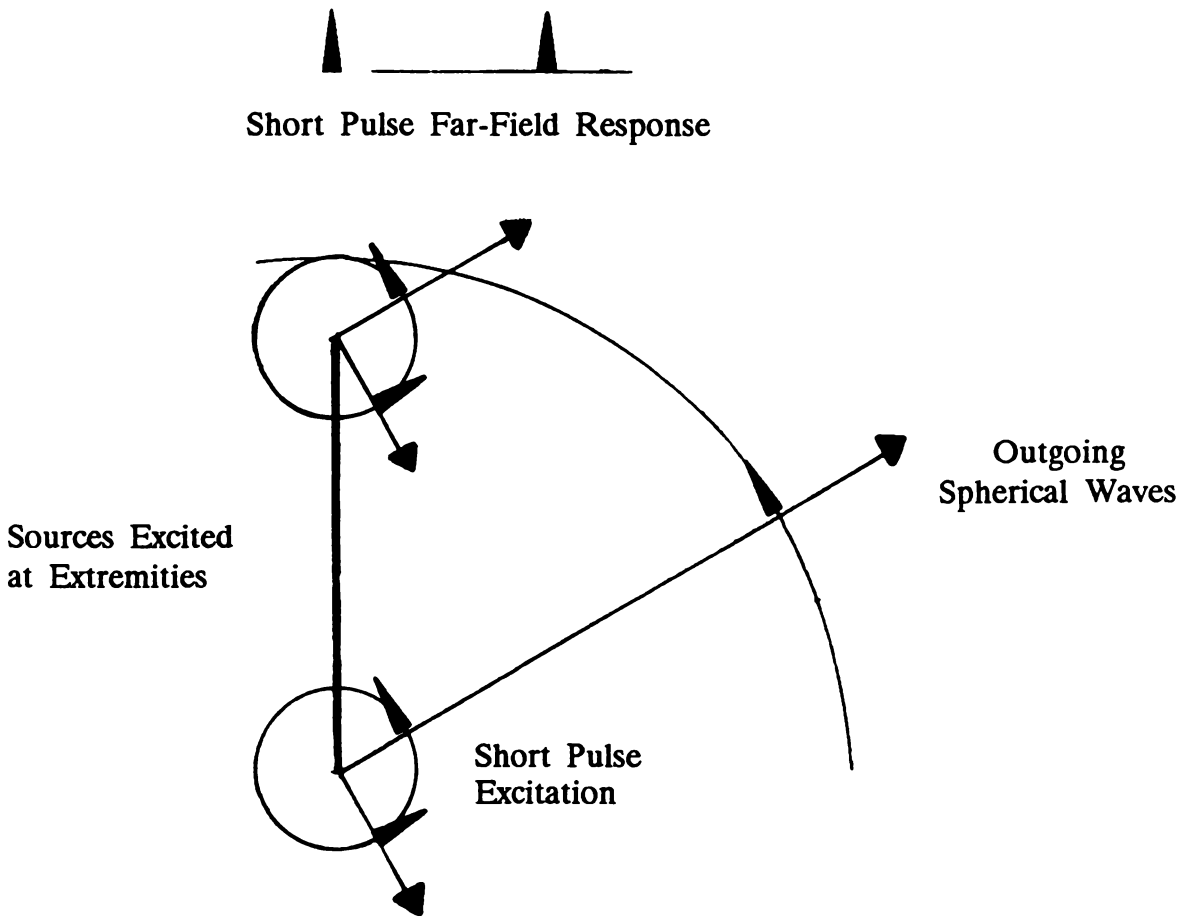


**Figure 3.28** The Radiated Field of a Long, Thin, Wire Antenna with Short Pulse Excitation

This introductory material, with its far-reaching theoretical implications, can be pursued by in-depth study of Schelkunoff's mode theory of antennas, and making further extensions into scattering theory. A short note on radiation patterns of long thin antennas by Bolle and Jacobs, covering short-pulse excitation, is also applicable. The inclusion of this material in our discussions is directed toward specific scattering applications covered later, with the introduction of spherical-wave formulations best accomplished from an antenna point of view. We hope the reader will appreciate the antenna and scattering descriptions, which are excellent examples of interpretations of scattering centers that are fundamental in many aspects of the properties of observable radar targets.



### *Spherical Waves on Wires*

Our discussions conclude with a summary of principal wave propagation along thin-wire structures. Radiated fields will be described in a summation of principal waves for a number of thin-wire antennas, including the ones already discussed. The following additional notation will be applied:

$$m_{-}(r, \theta) = \frac{1 - \cos \theta}{\sin \theta} \left[ \frac{\exp(-jkr)}{4\pi r} \right] \quad (3.208)$$

and

$$m(r, \theta) = m_{+}(r, \theta) + m_{-}(r, \theta) = \frac{2}{\sin \theta} \left[ \frac{\exp(-jkr)}{4\pi r} \right] \quad (3.209)$$

The antenna formulas are as follows.

<i>SPHERICAL WAVES ON WIRES</i>	
<i>Positive, Semi-Infinite Thin Wire</i>	$E(r, \theta) = \eta I m_{+}(r, \theta)$
<i>Negative, Semi-Infinite Thin Wire</i>	$E(r, \theta) = \eta I m_{-}(r, \theta)$
<i>Current Element</i>	$E(r, \theta) = \eta I [m_{+}(r, \theta) - m_{+}(\tilde{r}, \tilde{\theta}) \exp(-jkl)]$ $\left\{ \begin{array}{l} r \cos \theta = l + \tilde{r} \cos \tilde{\theta} \\ r \sin \theta = \tilde{r} \sin \tilde{\theta} \end{array} \right\}$
<i>Traveling Wave Antenna Dipole, Length 2L</i>	$E(r, \theta) = \eta I [m_{+}(r, \theta) - m_{+}(\tilde{r}, \tilde{\theta}) \exp(-jkL)]$ $E(r, \theta) = \eta I \{m(r, \theta)[1 + \exp(-j2kL)] - [m(\tilde{r}_1, \tilde{\theta}_1) + m(\tilde{r}_2, \tilde{\theta}_2)] \exp(-jkL)\}$

The coordinates  $(\tilde{r}_1, \tilde{\theta}_1)$  and  $(\tilde{r}_2, \tilde{\theta}_2)$  are referenced to the ends of the dipole on the positive and negative z-axis terminations, respectively. Extensions to other wire antennas follow the same procedure.

### **Fourier Transform Methods**

The radiated fields or antenna patterns of large aperture antennas, similar to their scattering counterparts, are usually determined from mathematical formulations derived from Kirchhoff's theory. In its most common form, the diffraction integral for rectangular apertures may be placed in the form of a Fourier transform, relating the aperture to the radiated field distributions. Circular apertures can likewise be

expressed as transforms, and because of the geometrics, can reduce the diffraction integrals to Hankel transforms. These methods of scalar diffraction theory can be used for the computation of near and far fields of large aperture antennas. The scalar theory and consideration of field equivalence principles allows applications for any antenna aperture, within constraints of the Kirchhoff boundary conditions. Practically, beamwidth, gain, and sidelobe relations may be estimated from the transform formulations. For analysis purposes, use of fast Fourier transform provides simple and efficient numerical solutions.

### *The Rectangular Antenna*

Consider a rectangular aperture positioned in the  $(x,y)$  plane of a rectilinear system  $(x,y,z)$  as shown in Figure 3.29. Let the aperture coordinates be normalized  $(\xi,\eta) = (x/a,y/b)$ , where  $a$  and  $b$  are the dimensions of the antenna. The aperture distribution is separable, that is  $f(\xi,\eta) = f(\xi)g(\eta)$ , where, for generality, the distributions in the  $(\xi,\eta)$  coordinates are different.

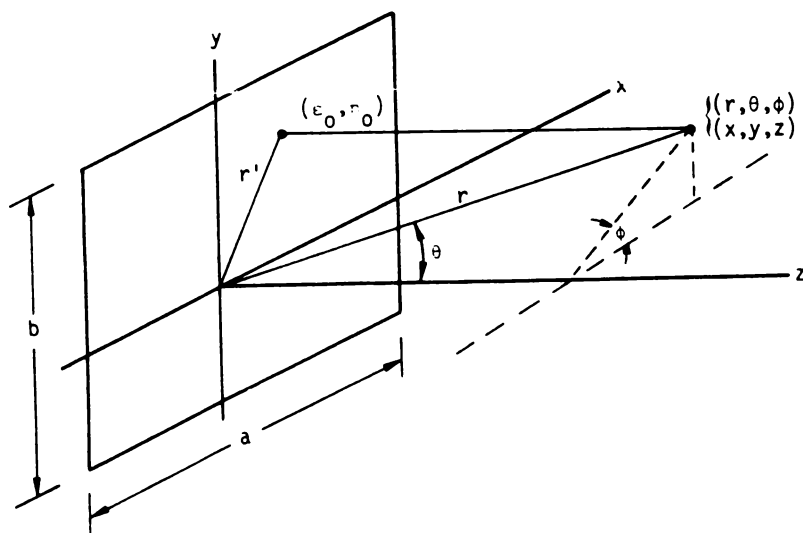


**Figure 3.29** Planar Rectangular Aperture and Coordinate System. (From Bogush and Elkins)

From Appendix B, where diffraction integrals compiled from Hu are contained, the far radiated fields of the antenna are

$$E(r, \theta, \phi) = j \frac{kab}{4\pi r} (1 + \cos\theta) \exp(-jkr) \int_{-1/2}^{+1/2} f(\xi) \exp(ju\xi) d\xi \int_{-1/2}^{+1/2} g(\eta) \exp(jk\eta) d\eta \quad (3.210)$$

where the variables:

$$u = ka \sin\theta \cos\phi \quad (3.211)$$

$$v = kb \sin\theta \sin\phi \quad (3.212)$$

have been introduced. We use the transform pair, as it usually appears in time and frequency variables:

$$f(t) = \frac{1}{2\pi} \int_{-\infty}^{+\infty} F(\omega) \exp(j\omega t) d\omega \quad (3.213)$$

and

$$F(\omega) = \int_{-\infty}^{+\infty} f(t) \exp(-j\omega t) dt \quad (3.214)$$

or in shortened notation:

$$f(t) \leftrightarrow F(\omega) \quad (3.215)$$

which is a statement of  $F(\omega)$  being the Fourier transform of  $f(t)$  given by Equation (3.214), and its inverse given by Equation (3.213). Some Fourier transform theorems are as follows.

---

#### FOURIER TRANSFORM THEOREMS

---

Given functions ( $f(t)$ ) and  $F(\omega)$  that are Fourier transformable, applications of Fourier transform theory are simplified by the use of several theorems. From Papoulis,

$$f(at) \leftrightarrow \frac{1}{|A|} F\left(\frac{\omega}{a}\right)$$

$$f^*(t) \leftrightarrow F^*(-\omega)$$

$$F(t) \leftrightarrow 2\pi f(-\omega)$$

$$f(t - t_0) \leftrightarrow F(\omega) \exp(-jt_0\omega)$$

$$f(t) \exp(j\omega_0 t) \leftrightarrow F(\omega - \omega_0)$$

$$f(t) \cos(\omega_0 t) \leftrightarrow \frac{1}{2} [F(\omega + \omega_0) + F(\omega - \omega_0)]$$

$$f(t) \sin(\omega_0 t) \leftrightarrow \frac{1}{2} [F(\omega + \omega_0) - F(\omega - \omega_0)]$$

$$\int_{-\infty}^{+\infty} f_1(\tau) f_2(t - \tau) d\tau \leftrightarrow F_1(\omega) F_2(\omega)$$

$$f_1(t) f_2(t) \leftrightarrow \frac{1}{2\pi} \int_{-\infty}^{+\infty} F_1(y) F_2(\omega - y) dy$$

$$\frac{d^n f(t)}{dt^n} \leftrightarrow (j\omega)^n F(\omega)$$

$$(-jt)^n f(t) \leftrightarrow \frac{d^n F(\omega)}{d\omega^n}$$

The last two entries are particularly useful when aperture distributions are expansions of Gaussian functions.

Now, referring to Equation (3.210) in view of (3.213), (3.214), and (3.215), we let

$$F(u) = \int_{-1/2}^{+1/2} f(\xi) \exp(j\omega\xi) d\xi \quad (3.216)$$

and

$$G(v) = \int_{-1/2}^{+1/2} g(\eta) \exp(j\omega\eta) d\eta \quad (3.217)$$

then  $f(\xi) \leftrightarrow F(u)$  and  $g(\eta) \leftrightarrow G(v)$ . The radiated fields can hence be written as Fourier transforms of the aperture distribution:

$$E(r, u, v) = j \frac{kab}{4\pi r} (1 + \cos\theta) \exp(-jkr) \left\{ F(u) G(v) \right\} \quad (3.218)$$

The antenna patterns are normally expressed by Equations (3.216) and (3.217), the Fourier transforms of the aperture distributions.

Because the aperture distributions are separable, the antenna pattern is the product  $F(v)$  and  $G(v)$ . For analysis purposes, without loss in generality, the properties of the antenna can be obtained from separate consideration of  $F(v)$  and  $G(v)$ . Several patterns of readily transformable antenna distributions are as follows:

---

*EXAMPLES OF ANTENNA PATTERNS*

---

*Uniform Antenna*

$$f(\xi) = \mathcal{U}(\xi + 1/2) + \mathcal{U}(\xi - 1/2)$$

$$F(u) = \frac{\sin(u/2)}{(u/2)}$$

*Triangular*

$$f(\xi) = 1 - 2|\xi|$$

$$F(u) = \frac{\sin^2(u/4)}{(u/4)^2}$$

*Gaussian*

$$f(\xi) = \exp(-\xi^2)$$

$$F(u) = \sqrt{2\pi} \exp(-u^2/2)$$

*Cosine*

$$f(\xi) = \cos(\pi\xi)$$

$$F(u) = \left(\frac{\pi l}{2}\right) \frac{\cos u}{(\pi/2)^2 - u^2}$$

*Cosine Squared*

$$f(\xi) = \cos^2(\pi\xi)$$

$$F(u) = \left(\frac{l}{2}\right) \left(\frac{\sin u}{u}\right) \left(\frac{\pi^2}{\pi^2 - u^2}\right)$$


---

The antenna pattern for the cosine antenna is plotted in Figure 3.30. The beamwidth of this antenna is

$$\theta_3 = 1.189 \left(\frac{\lambda}{L}\right) \quad (3.219)$$

with a corresponding sidelobe level of  $-23$  dB. Although they may be interesting, antennas with the distributions given above are physically unrealizable because discontinuities (or zero-field intensities), at the edges of antenna can only be approximated, while Gaussian distributions are infinite in extent and must be truncated. They are, however, useful for analysis purposes.

For radar applications, a desire to achieve an optimal gain for the smallest possible antenna leads to a choice of aperture distributions that yield the narrowest beamwidth for a given sidelobe level and antenna dimensions. Most modern radars will employ optimal Taylor aperture illumination functions. Exceptions occur when low to ultralow antenna designs are attempted; compromises may be made in aperture size, and thus efficiency, to achieve desired sidelobe levels. Antenna patterns, in particular the sidelobe structure, also become degraded due to phase errors that occur at the surface of the antenna and in the feeding networks, and aperture distributions are susceptible to perturbations due to edge effects or coupling between elements in an array.

The antenna parameters of concern therefore are the aperture distribution, beamwidth, sidelobe level, aperture efficiency, gain, and effective area. Collecting formulas, and repeating a few for convenience, the beamwidth of the antenna is proportional to the wavelength and inversely proportional to the aperture dimension:

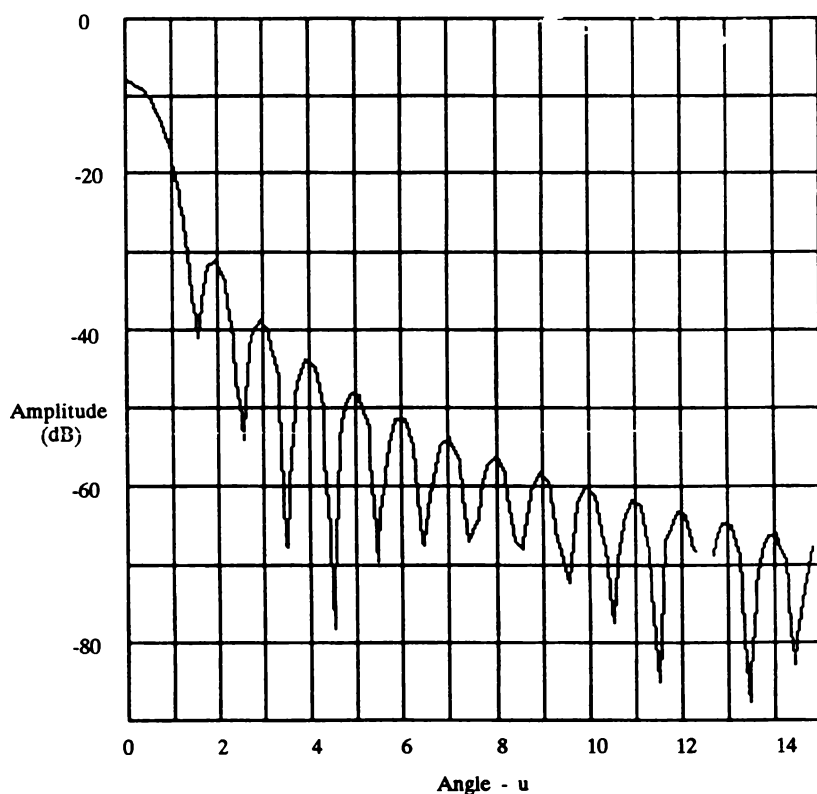


**Figure 3.30** Antenna Pattern for Cosine Aperture Distribution

$$\theta_3 = K \left( \frac{\lambda}{a} \right) \quad (3.220)$$

The parameter  $K$  depends on the aperture distribution, and is related to the sidelobe level. The gain of the antenna is proportional to its area:

$$G = \frac{4\pi}{\lambda^2} A_e \quad (3.221)$$

where  $A_e$  is the effective area of the antenna, defined as

$$A_e = \eta A \quad (3.222)$$

where  $\eta$  is the aperture efficiency.

A compilation of parameters for a number of aperture distributions is provided in Table 4.1 in Chapter 4.

### Near Fields

In Figure 3.29, the near-field diffraction integral, from Appendix A, can, with the substitutions  $\xi \rightarrow \xi/a$ ,  $\eta \rightarrow \eta/b$ ,  $x' = x/a$  and  $y' = y/b$ , be placed in the form:

$$E(x', y', z) = j \frac{kab}{4\pi r} \left( 1 + \frac{z}{r} \right) \exp(-jkr) \int_{-1/2}^{+1/2} f(\xi) \exp[-jka^2(x' - \xi)^2/2z] dx' \int_{-1/2}^{+1/2} g(\eta) \exp[-jkb^2(y' - \eta)^2/2z] dy' \quad (3.223)$$

The cross range  $(x, y)$  normalization is a convenient choice of variables since the near fields are confined to regions close to the beam axis. Equally convenient is a measure of range along the beam axis expressed in units of  $a^2/\lambda$  or  $b^2/\lambda$ . Let

$$r = ga^2/\lambda \quad (3.224)$$

where  $a > b$  and where the extent of the near field is of concern. Now consider the following additional substitutions  $X = x'/g/2\pi$  and  $Y = y'/a^2g/2\pi b^2$ ; how the integrals in Equation (3.223) can be expressed as the Fourier transform pairs,

$$f(\xi) \exp\left(j \frac{\pi \xi^2}{g}\right) \leftrightarrow F(X) \quad (3.225)$$

and

$$g(\eta) \exp\left(j \frac{\pi \eta^2 b^2}{a^2 g}\right) \leftrightarrow G(Y) \quad (3.226)$$

The near fields can now be expressed as Fourier transforms, from (3.223):

$$E(X, Y, g) = j \frac{kab}{4\pi r} (1 + ga^2/\lambda r) \exp[-j/4\pi (X^2 + a^2 Y^2/b^2)] \times F(X)G(Y) \exp(-jkr) \quad (3.227)$$

Further simplification of this equation is possible. For a square antenna with  $f(\xi) = g(\eta)$ ,  $F(X) = G(Y)$ , with the fields of interest confined to a region close

to the beam axis, then the magnitude of the field is

$$|E(X, Y, g)| = \frac{1}{g} F(X)G(Y) \quad (3.228)$$

which is a useful result.

Numerical computations of near fields can be performed using (3.226) or (3.227). Closed-form solutions of either are possible for a number of aperture distributions by expressing the integrals as Fresnel integrals, a task requiring only changes in variables. When obtainable, however, the results are not convenient for computations, numerical integrations being the preferred choice. Later, we will show examples of numerical integrations of the diffraction integrals, when Gaussian field expansions are described. Examples of Fresnel integral solutions can be found in the bibliography.

### Hankel Transform Methods

Hankel transforms are encountered in the analysis of large aperture, circular antennas. Formulas for the far and near fields are given. Aperture illuminations with radial dependence are also considered.

The circular antenna is shown in Figure 3.31. From Appendix A, the far-field diffraction integral is

$$\begin{aligned} E(r, \theta, \phi) = & j \frac{k}{4\pi r} (1 + \cos\theta) \exp(-jkr) \\ & \times \int_0^a f(\rho) \int_{-\pi}^{+\pi} \exp[jk\rho \sin\theta \cos(\phi - \phi')] d\phi' \rho d\rho \end{aligned} \quad (3.229)$$

but the Bessel function  $J_0(x)$  is defined as

$$J_0(x) = \frac{1}{2\pi} \int_{-\pi}^{+\pi} \exp[jx \cos(x - \alpha)] dx \quad (3.230)$$

Now, let  $\zeta = \rho/d$  and  $u = kd \sin\theta$ . Then, substituting into Equation (3.229) and applying (3.230), we have

$$E(r, \theta) = j \frac{kd^2}{2r} (1 + \cos\theta) \exp(-jkr) \int_0^{1/2} f(\zeta) J_0(u\zeta) \zeta d\zeta \quad (3.231)$$



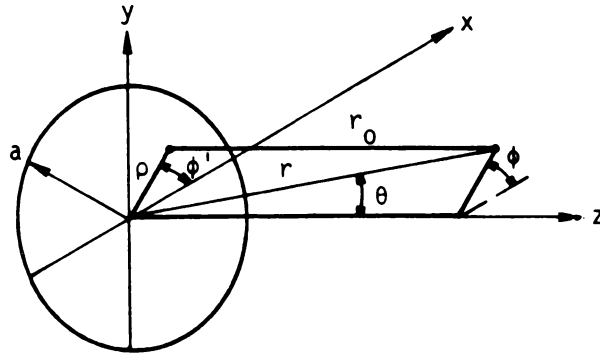


**Figure 3.31** Planar Circular Antenna and Coordinate Systems. (From Bogush and Elkins)

The Hankel transform, (given  $f(r)$  and a real constant  $w$ ) is, from Papoulis, defined as

$$\bar{f}(w) = \int_0^\infty r f(r) J_0(wr) \, dr \tag{3.232}$$

with inversion, we obtain

$$f(r) = \int_0^\infty w \bar{f}(w) J_0(rw) \, dw \tag{3.233}$$

or in shortened notation:

$$\bar{f}(r) \stackrel{\mathcal{H}}{\leftrightarrow} f(w) \tag{3.234}$$

The far-field pattern of the circular antenna can now be expressed as

$$E(r,\theta) = j \frac{kd^2}{4\pi r} (1 + \cos\theta) \exp(-jkr) F(u) \tag{3.235}$$

where

$$f(\xi) \leftrightarrow F(u) \tag{3.236}$$

From Papoulis, and for computational purposes, the Hankel and Fourier transforms are related. Let the function  $\Psi(x)$  be defined as

$$\Psi(x) = \int_{-\infty}^{+\infty} f[(x^2 + y^2)^{1/2}] \, dy \tag{3.237}$$

then,

$$\Psi(x) \leftrightarrow 2\pi F(u) \quad (3.238)$$

which enables the Hankel transforms to be determined from the Fourier transforms; numerically, advantage can be taken of Fourier computational methods in determining the fields of a circular antenna.

In the near field, from Appendix A, and following the procedures used for the far-field derivations, we obtain

$$E(r, \theta) = j \frac{kd^2}{2r} (1 + \cos\theta) \exp(-jkr) \bar{F}(u) \quad (3.239)$$

where

$$f(\zeta) \exp\left(-j \frac{ka^2 \zeta^2}{2r}\right) \xleftrightarrow{h} \bar{F}(u) \quad (3.240)$$

Computation of the near fields of the circular antenna follows the far-field method, subject to Equation (3.240).

The gain, effective area, and aperture efficiency can be determined by using the general field relationships. A useful formula for the maximum gain is

$$G_m = \eta G_0 = \left( \frac{\pi d^2}{\lambda^2} \right) \quad (3.241)$$

A compilation of circular antenna parameters, from Barton and Ward, is contained in Table 3.2.

### Gaussian Field Expansions

It is common in many radar applications to use a Gaussian function to approximate an antenna beam within its half-power, 3-dB points. The advantage of such approximations is in computations where simple functions replace the considerably more complicated ones that were obtained from measurement or theory. The Gaussian theory of large aperture antennas formalizes this approximation. Through expansion of aperture distributions in orthogonal Hermite-Gaussian or Laguerre-Gaussian functions for rectangular and square antennas, respectively, the resultant field expansions yield a Gaussian function as the first term of an infinite series. It approximates the peak of the antenna beam, and the peak of the near-field and

aperture distributions. Therefore, application of the Gaussian beam approximations in the far field, within the theory, also establishes the first estimates of the near field. The resultant field description, in Gaussian terms, is equally simple to use, much the same as its far-field counterpart. In fact, it is, in some instances, convenient to establish the near-field formula, which reduces appropriately to aperture and far fields. These one-term series (or one-term partial sum) representations of the radiated fields are called *Gaussian equivalents*.

Table 3.2 Circular Antenna Parameter\*\*

APERTURE FIELD	SLL* (.dB)	$(a/\lambda)\theta_3$	$\eta$
TRUNCATED GAUSSIAN n = 1.0	19.2	1.010	0.990
TRUNCATED GAUSSIAN n = 1.7	23.3	1.085	0.922
TRUNCATED GAUSSIAN n = 2.4	34.5	1.322	0.757
TRUNCATED GAUSSIAN n = 2.8	43.3	1.567	0.638
TRUNCATED GAUSSIAN n = 3.2	49.1	1.905	0.525
30 dB TAYLOR n = 4	31.2	1.182	.846
40 dB TAYLOR n = 6	41.0	1.416	.706

\* Sidelobe level  
\*\*Data Compiled from Barton and Ward.

It has been found that through proper choice of scaling parameters in the aperture field expansions, the order of the partial sum is one greater than the number of sidelobes approximated in the far field. While a single term approximates the peak of the beam, a two-term expansion approximates the entire main beam, while maintaining simple functional relationships, thus providing simple beam representations for analysis purposes. It also provides a theoretical, infinite-aperture antenna with a single sidelobe, which is analogous to a theoretical antenna pattern without sidelobes being an infinite Gaussian antenna. Real-world applications involve the assessment of truncation and its effects on the one-sidelobe antenna pattern. The same principles apply to higher-order partial sums, but as each term

is added, the aperture field series approaches the one being approximated, and truncations, for whatever reason, approach the actual antenna dimensions. The theory of field expansions of large-aperture antennas was developed by Bogush and Elkins, and described as an approximate theory within the constraints of the Kirchhoff diffraction formulation. This theory is reviewed, but placed within the context of a generalization of the Gaussian beam approximation. Sufficient examples are provided to demonstrate the usefulness of the theory in these delineations, as well as the derivation of a Gaussian form of the radar equation, which is described in the next chapter. Appendix A contains supporting antenna and mathematical material.

### *The Rectangular Antenna*

We will now let the aperture distribution for the rectangular antenna of Figure 3.29 be separable, with  $f(\xi\eta) = f(\xi)y(\eta)$ ; the first step is to let  $f(\xi)$  be expanded in the series

$$f(\xi) = \sum_{n=0}^{\infty} C_n \psi_n(\alpha\xi) \quad (3.242)$$

where  $\alpha$  is a scaling factor and  $\psi_n(\alpha\xi)$  is given by

$$\psi_n(\alpha\xi) = H_n(\alpha\xi) \exp(-\alpha^2\xi^2/2) \quad (3.243)$$

Here,  $H_n$  and  $(\alpha\xi)$  are the Hermite polynomials:

$$\begin{aligned} H_0(\alpha\xi) &= 1.0 \\ H_1(\alpha\xi) &= 2\alpha\xi \\ H_2(\alpha\xi) &= 4\alpha^2\xi^2 - 2 \\ &\vdots \\ &\vdots \\ &\vdots \\ H_n(\alpha\xi) &= 2\alpha\xi H_{n-1}(\alpha\xi) - (2n - 2)H_{n-2}(\alpha\xi) \end{aligned} \quad (3.244)$$

The products of the Gaussian function and the Hermite polynomials are called *Hermite-Gaussian functions*. The aperture distribution of Equation (3.242) is also referred to as the *aperture field expansion*. Hermite functions are plotted in Figure 3.32. Note that even-function distributions will require odd-ordered Hermite functions, with even-ordered functions corresponding to odd distribution. A mixed presence indicates asymmetry in the fields.

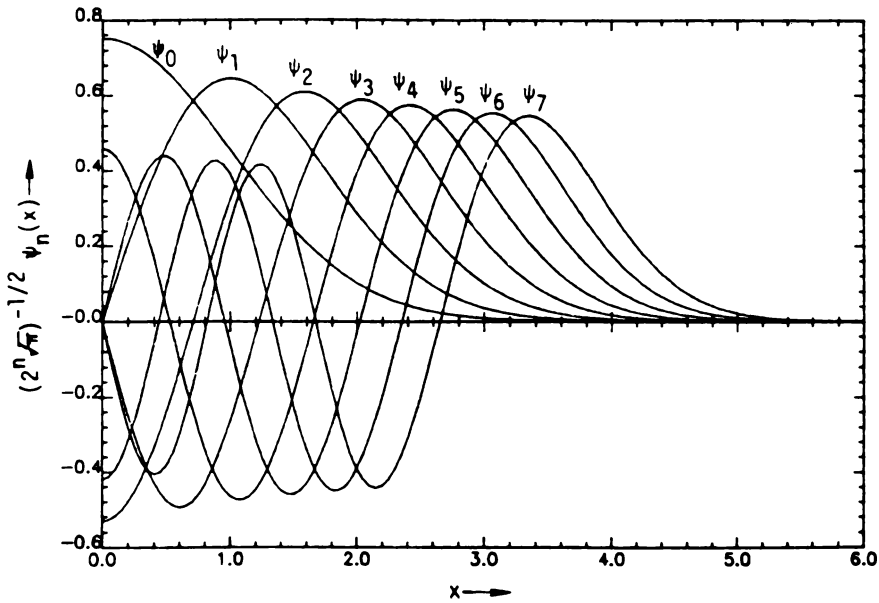


**Figure 3.32** Normalized Hermite-Gaussian Functions. (From Bogush and Elkins)

The constant  $C_n$  of the aperture field expansion, from the orthogonality relationship of the Hermite-Gaussian functions is

$$C_n = \frac{\alpha}{2^n n! \pi} \int_{-1/2}^{+1/2} f(\xi) \psi(\alpha \xi) d\xi \quad (3.245)$$

The effectiveness (or merit) of the approximation of Equation (3.242) for  $f(\xi)$  depends on choice of scale. Choice of a small  $\alpha$  gives a Gaussian function with half-power width that is much larger than the aperture, while choice of a very large  $\alpha$  gives a Gaussian function with half-power width much smaller than the aperture. The scaling factors have been selected in two ways. In the first and general approach, the scale is optimized so that the radiated power of the aperture best matches the radiated power of the actual distribution. Let the radiated power of the one-dimensional aperture distribution be

$$P = C \int_{-1/2}^{+1/2} f^2(\xi) d\xi \quad (3.246)$$

where  $C$  is a constant of proportionality. If we consider the  $N$ th partial sum representation of  $f(\xi)$ , we have

$$P_N(\alpha) = C \int_{-1/2}^{+1/2} \left[ \sum_{n=0}^{\infty} C_n \psi_n(\alpha \xi) \right]^2 d\xi \quad (3.247)$$

$P_n(\alpha)/C$  is plotted in Figure 3.33 for  $f(\xi) = 1.0$ , the uniform distribution. It has been found for this and other common aperture distributions that the maximum corresponding to the largest choice of scale results in a qualitatively best structured description of the sidelobe structure in the far field. The extremes of  $P_n(\alpha)$  satisfy the following:

$$\int_{-\infty}^{+\infty} f(x) \psi_{N-1}(\alpha x) dx \int_{-\infty}^{+\infty} f(y) \psi_{N+1}(\alpha y) dy = 0 \quad (3.248)$$

for  $f(x)$  as an odd function, and

$$\int_{-\infty}^{+\infty} f(x) \psi_N(\alpha x) dx \int_{-\infty}^{+\infty} f(y) \psi_{N+2}(\alpha y) dy = 0 \quad (3.249)$$

for  $f(x)$  as an even function. Tables of optimal scale factors and corresponding series coefficients for cosine, truncated Gaussian, and Taylor aperture distribution are provided in Appendix A. The first four optimal Hermite-Gaussian approximations to a cosine aperture distribution, chosen for illustrative purposes, are plotted in Figure 3.34. A second choice of scaling factor pertains only to one-term expansions or Gaussian equivalents, where  $\alpha$  is chosen to yield a given far-field beamwidth.

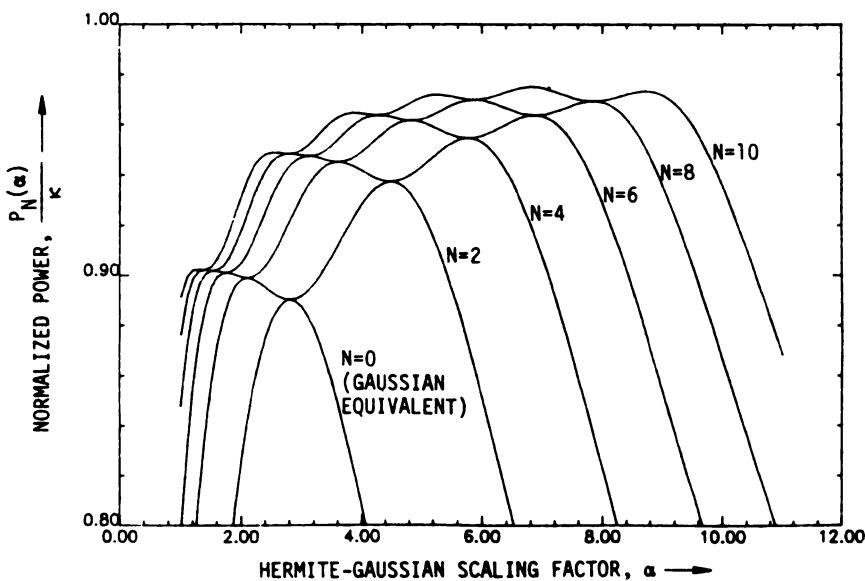


**Figure 3.33** Normalized Power Radiated by a Truncated Hermite-Gaussian Series Approximating a Uniform Aperture Distribution (From Bogush and Elkins)

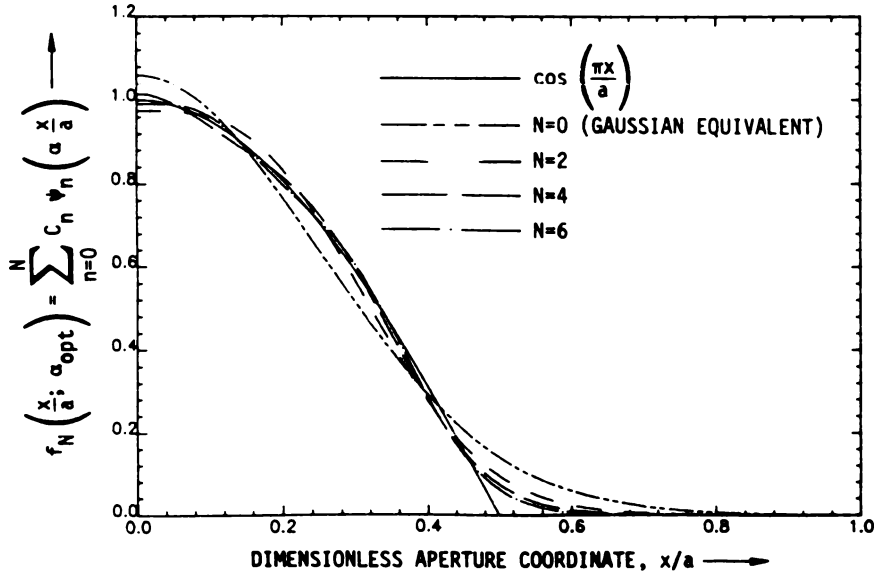


**Figure 3.34** First Four Optimal Hermite-Gaussian Approximations to a Cosine Aperture Distribution. (From Bogush and Elkins)

The far-field diffraction integral from Appendix A applies with the aperture distribution given by the Hermite-Gaussian expansion of (3.242). The Fourier transforms of the aperture distribution can be obtained by treating each term separately, and applying the frequency differentiation theorem of Fourier transform theory. Proceeding, we obtain

$$\begin{aligned}
 H_0(\alpha\xi) \exp(-\alpha^2\xi^2/2) &\leftrightarrow j^0\sqrt{2\pi/\alpha} \, H_0(u/\alpha) \exp(-u^2/\alpha^2) \\
 H_1(\alpha\xi) \exp(-\alpha^2\xi^2/2) &\leftrightarrow j^1\sqrt{2\pi/\alpha} \, H_1(u/\alpha) \exp(-u^2/\alpha^2) \\
 &\vdots \\
 &\vdots \\
 &\vdots \\
 H_n(\alpha\xi) \exp(-\alpha^2\xi^2/2) &\leftrightarrow j^n\sqrt{2\pi/\alpha} \, H_n(u/\alpha) \exp(-u^2/\alpha^2)
 \end{aligned}
 \tag{3.250}$$

so that

$$C_n y_n(\alpha\xi) \leftrightarrow \sqrt{2\pi/\alpha} \, j^n \, C_n \psi_n\left(\frac{\mu}{\alpha}\right)
 \tag{3.251}$$

and

$$D_n \psi_n(\beta \eta) \leftrightarrow \sqrt{2\pi/\beta} j^n D_n \psi_n\left(\frac{v}{\beta}\right) \quad (3.252)$$

where  $D_n$  is the  $n$ th coefficient of the expansion of  $g(\eta)$  and  $\beta$  is the associated scaling factor. The far-field expansion can be written as

$$E(r, u, v) = j \frac{kab}{2\alpha\beta r} (1 + \cos\theta) \exp(-jkr) \left( \sum_{n=0}^{\infty} j^n C_n \psi_n\left(\frac{u}{\alpha}\right) \right) \left( \sum_{m=0}^{\infty} j^m D_m \psi_m\left(\frac{v}{\beta}\right) \right) \quad (3.253)$$

The aperture fields are directly transformable, and thus the aperture distribution, except for multiplicative constants, is its own Fourier transform. The choice of the form of (3.242) allows for this occurrence. As a result, in this approximate theory, the diffraction integral has been replaced by the field expansions.

Far-field plots are provided for the cosine aperture distributions in Figures 3.35 and 3.36. The examples demonstrate a structured property, where sidelobes are added sequentially as more terms in the series are utilized. This property is attributed to the optimization procedure that was chosen.

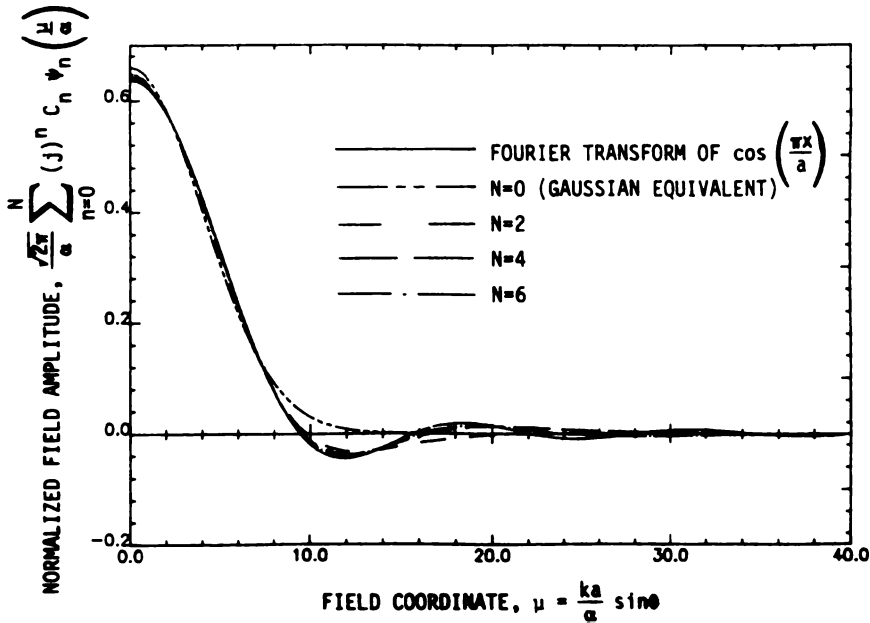


**Figure 3.35** First Four Optimal Hermite-Gaussian Approximations to the Fraunhofer Field of a Cosine Aperture Distribution. (From Bogush and Elkins)



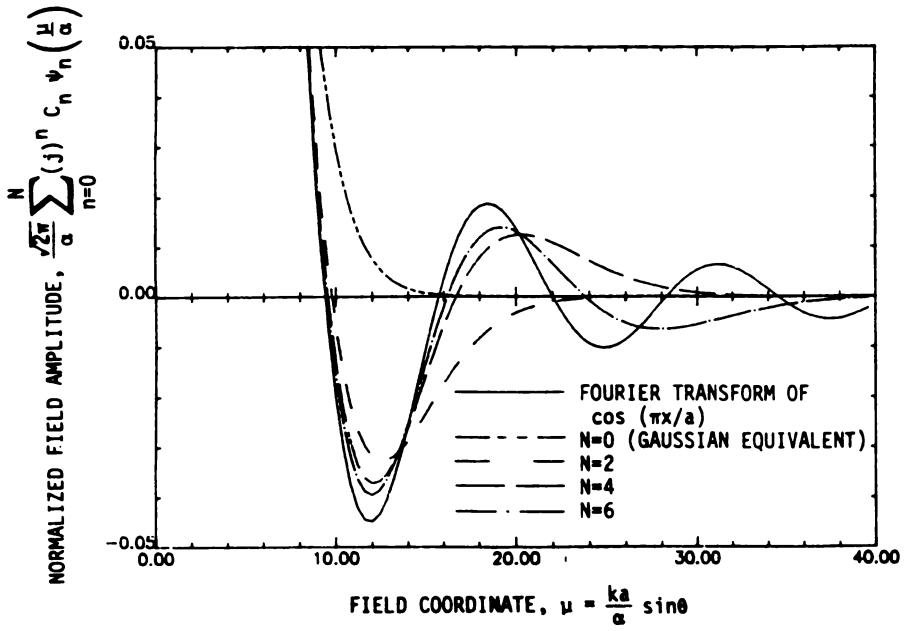


Figure 3.36 Detail of Sidelobe Region from Figure 3.35. (From Bogush and Elkins)

In the near fields, introduction of the complex scaling factors yields

$$\rho = \sqrt{1 + j \frac{ka^2}{\alpha^2 z}}, \quad \gamma = \sqrt{1 + j \frac{kb^2}{\beta^2 z}} \quad (3.254)$$

the two field variables:

$$v = \frac{k \alpha \rho x}{\alpha z}, \quad \nu = \frac{k b \gamma y}{\beta z} \quad (3.255)$$

The transform pair:

$$H_n(\rho \xi) \exp(-\xi^2/2) \leftrightarrow \sqrt{2\pi} j^n H_n(\rho v) \exp(-v^2/2) + O[\rho^{n-2} - \rho^n] \quad (3.256)$$

leads to

$$\begin{aligned} E(x, y, z) &\approx \frac{1}{2} \left( \frac{\rho \gamma a b}{\alpha \beta} \right) \left( j \frac{k}{r} \right) \left( 1 + \frac{z}{r} \right) \exp(-jkr) \exp \left[ -jk \frac{(x^2 + y^2)}{2z} \right] \\ &\times \sum_{n=0}^{\infty} C_n j^n H_n(\rho v) \exp(-v^2/2) \\ &\times \sum_{m=0}^{\infty} D_m j^m H_m(\gamma \nu) \exp(-\nu^2/2) \end{aligned} \quad (3.257)$$

As range  $z$  increases, the scales  $\rho$  and  $\gamma$  approach unity, and the higher-order terms become negligible. As  $z \rightarrow \infty$ , Equation (3.257) reduces to the far-field result of (3.253). In the near field, its accuracy depends on the complex parts of  $\rho$  and  $\gamma$ . Equation (3.254) suggests that large values should be chosen for the aperture scales  $\alpha$  and  $\beta$ . This does not appear to be a very restrictive requirement, as numerical experiments on various aperture distributions have given good results throughout the near fields, for optimal aperture scales. The Gaussian character of the near fields can be seen in the form of Equation (3.257).

Examples of Fresnel field computations are provided in Figure 3.37, where the cross-range dimension is units of  $X = x/a$ , and the down-range dimension is in units of  $g = z\lambda/a^2$ . Amplitude is in decibels, covering a total range of about 50 dB. The structured property of the fields is evident throughout the near-fields, with the results obtained using a five-term expansion, which compares well with numerical integration results.

The zero-order approximation, plotted in Figure 3.37 for the cosine aperture distribution, is referred to as a Gaussian equivalent because it provides first-order estimates for the aperture, Fresnel, and far fields in a very simple Gaussian form. A formula useful for Fresnel region computations, especially when power computations such as radar range equation calculations are involved, is

$$|E_0(x,0,z)| = \frac{C_0^2}{2}(1 + \chi^2)^{-1/2} \exp\left[-\frac{1}{2}\frac{\alpha^2\chi^2}{\alpha^2(1 + \chi^2)}\right] \frac{z}{r}\left(1 + \frac{z}{r}\right) \quad (3.258)$$

where  $C_0$  is the lead term in the Hermite function expansion of  $f(\xi)$ , and

$$\chi = \frac{\alpha^2 z}{ka^2} \quad (3.259)$$

At large ranges,  $z/r$  approaches unity and Equation (3.258) approaches the zero-order expression for the far fields. In the near field, Equation (3.258) is a Gaussian, modified by the factor  $z/r(1 + z/r)$ . Expanding the factors in a power series reveals that the Gaussian character dominates as long as

$$\frac{\alpha^2 z^2}{a^2(1 + \chi^2)} \gg 1.0 \quad (3.260)$$

Because this condition is nearly always satisfied by real antennas, any antenna with a far field well approximated by a Gaussian can be expected to have a Fresnel field that is also well approximated by a Gaussian. This observation can also be interpreted to mean that once a beam is approximated by a Gaussian function, this approximation is extended to the near and aperture fields through Equation

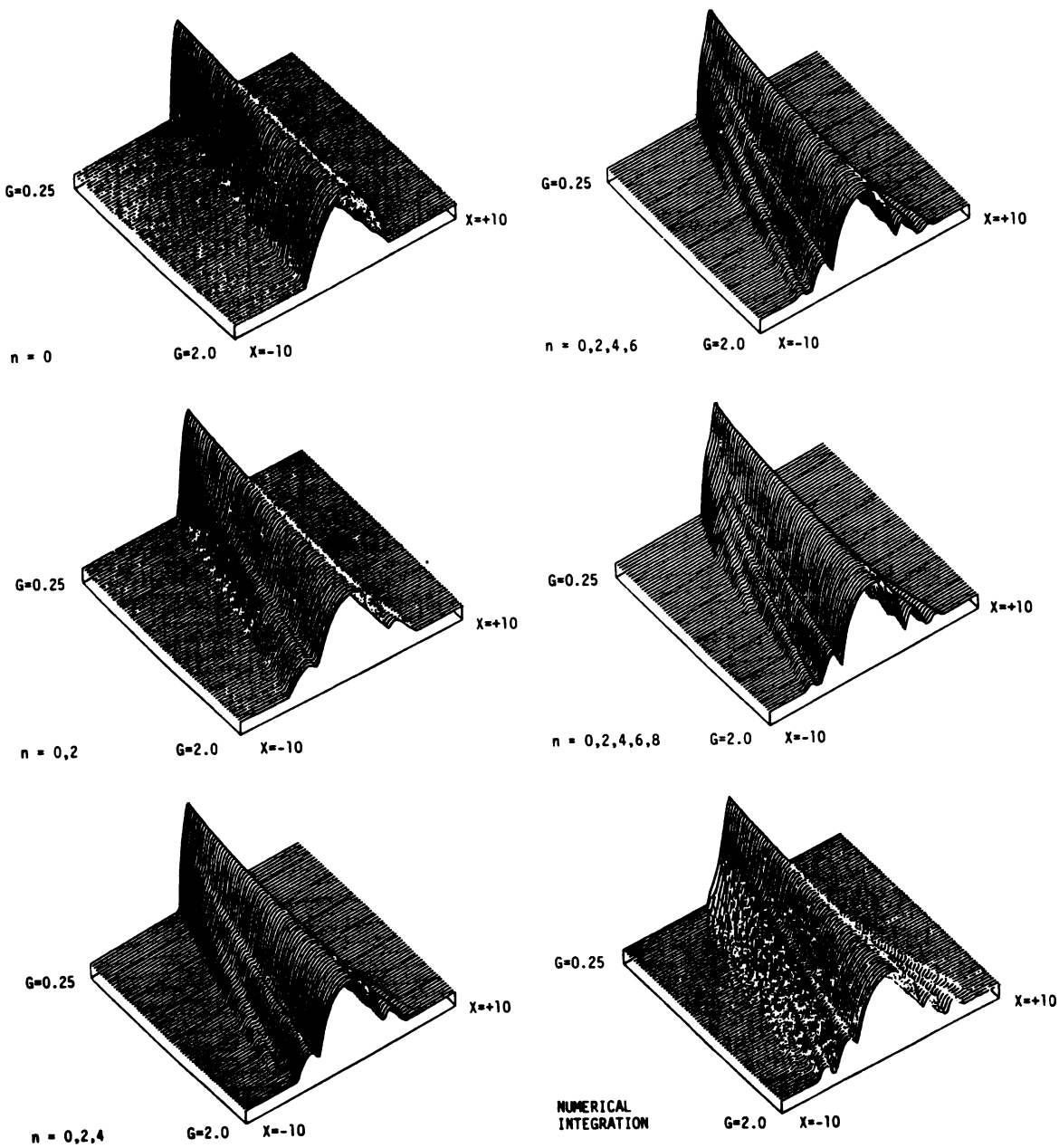


**Figure 3.37** Fresnel Region Field Distributions for a Cosine Aperture Distribution. (From Bogush and Elkins)

(3.258). For this reason, it is appropriate to designate the fields as Gaussian equivalents of the approximated fields.

When applying the Gaussian beam approximation, it is convenient to choose the scaling factor by setting the first partial sum pattern equal to

$$F(\theta) = \exp \left[ -2 \ln 2 \left( \frac{\theta}{\theta_3} \right) \right] \quad (3.261)$$

which is the normal Gaussian beam representation. This amounts to

$$\frac{1}{2} \left( \frac{ka\theta}{\alpha} \right)^2 = -2 \ln 2 \left( \frac{\theta}{\theta_3} \right) \quad (3.262)$$

which yields

$$\alpha = \frac{\pi}{\sqrt{\ln 2}} \left( \frac{a}{\lambda} \right) \quad (3.263)$$

Substitution of this result into Equation (3.258) extends the Gaussian beam approximation to the near and aperture fields because of the convergence properties of the near-field formula when  $z > 0$  and  $z \rightarrow \infty$ . The approximation applies to the fields in the vicinity of the beam axis for all ranges. The merit of the approximation depends on the aperture distribution and requires validation by other means (such as a numerical integration of the diffraction integrals). For higher-order partial sums, the choice of a power-dependent (rather than beamwidth-dependent) scaling factor will yield total far-field beam representations for two or more terms in the field expansions, with the accompanying structuring of the sidelobes.

For the rectangular antenna, and in a similar way for the circular antenna (to be discussed next), if we refer to the structuring of the antenna patterns shown in the figures, the following procedure for use of the field expansions is evident:

1. Given an antenna with beamwidth  $\theta_3$ , the Gaussian beam is given by Equation (3.261). The field describes the peak of the beam, and the remaining angular dependence is infinite in extent.
2. The near fields are found by computing  $\alpha$  from Equation (3.263), then computing  $E(x, 0, z)$  from (3.258).
3. The Gaussian approximation of the aperture distributions is found from Equation (3.242), using  $\alpha$  of Equation (3.263). Like the far fields, the distributions for the aperture and near fields are infinite in cross-range extent, confining their usefulness to regions about the beam axis. The lower the sidelobes, the better the approximation, and the larger the cross-range extent becomes.
4. The entire far-field beam may be approximated using a two-term expansion. For even-function distributions, the first two terms contain the Hermite polynomials  $H_0(x) = 1.0$  and  $H_2(x) = 4x^2 - 2$ . Scaling factors and

series coefficients are given in Appendix A for a number of aperture distributions. The fields are found from Equations (3.242) (aperture distribution), (3.257) (near fields) and (3.253) (far fields). A one-sidelobe, far-field antenna pattern results, infinite in cross-range extent. The approximation is useful for beam descriptions, including one for the vicinity of the first null.

5. For higher-order structured antenna patterns, use the procedure of step 4, with the addition of terms in the series. The procedures provided for computing the optimal scale factors and series coefficients can be applied if the tabulated values of Appendix A are incomplete.

### *The Circular Antenna*

Gaussian field expansion for circular antennas are obtained in the same way as for rectangular antennas, with two procedural changes: Hankel transforms are encountered instead of Fourier transforms, and Laguerre, not Hermite, polynomials are used. The derivations are considerably simpler than those developed for the rectangular apertures.

Circular aperture and coordinate systems are shown in Figure 3.31. We let the aperture distribution  $f(\rho, \phi') = f(\rho)$  (with  $\rho$  normalized,  $\zeta = \rho/\alpha$ ) to yield the distribution  $f(\zeta)$ . Now we consider the Laguerre-Gaussian function  $\psi_n(\zeta)$ :

$$\Psi_n(\zeta) = L_n(\zeta^2) \exp(-\zeta^2/2) \quad (3.264)$$

where  $L_n(\zeta^2)$  is the  $n$ th Laguerre polynomial, and

$$\begin{aligned} L_0(\zeta^2) &= 1 \\ L_1(\zeta^2) &= -\zeta^2 + 1 \\ L_2(\zeta^2) &= \zeta^4 - 4\zeta^2 + 2 \end{aligned} \quad (3.265)$$

$$L_{n+1}(\zeta^2) = (2n + 1 - \zeta^2)L_n(\zeta^2) - n^2L_{n-1}(\zeta^2)$$

We now let the aperture field be expanded in a series of Laguerre-Gaussian functions:

$$f(\zeta) = \sum_{n=0}^{\infty} C_n \Psi(\alpha \zeta) \quad (3.266)$$

where, as before,  $\alpha$  is a scaling factor. The coefficients  $C_n$  follow from the orthogonality relationship for the Laguerre-Gaussian functions:

$$C_n = \frac{2\alpha}{n!} \int_0^{\infty} \zeta f(\zeta) \exp\left(-\frac{\alpha^2 \zeta^2}{2}\right) L_n(\alpha^2 \zeta^2) d\zeta \quad (3.267)$$

Equation (3.266), with coefficients given by (3.267), is the aperture field expansion.

If we let  $u = kd \sin\theta$ , placement of the aperture distribution of Equation (3.266) into the diffraction integral

$$\begin{aligned} E(r, \theta, \phi) &= j \frac{C_n k a^2}{2r} \exp(-jkr)(1 + \cos\theta) \\ &\times \int_0^{\infty} \exp\left(-\frac{\alpha^2 \Omega^2 \zeta^2}{2}\right) L_n(\alpha^2 \zeta^2) J_0(u\zeta) \zeta d\zeta \end{aligned} \quad (3.268)$$

where

$$\Omega^2 = \left(1 + j \frac{ka^2}{r\alpha^2}\right) \quad (3.269)$$

Using the Hankel transform pair deduced from Gradshtegn and Ryzhik, we have

$$\exp\left[-\left(\frac{\alpha^2 \Omega^2}{2}\right)\right] L_n(\alpha^2 \zeta^2) \xleftrightarrow{h} \exp\left[-\left(\frac{u^2}{2\alpha^2 \Omega^2}\right)\right] L_n\left[\frac{u^2}{\alpha^2 \Omega^2 (2 - \Omega^2)}\right] \quad (3.270)$$

The near fields of the circular aperture become

$$\begin{aligned} E(r, \theta) &= j \frac{k}{2r} \left(\frac{d}{\alpha \Omega}\right)^2 \exp(-jkr)(1 + \cos\theta) \\ &\times \sum_{n=0}^{\infty} C_n (1 - 2\Omega^{-2})^n L_n\left[\frac{u^2}{\alpha^2 \Omega^2 (2 - \Omega^2)}\right] \exp\left[-\frac{u^2}{2\alpha^2 \Omega^2}\right] \end{aligned} \quad (3.271)$$

In the far field,  $r \rightarrow \infty$ , and  $\Omega \rightarrow 1.0$ , so Equation (3.271) reduces to:

$$E(r, \theta) = j \frac{k}{2r} \left( \frac{d}{\alpha} \right) \exp(-jkr)(1 + \cos\theta) \times \sum_{n=0}^{\infty} (-1)^n C_n L_n \left( \frac{u^2}{\alpha^2} \right) \exp \left( -\frac{u^2}{2\alpha^2} \right) \quad (3.272)$$

The truncation of either field expansion results in a structured approximation of the fields, identical to those obtained for the rectangular antenna. The optimization procedure likewise follows the previous derivations, where the scaling factor is determined by optimizing the power radiated by the  $n$ th partial sum distribution for partial sums exceeding one term. For single terms, or when the Gaussian beam approximation is applied, the scaling factor is chosen to yield the far-field beamwidth; then, as before, the aperture and near fields are also approximated.

For power optimization, the power radiated by the circular antenna is

$$P = q \int_0^{\infty} \zeta [f(\zeta)]^2 d\zeta \quad (3.273)$$

For the  $n$ th partial sum, the radiated power is

$$P_N = q \int_0^{\infty} \zeta \left[ \sum_{n=0}^{\infty} C_n(\alpha) \phi_n(\alpha\zeta) \right]^2 d\zeta \quad (3.274)$$

The maximum of  $P_n$  will occur when  $C_{N+1} = 0$ , or when

$$\int_0^{1/2} x \phi(\alpha x) f(x) dx = 0 \quad (3.275)$$

repeating  $\phi_n(\alpha\xi) = L_n(x^2) \exp(-x^2/2)$ . Equation (3.275) will require numerical integration. Optimal scale factors and series coefficients for truncated Gaussian and cosine-distributed circular antennas are tabulated in Appendix A.

Figure 3.38 shows optimal approximations to a cosine aperture distribution for one-, two-, three-, and four-term series. Figure 3.39 shows those same approximations in the far field. The approximations converge rapidly toward a good representation of the main lobe as terms are added to the series. This occurs because the Gaussian nature of the approximating functions is matched to the Gaussian nature of the far-field distribution. Figure 3.40 details the sidelobe region of the far field. We see that the number of sidelobes represented in the approximation is one less than the number of terms in the approximating series. This parallels the structured behavior of rectangular antenna distributions. Figure 3.41 illustrates a four-term approximation of the Fresnel field magnitude for a cosine-distributed antenna. That such detail of structure can be reproduced from a series involving only elementary functions and readily calculated parameters underscores the usefulness and versatility of the Gaussian field expansion.

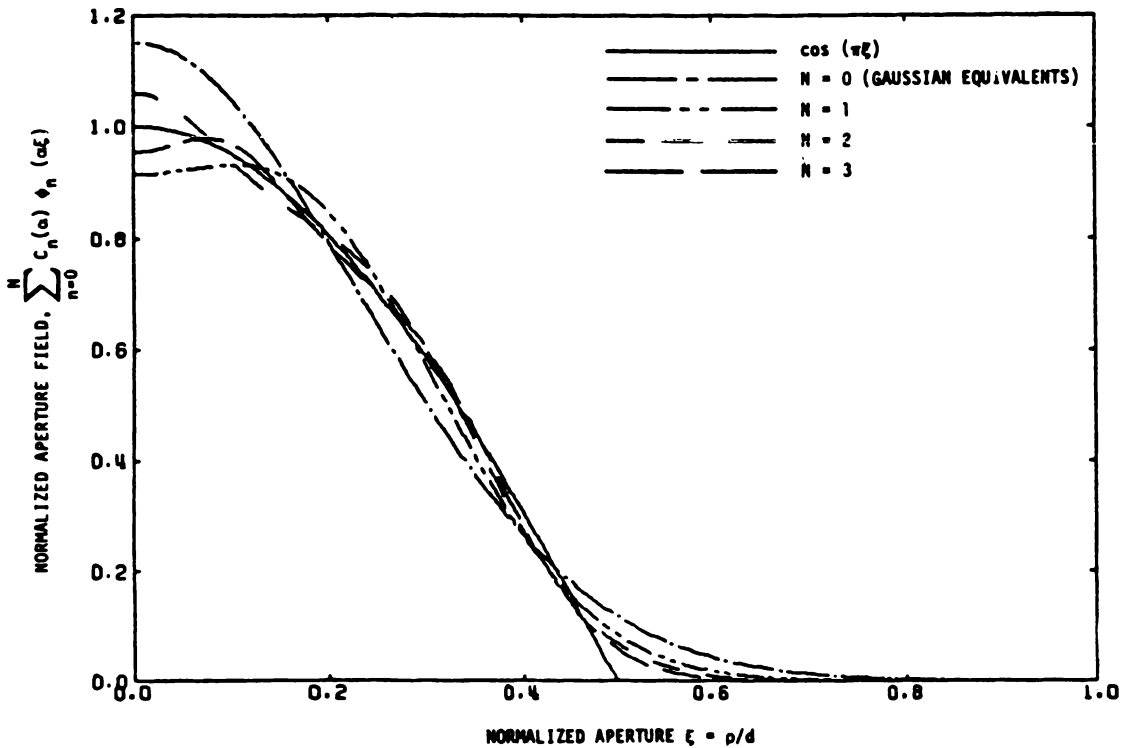


Figure 3.38 First Four Optimal Laguerre-Gaussian Approximations to a Cosine Aperture Distribution. (From Elkins, Bogush, and Jordan)

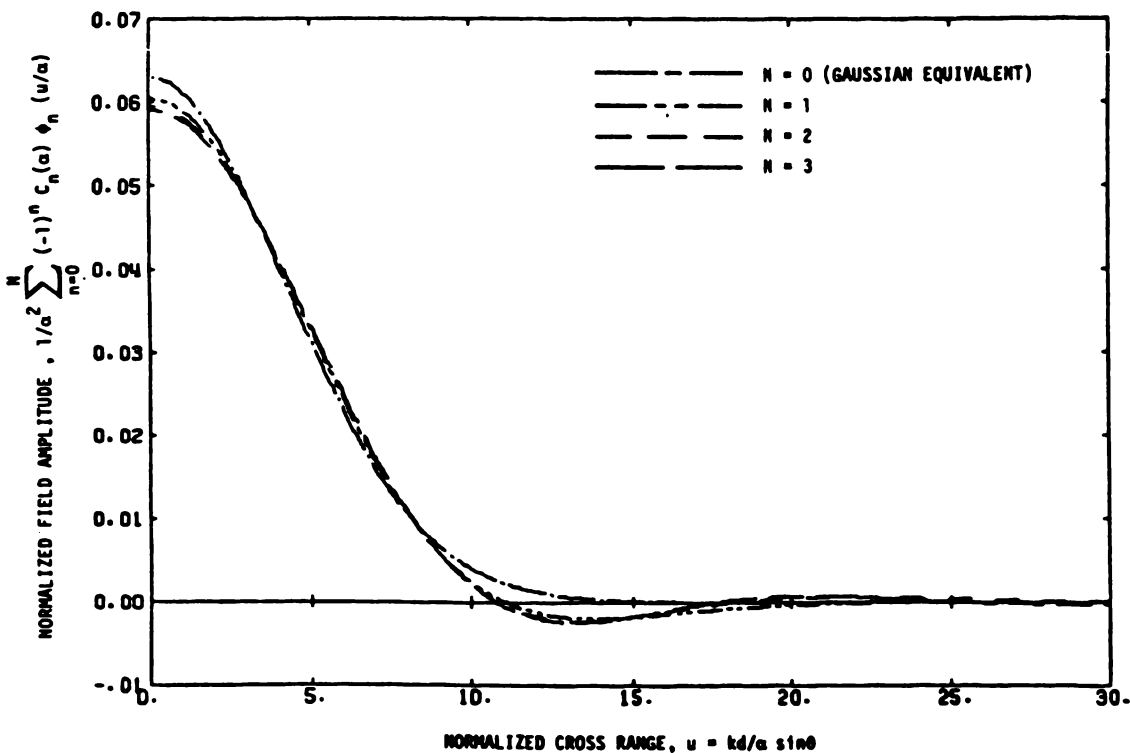


Figure 3.39 First Four Optimal Laguerre-Gaussian Approximations to the Far Field. (From Elkins, Bogush, and Jordan)



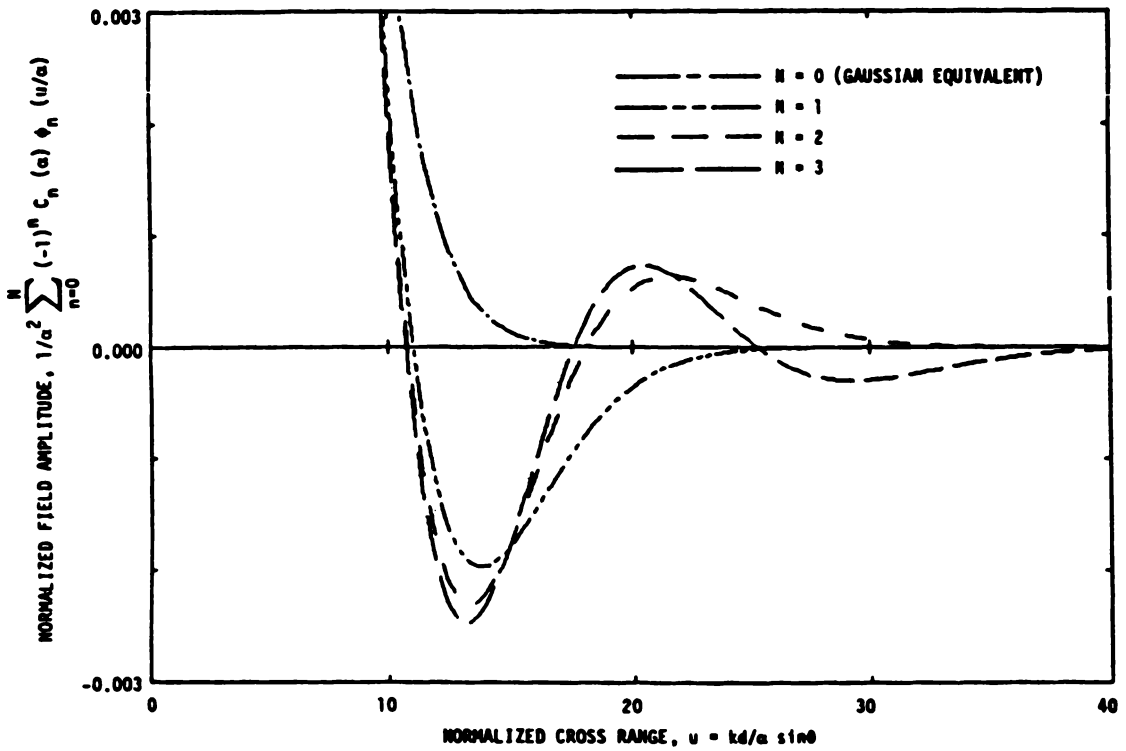


Figure 3.40 Detail of Sidelobes Region. (From Elkins, Bogush, and Jordan)

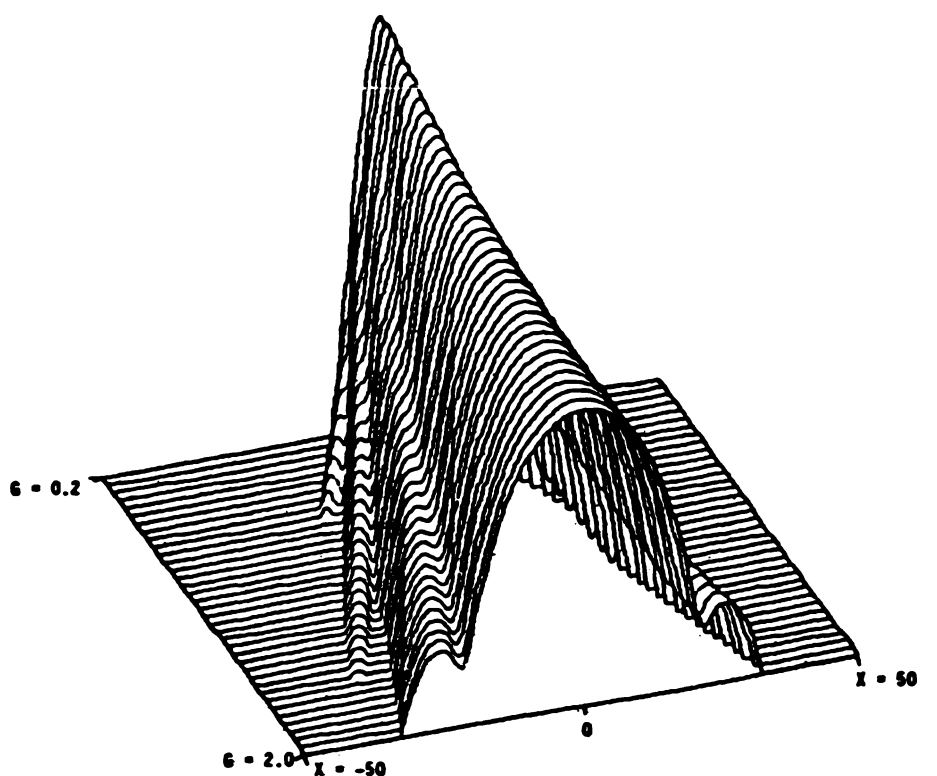
The Gaussian equivalent (or one-term partial sum) is a reduction of the near-field expansion for  $N = 0$ . The result is identical to Equation (3.258) for the fields of the square antenna, with  $d$  (the diameter of the aperture) replacing the dimension  $a$ . The result of this derivation is:

$$|E(r, \theta)| = \frac{k(\phi/\alpha)^2}{r} (1 + \chi^2)^{-1/2} \exp\left[-\frac{u^2}{2\alpha^2(1 + \chi^2)}\right] \quad (3.276)$$

where  $\chi = kd^2/\alpha^2 r$  is the Gaussian equivalent. When used for near-field estimates of specific antennas, it is convenient to choose  $\alpha$  to approximate the far-field beamwidth. Then, as with the rectangular antenna, Equation (3.276) describes the fields in the vicinity of the beam axis for the aperture, near, and far fields, thereby extending the usefulness of Gaussian beam approximation. This result and the comparable Equation (3.258) are useful for range equation calculations when the near fields are encountered.

### The Infinite Gaussian Antenna

Three antennas are now given special consideration, and all are special cases of the general Gaussian field expansions. We will consider the infinite Gaussian an-



NOTE: CROSS RANGE IS IN UNITS OF  $x/a$ , DOWN RANGE IS IN UNITS OF  $x\lambda/a^2$ . AMPLITUDE IS IN dB, WITH THE FLOOR SET AT -50 dB.

**Figure 3.41** Fresnel Field Distributions for a Circular Cosine Aperture Distribution. (From Elkins, Bogush, and Jordan)

tenna, the first term of the field expansion; the truncated Gaussian; and the truncated second partial sum, a special class of an antenna approaching a single-sidelobe pattern. Square antennas are considered, with their possible generalization to other shapes.

The derivation of the Gaussian field expansion is primarily dependent on infinite limits of integration. The transformations of the Gaussian functions are kept in the bounds of self-reciprocity, where the field distributions are their own Fourier transforms. As a result, field quantities (for all partial sums) are approximate, and theoretically represent antennas that are of infinite extent, which are academically interesting, but not physically realizable. However, as the number of terms in the series increases, the aperture fields converge to the actual distribution and, in the limit as  $N \rightarrow \infty$ , is representative of a real-world antenna.

When  $n$  is small, aperture dimensions referenced to some low value (i.e., the width between the 30 dB points of  $n$ th partial sum aperture field) are larger than the aperture described. Particularly, when antenna sidelobes are of moderate depth (e.g., 20 to 30 dB), one-term representations of the aperture fields are characterized by high values outside of the aperture extent. In general, as the sidelobes decrease,

aperture distributions become tapered to higher degrees and the field expansions converge more rapidly to the aperture fields.

We illustrate this, while describing the infinite Gaussian antenna and its usefulness, as we consider an aperture with distribution  $f(\xi) f(\eta)$ . Let

$$f(x) = \exp \left[ -2 \ln 2 \left( \frac{x}{a_3} \right)^2 \right] \quad (3.277)$$

where  $a_3$  is the width of the Gaussian function at the 3 dB points. Now we introduce an arbitrary scale  $a$ , an aperture dimension in a Gaussian equivalent representation. Then, with  $\xi = x/a$

$$f(\xi) = \exp \left[ -2 \ln 2 \left( \frac{a}{a_3} \right)^2 (\xi)^2 \right] \quad (3.278)$$

which is an infinite Gaussian antenna distribution normalized to a scale  $a$  and expressed in terms of the 3 dB-width  $a_3$ . Note that  $f(\epsilon) = 0.707$  when  $x = a_3/2$ . This choice of aperture distribution is convenient when comparisons are made to a finite antenna of size  $a$ . The physically realizable antenna is of finite dimensions; the Gaussian representation is not, but it is scaled to the real quantity  $a$ .

In the Gaussian equivalent representation, the far-field beam is extended to the aperture fields, but is in general confined to a region about the beam axis, the extent of which depends on the particulars of the antenna. Normally when infinite antennas are described, a variable convenient for transferability is chosen, (i.e.,  $f(x) = \exp(-x^2/2)$ ), requiring scaling for specific applications. Equation (3.278) is scaled, but care must be taken in its use to assure proper use of units and dimensions.

Gaussian aperture distributions are plotted in Figure 3.42 for  $1 < a/a_3 < 6$ . Clearly, when viewed in this fashion, representations of antennas for  $a/a_3$  greater than about 3.5 can be expected to yield effective field representations for  $n$ -term expansions of small order. Plots of infinite Gaussian antennas are contained in Figure 3.37 and Figure 3.41, where the near fields of rectangular and circular antennas are displayed.

The infinite Gaussian antenna is sometimes referred to as a limiting, unrealizable antenna, without sidelobes.

### *The Truncated Gaussian Antenna*

When an infinite Gaussian antenna is truncated, it is physically realizable and may be described by an aperture distribution of the form of Equation (3.278), which

is plotted in Figure 3.42. Classical solutions for the antenna pattern may be obtained directly from the diffraction integrals. The results are expressed as complex error functions, which, although readily derived, are difficult to apply. Therefore, numerical integration of the diffraction integral or the use of Fourier transform methods is advocated.

The Gaussian field expansions provide an alternate solution to this classical antenna problem. Appendix A contains optimal scaling factors and series coefficients for truncated Gaussian antennas of rectangular and circular geometries. An example of pattern computations is displayed in Figure 3.42 for  $a/a_3 = 2.0$ . The structuring of the antenna pattern is evident as terms are added to the series.

Several examples of the properties of the infinite and truncated Gaussian antenna are shown in Figure 3.43 and Figure 3.44. The beamwidth comparison shows compatibility between the infinite and truncated antenna for  $a/a_3 > 3.0$ . As  $a/a_3 > 0$  for the infinite antenna, the beamwidth tends to zero, while large ratios for the finite antenna reduce to the the uniform aperture, and  $\theta_3 (a/\lambda) > 0.88$ . When Gaussian equivalents are used, adjusting far-field beamwidths yields large aperture sizes for  $a/a_3 < 3.0$ .

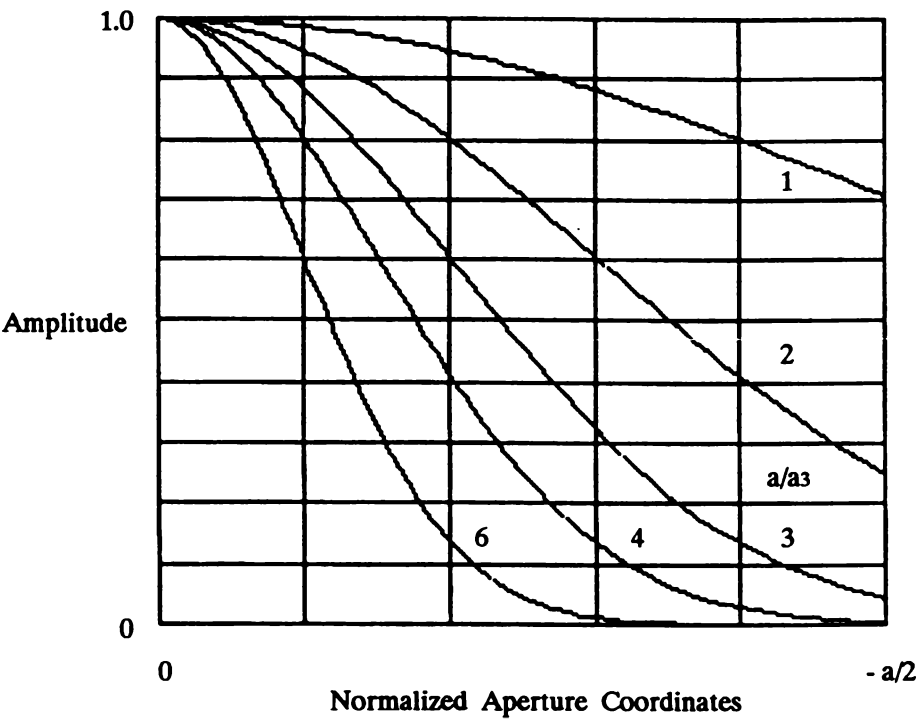


Figure 3.42 Gaussian Antenna Distributions

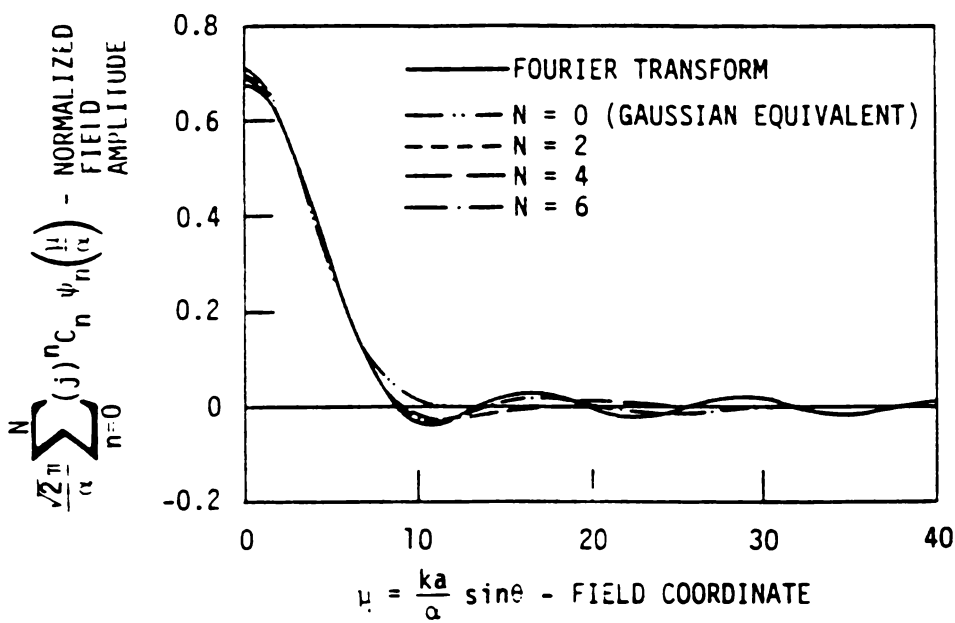


Figure 3.43 First Four Optimal Hermite-Gaussian Approximations to the Far Field. (From Bogush and Elkins)

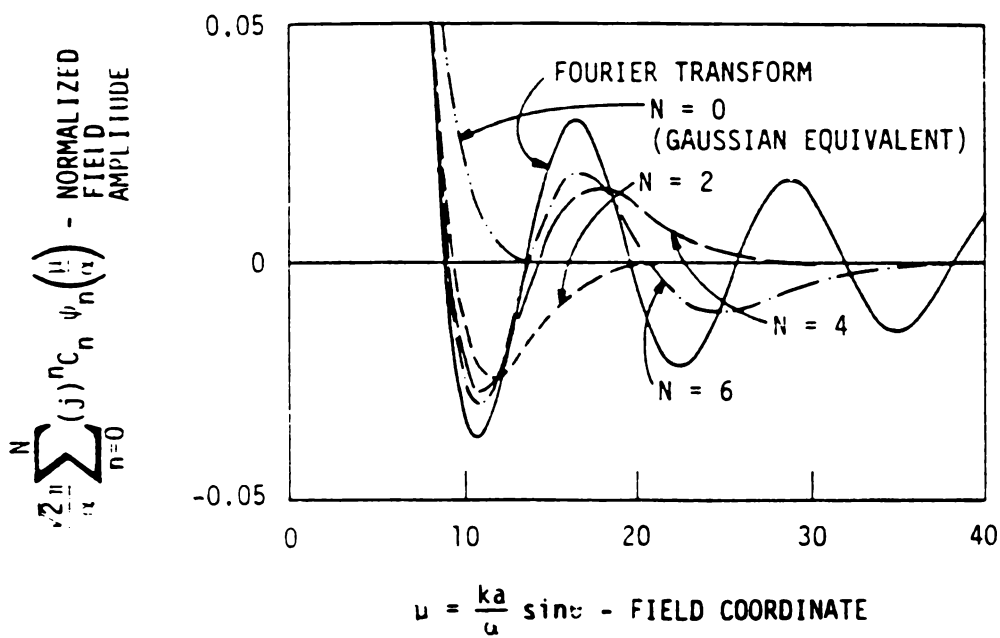


Figure 3.44 Fields of a Truncated Gaussian Antenna,  $a/a_3 = 2.0$ . (From Bogush and Elkins)

An interesting result is plotted in Figures 3.45 and 3.46, where beamwidth and sidelobe relationships are displayed for the optimal Taylor, truncated Gaus-

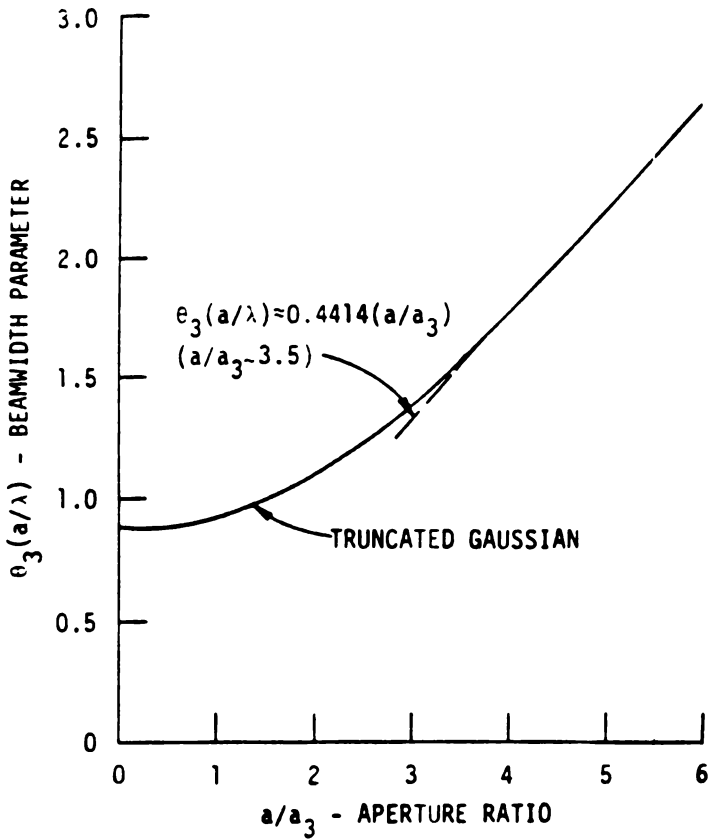
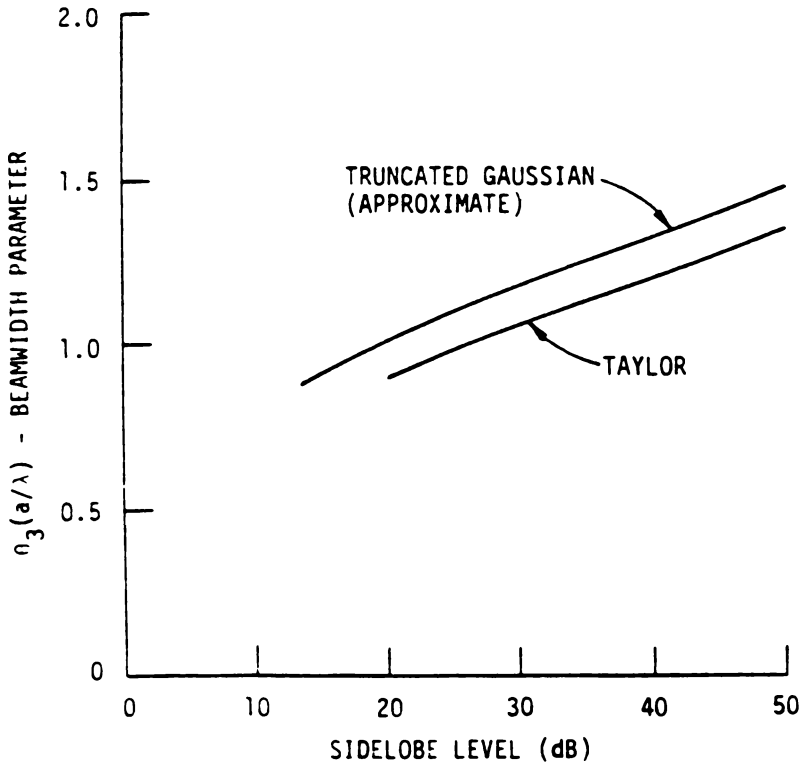


Figure 3.45 Beamwidth of the Truncated Gaussian Antenna. (From Bogush and Elkins)

sian, and other antennas. The Taylor distribution clearly yields optimal beamwidth and sidelobe values. The truncated Gaussian distributions are not optimal, but follow similar increases in beamwidths as sidelobe levels decrease. Other antennas deviate drastically from the optimal to negate their usefulness, except, perhaps, when subjected to severe constraints.

In the design of large aperture antennas, allowing for sidelobe and beamwidth degradation due to fabrication and design practices is not uncommon. For example, a 25-dB sidelobe requirement may lead to the use of a 30-dB Taylor aperture distribution. The antenna that results is not necessarily optimal in the Taylor sense, degrading probably to a more realistic truncated Gaussian description. It is best for analysis and design purposes to combine measurements, theory, and modeling with due consideration given to optimal and near-optimal distributions. The truncated Gaussian distribution is useful in that regard for antenna simulations and analysis when certain beamwidth and sidelobe degradations are anticipated.



**Figure 3.46** Beamwidth and Sidelobe Relationships for the Truncated Gaussian and the Taylor Antenna. (From Bogush and Elkins)

### *The Two-Term Expansion*

The infinite Gaussian antenna, in general, is the first term of a Gaussian field expansion and is an antenna without sidelobes. A two-term expansion is an antenna with a single sidelobe. When viewed as an infinite aperture, the finite antenna, as represented, includes the main beam, the first null position, and an estimate of the first sidelobe. Of interest is the effect of truncation of the infinite aperture, and the resulting sidelobe levels of the antenna pattern.

Consider a truncated Gaussian antenna with the following defining parameters:

$$a/a_3 = 2.0$$

$$\text{sidelobe} = -26 \text{ dB}$$

$$\theta_3(a/\lambda) = 1.086$$

$$\alpha = 4.90224$$

$$C_0 = 1.16619$$

$$C_2 = 0.059658$$

Then, we may obtain

$$f(\xi) = \left\{ C_0 + 2C_2 \left[ 2 \left( \frac{\alpha^2 \xi}{2} \right) - 1 \right] \right\} \exp \left( - \frac{\alpha^2 \xi^2}{2} \right) \quad (3.279)$$

with a far-field pattern for  $\phi = 0$ , such that

$$F(u) = \left\{ C_0 - 2C_2 \left[ 2 \left( \frac{k^2 a^2 \sin^2 \theta}{\alpha^2} \right) - 1 \right] \right\} \exp \left( \frac{k^2 a^2 \sin^2 \theta}{2\alpha^2} \right) \quad (3.280)$$

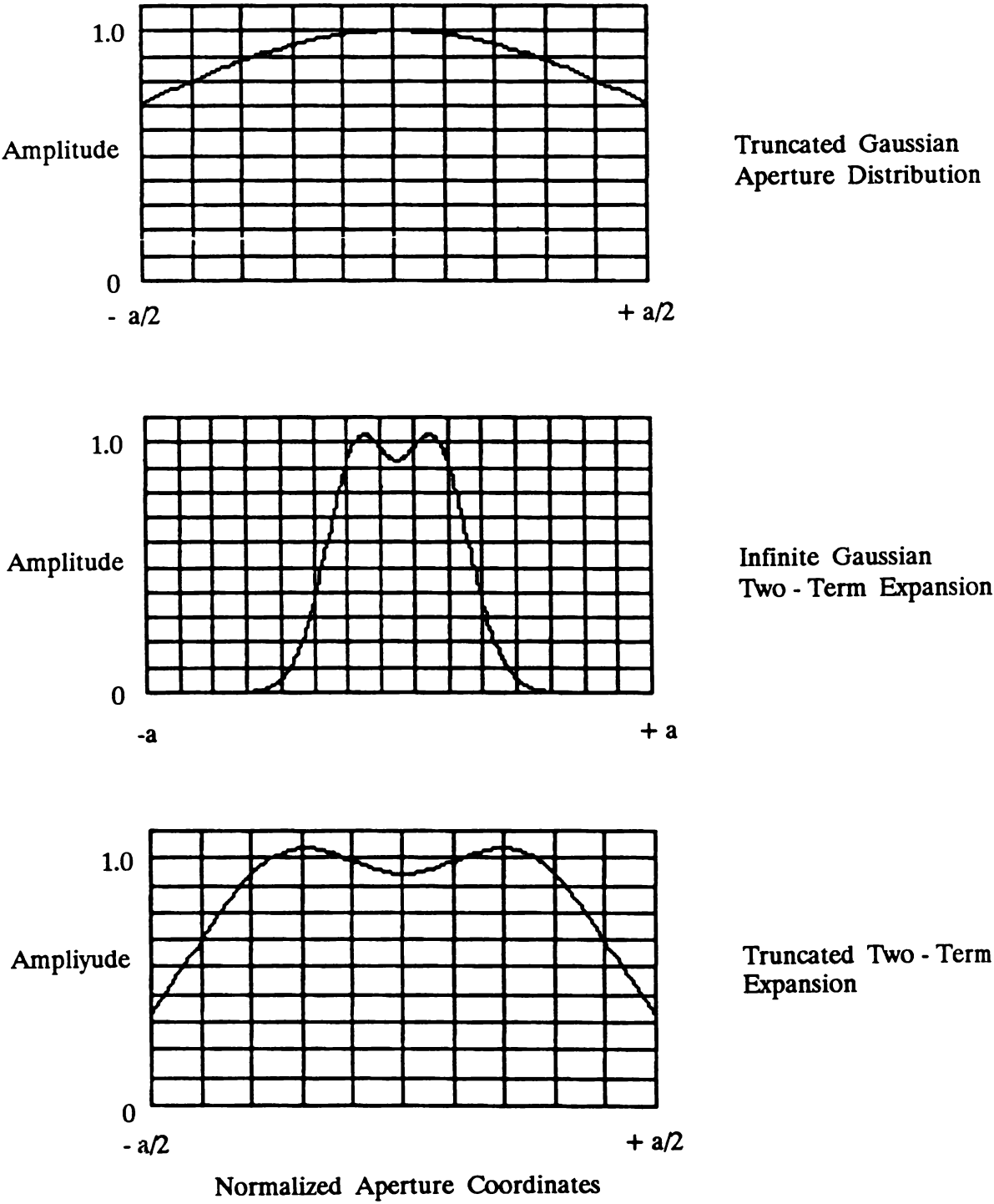
The aperture distribution, a far-field pattern for an infinite antenna and a far-field pattern for a truncation at  $\xi = 0.6$ , are plotted in Figure 3.47. The resulting pattern maintains a near-in or first sidelobe of nearly 26 dB, but has suppressed outer lobes. Antennas of this type yield the low outer sidelobe at the expense of an increased antenna size. Also, note the slight perturbation at the center of the aperture distribution, which will become more pronounced at lower-design first sidelobes. Extensions to higher-order partial sums may be of benefit in maintaining the low outer lobes, but with smaller apertures remaining larger than the original one.

The far-field antenna pattern of Equation (3.280) is another example of the extension of the Gaussian beam approximation to include an approximation of the entire mainbeam.

## Introduction To Arrays

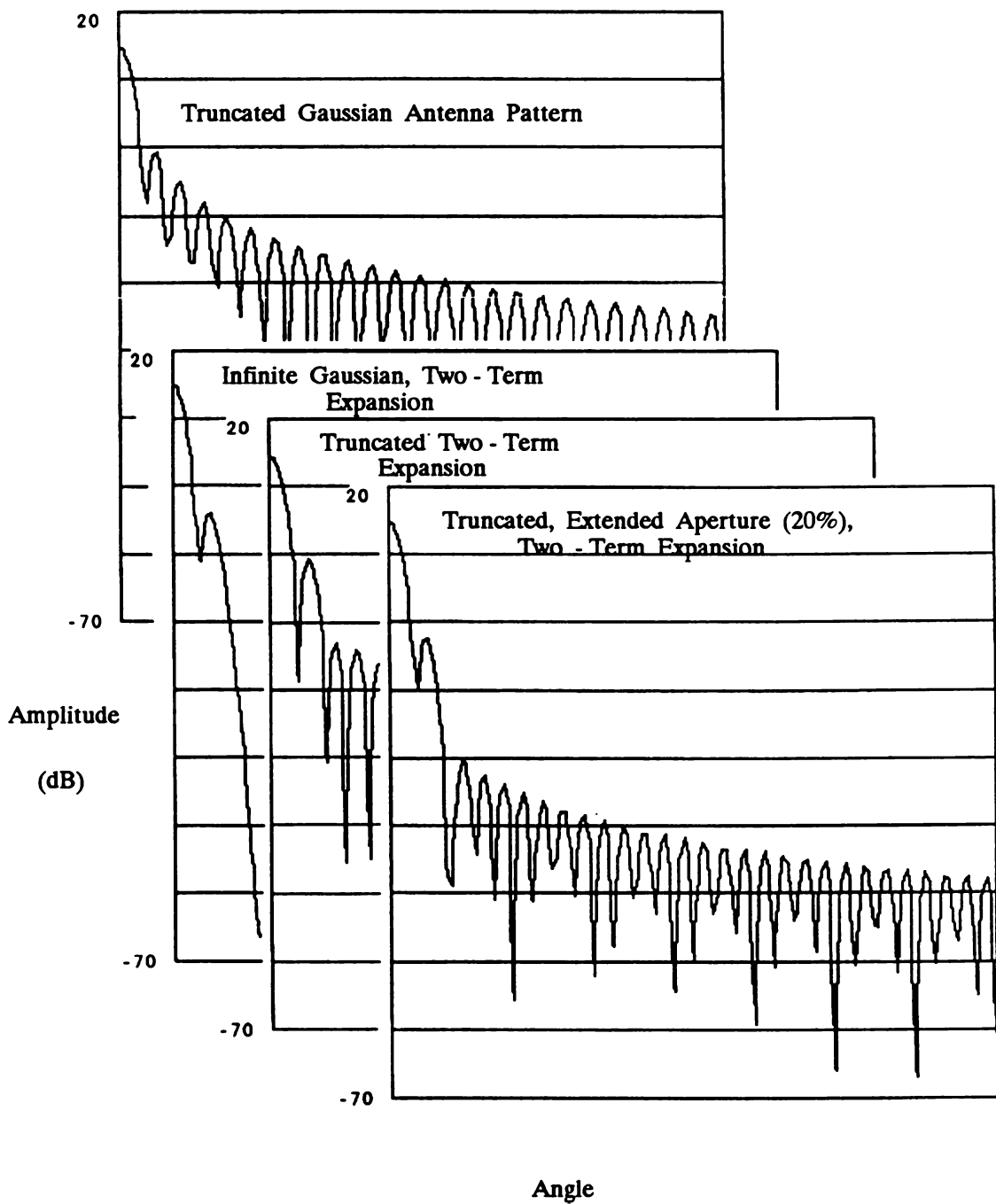
An introduction to array antennas follows directly in a formal way from a superposition of spherical waves. Although simple in concept with a readily understood physical basis, array designs are complicated by coupling between elements, edge effects, phase errors, and scanning limitations. We intend to develop the theory, provide an array model for analysis purposes, and summarize some properties of practical arrays.





(a)

**Figure 3.47** Properties of a Truncated Single-Sidelobe Gaussian Antenna: (a) Aperture Distributions



(b)

**Figure 3.47** Properties of a Truncated Single-Sidelobe Gaussian Antenna (b) Antenna Patterns

### Derivation

We will now consider a point source with field component  $E_\theta$  or  $E_\phi$  that radiates uniformly. Referring to Figure 3.48, we let the field components at  $\mathbf{r}$  be denoted by  $E(r)$ . The field of the isotropic source can hence be written as

$$E(r) = \frac{A_0 \exp(-jkr)}{r} \quad (3.281)$$

which is an outwardly expanding spherical wave. Now, referring to Figure 3.49, the field  $E(r)$  due to  $N$  sources positioned in the  $(x, y)$  plane is

$$E(\mathbf{r}) = \sum_{n=0}^N \frac{A_n}{r_n} \exp(-jk\tilde{r}) \quad (3.282)$$

Now, we let  $A_n$  be expressed as the product of a complex excitation  $a_n$  and field pattern  $f_n(\mathbf{r})$ . Thus,

$$E(r) = \sum_{n=0}^N \frac{a_n f_n(\mathbf{r})}{\tilde{r}} \exp(-jk\tilde{r}) \quad (3.283)$$

Proceeding, we consider the far radiated fields:

$$r_n = r - \mathbf{r}_n \cdot \mathbf{r} \quad (3.284)$$

and

$$E(r) = \frac{\exp(-jkr)}{r} \sum_{n=0}^N a_n f_n(\mathbf{r}) \exp(+jk\mathbf{r}_n \cdot \mathbf{r}) \quad (3.285)$$

The far-field array antenna pattern is

$$F(r) = \sum_{n=0}^N a_n f_n(\mathbf{r}) \exp(+jk\mathbf{r}_n \cdot \mathbf{r}) \quad (3.286)$$

When  $a_n = 1$ , and  $f_n(\mathbf{r}) = 1$ , an integration over a surface  $A$  containing isotropic sources is

$$F(r) = \iint_A \exp(+jk\mathbf{r}_n \cdot \mathbf{r}) dA \quad (3.287)$$

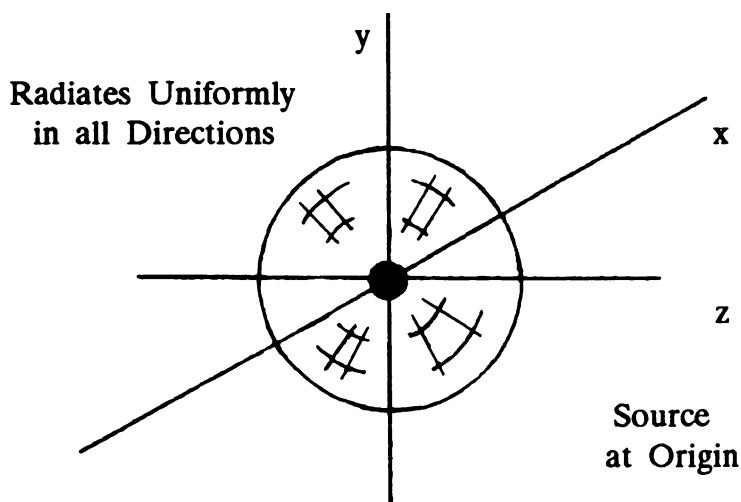


Figure 3.48 An Isotropic Source

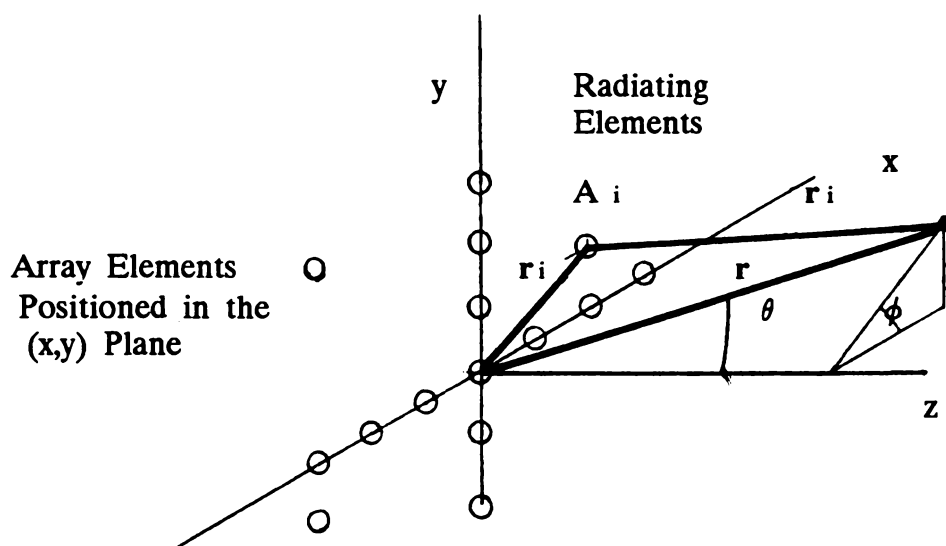


Figure 3.49 Planar Array and Coordinates

which is the pattern of a uniformly distributed antenna of area  $A$ . This limiting case of the array formula is a demonstration of Huygen's principle, which states that every point on a wavefront (in this case, the surface  $A$ ) can be considered as the source of spherical wavelets that gives rise to fields at a later time. Equation (3.286) is an approximation of a diffraction integral, yielding antenna patterns with similar basic properties. As stated, Equation (3.286) will yield a directive antenna pattern positioned along the  $z$  axis in Figure 3.49 when the extent of the source distributions is large compared to a wavelength,  $n$  is large, and  $f_n(\mathbf{r})$  is nonzero in the  $z$  direction.

The beam can be scanned to a direction  $\mathbf{r}_0$  by placing the excitation  $A_n$  in the form:

$$A_n = a_n \exp(-jk\mathbf{r}_n \cdot \mathbf{r}_0) \quad (3.288)$$

Then, the final form of the array formula becomes

$$F(\mathbf{r}) = \sum_{n=0}^N a_n f_n(\mathbf{r}) \exp(jk\mathbf{r}_n \cdot \mathbf{r}) \exp(-jk\mathbf{r}_n \cdot \mathbf{r}_0) \quad (3.289)$$

where the vector notation has been maintained for generality and convenience.

### *Model for Analysis*

Array patterns are usually computed in scalar fashion, where the radiated fields maintain the same polarization as the sources. Thus,

$$F(\mathbf{r}) = F(\theta, \phi) \quad (3.290)$$

The coefficients  $A_n$  are (in most instances) chosen to yield optimal beamwidth-to-sidelobe relationships. Such coefficients are usually Taylor distributions (available in tabular form) or are computed for special cases. Sources of this data are provided in the bibliography.

The dot products indicated in Figure 3.49 are readily expanded. For sources in the  $(x, y)$  plane,

$$\mathbf{r}_n = x_n \mathbf{i} + y_n \mathbf{j} \quad (3.291)$$

and

$$\mathbf{r} = \sin\theta \cos\phi \mathbf{i} + \sin\theta \sin\phi \mathbf{j} \quad (3.292)$$

For scanning in the direction  $(\theta_0, \phi_0)$ , we have

$$\mathbf{r}_0 = \sin\theta_0 \cos\phi_0 \mathbf{i} + \sin\theta_0 \sin\phi_0 \mathbf{j} \quad (3.293)$$

Then, we obtain

$$\mathbf{r}_n \cdot \mathbf{r} = X_n \sin\theta \cos\phi + Y_n \sin\theta \sin\phi \quad (3.294)$$

and,

$$\mathbf{r}_n \cdot \mathbf{r}_0 = X_n \sin\theta_0 \cos\phi_0 + Y_n \sin\theta_0 \sin\phi_0 \quad (3.295)$$

The inclusion of errors in all array computations is also useful. We will let the phase errors due to array fabrication, feed system design, and other sources be designated as  $\delta_n$ . These errors are usually a random draw taken from a normal distribution of zero mean and variance  $\sigma$ , or they may be of some other distribution. Then, the phase distribution in the array formula will be perturbed by  $j\delta$ . Combining these observations, we have

$$F(\theta, \phi) = \sum_{n=0}^N a_n f(\theta, \phi) \exp(-jk\mathbf{r}_n \cdot \mathbf{r}) \exp(-jk\mathbf{r}_n \cdot \mathbf{r}_0) \exp(-j\delta) \quad (3.296)$$

where the dot products are defined by Equations (3.294) and (3.295). Care must be taken in the use of the formula for the following reasons:

1. Arrays may be of rectangular or circular geometries, with a variety of grid patterns, (i.e., rectangular, square or triangular), dictating  $(X_n, Y_n)$ .
2. The element patterns, whether of slot or wire form, should be measured, and (ideally) validated for all element positions.
3. The coefficients  $a_n$  are most accurately described when mutual impedance is taken into account and expressed as a function of frequency and scan angle.
4. The errors,  $\delta$ , should reflect the real antenna design.
5. Many radars are subarrays, which first requires a field computation for the subarray; then, using the subarray as an element pattern, computation of the array fields may be done.
6. Arrays may be thinned, and spatially distributed, influencing the element position  $(X_n, Y_n)$ .

Effective array simulations are possible if we apply carefully chosen combinations of measurement and theory. Element patterns and array patterns, for validation, and a quantitative estimate of the excitation coefficients, are needed.

### Properties

Some properties of arrays are summarized as follows.

---

#### ARRAY PROPERTIES

---

##### PATTERN MULTIPLICATION

As specified, the array pattern formula in Equation (3.289) is the product of the element pattern that can be taken outside the summation and the summed, weighted amplitude of an array of isotropic sources. The magnitude of this array contribution to the radiated fields is called a *space factor*. The product of the array

**NUMBER OF ELEMENTS— $N$** 

factor and space factor demonstrates a principle of pattern multiplication that is fundamental to antenna theory.

Given an antenna element (or subarray) of area  $a$ , with total antenna area of  $A$ , then

$$N = A/a$$

**GAIN—UNIFORM ARRAY**

The optimal gain of an array in the product,

$$G_0 = G_e N$$

where  $G_e$  is the gain of the radiating element.

**GAIN**

The maximum gain of a tapered array is

$$G = n G_e N$$

where  $n$  is the aperture efficiency.

**APERTURE EFFICIENCY**

The aperture efficiency is

$$\eta = \frac{\left(\sum a_n\right)^2}{\sum (a_n)^2}$$

where  $a_n$  are the excitation coefficients, and  $\eta$  is a tabulated quantity.

**SCANNING LOSS**

The element patterns generally radiate broadside to the array. From the pattern multiplication principle, losses in gain referenced to the broadside maximum will occur. In general,

$$G(\theta) = G \cos^n \theta$$

where  $1 < n < 2$  with  $n = 1$  being the ideal, projected area case;  $n \approx 3/2$

**BEAMWIDTH**

The beamwidth of an array is proportional to the ratio of the wavelength and aperture dimension:

$$\theta_3 = K(\lambda/a)$$

where  $K$  depends on the aperture distribution.

**BEAMWIDTH—SCAN VARIATION**

The beamwidth will increase with scan angle as follows:

$$\theta_3 \approx \theta_{30}/\cos\theta_0$$

**GRATING LOBES**

Grating or spurious scanning lobes will occur if the elements are spaced far apart. Grating lobes can be restricted to angles of  $90^\circ$  when

$$d/\lambda < 1/(1 + \sin\theta_0)$$

where  $d$  is the element spacing.

We have used an introductory context and directed the reader toward quantitative, effective system analysis. Each topic, however, is worthy of further consideration; interested readers should consult the bibliography.

### 3.6 RADAR CROSS SECTIONS

There are three important considerations in the analysis or estimation of radar cross section for radar applications. They are the target *static* cross section, the *dynamic* cross section, and the *modeling* or representation of static or dynamic cross sections in a convenient form. Radar cross sections are either measured or estimated by using a number of analytical methods and prediction programs that have been recently derived. Careful analysis of target signature, or modeling of static or dynamic cross sections, requires a combination of theory and experiment, with consideration given to intended radar and applications and the specifics of the measurements.

Of fundamental importance is the representation of the radar cross section as the summation of contributions from discrete scatterers called *scattering centers*, located on the target. Knowledge of the amplitude and phase properties of these centers provides the static radar cross section. Knowledge of the movements of the centers provides the dynamic cross section. Analysis of the static and dynamic characteristics of the cross section provides the basis for models for target detection, identification discrimination, and other radar functions.

In the introductory summaries to follow, radar cross sections are described from a scattering center point of view. Basic formulations of Rayleigh, physical optics, and geometric optics are reviewed and placed in a scattering center context. Special attention is given to the scattering from long thin wires, where the notion of a scattering center is vividly displayed. A summary of target models is included in the discussions. The topic of volume scattering, which is important in meteorological applications as well as for other radar environments, is covered in Chapter 4, where a Gaussian, structured approach is described.

#### Scattering Centers

For most radar targets, the scattering will appear to be localized, emanating from discrete points on the target. When viewed by a short pulse radar with sufficient



bandwidth, the centers are resolvable. They are related to the target geometry, and, when the dynamic properties are known, they give rise to a complete description of the cross sections. The scattering center formulation is introduced, with its basic properties provided.

Consider a target complex of  $N$  scatterers with cross sections  $\sigma_1, \sigma_2, \sigma_3 \dots \sigma_n$ . If we let  $\phi_n$  be a phase reference for the  $n$ th scattering center, the radar cross for the complex is

$$\sigma_t = \left| \sum_{n=1}^N \sqrt{\sigma_n} \exp(j\phi_n) \right|^2 \quad (3.297)$$

Now, consider the scattering center arrangement in Figure 3.50. if we let the phase reference be a plane normal to the direction of propagation, then

$$\sigma_t = \left| \sum_{n=1}^N \sqrt{\sigma_n} \exp(j2kd_i) \right|^2 \quad (3.298)$$

where  $d_i$  is the distance, parallel to the propagation path, from the scattering center to the reference plane. The factor of 2 in the phase term is needed to account for the two-way path.

When target motion is considered, and a uniform random distribution of phase between the limits of 0 and  $2\pi$  occurs, the average radar cross section is the sum of the cross sections of each scattering center:

$$\bar{\sigma}_t = \sum_{n=1}^N \sigma_n \quad (3.299)$$

The rms variation of the cross section about the mean is

$$\sigma_t = \sigma_t \pm \left[ \left( \sum_{n=1}^N \sigma_n \right)^2 - \sum_{n=1}^N \sigma_n^2 \right] \quad (3.300)$$

The radar cross section of a target depends on frequency, orientation of the scatterer, and the material. The complexities of the cross sections depend on their number, location, and dynamics. Scattering center cross sections are generally slowly varying functions of frequency and aspect angle, are deterministic in behavior, and may be characterized individually as point targets. By virtue of the phase dependence of the total cross section and the common occurrence of targets with large characteristic dimensions (when compared to a wavelength), the resultant scattered signals are rapidly fluctuating and statistical in behavior. The statistics of the return of a moving target constitute the basis for target models

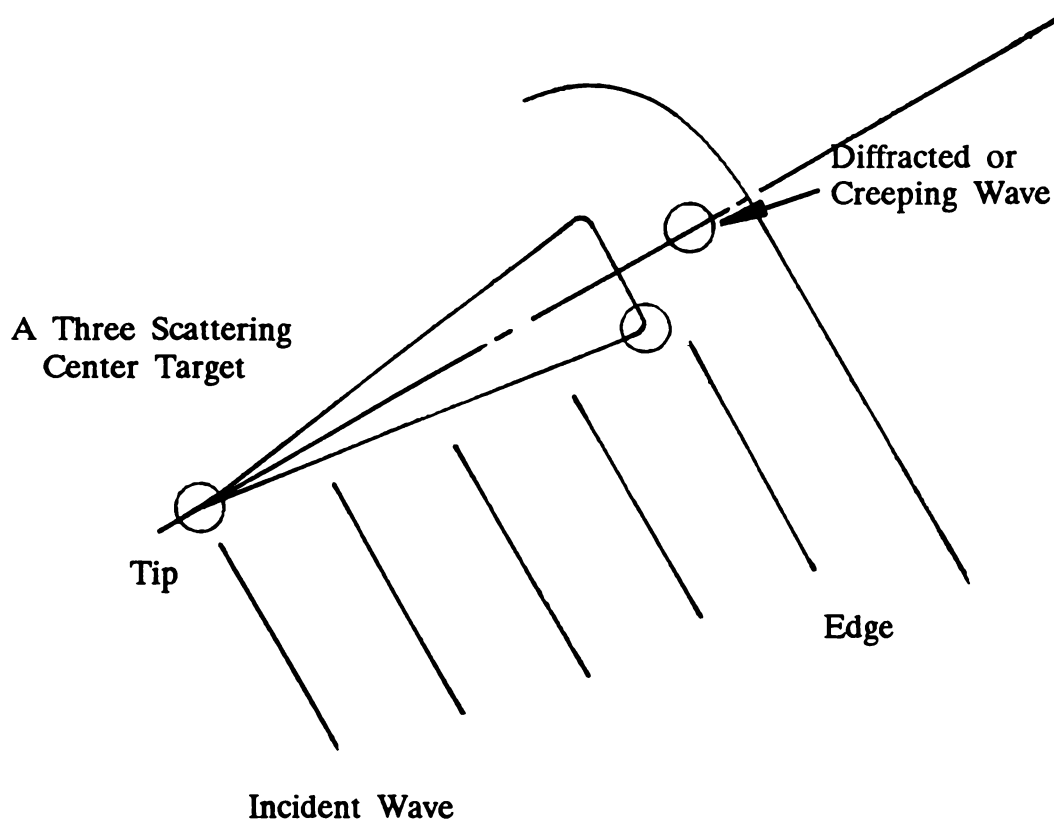


**Figure 3.50** Scattering Center Representation

such as the Swerling class I to IV. Knowledge of the scattering center properties constitutes the basis for target identification and discrimination developments. Increasing the target cross section or its augmentation for test purposes involves the addition of one or more scattering centers with expected results described by Equation (3.298). Radar cross section reduction likewise involves control of scattering center amplitudes and choice of materials.

Scattering centers arise from:

- *Specular or surface scattering center*—the incident wave is normal to a curved surface;
- *Edges*—a point where the incident wave is normal to an edge;
- *Discontinuity*—a discontinuity in the surface of the scatterer;
- *Creeping wave*—a wave diffracted about the scattering with origin appearing behind the object.

The scattering centers are excited directly by the incident wave. Depending on target geometries and materials, scattering centers may interact, where, for example, the  $n$ th scattering center exits the  $(n + 1)$ th center, which the radar sees as a separate return.

Structure of a scattering center model is accomplished through choice of path length, as related to the target geometry and direction of the incident wave. Physical interpretations of scattering center formations may be difficult, and their separation into single and multiple bounce returns may be troublesome.

Scattering center representation is formed from theory and experiment. Several examples, described below, review commonly applied analytical methods and place them in a scattering center context.

## Formulations

Three approximate scattering formulations will now be reviewed. At low frequencies (or when the characteristic dimensions of the scatterer are small in comparison to a wavelength), the radar cross section is proportional to the volume and inversely proportional to the fourth power of the wavelength. In these instances, *Rayleigh scattering* occurs. At higher frequencies, when the surface current of a metallic scattering is related to the magnetic field of the incident wave (and assumed to occur in an illuminated region), the cross sections are frequency-dependent, with solutions being within a *physical optics approximation*. At higher frequencies, cross sections depend on the radii of curvature, are independent of frequency, and are described as *geometric optics radar cross sections*. Each approximate method will be reviewed.

## Long, Thin Bodies of Revolution

Scatterers of this form are representative of long targets with small cross sections as viewed toward an edge. The summary description provided exemplifies the notion of a scattering center, where the discrete points coincide with the ends of the target.

Scattering from long, thin conducting bodies of revolution has been examined by Peters; these bodies include objects such as wires, thin cones, ogives, and others. A traveling wave connotation is adopted in interpretation of the formulas.

In deriving the radar cross section of scatterers of this type, it is convenient to treat the object as a traveling wave antenna with short-circuited terminals that accept energy from the incident wave and radiate the signal back toward the radar. Figure 3.51 shows the scatterer and its orientation. In this formulation, from Equation (2.28), the cross section is

$$\sigma = A_e G = \frac{\lambda^2}{4\pi} G^2 \quad (3.301)$$

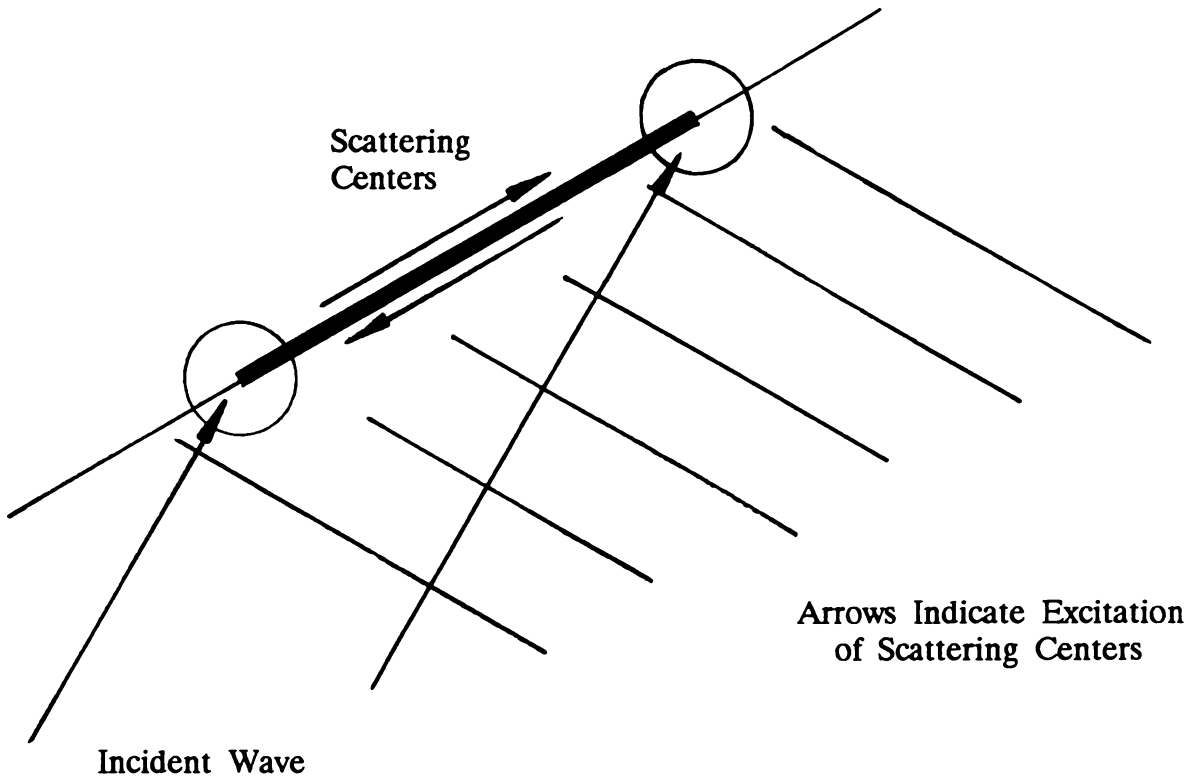


**Figure 3.51** Scattering from a Long, Thin Wire

By considering traveling waves of a dominant (or lowest-order) transverse magnetic mode, the related phase velocities, and the details of the back end of the scatterer (in the form of a reflection coefficient), the backscatter cross section as determined by Peters is

$$\sigma = \frac{\lambda^2 \gamma^2 Q^2}{\pi} \left\{ \left[ \frac{\sin \theta}{1 - p \cos \theta} \right] \left[ \sin(kl/2(1 - p \cos \theta)) \right] \right\}^4 \quad (3.302)$$

where

$p$  = phase velocity of the traveling wave

$\gamma$  = rear-end reflection coefficient

$l$  = length of scatterer

and the parameter  $Q$  for  $Kl \gg 1$  and  $p = 1$  is

$$\frac{1}{Q} \approx \ln(2kl) - 0.4228 \quad (3.303)$$

In this form, Equation (3.298) becomes

$$\sigma = \frac{\lambda^2 \gamma^2 Q^2}{\pi} \left\{ \left[ \frac{\sin \theta}{1 - \cos \theta} \right] \left[ \sin(kl/2(1 - \cos \theta)) \right] \right\}^4 \quad (3.304)$$

Calculated and measured cross sections for a rod of length  $39\lambda$  and radius  $\lambda/8$  are shown in Figure 3.52. The lobe structure of cross sections in the vicinity of a  $10^\circ$  aspect angle is that of a traveling wave antenna (a distinct physical interpretation). Taking into account the discussions of thin wire antennas of Section 3.5, the first term within the brackets in equation (3.300) is the field distribution of a spherical wave excited at the ends of the scatterer. The second term within the brackets, when expanded, yields phase terms  $\theta_n$ , related to the length of the scatterer  $l$ , and the incident angle ( $l \cos \theta$ ). Therefore the total cross section, like thin wire antennas, is described as the summation of principal modes, excited at the extremities, and traveling along the thin structure. Similar observations were made by examination of thin wire scattering, as described by Ufimtsev.

Long and thin geometries other than cylindrical ones have similar scattering cross sections and are characterized by the same scattering mechanisms. Changes in the parameter  $\theta$  and reflection coefficient  $\gamma$  in Equation (3.298) are necessary.

### *Physical Optics*

Physical optics methods in radar cross section estimation are a consequence of Kirchhoff's principles. The theory applies to scatterers with large characteristic dimensions and induced current, obtained directly from the magnetic field component of the incident wave. Because edge or shadow boundary effects are ignored, diffraction about the extremities of the target is excluded in the formulation. Scattering center properties of specular, edge, and discontinuous forms may be determined from physical optics theory.

The physical optics theory of scattering has been discussed in Section 3.3, where the radar equation is derived. Equation (3.118) is applicable for radar cross section estimates; however, a useful form of the scattering integral is as follows:

$$\sigma = \frac{4\pi}{\lambda^2} \left[ \int_A \int \frac{\partial A}{\partial \zeta} \exp(2jk\zeta) d\zeta \right]^2 \quad (3.305)$$

Integration is applied over the illuminated portion of the object, with induced currents forced to zero in the shadow region. The parameters  $A$  and  $\delta$  are defined as follows:

$A$  = area projection

$\delta$  = distance parallel to propagation path

For a sphere, we may calculate

$$\begin{aligned}\sigma &= \frac{4\pi}{\lambda^2} \int_{-a}^0 (-2\pi\zeta) \exp(2jk\zeta) d\zeta \\ &= \frac{4\pi}{\lambda^2} \left\{ j \frac{\pi A}{f} \exp(-2jka) + \frac{\pi}{2k^2} [\exp(-2jka) - 1] \right\}\end{aligned}\quad (3.306)$$

which reduces to  $\pi a^2$  for large  $k$ . The value is the leading-edge scattering center for radar targets of spherical form.

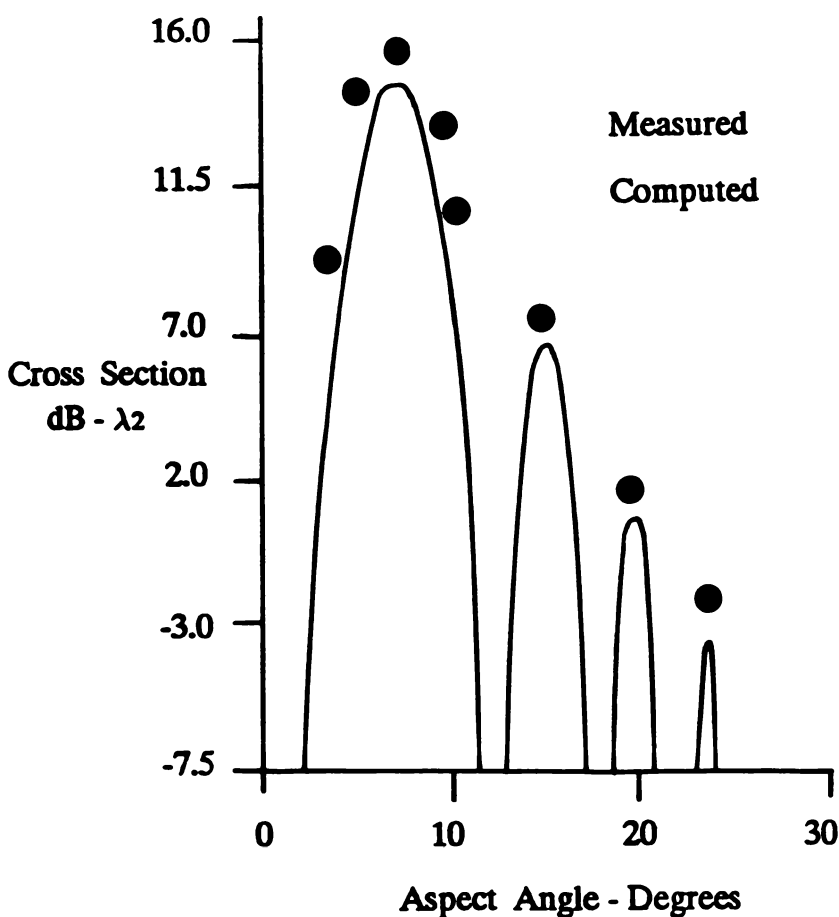


**Figure 3.52** Calculated and Measured Cross Section of a Long, Thin Wire. (From Peters)

Physical optics methods also apply to bistatic cross sections. From Equation (3.118) or (3.305), we derive the forward scatter result:

$$\sigma_p = \frac{4\pi A^2}{\lambda^2} \quad (3.307)$$

where  $A$  is the projected area in the direction of propagation. For bistatic cross sections with separations less than  $180^\circ$  (from Crispin, *et al.*), is the following theorem:

In the limit of vanishing wavelength, the bistatic cross section for transmitter direction  $\mathbf{k}$  and receiver direction  $\mathbf{n}_0$  is equal to the monostatic cross section for the transmitter. Receiver direction  $\mathbf{k} + \mathbf{n}_0$  with  $\mathbf{k} \neq \mathbf{n}_0$  for bodies which are sufficiently smooth.

Table 3.3 contains a compilation of target cross section. It may be used as given, or separated and combined with other scatterers to form a scattering center, radar cross section, or target representation.

Table 3.3 Radar Cross Sections of Typical Targets

TARGET	CROSS SECTION	DEFINITIONS
Sphere	$\sigma = \pi a^2$	$a$ = radius
Curved Surface	$\sigma = \pi a_1 a_2$	$a_1, a_2$ = radii
Flat Plate	$\sigma = 4\pi \left(\frac{A}{\lambda}\right)^2$	normal incidence $A$ = area
	$\sigma = \frac{4\pi a^4}{\lambda^2} \left(\frac{\sin u}{u}\right) \cos^2 \theta$	square plate, edge $a$ $u = ka \sin \theta$ , $\theta$ from normal
Circular Plate	$\sigma = \frac{4\pi^3 a^4}{\lambda^2} \left[ 2J_1 \left(\frac{\sin u}{u}\right) \right]^2$	$J_1$ = 1st order Bessel function $u = ka \sin \theta$
Corner Reflector	$\sigma = \frac{12\pi a^4}{\lambda^2}$	square $a$ = edge
Dipole	$\sigma = .88\lambda^2$	resonant, maximum
Cylinder	$\sigma = \frac{2\pi a L^2}{\lambda}$	normal incidence $a$ = radius, $L$ = length
	$\sigma = \frac{2\pi a L^2}{\lambda} \left(\frac{\sin u}{u}\right) \cos \theta$	$u = kL \sin \theta$
Infinite Cone (Conical Tip)	$\sigma = \frac{\lambda^2}{16\pi} \tan^4 \alpha$	$\alpha$ = cone half-angle

Rayleigh Scattering

The Rayleigh theory of scattering applies to spheroids, spheres, cylinders, and other objects with characteristic dimensions of much less than a wavelength. Although from an approximate theory, the usefulness of Rayleigh cross section estimates have been demonstrated in individual radar target returns, and as constituents of cluttered environments.

When the characteristic dimension of the scatterer is small in comparison to a wavelength, the radar cross sections, based on Rayleigh theory are as follows:

$$\sigma = \frac{4}{\pi} k^4 V^2 \quad (3.308)$$

where  $V$  is the volume and  $k$  is  $2\pi/\lambda$ . The inverse fourth-power relationship is evident, as is the volume-squared dependence. Crispin and Siegal have introduced a shape correction factor to account for a variety of shapes and to achieve agreement with measurement. If we let this factor be  $F$ , then

$$\sigma = \frac{4}{\pi} k^4 V^2 F^2 \quad (3.309)$$

where

$$F = 1 + \frac{1}{\pi y} \exp(-y) \quad (3.310)$$

and  $y$  depends on the geometry of the scatterer.

For spheroids with semiaxis  $(a, a, b)$ ,  $y = b/a$ . For a sphere, we have  $a = b$ , and

$$\sigma \approx \frac{4}{\pi} k^4 V^2 \left( 1 + \frac{1}{\pi e} \right) \quad (3.311)$$

which compares favorably with the general result:

$$\sigma = 9\pi a^6 k^4 \quad (3.312)$$

that is derived from Mie theory. Tables of Rayleigh cross sections for conducting bodies of revolution can be found in Ruck, *et al.*, *Radar Cross Section Handbook*.

Rayleigh scattering may appear as targets or portions of target complexities when the scatterers are small. However, most Rayleigh scatterers appear as clutter constituents, with rain as a good example. Equation (3.304) is fundamental and is useful for cross section estimates, but should be supported by measurements, especially when unusual shapes are encountered.

### *Geometric Optics*

The geometric optics theory of scattering applies to scattering from large convex surfaces in the limit when  $Kd \rightarrow \infty$ , with  $d$  being the characteristic dimension.



Useful leading-edge scattering center cross sections are obtained by using the theory.

When  $f \rightarrow \infty$ , or  $\lambda \rightarrow 0$ , or as the characteristic dimension of the scatterer becomes large (when  $a/\lambda \rightarrow \infty$ ), the cross section depends on the geometry. Incident waves are represented by ray paths, which are reflected at the surface, and for the usual convex surfaces, spread away from a referenced ray path. For a curved surface with principal radii of curvature,  $a_1$  and  $a_2$ , the backscatter cross section is

$$\sigma = \pi a_1 a_2 \quad (3.313)$$

The formula is applicable to surfaces describable by second-degree polynomials, and does not apply to flat or cylindrical geometries. For a sphere,  $a_1 = a_2 = a$  and

$$\sigma = \pi a^2 \quad (3.314)$$

which is a classical result. For an ellipsoid described by the surface,

$$\frac{x^2}{a^2} + \frac{y^2}{b^2} + \frac{z^2}{c^2} = 1 \quad (3.315)$$

The cross section for a wave incident along the  $z$ -axis is

$$\sigma = \frac{\pi b^2 c^2}{a^2} \quad (3.316)$$

which is a form similar to the sphere result. Radar targets are describable by geometric optics in special situations when large spherical conducting targets are observed with narrow band signals, or in instances when targets with curved surfaces are observed with wideband signals. Scattering center cross sections of the form of Equation (3.313) will appear, a classical example being the wideband scattering from a sphere where the first return of a short pulse response is  $\pi a^2$ .

Geometric optics, Rayleigh, and physical optics theories of scattering are the foundation of radar cross section estimation. Their usefulness is best realized in a scattering center way. Other proven analytical methods exist, and include Mie scattering and the geometrical theory of diffraction, both yielding diffraction contributions to the total radar cross section for a number of radar targets. The work of Rheinstein in the analysis and application of Mie scattering for estimation of creeping wave components of spheres and cone-sphere targets and the original work of Keller in the formulation of the geometrical theory are notable. Both sources are recommended for further study.

## Target Models

It is appropriate to include a summary of radar target models within the summaries of target cross sections, because the scattering center properties and their dynamics are the basis of the formulations. The Swerling models are reviewed, with reference made to a random-number-generation scheme, where perturbations of standard models may be achieved for special applications and for analysis purposes.

Let the targets be classified as nonfluctuating or fluctuating, with both subjected to considerable examination over an extended period of time. The non-fluctuating or point target model, supported by a quantitative detection probability data base, is applicable for normal radar operation (i.e., narrow-band in the sense that the scattering centers are not resolvable), or for wideband radars when the scattering centers are resolvable and operated upon within the functioning of the radar. Fluctuating targets have eluded a thorough and acceptable representation because of the complexity of the target cross section resulting from the scattering center structure, frequency, polarization, viewing angles, and materials, in addition to the motion of the target.

The Swerling models provide representations of many radar targets, with the scattering properties conducive for mathematical representation. The Swerling I model relates to a conglomeration of scatterers that are roughly of equal amplitude, large in number, and randomly positioned. In this instance, radar signal amplitudes are Rayleigh distributed, with the signal intensities being exponentially distributed. The density function for a single sample is given by:

$$f(\sigma) = \frac{1}{\bar{\sigma}} \exp\left(-\frac{\sigma}{\bar{\sigma}}\right) \quad (3.317)$$

where  $\bar{\sigma}$  is the mean of  $\sigma$ . Target detection probabilities have been compiled for slow target fluctuations, where a pulse-to-pulse correlation occurs (Class I) and fast target fluctuations, where an independence between pulse-to-pulse returns is assumed. Aircraft targets are, in many instances, represented by this class of target. When the scattering centers are characterized by a dominant scatterer, the Swerling Class III and IV models are based on cross section statistics described by a Chi-square distribution with four degrees of freedom. The density function for a single sample is

$$f(\sigma) = \frac{4\sigma}{\bar{\sigma}^2} \exp\left(-\frac{2\sigma}{\bar{\sigma}}\right) \quad (3.318)$$

Class III and IV models carry the same correlation designations as the I and II targets. Radar targets such as large cylinders or other large targets, when viewed in the vicinity of a specular return, are adequately represented by this class of target.

Data compilations that yield detection probabilities, false alarm probabilities, signal-to-noise ratios, and numbers of pulses integrated are extensive. Reference is made to Meyer and Mayer for a comprehensive treatment of the models, supplemented by numerous tables.

Radar models are of perpetual concern in radar system and cross section analysis. Besides Swerling models, log-normal Weibull distributions have been important for the modeling of a number of target and clutter environments. It is also important to realize that the cross section representation of targets as a complex of discrete scattering centers allows mathematical formulation of cluttered environments, where the constituents contribute in a position and phase-dependent way, much like the scattering centers to be applied. In this regard, the Weibull distribution has been found to be useful in describing certain radar ground clutter returns.

For analysis and simulation purposes, the generation of random sequences with defined statistics such as Rayleigh, exponential, Gaussian, log-normal and Weibull is necessary. Generation of such sequences using an inverse probability approach is possible through variations of integrations of the function  $1/x$ . When fractal models are applied, hyperbolic distributions of the form of  $1/x^\alpha$ , where  $\alpha$  is a positive real number, are encountered. Random sequences can also be generated with these distributions by an integration of the form of  $1/x^\alpha$ . A random-number scheme provided in Appendix B can be used for the hyperbolic and standard radar distributions listed above. The integrations included in the number-generation scheme are fractional, and yield perturbations through control of a fractional order of integration from the standard distributions. Although developed for fractal applications, the methodology is of value in the analysis and interpretation of target and clutter data. An introduction to fractal modeling is provided in Chapter 8.

### 3.7 THE RADAR SIGNAL

In the derivation of the radar equation and the supplementary discussions of plane waves, antennas, and scattering, a field theory basis was used. However, the functioning of the radar, for whatever purpose, is dependent on its response to a scattered signal from which information about the target is extracted. This final discussion of elements of the radar equation examines several basic properties of the radar signal. Topics include the matched receiver, classes of waveforms, and ambiguity functions. The ambiguity function provides, through interpretation, a vivid portrayal of the performance of a radar subjected to complicated target complexes and operating environments.

The material provided is composed of short summaries of several topics contained within *Modern Radar* by R.L. Berkowitz, Chapter 4 by G.W. Deley in

*Radar Handbook* edited by M.I. Skolnik, *Systems and Transforms with Applications in Optics* by A. Papoulis, and *Introduction to Defense Radar System Engineering* by J.N. Constant. As do our previous discussions, the material emphasizes basics, which we present in an introductory manner, and it is intended for reference purposes as well as a preparation for further study.

## Basics

Signals are generated in the transmitter, propagated in the atmosphere, scattered by the target and processed in the receiver. The received signal, a replica of the transmitted one, is delayed in time, and shifted in frequency by the radial velocity and acceleration of the target. The principal target parameters measured are range, azimuth and elevation angles, and velocity. Parameters estimated from the properties of the signal include size, shape, and orientation for target identification, discrimination, and other purposes. Fundamentals relate to the analysis of the received signals and their relationship to the radar cross section signatures of the target.

Consider the linear time-invariant system of Figure 3.53. We will let the input signal be a complex representation of the form:

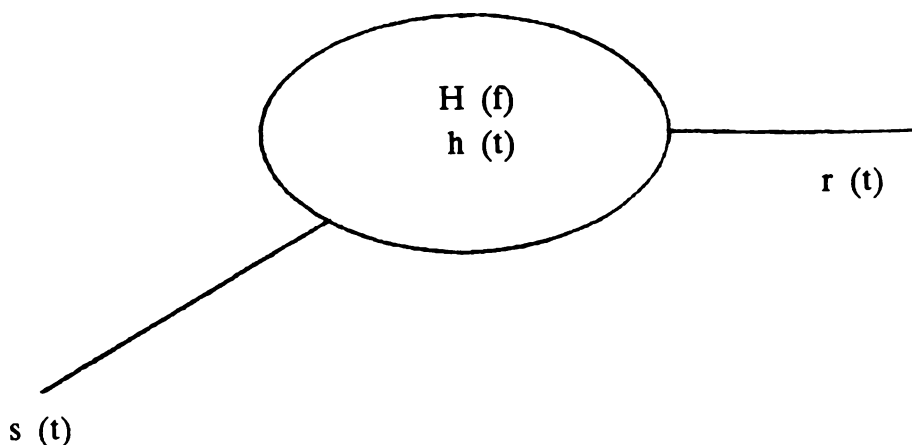


Figure 3.53 A Linear System

$$s(t) = au(t) \exp(jf_0 t) \quad (3.319)$$

where  $a$  is amplitude,  $f_0$  is the carrier frequency and  $u(t)$  is a complex modulation of the form:

$$u(t) = a(t) \exp[j\phi(t)] \quad (3.320)$$

where  $a(t)$  and  $\phi(t)$  are amplitude and phase modulation functions.

The transfer (or system) function of the linear system is  $H(\omega)$ . Starting with the definition of a delta function, from Papoulis, we have

$$\int_{-\infty}^{+\infty} \delta(t) dt = 1 \begin{cases} \delta(t) = 0, \\ t \neq 0 \end{cases} \quad (3.321)$$

$$\int_{-\infty}^{+\infty} f_n(t) dt = 1 \begin{cases} \lim_{n \rightarrow \infty} f_n(t), t \neq 0 \end{cases} \quad (3.322)$$

$$\int_{-\infty}^{+\infty} \delta(t)f(t) dt = f(0) \quad (3.323)$$

which also provides some properties of the function  $\delta(t)$ . Given the transform pair:

$$h(t) \leftrightarrow H(\omega) \quad (3.324)$$

the response of the system  $r(t)$  to the input  $s(t)$  is

$$r(t) = \int_{-\infty}^{+\infty} s(\tau)h(t-\tau) d\tau \quad (3.325)$$

or with  $s(t) \leftrightarrow S(\omega)$ ,

$$r(t) \leftrightarrow S(\omega)H(\omega) \quad (3.326)$$

The function  $h(t)$  is the impulse response of the system. The response  $r(t)$  can be interpreted as the correlation of the input signal with the impulse response.

Equations (3.225) and (3.226) form the basis of the analysis of deterministic signals, characterized by their point properties of  $s(t)$ , energy content and band-limited properties. Random signals are characterized by their average values, with their band-limited properties determined by the power spectrum. If we let an input random signal be  $n(t)$ , the time average value of the signal is

$$\langle n(t) \rangle = \lim_{T \rightarrow \infty} \frac{1}{2T} \int_{-T}^{+T} n(t) dt \quad (3.327)$$

The autocorrelation of  $n(t)$  is

$$R(t) = \lim_{T \rightarrow \infty} \frac{1}{2T} \int_{-T}^{+T} n(t+\tau)n(\tau) d\tau \quad (3.328)$$

The power spectrum of the signal is the transform of the autocorrelation function:

$$R(t) \leftrightarrow N(\omega) \quad (3.329)$$

The power spectrum of the output signal  $S_0(\omega)$  is

$$S_0(\omega) = S(\omega)|H(\omega)| \quad (3.330)$$

The spectrum of a random signal is found from a Fourier transform of a correlation function, while the deterministic signals may be transformed from a time dependent function  $S(t)$ . A system is *linear* when the response to  $a_1s_1(t) + a_2s_2(t)$  is  $a_1r_1(t) + a_2r_2(t)$ , *time-invariant* when the response to  $s(t - t_1)$  is  $r(t - t_1)$ , *stable* when the response to a bounded signal  $|s(t)| < IM$ , where  $I$  is a constant independent of input, and *causal* if  $s(t) = 0$  for  $t < t_1$ , and  $r(t) = 0$  for  $t < t_1$ .

### The Matched Filter

We will now consider a linear system with inputs  $s(t)$ , and  $n(t)$ . The signal-to-noise at the output from Equations (3.226) and (3.230) is

$$\frac{S}{N} = \frac{|r(t)|^2}{N} = \frac{|\int S(\omega)H(\omega) d\omega|^2}{\int S_0(\omega)|H(\omega)|^2 d\omega} \quad (3.331)$$

When the transfer function of the linear system is the complex conjugate of the spectrum of the input signal, then the signal-to-noise ratio at the output is a maximum given by

$$\frac{S}{N} = \int \frac{|S(\omega)|^2}{S_0(\omega)} d\omega \quad (3.332)$$

Equation (3.232) defines the output of a matched filter. It yields the maximum signal-to-noise ratio for detecting signals in white noise (characterized by a power spectrum that is infinite in extent and uniform in amplitude).

The output of a matched filter is the autocorrelation of the input signal:

$$r(t) = \int_{-\infty}^{+\infty} S(\tau)S(t + \tau) d\tau \quad (3.333)$$

which is a fundamental result. An input signal with a rectangular amplitude modulation of width  $\tau_p$  will yield an output pulse of triangular shape of width  $2\tau_p$ .

For radar equation computations, matched receivers are usually assumed ( $\beta_n\tau = 1$ ). Mismatches in the filter give rise to losses that must be accounted in the compilation of total system losses.

## The Ambiguity Function

The ambiguity function, characteristic of a matched filter, describes the range and doppler response of targets and clutter to specific incident waveforms. If the knowledge of the target scattering center's properties and motions are complete, the receiver response is then known to a high-confidence level. The ambiguity function provides a quantitative description of the resolution, accuracies, range and doppler ambiguities, and clutter rejection capabilities of the radar.

The ambiguity function will be defined first, then waveform classes will be described, with their properties related to the associated ambiguity surface.

Following Deley, we let the transmitted signal  $s(t)$  be delayed in time by  $\tau_r$  and doppler  $\phi_r$  and introduce the variables  $\delta = n - \tau_r$ ,  $\phi = \phi_r - \phi_m$ , where  $\tau = T_0 - t + \tau_r - \tau_m$ , and we have

- $\tau$  = time between signal arrival and time reference of filter
- $\phi$  = phase between signal arrival phase and phase reference of filter
- $n$  = time variable
- $\tau_m$  = matched filter delay
- $\phi_m$  = matched filter doppler
- $T_0$  = filter delay time

If we let  $A$  be the amplitude of the received signal, then from Equation (3.233), using (3.319), we obtain a filter output response:

$$r(t) = A \chi(\tau, \phi) \exp[-j2\pi(f_0 - \phi_m)\tau] \quad (3.334)$$

Where  $\psi(\tau, \phi)$  is the ambiguity function, we have:

$$\chi(\tau, \phi) = \int_{-\infty}^{+\infty} u(t) u^*(t + \tau) \exp(-j2\pi\phi t) dt \quad (3.335)$$

The ambiguity function is the correlation of the transmitted signal, with its replica shifted in doppler frequency. The receiver response is the weighting of the signal scattered by the target, described in range-doppler space, by the ambiguity surface.

## Waveforms

Radar waveforms, grouped into classes by Rihaczek and described by Mitchell, are characterized as *Class A*—simple pulses; *Class B*—pulse-compression waveforms and *Class C*—coherent pulse trains.

The Class A waveforms are amplitude modulated, with carrier frequency  $f_0$ . The pulses may be long, corresponding to a narrowband signal approaching CW, or may be short in duration, representing a wideband or short pulse signal. Figure 3.54 shows a sketch of the pulse and ambiguity functions for narrow-band and wideband signals. A short pulse is characterized by good range but poor doppler resolution. The opposite is true for the narrow-band signal. The bandwidth of the pulse is approximately  $1/\tau_p$ . The range resolution is  $C\tau_p/2$ . Ambiguity surfaces of this type are sometimes referred to as *knife-edge forms*.

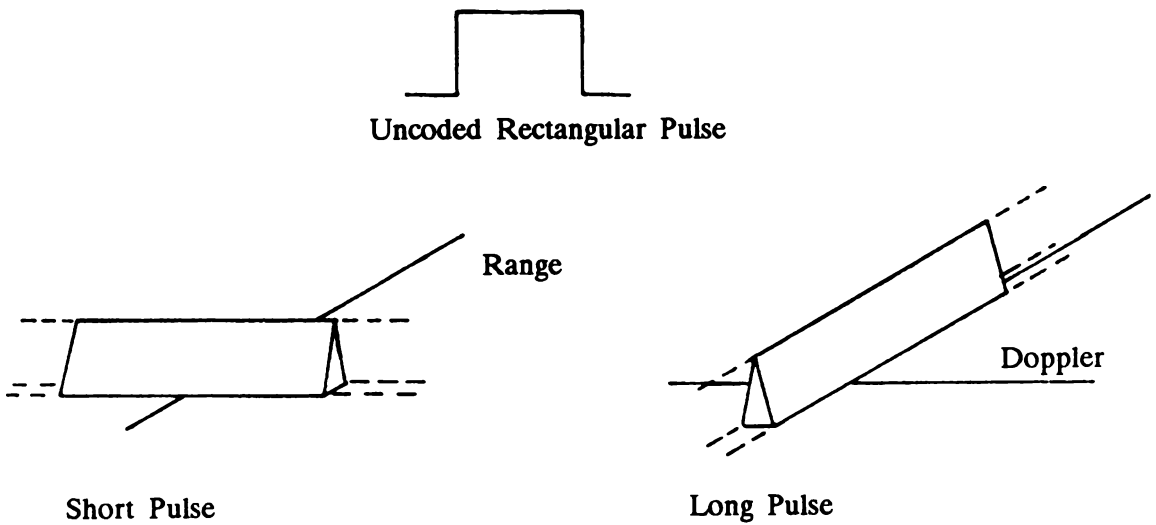


**Figure 3.54** Simple Pulse and Ambiguity Surface

Compressed waveforms include the linear FM or LFM signals characterized by a linear frequency modulation of extent  $B$ . The resolution capabilities of the waveform are dependent on  $1/B$ . The detectability of the radar is dependent on the pulse length  $\tau_p t$ . This signal, and the ambiguity surface, are shown in Figure 3.55. The surface is similar in appearance to the simple pulse surfaces, but rotated, and maintaining a knife-edge description. Targets shifted in doppler from the matched frequencies will appear along the ridge.

Coded waveforms of several forms are also within the Class B category. Examples of such waveforms include pseudorandom binary phase shift, Barker, and Frank polyphase codes. Figure 3.56 displays a pseudorandom compressed pulse and ambiguity surface, characterized by a single peak and a time-velocity sidelobe structure. The sidelobe level is a measure of clutter degradations for responses that may occur at frequencies removed from the matched one. Ambiguity surfaces of this type are sometimes called *thumbtack forms*.



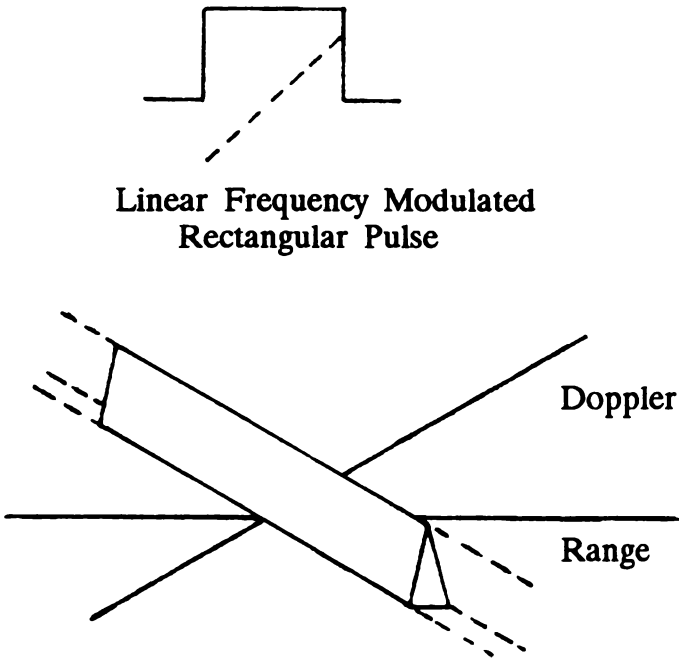


**Figure 3.55** LFM Pulse and Ambiguity Surface

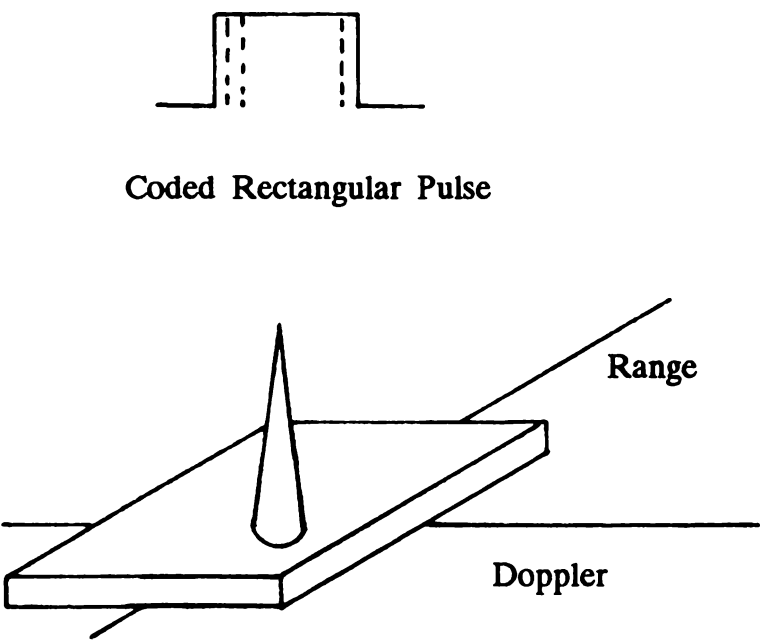
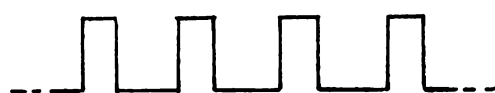


**Figure 3.56** Coded Pulse and Ambiguity Surface

Coherent pulse trains allow simultaneous measurement of range and doppler. Depending on the specifics of the waveform design, targets may be separated in range and doppler while suppressing clutter, with defined spectral behavior. Pulses

are generally weighted to achieve optimal clutter suppression and resolution in much the same way an antenna beamwidth and sidelobe are optimized. Figure 3.57 is a sketch of a uniformly weighted train of four coherent pulses. The ambiguity surface appears as a bed of spikes, with ambiguous range and doppler responses. Using waveforms of this type requires special processing for removal of range ambiguities, and parameters must be chosen to keep expected clutter responses between the matched and first doppler ambiguity responses. A measure of the clutter rejection capabilities of the waveform is the amplitude of the ambiguity function referenced to the peak response between the ambiguous responses.



Rectangular Pulse Train

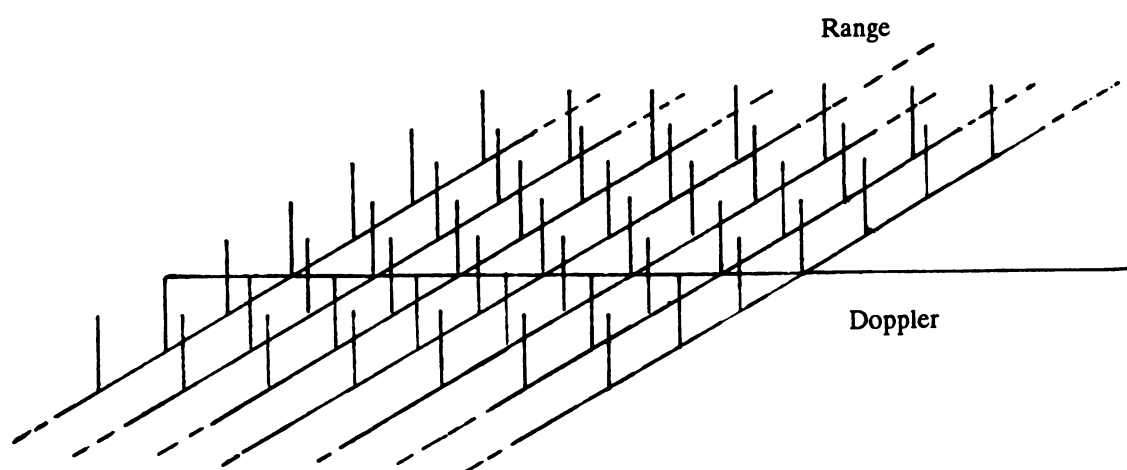


Figure 3.57 Four-Pulse Train and Ambiguity Surface

For range equation computations for Class A and B waveforms, matched filters are assumed with  $B_n = 1/t/\tau_p$ . The resolution of the simple (Class A) waveforms depends on the pulse length, while the resolution depends on the compressed pulses for Class B forms. For  $n$  uniformly weighted pulse bursts, the signal-to-noise ratio is proportional to  $n$  times the single-pulse response.

### 3.8 SYNOPSIS

A comprehensive outline of the material covered is now provided in tabular form. In the process of deriving the radar equation from the basic theory formulations,

many fundamental aspects of radar antennas, propagation, and scattering were explicitly described and are an inherent part of the derivations. It is a collection of these observations, stressing basic considerations, that we now summarize.

SYNOPSIS OF RADAR EQUATION BASICS

<i>ELECTROMAGNETIC FIELDS</i>	Described by four vector quantities <b>E</b> , <b>H</b> , <b>D</b> , and <b>B</b> .
<i>E, H, D, B</i>	Electric field intensity, magnetic field intensity, electric flux density, and magnetic flux density.
<i>MAXWELL'S EQUATIONS</i>	Field equations, stating physical laws of electromagnetic field theory.
<i>FORMS OF MAXWELL'S EQUATIONS</i>	Integral forms are statements of physical laws; differential forms are most often applied.
<i>PHYSICAL LAWS</i>	Maxwell's equations are derived from the laws of Gauss, Faraday, Ampere, and Maxwell.
<i>BOUNDARY CONDITIONS</i>	Material parameters $\epsilon$ —permittivity, $\mu$ —permeability, and $\sigma$ —conductivity; physical laws defining fields at a boundary between two dissimilar materials.
<i>VECTOR POTENTIALS</i>	Relate radiated fields to electric and magnetic sources.
<i>CURRENT ELEMENT</i>	Fields of an infinitesimal current element follow directly from a vector potential formulation; integration of current elements over surfaces or volumes yields radiated fields of antennas when current distributions are known.
<i>EQUIVALENCE THEOREM</i>	Relates fields emanating from current sources within an enclosed volume to equivalent sources on the surface.
<i>STRATTON-CHU DIFFRACTION FORMULAS</i>	Relates fields in a source-free region to fields on a closed surface; applicable to antenna and scattering problems.
<i>KIRCHHOFF DIFFRACTION FORMULA</i>	An approximation to general diffraction formula, subject to Kirchhoff's boundary conditions, forming the basis of Kirchhoff's diffraction theory. For an antenna, fields are specified on the aperture and are zero elsewhere. For a scatterer, the fields are specified within the illuminated region and are zero elsewhere.
<i>SCALAR THEORY</i>	Radiated fields have the same polarization as the sources. Kirchhoff theory is a scalar one; Stratton-Chu, in its general form, is a vector theory.
<i>DIFFRACTION INTEGRALS</i>	Integrals for radiated fields of large aperture antennas, subject to Kirchhoff's conditions.
<i>POYNTING'S THEOREM</i>	Defines power flow in an electromagnetic field.
<i>RECIPROCITY</i>	Relates interchangeability of fields and sources. Equivalence of transmitting and receiving antenna patterns is a consequence of reciprocity.
<i>RADAR EQUATION</i>	Shown to be a consequence of reciprocity and Kirchhoff's law.
<i>RADIATED EQUATION</i>	Antennas radiate spherical waves with $1/r$ dependence, power flow propagates as $1/r^2$ . At large distances, propagation is nearly planar.
<i>VELOCITY</i>	Waves in free space travel at the speed of light ( $c$ ); waves in a lossless dielectric travel at a velocity slower than $c$ .
<i>FREE-SPACE WAVELENGTH</i>	The ratio of $c$ to the carrier frequency.

---

<i>INDEX OF REFRACTION</i>	The square root of the dielectric constant.
<i>LARGE-APERTURE ANTENNA</i>	Characteristic dimensions are much larger than a wavelength.
<i>FOURIER TRANSFORM METHODS</i>	Directly relates the aperture distribution to the antenna pattern for rectangular geometrics.
<i>HANKEL TRANSFORM METHODS</i>	Directly relates the aperture distribution to the antenna pattern for circular geometrics.
<i>GAUSSIAN FIELD EXPANSIONS</i>	Generalization of the Gaussian beam approximation within constraints of Kirchhoff diffraction theory.
<i>GAUSSIAN EQUIVALENT</i>	A Gaussian representation of an antenna pattern for aperture, near and far fields.
<i>ARRAY</i>	An antenna consisting of an arrangement of identical radiating elements.
<i>ARRAY ELEMENT</i>	The radiating element or elements in an array.
<i>SCATTERING CENTER</i>	The localized regions of a target that give rise to a scattered field.
<i>PHYSICAL OPTICS</i>	A scattering formulation based on Kirchhoff theory, where the scatterer characteristic dimensions are much larger than a wavelength.
<i>RAYLEIGH SCATTERING</i>	Theory applies to scatterers with characteristic dimensions much smaller than a wavelength.
<i>GEOMETRIC OPTICS</i>	Theory applies to scattering from large convex surfaces in the limiting case of $kd \rightarrow \infty$ .
<i>MATCHED FILTER</i>	A filter that optimizes the output ratio of peak signal power to mean noise power.
<i>AMBIGUITY FUNCTION</i>	Describes the response of a radar receiver to targets and clutter, displaced in range and doppler, from a reference matched position.

---

In this formal treatment of the range equation, a field theory perspective of radar has been provided. A complete theory of radar in combination with signal theory will then generate a comprehensive description radar and its operating environment.



## *Chapter 4*

### *The Radar Equation—Gaussian Forms*

Previously, the radiated fields of large-aperture antennas were described as a generalization of the Gaussian beam approximation. In this chapter, the radar equation will be placed in a general Gaussian form. Our discussions begin with a review of radiated power density formulas, gain, aperture efficiency, beamwidth of Gaussian equivalent aperture distributions, and power transfer. Square and circular antennas are treated separately; bistatic and monostatic equations are provided; near fields and far fields are included; and the meteorological radar equation is derived from a general Gaussian representation. Examples are provided to demonstrate the use of the formulas.

For radar equation applications, Gaussian equivalents are introduced that extend current beam approximations into the near and aperture fields. Computations are easily performed, and provide good field estimates, especially when low-sidelobe antennas are involved. The meteorological equation derivations are likewise based on single Gaussian representations. However, its generalization is introduced by successive additions of terms within the Gaussian field expansions. Advantage is taken of the structured properties of the field descriptions, enabling approximations to be made in a regimented manner that may be associated with the beam properties of the radar. Aside from the meteorological applications, these mathematical formulations are of value in the general area of volume scattering. The additional forms of the radar equations can be similarly applied.

#### **4.1 RATIONALE**

The use of the Gaussian field expansions in the radar range equation provides a simple means of including the near fields in radar equation calculations. Gaussian field expansions provide series representations of the aperture, near field, and far field as products of Hermite or Laguerre polynomials and Gaussian functions. The first term of the far-field expansion approximates the nose of the antenna beam

as a Gaussian function. We have already demonstrated that the use of Gaussian functions in this way is justifiable on a theoretical basis. Theory also shows that the direct transformation of the fields from the aperture to the near or far fields yields the same form of representations. Thus, a Gaussian beam approximation in the far field establishes a similar representation in the near and aperture fields. As a result, it is convenient, when estimating radiated power densities, to use near-field approximations instead of the usual far-field ones. The resulting radar equation now reduces to a far-field equation when the range to the target is large, with the power densities reducing to aperture values when the range is small. The resulting formula is simple in form, easy to use, and versatile.

The Gaussian fields are also structured, which allows for the addition of sidelobes in a sequential way, through the use of the  $N$ th partial sums. The formulas yield the nose of the beam when the first term is used, the main beam and an approximation to the first sidelobe with the addition of a second term, an improved approximation to the first sidelobe, and the addition of a second sidelobe with another term, and so forth. In many instances, range-equation calculations involve target positions at or near the peak of the beam, where single-term expansions are applicable. Although total field expansions are used in the following equation derivations, emphasis is placed on single-term expansions for clear and rain environments. These expansions are especially useful for radar equation calculations, because of their simple and effective representation of the power densities in the vicinity of the beam axis, a region where most calculations are performed.

Radar beams, especially directive ones, are, in general, elliptic, but are often circularly symmetric. Implied here are antennas of square or circular geometry. Real-world antennas may be circular when parabolic or dish antennas are used. Planar-array antennas can be square in appearance, and depending on the antenna element design, can be of circular or square geometries that may have irregular outer edges. Therefore, the primary square and circular antenna geometries (to be considered separately) are most useful.

## 4.2 FORMULATIONS

In previous derivations, the power density along the beam axis was expressed in the following way:

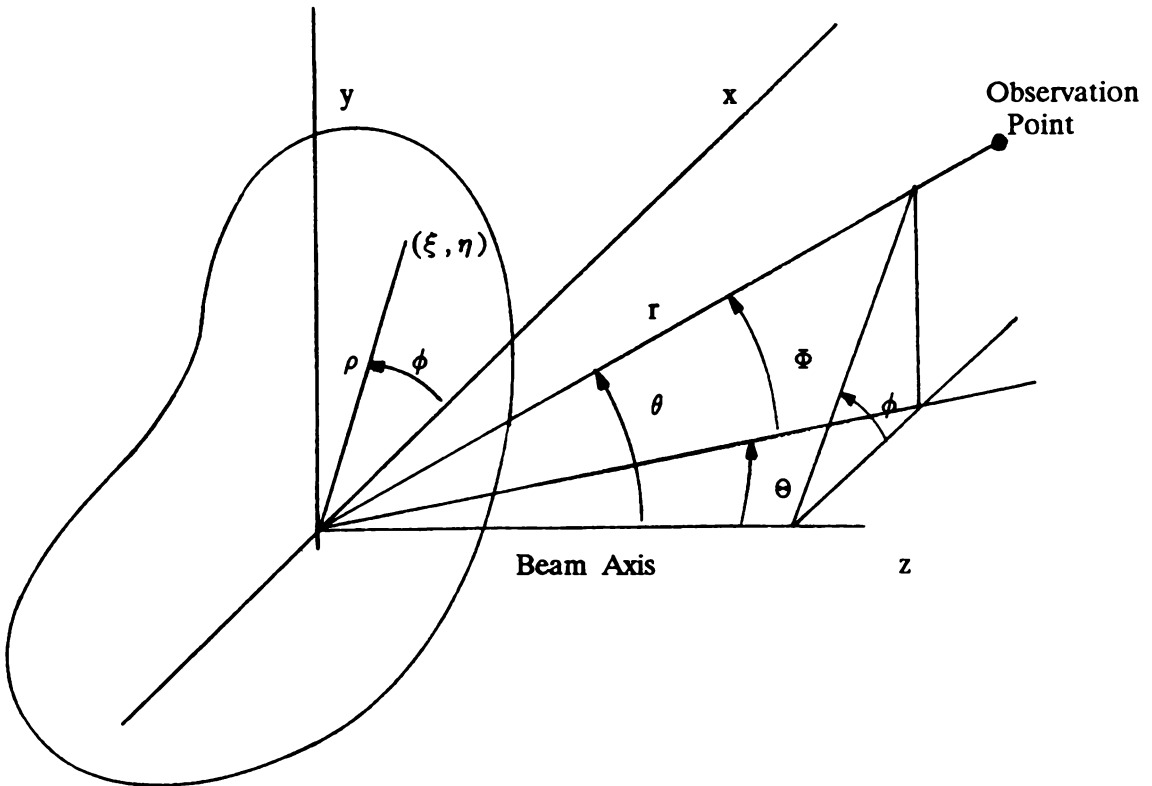
$$S = \frac{PG}{4\pi r^2} \quad (\text{W/m}^2) \quad (4.1)$$

The gain will now be expressed in terms of field quantities. We will now review this process. Later, the field quantities will be placed in Gaussian form.

## Power Densities

Referring to Figure 4.1, we let an antenna with aperture distribution  $f(x,y)$  be positioned in the  $(x,y)$  plane with the beam directed along the  $z$  axis. If we let the power applied to the antenna be  $P$ , then we have:

$$S_a = \mathcal{E}|f(x,y)|^2 \quad (4.2)$$



Radar Coordinates	$(r, \theta, \Phi)$
Spherical Coordinates	$(r, \theta, \phi)$
Rectangular Coordinates	$(x, y, z)$
Circular Aperture Coordinates	$(\rho, \phi), (\rho, \phi')$
Rectangular Aperture Coordinates	$(x, y), (\xi, \eta)$

**Figure 4.1** Antenna, Coordinates, and Beam Position



where  $S_a$  is the power density at the aperture and  $\mathcal{C}$  is a constant. An integration yields

$$\mathcal{C} = \frac{P}{\iint |f(x,y)|^2 dx dy} \quad (4.3)$$

We now consider the power density along the beam axis. In general,

$$S(0,0,z) = \frac{P|E(0,0,z)|^2}{\iint |f(x,y)|^2 dx dy} \quad (4.4)$$

In the far-field, from Chapter 3 with  $\cos\theta \approx 1$ , the field quantity in Equation (4.4) is

$$|E(0,0,z)|^2 = \frac{1}{\lambda^2 r^2} |\iint f(x,y) dx dy|^2 \quad (4.5)$$

Substituting Equation (4.5) into Equation (4.4) yields

$$S(0,0,z) = \left( \frac{P}{4\pi r^2} \right) \left( \frac{4\pi}{\lambda^2} \right) \frac{|\iint f(x,y) dx dy|^2}{\iint |f(x,y)|^2 dx dy} \quad (4.6)$$

However, by definition, the gain is represented as follows:

$$G = \left( \frac{4\pi}{\lambda^2} \right) \frac{|\iint f(x,y) dx dy|^2}{\iint |f(x,y)|^2 dx dy} \quad (4.7)$$

Thus, Equations (4.5) and (4.4) are equivalent to Equation (4.1), in view of the defining equation (4.7). For off-axis fields, the equivalent to Equation (4.5), also from Chapter 3, is

$$|E|^2 = \frac{1}{\lambda^2 r^2} |F|^2 \quad (4.8)$$

where  $F$  is the antenna pattern. Equation (4.4) can now be written in one of these more general forms:

$$S = \frac{P|E|^2}{\iint |f(x,y)|^2 dx dy} \quad (4.9)$$

or

$$S = \frac{P}{4\pi r^2} \left[ (4\pi r^2) \frac{|E|^2}{\iint |f(x,y)|^2 dx dy} \right] \quad (4.10)$$

or

$$S = \frac{P}{4\pi r^2} \left[ \left( \frac{4\pi}{\lambda^2} \right) \frac{|F|^2}{\iint |f(x,y)|^2 dx dy} \right] \quad (4.11)$$

For the near fields, the equation comparable to Equation (4.8), from Chapter 3, is

$$|E|^2 = \frac{1}{4\lambda^2 r^2} \left( 1 + \frac{z}{r} \right)^2 |F|^2 \quad (4.12)$$

Equations (4.9) and (4.10) are applicable in the near field, but Equation (4.11) becomes

$$S = \frac{P}{4\pi r^2} \left[ \frac{\pi}{\lambda^2} \left( 1 + \frac{z}{r} \right)^2 \frac{|F|^2}{\iint |f(x,y)|^2 dx dy} \right] \quad (4.13)$$

where  $F$  is the near-field antenna pattern. If the fields are confined to the vicinity of the beam axis,  $z \approx r$ , and Equations (4.13) and (4.11) are equivalent.

In view of Equation (4.1), the quantity within the brackets in Equations (4.10), (4.11) and (4.13) are interpreted as antenna gains. Their applicability depends on the field quantities that are used.

## Power Transfer

Power density estimates can be made using the appropriate (or the most convenient) formula given above. The correct choice of far-field or near-field quantities for a particular application is sometimes confusing, but can be made by interpretation of the general power transfer formula. Consider a power transfer between two antennas or arbitrary separation. Let the gain of the receiving antenna be  $G_2$ , with antenna 2 positioned in the near field of antenna 1, and antenna 1 positioned in the far field of antenna 2. Then, from Section 3.3 of Chapter 3, the power  $P_{12}$  received at antenna 2, resulting from an applied power  $P$  at antenna 1, is

$$P_{12} = \frac{P}{4\pi r^2} \left[ \left( \frac{4\pi}{\lambda^2} \right) \frac{|F|^2}{\iint |f(x,y)|^2 dx dy} \right] \left( \frac{\lambda^2 G_2}{4\pi} \right) \quad (4.14)$$

Following the procedures of Chapter 3, and applying Equation (4.11) for a two-way power transfer, yields

$$S = \frac{P\lambda^2\sigma}{(4\pi)^3 r^4} \left[ \left( \frac{4\pi}{\lambda^2} \right) \frac{|F|^2}{\iint |f(x,y)|^2 dx dy} \right]^2 \quad (4.15)$$

Near-field quantities are necessary for both propagation paths because antenna reciprocity requires that

$$\frac{P_{11}}{P_{12}} = \frac{P_{22}}{P_{21}} \quad (4.16)$$

Monostatic radar considerations are of primary importance. However, many radar situations occur where obstacles in the near field degrade system performance. Bistatic radar equations are useful for those applications, and will be included in the following derivations. Equation (4.14) will be applied to bistatic derivations, while Equation (4.15) will be used for monostatic radar developments.

### Beamwidth, Gain, and Aperture Efficiency

The use of a Gaussian function to approximate the nose of a far-field antenna pattern, by virtue of its self-reciprocal transform properties, also yields a similar representation of the near and aperture fields. Because of this occurrence, it is convenient to refer to the approximate field representation as a Gaussian equivalent of the antenna of concern. Associated with the Gaussian equivalent are beamwidths, gains, and aperture efficiencies, which we will now define.

We let the far-field pattern of a directive antenna be expressed in the following way:

$$E(\theta) = \exp \left[ -2\ln 2 \left( \frac{\theta}{\theta_3} \right)^2 \right] \quad (4.17)$$

where  $\theta_3$  is the 3dB beamwidth. Here, the Gaussian function describes the principal plane antenna pattern of a large-aperture antenna. In a Gaussian field expansion formulation for square and circular apertures, the equivalent far-field antenna pattern is expressed as:

$$E(\theta) = \exp \left[ -\frac{1}{2} \left( \frac{ka\theta}{\alpha} \right)^2 \right] \quad (4.18)$$

where, as before,  $k = 2\pi/\lambda$ ,  $\alpha$  is a scaling factor, and  $a$  is the side of a rectangular antenna (or the diameter of a circular one). The scaling factor is related to the 3-dB beamwidth by

$$\alpha = \frac{\pi}{\sqrt{\ln 2}} \left( \frac{a\theta_3}{\lambda} \right) \quad (4.19)$$

In this generalization of the Gaussian beam approximation, it is also convenient to relate the scaling factor  $\alpha$  to the aperture dimension  $a$  in a specific way. This is accomplished by writing the first term of the aperture field expansion as follows:

$$\exp\left(-\frac{\alpha^2 x^2}{2a^2}\right) = \exp\left[-2\ln 2 \left(\frac{a}{a_3}\right)^2 \left(\frac{x}{a}\right)^2\right] \quad (4.20)$$

where, analogous to  $\theta_3$ ,  $a_3$  is the 3dB width of the Gaussian aperture distribution. Then, we have

$$\alpha = 2\sqrt{\ln 2} \left( \frac{a}{a_3} \right) \quad (4.21)$$

The ratio of the aperture dimension  $a$  to the width  $a_3$  is found in truncated Gaussian aperture distribution representations. Their use in describing the equivalents follows those descriptions in this context of general field expansions for an arbitrary antenna.

Antenna gain, by definition, is a far-field quantity. In this formulation, the antenna gain is found from Equation (4.7), using the aperture distribution in Equation (4.20). Antenna efficiencies are found using the defining relationship:

$$\eta = \frac{G}{G_0} \quad (4.22)$$

where

$$G_0 = \frac{4\pi A}{\lambda^2} \quad (4.23)$$

where  $A$  is the area of the antenna.

In summary, given an antenna with beamwidth  $\theta_3$ ,

1. The Gaussian antenna beam is given by Equation (4.15).

2. The scaling factor for the Gaussian equivalent antenna is computed by using Equation (4.19).
3. The Gaussian equivalent aperture distribution is given by Equation (4.20), with aperture parameters determined by using Equation (4.21).
4. Antenna gain and aperture efficiency are defined in Equations (4.7), (4.22), and (4.23).

Equations (4.1) through (4.23) provide the basis for the derivation of range equations in Gaussian form. They will now be applied.

### 4.3 THE SQUARE ANTENNA

Referring to Figure 4.1, we let a square antenna of dimensions  $(a, a)$  be positioned in the  $(x, y)$  plane. From Chapter 3, the aperture distribution or field expansion is

$$f(\xi, \eta) = \left[ \sum_0^N C_n H_n(\alpha \xi) \exp\left(-\frac{\alpha^2 \xi^2}{2}\right) \right] \times \left[ \sum_0^M D_m H_m(\beta \eta) \exp\left(-\frac{\beta^2 \eta^2}{2}\right) \right] \quad (4.24)$$

where  $C_n$  and  $D_m$  are the series coefficients,  $\alpha$  and  $\beta$  are scaling factors,  $H_n$  and  $H_m$  are Hermite polynomials, and  $\xi$  and  $\eta$  are normalized aperture coordinates  $x/a$ ,  $y/z$ . For symmetrical antenna patterns and a square aperture,  $C_i = D_i$ ,  $\alpha = \beta$ , and  $N = M$ .

From Chapter 3, the near-field expansion can be written in the form:

$$|E| = \left\{ \left( \frac{1}{1 + \chi^2} \right)^{1/2} \exp\left[ -\frac{\alpha^2}{2a^2} \left( \frac{1}{1 + \chi^2} \right) (x^2 + y^2) \right] \right\} \times \left[ \sum_0^N C_n j^n H_n(\rho \nu) \right] \left[ \sum_0^M D_m j^m H(\gamma \nu) \right] \quad (4.25)$$

where

$$\begin{aligned}
\rho &= \left(1 + j \frac{ka^2}{\alpha^2 z}\right)^{-1/2} & \gamma &= \left(1 + j \frac{kb^2}{\alpha^2 z}\right)^{-1/2} \\
u &= \frac{k \alpha \rho x}{\alpha z} & v &= \frac{k b \gamma y}{\alpha z} \\
\chi &= \frac{\alpha^2 z}{k a^2}
\end{aligned} \tag{4.26}$$

Now the following quantities are defined:

$$Q = \frac{1}{1 + \chi^2} \tag{4.27}$$

$$U = \exp \left[ - \frac{\alpha^2}{a^2} \left( \frac{1}{1 + \chi^2} \right) (x^2 + y^2) \right] \tag{4.28}$$

$$\mathcal{H}_N = \sum_0^N C_n j^n H_n(\rho v) \tag{4.29}$$

$$\mathcal{H}_M = \sum_0^M D_m j^m H_m(\gamma v) \tag{4.30}$$

Then, in abbreviated form, Equations (4.25) and (4.27) through (4.30) become

$$|E|^2 = Q U |\mathcal{H}_N|^2 |\mathcal{H}_M|^2 \tag{4.31}$$

Equation (4.31) is a general Gaussian field expression. Although not explicit, the field exhibits a  $1/r^2$  dependence for large  $r$  contained within the factor  $Q$ , a result of the near-field generalization. The total field is described when  $N \rightarrow \infty$ . Otherwise, the radiated fields are structured with sidelobe limits depending on the choice of  $N$ .

### Gaussian Equivalents

When  $N = M = 0$ ,  $H_0 = 1.0$ , and  $C_0 \approx 1.0$ , the aperture distribution becomes

$$f(\xi, \eta) = \exp\left[-\frac{\alpha^2}{2}(\xi^2 + \eta^2)\right] \quad (4.32)$$

while Equation (4.25), the near-field expansion, reduces to

$$|E(x, y, z)| = \left(\frac{1}{1 + \chi^2}\right)^{1/2} \exp\left[-\frac{\alpha^2}{2a^2}\left(\frac{1}{1 + \chi^2}\right)(x^2 + y^2)\right] \quad (4.33)$$

In the far field, from Equation (4.33), we have

$$|E(r, u, v)| = \frac{a^2 k}{\alpha^2 r} \exp\left[-\frac{a^2}{2\alpha^2}(u^2 + v^2)\right] \quad (4.34)$$

where, as before,  $u = k \sin\theta \cos\phi$  and  $V = K \sin\theta \sin\phi$ . Although derived from the field expansions, Equations (4.32), (4.33), and (4.34), all Gaussian in character, may be derived directly from the diffraction integrals, using the aperture distribution of Equation (4.32). Equation (4.33), the near field, reduces to the far field of Equation (4.34) when  $Z \rightarrow r \rightarrow \infty$ , and reduces to Equation (4.31) when  $z \rightarrow r \rightarrow 0$ . For range-equation applications, it is convenient to use the near-field formula, without appreciable added complexities, while increasing its usefulness.

### EXAMPLE: NEAR-FIELD LIMITS

When  $Z \rightarrow 0$ ,  $X \rightarrow 0$ , and  $Q \rightarrow 1.0$ , the near field of Equation (4.33) reduces to the aperture distribution of Equation (4.32). Conversely, when  $Z \rightarrow \infty$  (with  $Z \approx r$ ), a reasonable assumption for the far field of a directive antenna is

$$\frac{1}{\chi} = \frac{ka^2}{\alpha^2 r}$$

and

$$\begin{aligned} \frac{\alpha^2}{2a^2} \left(\frac{ka^2}{\alpha^2 z}\right)^2 (x^2 + y^2) &\rightarrow \frac{k^2 a^2}{2\alpha^2} (\sin^2\theta \cos^2\phi + \sin^2\theta \sin^2\phi) \\ &= \frac{a^2}{2\alpha^2} (u^2 + v^2) \end{aligned}$$

Thus, the near field of Equation (4.33) approaches (as a limit) the far field of Equation (4.34), when  $r \rightarrow \infty$ . Given the scaling factor  $\alpha$  and the Gaussian equivalent formulas of Equations (4.17) through (4.23), this example demonstrates that a Gaussian beam approximation provides estimates of the near field, and a Gaussian equivalent representation of the aperture distribution. The first partial sum field expansions formalize this procedure, although, as we have pointed out, the same result can be achieved by assuming an infinite Gaussian aperture distribution and deriving the near- and far-field formulas directly from the diffraction integrals.

When on-axis fields are of interest, the Gaussian functions in Equations (4.32), (4.33), and (4.34) reduce to unity. The field expressions become 1.0,  $(1 + 1/\chi^2)^{1/2}$  and  $a^2 k/\alpha^2 r$  for aperture, near, and far fields, respectively.

### Radar Equations—Gaussian Equivalents

The radiated power density is given by Equation (4.4). Because

$$\int_0^\infty \exp(-x^2) dx = \frac{\pi}{2} \quad (4.35)$$

we have

$$\iint |f(x,y)|^2 dx dy = \int_0^\infty \int \exp\left(-\frac{\alpha^2 x^2}{a^2}\right) \exp\left(-\frac{\alpha^2 y^2}{a^2}\right) dx dy = \frac{a^2 \pi}{\alpha^2} \quad (4.36)$$

In abbreviated form, the power density is

$$S = \left(\frac{4P}{\eta A}\right) QU \quad (4.37)$$

where  $\eta$  is the aperture efficiency of the Gaussian equivalent antenna ( $4\pi/\alpha^2$ ), and

### EXAMPLE: ANTENNA GAIN

The gain of the infinite antenna is readily determined from Equation (4.7). Solving the integrals, we obtain



$$\left| \int_{-\infty}^{+\infty} \int \exp\left(-\frac{\alpha^2 x^2}{2a^2}\right) \exp\left(-\frac{\alpha^2 y^2}{2a^2}\right) dx dy \right|^2 = \frac{4a^4 \pi^2}{\alpha^4}$$

$$\int_{-\infty}^{+\infty} \int \left| \exp\left(-\frac{\alpha^2 x^2}{2a^2}\right) \exp\left(-\frac{\alpha^2 y^2}{2a^2}\right) \right|^2 dx dy = \frac{a^2 \pi}{\alpha^2}$$

Substituting the results of the two integrations into Equation (4.7) yields the gain:

$$G = \left[ 4\pi \left( \frac{a^2}{\lambda^2} \right) \right] \left( \frac{4\pi}{\alpha^2} \right)$$

Applying Equations (4.22) and (4.23), we obtain

$$\eta = \frac{4\pi}{\alpha^2}$$

From Equation (4.37), when  $r \rightarrow \infty$ ,

$$S = \frac{P}{4\pi r^2} \left\{ \left[ 4\pi \left( \frac{a^2}{\lambda^2} \right) \right] \left( \frac{4\pi}{\alpha^2} \right) \right\} = \frac{PG}{4\pi r^2}$$

which agrees with the gain derived from the aperture field integrations, and reaffirms the equivalence of Equations (4.37) and (4.1).

We will now consider the general radar deployment of Figure 4.2. For a bistatic radar deployment with  $\sigma_b$  the bistatic cross section,  $r_1$  the range from a target, obstacle, or obstruction positioned in the near field of the primary radar to a second radar, and  $G_1$  the gain of the receiving radar, the radar equation is

$$S_b = \left( \frac{4P}{\eta A} \right) Q U \left( \frac{\sigma_b}{4\pi r_1^2} \right) \left( \frac{\lambda^2 G_1}{4\pi} \right) \quad (4.38)$$

or,

$$S_b = \left( \frac{4P}{\eta A} \right) \frac{QUG\lambda^2\sigma_b}{(4\pi r_1)^2} \quad (4.39)$$

For on-axis conditions,  $U = 1.0$ , and Equation (4.39) becomes

$$S_b = \left( \frac{4P}{\eta A} \right) \frac{QG\lambda^2\sigma_b}{4\pi r_1^2} \quad (4.40)$$

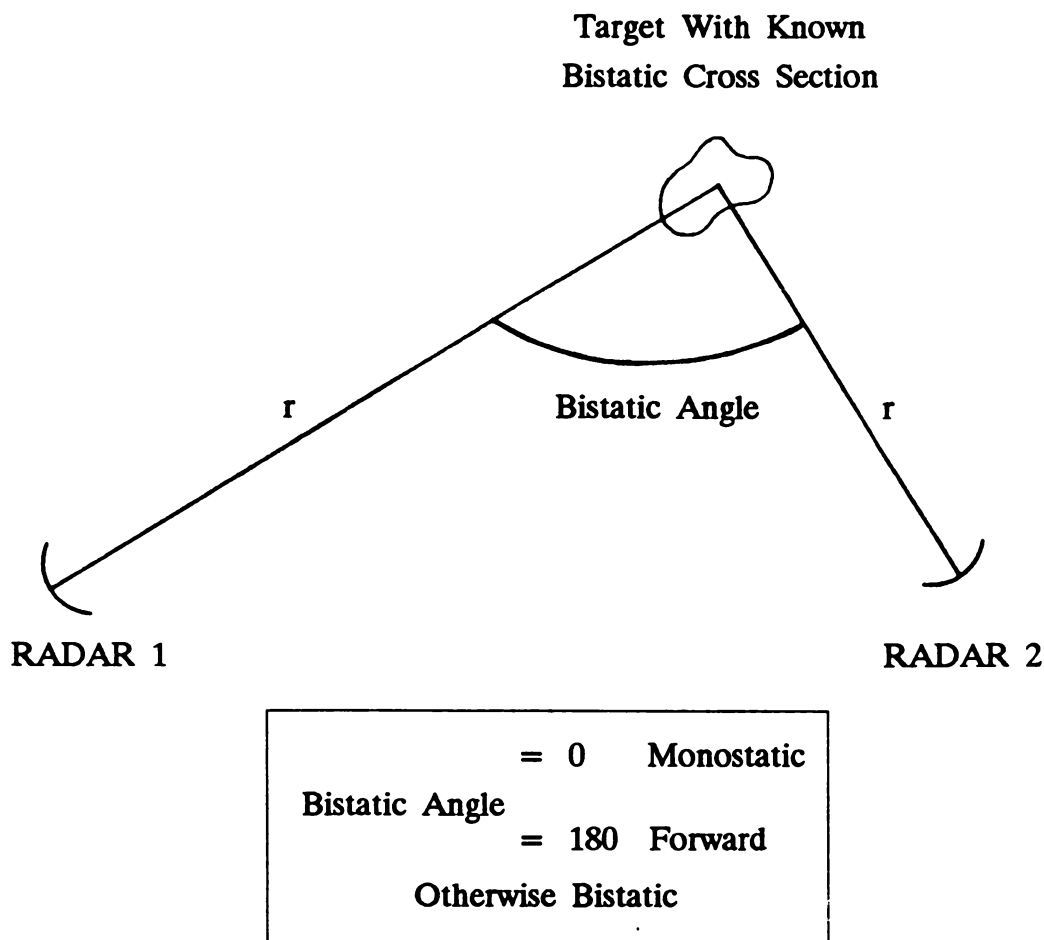


**Figure 4.2** A General Radar Deployment

In the far field, by direct reduction of Equation (4.40), or by extension of the classical form of the monostatic radar equation to a bistatic form, the radar equation becomes

$$S_{cb} = \frac{PGG_1\lambda^2\sigma_b}{4\pi r_1^2} \quad (4.41)$$

where  $G$  is the gain of the primary radar antenna.

Consider the ratio  $\mathcal{R}$  of (4.40) to (4.41), with  $z = g\lambda^2/a$ :

$$\mathcal{R}_b = \frac{\eta A}{\eta_1 A_1} \left( \frac{1}{1 + (\eta/2g)^2} \right) \quad (4.42)$$

which is plotted in Figure 4.3 for  $\eta_1 = \eta$ . Shown are the errors expected in range-equation computations when far-field instead of near-field gains are used.

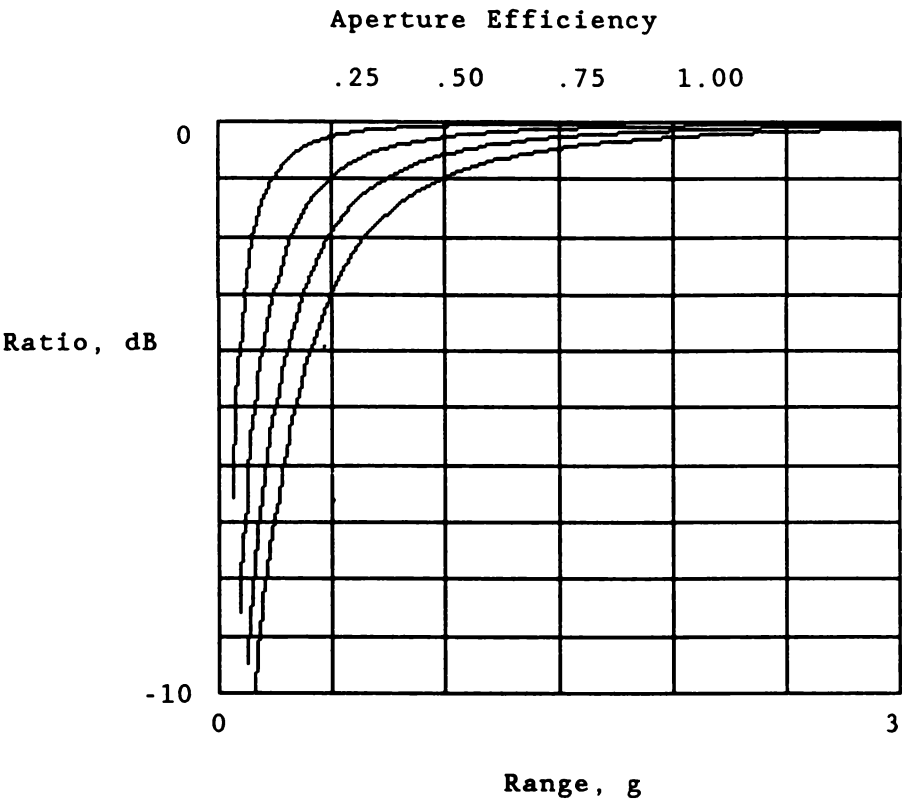


**Figure 4.3** A Comparison of Near- and Far-Field Radar Equation Estimates for a Bistatic Deployment

For forward scatter, a bistatic radar deployment with  $\psi = 180^\circ$ , the forward radar cross section for characteristic dimensions large in comparison to a wave-length is

$$\sigma_f = \frac{4\pi A_t^2}{\lambda^2} \tag{4.43}$$

The power density in the forward direction, resulting from a scatterer positioned in the near-field of the radar is

$$S = \frac{4PA_t^2QU}{\eta a^2 r_1^2 \lambda^2} \tag{4.44}$$

Placement of a radar with antenna gain  $G_1$ , a distance  $r_1$  forward of the scatterer yields the radar equation:

$$S_f = \left( \frac{4P}{\eta a^2} \right) \frac{QUG_1 A_t^2}{4\pi r_1^2} \quad (4.45)$$

In particular, Equation (4.44) has been useful in estimating radar performance degradations due to interference from scatterers positioned in the near field of the antenna.

Using Equations (4.15) and (4.37), the monostatic radar equation for a small scatterer positioned in the near field of the antenna is

$$S_m = \left( \frac{P}{\eta^2 A^2} \right) \frac{4Q^2 U^2 \lambda^2 \sigma}{\pi} \quad (4.46)$$

In the far field, Equation (4.46) reduces to:

$$S_c = \frac{PG^2 \lambda^2 \sigma}{(4\pi)^3 r^4} \quad (4.47)$$

which is the classical monostatic radar Equation. Taking the ratio of equation (4.46) to (4.47) yields,

$$\mathcal{R}m = \frac{\eta^2 A^2}{\eta_1^2 A_1^2} \left( \frac{1}{1 + (\eta/2g^2)} \right)^2 \quad (4.48)$$

These results, interpreted in the same way as before, are plotted in Figure 4.4.

### Radar Equations—General Forms

General forms of the radar equation follow directly from the Gaussian equivalent formulas, the defining field relationships, and the orthogonal properties of the Hermite polynomials. Given

$$\int_{-\infty}^{+\infty} \Psi_n(x) \Psi_m(x) dx = 2^n n! \sqrt{\pi} \quad (4.49)$$

then

$$\int_{-\infty}^{+\infty} \Psi_n\left(\frac{\alpha x}{a}\right) \Psi_m\left(\frac{\alpha x}{a}\right) dx = \frac{a}{\alpha} \sqrt{\pi} \sum_n^N C_n^2 2^n n! \quad (4.50)$$

Using the abbreviated form of the field intensity and Equation (4.9), we have

$$S = \left( \frac{4P}{\eta \alpha^2 \mathcal{G}} \right) QU \quad (4.51)$$

where

$$\mathcal{G} = \left( \sum_n^N C_n^2 2^n n! \right)^2 \quad (4.52)$$

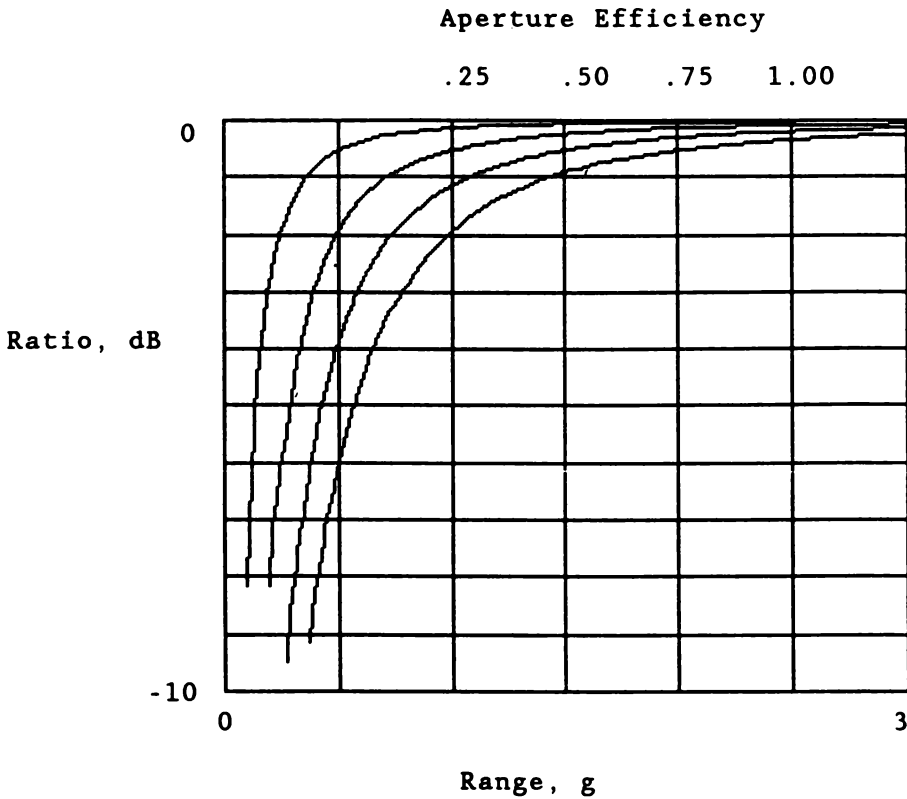


**Figure 4.4** A Comparison of Near- and Far-Field Radar Equation Estimates for a Monostatic Deployment

Applying Equation (4.9), and using Equation (4.25), the defining parameters in Equation (4.26), and the abbreviated notation of Equations (4.27) through (4.31) yields

$$S = \left( \frac{P}{\eta a^2 \mathcal{G}} \right) QU |\mathcal{H}_N|^2 |\mathcal{H}_M|^2 \quad (4.53)$$

The radar equations now follow directly from Equations (4.39), (4.45), and (4.46). Hence,

$$S_b = \left( \frac{P}{\eta A^2 \mathcal{G}} \right) \frac{QUG_1 \lambda^2 \sigma_b |\mathcal{H}_N|^2 |\mathcal{H}_M|^2}{2\pi r_1^2} \quad (4.54)$$

and

$$S_f = \left( \frac{P}{\eta A^2 \mathcal{G}} \right) \frac{QUG_1 A_i^2 |\mathcal{H}_N|^2 |\mathcal{H}_M|^2}{\pi r_1^2} \quad (4.55)$$

with the monostatic form:

$$S_m = \left( \frac{4P}{\eta^2 A^2 \mathcal{G}^2} \right) \frac{Q^2 U^2 \lambda^2 \sigma |\mathcal{H}_N|^2 |\mathcal{H}_M|^2}{\pi} \quad (4.56)$$

Computations are best performed using the recurrence relationship:

$$H_n(x) = 2nH_{n-1} - 2(n-1)H_{n-2} \quad (4.57)$$

and the zero- and first-order Hermite polynomials,  $H_0(x) = 1.0$  and  $H_1(x) = 2x$ .

In the far field, the Hermite polynomials are real. From Equation (4.25), the complex arguments of the Hermite polynomials reduce to real values in the following way:

$$\rho v = \left( \frac{1}{1 + jka^2/\alpha_2 z} \right) \left( \frac{ka}{\alpha z} \right) \rightarrow \left( \frac{1}{j + \alpha^2 z/ka^2} \right) \left( \frac{\alpha}{a} \right) \xrightarrow{r \rightarrow \infty} \left( \frac{ka}{\alpha r} \right) x \quad (4.58)$$

For even-function aperture distributions, the summations in Equation (4.25) include even-numbered terms. In those instances, they may be placed in the form:

$$\mathcal{H}_N = \sum_0^\infty (-1)^{n/2} C_n H_n \left[ \left( \frac{ka}{\alpha} \right) (\sin\theta \cos\phi) \right] \quad n \text{ even} \quad r \rightarrow \infty \quad (4.59)$$

and

$$\mathcal{H}_M = \sum_0^{\infty} (-1)^{m/2} C_m H_m \left[ \left( \frac{ka}{\alpha} \right) (\sin\theta \sin\phi) \right] \quad n \text{ even} \quad r \rightarrow \infty \quad (4.60)$$

Similar reductions occur for odd-function distributions. Because  $j^n$  for odd-numbered  $n$  can be written as  $j(-1)^{(n+1/2)}$ , and the magnitudes of the fields are of interest, we thus have

$$\mathcal{H}_N = \sum_0^{\infty} (-1)^{(n+1/2)} C_n H_n \left[ \left( \frac{ka}{\alpha} \right) (\sin\theta \cos\phi) \right] \quad n \text{ odd} \quad r \rightarrow \infty \quad (4.61)$$

and

$$\mathcal{H}_M = \sum_0^{\infty} (-1)^{(n+1)/2} C_n H_n \left[ \left( \frac{ka}{\alpha} \right) (\sin\theta \cos\phi) \right] \quad n \text{ odd} \quad r \rightarrow \infty \quad (4.62)$$

Although even- and odd-function separations are necessary for computations, the reduction to real arguments simplifies these computations. Given the series coefficients  $C_n$ , far-field computations are within reasonable bounds using a hand calculator. The Gaussian forms are usually simpler to use than the functions being expanded and integrated to determine the near or far fields.

With the general forms of the Gaussian field expansions in radar equation formats, complex quantities occur in the Hermite polynomials. Thus, computations, especially when large-order partial sums are necessary, are more extensive than required for the far fields. However, if we take advantage of the structured property of the fields, then adequate radar-range equation estimates can be made with relatively simple functions which are preferred over conventional analysis procedures.

#### 4.4 THE CIRCULAR ANTENNA

In the Gaussian theory of large-aperture antennas, Hermite polynomials occur when rectangular geometrics are encountered. For circular antennas, Laguerre orthogonal polynomials constitute the basis for the field expansions. The resulting range equations are similar to the ones derived for the square antennas. We will point out the similarities and differences in the compilation of formulas in the following sections.

##### Gaussian Field Expansions

Referring once again to Figure 4.1, we let a circular aperture of diameter  $d$  be

positioned in the  $(x,y)$  plane, with the antenna beam positioned along the  $z$  axis. The aperture distribution, repeated for convenience, is

$$f(\rho) = \sum_0^{\infty} E_n L_n(\zeta^2 \rho^2) \exp\left(-\frac{\zeta^2 \rho^2}{2}\right) \quad (4.63)$$

where, as shown in previous derivations in Chapter 3, circular symmetry is assumed.  $E_n$  are the series coefficients,  $\zeta$  is the scaling factor, and  $\rho$  is the normalized aperture coordinate  $r/a$ .

The magnitude of the radiated near field of a circular antenna in Gaussian form can be written as

$$|E| = \left\{ \left( \frac{1}{1 + \chi^2} \right) \exp \left[ -\frac{d^2 u^2}{2d^2} \left( \frac{1}{1 + \chi^2} \right) \right] \right\} \\ \times \sum_0^{\infty} E_n (1 - 2\Omega)^{-2} L_n \left[ \frac{d^2 u^2}{2\zeta^2 \Omega^2 (1 - \Omega^2/2)} \right] \quad (4.64)$$

where, repeating,

$$\Omega^2 = 1 + j \frac{kd^2}{\zeta^2 r} \quad (4.65)$$

$$\chi^2 = \frac{\zeta^2 r}{kd^2} \quad (4.66)$$

$$u = k \sin \theta \quad (4.67)$$

In shortened notation, we have

$$W = \frac{1}{1 + \chi^2} \quad (4.68)$$

$$V = \exp \left[ -\frac{d^2 u^2}{\zeta^2} \left( \frac{1}{1 + \chi^2} \right) \right] \quad (4.69)$$

and

$$\mathcal{L} = \sum_0^N E_n (1 - 2\Omega^2)^{-2} L_n \left[ \frac{d^2 u^2}{2\zeta^2 \Omega^2 (1 - \Omega^2/2)} \right] \quad (4.70)$$



Then, for convenience in deriving the radar equation, we have

$$|E|^2 = WV |\mathcal{L}_N|^2 \quad (4.71)$$

These field expressions are in the same form as previous ones, with the notation changed to reflect the different geometry and orthogonal polynomials. The fields maintain the structured property.

### Gaussian Equivalents

Proceeding as before, when  $N = 0$ ,  $L_0 = 1$ , and  $E_n \approx 1, 0$ , the aperture distribution becomes

$$f(\rho) = \sum_0^\infty E_n \exp\left(-\frac{\zeta^2 \rho^2}{2}\right) \quad (4.72)$$

For the near field expansion, Equation (4.64) reduces to

$$|E(r, \theta)| = \left(\frac{1}{1 + \chi^2}\right)^{1/2} \exp\left[-\frac{\zeta^2 r^2 \sin^2 \theta}{2d^2(1 + \chi^2)}\right] \quad (4.73)$$

or, for fields in the vicinity of the beam axis, where  $r \approx z$ ,

$$|E(x, y, z)| = \left(\frac{1}{1 + \chi^2}\right)^{1/2} \exp\left[-\frac{\zeta^2}{2d^2}\left(\frac{1}{1 + \chi^2}\right)(x^2 + y^2)\right] \quad (4.74)$$

which is equivalent in form to Equation (4.33), the result obtained for the square antenna. The on-axis fields are

$$|E(0, 0, z)| = \left(\frac{1}{1 + \chi^2}\right)^{1/2} \quad (4.75)$$

which reduces to 1.0 when  $r \rightarrow 0$ , and the far-field on-axis field  $d^2 K / \zeta^2 r$  when  $r \rightarrow \infty$ .

### Radar Equations—Gaussian Equivalents

Referring to Equation (4.4), use of the identity:

$$\int_0^\infty r \exp(-r^2) dr = \frac{1}{2} \quad (4.76)$$

results in

$$2\pi \int_0^\infty |f(r)|^2 dr = 2\pi \int_0^\infty r \exp\left(-\frac{\zeta r}{d}\right) dr \quad (4.77)$$

which is the same result as before, when the aperture length  $a$  is replaced by the diameter  $d$ . Power densities and the resulting range equations will therefore be equivalent to the square antenna results. However, in view of Equations (4.22) and (4.23), the aperture efficiencies differ. Thus, for the circular antenna:

$$\eta = \frac{16}{\zeta^2} \quad (4.78)$$

where equivalence of antenna gains dictates equivalence of the products of antenna efficiencies and areas. Thus, bistatic (4.39), forward scatter (4.45), and monostatic (4.46) radar equations are applicable for Gaussian equivalent circular antennas by simply replacing  $\eta A$  products with the appropriate circular antenna values, and the square antenna dimension  $a$  with the diameter  $d$ , which has already been accomplished in defining the abbreviated form of the field equations.

A convenient, abbreviated form of the radar equations for large-aperture circular antenna can be obtained directly from the previous results. Thus,

$$\text{Bistatic} \quad S_b = \left(\frac{P}{\eta A}\right) \frac{WVG_1 \lambda^2 \sigma_b}{2\pi r_1^2} \quad (4.79)$$

$$\text{Forward} \quad S_f = \left(\frac{P}{\eta A}\right) \frac{WVG_1}{\pi r_1^2} \quad (4.80)$$

$$\text{Monostatic} \quad S_m = \left(\frac{P}{\eta^2 A^2}\right) \frac{4W^2 V^2 \lambda^2 \sigma}{\pi} \quad (4.81)$$

The behavior of the radiated power densities and the resultant radar equations remain the same as before.

### Radar Equations—General Forms

Resulting from the orthogonality of the Laguerre polynomials are:

$$\int_0^\infty \exp(-x)[L_n(x)]^2 dx = (n!)^2 \quad (4.82)$$

$$\int_0^\infty r \exp\left[-\left(\frac{\zeta r}{d}\right)^2\right] \left\{L_n\left[\frac{\zeta r}{d}\right]^2\right\}^2 dr = \frac{d^2(n!)^2}{2\zeta^2} \quad (4.83)$$

and

$$\int_0^{2\pi} \int_0^\infty r \exp\left[-\left(\frac{\zeta r}{d}\right)^2\right] \left\{L_n\left[\frac{\zeta r}{d}\right]^2\right\}^2 dr = \frac{d^2\pi}{\zeta^2} \sum_0^N E_n^2(n!)^2 \quad (4.84)$$

Now we let

$$\mathcal{E} = \sum_0^N E_n^2(n!)^2 \quad (4.85)$$

The general radar equations also follow from previous results. Thus, we have:

$$\text{Bistatic} \quad S_b = \left(\frac{P}{\eta A \mathcal{E}}\right) \frac{WVG_1 \lambda^2 \sigma_b |\mathcal{L}_N|}{2\pi r_1^2} \quad (4.86)$$

$$\text{Forward} \quad S_f = \left(\frac{P}{\eta A \mathcal{E}}\right) \frac{WVG_1 A_i^2 |\mathcal{L}_N|}{\pi r_1^2} \quad (4.87)$$

$$\text{Monostatic} \quad S_m = \left(\frac{P}{\eta^2 A^2 \mathcal{E}^2}\right) \frac{W^2 V^2 \lambda^2 |\mathcal{L}_N|^2}{\pi} \quad (4.88)$$

Computations are best performed using the recurrence relationship:

$$L_{n+1}(x) = (2n + 1 - x)L_n(x) - nL_{n-1}(x) \quad (4.89)$$

and the first two ordered functions,  $L_0(x) = 1$  and  $L_1(x) = -x + 1$ . In the far field, the Laguerre polynomials are real, with arguments  $d^2 u^2 / \zeta^2$ , thus simplifying computations.

#### 4.5 The Meteorological Radar Equation

We will now use radar equation derivations for the square antenna. Although meteorological applications (namely rain) are of interest, the volume scattering problem is treated in a general way, thus extending the usefulness of the results, with rain reflectivity formulations inserted for rain applications. The equations

provide the means to extend current Gaussian approximations to include main beam and sidelobes in the estimates of rain clutter responses. The derivations begin with the Gaussian equivalent formulation for near fields, reduced to the familiar far field expression currently in use. The far-field results are then placed in a general Gaussian form.

## Derivations

Gaussian forms of the meteorological radar equation follow directly from previous derivations. Let the cross section of a volume  $V$  containing scatterers of reflectivity  $n_v$  be

$$\sigma_v = \eta_v \quad (4.90)$$

Let the radar resolution cell be characterized by a uniform distribution of scatterers in all directions. Then, the radial dimension of the cell can be expressed as  $c\tau/2$ , where  $c$  is the velocity of the propagating signal and  $\tau$  is the pulsewidth. For the angular transverse dimensions, weighted integrated values are considered with Equation (4.90) expressed as follows:

$$\sigma_v = \frac{\eta_v c \tau}{2} \iint \frac{|F(\Theta, \Phi)|}{|F(0, 0)|} d\Theta d\Phi \quad (4.91)$$

where  $F$  is the antenna pattern, with the integration being a normalized weighting of the scatterer cross sections in the angular directions. Previous antenna derivations have used a spherical system of units. Here, the use of radar coordinates is advantageous, where  $\Theta$  and  $\Phi$  are the azimuth and elevation angles, respectively. In this formulation and in the far field

$$\begin{aligned} \sin\theta \cos\phi &\rightarrow \sin\Theta \rightarrow \Theta \\ \sin\theta \sin\phi &\rightarrow \sin\Phi \rightarrow \Phi \end{aligned} \quad (4.92)$$

where high gain antennas are assumed. Thus, independent of the order of the partial sum of the field expansions ( $N$ ), the limits of integration in Equation (4.91) are infinite because of the exponential decay of the transverse fields and sidelobe levels of normal to low are tacitly assumed, and are expected to decrease rapidly with increasing angle; thereby confining the radiated power densities close to the mainbeam.

Now, consider a one-term Gaussian equivalent field expansion. Using Equation (4.46), and appreciating that only on-axis radar equations are of concern for volume scattering elements, then, with  $C_v$  being the scattered power density at the

radar in a monostatic deployment, we have

$$C_v = \left( \frac{P}{\eta^2 A^2} \right) \frac{2Q^2 \lambda^2 \eta_v c \tau}{\pi} \int_{-\infty}^{+\infty} \int \exp \left[ - \frac{2\alpha^2}{a^2} \left( \frac{x^2}{1 + \chi^2} \right) \right] \exp \left[ - \frac{2\alpha^2}{a^2} \left( \frac{y^2}{1 + \chi^2} \right) \right] dx dy \quad (4.93)$$

All parameters are as previously defined, and in this initial derivation, near fields are considered. Because

$$\int_{-\infty}^{+\infty} \exp \left[ - \frac{2\alpha^2}{a^2} \left( \frac{x^2}{1 + \chi^2} \right) \right] dx = \frac{a}{\alpha} \sqrt{\frac{\pi}{2}} \sqrt{1 + \chi^2} \quad (4.94)$$

then,

$$C_v = \left( \frac{P}{\eta^2 A^2} \right) \left( \frac{2Q^2 \lambda^2 \eta_v c \tau}{\pi} \right) \left[ \frac{a^2 \pi (1 + \chi^2)}{4\alpha^2} \right] \quad (4.95)$$

which is an extension of the far-field volume scattering estimate, where Gaussian beam approximations are used in the near field.

In the far field, Equation (4.95) reduces to

$$C_v = \left[ \frac{PG^2 \lambda^2}{(4\pi)^3 r^2} \right] \left( \frac{\eta_v c \tau}{2} \right) \left( \frac{\alpha^2 \lambda^2}{8\pi a^2} \right) \quad (4.96)$$

Or, using Equation (4.19), is equivalent to

$$C_v = \left[ \frac{PG^2 \lambda^2}{(4\pi)^3 r^2} \right] \left( \frac{\eta_v c \tau}{2} \right) \left( \frac{\pi}{8 \ln 2} \Theta_3^2 \right) \quad (4.97)$$

which is also identical to the results in Chapter 2, where the classical form of the meteorological radar equation was given. The factor  $\pi/8 \ln 2$  can be interpreted as the ratio of a pattern-propagation factor and the beam shape loss in recent descriptions of the volume clutter radar equation described by Barton. Although Gaussian fields are of interest, the methodology is of general applicability, providing that the pattern and reflectivity constants are known to an acceptable degree of accuracy.

The behavior of the meteorological radar equation in the near field, when Gaussian beam assumptions are applied, can be seen from the ratio of Equations (4.95) and (4.96). Performing these manipulations yields

$$\mathcal{R}_{cm} = \frac{1}{1 + (\eta/2g)^2} \quad (4.98)$$

The result is identical to the bistatic one of Equation (4.42) when  $\eta_1 A_1 = \eta A$ ; thus, the plots in Figure 4.3 are applicable. Near-field measurements of rain, for example, can be expected to decrease with range according to Equation (4.98), a result of the smaller clutter volumes present in the near field.

Specifically for rain,  $n_v = n_r$ , which is given in Equation (2.14), once again maintaining the reflectivity units of  $m^6$  per  $m^3$  that require a multiplying factor of  $10^{-18}$  in the radar equation. The general result for the one-term expansion is

$$C_v = \left( \frac{P}{\eta A} \right) \frac{Q \lambda^2 \eta_r c \tau 10^{-18}}{8 \pi L L_p} \quad (4.99)$$

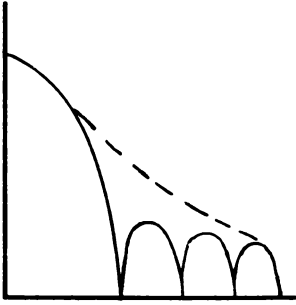
where system and propagation path losses have been included. For large  $r$ , Equation (4.99) reduces to the far-field result of Equation (2.20).

## A General Form

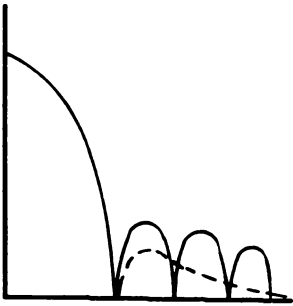
The results achieved thus far and the intention of the general form of the Gaussian meteorological radar equation to follow them are depicted in the sketch in Figure 4.5. The first-term expansion approximates the beam, as shown, when  $N = 1$ . A better approximation occurs when  $N = 2$ , where the mainbeam between the first nulls is approximated. Then, as is characteristic of the Gaussian field expansion, sidelobes are added in a structured, sequential way. For low-sidelobe antennas, for many analysis purposes, a choice of small  $n$  is apparent, because of sidelobe level reductions away from the beam axis, yielding negligible field effects.

Concentrating on the far fields, the general Gaussian form can be written directly as

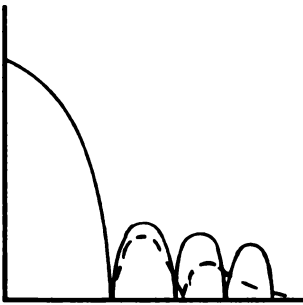
$$S_c = \frac{P G \lambda^2 \eta c \tau}{(4\pi)^3 r^2} \mathcal{J}_{NM} \quad (4.100)$$



One -Term Gaussian Beam Approximation



Two-Term Gaussian Beam Approximation



Three-Term Gaussian Beam Approximation

**Figure 4.5** Gaussian Formation of the Radiated Power Densities

where the integral  $\mathcal{J}_{NM}$  is

$$\mathcal{J}_{NM} = \int_{-\infty}^{+\infty} \frac{\left( \mathcal{H}_N \left[ \left( \frac{ka}{\alpha} \right) \Theta \right] \right)^4}{(\mathcal{H}_N[0])^4} \exp \left[ -\frac{8\pi^2}{\alpha^2} \left( \frac{a^2}{\alpha^2} \right) \Theta^2 \right] \\ \times \frac{\left( \mathcal{H}_M \left[ \left( \frac{ka}{\alpha} \right) \Phi \right] \right)^4}{(\mathcal{H}_M[0])^4} \exp \left[ -\frac{8\pi^2}{\alpha^2} \left( \frac{a^2}{\alpha^2} \right) \Phi^2 \right] d\Theta d\Phi \quad (4.101)$$

Usually, even-function aperture distributions are present; then the Hermite polynomial expansions of Equations (4.59) and (4.60) are applicable. Equation (4.101) reduces to (4.96) or (4.97) when  $N = M = 0$ .

Closed-form solutions of Equation (4.101) are possible in two forms. First, the summation of Hermite polynomials can be expanded and arranged in such a way as to encounter integrals of the form of

$$\int_{-\infty}^{+\infty} \exp\left(-\frac{x^2}{2}\right) H_N(x) H_M(x) \dots dx$$

Solutions are possible, but the results are impractical for computation. Another method of solution is to expand the individual Hermite polynomials, then integrate term by term. In this instance the integrals are unnecessarily numerous with the results, as before, being impractical.

A numerical integration is an acceptable approach, with the values of the Hermite polynomials obtained using the recurrence formulas of Equation (4.57). An example of such computation is provided in Figure 4.6, where a square antenna with a truncated Gaussian aperture distribution is examined. The results, normalized to  $\pi/8\ln 2$ , the solution for  $N = M = 0$ , show discrepancies that are expected in range-equation calculations when a one-term Gaussian beam approximation is used instead of the more complete  $N$ th term representation of the radiated power densities. A low-sidelobe antenna is considered, where, in general, Gaussian characteristics are prominent in the aperture, near and far fields.

Further extensions of the radar equations are possible. Included would be equations for clutter to noise,  $C_v/N$ , or target to clutter ratios  $S_m/C_v$ . These formulas follow directly from the formulas provided. Also, extensions to general rectangular and circular antennas are possible, following the procedures demonstrated.

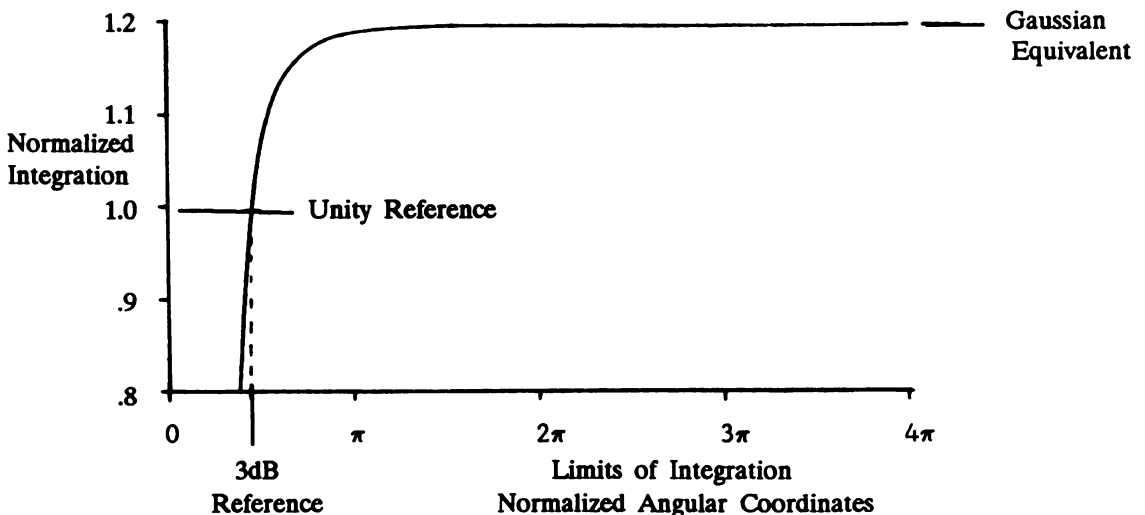


**Figure 4.6** Gaussian Factors for Radar Meteorological Equation Extensions



## 4.6 APPLICATIONS

The use of the Gaussian radar equation formulas are placed in three categories: radiated power densities, pattern degradations and two-term expansions. Each category is representative of a number of radar problems that share a common approach and methodology. A representative example is provided in each case, with extensions to other applications discussed.

### The Radiated Power Density

The radiated power densities in the vicinity of the beam axis of a large-aperture antenna can be estimated using Equation (4.37) for the aperture, near, and far fields, within the limits of the Gaussian equivalent representations. Table 4.1 contains such representations for several cosine, truncated Gaussian, and Taylor aperture distributions. The antenna data provided in the first four columns are from Barton and Ward. The remaining data are computed using the Gaussian-equivalent formulas of Equations (4.17) through (4.23). The effectiveness of a single-term Gaussian representation is indicated in the ratios of aperture efficiencies, which are nearly unity for all of the aperture distributions. The Gaussian character is more pronounced as the sidelobes decrease, or, equivalently, as the aperture efficiency decreases, an observation found to be generally applicable, regardless of the aperture distribution.

The use of Equation (4.37) to approximate the radiated-power densities of the cosine aperture distributions is demonstrated in Figure 4.7 for the aperture fields, Figure 4.8 for the on-axis power densities, and Figures 4.9 through 4.12 for the near and far fields. Comparison is made to computed results obtained from a numerical integration of the diffraction integrals for all except the aperture fields. Near-field comparisons are especially impressive, with the exception of the characteristic peak-power density present in the cosine on-axis results, at a range of about  $0.25 a^2/\lambda$ , where additional terms of the field expansions are needed for better representations. For the higher-order cosine antennas, the near-field estimates are good for most of the near-radiated beam. In the far field, as expected, the results are excellent, especially within the 3dB positions.

These data demonstrate the extension of the Gaussian far-field beam approximation to the near and aperture fields. Once the far-field Gaussian field parameters are determined, the remaining two field descriptions are described in a single formula (4.33). This capability provides the means for estimating the radiated fields in a simple way, by an extension to the Gaussian beam approximation. Although cosine aperture distributions are used in this example, the same properties are evident in other common distributions.

**Table 4.1** Gaussian Equivalent Antenna Pattern Parameters

<i>Aperture Field</i>	$S_l$ (dB)	$\left(\frac{a}{\lambda}\right)\Theta_a$	$\eta_x$	$\eta_x^2$	$\alpha$	$\left(\frac{a}{a_3}\right)$	$\eta_e$	$\eta_e/\eta_x^2$
$\cos\left(\frac{\pi x}{a}\right)$	23.0	1.189	0.802	0.643	4.487	2.695	0.624	0.970
$\cos^2\left(\frac{\pi x}{a}\right)$	31.5	1.441	0.660	0.436	5.438	3.266	0.425	0.975
$\cos^3\left(\frac{\pi x}{a}\right)$	39.0	1.659	0.571	0.326	6.260	3.760	0.321	0.985
$\cos^4\left(\frac{\pi x}{a}\right)$	47.0	1.849	0.509	0.259	6.977	4.190	0.257	0.991
<i>Truncated Gaussian</i> $n = 1.0$	15.5	0.920	0.990	0.980	3.472	2.085	1.042	1.064
<i>Truncated Gaussian</i> $n = 1.7$	20.8	1.025	0.930	0.865	3.868	2.323	0.840	0.971
<i>Truncated Gaussian</i> $n = 2.4$	32.1	1.160	0.808	0.653	4.377	3.157	0.656	1.005
<i>Truncated Gaussian</i> $n = 3.2$	47.5	1.444	0.650	0.423	5.449	3.931	0.423	1.000
<i>Taylor</i> 30 dB $\tilde{n} = 4.0$	30.9	1.115	0.850	0.723	4.207	3.035	0.710	0.982
<i>Taylor</i> 40 dB $\tilde{n} = 6.0$	40.9	1.250	0.763	0.582	4.717	3.403	0.565	0.970

$n$  = Truncated Gaussian Antenna Parameter ( $a/a_3$ ).

$\tilde{n}$  = Taylor Distribution Parameter (Defined in Appendix A).

Now consider the radiated power of a large antenna, expressed in contours of constant densities. Then, with  $\Omega$  being the power density, Equation (4.37) can be written as

$$(x^2 + y^2) \left[ \frac{\alpha^2}{2a^2} \left( \frac{1}{1 + \chi^2} \right) \right] = \ln \left( \frac{4P}{\eta A} \right) + \ln Q - \ln \Omega \quad (4.102)$$

It is convenient when using this formula, and for near-field computations in general, to express the range  $z$  in units of  $a^2/\lambda$ , or as  $z = ga^2/\lambda$ , and the cross range as multiples of the antenna dimensions,  $x/a$ , and  $y/a$ .

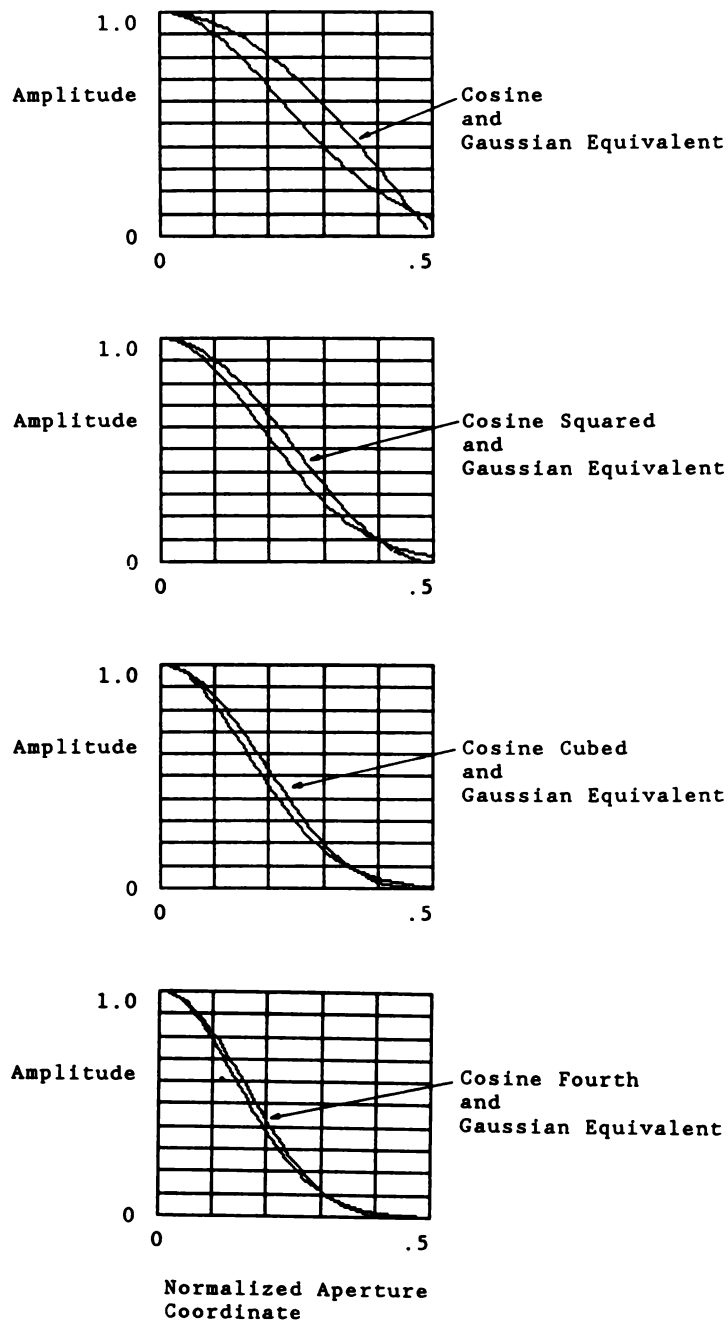


**Figure 4.7** Gaussian Equivalent Aperture Distributions For Cosine Antennas

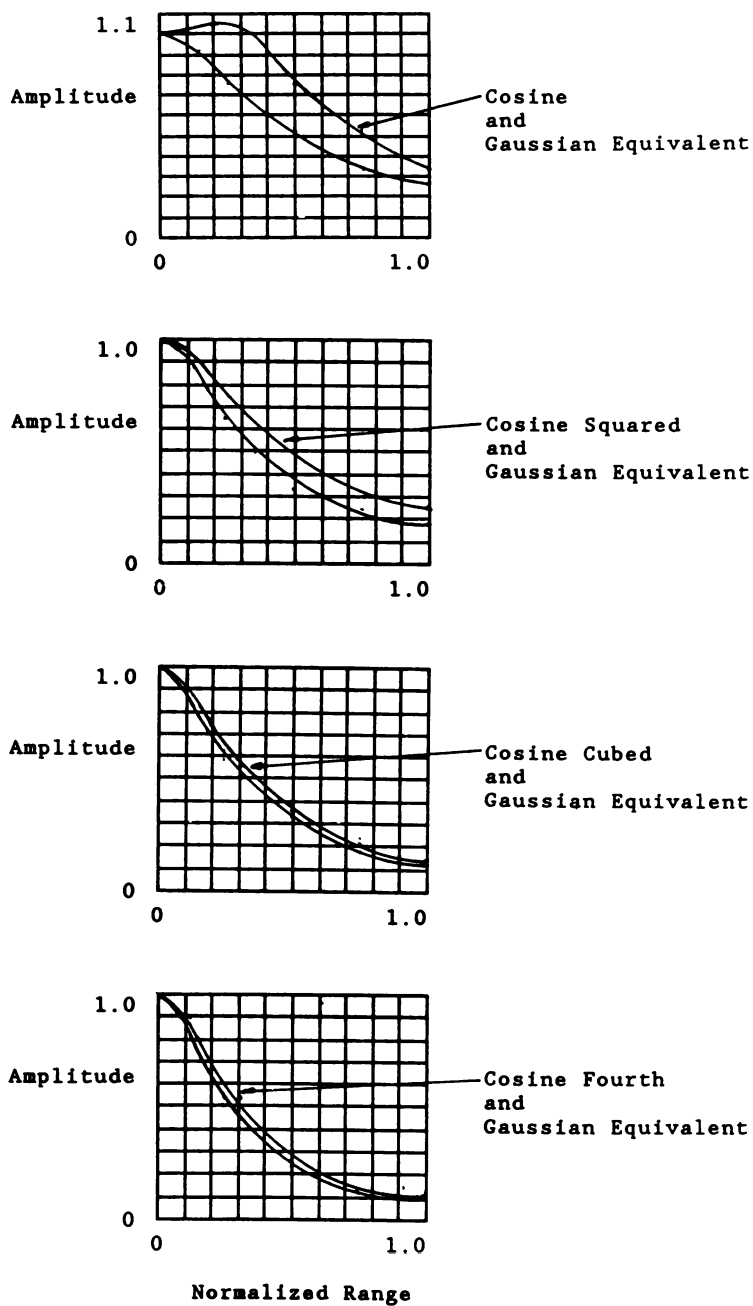


**Figure 4.8** On-Axis Field Comparisons

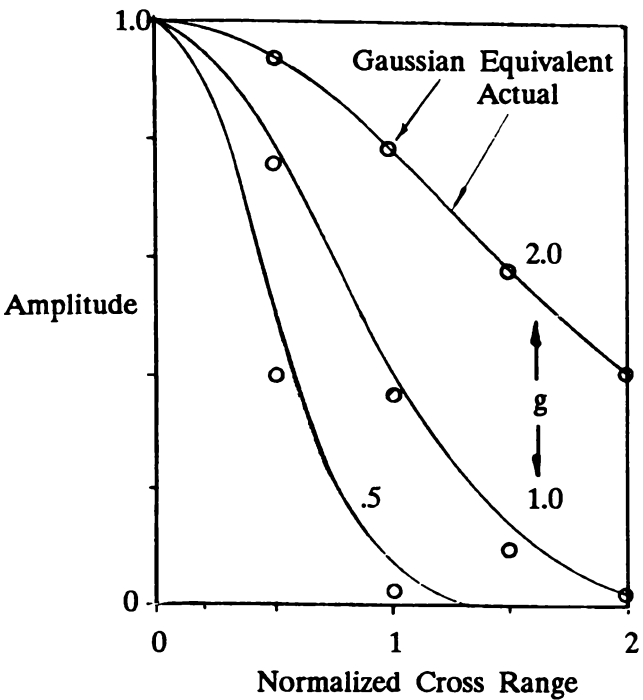


Figure 4.9 Normalized Field Plots for the Cosine Aperture Distribution and the Gaussian Equivalent

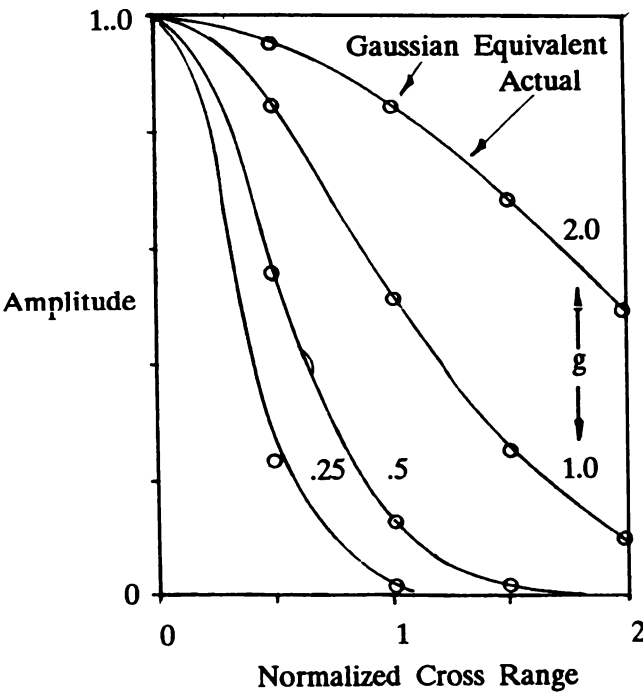
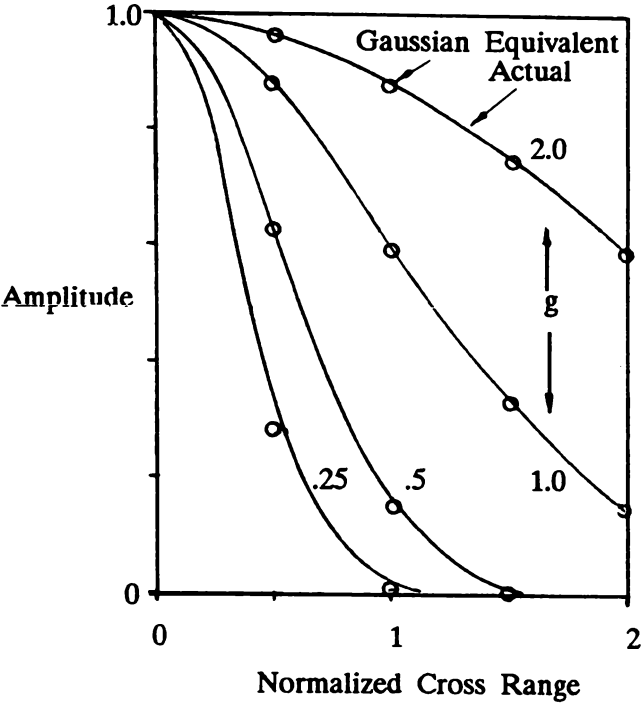
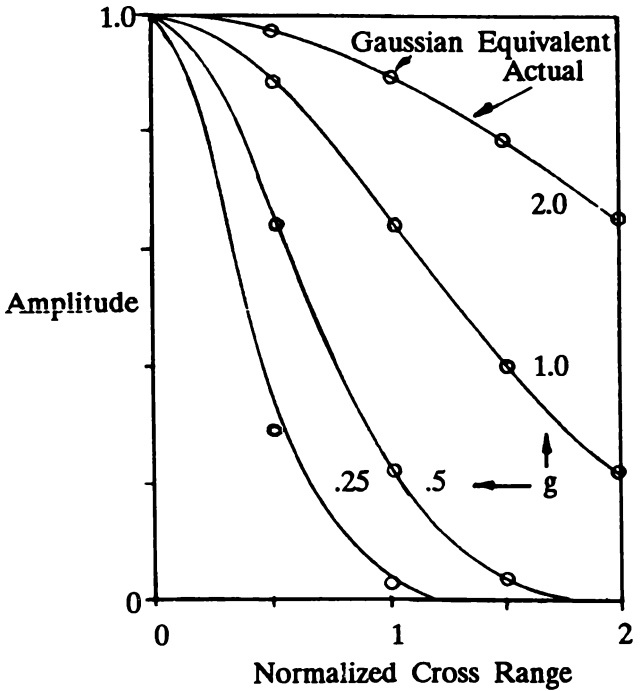


Figure 4.10 Normalized Field Plots for the Cosine Squared Aperture Distribution and the Gaussian Equivalent



**Figure 4.11** Normalized Field Plots for the Cosine Cubed Aperture Distribution and the Gaussian Equivalent



**Figure 4.12** Normalized Field Plots for the Cosine Fourth Aperture Distribution and the Gaussian Equivalent

As an example, consider a large square antenna with aperture dimension  $a = 25.6$  m (84 feet), a frequency of about 3 GHz, with a corresponding wavelength of 0.1 m, and a peak power of about 1.6 MW. If we let the Gaussian parameters be  $(a/a_3) \approx 2.0$ ,  $\alpha \approx 3.472$ , and  $n_e \approx 1.0$ , then the peak-power density in the aperture plane is about 1000 mW/cm<sup>2</sup>. The use of Equation (4.37) for computation of the on-axis power density yields the results in Figure 4.13. For the selected example, absolute power densities are in excess of 10 mW/cm<sup>2</sup>, an upper boundary of an acceptable safe power density for personnel exposure, at ranges in excess of the far-field limit of  $2a^2/\lambda$ . Contour plots, expressed in absolute and relative power densities, are displayed in Figure 4.14. The power densities follow a definite characteristic pattern, with the higher-power values confined (as expected) to areas in close proximity to the beam axis. However, in this instance, the considered high power density of 10 mW/cm<sup>2</sup> extends outward in range beyond near-field limits and outward in cross range beyond the extremities of the aperture (i.e.,  $x \geq a/2$ ).

It is important, therefore, in establishing “keep-out” regions in the vicinity of high-power radars for personnel safety reasons to estimate on-axis and cross-range radiated power levels. This power density contour formulation provides the means toward that end.

This methodology and the use of Gaussian range equation formulas can be applied to several related radar problems. They are provided in the summary example given below.

#### **EXAMPLE: FURTHER APPLICATIONS OF THE POWER DENSITY FORMULATIONS**

*Interference Susceptibilities*—Radars are subjected to interference of many forms that increases the receiver noise levels, thus degrading target detection. Near-field as well as far-field considerations may be involved. In those instances, a convenient analysis procedure follows first from the use of Equation (4.14), the Friis’ transmission formula, to obtain the power density at the radar we let

$$P_2 = \left( \frac{P_I G_I}{4\pi r^2} \right) \left( \frac{\lambda^2}{4\pi} \right) \left( \frac{4\alpha^2 z^2}{a^2} Q U \right)$$

which is a general near-field position of the source of interference. Then the far-field monostatic radar equation can be applied to obtain the target response. The ratio of the interference response to target response is

$$\frac{S_I}{S} = \left( \frac{16\pi\alpha^2 z^2}{a^2} \right) \left( \frac{1}{\sigma} \right) \left( \frac{R^4}{r^2} \right) \left( \frac{P_I G_I}{G^2} \right) Q U$$

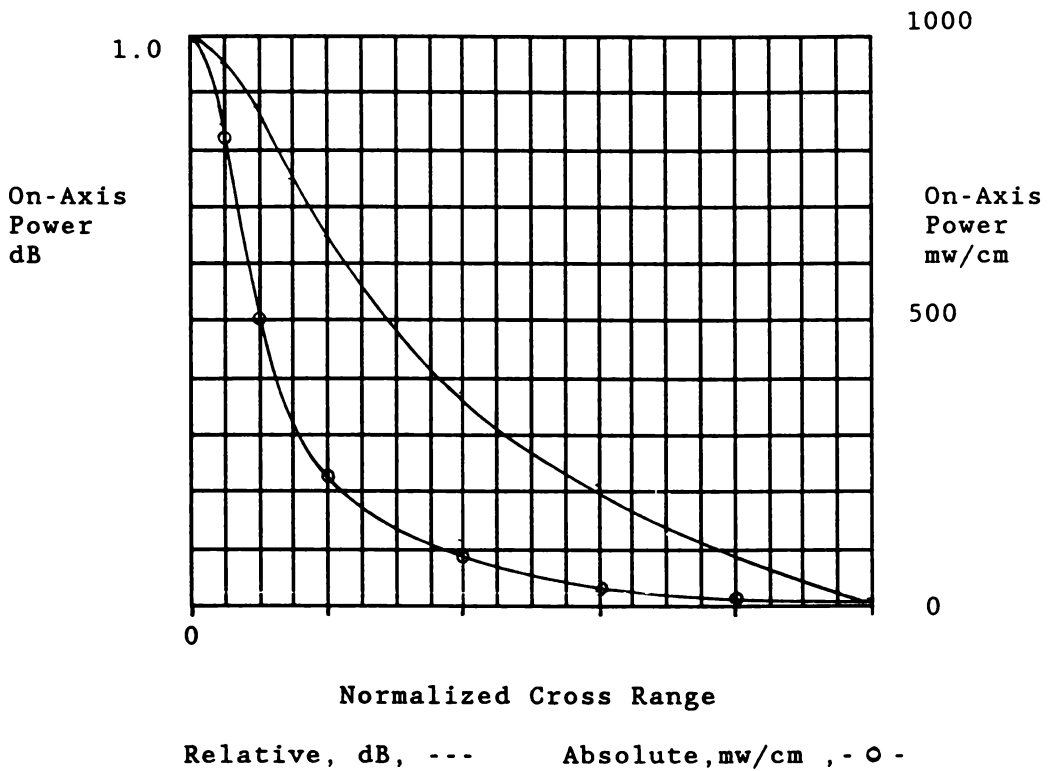


**Figure 4.13** Estimated Radiated On-Axis Power Densities for a Large, High-Power Radar Antenna

which can be expressed in the form of Equation (4.102). Thus,

$$\left[ \frac{\alpha^2}{2a^2} \left( \frac{1}{1 + \chi^2} \right) \right] (x^2 + y^2) = \ln \left( \frac{S}{S_I} \right) + \ln \left( \frac{P_I G_I}{G^2} \right) + \ln \left( \frac{1}{\sigma} \right) + \ln \left( \frac{16\pi\alpha^2 z^2}{a^2} \right) + \ln(Q)$$

When plotted, contours representing radar sensitivities to interference are obtained that display the same characteristics as those in Figure 4.14.

**Radar Siting**—Situations may occur, aside from personnel safety considerations (i.e., a reflection from a building), or when the radar is an interference with other equipment, requiring power densities in specified regions to be minimized. In these interference situations, the methodology used for the computation of power density contours is applicable.

**Radome Analysis**—In general, it is difficult to accurately estimate the radiated fields or power densities within confined areas such as a radome. Typically, fields in close proximity to the surface of the antenna are estimated by an extension in range of the aperture fields. Although a reasonable assumption, the Gaussian



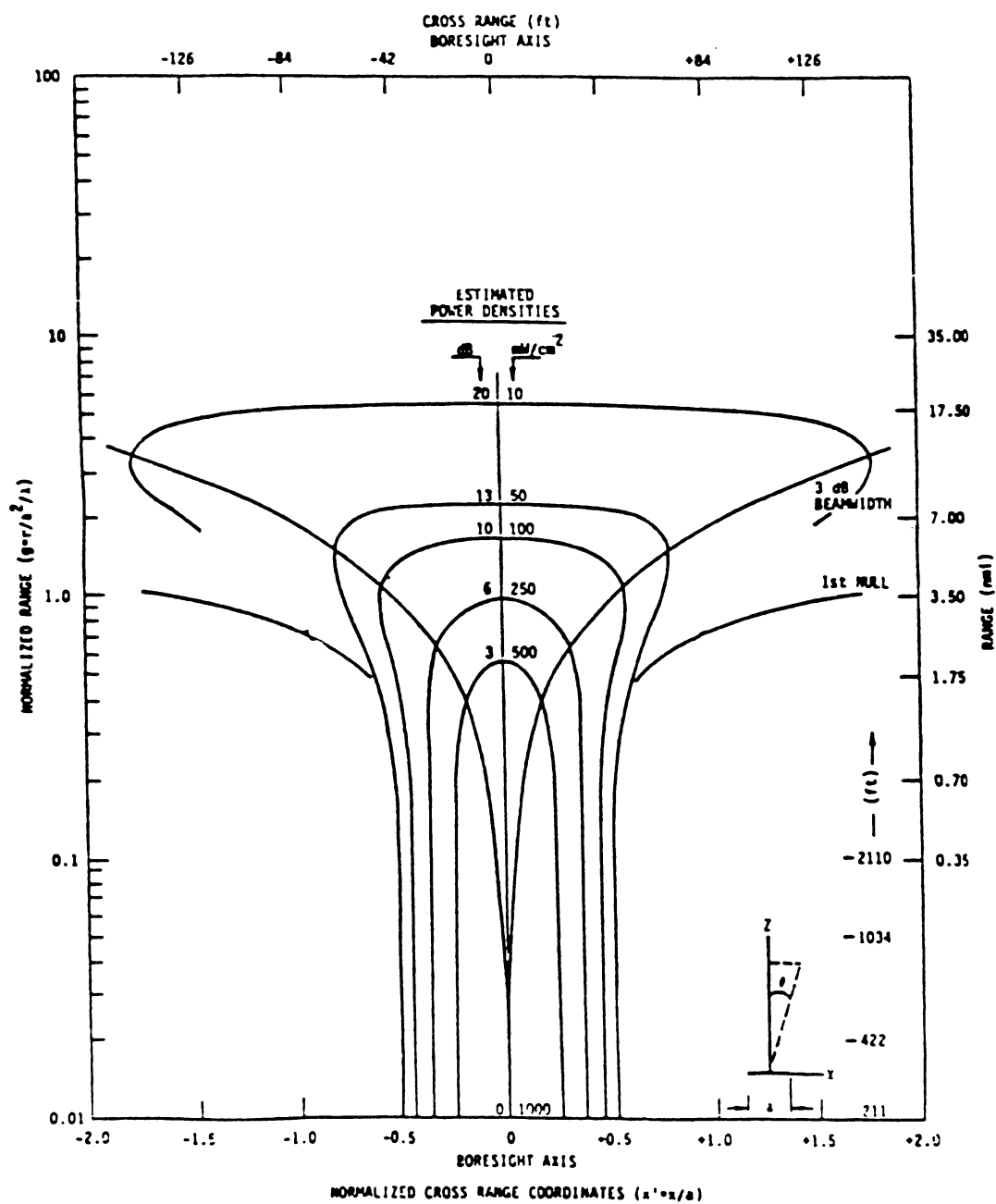
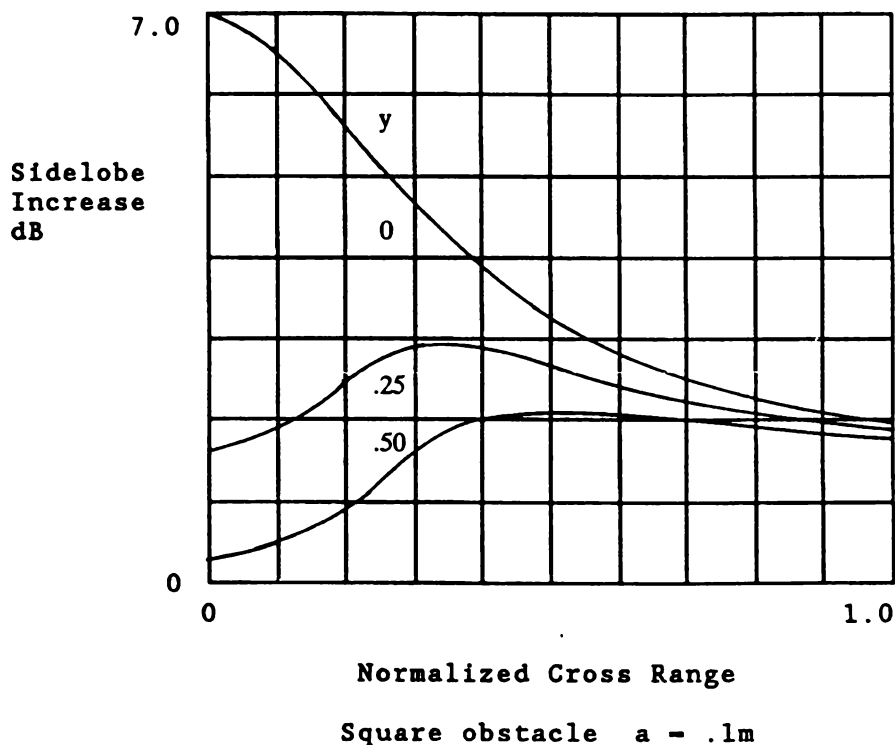


Figure 4.14 Estimated Radiated Power Densities for a Large, High-Power Radar Antenna

equivalent radar equation formulations provide a means for estimating cross-range, and range-dependent variations. Thus, as an example, power densities within and on the inner surface of the radome may be estimated.

## Pattern Degradations

In the examples to follow, obstructions with characteristic dimensions that are large in comparison to a wavelength, but small when compared to the antenna dimension, are arbitrarily positioned within the near-fields. Estimates of sidelobe degradations due to the presence of the obstacles are of concern. The three geometries shown in Figure 4.15 are considered.



**Figure 4.15** Obstacles Positioned in the Near Field

Problems of this type have been formulated by Silver as one of aperture blocking. Obstacles are considered to impart a phase error that reduces antenna gain and increases the level of the first sidelobe. The fields radiated from the obstacle are assumed to be  $180^\circ$  out of phase and referenced to the primary fields. In this initial derivation, an antenna formulation was developed, with uniformly-distributed circular apertures and blockage elements considered. This approach uses a scattering formulation rather than an antenna one and considers a general large aperture in Gaussian equivalent form.

Using Equation (4.1) and substituting for the antenna gain yields

$$S = \frac{P}{4\pi r^2} \left( \frac{4\pi A \eta}{\lambda^2} \right) \quad (4.103)$$

where, as stated previously,  $A = a^2$  is the area of the antenna and  $\eta$  is the aperture efficiency. Positioning an obstacle of cross-sectional area  $A_t$  with maximum characteristic dimension  $\delta$  in the near field of the antenna yields a scattered forward-power density (using Equation (4.44)), of

$$S_f = \left( \frac{4P}{\eta A} \right) \left( \frac{QU}{4\pi r^2} \right) \left( \frac{4\pi A_t^2}{\lambda^2} \right) \quad (4.104)$$

As postulated,  $A_t \ll A$  and  $\alpha \gg \lambda$ . Because sidelobe degradations in the far field are of interest, and the obstacle will be positioned in the near field, the range from the scatter to a far-field position is approximately equal to the radar range. Thus,  $r_1 \approx r$ , which is reflected in Equation (4.104).

#### EXAMPLE: ANTENNA, SCATTERING EQUIVALENCE

We will now consider the following forward scattered power density:

$$S_f = S_p \left( \frac{1}{4\pi r^2} \right) \left( \frac{4\pi A^2}{\lambda^2} \right)$$

If we let the power captured by the scatterer be

$$P = S_p A$$

then, by substitution for  $S_p$ ,

$$S = \left( \frac{P}{4\pi r^2} \right) \left( \frac{4\pi A}{\lambda^2} \right) = \frac{PG}{4\pi r^2}$$

which is Equation (4.1), the result of an antenna formulation. Thus, the equivalence of scattering and antenna approaches to the blockage problem is established.

The example also shows that the radiated power density of a large aperture antenna can be interpreted in a scattering way. In this example, a uniform aperture distribution is assumed where  $A = nA$  with  $n = 1.0$ . Use of the effective area would further generalize this interpretation.

If we let  $S_l$  be the antenna sidelobe level and  $s_l$  the degraded one, then,

$$s_l = \frac{S_l \frac{E}{E_f} + 1}{\frac{E}{E_f} - 1} \quad (4.105)$$

where  $E$  and  $E_f$  are the far antenna and scattered fields, respectively. Equivalently, we have

$$s_l = \frac{s_l \left( \frac{S}{S_f} \right)^{1/2} + 1}{\left( \frac{S}{S_f} \right)^{1/2} - 1} \quad (4.106)$$

Substituting  $S$  and  $S_f$  from Equations (4.103) and (4.106) yields

$$s_l = \frac{S_l \left( \frac{\eta A}{A_t} \right) + \sqrt{4QU}}{\left( \frac{\eta A}{A_t} \right) - \sqrt{4QU}} \quad (4.107)$$

which represents case three in Figure 4.15, where the obstacle is arbitrarily positioned in the near field. For case two, the on-axis positions,  $U = 1$  in Equation (4.107). For the aperture fields,  $r \rightarrow 0$ ,  $Q \rightarrow 1$ , and  $U$  is the aperture distribution. The particular case of  $x = y = 0$ , when the obstacle is centered in the aperture, and a uniform aperture distribution is assumed is Silver's aperture blockage result:

$$s_l = \frac{S_l \frac{A}{A_t} + 1}{\frac{A}{A_t} - 1} \quad (4.108)$$

As an example, consider a square aperture with dimension  $a = 3$  m, a frequency of 3 GHz with wavelength  $\lambda = 0.1$  m, and a truncated-Gaussian antenna with a sidelobe level of 47.5dB. Then, sidelobe degradations, for an obstacle with a cross-sectional area of 100 (or about 16 in<sup>2</sup>) is plotted in Figure 4.16. Thus, the obstruction positioned along the beam axis can be expected to raise the first sidelobe level by more than 5 dB.

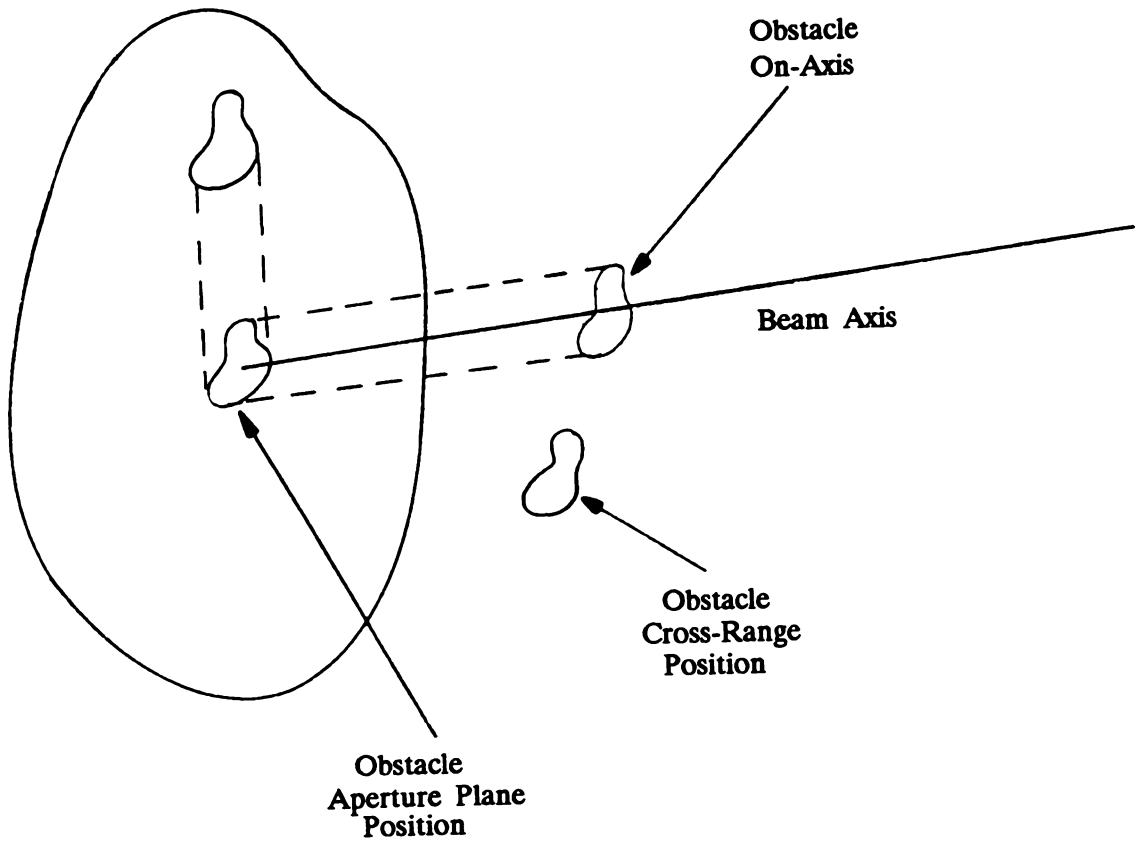


**Figure 4.16** Estimated Sidelobe Degradations due to Obstacles Positioned in the Near Field

### ***EXAMPLE: FURTHER APPLICATIONS OF PATTERN-DEGRADATION FORMULATION***

**Radar Siting**—The formulation may be used to estimate the effects of obstructions encountered in the siting of large, ground-based radars. Low-sidelobe antennas may be of particular concern.

**Radome Nose Tips**—Nose tips placed in radomes designed for airborne applications, when the aerodynamic environment is severe, may degrade antenna sidelobe levels. The formulation is directly applicable for estimating sidelobe degradations. In some instances, comparisons between antenna sidelobes with and without the radome present are useful.

**Airborne Radar Obstruction**—Airborne radars, in particular, may be subjected to obstacles of many forms in the nearfield. Long thin objects, for example, aligned parallel or nearly so to the beam axis may be treated as an antenna with specified gain. The power captured can be estimated from the product of the cross-sectional area of the obstruction and the radiated-power density of the radar. Then,

the Gaussian radar equations can be applied for the computation of scattered-power densities and resulting pattern degradations.

*Aperture Blockage*—An initial application of Silver's formulation was to estimate the effects of mounting structures, an inherent part of reflector antennas, on the sidelobes. A uniform circular aperture was considered. This extension includes aperture efficiencies in the results, the measure that allows extension of the original work to a broader class of antennas. Applications therefore follow, in the design of reflector type antennas, and the assessment of their performance as an element of the radar.

Although sidelobe degradations were considered, the formulas may also be used to estimate beam pointing errors that result from the near-field obstructions. In those instances, the scattered fields are added to the difference or odd function pattern of a monopulse beam structure to determine beam pointing errors. The addition of small signals to difference patterns with large null depths appear as small perturbations, but, in many cases, with large boresight axis shifts.

## Two-term Gaussian Expansions

In many instances, it is necessary to estimate beam null positions and the power densities in the immediate vicinity of the first null of an antenna beam. Two prominent examples are in the siting of a radar where a pattern null may be positioned in a specified direction and in determining beam positions, where received-power densities from interference sources may become excessive. An example of the use of two-term expansion is provided, where the entire antenna radar beam is estimated.

We will now consider a square antenna with a cosine-cubed aperture distribution. From Table XVIII of Appendix A, for a two-term Gaussian expansion:

$$\begin{aligned}\alpha &= 7.37349 \\ C_0 &= 1.12483 \\ C_2 &= 0.06571\end{aligned}\tag{4.109}$$

Because far fields are of interest, the general form of the radiated-power density Equation (4.53) is applicable with  $\mathcal{H}_N$  and  $\mathcal{H}_M$  given by Equations (4.59) and (4.60). Making the substitutions into (4.53), with  $r \rightarrow \infty$  and  $x = 0$ , yields

$$E^2(u) = \left\{ C_0 - C_2 \left[ 4 \left( \frac{u^2}{\alpha^2} \right) - 2 \right] \right\}^2 \exp \left( \frac{u^2}{\alpha^2} \right)\tag{4.110}$$

The radiated antenna pattern (expressed in dB) is plotted in Figure 4.17, where comparison is made to the computed value of Barton and Ward. Good beam estimates are provided by the two-term expansion, up to and including the first null of the antenna pattern. This example demonstrates the extension of the Gaussian beam approximation, limited to the beam peak, to include the entire main lobe of the antenna pattern.

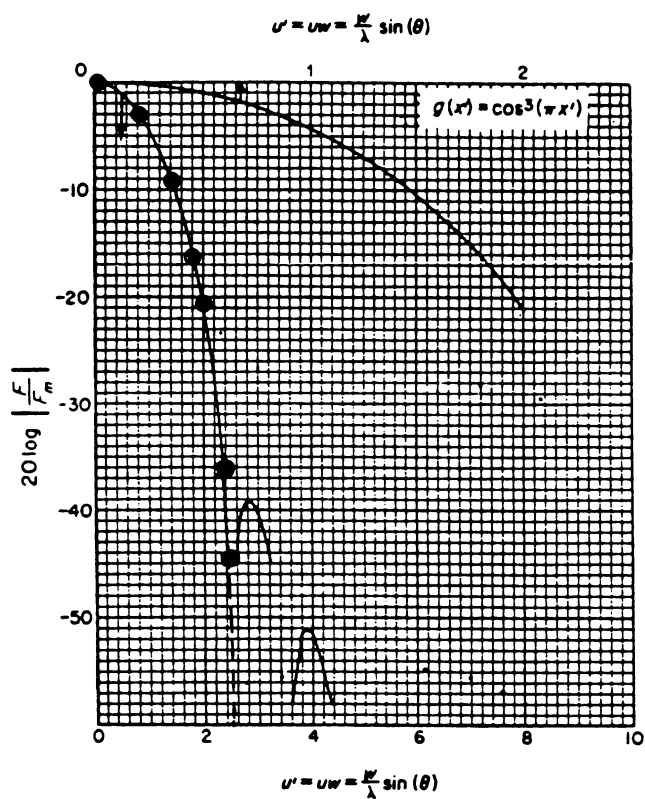


**Figure 4.17** Example of Two-Term Gaussian Beam Estimate. (Comparison with results of Barton and Ward)

### 4.7 FORMULAS

The radar equations derived in the previous two sections are listed below in the more familiar signal-to-noise form. The equations are provided in groups of two for general and Gaussian-equivalent forms covering bistatic, forward, and monostatic radar deployments. As in previous derivations,  $\tau$  is the transmitted pulse width,  $k$  is Boltzmann’s constant, and  $T_s$  is the system noise temperature.

For antennas of square geometries, the Gaussian form of the radar equations are as follows:

$$\text{Bistatic} \quad \frac{S_b}{N} = \left( \frac{P_\tau}{\eta A \mathcal{G}} \right) \frac{QUG_1 \lambda^2 \sigma_b |\mathcal{H}_N|^2 |\mathcal{H}_M|^2}{2\pi r_1^2 k T_s} \quad (4.111)$$

$$\frac{S_b}{N} = \left( \frac{P_\tau}{\eta A} \right) \frac{QUG_1 \lambda^2 \sigma_b}{2\pi r_1^2 k T_s} \quad (4.112)$$

$$\text{Forward} \quad \frac{S_f}{N} = \left( \frac{P_\tau}{\eta A \mathcal{G}} \right) \frac{QUG_1 A_i^2 |\mathcal{H}_N|^2 |\mathcal{H}_M|^2}{\pi r_1^2 k T_s} \quad (4.113)$$

$$\frac{S_f}{N} = \left( \frac{P_\tau}{\eta A} \right) \frac{QUG_1 A_i^2}{\pi r_1^2 k T_s} \quad (4.114)$$

$$\text{Monostatic} \quad \frac{S_m}{N} = \left( \frac{P_\tau}{\eta^2 A^2 \mathcal{G}^2} \right) \frac{4Q^2 U^2 \lambda^2 \sigma |\mathcal{H}_N|^4 |\mathcal{H}_M|^4}{\pi k T_s} \quad (4.115)$$

$$\frac{S_m}{N} = \left( \frac{P_\tau}{\eta^2 A^2} \right) \frac{4Q^2 U^2 \lambda^2 \sigma}{\pi k T_s} \quad (4.116)$$

For circular antennas:

$$\text{Bistatic} \quad \frac{S_b}{N} = \left( \frac{P_\tau}{\eta A \mathcal{E}} \right) \frac{WVG_1 \lambda^2 \sigma_b |\mathcal{L}_N|^2}{2\pi r_1 k^2 T_s} \quad (4.117)$$

$$\frac{S_b}{N} = \left( \frac{P_\tau}{\eta A} \right) \frac{WVG_1 \lambda^2 \sigma_b}{2\pi r_1^2 k T_s} \quad (4.118)$$

$$\text{Forward} \quad \frac{S_f}{N} = \left( \frac{P_\tau}{\eta A \mathcal{E}} \right) \frac{WVG_1 A_i^2 |\mathcal{L}_N|^2}{\pi r_1^2 k T_s} \quad (4.119)$$

$$\frac{S_f}{N} = \left( \frac{P_\tau}{\eta A} \right) \frac{WVG_1 A_i^2}{\pi r_1^2 k T_s} \quad (4.120)$$

$$\text{Monostatic} \quad \frac{S_m}{N} = \left( \frac{P_\tau}{\eta^2 A^2 \mathcal{E}^2} \right) \frac{4W^2 V^2 \lambda^2 \sigma |\mathcal{L}_N|^2}{\pi k T_s} \quad (4.121)$$

$$\frac{S_m}{N} = \left( \frac{P_\tau}{\eta^2 A^2} \right) \frac{4W^2 V^2 \lambda^2 \sigma}{\pi k T_s} \quad (4.122)$$



Applications of the formulas have been demonstrated for several representative radar problems. Two points are of significance in applying the formulas. Power densities should be chosen in a way that takes advantage of the structured properties of the Gaussian field expansions. Then, accuracies of the computations become an inherent part of the analysis procedure, when the order of the partial sum is selected. In addition, advantage should be taken of the real parameters that occur in the far-field expansions, thus reducing the complexity of the computations.

As a final example supporting the derivation of the Gaussian forms of the radar equation, we provide a methodology for use of the formulas. A square antenna is considered.

### ***EXAMPLE: A METHODOLOGY FOR USE OF THE GAUSSIAN RADAR EQUATION FORMULA***

The procedures are described in categories of Gaussian equivalents, two-term expansions, general forms, and meteorological, volume-scattering forms.

*Gaussian Equivalents*—The Gaussian equivalent formulation is the extension of the Gaussian beam approximation to include the near-field and aperture distributions. Procedurally, given a large-aperture radar antenna with known beamwidth, then

1. Place the antenna beam in Gaussian form using Equation (4.17).
2. Determine the Gaussian scaling factor  $\alpha$  using Equation (4.19). The aperture efficiency is  $4\pi/\alpha^2$ . The antenna pattern is given by Equation (4.18) or the more general form of Equation (4.34).
3. The antenna gain is computed using Equations (4.22) and (4.23).
4. Compute the aperture parameter ( $a/a_3$ ) from Equations (4.19) and (4.21). The aperture distribution is given by Equation (4.32). The power aperture distribution is proportional to the square of the exponential formula.
5. Determine the near fields using Equation (4.33). This field formula limits to the far field when  $r \rightarrow 0$  and the aperture distribution when  $r \rightarrow 0$ .

Thus far, the fields have been defined starting with the 3dB beamwidth of the antenna in Gaussian form. Table 4.1 contains some useful antenna data and Gaussian parameters, computed using the procedure given. For radar equation applications, the field quantities are used to estimate the radiated-power densities in the following way:

6. Establish the Gaussian parameters  $Q$  and  $U$ , using Equations (4.27) and (4.28), respectively.
7. Compute radiated-power densities using Equation (4.37). The formula is applicable for the aperture, near, and far fields.
8. Use Equation (4.39), Equation (4.40), Equation (4.45) or Equation (4.46) or their equivalents tabulated above for radar equation computations.

*Two-Term Expansions*—When estimates of the entire radiated far-field antenna beam are needed, a Gaussian two-term expansion may be applied. A recommended procedure is:

1. Determine the Gaussian scaling  $\alpha$ , and the series coefficients  $C_0$  and  $C_2$  for even-function antenna distributions, from the tables of Appendix A, or using the procedures described in Section 3.5 of Chapter 3.
2. Compute the magnitude of the radiated fields, using Equation (4.10). When normalized by division of  $C_0 + 2C_2$ , a normalized power pattern results.
3. For radar equation computations, use the formulas tabulated above for  $N$ ,  $M = 2.0$ .

*General Forms*—General forms of the Gaussian radar equation should be applied when a specified number of sidelobes are of concern. Then, the number of terms in the Gaussian expansions is one higher than the number of sidelobes. A reasonable procedure is

1. Determine the Gaussian scaling factor  $\alpha$  and the series coefficients from the Tables of Appendix A or using the methods of Section 3.5 of Chapter 3.
2. Use the Hermite expansions of Equations (4.59) through (4.62) for far-field computations. Otherwise, the general forms of the Hermite polynomials are necessary.
3. Use  $H_0(x) = 1.0$  and  $H_1(x) = 2x$  and the recurrence formula of Equation (4.5) for Hermite function computations.
4. Use the formulas tabulated above for radar equation computations.

*Meteorological Forms*—When volume scattering, such as rain is encountered, the structured properties of the Gaussian-radiated power densities are helpful. Also, in those instances, scattering measurements are desirable, and a thorough understanding of the radar performance, probably an instrumentation radar, is essential. The Gaussian formulas may be applied in the following way:

1. Place the antenna patterns in Gaussian form. Use the data in Appendix A and the procedures outlined in Chapter 3.
2. Solve Equation (4.101) to determine the effects of the structured antenna pattern on the scattering coefficients. Develop data similar to the data in Figure 4.16.
3. Use Equation (4.100) for volume radar equation calculations.



## ***PART III***

# ***THE ATMOSPHERIC ENVIRONMENT***

Discussions of the effects of the natural atmosphere on the design, analysis, and simulation of a radar are initiated with summary descriptions of the environment where a meteorological point of view is taken. In the two chapters which follow, summary descriptions of regions of the atmosphere, the standard atmosphere, cloud formations, and global rain distributions are provided. Later, when specific cross section and attenuation parameters are compiled, the data supplement the establishment of bounds of the environment and provide their global distributions. The range equation formulations and the accompanying theoretical developments of the previous chapters provide the means by which the data can be applied.

Included are discussions of temporal properties and principal features of the troposphere, stratosphere, mesosphere, and thermosphere. Special topics include discussions of the standard atmosphere, cloud families and genera, precipitation and fog.



## ***Chapter 5***

### ***The Atmosphere***

#### **5.1 REGIONS OF THE ATMOSPHERE**

The principal regions of the atmosphere and the approximate boundaries, characterized by the vertical distribution of temperatures, are shown in Figure 5.1. The principal thermal layers are the *troposphere*, the region of the atmosphere that is in contact with the earth, *stratosphere*, *mesosphere* and *thermosphere*, a high temperature region extending from an altitude around 80 km to the outer edge of the atmosphere. Intermediate regions, where changes in sign of the temperature gradient occur, are the tropopause, stratopause and mesopause.

The heights or altitudes represent average values of middle latitudes where most measurements are made. The data may be considered as a global, annual average. The vertical temperature distribution for the lower 120 km of the atmosphere, which shows the range of temperatures and the properties at the boundaries between the regions, is shown in Figure 5.2. These data are the yearly average conditions at 45° latitude. The temperatures can be expected to vary on a daily and yearly basis at given latitudes, depending on the weather.

#### **The Troposphere**

This lower layer of the atmosphere extends from the surface of the earth to a height of 10 to 16 km. Four-fifths of the mass of the atmosphere is contained in this layer, which is characterized by a decreasing temperature as height is increased above ground level.

The rate of decrease of temperature with altitude is expressed as a *lapse rate*, where, for the troposphere, based on the 1976 U.S. Standard Atmosphere, the average lapse rate is 6.5°C/km. This temperature characteristic results from heating of the atmosphere at the lower heights, the accompanying movement of air upward, and its subsequent cooling as pressure decreases. Because cloud formations are

associated with this movement, and water vapor concentrations are pronounced within the troposphere, most weather processes occur in this layer of the atmosphere.

The *tropopause* is the layer of the atmosphere separating the troposphere and stratosphere. The lower altitude of the tropopause is defined by a lapse rate of 2°C/km or less. The upper bound occurs when, at a given altitude, the lapse rate within the upper 2 km does not exceed 2°C/km. Although controversial, but simple in concept, the tropopause serves as a barrier between an exchange of air between the troposphere and stratosphere.

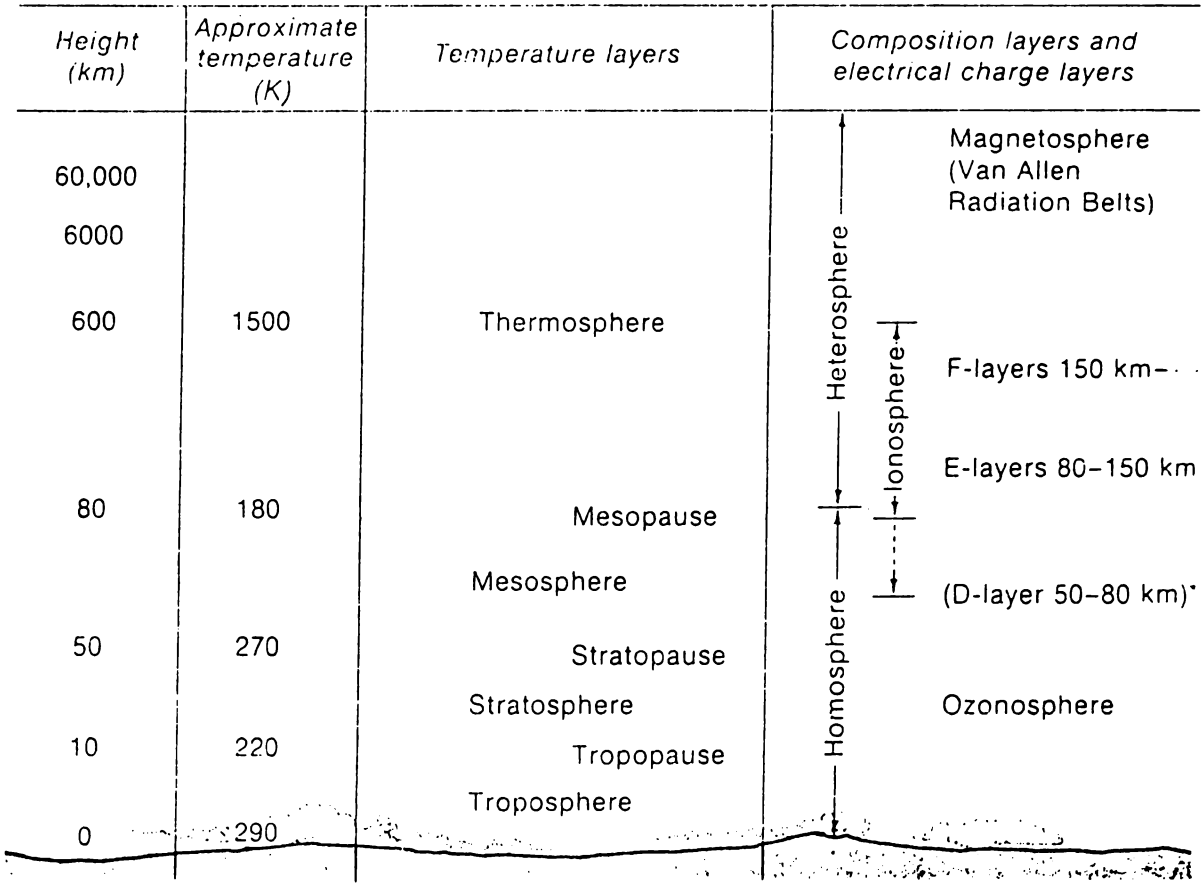
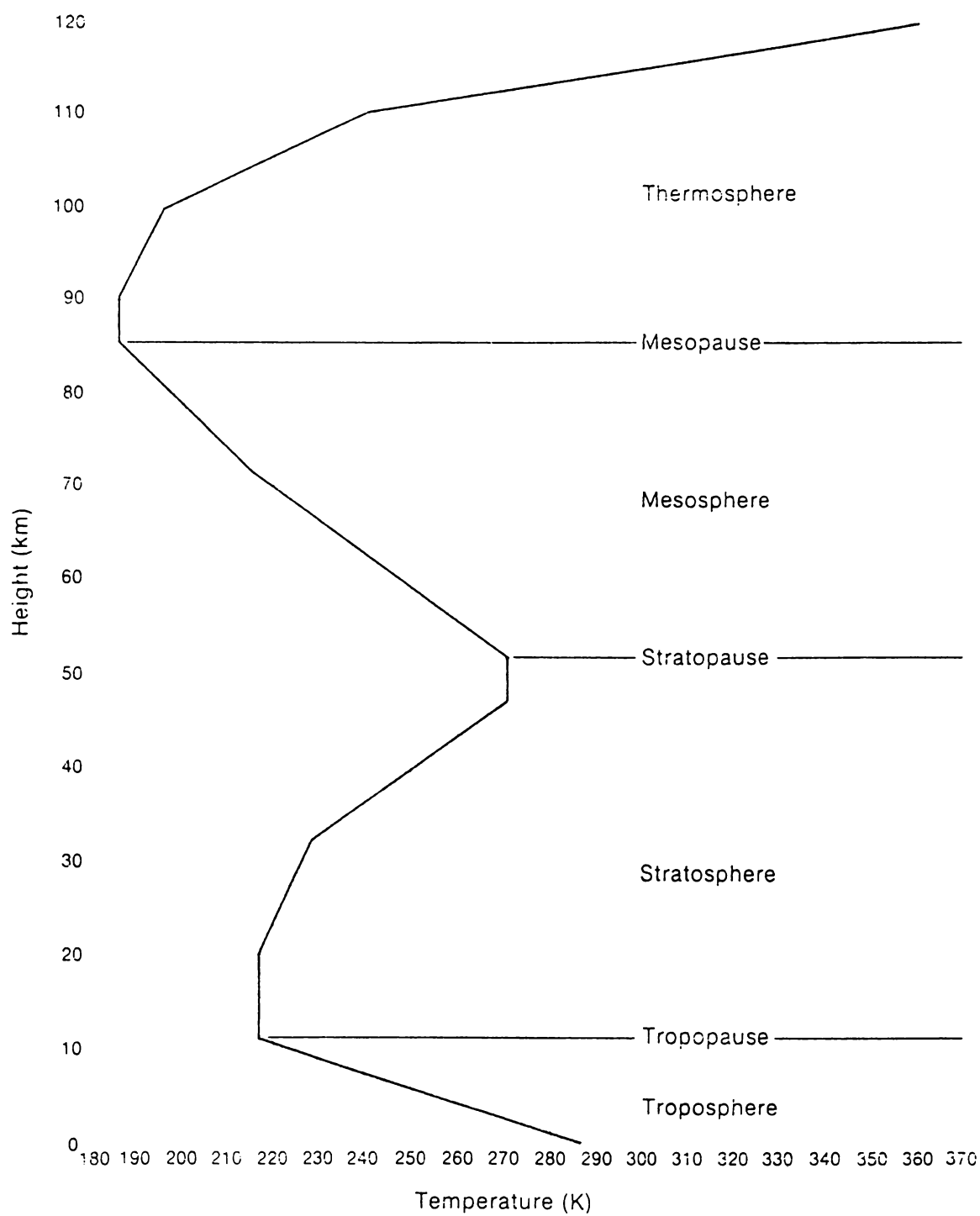


Figure 5.1 Regions of the Atmosphere. (From Neiburger, *et al.*)

The Stratosphere

Referring to Figure 5.2, the stratosphere is the layer of the atmosphere extending above the tropopause to a height of about 55 km. Below about 30 km, the temperature rises slowly, then increases at a higher rate in the upper stratosphere.



**Figure 5.2** U.S. Standard Atmosphere, Regions, and Temperatures. (From Neiburger, *et al.*)



Maximum temperatures around 270 K occur at the stratopause. The composition of the stratosphere is noted for the presence of an ozone layer and the occurrence of a low water vapor content.

The presence of ozone in the atmosphere is of interest for several reasons. Ozone absorbs ultraviolet light; thus, a large part of the ultraviolet radiation emanating from the sun is captured by the ozone layer, high in the atmosphere. The heating of the air at this height creates a warm region at a height of about 50 km above the ground. The amount of ozone in the atmosphere varies considerably from day to day. Although most of the ozone is situated above the tropopause, these changes are closely associated with variations in the weather. The ozone has an unexpected type of annual variation, and its distribution is equally unexpected. The seasonal and latitude variations have been related to the worldwide circulation of air between the troposphere and the stratosphere.

Because of the low water vapor content, few clouds are found in the stratosphere. Occasionally, the tops of very large cumulonimbus clouds rise so violently that they penetrate the tropopause and push up a kilometer or more into the stratosphere; otherwise no ordinary clouds are present. However, in certain cases mother of pearl clouds may form high above the tropopause at altitudes of about 27 km.

The *stratopause*, a layer of constant temperature, separates the stratosphere from the mesosphere. The absorption of solar ultraviolet radiation by ozone accounts for a temperature maximum at the stratosphere averaging about 270 K. In high latitudes during winter, the stratopause temperature may be much lower, and the distinction between stratosphere and mesosphere nearly disappears. The ozone concentration decreases rapidly with height, and the lack of absorbing gases should largely account for the general altitudinal decrease of temperature to an average value of about 185 K at the mesopause, the upper boundary of the mesosphere. Just above the mesopause, dissociation of molecular oxygen by solar ultraviolet rays (at wavelengths shorter than those reaching the stratopause) accounts for a rapid increase of temperature with heights.

## **The Mesosphere**

The mesosphere is the atmospheric layer between the stratopause and the mesopause. Like the troposphere, it is a layer where the temperature decreases with height. Special features of the mesosphere include a region of extremely strong winds centered near heights of 65 km, tidal oscillations and gravity waves of appreciable amplitude, meteors, and noctilucent clouds. In addition, the majority of the *D region* of the ionosphere, the lowest ionized layer of the atmosphere, is found in the mesosphere. Like the troposphere, the mesosphere is subject to strong seasonal variations of temperature at high latitudes. We think that many of the atmospheric variations encountered are linked to complicated physical processes

in the underlying layers.

In the middle to high latitudes, the mesospheric thermal structures vary between summer and winter months. In the summer, the temperature usually falls off smoothly with height at the rate of 3–5 K per kilometer; mesopause temperatures as low as 130 K have been measured. However, in the winter, alternating layers of decreasing and increasing temperatures are commonly encountered, resulting in a decrease in temperatures usually in the range of 180–250 K, at altitudes near 85 km. It appears that the winter thermal structure changes in some coherent way throughout the stratosphere and mesosphere. For example, when there is strong warming at a given level, warming also occurs at a level 40–50 km higher (or lower), with cooling at a level in the middle.

## The Thermosphere

The thermosphere is a high-temperature region extending upward from heights of about 80 km to the outer reaches of the atmosphere. Its high temperatures result from absorption of solar radiation at wavelengths below about 2000 Å. Responses to changes in solar radiation from night to day have been evident and related to sunspot cycles, placing this region of the atmosphere under direct solar influence. The motion within this region of the atmosphere appears to be one of thermally-induced solar tides with laminar and turbulent dynamic properties not clearly understood. The thermosphere contains the majority of the ionosphere, with auroras often seen in this region.

The *ionosphere* is an upper region of the earth's atmosphere in which many of the atmospheric atoms and molecules have become electrically charged by the addition, or (more often) the removal of electrons to produce ions, in which the ions and freed electrons coexist and become ionized. As a result, the ionosphere is sometimes defined as a *body of ionization*. The total population of ions and electrons is distributed throughout the ionospheric region. The lower boundary of the ionosphere lies at heights of about 55 km above the earth, where electron concentrations are sufficient by day to affect radio propagation. The concentration of electrons increases irregularly, with height to a maximum at elevations of 200–600 km. Above that, the concentration decreases again, but more slowly and over a much greater height span. Relative to the layered regions of the atmosphere, the ionosphere begins at a base near the stratopause, rises through the mesosphere to a peak in the thermosphere, and extends upward to overlap the *exosphere* (a region of relatively few particles). It terminates at heights of several earth radii in a complex of interactions with ionization flowing out from the sun. It was once thought that the ionosphere had a layered structure with distinct maxima of electron density occurring in layers called (in order of increasing altitude) *D layer*, *E layer*, *F layer* (in the daytime only), and *F2 layer*. The terms *D region*, *E region*, and *F region* are now used to refer to altitude regions below 90 km, between 90 and 140

km, and above 140 km, respectively. In the height range of 100–150 km, strong electric currents are generated by a process analogous to that of a conventional electric generator or dynamo. Thus, this region is often termed the *dynamo region*.

An important feature of the ionosphere is that it absorbs much of the sun's harmful radiation. The ionosphere's existence is, in fact, a direct consequence of this absorption in the earth's cover of air. Another important feature is the ionosphere's guidance of radio waves around the curvature of the earth. The E and F layers are most important in this regard, for they reflect radio signals in the broadcast and short-wave bands. Ionization of the D region acts to attenuate these signals by day, but effectively disappears when the sun sets, permitting broadcast reception over much greater regions. Ionization in the D region serves as a reflector for long-wave band signals by day, without introducing serious attenuation. This band provides stable communication as a result, and so is employed for special purposes. For example, accurate transoceanic navigation by ships and aircraft is accomplished with its aid.

## 5.2 U.S. STANDARD ATMOSPHERE

The vertical structure and properties of the atmosphere are described as the U.S. Standard Atmosphere. Initiated in the 1920s to meet aircraft needs, the atmospheric data compilations have been subject to review and extensions under international control. The U.S. Standard Atmosphere, formulated by the *National Advisory Committee for Aeronautics* (NACA) and European version generated by the *International Commission for Aerial Navigation* (ICAN) were unified by the *International Civil Aviation Organization* (ICAO) in 1952. Since then, properties of the atmosphere have appeared in 1962, and 1976, as U.S. Standard Atmosphere. The data provided below in the form of simple mathematical expressions are from the 1962 version. Tables of atmospheric properties are best obtained from the original sources. The formulas that follow are based on the formulations of Ulaaby.

### Pressure and Temperature

The atmospheric pressure decreases approximately exponentially with height reducing to one half its sea level value at 5.5 km altitude, one-fourth at 10 km, one-eighth at 15 km and one-sixteenth at 20 km. The pressure may be expressed in the following form:

$$p(h) = p_o e^{-h/H_p} \quad (5.1)$$

where  $h$  is the height above sea level,  $p_o$  is the sea level pressure and  $H_p$  is a constant.

Temperature as a function of height above sea level is estimated in the following way:

Troposphere	$T_0 - az$	$0 \leq h \leq 11 \text{ km}$
Tropopause	$T(h) = T$	$11 \leq h \leq 20 \text{ km}$
Lower Stratosphere	$T_1 + (h - 20)$	$20 \leq h \leq 32 \text{ km}$

where  $T_0$  is the temperature at sea level,  $T_1$  is the temperature at the propopause height of 11 km,  $h$  is the height or altitude and  $a$  is a constant. Changes in temperature with altitude or equivalently the temperature gradient  $-dT/dh$  where  $dT/dh$  is negative, is defined as the temperature lapse rate. Following this definition, the constant  $a$  is the temperature lapse rate in the lower 11 km of the atmosphere.

### Air Density

Air density, like pressure, varies exponentially with height. Following the format of Equation (5.1), with  $P_a$  being the density of dry air (expressed in  $\text{kg/m}^3$ ):

$$\rho_a = 1.225 e^{-h/H_1} \quad (5.2)$$

where  $H_1$  is a constant altitude set at 9.5 km. The results apply for heights between sea level and about 10 km. A better fit to the data, for heights up to 30 km, is obtained using

$$\rho_a = 1.225 e^{-h/H_2} [1 + 0.3 \sin(h/H_2)] \quad (5.3)$$

Aside from the addition of a sinusoidal weighting factor, the constant  $H_1$  in Equation (4.3) is reduced slightly to a value of  $H_2 = 7.3 \text{ km}$ .

### Water Vapor

Water vapor density at sea level will vary by about two orders of magnitude between cold day climates and hot humid days varying from about  $10^{-2} \text{ g/m}^3$  to  $30^{-2} \text{ g/m}^3$ . The average value of water vapor density as specified by the U.S. Standard Atmosphere 1976, is  $\rho_o = 7.72 \text{ g/m}^3$  for middle latitudes. With these stipulations, the altitude dependence of water vapor density is expressed in exponential form as

$$\rho_v(h) = e^{-h/H_3} \quad (5.4)$$

The constant  $H_3$  is set between 2 and 2.5.

As in previous examples the choice of constants, particularly the height constants  $H$  are somewhat arbitrary and should be adjusted to achieve better fits to the atmospheric data within specified boundaries if necessary.

### 5.3 CLOUDS

As we continue the summary descriptions of the atmosphere, but now concentrate on elements of the troposphere, a review of cloud forms and their basic properties is provided. The formation of clouds is considered first.

#### Formation of Clouds

Clouds form when moist air cools below its saturation point, releasing water vapor in the form of small water droplets or ice. When formed, the droplets are small and are suspended in the form of a cloud. As the damp air rises, it cools by expansion due to falling pressure. When condensation occurs, a number of aerosol particles are present to suspend the small droplets. Aerosol concentrations have been reported to vary from 100 particles or less per cubic meter to more than  $1065/\text{cm}^3$  in highly-polluted air. Water vapor droplets occur in sizes of about .01 mm in diameter with concentrations of about a few hundred per cubic centimeter.

When a thermal (i.e., a mass of warm air), rises above the condensation level, a trail of cloud occurs behind the upward movement. As we expect in the rather complicated structure of cumulus clouds, for example, more than one thermal occurs, giving rise a mixture of cloud forms of the same type. When confronted with a temperature inversion, and when the thermal penetrates the inversion level, a smooth cap or top of a cloud, defined as a *pileus*, is formed. When the inversion layer is not penetrated, the top of the cloud flattens out, covering a large area. Although treated here in a qualitative way, it is a combination of these and other basic mechanisms that give rise to an abundance of cloud forms.

#### Cloud Families

Let us begin with some abbreviated definitions of cloud formations. They are as follows:

- *Cirrus*—layered and fibrous in appearance;
- *Stratus*—layered without form;
- *Cumulo* or *Cumulus*—formed by convection;
- *Nimbo* or *Nimbus*—raining;

- *Castellanus*—high and oversized cumulus;
- *Pileus*—flat, capped;
- *Alto*—high;
- *Alto Cumulus*—short for alto stratocumulus;
- *Mamma*—bulging at base of cloud.

Clouds form in three distinct layers with four cloud families, by international classification, called high, medium, or low clouds, and clouds with vertical developments. Each family is divided into groups referred to as a *genera*. Each family contains two or three genera, which total ten for all families. Each genera is further divided into *species* and species into *varieties*. The International Cloud Atlas designates 10 genus, 20 species for 7 out of 10 genera, and 7 varieties that pertain to many of the species. Here we will concentrate on the first level of cloud classification, the cloud families and their associated genera, provided in Table 5.1

**Table 5.1** Cloud Families and Genera

<i>Family</i>	<i>Mean Low Altitude (KM)</i>	<i>Mean High Altitude (KM)</i>	<i>Genus</i>
High Clouds	6	—	(1) Cirrus (2) Cirrocumulus (3) Cirrostratus
Middle Clouds	2	6	(4) Altocumulus (5) Altostratus
Low Clouds	—	2	(6) Stratocumulus (7) Stratus (8) Nimbostratus
Clouds with Vertical Development	0.5	—	(9) Cumulus (10) Cumulonimbus

Beginning with high clouds and following the numbering of cloud genus in the table, some distinguishing features of the clouds are as follows:

- (1) *Cirrus*—detached clouds, fibrous in appearance, white in color, often of silky texture, composed of ice crystals with a degree of transparency which is dependent upon the crystal separations;
- (2) *Cirrocumulus*—layered or patched, contain small elements or globular masses and are arranged horizontally in regular fashion, often of wave-like or ripple structure;

- (3) *Cirrostratus*—thin optically transparent veils, smooth or fibrous in texture, often totally cover the sky, give rise to halos;
- (4) *Altostratus*—closely-spaced flattened globular masses arranged in line wave or group formations, white or gray in appearance, fibrous or diffuse, and layered;
- (5) *Altostratus*—resemble thick cirrostratus, layered and striated, bandlike appearance, cover large portion of sky, displays moon or sun, does not display halos;
- (6) *Stratocumulus*—separate or overlapping patches, gray or white with dark blotches, not fibrous but layered, rolled pattern resembles shallow cumulus, characterized by complete coverage with a defined base;
- (7) *Stratus*—gray cloud layer, resemble fog but above ground, uniform base, may contain drizzle, ice prisms, or snow, and when broken up form fractostratus clouds;
- (8) *Nimbostratus*—dark gray color, layered, continuous falling rain or snow usually reaching the ground, blot out sun, nearly uniform in composition;
- (9) *Cumulus*—thick clouds, dome-shaped, exhibit protuberances, horizontal base, detached, dense, white tops, dark bases, and may produce light rain;
- (10) *Cumulonimbus*—extensive vertical development, dense, produce rain, snow, and sometimes hail and thunderstorms, fibrous upper pileus structure, low ragged structure and overall mountain-like appearance.

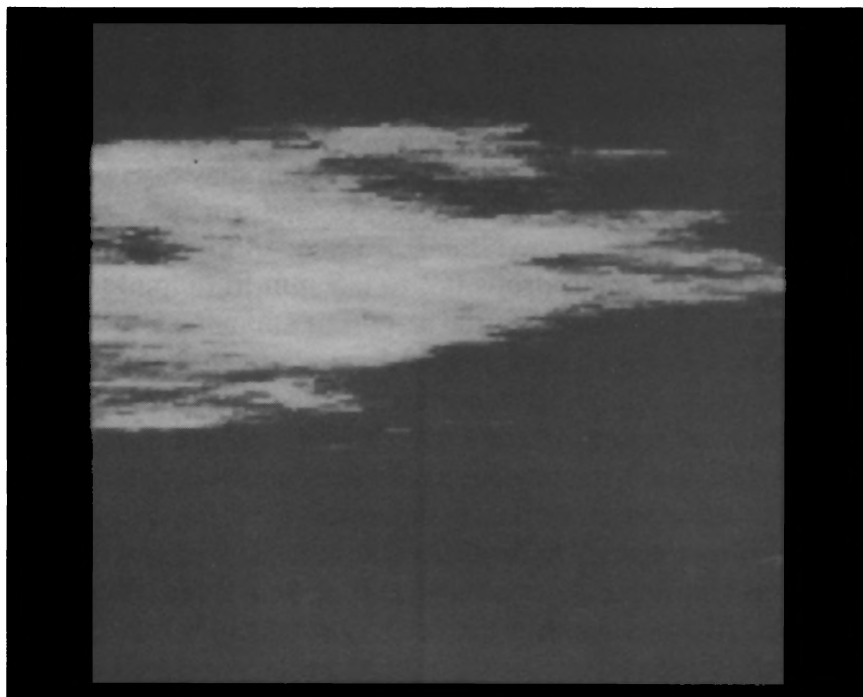
Additional abbreviated definitions that support the cloud features are as follows:

- *Anvil*—spreading out of cumulus cloud at a temperature inversion;
- *Billow*—wave-like appearance formed between two layers of air;
- *Contrail*—aircraft condensation trails, artificial cirrus;
- *Fallstreak*—sweeping trail, produced by falling ice crystals formed by wind variation at different height;
- *Fog*—stratus clouds formed at ground level;
- *Streets*—parallel lines of cumulus clouds;
- *Thermos*—mass of warm air;
- *Waves*—wave-like appearance resulting from condensation, level undulations over mountain or hilly terrain.

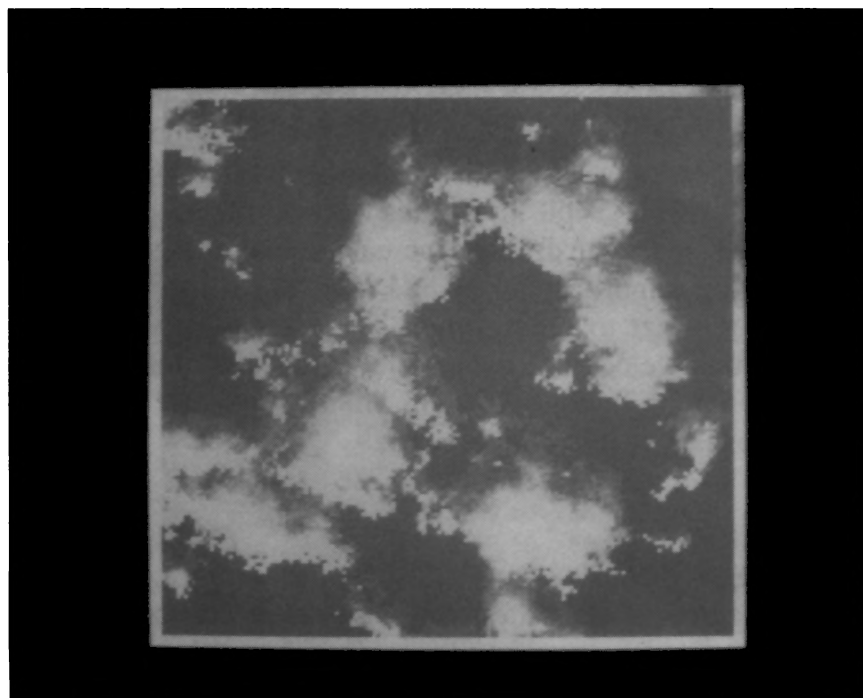
Examples of cirrus and cumulus cloud computed using a fractal formulation are shown in Figure 5.3.

## Precipitation

Cumulonimbus, nimbostratus, and altostratus clouds give rise to precipitation of various forms. Small amounts of precipitation may fall from cumulus, stratus,



(a)



(b)

**Figure 5.3** Fractal Display of Cloud Forms: (a) Cirrus, (b) Cumulus



stratocumulus or altocumulus. Generally, high altitude clouds formed of ice crystals produce little or no observable precipitation. As a rule, cumulonimbus clouds yield localized rain, snow or hail showers, thunderstorms and possibly tornadoes. A long-lasting steady rain is produced by nimbostratus and altostratus formations. Drizzle arises from stratus and cumulus clouds, which may also produce showers.

Precipitation occurs in the following forms:

- *Drizzle*—consists of small drops 0.2 to 0.5 mm in diameter, with rain rates of 1 mm/hr;
- *Rain*—consists of drops larger than 0.5 mm, upper diameter limits about 5 mm, instability is evident in larger diameters and the drops break up. Steady and near-uniform rain falls from layered clouds. Showers and rain storms with a marked cellular structure are characteristic of convective clouds. Light rain is characterized by rain rates of 1 mm/hr or less, moderate rain is 1–4 mm/hr, and heavy rain is 4 mm/hr or more;
- *Snow*—formed by aggregates of ice crystals as flakes, individual crystals or small pellets. Most snow is in the form of flakes that range in size from 1-2 mm to several centimeters. Snow accumulations are measured in depth of fall and equivalent water content. Ice crystals, when falling as precipitation, appear as fine dust. Ice pellets are observed as sleet resulting from the freezing of small rain drops;
- *Hail*—forms in strong updrafts in cumulonimbus clouds with high supercooled liquid content. Hailstones vary in size from 5 mm to 10 cm or more in diameter. Typically the diameters are about 1 cm.

Clouds are suspended or rise resulting from air currents that vary in velocity from 1–2 cm/s to 12 mm/s. Typically clouds consist of small water droplets with radii between 5 and 30  $\mu$ m. The droplets increase in diameter through a coalescence process, where falling raindrops will collide and fuse with other droplets. When the droplet increases in size to a point where the forces of gravity and air resistance are equal, the terminal velocity of the droplet is reached and rain will occur. The radii of drizzle drops are in excess of 0.1 mm while large raindrops in thunderstorms may have radii in excess of a few millimeters.

## Cloudiness

Estimates of the degree of cloudiness or *cloud cover* are expressed in tenths or percentages (i.e., one-tenth equals a 10% cloud cover), and are complicated by climatic, oceanic, and time-of-day factors. Furthermore, when considering radar applications, and in particular the formulation of environmental specifications, cloud cover distributions should include at least the ten cloud genus. We imply here the existence of an overwhelming data base that furnishes, for example, the

distribution of stratus clouds within a particular area of the world, for day and night conditions, where data may be sparse. The specifics of the cloud cover then require a careful review of cloud formations at locations related to the specifics of the radar, such as the frequency or bands of frequencies that are involved. Fortunately, the global distributions of rain are available in a form convenient for radar applications, and are based on quantitative data taken worldwide. Unfortunately, cloudiness can only be approximately correlated with rainfall because of the complexities noted above.

However, it is worthwhile to review here at least some basic global properties of cloudiness. Cool temperate regions receive a maximum of rainfall and minimum cloud cover in summer; the situation is reversed in winter. In regions of the Mediterranean, namely Egypt, summers are characterized by about one-tenth cloudiness, while in winter cloudiness increases to four-tenths. In hot tropical climates, rainfall and cloud distributions coincide, being maximal in summer and minimal in winter; An excess of water vapor occurs over oceans, forming clouds. The cloud formations are not only characteristic of ocean climates, but also influence cloudiness on the continents. Some properties of cloud cover include the occurrence of heavy cloud cover and rainfall near the polar regions, heavy rainfall and less cloudiness near tropical regions, and little cloudiness and rainfall in trade-wind subtropical regions.

Average global cloudiness compiled for 10° latitude bands on a monthly and yearly basis is given in Table 5.2. Note monthly averages being as low as 36 percent, and reaching values near 90 percent in some instances. Yearly averages vary from about 40 to 75 percent with global monthly averages exceeding 50 percent in all cases. Cloud cover is substantial and, as pointed out, requires separate evaluation when clouds are an issue in the radar design and deployment process.

**Table 5.2**  
Average Global Cloudiness Expressed in Percentage\*

<i>Latitude</i>	J	F	M	A	M	J	J	A	S	O	N	D	Yr
90-80 N	36	47	56	46	76	87	90	85	84	64	45	41	63
80-70 N	56	56	55	63	70	74	75	76	78	75	63	50	66
70-60 N	57	56	54	59	65	66	66	68	71	72	67	60	63
60-50 N	59	57	57	59	64	63	63	62	62	67	67	64	62
50-40 N	59	57	57	57	56	56	54	49	49	54	58	61	56
40-30 N	50	49	49	48	48	43	42	39	39	43	45	48	45
30-20 N	41	41	41	39	41	43	45	44	40	39	38	40	41
20-10 N	40	39	39	40	47	53	59	58	54	46	44	44	47
10-0 N	50	48	49	53	54	56	57	55	53	53	53	53	53
0-10 S	54	53	53	52	50	50	50	52	53	53	53	55	52
10-20 S	54	52	52	49	46	45	43	44	43	47	49	54	48
20-30 S	49	50	50	47	48	48	47	45	48	47	49	50	48

30-40 S	53	52	54	53	55	56	56	54	55	56	55	52	54
40-50 S	64	65	63	64	64	67	69	64	66	67	67	66	66
50-60 S	76	69	71	74	73	72	70	69	68	71	71	75	72
60-70 S	86	80	80	72	72	66	68	74	75	77	83	80	76
70-80 S	64	80	69	69	64	47	49	59	65	74	62	63	64
0-90 N	50	49	49	50	53	54	56	54	53	52	51	51	52
0-90 S	60	59	58	57	56	55	55	55	56	58	58	59	57
Continents	47	47	47	48	49	50	49	48	48	49	49	50	49
Oceans	59	58	58	57	58	58	59	58	58	59	58	59	58
Global	54	54	53	53	54	55	55	54	54	55	55	55	54

\*From Neiburger, *et al.*

Tabulated Cloud Characteristics

Cloud characteristics are summarized in Table 5.3. Aside from the key features of the 10 cloud genus, the table contains physical sizes, constituents and densities.

5.4 FOG

Fog is usually a result of a condensation process that occurs at or near the ground. Evaporation occurs, leading to a supersaturated condition and the formation of fog. Other occurrences of fog relate to clouds coming in contact with the ground, such as the drifting of a stratus cloud into a mountain slope. Fog is characterized as follows:

- *Steam fog*—results from cold air movements over warm water;
- *Warm-front fog*—evaporation of warm rain falling through cold air, usually associated with the movement of a warm front, under certain humidity conditions yields a supersaturated air mass at ground level;
- *Radiation fog*—results from radiational cooling of the earth’s surface below its dew level;
- *Ground fog*—radiation fog of small heights;
- *Valley fog*—radiation fog that forms in valleys;
- *Advection fog*—formed by cool air passing over a colder surface;
- *Up-slope fog*—results from the adiabatic cooling of air up-sloping terrain.

Fog consists of water droplets in most instances, but in cold climates may be composed of ice particles. Steam, dust, smoke, and other aerosols that may occur near ground levels are also associated with fog. Because of these variances and apparent complexities, care must be taken in deducing or interpreting fog data from meteorological sources.

**Table 5.3**  
Properties of Clouds

<i>Cloud Genus</i>	<i>Features</i>	<i>Color</i>	<i>Constituents</i>
Cirrus (High)	Thin, detached, fibrous in appearance	White, gray at low sun	Ice crystals
Cirrocumulus (High)	Layered or patched	White	Ice crystals
Cirrostratus (High)	Thin, smooth or fibrous in texture	White, gray at low sun	Ice crystals
Alto cumulus (Middle)	Globular masses arranged in formation	White or gray	Water droplets, ice crystal or snowflakes
Altostratus (Middle)	Layered and striated, band-like appearance	Light to dark gray	Ice crystals (thin), water droplets (thick)
Stratocumulus (Low)	Separate or overlapping patches, layered, rolled	Gray	Water droplets, 7 to 8 microns
Stratus (Low)	Layered, at low altitudes, fog-like appearance	Light to medium gray	Water droplets, about 4 microns
Nimbostratus (Vertical)	Layered, nearly uniform in composition	Medium gray	Ice crystals, water droplets about 10 microns
Cumulus (Vertical)	Thick, dome shaped	White from above, varying shades of gray from below	Water droplets, about 6 microns
Cumulonimbus (Vertical)	Thick, dome shaped, extensive vertical	White from above, gray to black from below	Water drops, ice, ice crystals and hail

Table 5.3 continued

Height of Base (km)	Thickness (km)	Precipitation
7-10	.100-.200 m, thin to 1, thick	None
6-8	0.2 to 0.4	None
6-8	0.1 to several	None
2-6	0.1 to 1	Rarely, light rain or snow
3-5	0.1 thin, 6 to 8	Light rain, light to moderate snow
about 0.5 to 1.5	0.2 to 0.8	Usually none, occasional light rain or snow
0.1 to 0.7	0.2 to 0.8	Drizzle, light rain or snow
0.1 to 1	to several km	Continuous rain or snow, light to heavy
0.8 to 1.5	0.15 to 1.5	Occasional light rain or snow
0.4 to 1.0	3 to 15	Moderate to heavy rain or snow, hail

Some specifics of fog formations include the presence of small drop sizes being less than 100  $\mu\text{m}$  in diameter. Because of the meteorological conditions associated with fog formations (for example, temperature and wind conditions), size distributions may vary considerably between fog formations, even at the same or similar locations. In addition, humidities of 95 to 100% are normally associated with fog, except over salt water, where humidities of 75 to 90% are common. Lastly, water concentration of fog formations is lower than typical water clouds (a few hundredths of a gram per cubic meter compared to values of 0.1  $\text{g}/\text{m}^3$  or more); droplet concentrations are less than  $100/\text{cm}^3$ . Fog appears to be denser than clouds because of the effectiveness of small droplets to absorb light, unlike the larger drops of typical water clouds.

Traditionally, fog forms are expressed as a visibility factor, determined by an observer's ability to see an object at a specified range. Typically, the visibility factors lie between about 400 and 1000 m. The judgments are also based on the ability of the observer to recognize the existence of fog at a specific area, giving rise to another difficulty in interpreting the data. The frequency of occurrence of fog on a global basis for visibilities less than 1000 m will be included in the global rain data distributions in the next chapter.



## *Chapter 6*

### *Global Rain Regions*

Global rain distributions are provided in four climatic categories, which are further subdivided into eight groups. The concept of *point rain rate* (PRR) is explained with accompanying probability of occurrence distributions. Examples of the use of the data as a first step in the formulation of a rain model for radar applications are included. Fog data are provided on a global scale showing yearly occurrence for one-kilometer visibilities.

#### **6.1 DEFINITIONS**

The global rain distributions to be described are placed in twelve climatic groups with eight divisions and four subdivisions. Associated with each group are probability distributions relating point rain rates and exceedance probabilities, each requiring special attention.

A PRR is the rate occurring at an observation point. Attenuation and backscatter values are associated with this rate. Normally, computation of radar performance in rain is based on a uniform, spatial rain-rate distribution. Attenuation and backscatter coefficients, that may be obtained from a number of sources, are point values usually distributed over the entire operating region of the radar. However, rainfall is rarely uniform over a typical radar propagation path. For example, when the PRR is low to moderate in intensity (within a rainstorm convective in character), the attenuation over a path length of more than several kilometers will exceed attenuation estimates, based on a uniform distribution of PRR and associated attenuation over the path. Conversely, a PRR of high intensity will lead to a lower path length attenuation estimate, because of the likelihood that the observation point is within a cell of the storm, with rain rates diminishing along a propagation path away from the observation point. The notion of point values forms the basis for taking the nonuniformities along a path into account.

The *exceedance probability* is expressed as a percentage of the year that a given rain rate will be equaled or exceeded. For example, an exceedance probability



of 0.1% related to a rain rate of 7 mm/hr, is interpreted to mean an occurrence of rain equal or exceeding 7 mm/hr, .012 months, .365 days, or about eight hours a year. The distributions given later plot rain rate as the ordinate (expressed in mm/hr) *versus* the exceedance probability.

## 6.2 CLIMATE REGIONS

Global rain distributions, compiled for communication systems applications, have evolved from climate regions based largely on temperature, terrain features, and types of vegetation, to the more realistic basis of global similarities in rain rate distributions. When initially formulated for the United States, five climatic regions were judged to be adequate. The regions were employed by the International Radio Consultative Committee (CCIR) on a global basis, later found to be inadequate for very intense rain areas, and expanded from five to eight regions. A five-region coverage of the United States was maintained, with one region subdivided into three areas for an improved description of observed rain rates.

The global distributions as described by Crane (see bibliography), are provided in Figure 6.1. The climate regions are *polar*, *temperate*, *subtropical* and *tropical*, each subdivided into two zones. The regions within the United States, shown in expanded form in Figure 6.2, are as follows: B, taiga moderate polar; C, maritime temperate; D, continental temperate; E, wet subtropical and; F, arid subtropical. The D region shown in Figure 6.2 is subdivided into D1, D2, and D3 groups and the B region is placed into B1 and B2 parts. Europe has similar climate regions, as shown in Figure 6.1 and in the expanded plot in Figure 6.3. The climate regions are B, C, D, and F.

Arid subtropical regions occur in Africa, Australia, the Middle East, and Far East; Large wet tropical regions are found in Africa and South America. Oceanic regions are also included in Figure 6.1 where, within the northern temperate zones, maritime temperate regions C occur. The C region also occurs in all of the United Kingdom, Eastern Europe and the upper northwest section of the United States.

Associated with each climatic region are the exceedance probability distributions (shown in Figure 6.4 and tabulated in Table 6.1). Comparing results within Figure 6.4 and referring to the numerical values in Table 6.1, an exceedance probability of 0.1 occurs for rain rates of 7.2 mm/hr in the maritime temperate zone C, 14.5 mm/hr in the continental zone D and in the extreme, 64 mm/hr in the wet tropical zone corresponding to the United Kingdom and Eastern Europe, a major portion of the United States, and the wet region of Africa and South America, respectively. European countries, by further comparison of Figures 6.2 and 6.3, have the same climatic regions, but they are distributed differently due to the influence of the maritime zone C.

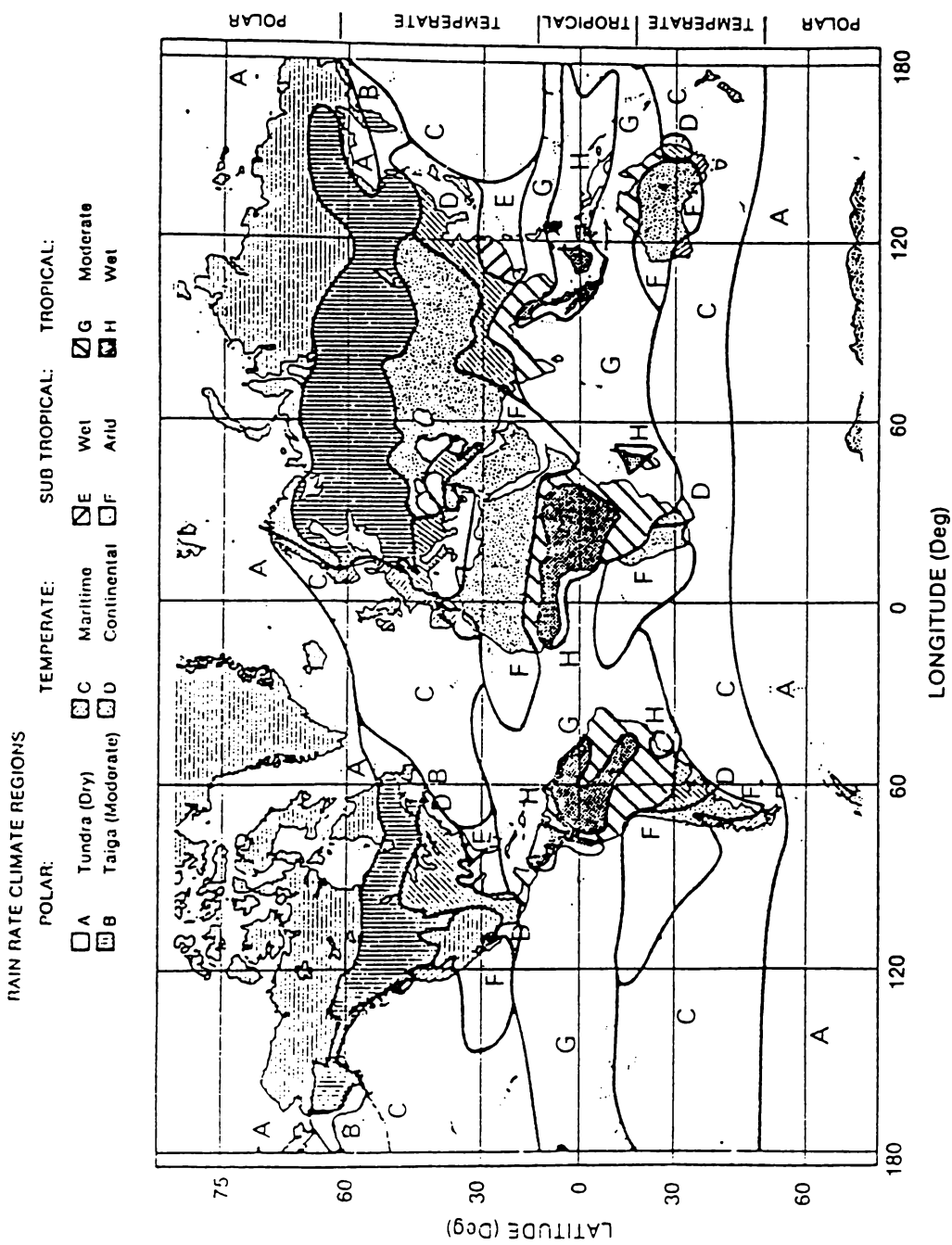
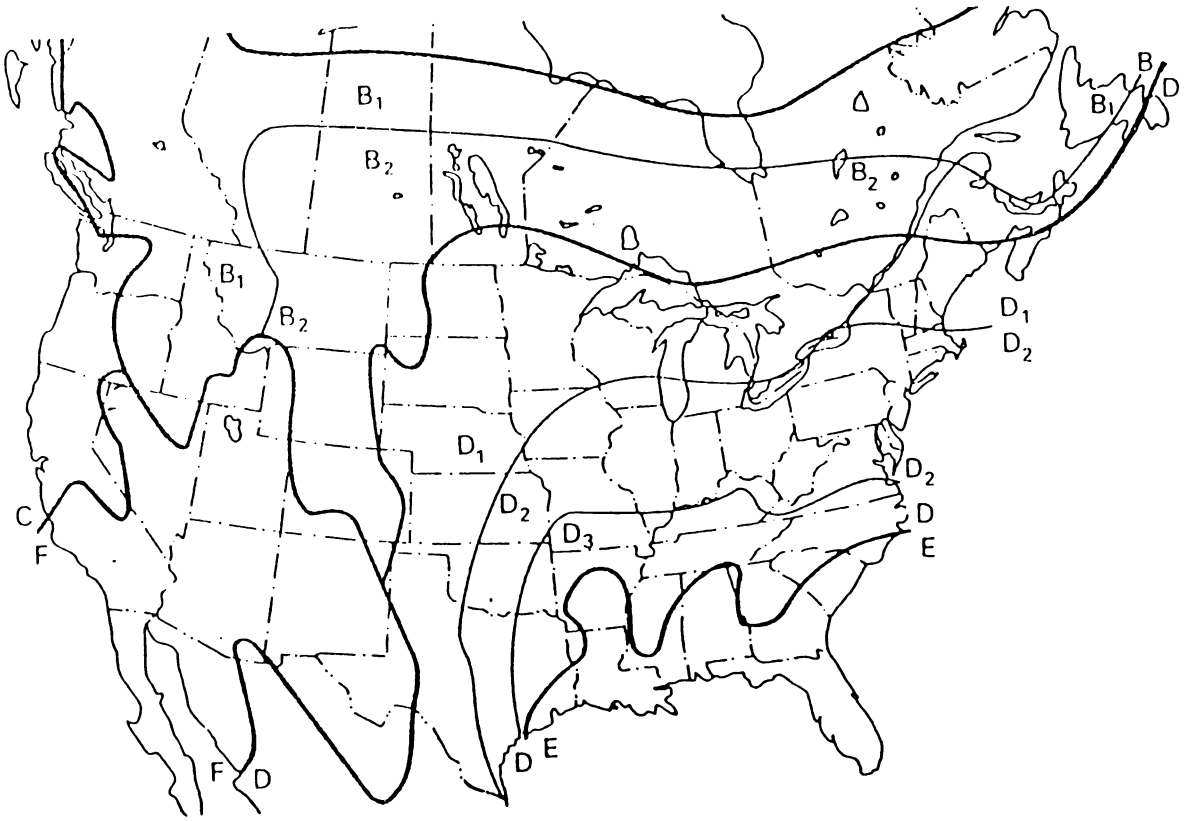


Figure 6.1 Global Climate Regions. (From Crane)



**Figure 6.2** Climate Regions for the Continental U.S. and Southern Canada. (From Crane)

### 6.3 FOG OCCURRENCES

Global fog occurrences are provided in Figure 6.5. The zones represent the average number of days per year that fog will occur sometime during a 24-hour period for a visibility of 1 km or less. These data are subjected to the judgments regarding their occurrences and the exactness of the visibility factor and do not distinguish between night or day, types of fog or times of occurrence.

The average daily occurrences of fog are most severe in coast regions of Asia, South America and Europe. The coastal fogs can be attributed to advection fogs forming over the oceans and drifting inland. The occurrences in Europe are radiation and up-slope fogs in the Alps, which have one of the highest daily occurrences in the world. Generally, the advection and frontal fogs in the coastal regions occur in the summer when warm air winds blows over colder water masses. The advection fogs are known to be widespread, dense, and deep. Radiation fogs are also dense, but vary in depth or heights above ground. When high radiation fogs occur, they may persist for long periods of time during daylight hours; Ground radiation fogs are usually nocturnal. Frontal fogs characteristic of water occurrences

**Table 6.1**  
Point Rain Rate Values for Exceedance Probabilities\*

Percent of Year	Rain Climate Region											Minutes per Year	Hours per Year
	A	B <sub>1</sub>	B	B <sub>2</sub>	C	D <sub>1</sub>	D = D <sub>2</sub>	D <sub>3</sub>	E	F	G	H	
0.001	28.5	45	57.5	70	78	90	108	126	165	66	185	253	5.26
0.002	21	34	44	54	62	72	89	106	144	51	157	220.5	10.5
0.005	13.5	22	28.5	35	41	50	64.5	80.5	118	34	120.5	178	26.3
0.01	10	15.5	19.5	23.5	28	35.5	49	63	98	23	94	147	52.6
0.02	7	11	13.5	16	18	24	35	48	78	15	72	119	105
0.05	4	6.4	8	9.5	11	14.5	22	32	52	8.3	47	86.5	263
0.1	2.5	4.2	5.2	6.1	7.2	9.8	14.5	22	35	5.2	32	64	526
0.2	1.5	2.8	3.4	4.0	4.8	6.4	9.5	14.5	21	3.1	21.8	43.5	1,052
0.5	0.7	1.5	1.9	2.3	2.7	3.6	5.2	7.8	10.6	1.4	12.2	22.5	2,630
1.0	0.4	1.0	1.3	1.5	1.8	2.2	3.0	4.7	6.0	0.7	8.0	12.0	5,260
2.0	0.1	0.5	0.7	0.8	1.1	1.2	1.5	1.9	2.9	0.2	5.0	5.2	10,520
5.0	0	0.2	0.3	0.3	0.5	0	0	0	0.5	0	1.8	1.2	26,298

\*From Crane.

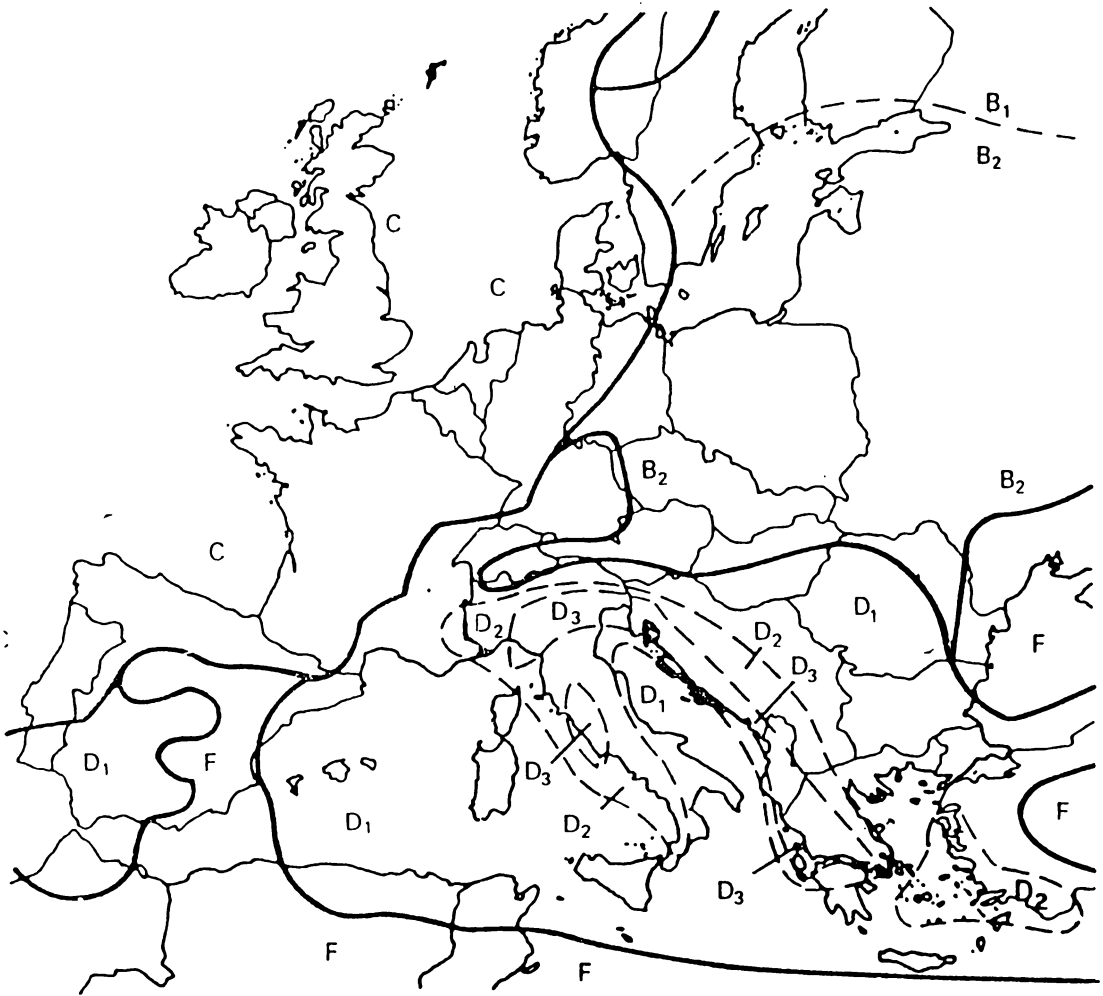


**Figure 6.3** Climate Regions for Europe. (From Crane)

are short-lived and infrequent when accompanying a cold front, but are persistent, deep, and expansive when accompanying a warm front with falling rain.

**6.4 EXAMPLES**

The data provided constitute the first step in the modeling process. Two examples are given that show the usefulness of the tabulated cloud characteristics of the previous chapter and the global distributions of rain and fog described above.

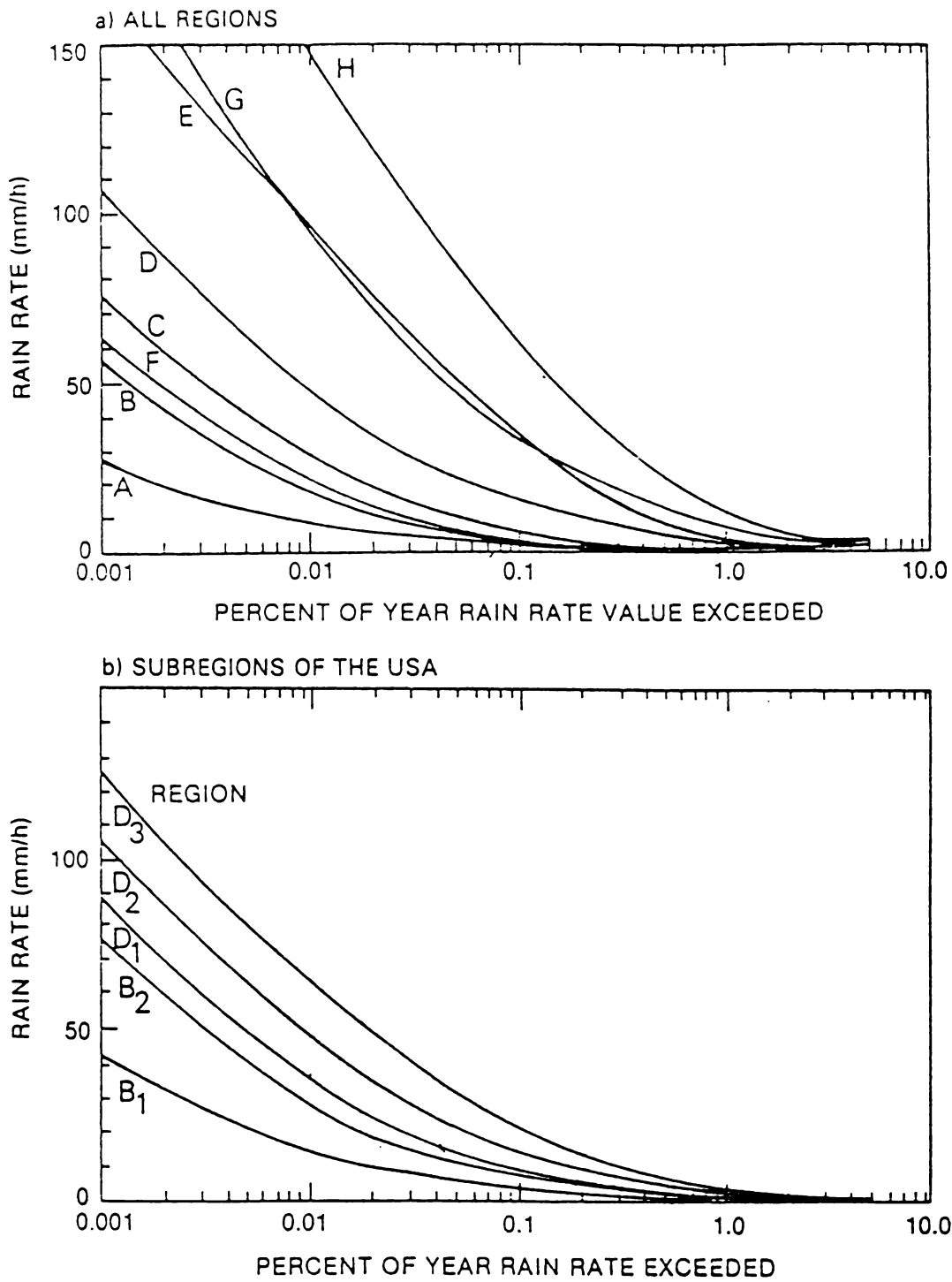


**Figure 6.4** Point Rain Rate Exceedance Probabilities. (From Crane)

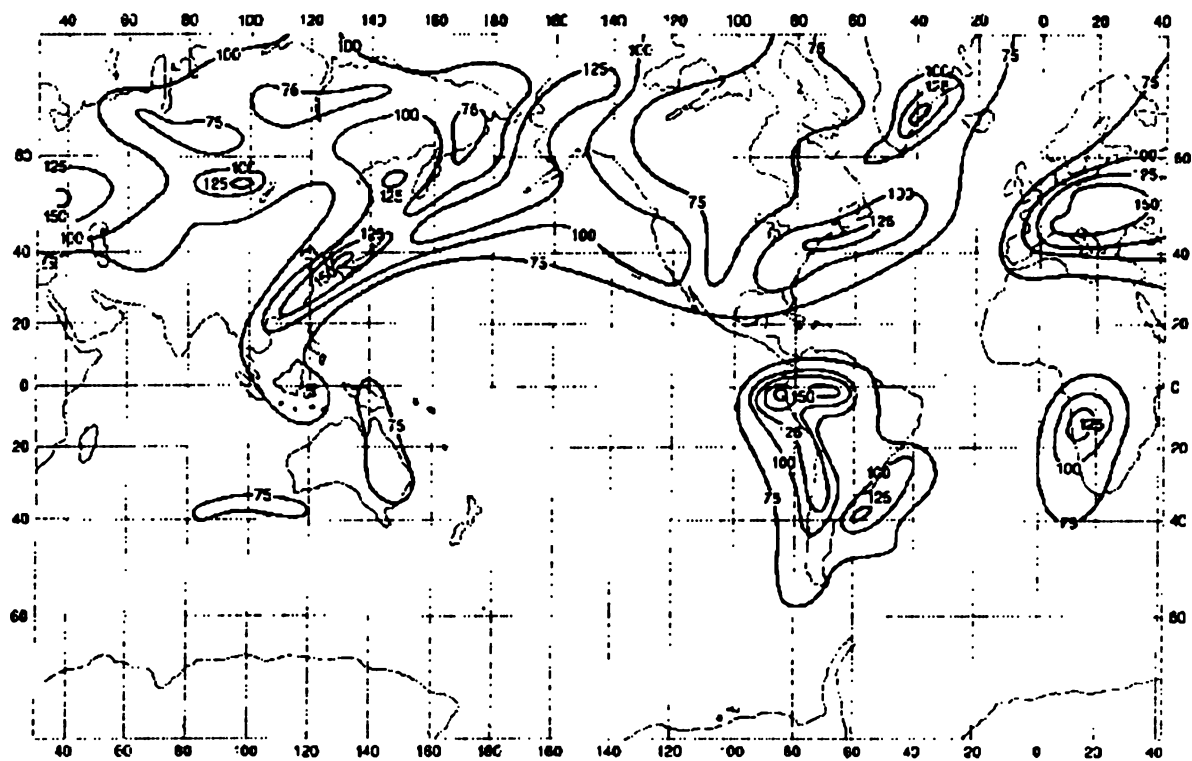


**Figure 6.5** Global Fog Occurrences for a Visibility of 1 Kilometer or Less During the Day. (From Neiburger, *et al.*)

*EXAMPLE: USE OF CLIMATE REGIONS*

A millimeter-wave tracking radar is designed to achieve acceptable sensitivity at the desired maximum range when subjected to a uniform rainfall of 4 mm/hr. Its estimated down time in hours per year when installed in Florida, Seattle or Minnesota is about 145, 55, and 45 hours, respectively. The rain climatic regions for the locations are E, C, and D, with the numerical values found by interpolation from Table 6.1, based on the selection of climatic regions from Figure 6.2.

*EXAMPLE: EXPECTED OPERATING ENVIRONMENT*

Consider a ground-based low-angle, millimeter-wave tracking radar with expected noticeable attenuation from cloud, fog, and light rain environments. Describe an expected operating environment for a Washington state coastal location.

From Table 6.1, consider the operating environment to consist of at least stratus clouds, with water composition bounded between a lower height of 0.1 to 0.7 km and an upper height of 0.3 to 1.5 km, with water contents of about

---

1 gm/m<sup>3</sup>. From Table 4.4, consider light rain of 1 mm/hr or less, resulting from nimbostratus clouds. The rain is expected to be uniform in distribution and observable from ground level to heights or altitude of several km (assumed to be about 2 km). From Figure 6.2, the rain climate region is the maritime temperate C (with an expected yearly occurrence of rain exceeding 1 mm/hr); Table 6.1 shows rain about 175 days per year. From Figure 6.5, advective and frontal fogs with 1 km visibility can be expected to form at least once a day for an average of 100 days per year. The fog will be characterized by a water content of 0.1 gm/m<sup>3</sup> and formed between ground level and heights of about 50 m.

The examples will be extended to include attenuation and backscatter values in Chapter 8, when data compilations and models are described.





## ***Part IV***

### ***Data Compilations and Models***

Data and models are provided for clear air, rain, and cloud environments. Emphasis is placed on rain, where attenuation and backscatter data are compiled. Models are described in three levels of sophistication designated as uniform, path-dependent, and fractal. Examples are provided that demonstrate the use of both the radar equations and the environmental descriptions of the previous chapters.



## *Chapter 7*

### *The Clear Environment*

Atmospheric constituents include nitrogen, oxygen, and several minor gases. The water content excludes rain and clouds. Atmospheric effects on propagation include absorption by gases and particles and, at millimeter and higher frequencies, scattering from the constituents. The index of refraction of clear air changes with air density and moisture content, and gradients in the index of refraction may lead to wave front distortion, phase delays, and bending of the propagation paths. Emphasis in this chapter is placed on these attenuation and refractivity properties of the atmosphere.

#### **7.1 ATTENUATION**

Values of clear air attenuation are provided for altitude and humidity variations. Zenith attenuations, the attenuations along a vertical line of sight passing through the entire atmosphere, are included.

Much of the data presented here are directed toward the higher regions of radar frequencies, where atmospheric effects are the most pronounced. This is particularly evident in the cloud data, where significant attenuation occurs at millimeter-wave frequencies. Radar signals are attenuated at low frequencies within the atmosphere and are adversely affected by rain. At frequencies below about 1.2 GHz, attenuation is a result of oxygen absorption with water vapor absorption being negligible but contributing to attenuation at higher frequencies. Extensive attenuation data were assembled by Blake for absorption by oxygen and water vapor constituents for frequencies of 100 MHz and above at varying elevation angles. These data are summarized in the graph of Figure 7.1a, where the lower frequencies are highlighted. Radars operating at frequencies between 1 and 10 GHz may experience signal attenuations in excess of one dB when transversing the entire atmosphere for elevation angles of 10° or less. The remaining graphs of Figure 7.1, from the Blake data base, provide separate attenuations due to oxygen and water vapor absorption, which are additive, for frequencies between about 1

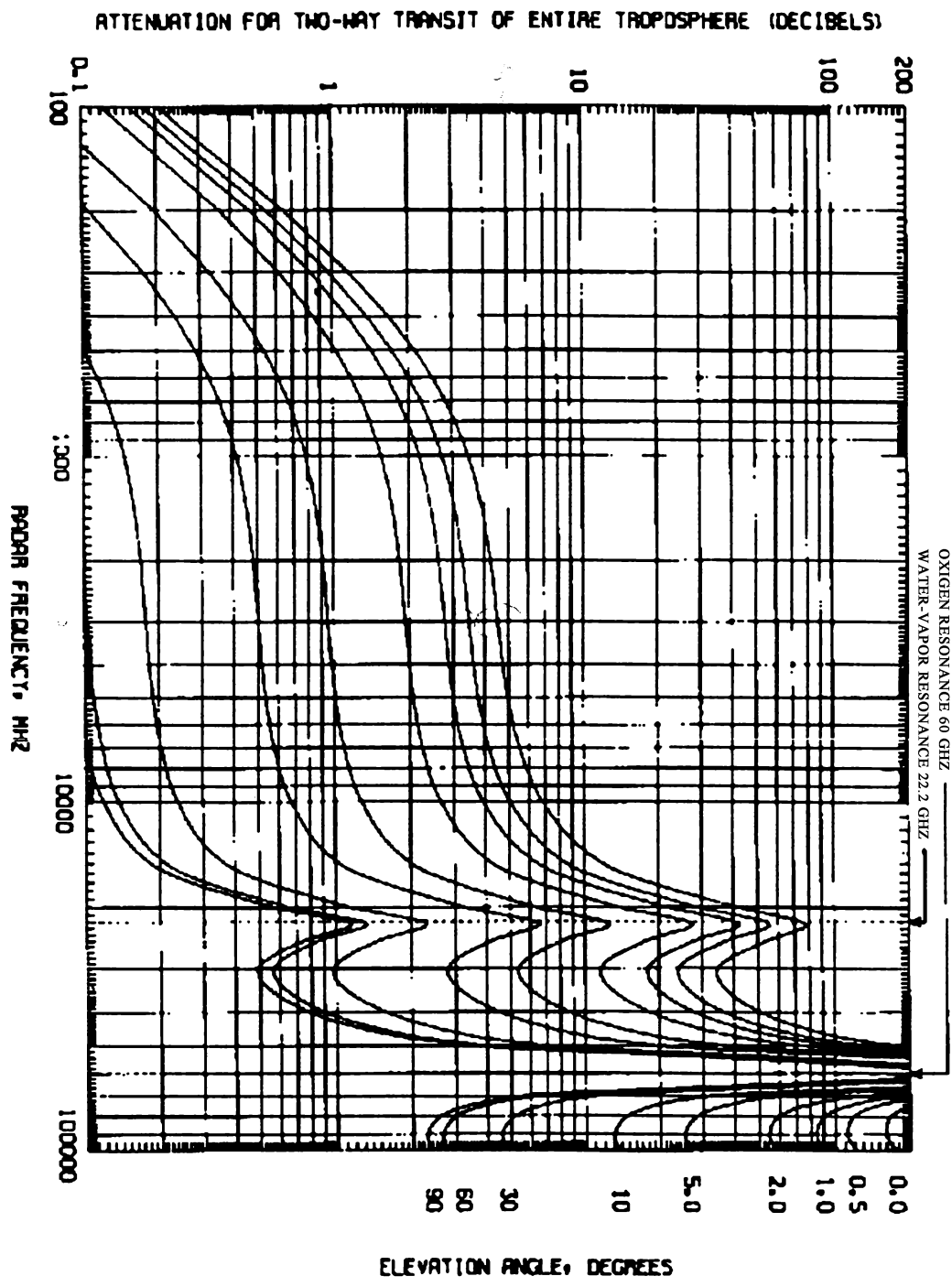


Figure 7.1(a)

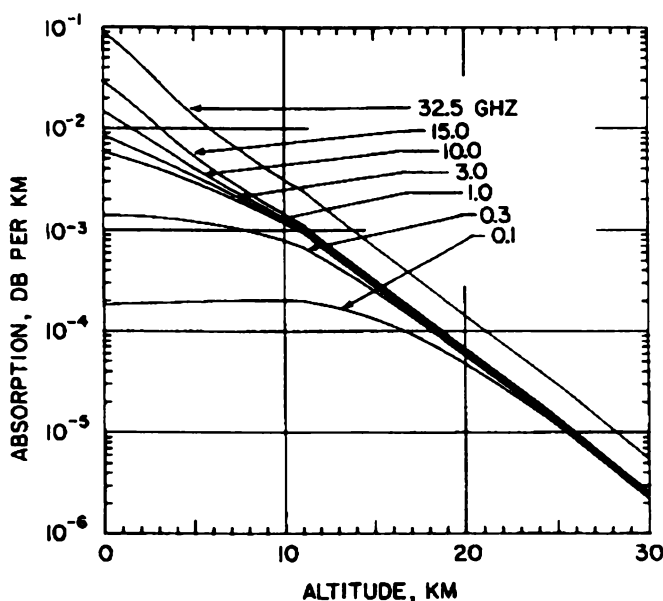


Figure 7.1(b)

**Figure 7.1** Clear Air Attenuations at Low Radar Frequencies, (a) total tropospheric and (b) dB per km at  $0^\circ$  elevation angle. (From Blake)

GHz and 10 GHz. Clear air attenuation is significant for long radar systems operating at low elevation angles, and may degrade overall sensitivity.

## Properties

Clear air attenuations at sea level are plotted in Figure 7.2 as attenuation per length (dB/km) *versus* frequency (GHz) for several relative humidities. Fog and rain attenuations are also included, for comparative purposes. As indicated, attenuation due to fog is similar to that of a high-humidity, clear environment, increasing attenuation within the windows, and following the frequency-dependent trends of the molecular absorption curves. Rain, however, is characterized by a different frequency dependence, as would be expected by the occurrence of different wavelength to particle size ratios.

The effects of diatomic oxygen and water molecules can be discerned in Figure 7.2. Oxygen has numerous overlapping magnetic dipole transitions near 60 GHz, seen as a high and broad absorption peak. Also, oxygen has an isolated line near 118 GHz, best seen as the narrower peak on the zero relative humidity curve. At sea level, the attenuation rate at the 60 GHz absorption is about 15 dB/km, and the zenith attenuation is about 156 dB. Water has two pronounced resonance

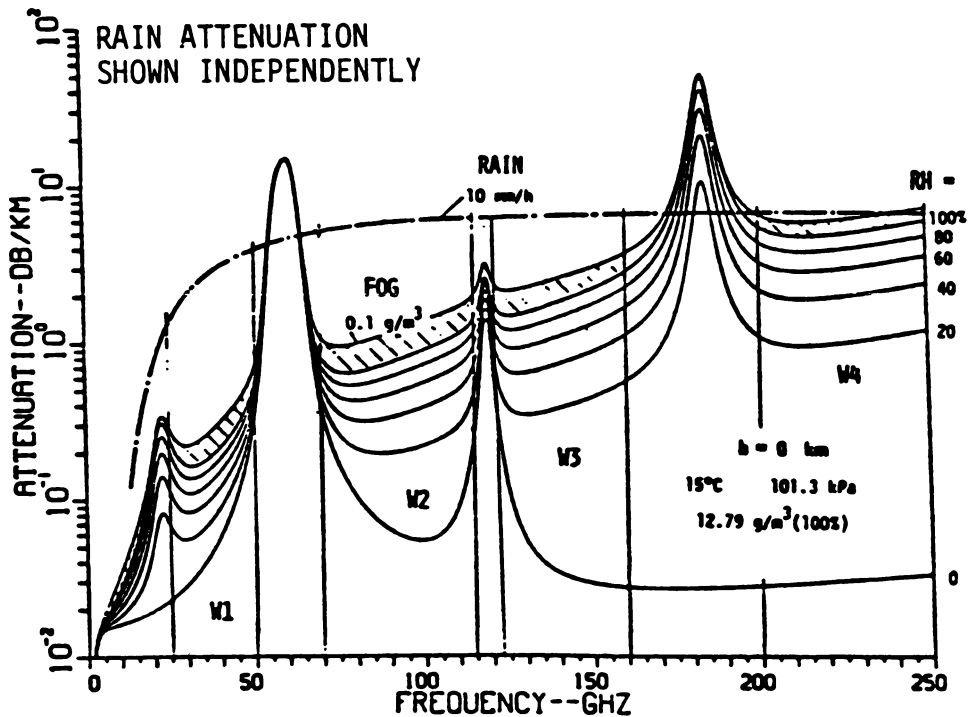


Figure Figure 7.2 Clear Air Attenuation at Sea Level. (From Liebe)

absorption lines occurring near 22 and 183 GHz. As expected, the effects of those lines are observed to increase as relative humidity increases. Table 7.1 gives the sea level, 50 percent relative humidity attenuation rate and zenith attenuation at these four molecular transitions. Atmospheric propagation windows occur between the attenuation maxima corresponding to the transitions. The minimum attenuations in the windows occur near 35, 94, 140, and 220 GHz. Table 7.2 contains the widths and attenuation rates of those windows.

Attenuation rates increase considerably in the windows with increasing relative humidity. The increase may be due in part to the uncertainties in the wings or drop-offs of strong oxygen and water lines, or to the idealized use of Mie scattering theory for water droplets. The resulting additional absorption is included in the data presented in Tables 7.1 and 7.2.

Altitude Dependence

Figures 7.3, 7.4, and 7.5 include plots of attenuation *versus* frequency between 30 and 100 GHz for altitudes at sea level, 5 km, and 10 km. Each figure provides curves for 5 percent, 50 percent, and 100 percent relative humidities. As expected,

**Table 7.1**  
Attenuation at Molecular Transitions for a Relative Humidity of 50%\*

<i>Molecule</i>	<i>Frequency (GHz)</i>	<i>Sea Level Attenuation Coefficient (dB/km)</i>	<i>Zenith Attenuation (dB)</i>
O <sub>2</sub>	60 (30 Lines)	15	156
	118 (Single Line)	2	60
H <sub>2</sub> O	22 (Single Line)	0.17	0.54
	183 (Single Line)	26	93

\*Compiled from Liebe.

**Table 7.2**  
Width of Millimeter-Wave Windows\*

<i>Absorption Feature</i>		<i>Window Range (GHz)</i>	<i>Attenuation Range at Sea Level (dB/km)</i>
22-GHz H <sub>2</sub> O Line	W1	24–48	0.1–0.3
60-GHz O <sub>2</sub> Line Complex	W2	70–110	0.1–1.0
119-GHz O <sub>2</sub> Line	W3	120–155	1.0–2.5
183-GHz H <sub>2</sub> O Line	W4	190–300	2–10
325-GHz H <sub>2</sub> O Line	W5	335–355	5–20
380-GHz H <sub>2</sub> O Line (and 1823 more lines of the rotational band up to 25 GHz)			

\*Compiled from Liebe.

attenuation coefficients decrease with increasing altitude. By comparing the three sets of figures, we can see that relative humidity affects the attenuation at lower altitudes. For example, at sea level, increasing the relative humidity from 5 to 100 percent increases the attenuation at 40 GHz from 0.06 dB/km to 0.19 dB/km. At a 5 km altitude, on the other hand, the same change in relative humidity results in a smaller increase in attenuation, from 0.022 dB/km to 0.03 dB/km; at a 10 km altitude, relative humidity has no effect, as the attenuation remains constant at 0.008 dB/km. At higher altitudes, the concentration of water is so low that its contribution to attenuation is negligible compared to that of oxygen.

Figures 7.6 and 7.7 contain plots of attenuation *versus* altitude for the window frequencies of 35 GHz, 94 GHz, 140 GHz and 220 GHz. Separate curves are given for 5, 50, and 100 percent relative humidities. Note that the attenuations in the windows are less than 0.1 dB/km for altitudes in excess of about 7 km.



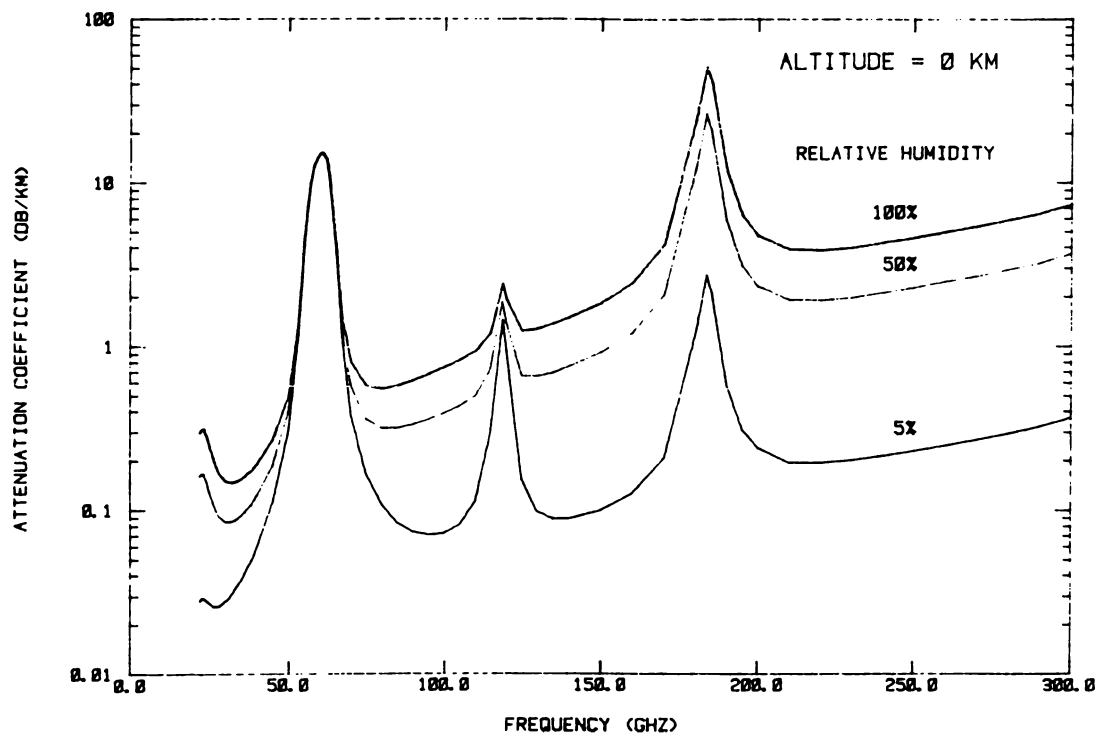


Figure 7.3 Atmospheric Attenuation *versus* Frequency; Altitude = 0 km. (From Liebe)

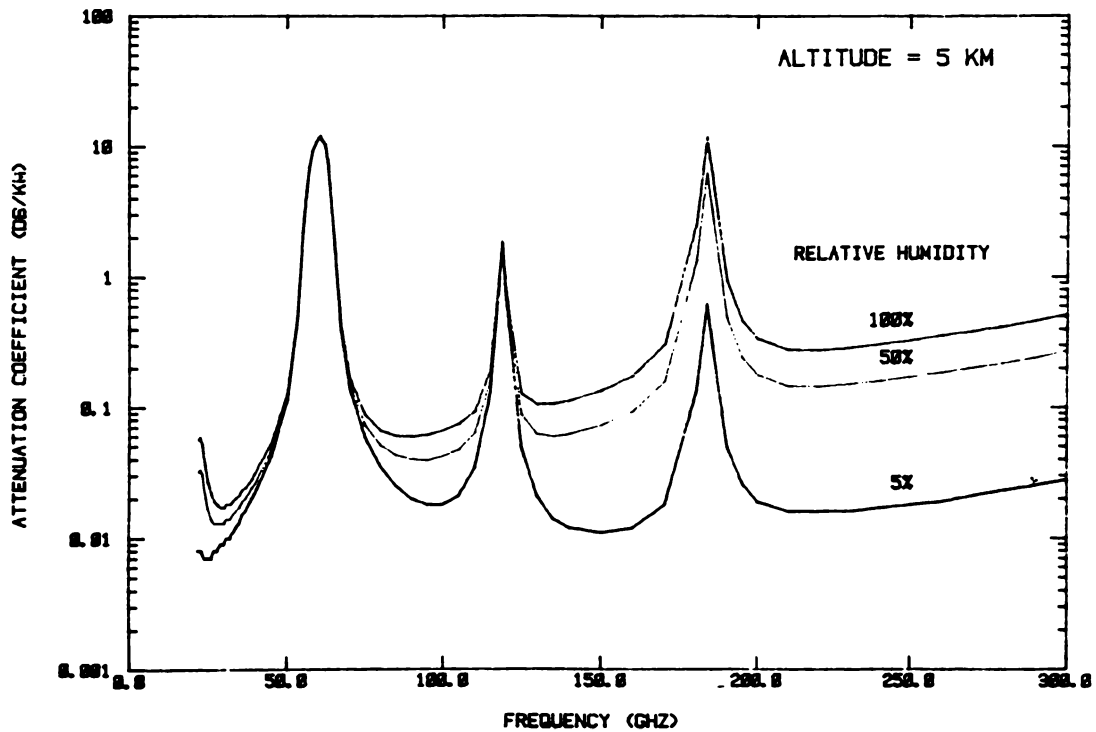


Figure 7.4 Atmospheric Attenuation *versus* Frequency; Altitude = 5 km

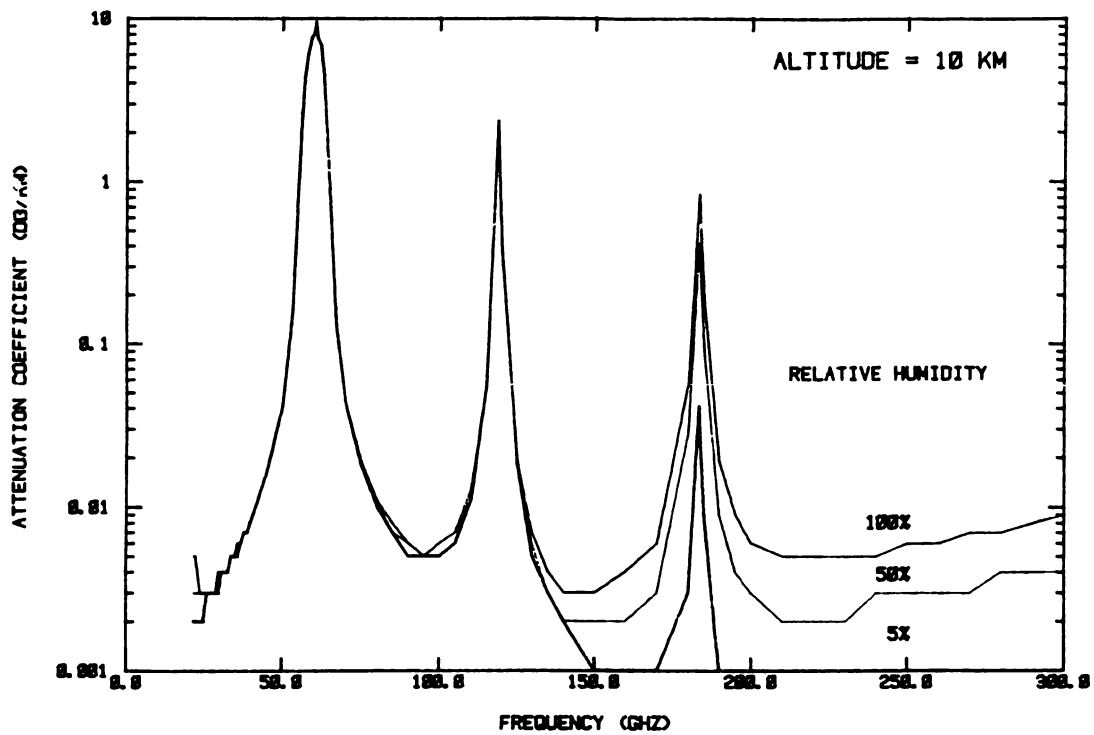


Figure 7.5 Atmospheric Attenuation *versus* Frequency; Altitude = 10 km

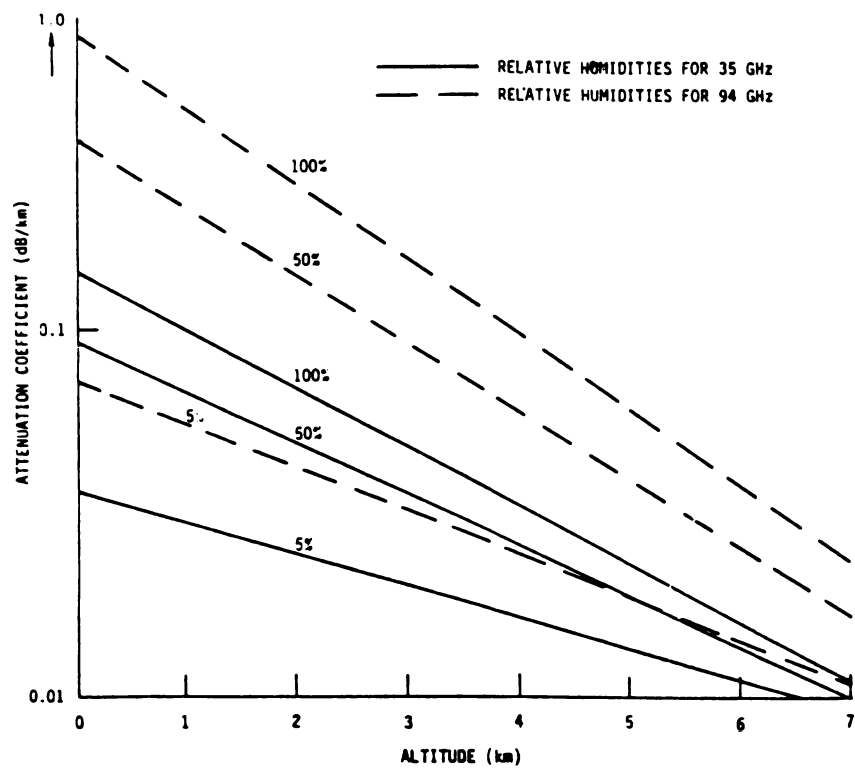


Figure 7.6 Clear Air Attenuation at Altitudes of 0 to 7 km for 35 and 94 GHz

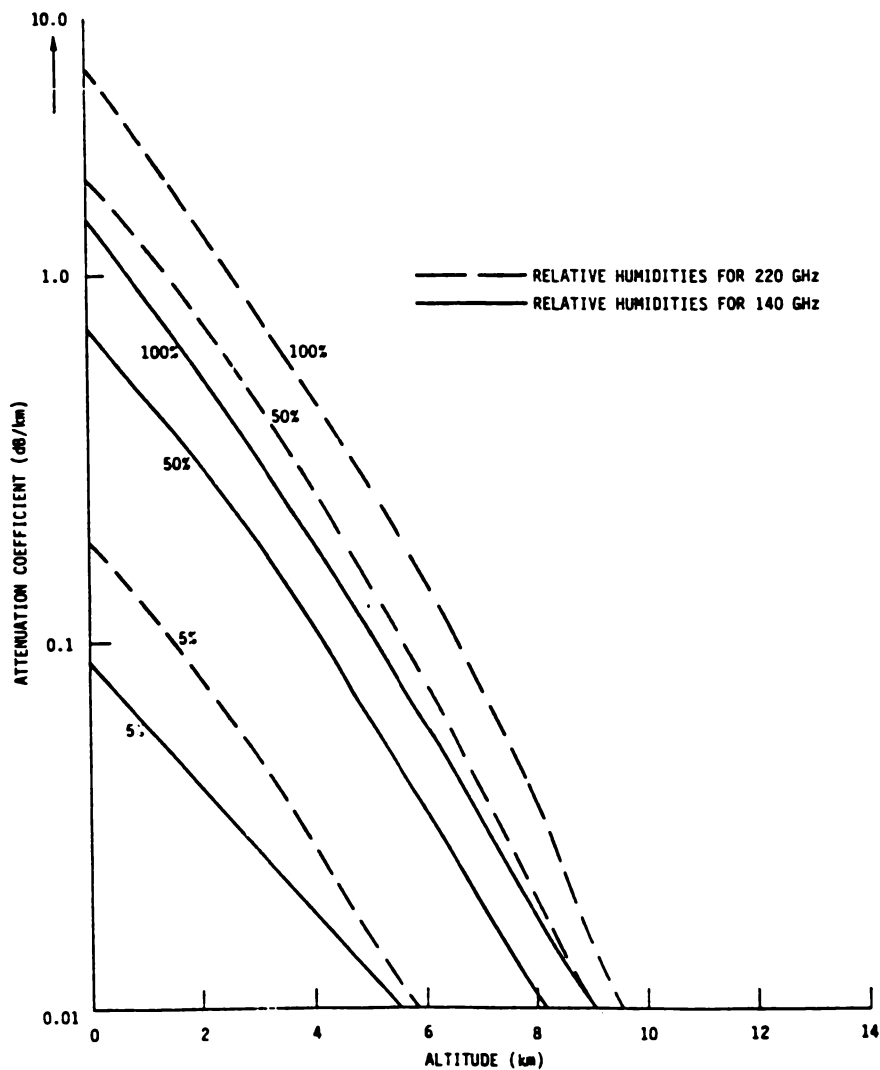


Figure 7.7 Clear Air Attenuation at Altitudes of 0 to 14 km for 140 and 220 GHz

Zenith Attenuation and Phase Delay

Table 7.3 contains integrated attenuations and relative phase delays for zenith (vertical) rays passing through the entire atmosphere. The *relative phase delay* is the phase difference between the zenith ray path and an equivalent ray path in a vacuum. Total attenuations are given in decibels for frequencies between 25 and 300 GHz, in intervals of 5 or 10 GHz. Interpolation between frequencies given in the table may give erroneous results because resonance absorptions can occur over narrow frequency intervals. Papers by Liebe should be consulted for such cases.

**Table 7.3**  
Zenith Attenuation (Decibel) and Relative Phase Delay (Radians)\*

<i>Frequency (GHz)</i>	<i>Relative Humidity</i>					
	<i>5%</i>		<i>50%</i>		<i>100%</i>	
	<i>Decibel</i>	<i>Radians</i>	<i>Decibel</i>	<i>Radians</i>	<i>Decibel</i>	<i>Radians</i>
25	0.11	1202	0.35	1251	0.57	1296
30	0.12	1442	0.24	1501	0.36	1556
35	0.18	1683	0.29	1751	0.40	1815
40	0.29	1923	0.42	2001	0.54	2074
45	0.55	2163	0.70	2251	0.85	2333
50	1.49	2404	1.68	2501	1.85	2594
55	27.31	2644	27.55	2752	27.77	2852
60	155.96	2884	156.10	3002	156.24	3111
65	22.21	3125	22.59	3252	22.94	3370
70	1.77	3365	2.18	3502	2.57	3629
75	0.76	3605	1.16	3752	1.54	3889
80	0.47	3846	0.91	4002	1.32	4148
85	0.34	4086	0.83	4252	1.30	4407
90	0.28	4327	0.83	4503	1.35	4666
95	0.26	4567	0.87	4753	1.44	4926
100	0.26	4807	0.94	5003	1.57	5185
105	0.31	5047	1.05	5253	1.75	5444
110	0.48	5288	1.30	5503	2.07	5703
115	1.64	5528	2.55	5753	3.39	5903
120	8.21	5769	9.19	6003	10.11	6222
125	0.67	6009	1.75	6253	2.77	6481
130	0.33	6249	1.50	6504	2.61	6740
135	0.25	6490	1.54	6754	2.75	7000
140	0.23	6730	1.64	7004	2.97	7518
145	0.23	6971	1.78	7254	3.25	7518
150	0.24	7211	1.97	7504	3.59	7777
155	0.26	7451	2.21	7754	4.06	8037
160	0.29	7692	2.57	8005	4.73	8296
165	0.34	7932	3.17	8255	5.86	8555
170	0.46	8172	4.43	8505	8.23	8814
175	0.83	8413	8.22	8755	15.30	9074
180	3.02	8653	30.13	9005	55.56	9333
185	6.04	8893	59.63	9255	108.53	9592
190	1.30	9134	13.03	9505	24.27	9851
195	0.68	9374	6.69	9755	12.44	10111
200	0.51	9615	4.98	10006	9.24	10369
210	0.42	10095	4.12	10506	7.61	10888
220	0.42	10576	4.06	11006	7.50	11450
230	0.43	11057	4.23	11507	7.80	11925
240	0.46	11537	4.50	12007	8.30	12444
250	0.49	12018	4.83	12507	8.91	12962

Table 7.3 continued

Frequency (GHz)	Relative Humidity					
	5%		50%		100%	
	Decibel	Radians	Decibel	Radians	Decibel	Radians
260	0.53	12499	5.22	13007	9.61	13481
270	0.57	12980	5.65	13508	10.42	13999
280	0.62	13460	6.16	14008	11.36	14518
290	0.69	13941	6.80	14508	12.54	15036
300	0.78	14422	7.72	15009	14.27	15555

\*From Liebe.

The attenuation for nonvertical rays whose elevation above the horizon is greater than about 6° can be estimated simply from

$$A(\phi) = \frac{A(90^\circ)}{\sin\phi}$$

(7.1)

where  $A(\phi)$  is the attenuation of slant ray,  $A(90^\circ)$  is the zenith attenuation, and  $\phi$  is the ray's elevation above the horizon. The same formula can be used to calculate relative phase delays. These formulas tacitly assume ray or propagation paths that are straight lines. The phase delay computations will be generalized later.

7.2 REFRACTIVITY

Clear air refractivity data are summarized here. The data are provided in a number of graphs and tables with several mathematical formulations provided for analytical purposes. The compilations and formulas are useful for estimating radar performance parameters such as beam pointing errors, phase delays, and time delays resulting from variations in the propagating paths.

Propagation Constant

The lower clear air atmosphere is characterized by an index of refraction ( $n$ ) that is greater than unity and decays toward unity in an exponential way as a function of altitude. Furthermore, the index of refraction, even at lower altitudes, is nearly equal to unity. As a result, and for convenience in analysis and performing computations, the refractivity ( $N$  has been adopted in past propagation analyses). It is defined as

$$\mathcal{N} = (\eta - 1)10^6 \quad (7.2)$$

As we will show, the refractivity depends on the dry air pressure, temperature, and water vapor content, all of which vary with altitude. From an analysis point of view, the lower atmosphere is considered a horizontally-stratified medium.

From Liebe, the propagation of a plane wave in the atmosphere is expressed in the following way:

$$E = E_0 \exp(\Gamma L) = E_0 \exp[j0.02096f(\mathcal{N} + 10^6)] \quad (7.3)$$

where

$E_0$  = electric field strength

$\Gamma$  = propagation constant ( $\text{km}^{-1}$ )

$L$  = path length (km)

$f$  = frequency (GHz)

Usually, the distance ( $L$ ) is a coordinate variable (i.e., typically rectangular) ( $x$ ,  $y$ , or  $z$ ) for plane-wave propagation. However, in propagation analysis, the end points of a path of length  $L$  are of primary importance; thus, the form of Equation (7.3) is convenient. Also, the constant 0.02096 results from the choice of units and the definition of refractivity given in Equation (7.2). The refractivity ( $\mathcal{N}$ ) is further defined as a complex quantity having real and imaginary parts with the real part expressed as the sum of frequency-independent and frequency-dependent (i.e., dispersive) parameters. The formulation from Liebe is as follows:

$$\mathcal{N} = N_0 + D(f) + jN''(f) \quad (7.4)$$

where

$N_0$  = frequency independent refractivity

$D(f)$  = refractive dispersion

$N''(f)$  = absorption coefficient

The propagation constant ( $\Gamma$ ) now becomes

$$\Gamma = -0.02096fN''(f) + j0.02096f(N_0 + D(f) + 10^6) \quad (7.5)$$

The absorption  $N''(f)$  is proportional to the specific attenuation  $\alpha$  in the following way:

$$N''(f) = \frac{\alpha}{0.1820f} \quad (7.6)$$

where, as before,  $f$  is the frequency expressed in GHz. The specific attenuation or point attenuation  $\alpha$  is the attenuation expected at a given point along a ray path, and is expressed in units of decibels per kilometer. The plots provided in Figures 7.2 through 7.7 display specific (or point) attenuations. Substituting Equation (7.6) into Equation (7.5) yields a more usable form of the propagation constant:

$$\Gamma = 0.1152\alpha + j0.02096f(N_0 + D(f) + 10^6) \quad (7.7)$$

The propagation constant forms the basis for the estimation of propagation effects or phenomena such as beam position errors, phase delays, and delay times. Frequency-independent refractivity and dispersive refractivity are discussed separately in the next two sections. A collection of formulas are given that use these basic formulations.

### Frequency-Independent Refractivity

The frequency-independent refractivity is a function of the following atmospheric parameters:  $p$  = dry air pressure (kPa = kilopascals),  $\psi$  = temperature parameter =  $300/T$ , and  $e$  = water vapor partial pressure (Pa = pascals). The refractivity is given by

$$N_0 = 2.589p\psi + 41.600e\psi + 2.390e\psi^2 \quad (\text{ppm}) \quad (7.8)$$

The temperature  $T$  in this formulation is in units of kelvin (K). The atmospheric parameters are provided in Table 5.4 of Chapter 5.

To illustrate the use of Equation (7.8) while providing useful refractivity data, an upper bound for the frequency-independent refractivity can be found by setting the water vapor partial pressure ( $e$ ) equal to the saturation pressure ( $e_s$ ). Substituting parameter values from Table 5.4 into Equation (7.8) yields the refractivities contained in Table 7.4. The indices of refraction are also included in the tabulations. The refractivity decreases from a value of 354 ppm at sea level to nearly zero at an altitude of 30 km.

The refractivity is usually represented in an exponential form. For the data provided in Table 7.4, a reasonable exponential representation is

$$N_0 = N_{0s} \exp(-0.1429h) \quad (7.9)$$

The altitude ( $h$ ) is expressed in kilometers and  $N_{0s}$  is the frequency-independent refractivity at sea level. For the example given in Table 7.5,  $N_{0s} = 354$ . The refractivities obtained from Table 7.4 and Equation (7.9) are plotted in Figure 7.8.

**Table 7.4**  
Computed Values of Refractivity and Index of Refraction\*

<i>Altitude (km)</i>	<i>Refractivity (ppm)</i>	<i>Index of Refraction</i>
0	354.23	1.000354
1.6	276.87	1.000276
3	226.47	1.000226
6	152.75	1.000153
10	92.71	1.000093
16	37.26	1.000037
20	19.97	1.000020
30	4.82	1.000005

\*From Liebe.

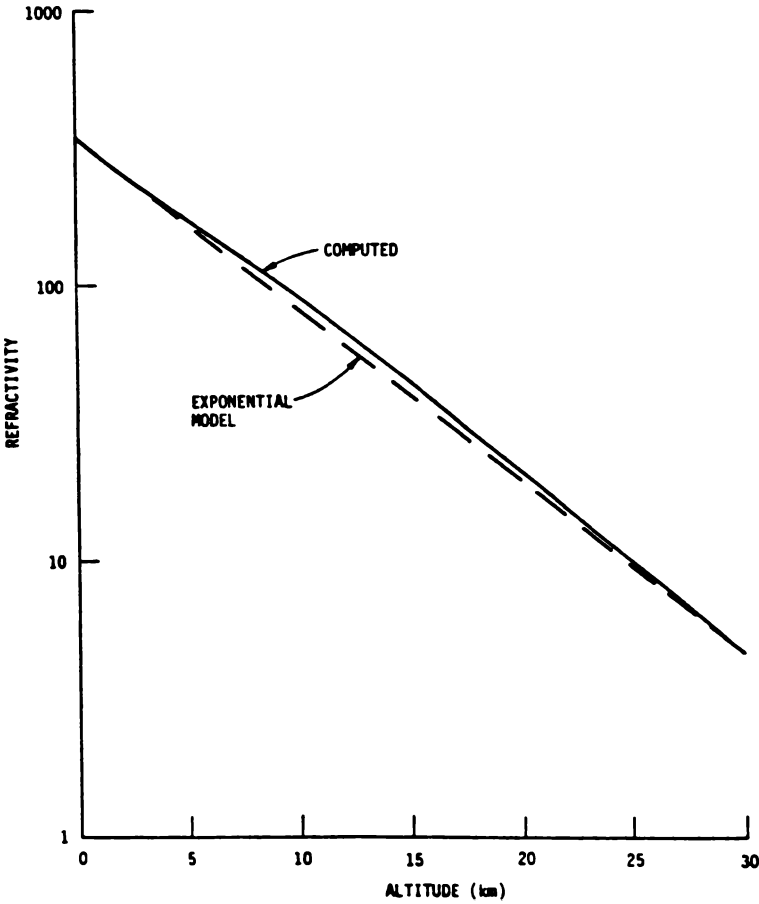


**Figure 7.8** Frequency Independent Refractivity Plotted as a Function of Altitude for Maximum Relative Humidity



## Frequency-Dependent Refractivity

The dispersive quality of the atmosphere gives rise to a frequency-dependent refractivity. Figure 7.9 shows the dispersive properties of the refractivity for a clear air environment at sea level and for relative humidities of 0–100%. Within the frequency range of 0 to 1000 GHz, the peak refractivity of about 150 ppm occurs at a frequency of 557 GHz. At lower frequencies, a maximum value of 10.6 occurs at about 450 GHz and reduces to less than 1.2 ppm within the millimeter-wave spectrum of 30 to 300 GHz. Therefore, for radar design considerations within the millimeter-wave region, the dispersive component of the refractivity may be neglected.

## 7.3 ADDITIONAL FORMULATIONS AND PROCEDURES

A useful equation for the propagation or ray paths in a layered medium is derived. Additional formulas are given for estimating beam position errors, phase delays, and time delays.

### Ray Paths

The atmosphere can be considered a layered medium with an altitude-dependent refractivity. Formulas for refraction along ray paths are readily developed from Snell's law. Referring to Figure 7.10, let the index of refraction equal  $\eta(z)$ ; then, with an index of refraction of  $\eta_0$  at the origin of the ray path, a direct application of Snell's law yields

$$\eta(z) \sin\theta = \eta_0 \sin\theta_0 \quad (7.10)$$

At any point along the ray path:

$$\tan\theta = \frac{dx}{dz} \quad (7.11)$$

and

$$\sin\theta = \left[ 1 + \left( \frac{dz}{dx} \right)^2 \right]^{1/2} \quad (7.12)$$

from which

$$\frac{dx}{dz} = \left[ \left( \frac{\eta(z)}{\eta_0 \sin \theta_0} \right)^2 - 1 \right]^{-1/2} \quad (7.13)$$

Integrating, we obtain

$$x = \int_0^z \left[ \left( \frac{\eta(z)}{\eta_0 \sin \theta_0} \right)^2 - 1 \right]^{-1/2} dz \quad (7.14)$$

which is the equation for the ray paths.

Replacing the index of refraction  $\eta(z)$  by the refractivity  $N_0(z)$  yields, instead of Equations (7.11) and (7.12),

$$\tan \theta = \left\{ \left[ \frac{N_0(z) + 10^6}{(N_0(0) + 10^6) \sin \theta_0} \right]^2 - 1 \right\}^{-1/2} \quad (7.15)$$

Equation (7.14) becomes,

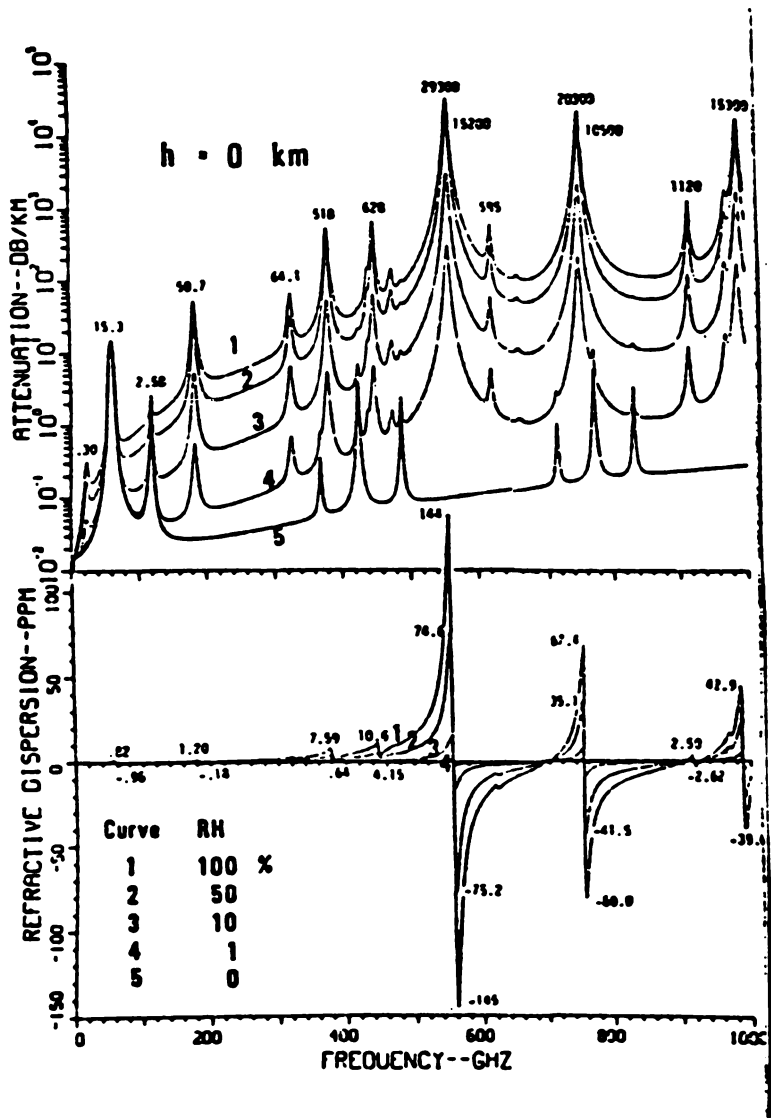
$$x = \int_0^z \left\{ \left[ \frac{N_0(z) + 10^6}{(N_0(0) + 10^6) \sin \theta_0} \right]^2 - 1 \right\}^{-1/2} dz \quad (7.16)$$

The altitude-dependent refractivity is given by Equation (7.8) or (7.9). Ray paths within an atmosphere modeled in this way are known to be approximately parabolic in shape. However, for short ray paths, straight-line propagation paths can be expected. The tolerable deviation of the parabolic path from a straight line depends on the accuracy of the radar being considered. For computational purposes, the slope of the path is found directly from Equation (7.15) while the ray path is best found by numerically integrating Equation (7.16).

For long propagation paths, considering the numerical values of the index of refraction is nearly unity, the curvature of the earth must be taken into account. In these instances, Equations (7.13) and (7.14) are applicable, with  $z$  being the altitude as before,  $x$  being the arc distance along the surface of the earth, and with the index of refraction  $n(z)$  being replaced by

$$\eta_s(z) = \eta(z) \left( 1 + \frac{z}{a} \right) \quad (7.17)$$

where  $a$  is the earth's radius.



f, GHz	α, dB/km		
	RH = 0	10	100%
10	0.016	0.017	0.028
50	0.299	0.322	0.527
100	0.054	0.136	0.886
200	0.028	0.546	5.38
300	0.040	0.982	9.71
500	0.108	11.1	116
1000	0.284	124	1313

**Figure 7.9** Attenuation and Refractive Dispersion for Relative Humidities 0–100% at Sea Level Over a Frequency Range of 1–1000 GHz. (From Liebe)

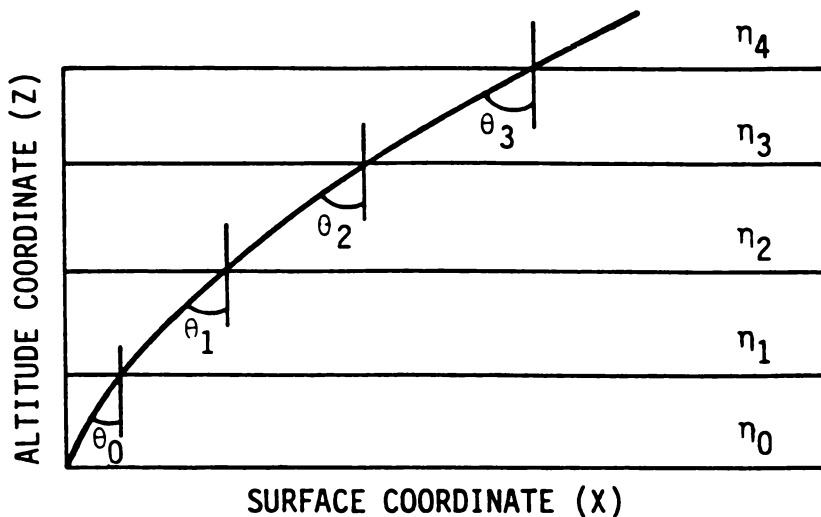


**Figure 7.10** Layered Medium with Varying Index of Refraction

### Formulas for Beam Position Errors

Let the beam position error be defined as

$$\delta\theta = \theta - \theta_0 \quad (7.18)$$

where  $\tan\theta$  is the slope of the ray path and  $\theta_0$  is the beam pointing direction at the origin of the path. Using Equation (7.13) yields

$$\delta\theta = \tan^{-1} \left[ \left( \frac{n(z)}{N_0} \right)^2 \sec^2\theta - 1 \right]^{-1/2} - \theta_0 \quad (7.19)$$

where, repeating, the index of refraction is related to the refractivity through Equation (7.2), with the refractivity determined using Equation (7.8) or (7.9).

### Phase Delays

Let  $\phi$  be the phase difference between the end points of a propagation path, then

$$\phi = \int_a^b \mathbf{k} \cdot d\mathbf{s} \quad (7.20)$$

where  $\mathbf{k}$  is the propagation constant and  $d\mathbf{s}$  is a segment of the propagation path;  $a$  and  $b$  designate the end points.

Let  $k = \omega n(z)/c$ , then with

$$ds = \sqrt{1 + \left(\frac{dx}{dz}\right)^2} \quad (7.21)$$

and  $(dx/dz)$  given by (7.13), Equation (7.20) becomes

$$\phi = \frac{\omega}{c} \int_0^{z_0} n(z) \sqrt{\frac{1}{1 + \left(\frac{\eta_0}{\eta(z)}\right)^2 \sin^2 \theta}} dz \quad (7.22)$$

where  $z_0$  is the altitude at the termination of the propagation path. The integral can be simplified. First, for  $\eta(z) = \eta_0 = 1$ ,

$$\phi = \frac{\omega}{c \cos \theta_0} \quad (7.23)$$

which is the expected result. If  $(\eta_0/\eta(z))^2 = 1$ , then

$$\phi = \frac{\omega}{c \cos \theta_0} \int_0^{z_0} \eta(z) dz \quad (7.24)$$

If the propagation path includes the entire atmosphere, the phase  $\phi$  is the zenith phase, corrected for the incident angle by  $1/\cos \theta_0$ . This result conforms to the observations made previously. Straight-line ray paths have been tacitly assumed in both approximations.

If the detail implied here is necessary, then use Equation (7.14) or (7.16); Equation (7.21) is recommended with integrals in all cases best solved numerically. Phase is usually expressed as a delay  $\delta\phi = \phi - \phi_v$ , where  $\phi_v$  is the phase along an equivalent path with  $n = 1.0$ .

## Time Delays

Proceeding as before, the time delay along a propagation path is

$$t = c \int_0^{z_0} n(z) \left[ 1 - \left(\frac{n_0}{n(z)}\right)^2 \sin^2 \theta_0 \right]^{-1/2} dz \quad (7.25)$$

Also as before, the propagation time is usually expressed as a delay  $\delta t = t - t_v$  where  $t_v$  is the propagation time along a reference path with  $\eta = 1.0$ .

## 7.4 SUMMARY

The data provided here constitute the basis for clear air environment considerations in radar analysis and simulation. The formulas provided will assist us in understanding the effects of the clear atmosphere on radar. It will also provide a method for using atmospheric data directly when needed. The reader should refer to the tutorial discussions of Chapter 3 or an equivalent for examples showing application-analogous plane-wave formulations. The data compilations can be used directly.



## ***Chapter 8***

### ***Rain Data Compilations***

Background material covering types of rain, vertical profiles and heights, drop size distributions, and model considerations is covered first; then, three models of varying complexity and applicability are described. The first model provides attenuation and backscatter estimates on a global basis for given upper-altitude bounds of an assumed uniform rain, and simple formulas for radar analysis and simulation are provided. The second model includes nonuniform clutter with cellular structure taken into account using a path-corrected attenuation. In this formulation, path-dependent attenuation will exceed specific attenuation values when rain rates are low, but will decrease when rain rates are moderate to heavy in intensity. The model includes statistical descriptions of the cellular structure of rain storms where rain rates for cells and debris are compiled. Fractal formulations are introduced into the modeling process. The definition of a fractal is approached first from a geometrical point of view, where comparisons to Euclidean geometry are made and the notions of self-similarity and fractal dimension are delineated. The deterministic fractals are then extended to statistical ones and attention is given to fractional Brownian motion and  $1/f$  noise. A quantitative introduction to fractional differentiation and integration is provided. Two fractal models are described, the first being a fractional Brownian sheet, a two dimensional representation of Brownian motion. The second, a fractional sum-of-pulses algorithm formed on a elliptical basis with hyperbolic statistics, is described with outputs characterized as hyperbolic fractal sheets. Anisotropy, introduced by the elliptical structure, provides control of the elongation properties of the fractals, a useful provision for modeling many radar environments. Special attention is given to the hyperbolic distribution, its properties and formation of a random number generator capable of producing sequences with Rayleigh, exponential, and Gaussian distributions. Although specific rain and cloud environments are considered, the introductory material is applicable for general radar target and clutter modeling applications.



## 8.1 INTRODUCTION

Degrading effects on signals propagating through rain environments are a result of macroscopic and microscopic properties of the storms. Macroscopic characteristics include size, distribution and movements of rain cells, height of melting layers, and presence of ice crystals. Microscopic characteristics include size, distribution, density, and oblateness of rain drops and ice crystals. It is necessary to assess the combined effects in order to obtain a thorough understanding of their influence on the signals. Unfortunately, the representation of all significant macroscopic and microscopic rain parameters in a way that will yield acceptable estimates of resulting signal degradations is difficult, and models for radar applications that are generic in form are not currently available. What we can do, however, is compile the current rain representations in a context appropriate for making best estimates, and update the representations as new descriptions or models become available. The models provided will at least extend the most-used uniform clutter assumptions to more realistic descriptions for both radar analysis and simulation investigations. The background material and model descriptions that follow have been assembled sequentially in order of complexity to allow for further updates as models are improved. The fractal models in particular are useful now and serve to indicate future anticipated model developments.

### Types of Rain

Two types of rain are of primary importance. They are widespread or stratiform, and convective or thundershower rains. *Stratiform rainfall* is characterized by horizontal extents of hundreds of kilometers, durations of more than one hour and rain rates of less than about 25 mm/hr. Rainfall of this type is common to mid-latitude regions, occurs mostly during spring and fall months, and reaches vertical heights of 4 to 6 km. *Convective rains* occur in cells usually associated with weather fronts. Rains of this type are characterized by high rain rates of short duration (i.e., several minutes) with storm heights usually exceeding the average freezing layer altitudes. High rain rates exceeding 25 mm/hr within the continental United States are, in most cases, the result of convective storms.

*Cyclonic storms* (hurricanes), not of concern here, are a third type of rain, and are 50 to 200 km in extent with storm movements of 10 to 20 km/hr. Typically, rain rates exceed 25 mm/hr and extend in altitude to the melting layer (i.e., up to about 8 km).

For radar applications, it is important to consider that rain is rarely uniform. Stratiform rain yields similar long-time-averaged rain rates for widely separated locations, but radar observations of such rains indicate that they are spatially inhomogeneous. Convective storms, on the other hand, are by their very nature

spatially nonuniform. This is confirmed by radar observations made over long periods of time. However, most rain clutter models used in radar system design or simulation investigations incorporate uniform clutter assumptions that may lead to unrealistic performance estimates, especially for sensitivity computations where long path lengths are of concern.

Figure 8.1 illustrates typical spatial properties of a convective storm. The data show rain rate occurrences of 1 to 100 mm/hr within a single rain storm with horizontal extents of about 35 km<sup>2</sup>. The cells containing the highest rain rates are a maximum of about 2 km in the largest horizontal dimension. Later, fractal representation of cells of this form will be described.

The largest area of the storm (i.e., within the contours) appears to have rain rates below 6 mm/hr. A 35 GHz radar observing this storm, depending upon its location, would be subjected to attenuations varying from about 0.1 dB/km to over 10 dB/km with backscatter values between about 10<sup>-5</sup> and 10<sup>-3</sup>m<sup>2</sup>/m<sup>3</sup>. Stratiform storms can be expected to yield similar general characteristics, but the variance in observables is reduced. We will also discuss fractal methods that will provide signal estimates for radar clutter of this type.

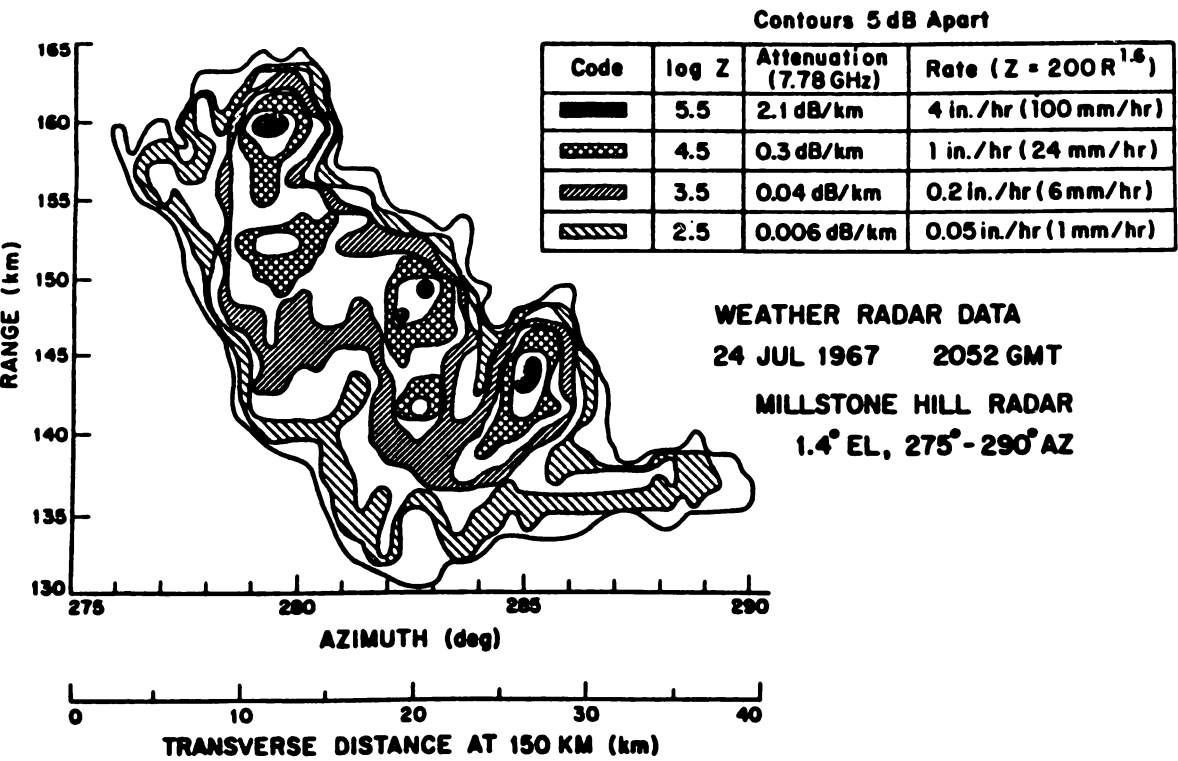


Figure 8.1 Rain-Rate Inhomogeneities for a Convective Storm. (From Crane)

Vertical Profiles

Vertical profiles pertain to vertical variations in raindrop concentration. Relatively recent radar measurements show that rain can be characterized, on the average, by a constant reflectivity related to the rain rate from ground level to the height of the zero-degree isotherm. Above this altitude a so-called bright band exists that consists of ice, snow, and aggregated snow crystals. In this band, attenuation decreases rapidly as altitude increases, but there may be depolarization effects. The experimental results that show these observations are contained in Figure 8.2. The numbers in parentheses are the number of rain cells measured at the rain rates indicated. Data of this type are sometimes plotted as a function of reflectivity rather than rain rate. When data are present in that form, the horizontal axis is placed in units of reflectivity, where a commonly used value of  $Z = 200R^{1.6}\text{mm}^6/\text{m}^3$  is applied. The rain rate  $R$  given in Figure 8.2 provides the means for this conversion of parameters.

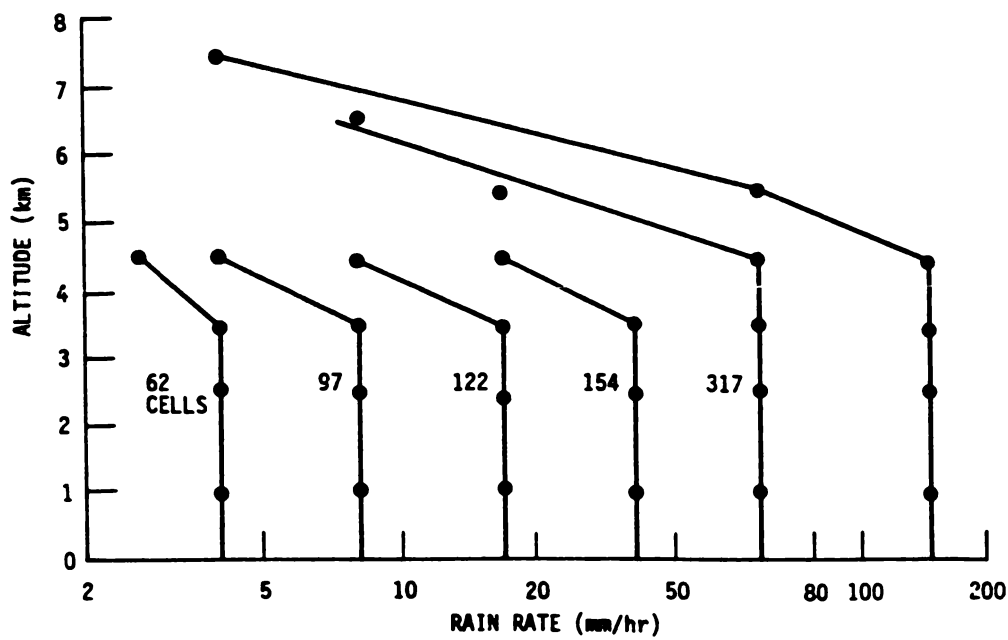
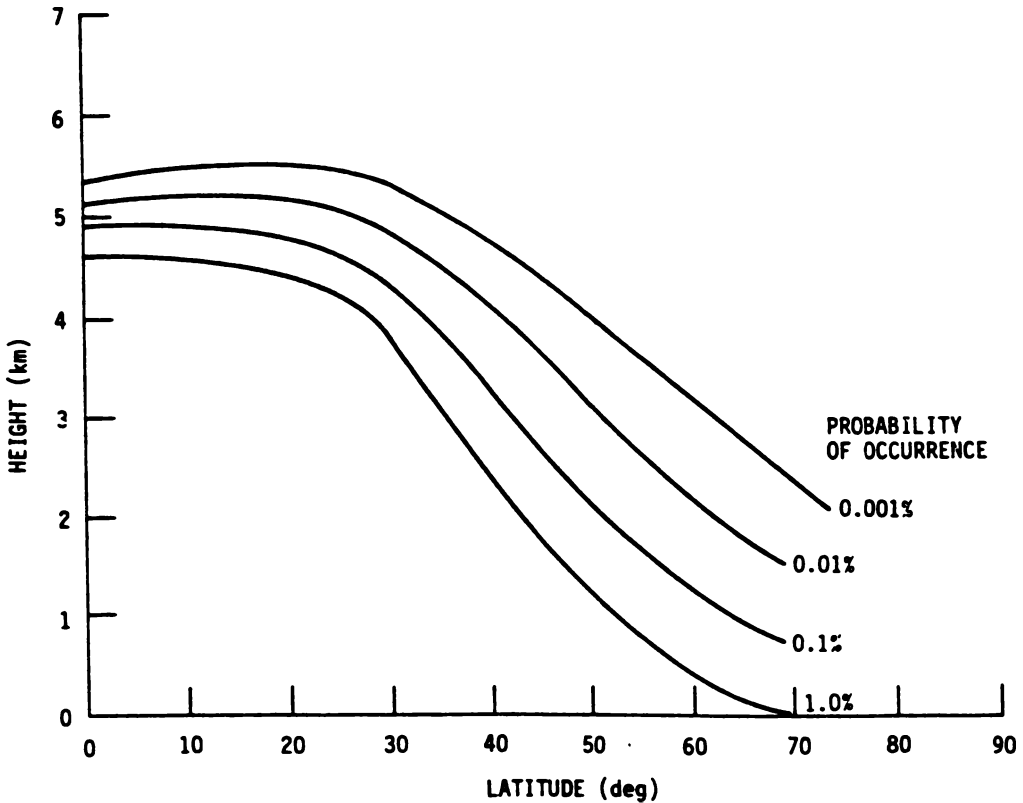


Figure 8.2 Measured Vertical Rain Rate Profiles. (From Goldhirsh)

Data compilations from Crane on the dependence of the melting layer or zero-degree isotherm height on latitude, and its probability of occurrence are contained in Figure 8.3. The seasonal uncertainty in zero-degree Celsius isotherm height is assumed to be 500 m or about 13% of the average height. Values for altitudes ( $H$ ) corresponding to probabilities ( $P$ ) between 0.001 and 1.0% can be found by interpolation using

$$H = p + q \log P \quad (8.1)$$

where  $p$  and  $q$  are constants determined from the 0.001 and 1.0% altitudes for the latitude of interest. For example, at a latitude of  $50^\circ$ ,  $p \approx 1.2$  and  $q \approx 1.0$ .



**Figure 8.3** Height of the Zero-degree Isotherm Expressed as an Annual Probability of Occurrence. (From Crane)

These data apply to moderate to low rain rates of stratiform and convective forms. For high rain rates and convective storms, cells usually extend to altitudes exceeding the zero-degree thermal heights where liquid raindrops are carried upward by strong updrafts. For analysis or simulation purposes, use of the zero-degree isotherm upper bound for stratiform and convective storms is encouraged, unless otherwise specified for the rain storms encountered.

### Drop Size Distributions

Two distributions that relate raindrop sizes to rain rates are prominent. These are the well known *Laws and Parsons* (L-P) and the M-P distributions. The early work

of Laws and Parsons, which has been favorably compared to measurements of stratiform and convective rain, is the most widely used. The later work of Marshall and Palmer resulted in an exponential representation of drop sizes expressed in the following way:

$$N_D = N_0 \exp(-\Lambda r) \tag{8.2}$$

where  $N_D$  is the number of drops per unit volume with radii in the interval  $r$  to  $r + dr$ , and  $N_0$  is an empirically derived constant. The parameter  $\Lambda$  is defined as

$$\Lambda = cR^{-d} \tag{8.3}$$

where  $c$  and  $d$  are also empirically derived constants and  $R$  is the rain rate expressed in mm/hr. For the M-P distribution,  $N_0 = 8 \times 10^3$  (1/m<sup>3</sup> mm),  $c = 8.2$ , and  $d = 0.21$ .  $\Lambda$  is expressed in units of mm<sup>-1</sup>.

Figure 8.4 shows examples of the L-P (dashed lines), the M-P (solid lines), and M-P measured (dotted lines) distributions. The results are essentially equivalent for drop size diameters greater than 1.0 to 1.5 mm. For attenuation and backscatter calculations, larger drop sizes tend to dominate; thus the exponential formulation is applicable.

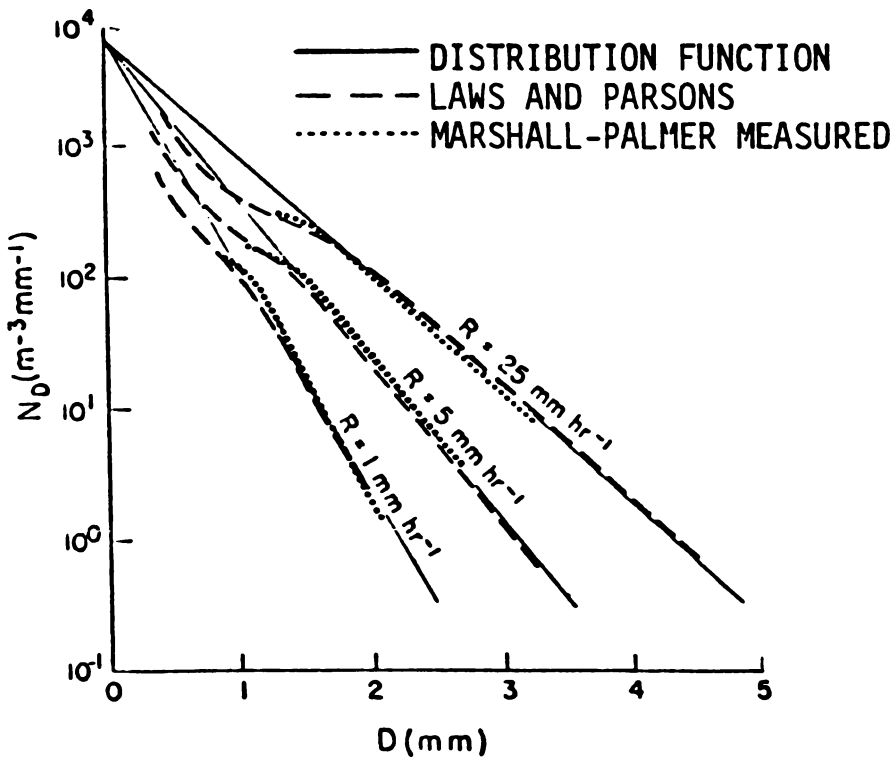


**Figure 8.4** Distribution Functions Compared with the Results of Laws and Parsons and Measurements. (From Crane)

The measured L-P distribution is provided in Table 8.1. Since its initial publication, the distribution has appeared in a number of forms, all of which describe the size of the raindrops as a percentage of a total volume. The data provided in Table 8.1 are in a convenient form.

Use of the tabulated L-P distribution usually requires that the distribution be expressed in terms of the number of droplets within specific size ranges per unit volume. To accomplish this transformation, let  $N(d_{i+1}, d_i)$  be the distribution in units of droplets per unit volume in the range  $\Delta r_i = d_{i+1} - d_i$ , then

$$N(d_{i+1}, d_i) = \frac{RP(d_{i+1}, d_i)}{V(\bar{r})V_0(\bar{d})} \quad (8.4)$$

where  $R$  is the rain rate expressed in mm/hr,  $P(d_{i+1}, d_i)$  is the distribution of the volume percentage rain rate in  $\Delta d_i$  range of diameters as described in Table 8.1,  $V(\bar{r})$  is the volume of a sphere with an average diameter within  $\Delta d_i$ , and  $V_0(\bar{d})$  is the terminal velocity of a spherical raindrop of diameter  $d_i$ . Table 8.2, from Setzer, contains values for the terminal velocity.

**Table 8.1**  
Laws and Parsons Drop Size Distributions for Various Precipitation Rates\*

Drop Diameter	Rain Rate (mm/hr)								
	0.25	1.25	2.5	5.0	12.5	25.0	50.0	100.0	150.0
(cm)	Percent of Total Volume								
0.05	28.0	10.9	7.3	4.7	2.6	1.7	1.2	1.0	1.0
0.10	50.1	37.1	27.8	20.3	11.5	7.6	5.4	4.6	4.1
0.15	18.2	31.3	32.8	31.0	21.5	18.4	12.5	8.8	7.6
0.20	3.0	13.5	19.0	22.2	25.4	23.9	19.9	13.9	11.7
0.25	0.7	4.9	7.9	11.8	17.3	19.9	20.9	17.1	13.9
0.30		1.5	3.3	5.7	10.1	12.8	15.6	18.4	17.7
0.35		0.6	1.1	2.5	4.3	8.2	10.9	15.0	16.1
0.40		0.2	0.6	1.0	2.3	3.5	6.7	9.0	11.9
0.45			0.2	0.5	1.2	2.1	3.3	5.8	7.7
0.50				0.3	0.6	1.1	1.8	3.0	3.6
0.55					0.2	0.5	1.1	1.7	2.2
0.60						0.3	0.5	1.0	1.2
0.65							0.2	0.7	1.0
0.70									0.3

\*From Setzer.

The use of Equation (8.4) to obtain drop size distributions is demonstrated in Figures 8.5 through 8.14. The average diameters are the inserts in Table 8.1 with a constant  $\Delta d_i$  of 0.5 mm. Care must be taken to assure a consistent set of units. It is tacitly assumed that the raindrops are uniformly distributed within a volume and within the  $\Delta d_i$  increments.

Table 8.2  
Raindrop Terminal Velocity\*

<i>Radius (cm)</i>	<i>Velocity (m/s)</i>
0.025	2.10
0.050	3.90
0.075	5.30
0.100	6.40
0.125	7.30
0.150	7.90
0.175	8.35
0.200	8.70
0.225	9.00
0.250	9.20
0.275	9.35
0.300	9.50
0.325	9.60

\*From Setzer.

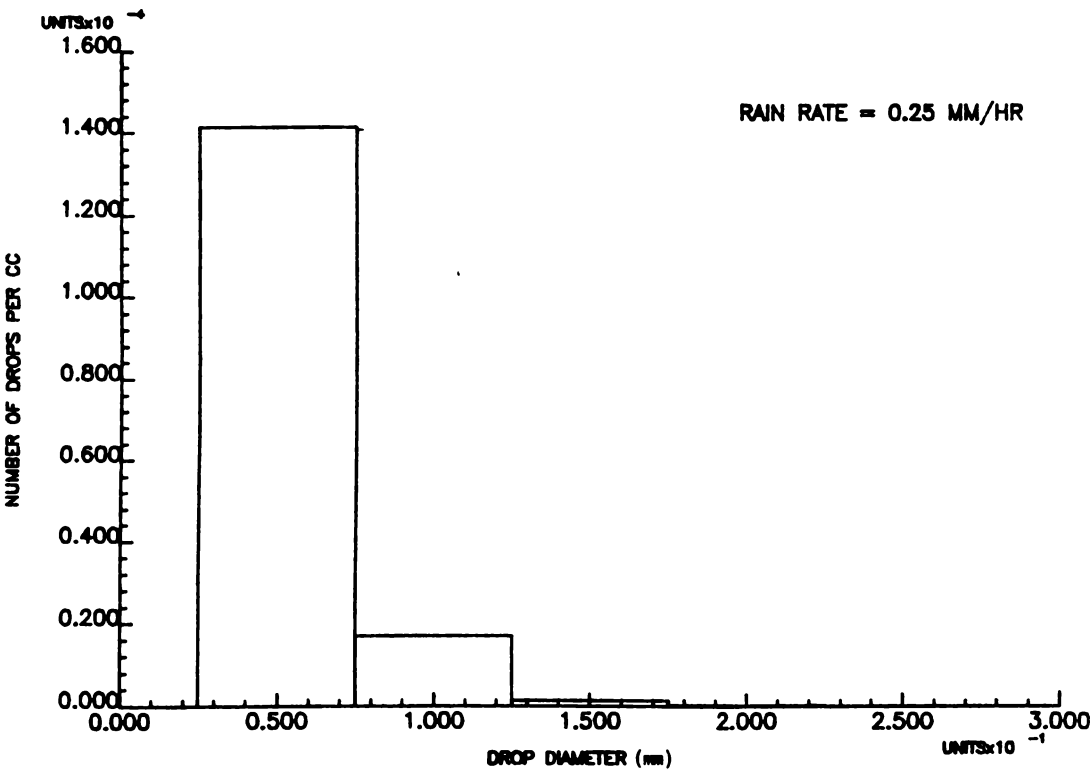


Figure 8.5 Laws and Parsons Drop-Size Distributions; 25.0 mm/hr Rain Rate

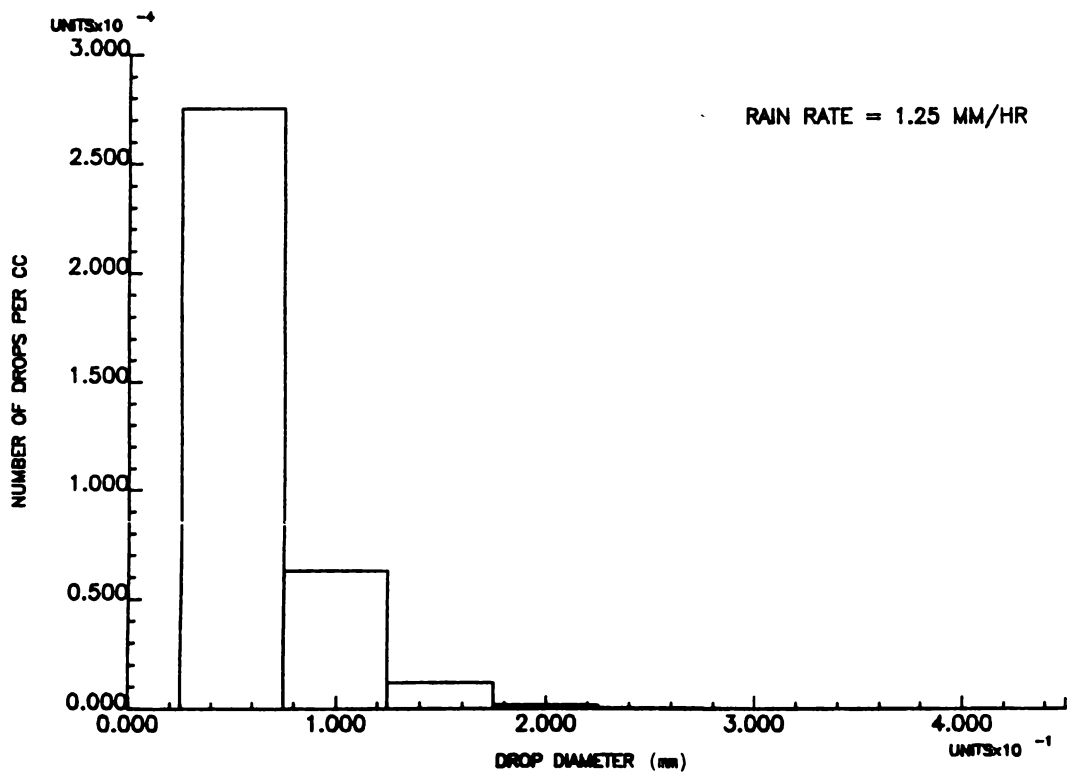


Figure 8.6 Laws and Parsons Drop-Size Distributions; 1.25 mm/hr Rain Rate

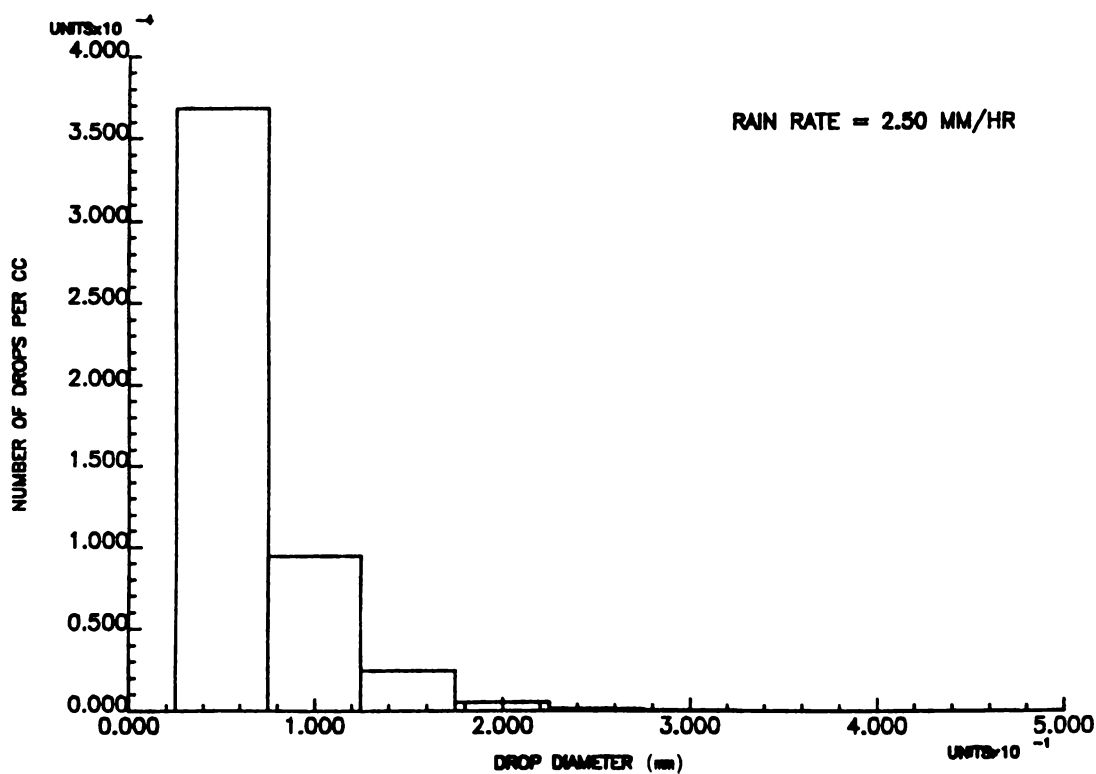


Figure 8.7 Laws and Parsons Drop-Size Distributions; 2.50 mm/hr Rain Rate



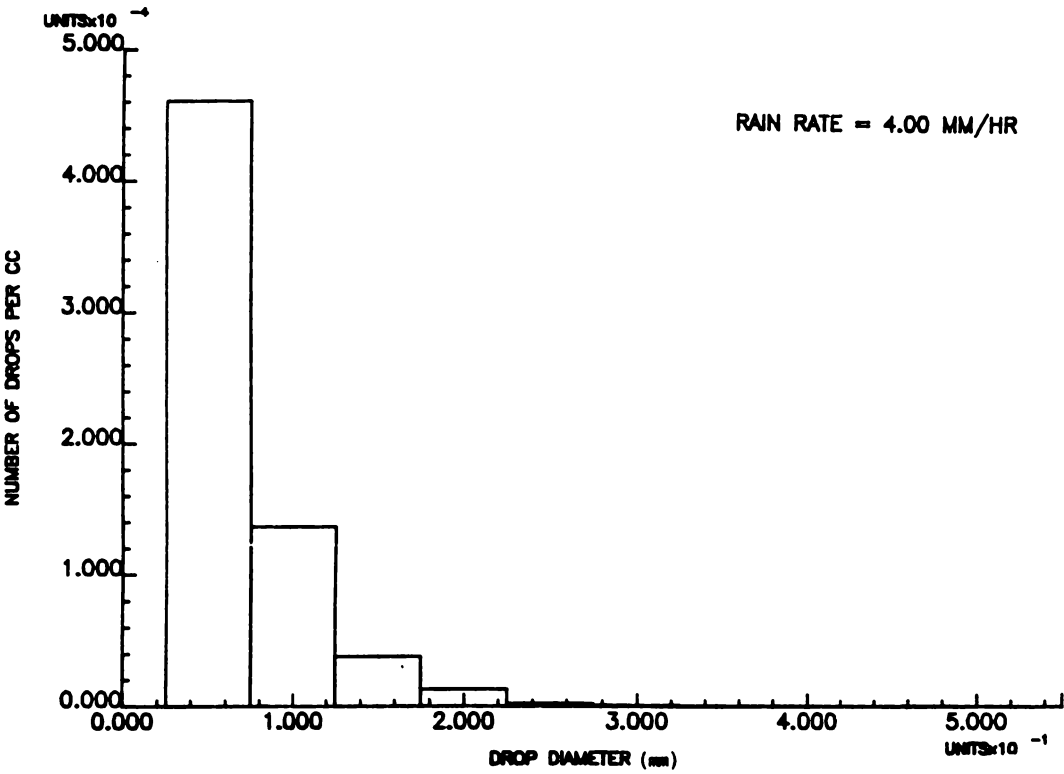


Figure 8.8 Laws and Parsons Drop-Size Distributions; 4.00 mm/hr Rain Rate

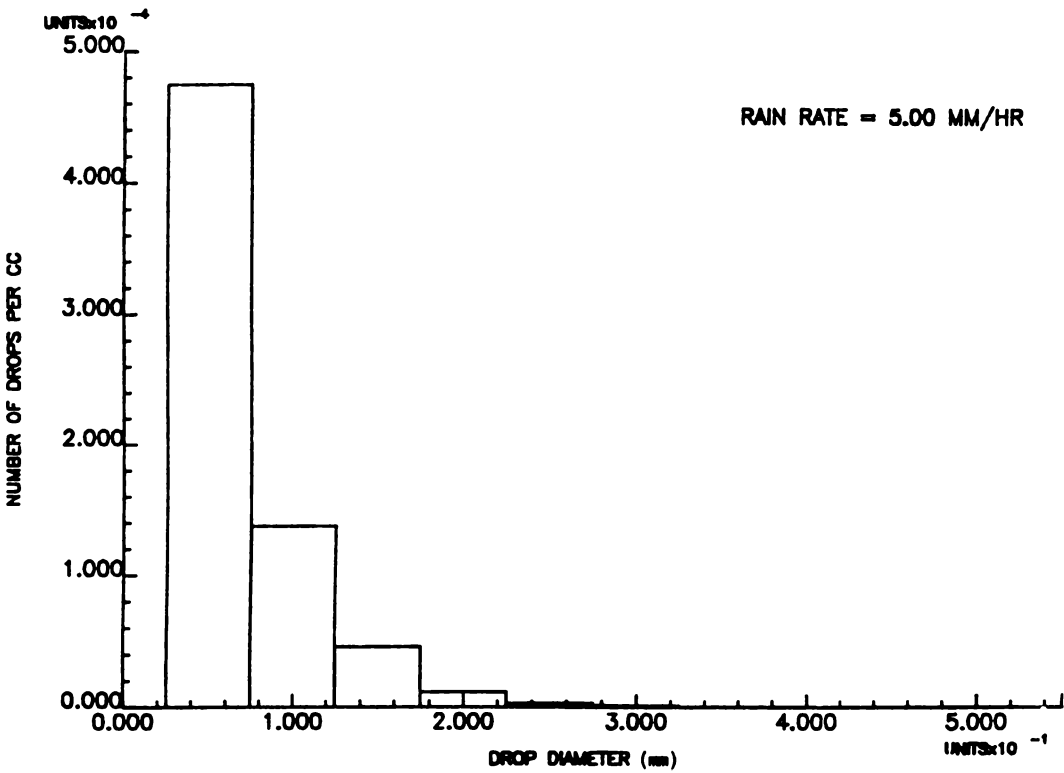


Figure 8.9 Laws and Parsons Drop-Size Distributions; 5.00 mm/hr Rain Rate

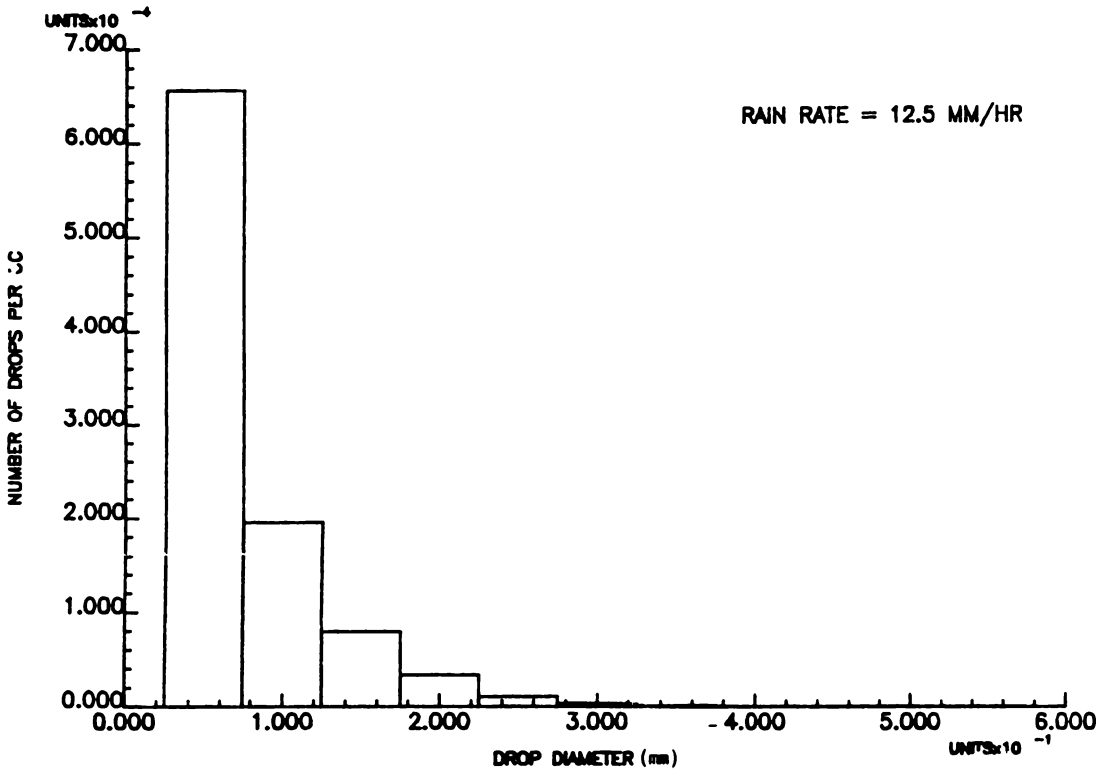


Figure 8.10 Laws and Parsons Drop-Size Distributions; 12.5 mm/hr Rain Rate

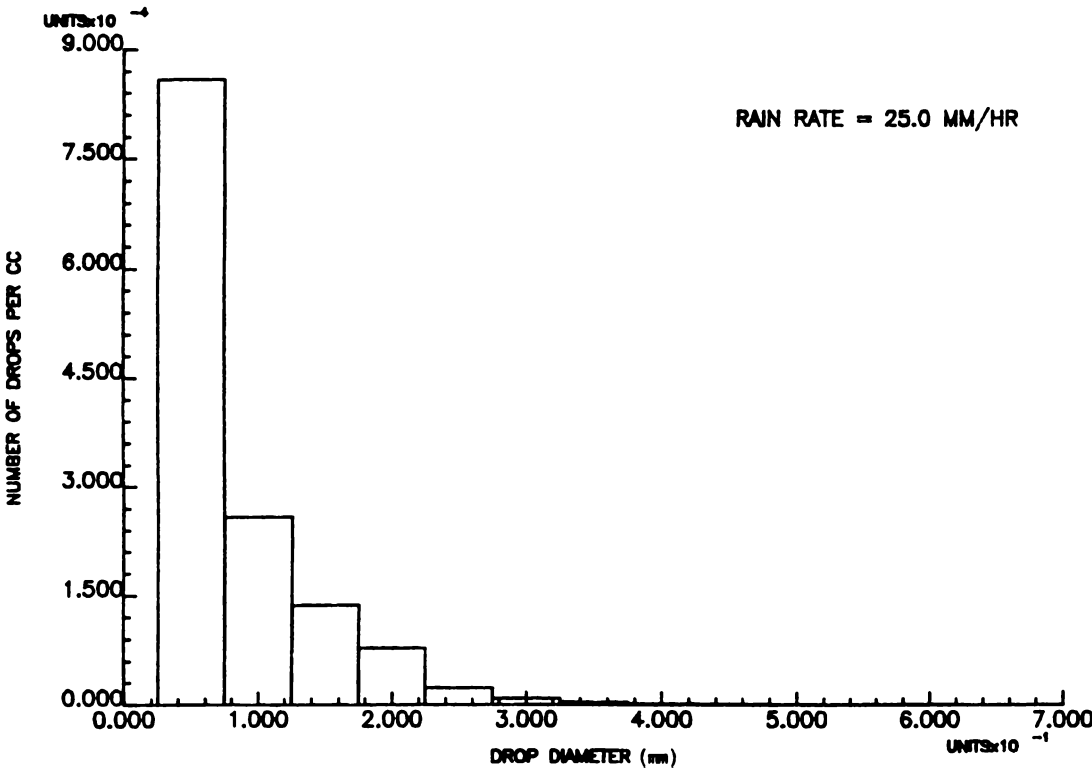


Figure 8.11 Laws and Parsons Drop-Size Distributions; 25.0 mm/hr Rain Rate

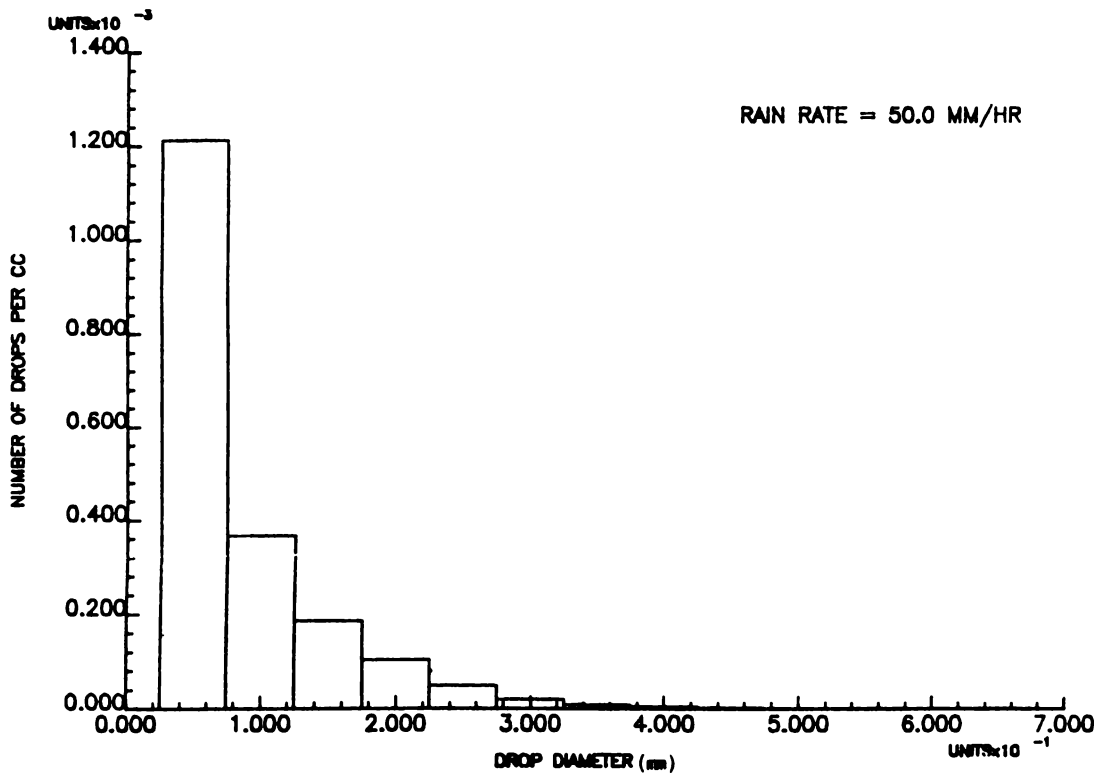


Figure 8.12 Laws and Parsons Drop-Size Distributions; 50.0 mm/hr Rain Rate

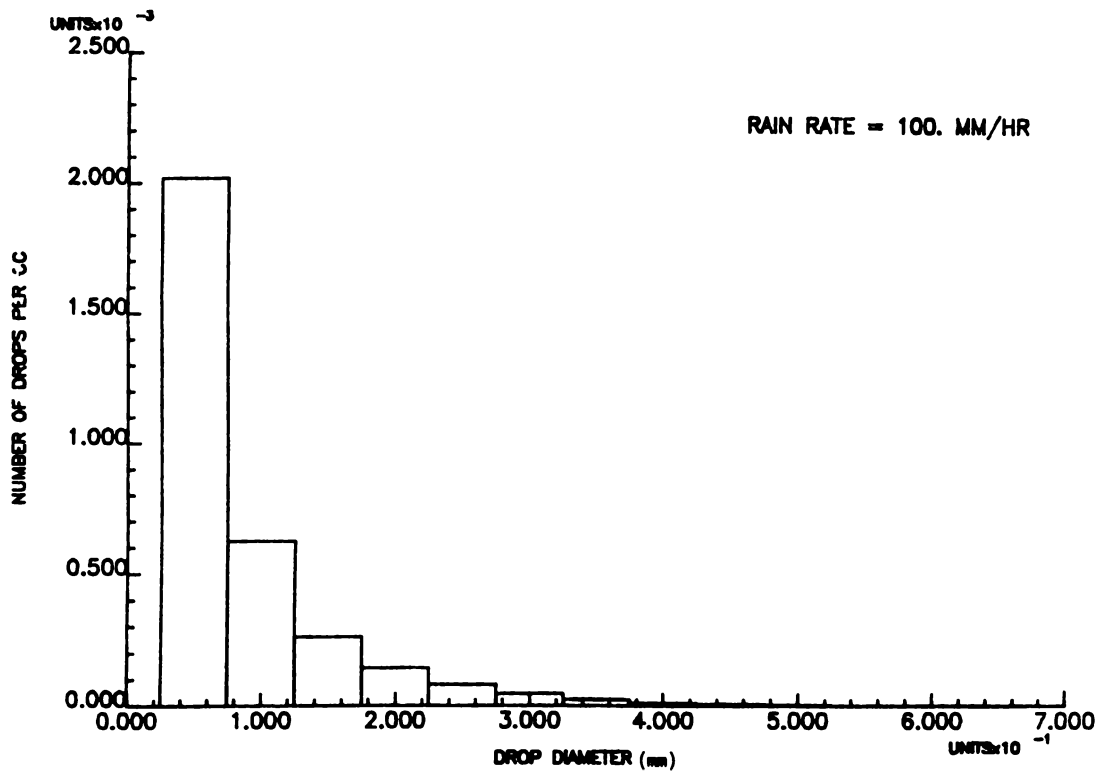


Figure 8.13 Laws and Parsons Drop-Size Distributions; 100.0 mm/hr Rain Rate

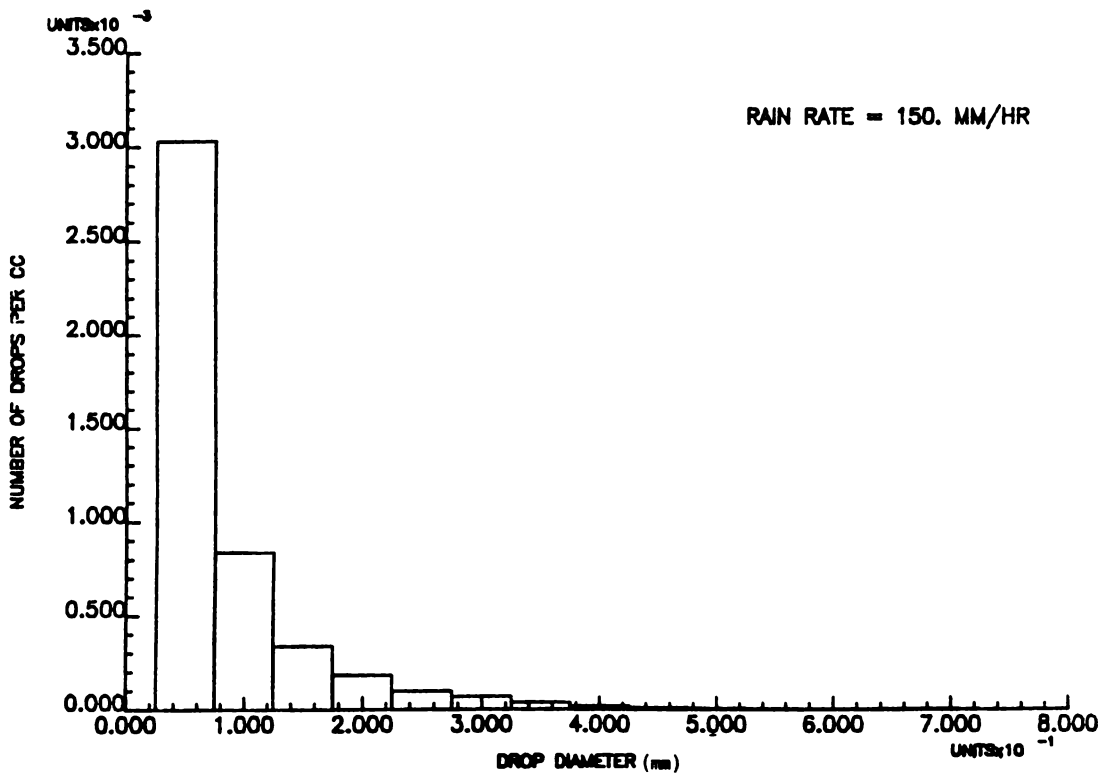


Figure 8.14 Laws and Parsons Drop-Size Distributions; 150.0 mm/hr Rain Rate

### Additional Background

There are a number of models available for estimating rain rates and signal attenuations for each space communication paths assembled for global applications. The published models available are summarized in Table 8.3, where key features of seven models are provided. For the applications considered here, Crane’s work (included in inserts 3, 4, and 5 in Table 8.3) is most applicable. Further discussions of the remaining formulations can be found in the papers cited in the bibliography, particularly the work of Ippolito.

In several papers, Crane developed surface point rain rate distributions from long-term observations of rain accumulations. For global applications, considering climates that range from dry desert regions to wet tropical areas, eight climate regions were found necessary to adequately characterize observed rain rate distributions. The rain-rate distribution functions provided relate rain rate to a percentage of occurrence on a yearly basis. These distributions, when integrated, yield *yearly average rainfalls*. The rain rates then lead to attenuation and backscatter estimates.

The procedures developed by Crane for global rain-rate estimates constitute a good first step in developing any rain model because of the global estimates of

**Table 8.3**  
Summary of Model Parameters\*

<i>Model</i>	<i>Inputs</i>	<i>Outputs</i>	<i>Comments</i>
Rice-Holmberg	Climate or site-specific mean annual rainfall plus ratio of thunderstorm-to-total rain	Cumulative time distribution of rainfall	Two rain modes considered: Thunderstorm and uniform rains. Probability of rain rate exceedance for either or both modes is available.
Dutton-dougherty	Same as Rice-Holmberg and line parameters (e.g., frequency, elevation angle)	Rain or gaseous attenuation associated with a given exceedance time percentage	Utilizes modified Rice-Holmberg rain model. Provides confidence limits, given two additional rain rate distributions.
Global	Location and link parameters	Rain attenuation associated with a given exceedance time percentage	All rain attenuation parameter value are self-contained. Globally applicable.
Two-component	Same as global	Exceedance time percentage associated with a given rain attenuation	Same rain model (and comments) as global model. Two rain modes considered: Convective cell and debris rains.
CCIR	Same as global	Rain attenuation associated with a given exceedance time percentage	All rain attenuation parameter values are self-contained. Globally applicable.
LIN	Five-minute rain rate and link parameters	Attenuation associated with a given rain rate	Simple extension of terrestrial path rain attenuation model
Piecewise uniform	Rain statistics and link parameters	Attenuation associated with a given rain rate	Cross-polarization isolation and phase are available as outputs from the scattering model

\*From Ippolito

a rain parameter (i.e., a rain rate that forms the basis for size distributions), attenuation, and backscatter. It also lends itself to extensions for considering rain-rate distributions within the storms, and the further consideration of effects of inhomogeneities on the rain parameters. In view of these observations, the reference data provided in subsequent sections are placed in four forms or models, each having a different degree of complexity and each using the global rain-rate estimates provided in Chapter 6 as a starting point.

## 8.2 UNIFORM RAIN MODEL

While rain is rarely uniform within a storm, it is traditionally modeled as such. When this assumption is made, attenuation and backscatter estimates are constant in value, independent of path length, and infinite in extent. Backscatter coefficients are usually expressed as mean values with an assumed Rayleigh distribution. Rain modeled in this way may be applicable to certain stratiform rains where rain rates are low, convective storms with large debris areas, and short path lengths in a variety of types of rain. From a system point of view, uniform rain assumptions lead to upper and lower bounds from which realistic system performance may be determined.

An early model, developed by Crane for rain attenuation, makes use of point- and path-averaged rain rates where the cellular structure of the rain is taken into account to obtain path-dependent attenuation estimates. In this model, the point rain rates lead to a point or specific attenuation. These specific attenuation estimates constitute the basis for a uniform clutter model. Later, when the path-dependent model is described, the specific attenuation values are used to obtain the path-averaged ones.

### Attenuation

The specific attenuation is defined as

$$a = \alpha R^\beta \quad (8.5)$$

where  $a$  is the attenuation in decibels per kilometer,  $R$  is the rain rate, and  $\alpha$  and  $\beta$  are frequency-dependent parameters.

Table 8.4 contains parameters for computing the specific attenuation. These parameter values were derived using the L-P drop size distribution for a temperature of 0°C. The subscripts  $L$  and  $H$  pertain to rain rates of less than or more than 30 mm/hr, respectively. Although recommended, the 30 mm/hr division is not critical, and may occur anywhere between 25 and 50 mm/hr.

Specific attenuation is plotted in Figure 8.15 for frequencies between 30 and 100 GHz, and for rain rates between 0.25 and 100 mm/hr. These data are in general agreement with numerous published tabular data.

### Backscatter

The radar cross section of rain is determined by summing the independent contributions from each raindrop. Repeating from previous discussions in Chapter 2,

**Table 8.4**  
Parameters for Computing Specific Attenuation\*

Frequency (GHz)	$\alpha$		$\beta$	
	$LP_L$	$LP_H$	$LP_L$	$LP_H$
10	$1.17 \times 10^{-2}$	$1.14 \times 10^{-2}$	1.178	1.189
11	$1.50 \times 10^{-2}$	$1.52 \times 10^{-2}$	1.171	1.167
12	$1.86 \times 10^{-2}$	$1.96 \times 10^{-2}$	1.162	1.150
15	$3.21 \times 10^{-2}$	$3.47 \times 10^{-2}$	1.142	1.119
20	$6.26 \times 10^{-2}$	$7.09 \times 10^{-2}$	1.119	1.083
25	0.105	0.132	1.094	1.029
30	0.162	0.226	1.061	0.964
35	0.232	0.345	1.022	0.907
40	0.313	0.467	0.981	0.864
50	0.489	0.669	0.907	0.815
60	0.658	0.796	0.850	0.794
70	0.801	0.869	0.809	0.784
80	0.924	0.913	0.778	0.780
90	1.02	0.945	0.756	0.776
100	1.08	0.966	0.742	0.774

\*From Ippolito

but in summary form, the cross section per unit volume is expressed in the following way:

$$\eta = \left(\frac{\pi^5}{\lambda^4}\right)KZ(10^{-6}) \tag{8.6}$$

where  $\lambda$  is the wavelength in millimeters,  $K$  is a constant that depends on the dielectric constant of the raindrops and is numerically equal to  $0.90 \pm 0.315$ , and  $Z$  is defined as a reflectivity factor. For Rayleigh scattering

$$Z = \sum_i f_i D^6 N(D_i) \Delta D \tag{8.7}$$

where  $D_i$  is the diameter of an assumed spherical raindrop and  $N(D_i) \Delta D$  is the number of drops of diameter  $D_i$  within the increment  $\Delta D$ . As frequencies increase into the millimeter-wave region, the Rayleigh assumption becomes invalid and Mie scattering theory must be used. In that case

$$Z = \sum_i F_i D^6 N(D_i) \Delta D \tag{8.8}$$

where the factor  $F_i$  is the ratio of Mie to Rayleigh scattering for the spherical drop.

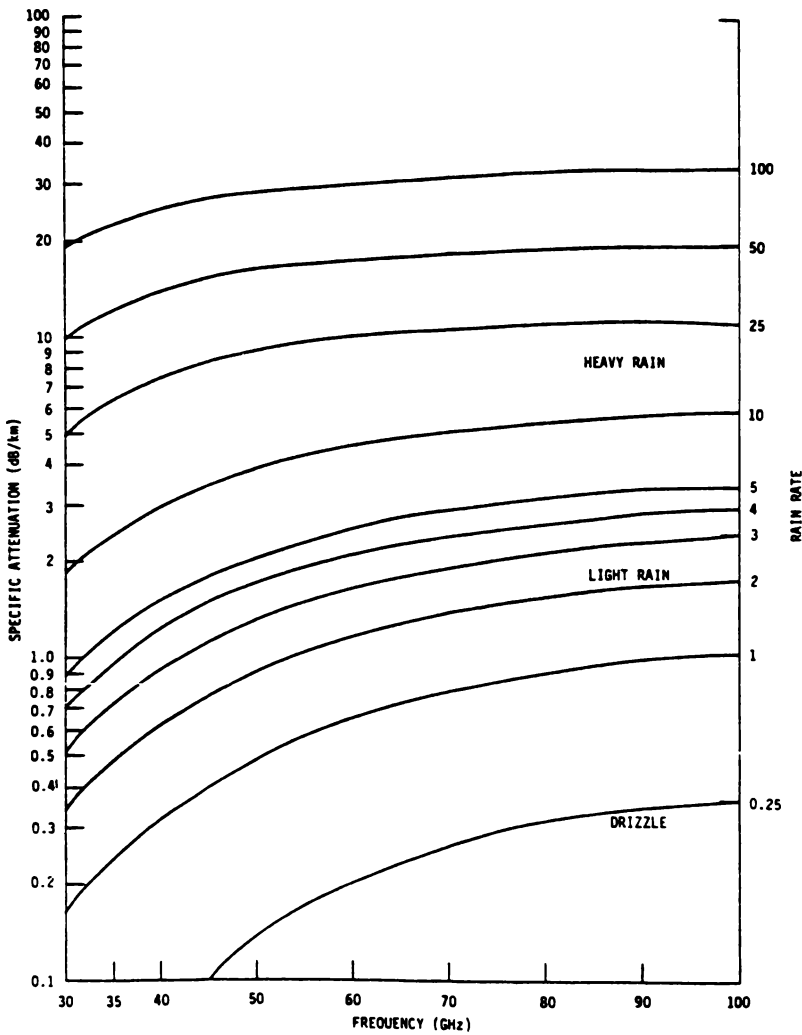


**Figure 8.15** One-Way Specific Attenuation *versus* Frequency for Rain. (Compiled from Ulaby)

Direct integration of the M-P drop size distribution for Rayleigh scattering yields a reflectivity factor of

$$Z = 296 R^{1.47} \quad (8.9)$$

In an original paper by Atlas, it was pointed out that discrepancies occur when wavelengths are below about 3.2 cm and that unique  $Z$ - $R$  relationships can be used only over restricted rain-rate intervals. From this early work, approximate  $Z$ - $R$  relations, obtained by using the M-P distribution and corrected for Mie scattering given in Table 8.5 were derived. The results given for a frequency of 35 GHz will yield estimates that are lower than more recently published theoretical and experimental values. The basic formulation used to determine the theoretical results and the resulting form of reflectivity factor is



$$Z = p R^q$$

(8.10)

where  $p$  and  $q$  are constants evident in Table 8.5 for ranges of frequency and rain rates.

Table 8.5  
Z-R Relations Corrected for Mie Scattering\*

Wavelength (cm)	R Interval (mm/hr <sup>-1</sup> )	M-P (°C)
0.62	0-5	240R <sup>1.1</sup>
	5-20	345R <sup>0.9</sup>
	20-100	540R <sup>0.75</sup>
0.86	0-5	350R <sup>1.32</sup>
	5-20	450R <sup>1.15</sup>
	20-100	780R <sup>0.95</sup>
1.24	0-5	356R <sup>1.5</sup>
	5-20	460R <sup>1.35</sup>
	20-100	820R <sup>1.15</sup>
1.87	0-20	330R <sup>1.54</sup>
	20-50	500R <sup>1.4</sup>
	50-100	750R <sup>1.3</sup>
3.21		275R <sup>1.55</sup>
4.67		280R <sup>1.45</sup>
5.5		280R <sup>1.45</sup>
5.7		
10.0		295R <sup>1.45</sup>

\*From Atlas

Backscatter cross sections ( $n$ ) expressed in units  $m^2/m^3$  are plotted in Figure 8.16 for rain rates between 2.5 mm/hr and 100 mm/hr. The actual cross section of the rain is related to  $(\eta)(v)$ , where  $v$  is the volume of the radar resolution cell. These data, from Crane, were computed using the M-P and L-P distributions.

Specific cross section data may be obtained by interpolation or extrapolation of the results plotted in Figure 8.16. Another preferred approach is to use the Z-R relationships provided in Table 8.5, or from other sources if needed, adjusted to data that become available. This approach is justifiable because the Z-R relationships provided are approximate and are continually being upgraded. When expressed in this form, they are particularly useful for simulation applications.

Use of Model

A step-by-step procedure for application of the uniform clutter model is provided below. The starting point is the use of global rain rate formulation.

1. Obtain the climatic region from Figures 6.1, 6.2, or 6.3 for the geographic longitude and latitude of interest. Using Figure 8.3 for the specific latitude, establish the altitude of the rain from the zero-degree isotherm data. Rain is assumed uniform throughout horizontal and bounded vertical extents.
2. Select a probability of exceedance for a percent of the year. Then, using Figure 6.4 or Table 6.1, determine the rain rate for the desired probability.
3. For the derived rain rate, use Equation (8.5) and the data in Table 8.4 to obtain the estimated attenuation in dB/km. The total system attenuation becomes this value multiplied by the path length.
4. For the derived rain rate, use Equation (8.10) and the data in Table 8.5 to obtain the estimated backscatter. An alternate approach is to interpolate or extrapolate between the data plotted in Figure 8.16. The total cross section is the obtained backscatter values multiplied by the volume of the resolution cell. Rayleigh fluctuations about these mean cross section values should be assumed.

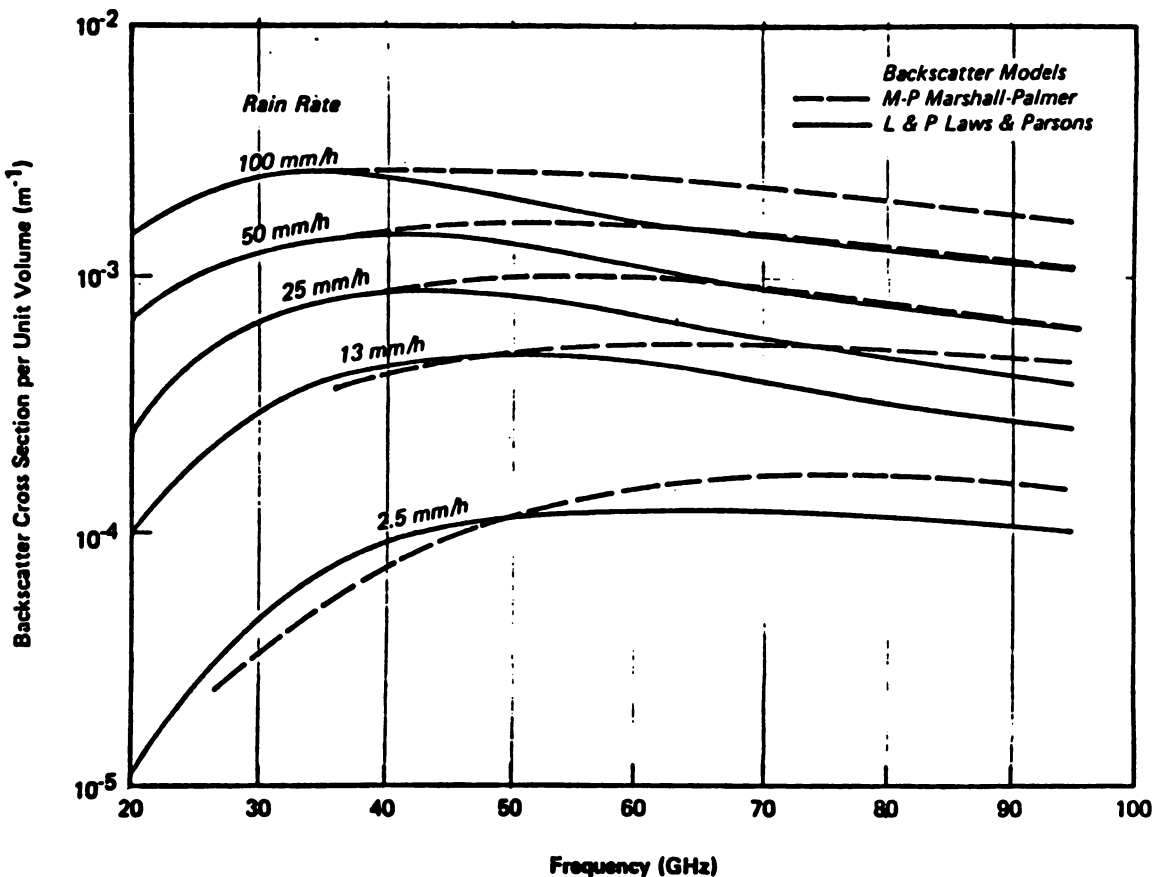


Figure 8.16 Reflectivity *versus* Frequency for Rain. (From Crane)

For simulation algorithm developments, use of Equations (8.5) and (8.10) is recommended. The number of constants utilized should be kept to a minimum and checked before using by comparing computed results with the data plotted in Figures 8.15 and 8.16. Algorithms for coverage of bands of frequencies would require tabulated data similar to the contents of Tables 8.4 and 8.5.

### 8.3 PATH-DEPENDENT MODEL

As indicated in the modeling work conducted by Crane, rain is characterized as inhomogeneous in the horizontal dimension and requires a statistical model to obtain reasonable attenuation and backscatter estimates. Crane first assembled data for path lengths of 5, 10, and 22.5 km, and accumulated path-averaged rain rate observations. From these data, path-averaged attenuation values were determined and related to the surface-point rain rate through a parameter referred to as an effective path average factor, expressed here as  $\delta = \bar{r}/r$ , where  $\bar{r}$  is the effective path length.

Because the cellular structure of a storm is taken into account, attenuation estimates exceed point values when the rain rates are low. Conversely, path-averaged attenuation falls below the specific values when rain rates are high. This basic characteristic of the model is expected, because a high specific (or point) rain rate implies a location within a cell with a corresponding high specific attenuation. Paths of reasonable length pointed in any direction will encounter lower rain rates and decreased path attenuations. The opposite occurs when the end point of a path is in a region of low rain rates; then, higher rain rates will likely occur over realistic path lengths, leading to total path attenuations higher than the point values.

Crane included the rain inhomogeneities in an attenuation model in a very simple but effective way. The starting point in describing the model is the specific (or point) attenuation described in the previous section and the path averaged factor defined above.

#### Path-Averaged Attenuation

From Crane but using a slightly different notation, let the path-averaged attenuation be expressed in the following way:

$$A = 2A\delta D \quad (8.11)$$

where  $A$  is total two-way path attenuation expressed in decibels,  $a$  is the specific attenuation ( $a = \alpha R^b$ ),  $\delta$  is the path average factor, and  $D$  is the one-way path length.

For  $d \leq D \leq 22.5$  km,

$$\delta = \frac{1}{D\beta} \left[ \frac{\exp(u\beta d) - 1}{u} + \frac{b^\beta}{c} \left( \exp(c\beta D) - \exp(c\beta d) \right) \right] \quad (8.12)$$

when  $0 \leq D \leq d$

$$\delta = \frac{1}{D\beta} \left[ \frac{\exp(u\beta D) - 1}{u} \right] \quad (8.13)$$

where

$$d = 3.8 - 0.6 \ln R \quad (8.14)$$

$$c = 0.026 - 0.030 \ln R \quad (8.15)$$

$$b = 2.3R^{-0.17} \quad (8.16)$$

$$u = \frac{\ln[\exp(cd)]}{d} \quad (8.17)$$

When  $\alpha$  and  $\beta$  are set equal to 1.0, the resulting  $\delta$  expresses the ratio of path-averaged rain rate to point rain rate. The parameters  $d$ ,  $c$ ,  $b$ , and  $u$  are empirically derived constants.

Equations (8.11) through (8.17) estimate path-averaged attenuation for horizontal paths. When slant paths are involved, corrections are needed and upper altitude bounds must be taken into account. If  $H_i$  is the zero-degree C isotherm height and  $H_0$  the altitude of the station or source, then the surface projected path length is

$$D = \frac{H_i - H_0}{\tan \theta}, \quad \theta \geq 10^\circ \quad (8.18)$$

where  $\theta$  is the elevation angle. When  $\theta < 10^\circ$ ,  $D$  is written as

$$D = E\Psi \quad (8.19)$$

where

$$\Psi = \sin^{-1} \left\{ \frac{\cos \theta}{H_i + 1} \left[ \sqrt{(H_0 + E)^2 \sin^2 \theta + 2E(H - H_0) + H^2 - H_0^2} - (H_0 + E) \sin \theta \right] \right\} \quad (8.20)$$

and  $E = 8500$  km, the effective radius of the earth. Use of  $D$  as in Equations (8.18) or (8.19) in Equations (8.11) through (8.17) yields the surface projected attenuation ( $A_s$ ). The attenuation along a slant path becomes

$$A = \frac{A_s}{\cos \theta} \quad (8.21)$$

or

$$A = \frac{A_s}{D} \sqrt{(E + H_0)^2 + (E + H_i)^2 - 2(E + H_i) \cos \Psi} \quad (8.22)$$

when  $\theta < 10^\circ$ .

Path length factors are plotted in Figure 8.17 for path lengths between 2 and 22.5 km. Therefore, total attenuation estimates would exceed the specific attenuation values for rain rates below about 10 mm/hr. For small path lengths, the path length factor is below one when moderate to high rain rates occur, leading to an attenuation that is less than the specific value. A convenient use of this formulation is to give upper and lower bounds for the estimates by specific and path-corrected attenuations. For path length factors greater than one, the specific attenuation estimate becomes the lower bound, while for factors less than one, the path-corrected estimates become the lower bound.

## Backscatter Formulation

In this model, the cross section or backscatter estimates can be made at the end-points of the path, where specific or point attenuation values occur. Then the backscatter is determined using the rain rate associated with the specific attenuation, in which case the formulation used in the uniform clutter model is applicable.

## A Methodology

A reasonable procedure for using the path-corrected model is as follows:

1. Obtain the climatic region from Figures 6.1, 6.2, or 6.3 for the geographic

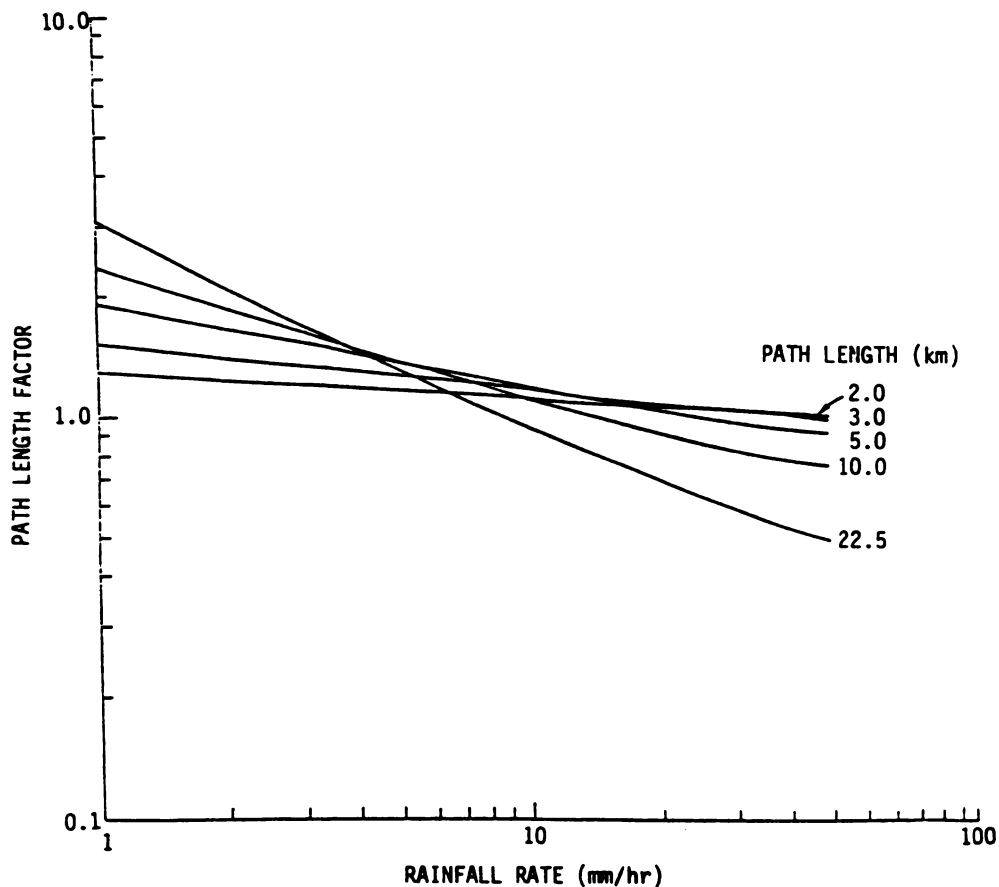


**Figure 8.17** Path Length Factors

longitude and latitude of interest. Using Figure 8.3 for the specific latitude, establish the altitude of the rain from the zero-degree isotherm data. Rain is assumed uniform within the bounded vertical extent and inhomogeneous in the horizontal directions.

2. Select a probability of exceedance for a percent of the year. Then using Figure 6.1 or Table 6.1, determine the rain rate for the given probability. This rain rate is used to estimate the specific attenuation and backscatter at the endpoints of the propagation path.
3. For the rain rate determined, use Equation (8.5) and the data in Table 8.4 to obtain the estimated specific attenuation.
4. Establish the surface projected path length  $D$  using the separation between antennas for terrestrial paths and Equations (8.13) to (8.22) for slant paths.
5. Compute the surface projected attenuation using Equations (8.11) to (8.17). The computed value is the path average attenuation for terrestrial paths. For slant paths and elevation angles greater than  $10^\circ$ , use Equations (8.18) to (8.22) to obtain the path-averaged attenuation. For angles less than  $10^\circ$ , use

Equations (8.4) to (8.22).

6. For the rain rate determined for estimates for the specific attenuation use Equation (8.10) or the data in Figure 8.16 to obtain the estimated backscatter.

In this model, the specific or point attenuation applies to the source point or end of the propagation path. The attenuation pertains to the total path and is a function of the path length. The backscatter procedure involving endpoints is an approximation that appears to be reasonable for low rain rates but serves as an upper bound when high rain rates with associated high specific attenuations are encountered.

For simulation applications, use of Equations (8.5) and (8.10) are recommended for specific attenuation and backscatter estimates, respectively. Then Equations (8.11) to (8.22) are readily programmable, leading to path-dependent attenuation estimates. It is convenient to bound the attenuation estimates by the path-averaged and specific values. Thus, upper and lower bounds are established, with the specific attenuation being the lower bound for rain rates below about 8 mm/hr. Use of this path-dependent model is recommended for all but low rain rates.

## **Two-component Dependence**

Two-component dependence, also developed by Crane, includes procedures for calculating the probabilities of occurrence of volume cells and widespread debris that yield varying attenuations along a propagation path. The model will be described and, following the format used previously, a procedure for its use will be discussed. This procedure, however, will be restricted to computing probabilities associated with cells, debris clutter, and their respective rain rates. As pointed out by Crane, the model is a first step in the consideration of more complex modeling problems. This is the case for radar analysis and simulation applications. Extension to a fractal model is accomplished in the next section. The two-component separations are considered as an extension or adjunct to Crane's path dependent model.

## *Summary Description*

Attenuation estimates involve separate treatment of rain showers (cells) and larger regions of light rain (debris) surrounding the showers. Figure 8.1 shows the structure of a typical storm with spatially inhomogeneous properties typical of all rainfall types. The horizontal area of a volume cell is small and the debris area surrounding the cells is large. Crane explicitly defines two rain properties as follows:

1. Volume Cell—Small volume surrounding a local reflectivity peak which has a reflectivity value greater than one half the peak value.

## 2. Debris—The larger region of lighter rain rate surrounding a volume cell.

Cells and debris are handled independently in the development of the model. It is assumed that a single cell or debris (or both) can occur along a propagation path. Thus, the resultant attenuation is due to combinations of contributions of cells and debris with the probabilities associated with each component determined and added independently to obtain the total probability of occurrence.

As in Crane's previous work, a global description of probability distributions of point-surface rainfall rate is provided. These revised versions have been described and used in the uniform and path-dependent models. Two notable additions occur in the two-component model. The first is the inclusion of distribution parameters  $P_c$ ,  $R_c$ ,  $P_D$ ,  $R_D$ , and  $\sigma_D$  for each region. They are defined as follows:

- $P_c$  = probability of the occurrence of a cell;
- $P_D$  = probability of the occurrence of debris;
- $R_c$  = average rain rate of cells;
- $R_D$  = average rain rate of debris;
- $\sigma_D$  = standard deviation of the natural logarithm of the rain rate.

Numerical values for the parameters are given in Table 8.6. The empirical rain-rate distribution functions are as follows:

$$P(r > R) = P_c(r > R) + P_D(r > R) \quad (8.23)$$

$$P_c(r > R) = P_c \exp\left(-\frac{R}{R_c}\right) \quad (8.24)$$

$$P_D(r > R) = P_D \mathcal{D} \mathcal{N}\left(\frac{\ln R - \ln R_D}{\sigma_D}\right) \quad (8.25)$$

where  $P(r > R)$  is the probability that the observed rain rate,  $r$ , exceeds the specified rain rate,  $R$ , and  $\mathcal{N}$  is the normal distribution function.

The second addition is to provide cell and debris heights based on measured averages. Figure 8.18 contains the latitude-dependent results. As might be expected, the cell height ( $H_c$ ) exceeds debris height ( $H_D$ ). The latitude dependence is expressed as

$$H_c = 3.1 - 1.7 \sin[2(\Lambda - 45^\circ)] \quad (8.26)$$

and

$$H_D = 2.8 - 1.9 \sin[2(\Lambda - 45^\circ)] \quad (8.27)$$



**Table 8.6**  
Two-Component Model Parameters for Each Rain Climate Region\*

Rain Zone	Cell Parameters		Debris Parameters		$\sigma_D$	$R$ for $P(r \geq R) = 0.01\%$ (mm/hr)
	$P_c$ (%)	$R_c$ (mm/hr)	$P_D$ (%)	$R_D$ (mm/hr)		
A	0.009	11.3	3.0	0.20	1.34	10
B <sub>1</sub>	0.016	15.2	9.0	0.24	1.26	15
B	0.018	19.6	7.0	0.32	1.23	18
B <sub>2</sub>	0.019	23.9	7.0	0.40	1.19	22
C	0.023	24.8	9.0	0.43	1.15	26
D <sub>1</sub>	0.030	25.7	5.0	0.83	1.14	36
D <sub>2</sub>	0.037	27.8	5.0	1.08	1.19	49
D <sub>3</sub>	0.100	15.0	5.0	1.38	1.30	62
E	0.120	29.1	7.0	1.24	1.41	100
F	0.016	20.8	3.0	0.35	1.41	10
G	0.070	39.1	9.0	1.80	1.19	95
H	0.060	42.1	9.0	1.51	1.60	245

\*From Crane

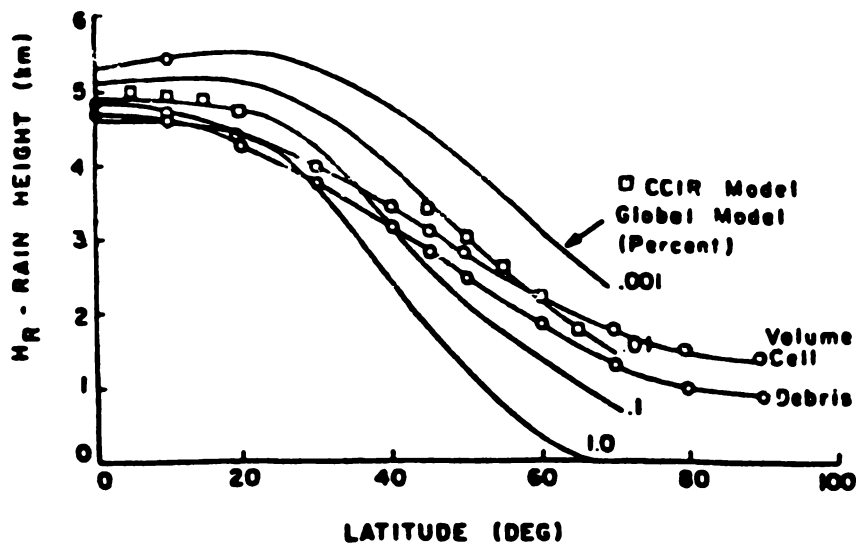


**Figure 8.18** Rain Height *versus* Latitude for the Global, CCIR, and Two-Component Models. (From Ippolito)

where  $\Lambda$  is the latitude in degrees.

Development of the rain models starts with the definition of the attenuation on a terrestrial path as,

$$a = \int_0^D \alpha [R(l)]^\beta dl \quad (8.28)$$

where  $a$  is the total attenuation along a propagation path of length  $D$ ,  $\alpha$  and  $\beta$  are parameters in the expression  $\alpha R^\beta$ , the specific or point attenuation.

The attenuation within a volume cell is written as

$$A = \frac{\alpha}{\bar{c}} R^\beta W_c \quad (8.29)$$

where  $\bar{c}$  is an adjustment factor necessary to account for attenuation outside of the volume cell, for the typical Gaussian cell representation,  $\bar{c} = 0.68$ .  $W_c$  is the average dimension of a cell having cross sectional area  $S_c$ ; it is assumed to be  $W_c = (S_c)^{1/2} \approx (5)^{1/2} = 2.2$  km.

The effective rain rate in the volume cell required to produce a specified attenuation value  $A$  or higher is

$$R' = \left( \frac{CA}{\alpha L_c} \right)^{1/\beta} \quad (8.30)$$

where  $L_c$  is the minimum of  $D$  or  $W_c$ . The probability of exceeding the specified attenuation value is

$$P_c(a > A) = P_c \left( 1 + \frac{D}{W_c} \right) \exp \left( -\frac{R'}{R_c} \right) \quad (8.31)$$

For debris, the scale length factor  $W_D$  is

$$W_D = 29.7^{[\beta/(\beta-0.34)]} \alpha^{[0.34/(\beta-0.34)]} A^{[-0.34/(\beta-0.34)]} \quad (8.32)$$

The effective rain rate is

$$R'' = \left( \frac{A}{\alpha W'_D} \right)^{1/\beta} \quad (8.33)$$

where  $W'_D$  is the minimum of  $W''_D$  or  $D$ . The resultant probability is

$$P_D(\beta > A) = P_D \left( 1 + \frac{D}{W''_D} \right) \mathcal{N} \left( \frac{\ln R'' - \ln R_D}{\sigma_D} \right) \quad (8.34)$$

where  $W_D'' = 29.7R''^{-0.34}$ . Adding Equations (8.31) and (8.34) yields

$$P(a > A) = P_c(a > A) + P_D(a > A) \quad (8.35)$$

For slant, earth-space paths,  $D$  is corrected using

$$D = \frac{\sqrt{2} (H - H_0)[2 - 2(H - H_0)/8500]^{1/2}}{\tan\theta + [\tan^2\theta + 2(H - H_0)/8500]^{1/2}} \quad (8.36)$$

where  $H_0$  is the station height and  $H$  is either  $H_c$  or  $H_D$  for cell or debris components, respectively, and  $\theta$  is the elevation angle. Then it is necessary to reduce the slant path attenuation ( $A_s$ ) before computing the probabilities:

$$A = A_s \cos\theta \quad (8.37)$$

$A$  is also referred to as the reduced attenuation.

### *Applications*

Two specific applications are considered. The first is the computation of a probability that an estimated attenuation value obtained from the first model is exceeded. The second application is directed to the estimation of the probability of a cell occurring in a propagation path and the association rain rate. Recommended methodologies are as follows:

1. Obtain the climatic region from Figures 6.1, 6.2, or 6.3 for the geographic longitude and latitude of interest. Using Figure 8.18 or Equation (8.26) and (8.27), establish the altitude of cell and debris rain. Rain is assumed uniform throughout the bounded vertical extent.
2. Establish the projected path lengths for cells and debris rain, using Equation (8.37). Reduce attenuation values if necessary, using Equation (8.28).
3. Calculate the effective rain rates  $R'$  and  $R''$  required to produce the specific attenuation values, using Equations (8.30) and (8.33).
4. Calculate the probability that the specified attenuation is exceeded, using Equation (8.36).

As pointed out explicitly by Crane, the two-component model includes the probability of exceeding a specified attenuation value. It can be used to determine an attenuation value corresponding to a specified probability by repeating the above procedure for varying attenuation values and interpolating between test cases. This procedure is recommended if the computed probabilities are small.

For the second consideration, the following procedure is suggested:

1. Follow steps 1 and 2 given above.
2. Compute the effective cell rain rate using Equation (8.30). Its probability of occurrence is given by Equation (8.31). The effective rain rate serves as an upper bound value along the propagation path.
3. Assume that the cells are circular in cross section with a diameter of 2.2 km. Also, assume that only one cell can exist and it can occur anywhere along the path, (i.e., a uniform probability distribution for the cell position).
4. Use the L-P distribution for the computed cell raindrop distribution. In this formulation, the resultant drop distribution will be more intense than the ones suggested for use in the first two models, where for most applications, the results are more indicative of debris rain.

This suggested procedure will yield worst-case situations based on a quantitative probabilistic description of rain structures.

For computational purposes or simulation applications, using Equations (8.23) through (8.25) is convenient to compute the point-rate distributions. This is particularly evident when the yearly percentages exceed one percent. The use of the formulas will yield separate distributions for the cell and debris rain rates. The sum of the two will yield the results plotted in Figure 6.4. Figures 8.19 through 8.30 contain the distributions for all the climatic regions. The dashed lines are the total distributions, the solid lines are the cell rain distributions, and the broken lines show debris distributions.

### 8.4 SNOW AND HAIL

Snow and hail differ from liquid hydrometeors in two ways. The index of refraction of ice is different from that of liquid water, shown in Table 8.7. In addition, snow and hail are generally composed of aspherical, crystalline particles. Because of these differences, snow and hail as clutter elements affect propagation in a fashion appreciably different than liquid hydrometeors.

**Table 8.7**  
Index of Refraction of Water and Ice\*

<i>Frequency (GHz)</i>	<i>State</i>	<i>Index of Refraction</i>
30	WATER 20°C	5.9–2.9i
	ICE	1.91–0.002i
100	WATER 20°C	3.505–2.007i
	ICE	1.88–0.00076i
150	WATER 20°C	3.039–1.575i
	ICE	1.88–0.00076i
300	WATER 20°C	2.587–0.937i
	ICE	1.88–0.00076i

\*From Gamble and Hodgens

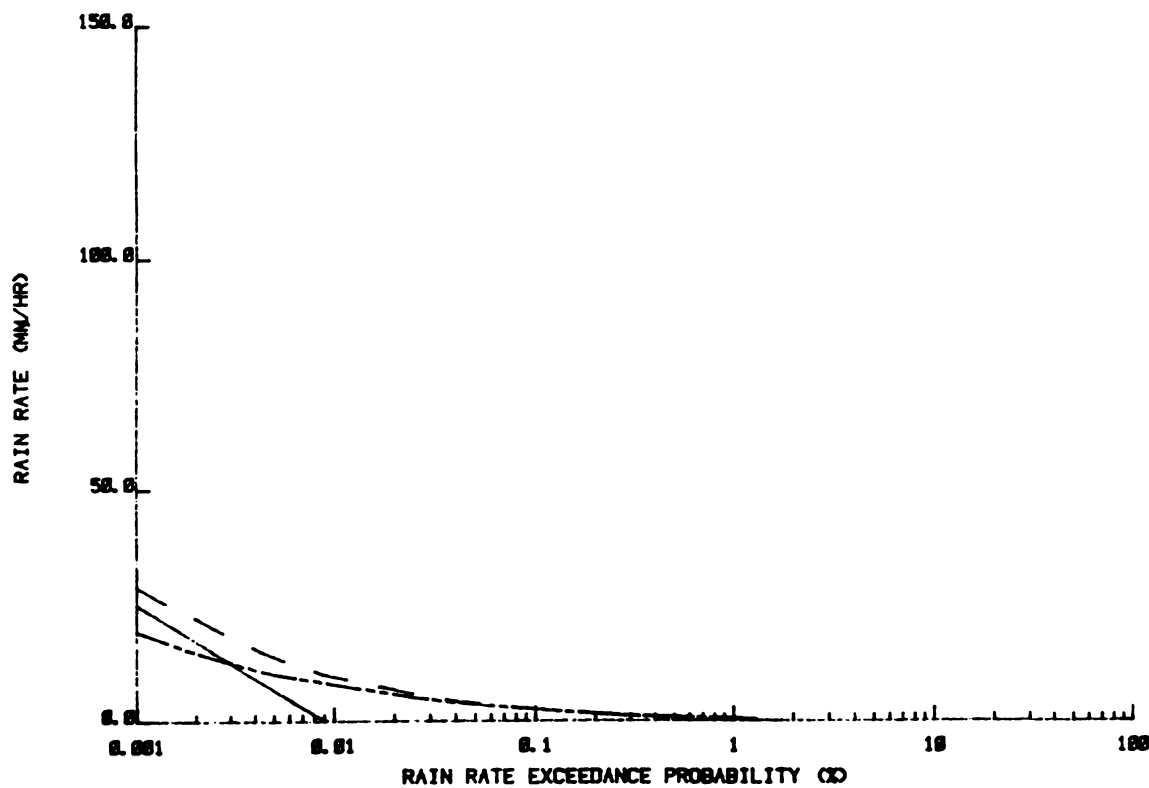


Figure 8.19 Debris and Cell Occurrence Probability—Region A

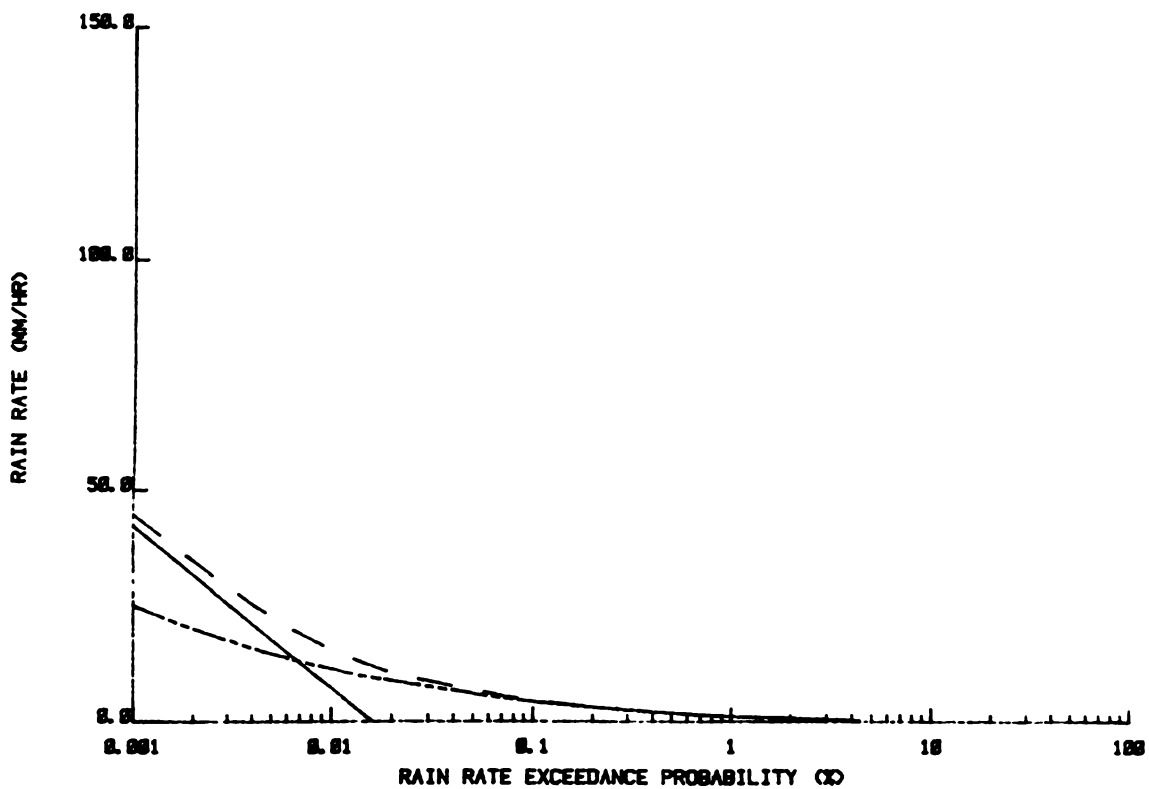


Figure 8.20 Debris and Cell Occurrence Probability—Region B1

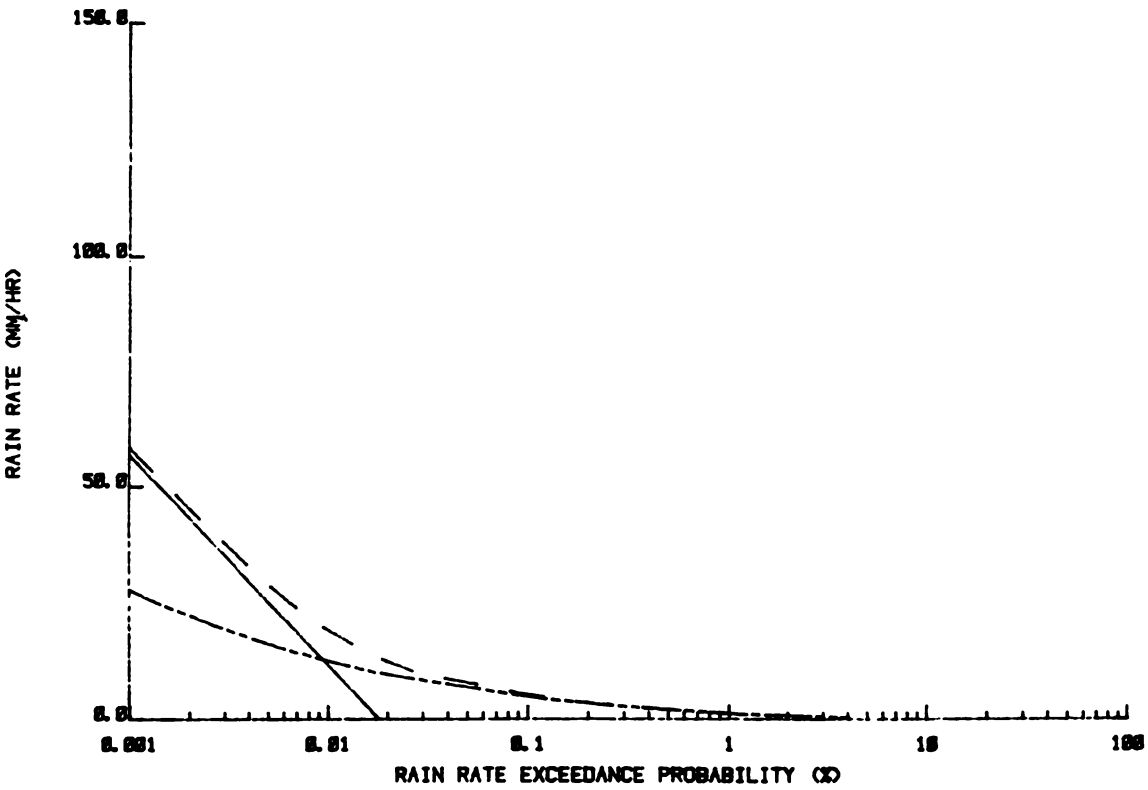


Figure 8.21 Debris and Cell Occurrence Probability—Region B

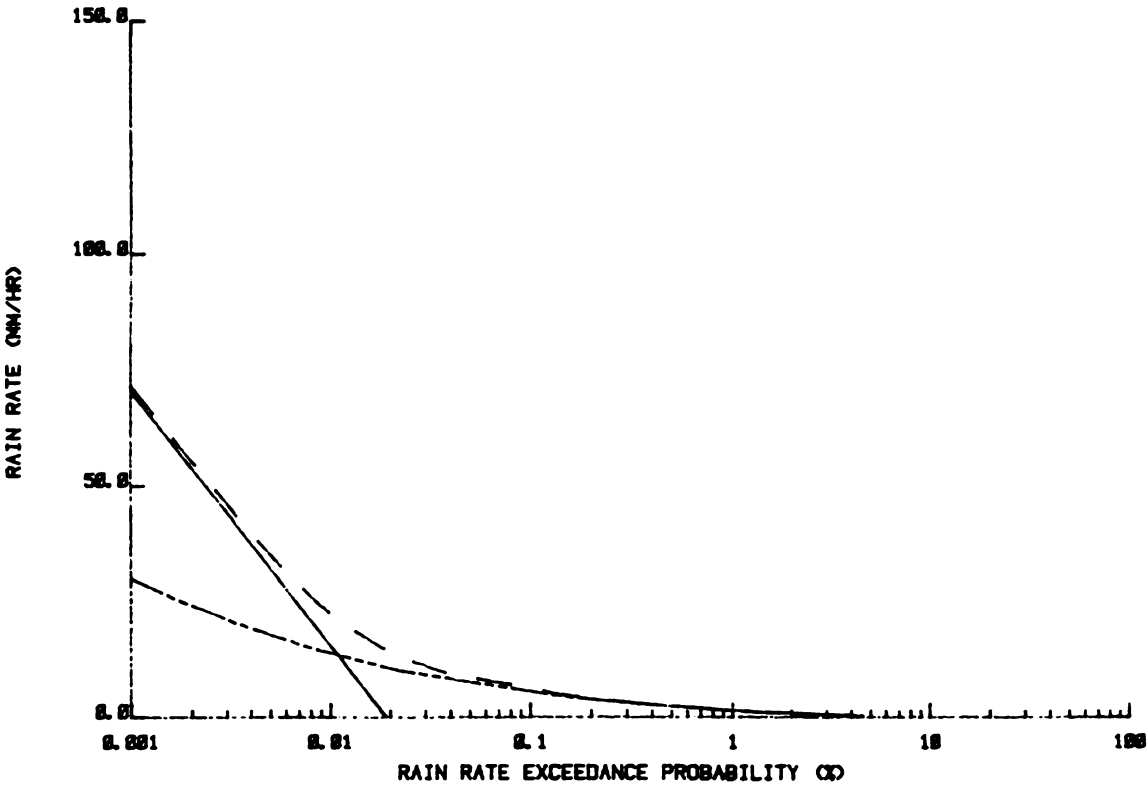


Figure 8.22 Debris and Cell Occurrence Probability—Region B2

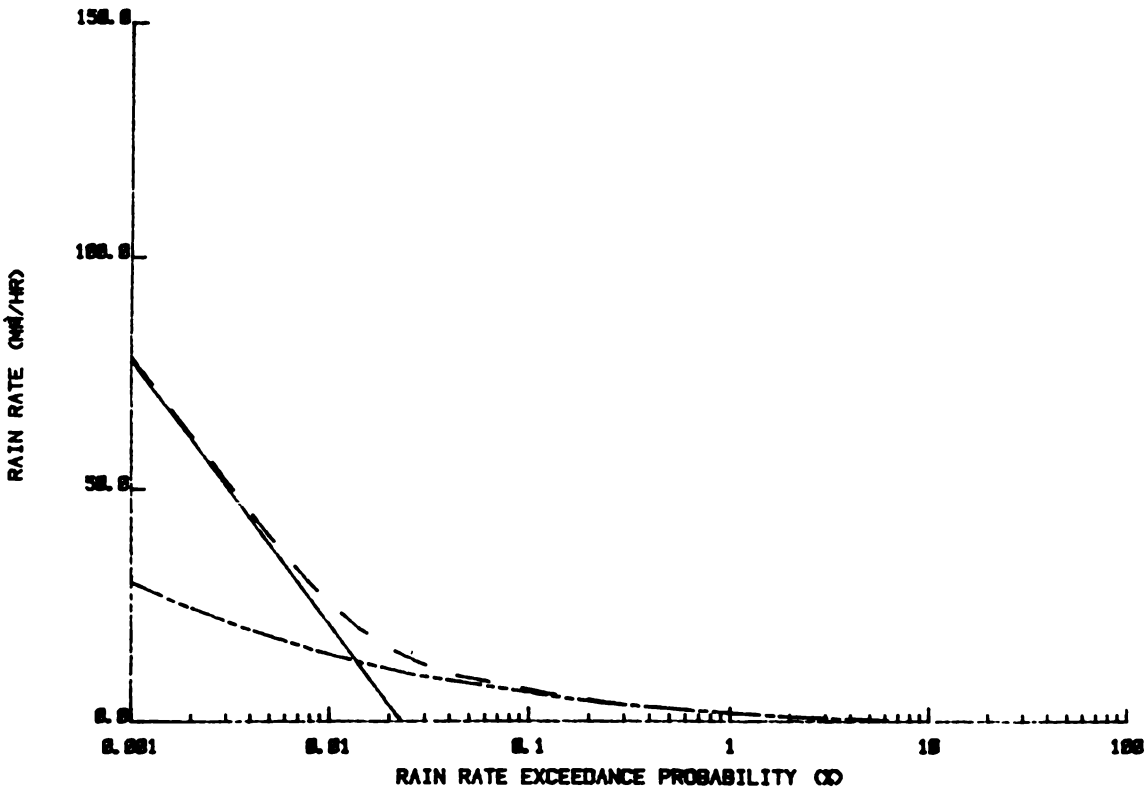


Figure 8.23 Debris and Cell Occurrence Probability—Region C

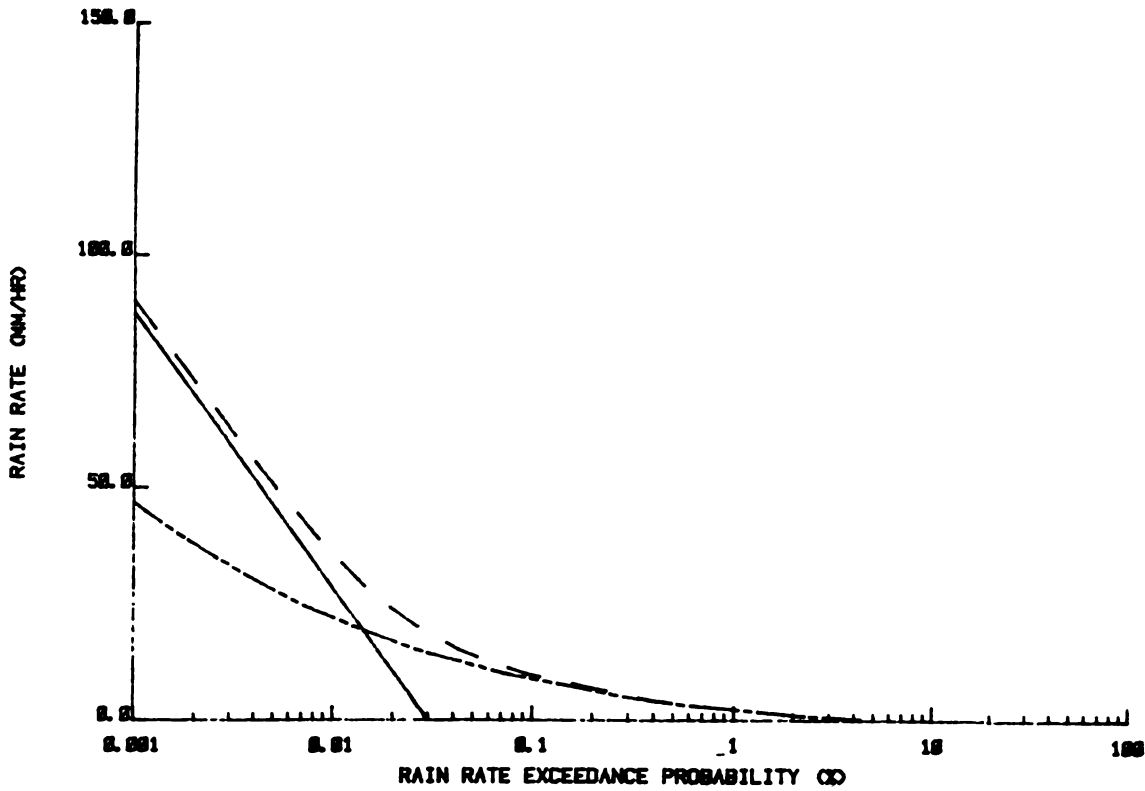


Figure 8.24 Debris and Cell Occurrence Probability—Region D1

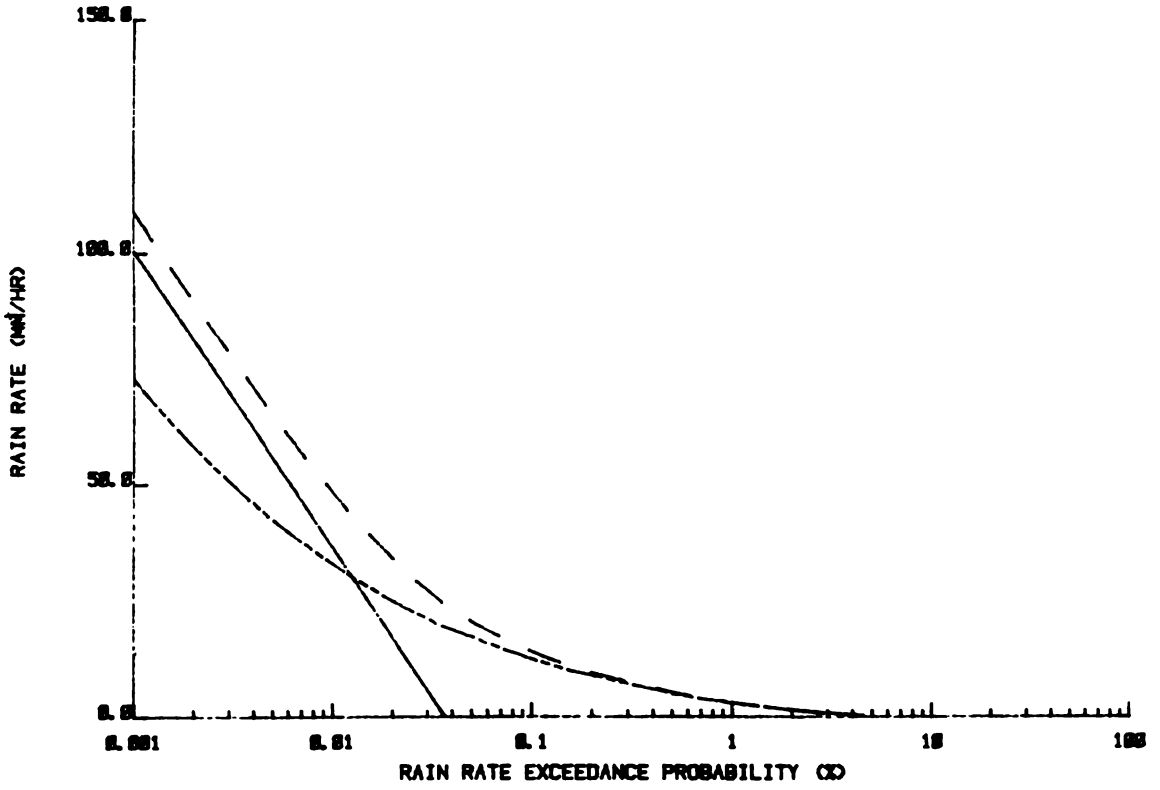


Figure 8.25 Debris and Cell Occurrence Probability—Region D2

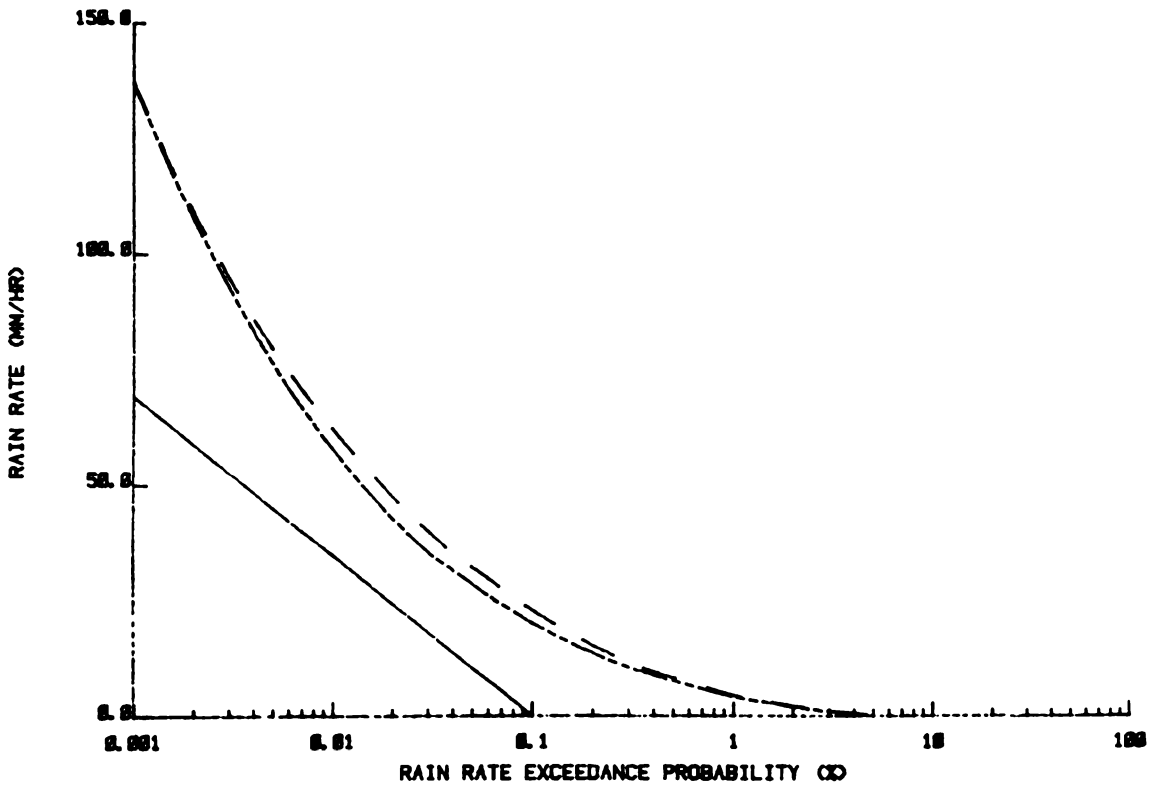


Figure 8.26 Debris and Cell Occurrence Probability—Region D3



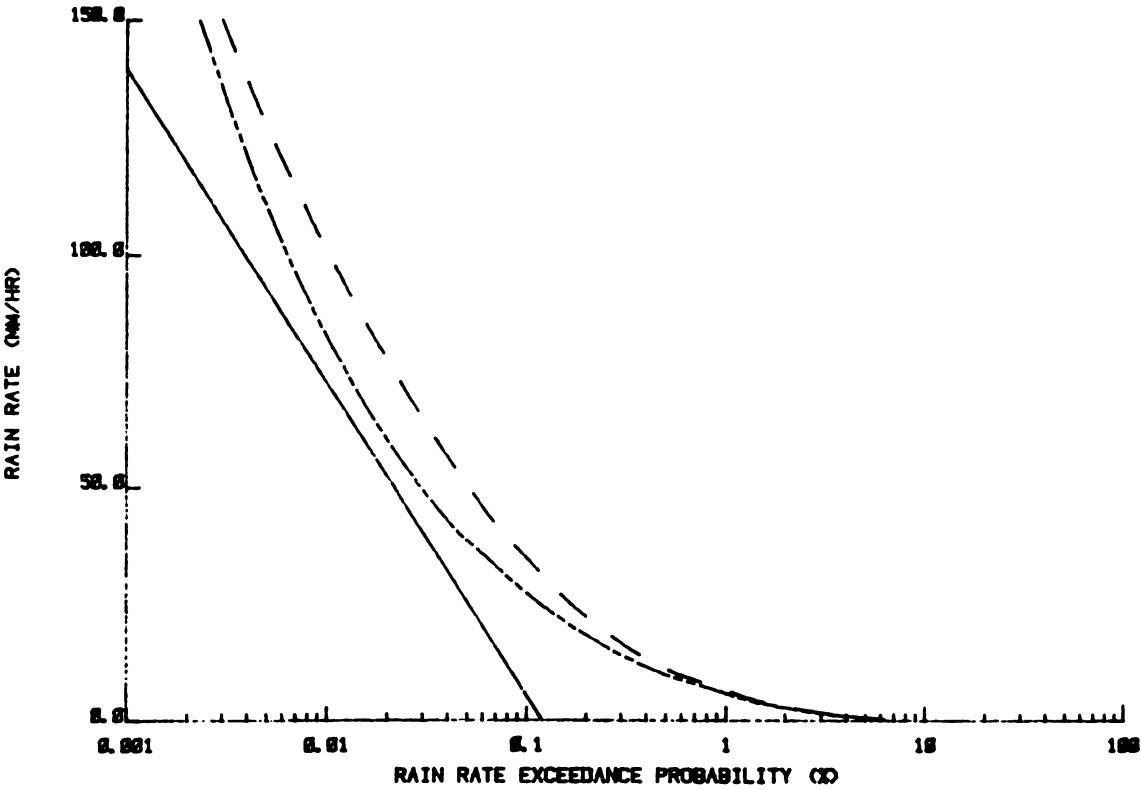


Figure 8.27 Debris and Cell Occurrence Probability—Region E

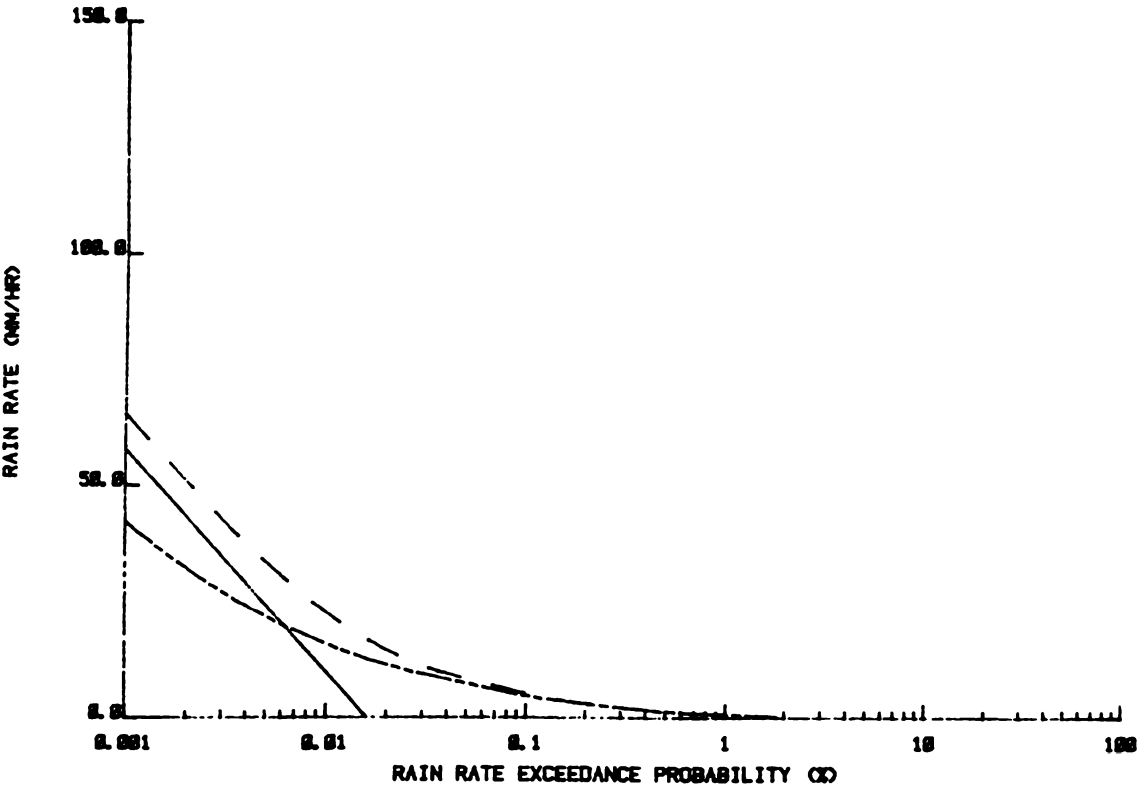


Figure 8.28 Debris and Cell Occurrence Probability—Region F

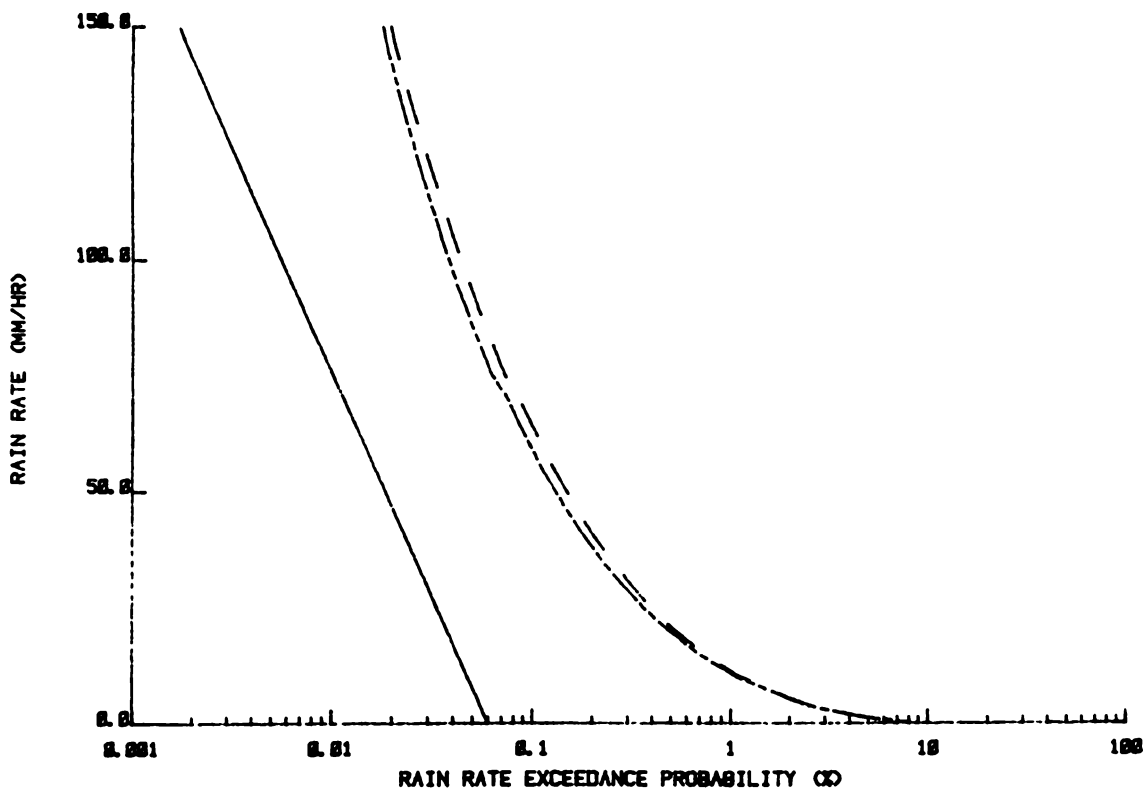


Figure 8.29 Debris and Cell Occurrence Probability—Region G

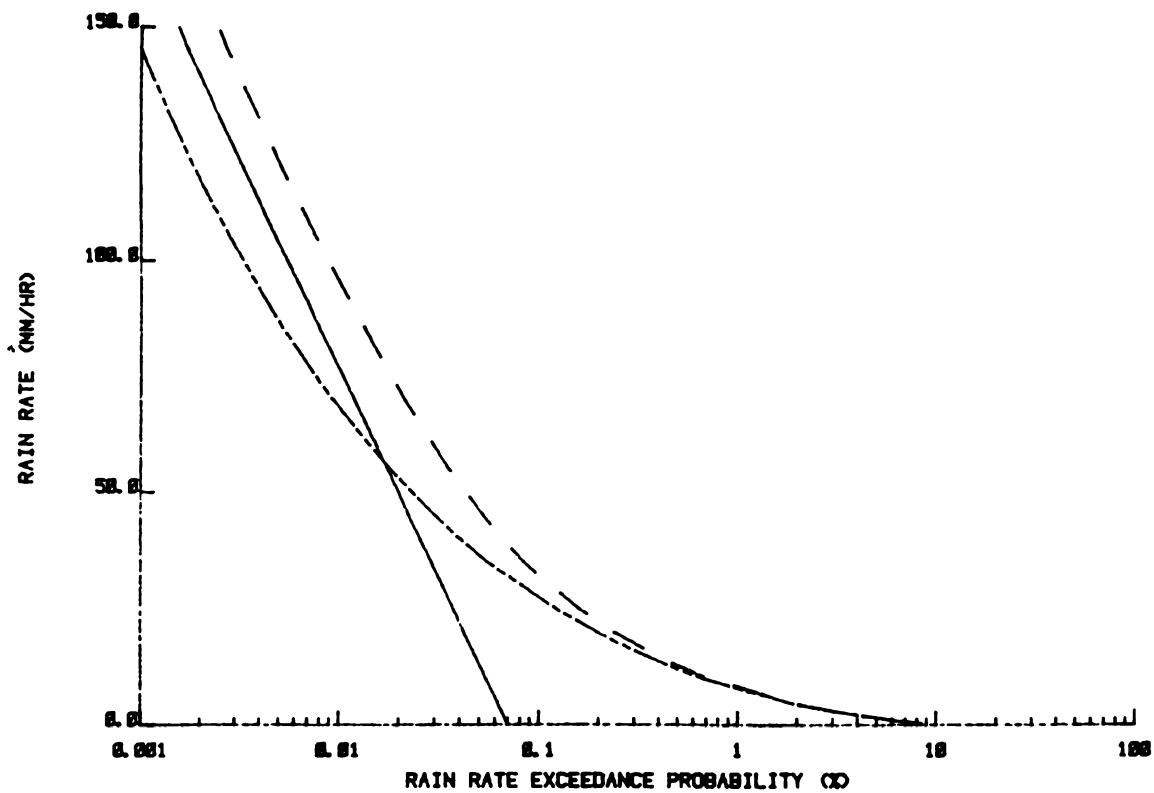


Figure 8.30 Debris and Cell Occurrence Probability—Region F

## Characteristics of Snow

There are few data describing size distributions, flake shapes, or liquid water content of snow. There are also few data describing millimeter-wave propagation through snow.

The classification of solid precipitation, as agreed upon by the International Commission on snow and ice in 1949, is shown in Table 8.8. The table provides 10 classes with remarks which generalize each class. In addition, the size,  $D$ , of the greatest dimension of the particle is classified in five groups from very small (0 – 0.49 mm) to very large (> 4 mm). The mean diameters for the values of the largest crystal dimension, mass, and fall velocity of six crystal types are given in Table 8.9. This information was determined from Nakaya and Terada, from their observations on Mt. Tokati, Japan, for air temperatures between  $-8^{\circ}$  and  $-15^{\circ}\text{C}$ . From their measurements, they determined that for plane dendrite particles, the thickness was about  $11\text{ }\mu\text{m}$  and was independent of particle size. The mean density of the graupel particles was found to be  $0.125\text{ gm/cm}^3$  and the maximum value was  $0.3\text{ gm/cm}^3$ . This density appears low compared to the density of hail, which is typically  $0.89\text{ gm/cm}^3$ .

Weickmann collected data on ice crystals from natural clouds at various heights in the troposphere. The findings of his work are summarized in Table 8.10.

The above efforts do not indicate the concentrations or size distributions of the solid precipitation, as is required for analysis and simulation studies. The aggregation of ice crystals, as indicated by Mason and other sources, appears to be most frequent for temperatures near  $0^{\circ}\text{C}$ . As expected, the cause of the aggregates is thought to be due to liquid water, which has a tendency to lead to adhesion of individual crystals.

The snow mass concentration may be converted to the equivalent rainfall rate by







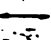
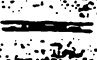






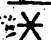





$$R_e = Xv \quad (8.38)$$

where  $X$  is the mass concentration of snow ( $\text{gm/m}^3$ ),  $v$  is the velocity of the snow or rainfall (m/s), and  $R_e$  is the equivalent rain rate (mm/hr). Therefore, a snow concentration of  $0.5\text{ gm/m}^3$  with a fall velocity of  $1\text{ m/s}$  would be equivalent to a  $1.8\text{ mm/hr}$  rainfall rate.

Significant available data include the work of Sekhon and Srivastava, where an empirical relationship for particle size distribution of snow is given as

$$N_D = 0.025R^{-0.94} \exp(-2.29R^{-0.45} D) \quad (8.39)$$

**Table 8.8**  
Classification of Solid Precipitation\*

CODE	GRAPHIC	TYPICAL FORMS	TYPES	REMARKS
1			Plates	also combinations of plates with or without very short connecting columns
2			Stellar crystals	also parallel stars with very short connecting columns
3			Columns	and combinations of columns
4			Needles	and combinations of needles
5			Spatial dendrites	spatial combinations of feathery crystals
6			Capped columns	columns with plates on either (or one) side
7			Irregular particles	irregular aggregates of microscopic crystals
8			Graupel (soft hail)	isometric shape, central crystal cannot be recognized
9			Ice pellets (Atm. sleet)	ice shell, inside mostly wet sleet
0			Hail	
Size of particle (D)		a 0-0.49 mm b 0.5-0.99 mm c 1.0-1.99 mm d 2.0-3.99 mm e 4.0 mm or larger	Very small Small Medium Large Very large	
The size D of the particle means the greatest extension of a particle ( or average when many are considered). For a cluster of crystals it refers to the average size of the crystals composing the flake.				

\*From the International Commission on Snow and Ice, 1949.

**Table 8.9**  
Mean Diameters, Masses and Fall Velocities of Snow Crystals\*

<i>Snow Crystals</i>	<i>Diameter (mm)</i>	<i>Mass (mg)</i>	<i>Fall Velocity (cm-s<sup>-1</sup>)</i>
Needle	1.53	0.004	50
Plane Dendrite	3.26	0.043	31
Spatial Dendrite	4.15	0.146	57
Powder Snow	2.15	0.064	50
Rimed Crystals	2.45	0.176	100
Graupel	2.13	0.80	180

\*From Nakaya

**Table 8.10**  
Observations of Predominant Crystal Forms in Different Cloud Types (due to Weickmann)

<i>Level of Observation</i>	<i>Temperature Range</i>	<i>Cloud Types</i>	<i>Crystal Forms</i>	<i>Remarks</i>
Lower Troposphere	0 to -15°C	Nimbostratus Stratocumulus Stratus	Thin Hexagonal Plates. Star-shaped crystals showing dendritic structure.	Hexagonal Plates Typical values Thickness < 50 μm Diameter < 500 μm
Middle Troposphere	-15 to -30°C	Altostratus Alto cumulus	Thick hexagonal plates. Prismatic columns— Single prisms and twins.	
Upper Troposphere	-30°C	Isolated cirrus	Clusters of prismatic columns containing funnel-shaped cavities. Some single hollow prisms.	Typical Prism Lengths: 0.5 mm Thickness: ≈ 0.1 mm
		Cirrostratus	Individual, complete prisms	

where

- $N_D$  = number of droplets per cm<sup>3</sup> volume per centimeter of size range;
- $R$  = snow rate in millimeters per hour of equivalent liquid water;
- $D$  = diameter in centimeters of a sphere of water formed from one of the snowflakes.

Although the particle size distribution is useful, information is readily available for particle size variations as a function of altitude and water content.

Propagation Effects

Kobayashi summarized the attenuation of snow at millimeter and submillimeter wavelengths. Figure 8.31 shows Kobayashi's summary for a number of frequencies between 11 and 312 GHz for dry and wet snow. Several observations can be made from this summary:

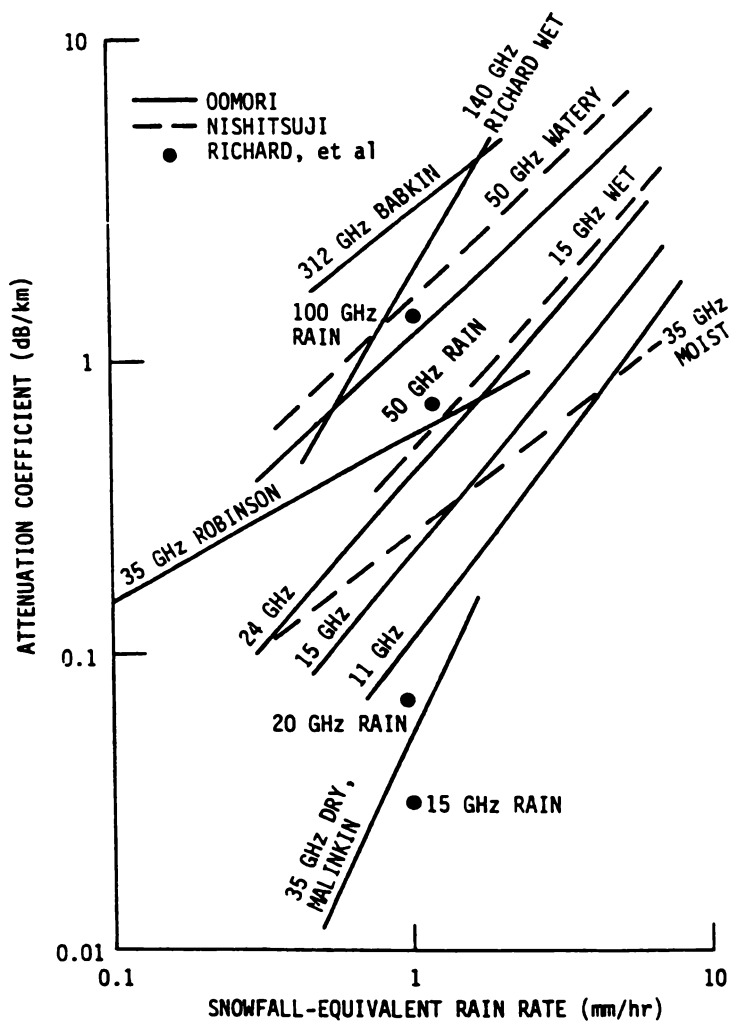


Figure 8.31 Summary of Measure Attenuation Coefficient through Falling Snow. (From Kobayashi)

1. The attenuation coefficient increases approximately linearly with snowfall rate for all frequencies considered.
2. Wet snow (snow containing liquid water) causes higher attenuation than dry snow for a given snowfall rate.
3. The attenuation generally increases with frequency for the frequencies considered.

More recent measurements by Wallace and Nemarich are discussed below, and indicate the significant spread in the data points.

Measurement of 96, 140, and 225 GHz attenuation coefficients in snow falling near the ground were made by Nemarich at the Snow One field tests in Vermont in 1981. Figure 8.32 shows attenuation coefficients plotted *versus* snow concentrations during one storm. Note that the 225-GHz data are plotted on a different scale. Attenuation coefficients were calculated from one-minute time averages of attenuation data. Snow concentrations were calculated from time averages at three stations along the propagation path. The attenuation coefficient increases most rapidly with snow concentration for 225-GHz signals, and least rapidly for 96-GHz signals. At 140 and 225 GHz, the attenuation coefficients for the 0°C to 1.5°C range are larger than the -0.5°C to 0°C range. A higher liquid water content or denser fog at the warmer temperature range may have caused this effect. The data for all three frequencies are more scattered for the -6°C to -0.5°C range. Blowing snow or increased variability in type, size, and orientation of flakes may have caused these fluctuations in the data.

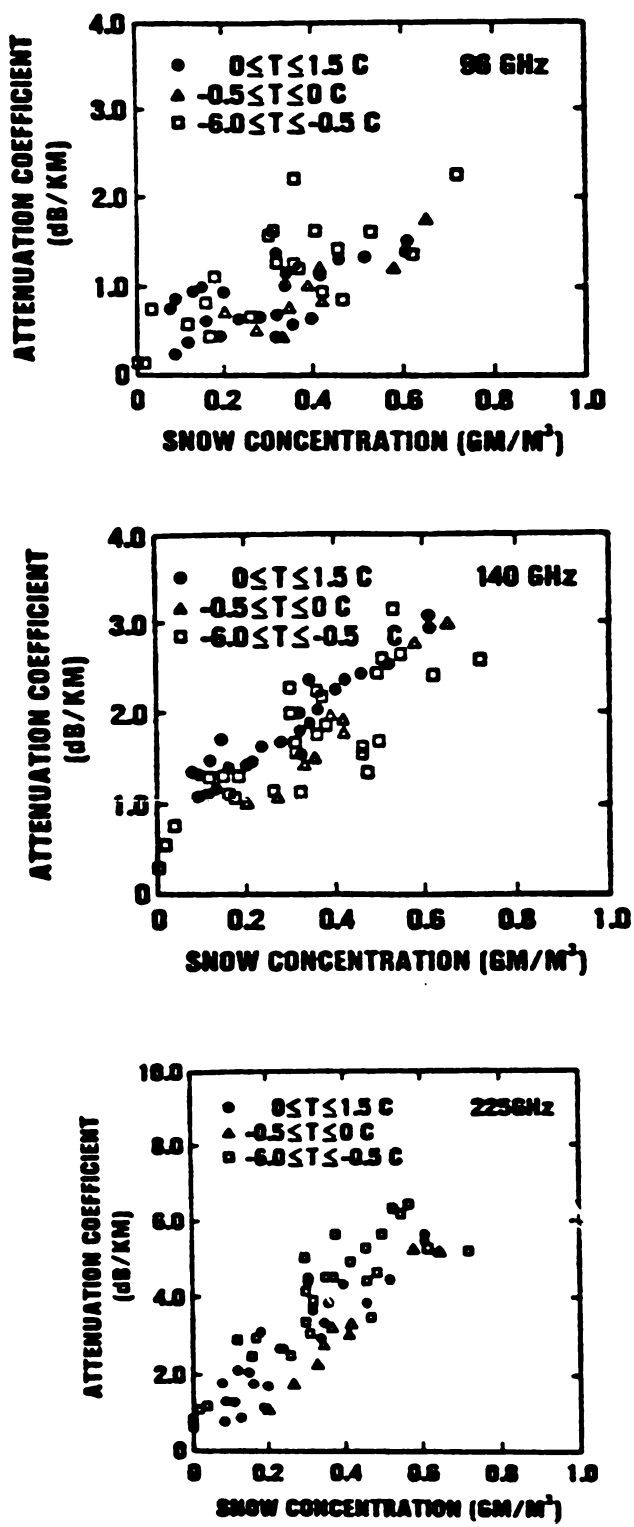
Backscatter measurements were made at 96 GHz for the same snowstorm in Figure 6.2. The backscatter cross section varied between  $2 \times 10^{-5} \text{ m}^2/\text{m}^3$  and  $6 \times 10^{-5} \text{ m}^2/\text{m}^3$ , and correlated with the snow concentrations.

Figure 8.33 shows Richard's data for attenuation coefficients *versus* equivalent rain rates. The data are for wet snow. Two sets of data are indicated in the figure: measurements made at an early time in the storm; measurements made at a later time. The early data show the attenuation coefficient to be proportional to equivalent rain rate, but the later data do not correlate. No explanation is given. The dashed line in Figure 6.3 represents the attenuation coefficient for rain. Note that rain causes less attenuation than snow at any given precipitation rate, according to Richard's research.

Figures 8.34 and 8.35 show Wallace's data for attenuation coefficients *versus* snow concentration for 35, 95, 140, and 217 GHz signals. While the data show considerable scatter, the attenuation coefficients generally increase as snow concentration and signal frequency increase. The lines drawn through the data are linear least-squares fits constrained to pass through the origins.

## Hail

Hail can form in cumulonimbus clouds when moisture is carried to altitudes above 20 kft and freezes to form nonspherical ice particles. Hailstones several centimeters



**Figure 8.32** Attenuation Coefficients Plotted Against Corresponding Snow Concentrations (Water Equivalent) for Several Temperature Ranges. (From Nemerich)



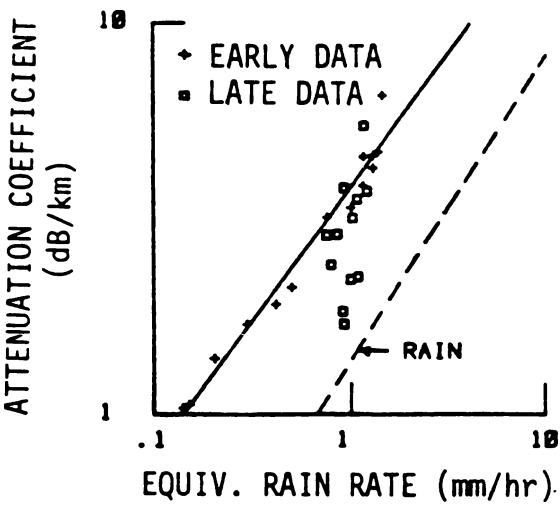


Figure 8.33 Attenuation from Snow. (From Richard's)

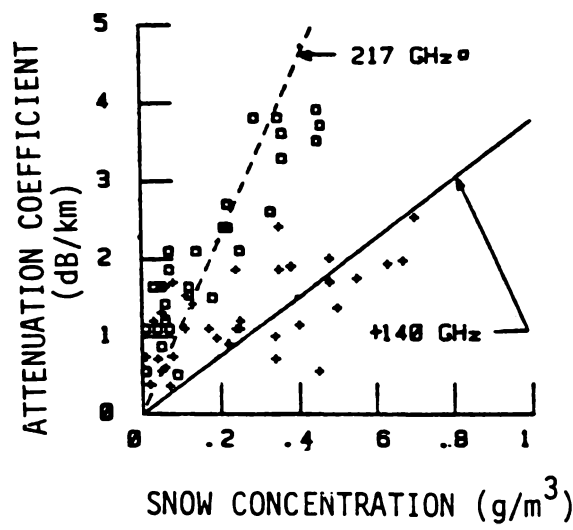


Figure 8.34 Snow Attenuation at 35 and 95 GHz. (From Wallace)

in diameter have been observed. Hail may significantly affect propagation of signals for frequencies above a few gigahertz. However, limited information is available describing the characteristics of hail and the resulting propagation effects.

Douglas gives an empirical relationship for number density of spherical hailstones as

$$N_D = 31 \exp(-3.09D) \tag{8.40}$$

where  $D$ , in units of centimeters, is the diameter of the hailstones, and  $N_D$  is the number of hailstones per cubic centimeter with diameters between  $D$  and  $D + dD$ .

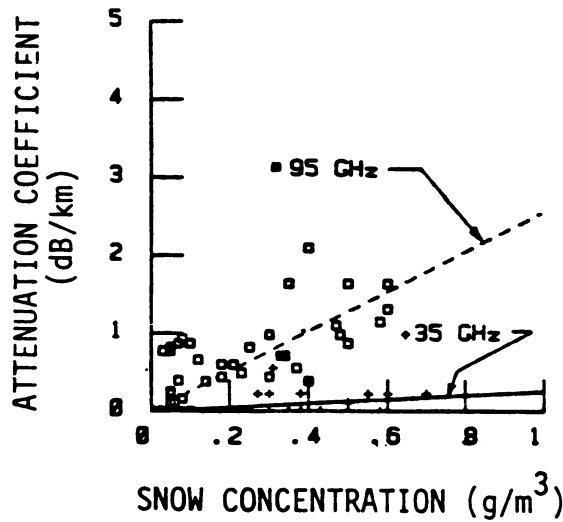


Figure 8.35 Snow Attenuation at 140 and 217 GHz. (From Wallace)

$\Delta D + D$  for  $\Delta D = 0.32$  cm (0.125 in). Battan uses this distribution and a maximum diameter of 2.89 cm to calculate an attenuation coefficient of approximately 5 dB/km for a 15-GHz signal. Larger attenuation coefficients are possible for higher frequencies. Douglas cites an attenuation coefficient of 1–2 dB/km at 15 GHz, measured in one storm where hail was assumed to be present.

An arbitrary scale, given in Table 8.11, has been used for reporting the size of hailstone. Beckwith has observed the frequency distribution of hailstone sizes for storms in the vicinity of Denver, Colorado, during the years 1949 to 1955. His findings indicate that pea-size hail occurs most often, and golf ball or larger size hail occurs at a frequency of 5% or less. Mason has reviewed information concerning the density of hailstones. According to his observations, the density of hailstones ranges between 0.85 and 0.91 gm/cm<sup>3</sup>, with the average density observed as 0.89 gm/cm<sup>3</sup>. Changnon and Stout reviewed the frequency of hail damage to wheat crops in the central and northwestern United States. Their results are summarized in Table 8.12. Although all months of the year are not indicated, the frequency of hailstorms clearly becomes larger later in the year for the more northern states.

One measure of the severity of cumulonimbus storm clouds is the height of the cloud tops. Radars can observe reflected-signals precipitation in these clouds. If a reflection is observed and has an origin above 30 kft, the possibility of hail exists. If the radar reflecting region is above 40 kft, hail and tornadoes are likely to be present.

## Summary

The data base containing the characteristics of snow environments is limited. For

**Table 8.11**  
Scale Used by Voluntary Observers in Reporting Size of Hailstones\*

<i>Kind of Hail</i>	<i>Approximate (Largest) Diameter (cm)</i>	<i>Description</i>
Ordinary or Small	< 0.5	Grain
	0.5–1.0	Pea
	1.0–1.5	Mothball, Small marble
Large	1.5–2.0	Cherry, Marble
	2.0–2.5	Large marble
	2.5–3.0	Walnut
	3.0–4.0	Golf ball
Giant	4.0–5.0	Small egg
	5.0–6.2	Egg
	6.2–7.5	Tennis ball
	7.5–9.0	
	> 9.0	

\*From Beckwith

**Table 8.12**  
Monthly Mean Number of Days of Hail Damage to Wheat Crops, 1957–1964\*

<i>State</i>	<i>April</i>	<i>May</i>	<i>June</i>	<i>July</i>	<i>Aug.</i>	<i>Sept.</i>
Texas	8	24	25	5	0	0
New Mexico	0	5	10	3	0	0
Oklahoma	11	25	22	3	0	0
Kansas	8	26	29	14	0	0
Colorado	0	13	21	20	4	0
Nebraska	2	19	28	24	4	0
Wyoming	0	2	11	14	4	0
South Dakota	0	6	23	28	15	1
North Dakota	0	0	23	29	25	6
Montana	0	2	20	25	20	4

\*From Mason

system applications, we recommend that rain rate equivalents be derived as described, and procedures contained in other chapters be utilized. This approach is reasonable until better descriptions or models become available. Using the basic formulations, models, and updates as they become available is important.

Hail can significantly degrade millimeter-wave propagation. However, only limited information is available describing the size distributions and their probabilities of occurrence. Although limited, the data sets provide at least first estimates for hail parameters, which are useful for a number of applications.

## 8.5 FRACTAL FORMULATIONS

Coastlines, island perimeters, cloud forms, and rain areas are prominent examples of naturally occurring fractals. Other examples include rivers, hydrological events, biological structures of many forms, turbulence on spatial or temporal scales, mountain ranges, distribution of galaxies, crater distributions, and the fractal structure of language, music, and stock market fluctuations. A snowflake is an excellent example of a deterministic fractal. Fractals commonly observed on a daily basis include clouds and mountainous silhouettes, which are examples of statistical fractals.

Fractals have received notoriety and visibility in the movie industry, where natural scenes have been created in several major movie productions. Similarly, striking simulations of clouds and terrain have appeared in a number of publications and were immediately recognized for their realism, but their scientific value was questioned. In the last several years, the theory and application of fractals has reached many mathematical, scientific, and engineering areas, thus marking the beginning of a rapidly expanding discipline.

The geometry of fractals, their deterministic and statistical behavior, modeling, and applications in radar including other engineering and scientific fields, are worthy of separate and definitive treatment. What seems to be implied here is an overabundance of mathematical and physical material that needs explanation before its usefulness can be realized. However, a fundamental characteristic of fractals is their descriptions, in the form of algorithms and models. Applications will then be very much in line with system analysis principles, where modeling and effectiveness in representing system observables and performance are paramount.

Two prominent applications of fractals to radar are evident. The first and most obvious is the modeling of radar targets and their natural and man-made environments for simulation purposes. The second is the introduction of hyperbolic probability distributions into the repertoire of Gaussian, Rayleigh, exponential and other probability density functions common in radar signal analysis.

Rain environments, specifically of interest here, have progressed to a point where a useful model has evolved from extensive data collection and analysis. Although not compete to a degree where, for example, a time-varying three-dimensional duplication of a weather radar ppi may be created, the extent of these activities provides a logical addition to past models, which extends their usefulness. Similar statements are applicable to other radar environments. However, new procedures recently made available for target, environment and background modeling will place radar simulations at a noticeably higher level of sophistication.

## Introduction

Fractals, introduced by Mandelbrot, are a class of mathematical objects or shapes that describe the irregularities and fragmented patterns of the natural occurrence of objects and phenomena. The basis of the theory of fractals is a geometrical one, with an extension of Euclid geometry to account for the uneven and unaligned properties of many commonly occurring shapes. Euclidean geometrical formulations are described by a set of definitive rules that govern the properties, measurement and relationships of points, lines, angles, and figures in space. Geometrical figures are two-dimensional (as in plane geometry) or three-dimensional (as in solid geometry). From their inception, geometrical formulations have provided accurate descriptions of simple shapes such as circles, squares, and cones that are characteristic of man-made objects. Although not prominent in descriptions of Euclidian geometry, but prompted by the development of fractal theory, are the scaling properties of the simple geometric figures. When magnified sufficiently, a circle, for example, will become segmented and approach a straight line. The propagation of Euclidean geometrical principles into other mathematical formulations, independent of the applications, reveals the simplicity of basic shapes and this scaling property.

In marked contrast to Euclidean geometry, fractal shapes are irregular and fragmented (without characteristic size or scale) and, when magnified, will also appear irregular and fragmented. The magnified curves are self-similar, and are exact replicas of the original fractal or a statistically equivalent one. Self-similarity, a prominent property of fractals, is representative of many real-world forms. While Euclidean geometry is characterized by a firm set of rules or formulas, fractals are described by algorithms or models that are usually computer generated. Theories associated with the creation of a fractal, or equivalently, the development of the algorithm, are therefore of a mathematical foundation. However, their application, by virtue of this modeling connotation, may in many respects be formulated as a system one, where observables are modeled, tested, validated, and used within acceptable practiced procedures or methodologies. The mathematical rigor or the underlying physical principles or phenomenologies are of concern in many applications of fractals, and they become an inherent part of the system methodology that evolves from the application of the fractals and the assessments of their validity.

The theory of fractals and the resulting algorithms and models abounds with hyperbolic probability distributions of the form of  $1/x^\alpha$ , where  $\alpha$  is, in general, a non-integer. Algorithms yield self-similar properties, and provide accurate statistical properties of the scenes being generated.

These statistics, in the form of  $1/f$  noise (i.e., noise obeying an inverse frequency power law), are a subject of considerable concern and investigation because of their occurrence in many electronic devices, and their resistance to an acceptable physical explanation. In the theory of fractals,  $1/f$  noise is generated through a

fractal integration of Brownian motion, yielding what is referred to as *fractional Brownian model*, a self-similar process constituting one of several fractal algorithms. Interpretation of this in a linear system view yields  $1/f$  noise as the output of a filter, with a transfer function of  $(j\omega)^{-1/2}$  excited by a white noise source. Thus, a physical interpretation of general  $1/f^\alpha$  noise is formulated. Also related to the fractal models is the generation of random sequences, where it is convenient to employ the inverse method (using uniformly distributed random sequences). Through fractional integration of the function  $1/x^\alpha$ , hyperbolic as well as conventional Gaussian, Rayleigh, and exponential sequences may be formed, with the fractional integrations allowing perturbations of the distributions about their nominal values, a potentially useful procedure for general radar analysis purposes. This procedure, resulting from fractal model developments, is indicated for further application of fractals in radar.

Fractional integration and differentiation methods are necessary to develop and describe the fractal models. Although the applicable theory has been in existence for some time, its applications have been limited. As a result, we have included an appendix covering principles of fractional calculus. The complexity of the theory is not overwhelming. In fact, it is interesting to observe common operations of integer order expressed as special cases of the more general ones of fractional order. Although the collection of this background material was motivated by its inclusion in fractal models, fractional integrations provide another avenue of control of the fundamental integration process, which may be especially useful in many system analysis applications. A single exploitation of this observation is taken in the generation of random numbers, where an algorithm for general computer analysis applications is provided (in Appendix B).

Several properties of fractals are described in the next section. The notion of self-similarity (or scaling) and fractal dimension are defined and described in a geometrical way. Examples are provided for clouds and rain cells that show fractional dimensions close to  $4/3$ , and may be justified on a theoretical basis. Brownian motion, a generalization of which is fractal Brownian motion, is prominent in the theory of fractals, and through it fractional integration is described. This constitutes one of two fractal algorithms that are provided. Also, fractal theory abounds with hyperbolic distributions, thus forming the basis for the remaining fractal model that is described. Supplementary material is provided (in Appendix B), with reviews of fractional differentiation and integration, the hyperbolic distribution, a random number generator, and references. Definitions are also provided, followed by a discussion of material that includes a view of radar applications, part of the background material, and a methodology for the use of fractals. While our discussions emphasize the modeling of rain environments, the theory and resulting models apply to the general area of radar target and clutter analysis and modeling.

Although specific references will be cited throughout the delineations, the majority of the material has been obtained from *The Fractal Geometry of Nature*

by B.B. Mandelbrot, and the recent publication “The Science of Fractal Images” by M.F. Barnsley, R.L. Devaney, B.B. Mandelbrot, H.O. Peitgen, D. Saupe and R.F. Voss. The path-dependent and two-component rain models, with their inherent data base and statistical models, are developed and referenced to Crane. The fractal displays are from R.E. Elkins and A.J. Bogush, Jr.

Definitions

A classic example of a fractal with exact self-similar properties is the von Koch curve, formed by a simple iterative procedure initiated with a straight line segment. Referring to Figure 8.36(a), the line segment is first subdivided into three parts, then the middle portion is replaced by two line segments in the form of an equilateral triangle, as shown in Figure 8.36(b). The new line segments consist of four parts, each one-third of the original line length. Treating each line segment in the same way leads to the curve in Figure 8.36(c). Further continuation of this process results in the von Koch curve of Figure 8.36(d).

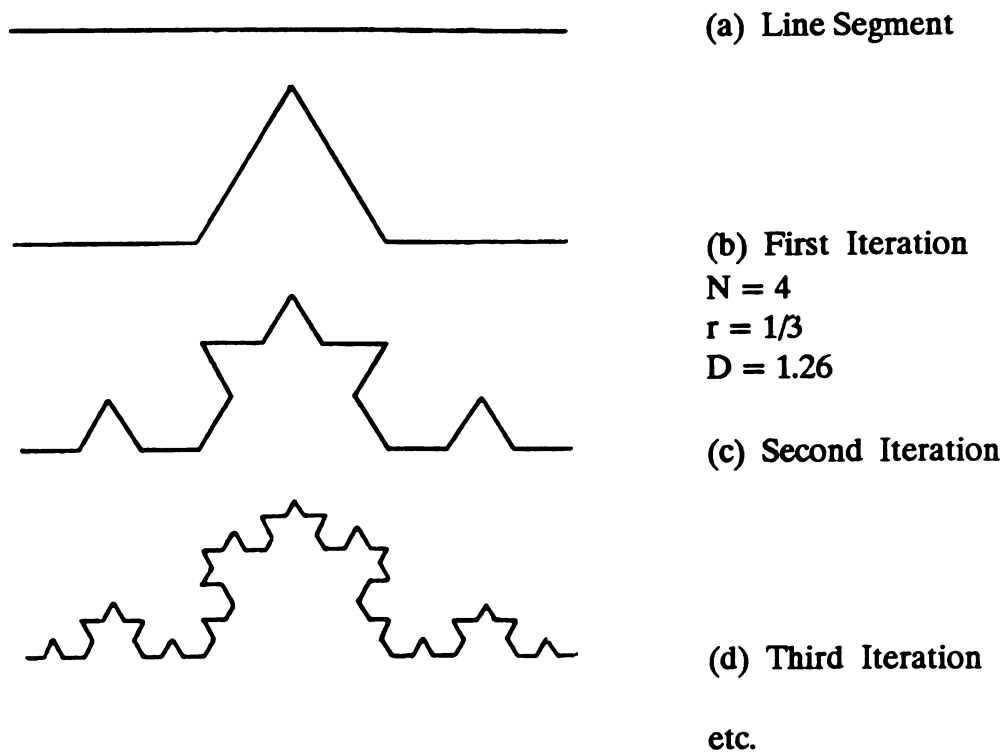


Figure 8.36 Forming the fractal von Koch curve.

Digressing for a moment, and concentrating on the notion of fractal dimen-

sion, if we let  $r$  be the ratio of the segment length to the whole, then

$$r = 1/N \quad (8.41)$$

for an area

$$r = 1/N^{1/2} \quad (8.42)$$

and volume

$$r = 1/N^{1/3} \quad (8.43)$$

In general, an object of dimension  $D$  displaying self-similar properties is characterized by:

$$r = 1/N^{1/D} \quad (8.44)$$

or

$$N = 1/r^D \quad (8.45)$$

which leads to

$$D = \frac{\log(N)}{\log(1/r)} \quad (8.46)$$

where  $D$  is the fractal dimension which, in general, is non-integer.

Referring again to Figure 8.36, since  $N = 4$ , and  $r = 1/3$ , use of Equation (8.44) yields a fractal dimension of 1.26 for the von Koch curve. The self-similar properties are evident from examinations of segments of the curve, which emulate varying degrees of magnification. Thus, dimension is associated with scaling and self-similarity, and related to an algorithm, in this case, a simple triangular manipulation of line segments. A deterministic fractal has been displayed, which demonstrates exact self-similarity.

Considering another classic example, a coastline representative of a readily visualized irregular curve, the notion of statistical self-similarity and fractal dimension can be described in an effective and comprehensive way. Proceeding as before, we let the length of the coastline be subdivided into  $n(r)$  segments, where  $r$  is a reference measurement length. The total measured length from Barnsley, *et al.* is  $rN(r)$  or, with  $n(r) = 1/r^D$ :

$$L \propto r \cdot \frac{1}{r^D} = \frac{1}{r^{D-1}} \quad (8.47)$$



The measured length depends on the fractal dimension and  $r$ , the size of the ruler used in the measurement. Practically, as the ruler is decreased in size and more of the intricate irregularities and fragmentations are measured, the total measured length becomes larger. Investigation of the specifics of coastlines show fractal behavior with about  $1.15 \leq D \leq 1.25$ . The coastline will vary in detail as different length scales are applied, but will maintain similar statistical properties, a fundamental property of fractals and many other naturally occurring forms.

As a final example, we will describe the fractal dimension and area perimeter relationships of two-dimensional fractals. We now consider the coastline as a closed fractal enclosing an area  $A$ , forming, for clarity and comparison, an island. The perimeter  $P$ , because of scaling, is proportional to the total length  $L$  as  $L^D$ . If the area of the island for  $D < 2$  is proportional to  $P^2$ , then the following area perimeter relationship results:

$$P \propto A^{D/2} \tag{8.48}$$

This equation is an important property of fractals. Elaborating, we first consider

Circle	$A = \frac{P^2}{4\pi}$	
Square	$A = \frac{P^2}{16}$	(8.49)
Rectangle (5 × 1)	$A = \frac{5P^2}{144}$	

The area of these common geometrical figures scale as the square of the perimeter. From the coastline example, the area scales nominally as  $2/1.2$ , or  $5/3$ . Lovejoy, in a characterization of rain and cloud areas in fractal form, obtained a fractal dimension of  $4/3$ , covering over six orders of magnitude of the area  $A$ . Combining these observations leads to the results of Figure 8.37. Aside from their differences, which are apparent, the examples demonstrate a useful procedure for estimating fractal dimensions from observables (in this case implying visual, radar, and optical data from Lovejoy).

**Fractal Models**

Two fractal algorithms, and their mathematical structure and examples, are described here, both from Mandelbrot. The first is a fractional Brownian sheet constructed from fractional integrations of white noise. The second, referred to as a *hyperbolic sheet*, is formed from a fractional sum of pulses. The algorithms, of

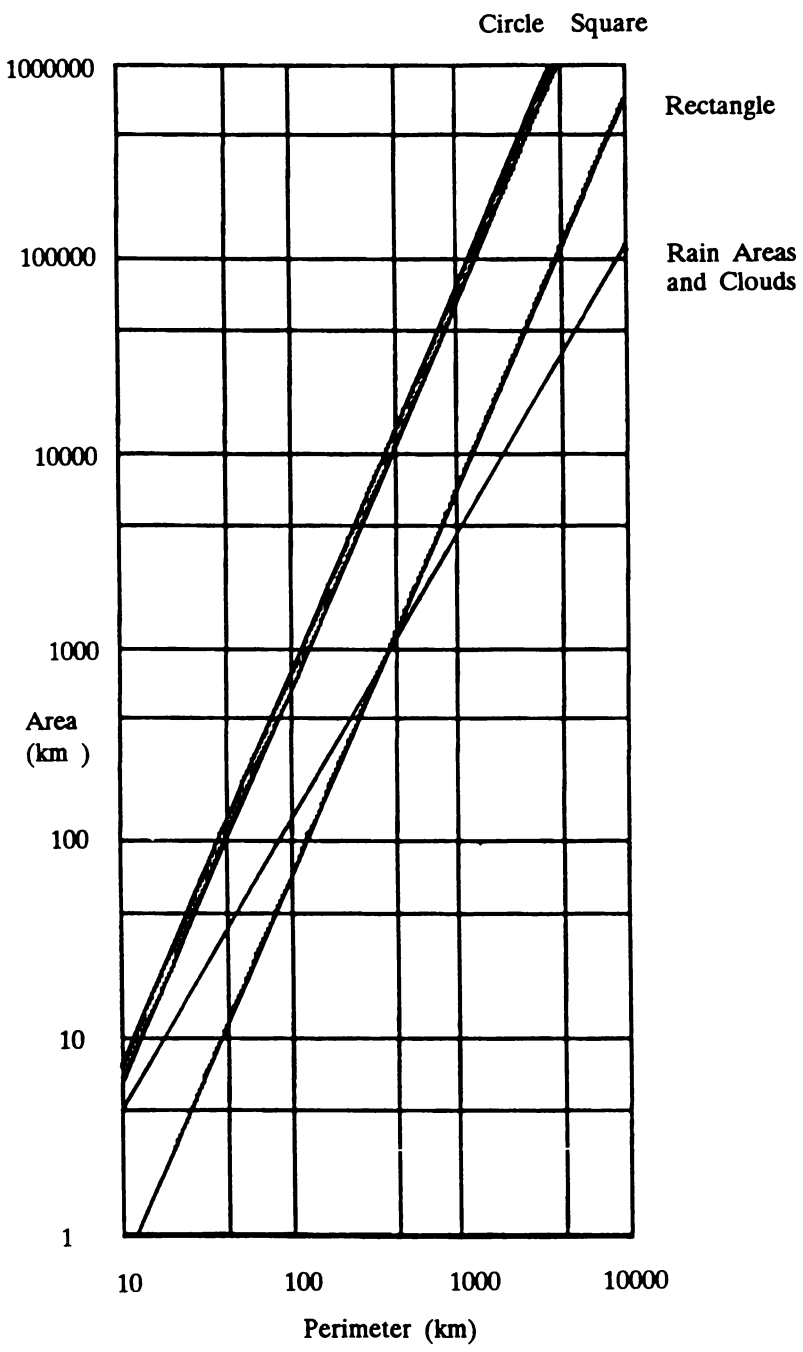


**Figure 8.37** Area Perimeter Relationships for Several Geometrical figures and fractals.

general applicability, are provided in sufficient depth for use in computer simulation. Further discussions of the algorithms (and additional ones) can be found in Barnsley, *et al.* Preliminary discussions focus on fractional integrations and Brownian motion are supplemented by reviews of fractional methods in Appendix B.

### FRACTIONAL BROWNIAN MOTION—FORMULATIONS

Mandelbrot introduced a family of Gaussian random functions as fractional Brownian motions, where past increments of ordinary Brownian motion are weighted by a kernel  $(t - s)^{H-1/2}$ .  $H$  is a parameter with value  $0 < H < 1$ . Implied here is a fractional, rather than integer order of integration of white noise for creating fractional Brownian motions. The spectrum of the resulting fluctuations demonstrates a  $1/f^\alpha$  behavior. It is interesting and reasonable to interpret the integer order integrations as a special case of the more general fractional ones and  $1/f$  noise as a specific fractional noise. Ordinary and fractional Brownian motions exhibit self-similar properties.

An ordinary Brownian motion is a Gaussian random function with mean zero and variance  $(t_2 - t_1)$ , which leads to

$$\langle B(t_2) - B(t_1) \rangle = 0 \quad (8.50)$$

and

$$\langle [B(t_2) - B(t_1)]^2 \rangle = (t_2 - t_1) \quad (8.51)$$

The Gaussian random variables are independent, so we have

$$\langle [B(t_2) - B(t_1)][B(t_4) - B(t_3)] \rangle = 0 \quad (8.52)$$

as long as the intervals  $(t_1, t_2)$  and  $(t_4, t_3)$  do not overlap.

A *fractional Brownian motion* is a random function which has increments  $B_H(t_2) - B_H(t_1)$  that are independent Gaussian random variables with mean zero and variance  $(t_2 - t_1)^{H-1/2}$ . The parameter  $H$  assumes the values  $0 < H < 1.0$ , and is the fractal dimension of the fractional Brownian motion. Similar to Equations (8.48) and (8.49) we have

$$\langle B_H(t_2) - B_H(t_1) \rangle = 0 \quad (8.53)$$

and

$$\langle [B_H(t_2) - B_H(t_1)]^2 \rangle = (t_2 - t_1)^{H-1/2} \quad (8.54)$$

Also from Mandelbrot, the increments of a function  $X(t)$  are self-similar with parameter  $H$  if

$$[X(t - \tau) - X(t)] = h^{-H}[X(t + h\tau) - X(t)] \quad (8.55)$$

By showing that the random functions  $B(t - \tau) - B(t)$  and  $h^{-1/2} [B(t + h\tau) - B(t)]$  have identical means and variances, we obtain

$$[B(t + \tau) - B(t)] = h^{1/2}[B(t + h\tau) - B(t)] \quad (8.56)$$

which states that an ordinary Brownian motion is self-similar with parameter  $1/2$ . In general, the fractional Brownian motion is self-similar with parameter  $H$ . Citing Equation (8.53), we have

$$[B_H(t + \tau) - B_H(t)] = \{h^{-H}[B_H(t + h\tau) - B_H(t)]\} \quad (8.57)$$

The Brownian function  $B(t)$  is further defined as the probability:

$$P\{[B(t + \Delta t) - B(t)]/|\Delta t|^H \leq x\} = \text{erf}(x) \quad (8.58)$$

When  $H = 1/2$ , Equations (8.48) and (8.49) are valid; otherwise, fractional motions are implied. In general,

$$\langle [B_H(t + \Delta t) - B_H(t)]^2 \rangle = |\Delta t|^{2H} \quad (8.59)$$

or with  $\Delta \rightarrow T$ , and  $H = 1/2$ ,

$$\langle [B_H(t + \tau) - B(t)] \rangle = T^{1/2} \quad (8.60)$$

which is referred to as the  $T^{1/2}$  Law.

### FRACTIONAL BROWNIAN SHEETS

If we let  $V_B(t)$  denote ordinary Brownian motion and  $W(t)$  white Gaussian noise, then  $V_B(t)$  is expressed in integral form as:

$$VB(t) = \int_{-\infty}^t dB(\tau) = \int_{-\infty}^t W(\tau)d\tau \quad (8.61)$$

From Papoulis and Maccone, we consider a linear system with impulse response  $h(t)$ , because the output process  $y(t)$  for an input  $x(t)$  is

$$y(t) = \int_{-\infty}^{+\infty} x(t-\tau)h(\tau)d\tau = \int_{-\infty}^{+\infty} x(\tau)h(t-\tau)d\tau \quad (8.62)$$

then, Equation (8.59) can be interpreted as the output of a linear system with impulse response

$$h(t) = U(t) \quad (8.63)$$

where  $U(t)$  is the unit step function. From Papoulis, for  $\alpha > -1$ , we have:

$$t^\alpha U(t) \leftrightarrow \frac{\Gamma(\alpha+1)}{|\omega|^{\alpha+1}} \exp\left[\pm \frac{j\pi(\alpha+1)}{2}\right] \quad (8.64)$$

where the argument of the exponent is positive when  $\omega < 0$ , and negative when  $\omega > 0$ . Because

$$h(t) \leftrightarrow H(\omega) \quad (8.65)$$

the transfer function is

$$|H(\omega)| = \frac{1}{\omega} \quad (8.66)$$

However, the spectrum of the output of a linear system is

$$S_{yy}(\omega) = S_{xx}(\omega)|H(\omega)|^2 \quad (8.67)$$

where

$$S_{xx}(\omega) \leftrightarrow R(t) \quad (8.68)$$

If  $R(t)$  is the autocorrelation of the input signal, equal to unity for white noise, then

$$S_{yy}(\omega) = \frac{1}{\omega^2} \quad (8.69)$$

Summarizing and concluding, *Brownian motion* is an integration of unity order of white noise. Brownian motion can be interpreted as the output of a linear filter with transfer function  $|H(\omega)| = 1/\omega$ , excited by white noise and characterized by a spectrum of  $1/\omega^2$  (i.e.,  $1/f^2$  noise).

Now referring to Appendix B, the references cited therein, and the recent work of Mandelbrot and Maccone, we let  $V_H(t)$  designate fractional Brownian motion defined as

$$V_H(t) = \frac{1}{\Gamma(H+1/2)} \int_{-\infty}^{+\infty} (t-\tau)^{H-1/2} W(\tau) d\tau \quad (8.70)$$

Formally, the integral is a Weyl fractional integration of order  $H + 1/2$ . The integration of Equation (8.59) can be considered as a special case of the fractional one by letting  $H = 1/2$  and  $\Gamma(1) = 1$ .

Fractional Brownian motion can also be placed in a linear system form following the procedure used above. Examining (8.68) in view of (8.60), we have:

$$h_H(t) = \frac{t^{H-1/2}}{\Gamma(H+1/2)} U(t) \quad (8.71)$$

Using the Fourier transform of Equation (8.62), the transfer function for the fractal filter is

$$|H(\omega)| = \frac{1}{\omega^{H+1/2}} \quad (8.72)$$

from which we determine

$$|H(\omega)|^2 = \frac{1}{\omega^{2H+1}} \quad (8.73)$$

and

$$S_{yy}(\omega) = \frac{1}{\omega^{2H+1}} \quad (8.74)$$

Therefore, *fractional Brownian motion* is a fractional integration of white noise. Fractional Brownian motion can be interpreted as the output of a linear filter with transfer function  $|H(\omega)| = 1/\omega^{H+1/2}$ , which is excited by white noise and characterized by a spectrum of  $1/\omega^{2H+1}$ . When  $H = 1/2$ , an output spectrum of  $1/\omega^2$  occurs. A spectrum of  $1/\omega$  (i.e., or  $1/f$  noise), occurs when  $H = 0$  with a transfer function of  $1/\omega^{1/2}$ . In this formulation,  $1/f$  and  $1/f^2$  noise are special cases of fractional Brownian motion related to filters with defined transfer functions.

Before providing examples which demonstrate the use of the formulas, consideration of an interpretation of the fractional integrations is worthwhile. An

ordinary unity order integration of the delta function  $\delta(t)$  is

$$\int_{-\infty}^{-\infty} \delta(t - 1)dt = U(t - 1) \tag{8.75}$$

Its more general integration of fractional order is

$$\frac{1}{\Gamma(-q)}\int_{-\infty}^{-\infty} (t - \tau)^{-q-1}\delta(t - 1)dt = \frac{(t - 1)^{-q-1}}{\Gamma(-q)} U(t - 1) \tag{8.76}$$

Plots of the fractionally integrated delta function are provided in Figure 8.38 where a unity order of integration yields the unit step or Heaveside function. Examining these results as a smoothing operator and considering the persistence of the effects of the integration, an ordinary unity order of integration yields for all  $t > 1$ , a unity weighting or smoothing. Fractional integration, however, yields a controlled persistence, which decreases as the order of the fractional integration is reduced. The motion of persistence is evident in Figure 8.39, where displays of fractional Brownian motion or equivalently fractional Gaussian noise are presented for varying fractal dimensions.

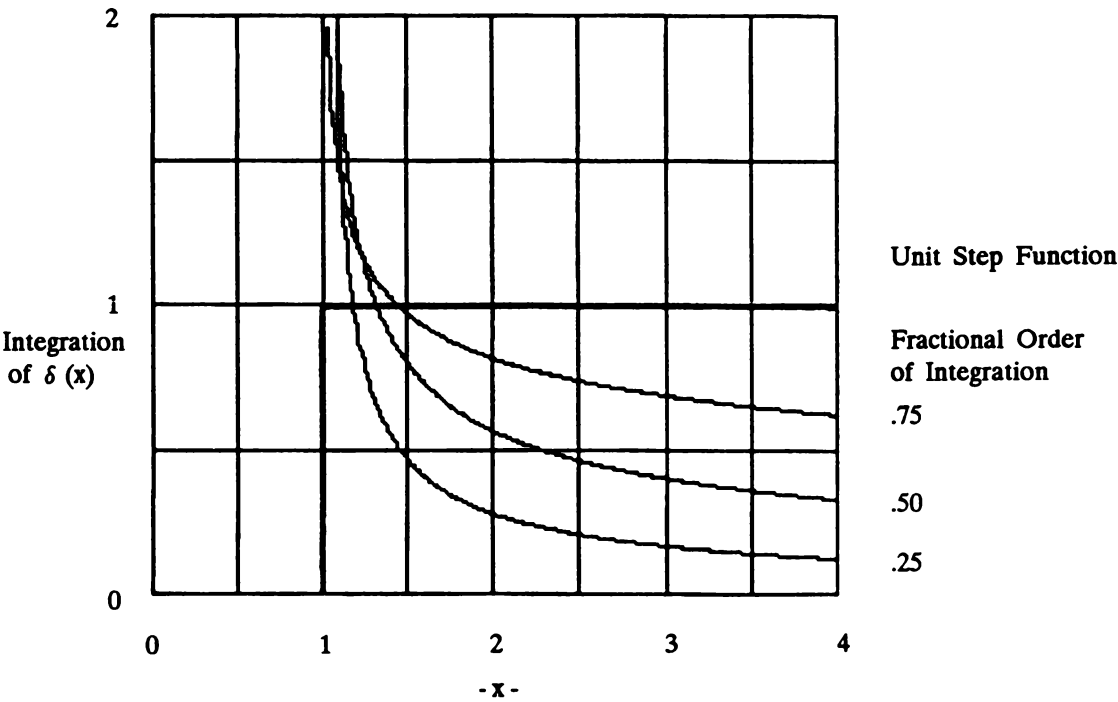
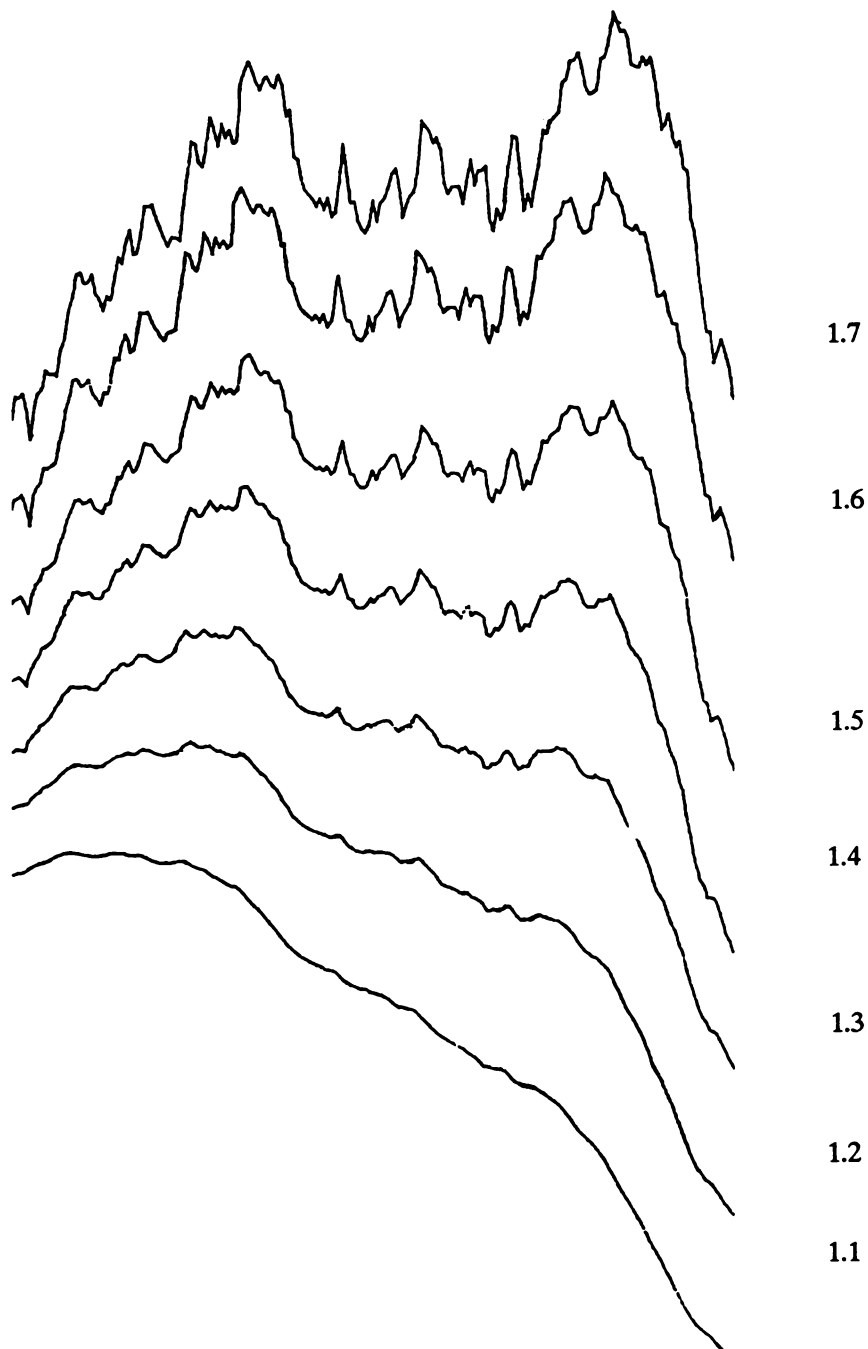


Figure 8.38 Fractional integration of the delta function.



**Figure 8.39** Fractional Gaussian noise.

For modeling purposes, self-similar Brownian motion sequences can be obtained directly from a numerical integration of Equation (8.68), the approach used to compute the results of Figure 8.39. In these computations, a Riemann integration



is employed, with  $W(t) = 0$  for  $t < 0$ . If solved directly, an algorithm for computation of the Gamma function is needed, which can be avoided using Grunwald's formula, an approximate numerical integration procedure for fractional integration and differentiation described in Appendix B. Similarly, a random number generator for white noise is needed, one method for which is also described in Appendix B. Fourier transform methods leading directly to random fractal algorithms are thoroughly described in Barnsley, *et al.* correlation. Properties of  $1/f^\alpha$  distribution have been derived by Maccone.

A fractional Brownian sheet is a generalization of  $B_H(t)$  to a function of two variables  $B_H(t,s)$  so that any slice of  $B_H(t,s)$  is a fractional Brownian motion. *Fractal sheets* are two-dimensional sheets, a section or slice of which is a fractal. An example is shown in Figure 8.40, where the fractal dimension lies between 2 and 3. Mandelbrot shows that the fractal dimension of a slice through a fractal sheet is one less than the fractal dimension of the sheet. For example, in order to generate shapes having perimeters of dimension 1.35 corresponding to rain and clouds, a fractal sheet having dimension 2.35 can be generated; it is then assumed to be filled with a liquid, and the resulting "islands" poking above the liquid will have shorelines with dimensions of 1.35. An illustration of the "island" formation is shown in Figure 8.41, where a fractal mountain scene is displayed. Using this approach, the cloud formations displayed in Figures 8.42, 8.43, and 8.44 can be realized. Although cumulus clouds are displayed, the results also pertain to rain areas because of the common fractal dimension. The fractal dimensions chosen and the results obtained conform to the findings by Lovejoy.

## HYPERBOLIC FRACTAL SHEETS

As shown, the Brownian functions  $B_H(t)$  exhibit statistical self-similarity. Statistical processes with increments described by a hyperbolic random variable are likewise self-similar. Formally, from Lovejoy and Mandelbrot, a random variable  $A$  is called hyperbolic if the tail probability  $P(A > a) \propto a^{-\alpha}$ . The hyperbolic distribution is characterized by a limit theorem, where the sum of  $N$  hyperbolic random variables is also hyperbolic. In fact, from Sussman and Mandelbrot, for a summation of  $K$  variables, with distribution  $\alpha t^{-\alpha-1}$ ,

$$g_k \approx K \alpha t^{-\alpha-1} \tag{8.77}$$

for  $K = 1, 2, \dots$ , and  $t \rightarrow \infty$ . Also, if a process consists of many interacting parts, at least one of which is hyperbolic, then the statistics of the total process are likely to be hyperbolic. Finally, the distribution has long tails, with related processes likely to be dominated by one or more extreme values. The  $1/f$  noise, previously discussed, falls into this category.

Hyperbolic fractal sheets are formed by uniformly distributing cylindrical step

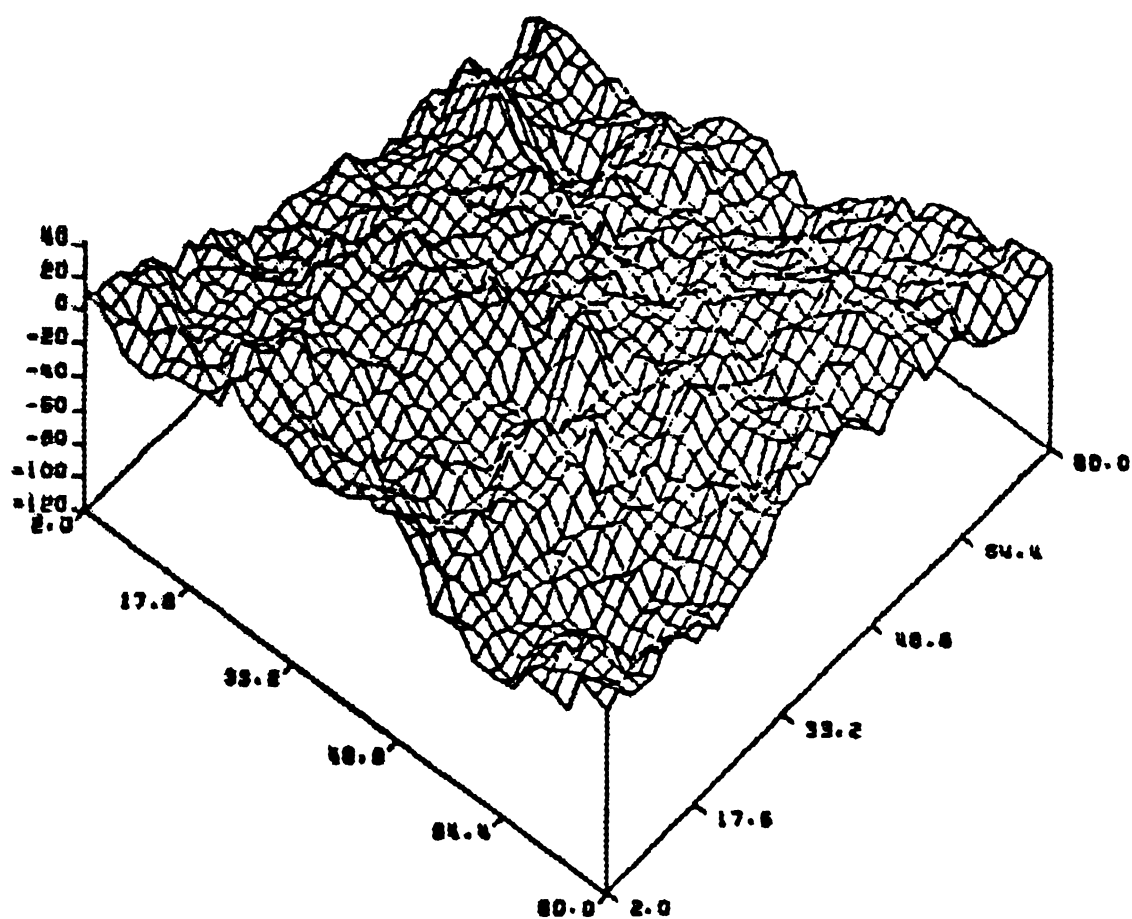


Figure 8.40 Fractal Brownian sheet.

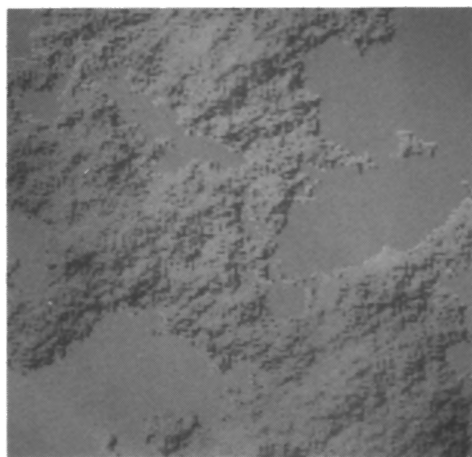
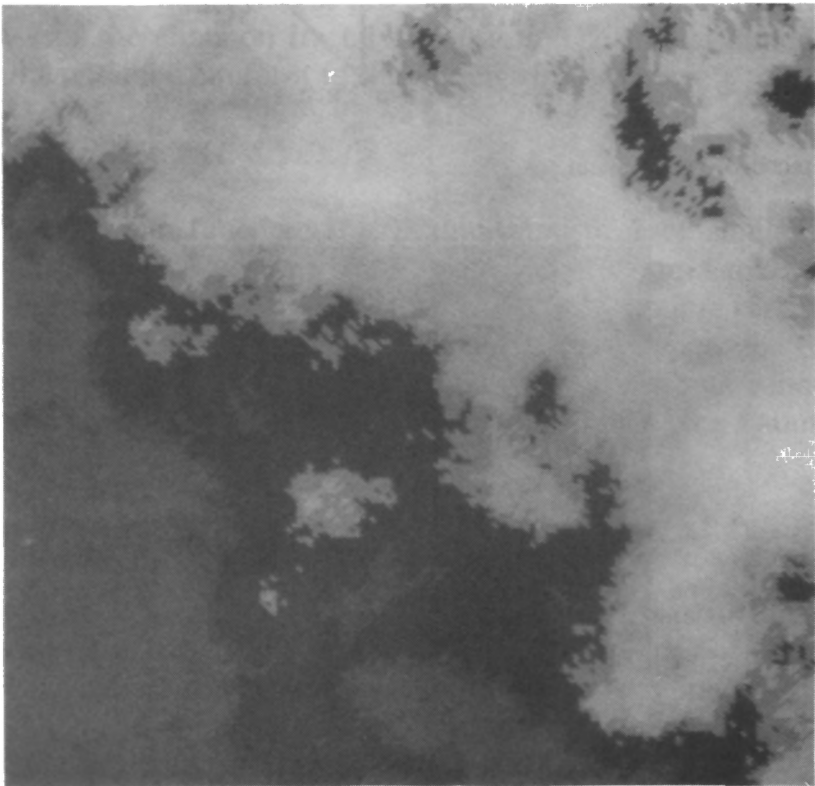


Figure 8.41 Fractal mountain scene.



**Figure 8.42** Cumulus clouds generated from fractional Brownian sheets.



**Figure 8.43** Fractocumulus cloud generated from fractional Brownian sheets.



**Figure 8.44** Cumulonimbus cloud generated from fractional Brownian sheets.

functions or “hats” on a flat plane. The area of the cylinders is the hyperbolic random variable:

$$P_r[A > a] \sim a^{-1} \quad (8.78)$$

The magnitude  $h$  of each cylinder is

$$h \sim \pm A^\alpha \quad (8.79)$$

The  $\pm$  signs of  $A$  are assigned with equal probability. The cylinders are positioned on a plane and summed. In the original form of the algorithm (described by Lovejoy and Mandelbrot), circular cylinders were used. Later, to control the lacunarity and bandlike or anisotropy character of rain areas, the circular base was changed to an annulus with defined inner and outer radii. A further extension to ellipses with varying eccentricities was made. The ellipses, when employed with restricted orientations, controlled anisotropy into the simulations and so were part of an effective method for rain and cloud environments. In all cases, the self-similar properties are maintained. The fractal displays of cumulus and cirrus cloud formations in Figure 5.3 were generated using a fractional sum of elliptical pulses, with a near-circular base used for the cumulus and elongated ellipse, and a restricted ( $\pm 10^\circ$ ) orientation for the cirrus emulations.

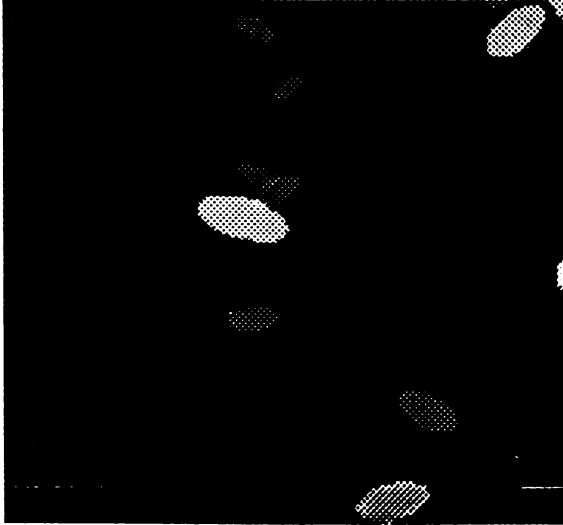
Several stages in the construction of a fractal using the fractional sum of pulse algorithm are displayed in Figure 8.45. This vivid portrayal of the procedure is intended for a cumulus cloud simulation using ellipses of low eccentricity and a broad  $90^\circ$  restriction of  $\pm 45^\circ$  referenced to the vertical. Although the results are impressive, the number of computations required are large. However, for radar clutter simulation of rain, the elliptical basis with specified eccentricity and controlled anisotropy may make the computational inefficiencies bearable. An algorithm for generating random numbers with hyperbolic distribution is contained in Appendix B.

### Methodology for Analysis and Simulation

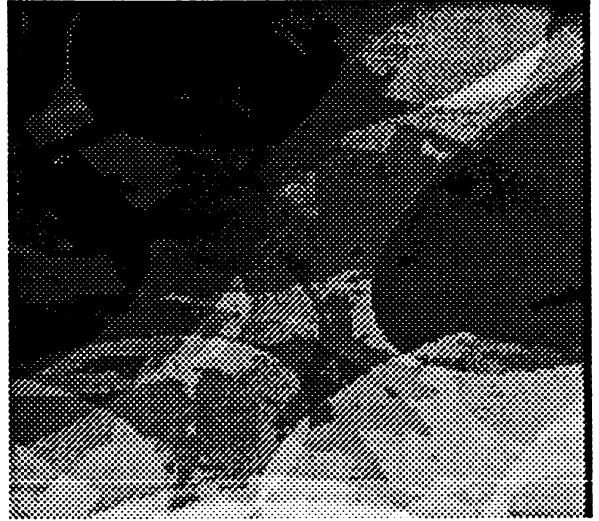
For radar analysis purposes, the theory of fractals introduces the hyperbolic distribution, and in general, the motion of self-similarity into the realm of target and clutter modeling. The fractal sum-of-pulse model, treated on an elliptical basis with its apparent control of anisotropy in radar observables (and its hyperbolic statistical framework), provides a useful tool for cloud and rain emulations, and has the potential for use with other clutter environments. The fractal Brownian sheets provide another analysis tool where radar responses or noise sources are characterized by spectral of  $1/f^\alpha$  form. Considering its definitive circuit or linear system analogy, the analysis and simulation of such signals arise within a real framework. Now, fractional integrations and differentiations are in the analysis procedures, which are not difficult to become acclimated, and providing new mathematical formulas and interpretations. One such example is the perturbation of Rayleigh statistics through fractional integrations that will also be useful for general target and clutter analysis.

Recent advances in the modeling of rain areas have been made using fractals by Lovejoy, Mandelbrot, and Schertzer. Although not complete to the extent of providing a total spatial and time varying representation, they do yield clutter characterizations that can be utilized to extend current rain models. It has been shown in this original work and verified by the examples provided here that: (1) certain spatial and temporal properties of clouds and rain environments exhibit a fractal behavior, (2) the fractional-sum-of pulse (FSP) model structured on an elliptical basis is effective in creating realistic cloud and rain environments in a simple way with realistic results, and (3) the fractal dimension of both environments is about  $4/3$ . The FSP model will provide a spatial distribution of the rain parameters (rain rates, backscatter, and attenuation) from which radar returns may be determined.

Procedurally, an environmental simulation will involve first a characterization (preferably from measurements) of the background. Data analysis would lead to a fractal dimension. Simulation of the environment may occur in several forms, with a varying number of control parameters, including the fractal dimension.



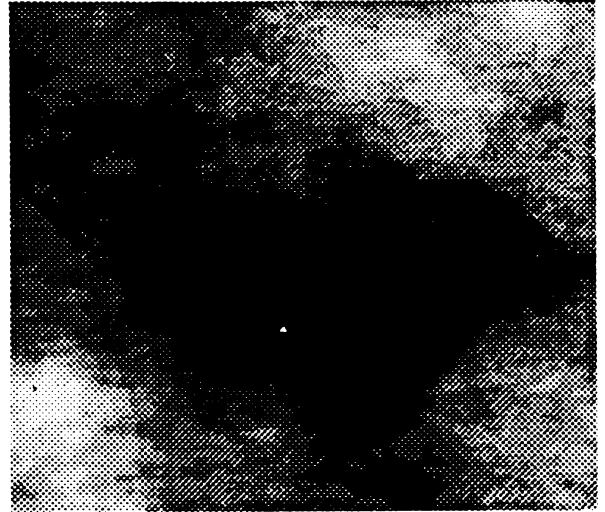
(a) 200 ellipses



(c) 20,000 Ellipses



(b) 2000 Ellipses



(d) 200,000 Ellipses

**Figure 8.45** Stages in the generation of a hyperbolic fractal sheet.

Scenes may then be generated that are statistically equivalent to the reference. Radar targets, especially extended statistical ones, may be treated in the same way. Consideration of multiple environments and specific targets lead to the structuring of a total simulated radar environment. Synthesis and analysis of the radar follows through simulation.

One immediate use of fractals in rain models is as an extension to the path-dependent model, formed in the following way. First, let the upper bound be the zero-degree isotherm. Then, consider a rain cell which extends to the zero-degree isotherm with a uniform rain rate distribution in the vertical dimension. Both conditions are reasonable for low to moderate rain rate storms. Using the data of Crane for cell size, debris, and cellular distributions, structure the cell or storm using the fractional sum of pulse model on a circular basis. If data is available, form the cell on an elliptical basis, adjusting the anisotropy to fit the measurements. Radar signals can be emulated from the structured weather scene taking into account rain rates, attenuation, and backscatter. Examples of the use of this methodology in order to form a rain cell are shown in Figure 8.46.

More specifically, referring to the fractal models of Lovejoy, Mandelbrot, and Schertzer, the data compilations of Crane, and the uniform and path-dependent models and descriptions of Sections 8.1, 8.2, and 8.3, we can consider a step-by-step procedure for the use of fractals. Following previous model formulations, the starting point is the global rain rate distributions.

1. Obtain the climatic region from Figures 6.1, 6.2, or 6.3 for the geographical longitude and latitude of interest.
2. For the specific latitude, use the data from Figure 8.3 for the altitude of the zero-degree isotherm.
3. Select a probability of exceedance for a percent of the year. Using Figure 6.4 or Table 6.1, determine the rain rate for the desired probability.
4. For the rain rate, use Equation (8.5) and the data of Table 8.4 to obtain the estimated point attenuation.
5. For the rain rate, use Equation (8.10) or the data in Table 8.5 to obtain the estimated point backscatter value.
6. Given cellular and debris structure from measurements, or form estimates using the statistical compilations of Crane used in the formulation of the path-dependent and two-component models, determine the fractal dimension by applying (8.46), or set the dimension at  $4/3$ .
7. Structure the cell using the fractal sum-of-pulse model of (8.76) and (8.77). Use a circular basis for cells with apparent distorted circular cross sections. Use an elliptical basis for elongated cellular structures common to rain frontal areas, the ellipticity constant, and angular restrictions controlling the elongation of the cell.

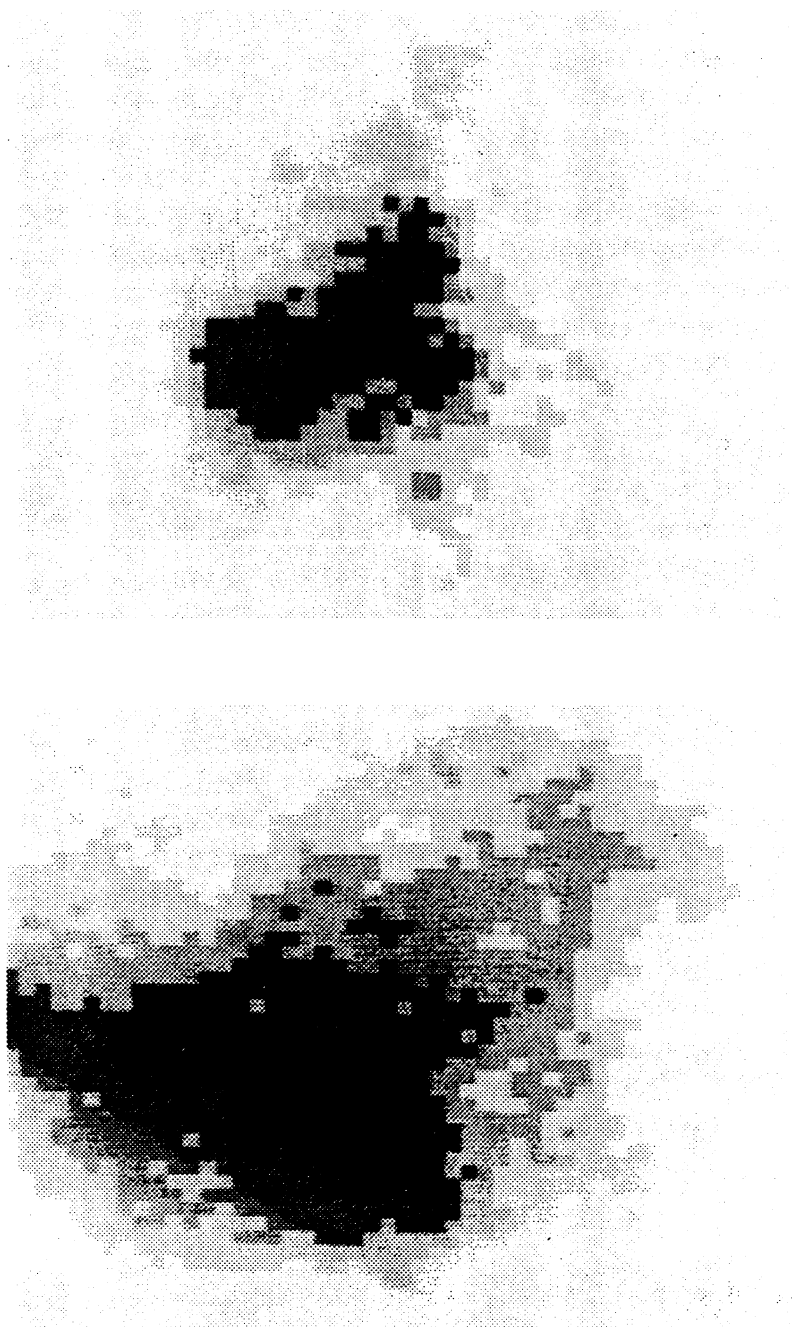


**Figure 8.46** Rain cell simulation.

8. Use the inverse method of generating sequences of random numbers provided in Appendix B. The resulting statistics of area and single responses



can be expected to be non-Rayleigh in character.

9. Since application of the fractal sum-of-pulse model involves cuts taken through three-dimensional forms, levels must be chosen to establish rain-rate levels that conform to observations or reasonable debris and cellular predictions.
10. Conversion of fractals expressed in rain rates to distribute attenuation or backscatter values may be accomplished using steps (4) and (5) given above.
11. Rain areas of similar statistical properties may be generated by changing the initiation (or seed) in the generation of uniformly distributed random numbers used in the fractal model.

The use of good measured data is advocated in all model developments, allowing for a thorough understanding of the functioning of the radar and a full appreciation of the properties of the environment. The fractal models in particular are, after accepting their theoretical basis, remarkably simple in structure and incredibly effective in the generation of sensor scenes.

## **8.6 FINAL REMARKS**

The rain data presented herein have been obtained from a number of recently published articles. Of these, the formulations that constitute the first two models have been used over a period of time and thus far been effective. Conversely, the last two models have not been used, although they appear to be more versatile than indicated in our discussions. Future work requires testing of several of the statistical formulations contained in the two-component model. The fractal formulations will also lead to advanced models requiring significant future work. Crane's global models have been found to be the most useful and realistic.

In all cases, simple formulas have been provided for determining fundamental rain parameters. These may indeed help to reduce the complexity of some difficult analysis and simulation problems.

### ***EXAMPLE: USE OF METHODOLOGIES***

The data provided and the models described extend previous, related radar models to include spatial bounds and the characteristic inhomogeneities of the atmospheric environment. This was accomplished in an evolutionary way by increasing the complexity of the models in well defined steps. Several important points in applying the methodologies are summarized below:

1. The zero-degree isotherm is a reasonable upper bound for rainstorms. They serve as a simple addition to a uniform rain clutter model and are needed in many radar applications.

2. There are numerous data available for rain attenuation and backscatter. Considering analysis and simulation applications, and the continuing updating of the data base, the use of the basic formulas and their frequency-dependent constants is advisable. In particular, for simulations applications, formulas may be more desirable than look-up tables.
3. The global distributions subjected to considerable review are an essential part of any rain model. They provide the essential data in establishing initial radar environment specifications and indicate periods of radar inoperability on a probabilistic basis.

Specifically, the methodologies provide the following benefits:

4. The uniform model extends to a definitive establishment of an upper bound. Rain attenuation and backscatter coefficients should be reviewed on a regular basis to ensure validity.
5. Path dependence introduces the spatial inhomogeneities of rain into the models in a simple way. Their use follows the formulas provided, or may establish rain attenuation increases or decreases of the point values.
6. Two-component considerations provide statistical data on the cellular and debris properties of rain. These data include modifications to the upper bounds of the rain, which, with the statistical data, may be of value in radar applications involving high rain rates and high radar frequencies.
7. The fractal models introduce methods for the modeling of the cellular and debris structure of a rain cell. In the initial model, the upper bounds of the rain maintain the zero-degree isotherm bounds with an assumed uniform vertical rain-rate distribution.

Future work should lead to sophisticated models for radar analysis and simulation applications.



## ***Chapter 9***

### ***Cloud Environments***

Clouds, haze, and fog are common atmospheric environments consisting of aerosols of water droplets in various size distributions. These environments can degrade radar performance. This section includes a discussion of propagation effects and data compilations for attenuation estimates, provides particle size distributions, and contains formulas for radar analysis and simulation. The material extends our discussions of the structure and occurrence of clouds and fog in Chapter 5.

#### **9.1 HAZE**

Haze consists of aerosols formed near the earth's surface when small droplets condense around hygroscopic particles. Generally, haze affects electromagnetic propagation less than fog but more than clear air. Many natural and man-made sources of haze-forming hygroscopic particles occur. Natural sources include micrometeorites, soil, and volcanic ash. Terpenes evaporating from vegetation can give rise to hazes above forests. Man-made sources include fires and industrial and vehicular emissions.

A size distribution typical of haze droplets is shown in Figure 9.1. As shown, the distribution peaks at less than 1  $\mu\text{m}$  radius, without the occurrence of droplets larger than 20  $\mu\text{m}$  in radius.

The density concentration of haze droplets is largest near sea level and drops by about two orders of magnitude at 5 km altitude. While haze is always present to some degree, its mass concentration (as compared to rain, fog, and hail) is small. As a result, its effect on signal propagation at frequencies between 30 and 300 GHz is insignificant.

#### **9.2 FOG**

Fogs occur when atmospheric water vapor condenses on small, pre-existing, atmospheric water droplets. Summarizing briefly, fog concentrations are defined in

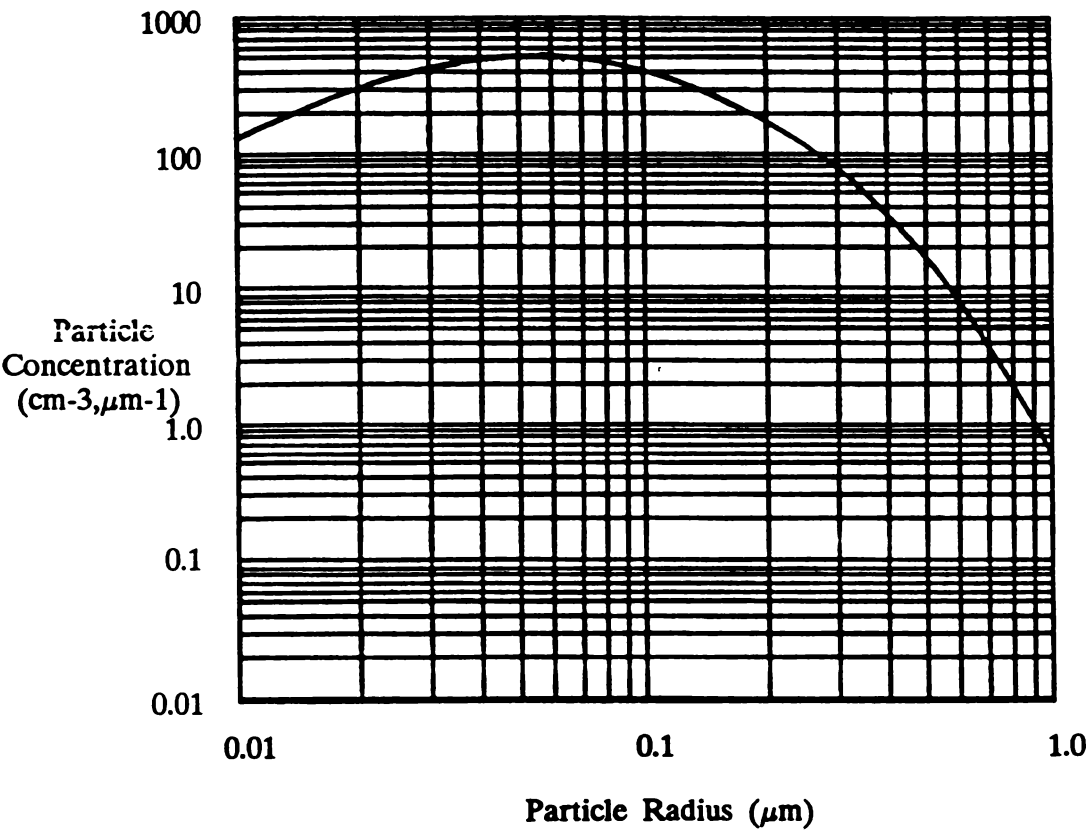


**Figure 9.1** Particle Size Distributions for Continental Aerosols. (From Deirmendjian)

terms of visibility (i.e., the distance at which a human eye can discern a black target against a sky background). By definition, a fog exists when visibility is less than 1 km. Fogs are classified as being of *advection* or *radiation*. Advection fogs occur in coastal areas when warm, moist air moves over cold water. The liquid water concentrations of advection fogs are usually less than  $0.4 \text{ g/m}^3$ . Radiation fogs typically occur in low-lying areas and along rivers when the ground cools radiatively and causes supersaturation of the air above. The liquid water concentrations of radiation fogs may be as large as  $1 \text{ g/m}^3$ .

The particle size distribution of a fog depends on atmospheric conditions, with the peak occurring between radii of 1 and  $10 \mu\text{m}$ . The largest droplets are usually no greater than  $70 \mu\text{m}$  in radius, but may occasionally be as much as  $100 \mu\text{m}$  in radius. Bimodal distributions frequently occur, having a secondary peak near the maximum droplet radius. Droplet number densities at the primary peak (between 1 and  $10 \mu\text{m}$ ) vary from  $30 \text{ cm}^{-3} \mu\text{m}^{-1}$  to several hundred  $\text{cm}^{-3} \mu\text{m}^{-1}$ . Number densities at the secondary peak are somewhat smaller.

Figure 9.2 contains attenuation coefficients, computed using a Rayleigh assumption, and expressed as a function of liquid water content. At a frequency of

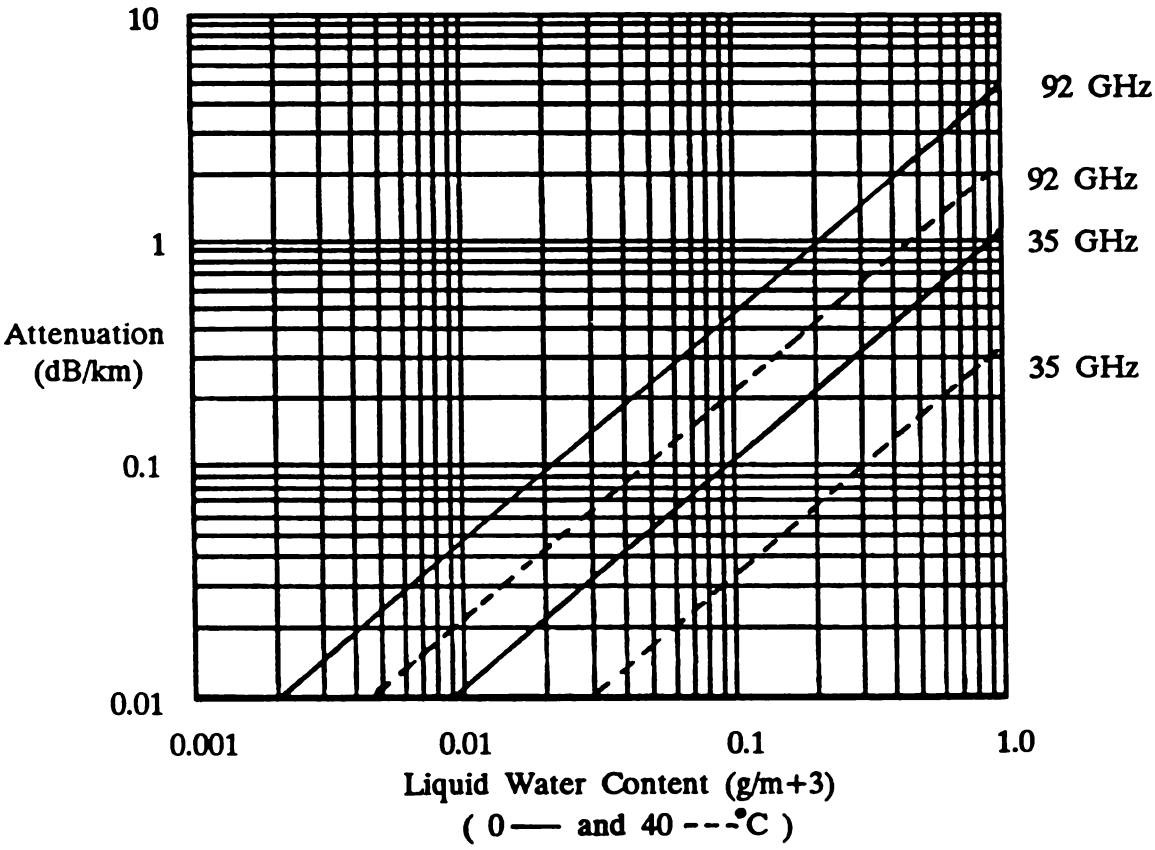


**Figure 9.2** One-Way Attenuation Coefficient in Fog as a Function of Liquid Water Content. (From Richard)

35 GHz, the attenuation is about 1 dB/km. Because a typical radar path length in fog may be less than 1 km, the one-way attenuation can be expected to be less than 1 dB. In similar circumstances, a 94-GHz signal is subjected to a loss of about 5 dB/km. An attenuation coefficient of this magnitude is significant in most radar system applications. At higher frequencies, when the maximum drop radii become comparable to the signal wavelength, the Rayleigh approximation is no longer valid. Thus, fogs will effect signal losses as frequencies increase beyond 100 GHz.

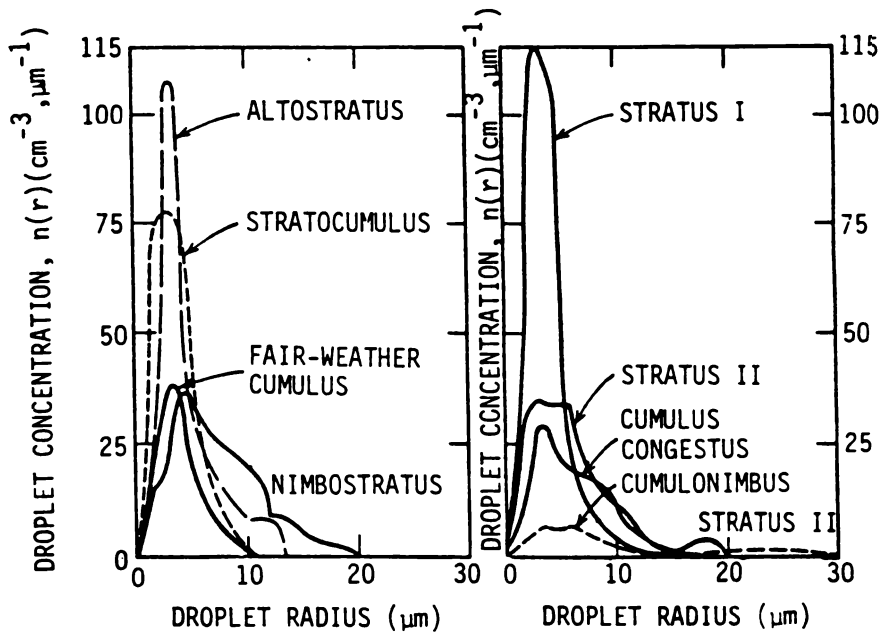
### 9.3 CLOUDS

Table 5.4 of Chapter 5 summarizes the characteristics of types of clouds. Table 9.1 lists typical values of number density  $N$ , mode radius  $r_c$ , minimum radius  $r_{min}$ , and maximum radius  $r_{max}$  of droplets for the size distributions shown in Figure 9.3. The size distributions of all clouds in Figure 9.3 are characterized by peaks between 3 and 5  $\mu\text{m}$  in radius. Only cumulonimbus clouds have droplets larger

**Table 9.1**  
Parameters of Droplet Size Distributions of Figure 9.3\*

Cloud Type	$N$ ( $\text{cm}^{-3}$ )	$r_c$ ( $\mu\text{m}$ )	$r_{min}$ ( $\mu\text{m}$ )	$r_{max}$ ( $\mu\text{m}$ )
Stratus I	464	3.5	0	16.0
Altostratus	450	4.5	0	13.0
Stratocumulus	350	3.5	0	11.2
Nimbostratus	330	3.5	0	19.8
Fair-Weather Cumulus	300	3.5	0.5	10.0
Stratus II	260	4.5	0	20.0
Cumulus Congestus	207	3.5	0	16.2
Cumulonimbus	72	5.0	0	30.0

\*From McCartney



**Figure 9.3** Droplet Size Distributions for Major Cloud Models. (From McCartney)

than 20  $\mu\text{m}$  radius, with the largest droplets indicated for cumulonimbus clouds being of 30  $\mu\text{m}$  radius. Cumulus and cumulonimbus clouds are expected to yield larger signal attenuations as a result of high water concentrations, large drop sizes, and the large vertical extents.

Experimental cloud data were assembled by A.W. Straiton and coworkers at 35 and 92 GHz using radiometric means. The measurements were obtained by observing the sun using radiometers with varying degrees of cloud cover. Cloud attenuation was estimated from the reduction in solar radiation. Seven cloud types were included in the observations.

Figure 9.4 shows the results of cloud measurements made by Straiton of a general overcast sky at different elevation angles. Observations were made along different lines of sight passing through varying extents of the earth's atmosphere. In the figure, an air mass,  $M_a$ , of 1 refers to the mass of the atmosphere seen on a vertical observation. Attenuations at angles removed from the vertical reference vary according to  $1/\sin\phi$ , where  $\phi$  is the elevation angle. Numerical values presented in Figure 9.4 for near vertical lines of sight are consistent with values presented in Table 7.1 (Chapter 7) for clear air attenuation. As expected, lines drawn through the data intersect at zero air mass and zero attenuation.

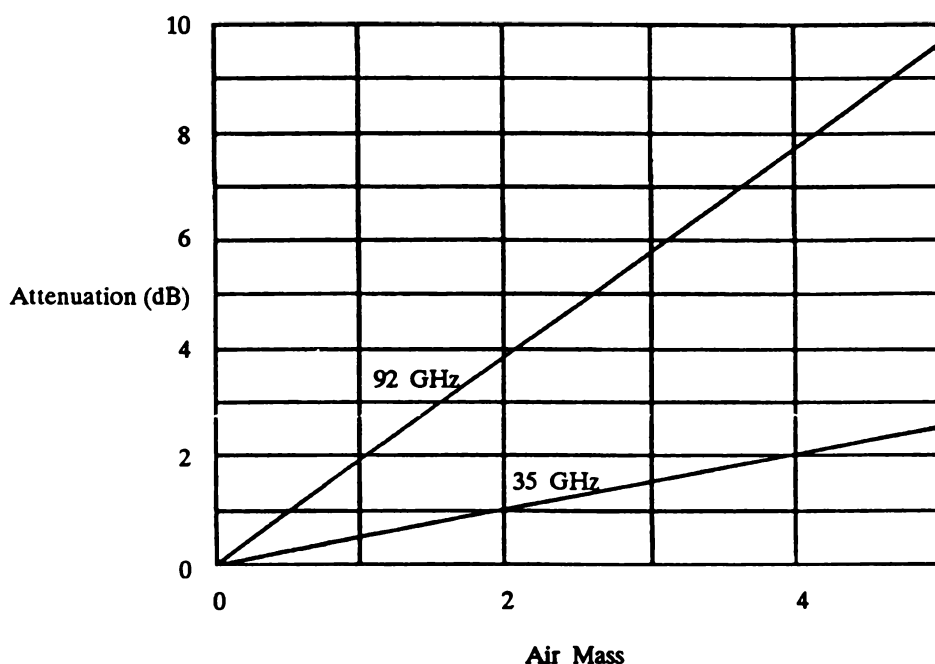


**Figure 9.4** Attenuation of General Overcast *versus* Air Mass (No Clouds) for 35 and 92 GHz. (From Straiton)

Figure 9.5 provides attenuation data for cumulus clouds. Attenuations between 0.5 and 1.0 dB generally occur at frequencies in the vicinity of 35 GHz. An absence of an attenuation dependence on elevation angle is evident, suggesting that radar observations of clouds indicate similar expected attenuations in vertical and horizontal directions. For modeling purposes, set reasonable bounds on the cloud forms of interest and assume a uniform environment for estimates of attenuation.

Straiton also used a Rayleigh assumption to calculate the ratio of absorption coefficient (i.e., decibels per kilometer), to mass concentration of suspended water (i.e.,  $\text{g/m}^3$ ). This ratio, sometimes called the *mass extinction coefficient*, is plotted



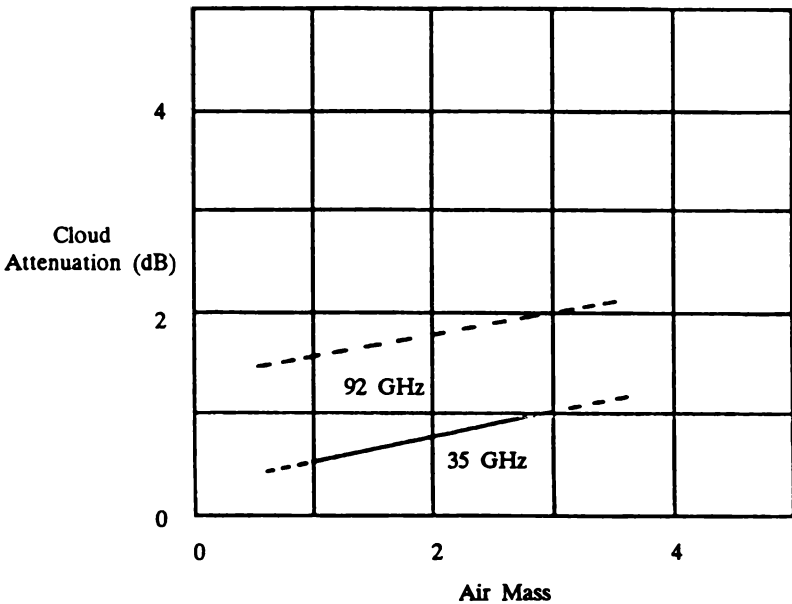
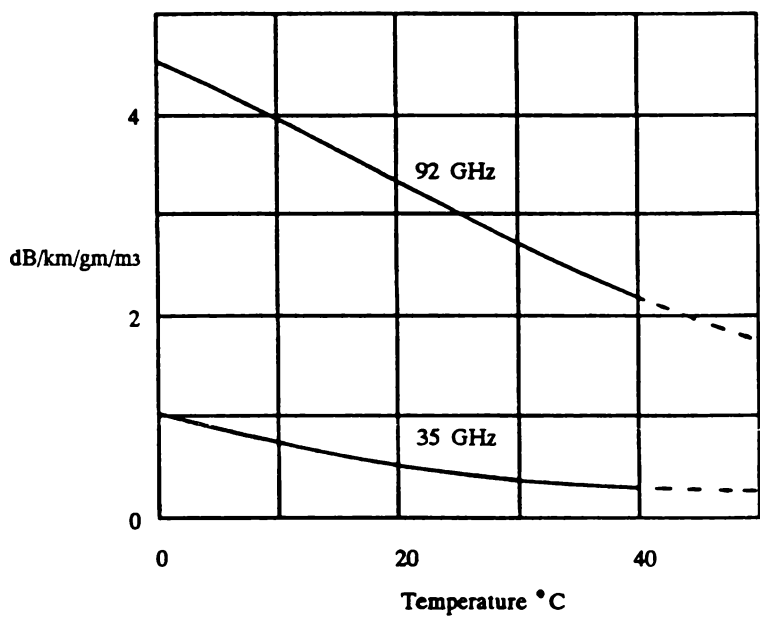


Figure 9.5 Cumulus Cloud Attenuation. (From Straiton)

in Figure 9.6 as a function of the water droplet temperature. Gunn and East have performed similar calculations at 33.3 GHz for liquid water and ice particles, with their results for liquid water confirming Straiton’s work. Their results for ice indicate that absorption by ice particles is less than 0.01 of liquid water on a per unit mass basis. High-altitude ice clouds yielding attenuations of significance is thus unlikely for most radar applications.

Attenuations of millimeter radiation through clouds will be dominated by absorption, as opposed to scattering from the cloud droplets. In those instances, the attenuation is expected to be proportional to frequency. Therefore, the attenuation at 95 GHz should be about three times the value at 35 GHz. However, Table 9.2, containing measured attenuation, shows a three to five dependence at 95 GHz. These data indicate the need for use of Mie scattering in the computations instead of the Rayleigh approximation.

Table 9.3 summarizes Lai-Ian’s data for zenith attenuation of different types of clouds. Ground level water vapor densities are also given. The ratio of attenuation at 95 to 35 GHz varies considerably within the data set, indicating varying droplet sizes and densities among the cloud forms. For stratus and nimbostratus clouds, larger attenuations are cited at 35 GHz than at 95 GHz. This is contrary to predictions of the Rayleigh approximation and may be an artifact of the statistics. An uncertainty factor of two should be employed when using values from this table.



**Figure 9.6** Liquid water Absorption as a Function of Temperature. (From Straiton)

**Table 9.2**  
Attenuation Due to Individual Fair Weather Cumulus Clouds\*

Cloud Attenuation (dB)		95/35 GHz Attenuation
35 GHz	95 GHz	
0.16	0.88	5.5
0.04	0.18	4.5
0.12	0.65	5.4
0.06	0.22	3.7
0.09	0.36	4.0
0.16	0.48	3.0
0.04	0.16	4.0
0.06	0.22	3.7

\*From Straiton.

**9.4 DUSTS AND SMOKE**

Dusts are composed of dry, solid particles originating from wind-blown dry soils and other sources. Their effects on signal propagation are less than water droplets and thus briefly covered.

**Table 9.3**  
Summary of Zenith Cloud Attenuation for Different Cloud Types\*

Cloud Type	Number of Days	Total Number of Observations	Ground Level Water Vapor Density (g/m <sup>2</sup> )		35/95 GHz Value (dB) Measured Cloud Attenuation	
			Mean	Standard Deviation	Mean	Standard Deviation
Alto cumulus	5	7	16.8	1.43	0.02/0.23	0.09/0.30
Alto stratus	2	2	14.7	1.53	0.15/0.30	0.04/0.05
Strato cumulus	8	22	18.9	1.68	0.18/0.61	0.13/0.41
Stratus	5	8	19.1	2.30	0.13/0.12	0.03/0.24
Nimbo stratus	2	5	20.8	0.31	0.14/0.11	0.06/0.24
Cumulus	13	20	18.7	1.81	0.12/0.34	0.14/0.36
Cumulo nimbus	2	6	18.1	2.39	0.34/2.36	0.22/1.86

\*From Lai-Ian

Seagraves characterizes several types of wind-blown dusts that can remain suspended for significant periods of time and are potentially important in many millimeter-wave applications. Suspended dusts occur when wind lifts particles from the earth's surface. Size distributions of the dusts typically have peak radii between 1 and 10  $\mu\text{m}$ . Within a given windstorm, one size distribution will usually characterize the dust cloud. After the strong winds of the storm have ceased, the number density of the dust cloud will fall off exponentially with increasing altitude. Seagraves used number densities between 3 and 58  $\text{cm}^{-3}$  to characterize dust clouds.

Thomson describes dust clouds generated by large chemical explosions. He states that path-integrated mass densities (integral of mass density along propagation path) between 10 and 20  $\text{g/cm}^2$  can occur at early times after the explosion, and lead to an attenuation of 20 dB or more for millimeter-wavelength signals. The size of the munition generating such a cloud is not given. Downs, on the other hand, reports no attenuation of 94-GHz and 140-GHz radar signals by explosion-generated dust clouds. Downs' observations might have been of more evolved clouds from which the larger particles had fallen out. Therefore, attenuation resulting from dust characterized by small particles is of little concern, at least for frequencies below about 100 GHz. However, special attention must be given to dust environments when particle sizes are large.

Smokes are generated from a variety of materials. Particle distributions for fog, oil, and white phosphorous smokes generally peak at particle diameters much smaller than 100  $\mu\text{m}$ . Therefore, large concentrations would be needed to attenuate millimeter radiation. Downs reports no attenuation of 94-GHz and 140-GHz radar signals by smokes of this type.

## 9.5 DATA COMPILATIONS AND SUMMARY

In this section, a summary of the characteristics of atmospheric environments and propagation effects, and simple models that predict attenuation in four millimeter-wave bands are provided. A review of simple models to predict attenuation in clear air, rain, snow, haze, fog, and cloud environments is provided first. Then, summaries of the characteristics of the particles in the atmosphere and propagation effects are given. The material is arranged to provide atmospheric properties in a readily accessible way that is useful for radar analysis and simulation applications.

### Basics

Hans Liebe of the Institute for Telecommunication Sciences has described some simple models that can be used to estimate the attenuation of four principal millimeter-wave regions. His work is summarized here.

Liebe points out that the physical state of air at a point along an arbitrary path can be identified by five basic meteorological parameters ( $p$ ,  $\theta$ ,  $v$ ,  $w$ , and  $R$ ). They are defined as follows:

$$1. \text{ Dry air pressure} = p(x) = p - e \text{ (kPa)} \quad (9.1)$$

where  $p$  is the barometric pressure and  $e$  the partial vapor pressure.

$$2. \text{ Relative inverse temperature} = \theta(x) = 300/T \quad (9.2)$$

where  $T$  is the temperature in kelvins.

$$3. \text{ Water vapor concentration} = v(x) = 7.219 e\theta \text{ (g/m}^3\text{)} \quad (9.3)$$

$$4. \text{ Relative humidity} = \text{RH}(x) \approx 29 e\theta^{1.8} \quad (9.4)$$

$$5. \text{ Liquid water concentration} = w(x) \approx 0.011/u^{1.7} \text{ (g/m}^3\text{)} \quad (9.5)$$

(suspended particles)

where  $u$  is the optical visibility. Table 9.4 contains values of  $w$  and  $u$  for several suspended hydrometers.

### Data

Useful formulas for attenuation estimates for several environments are provided below. The formulas are given first, followed by the necessary constants presented

in tabular form. Rain attenuation  $\alpha_R$  is estimated from

$$\alpha_R = aR^x \tag{9.6}$$

where  $a$  and  $x$  are constants, and  $R$  is the rainfall rate. Snow is difficult to model; however, first estimates of attenuation can be obtained by assuming an equivalent liquid concentration (i.e., between 0.2 and 0.8 g/cm<sup>3</sup>) and using the above equation.

Table 9.4  
Liquid Concentration Values\*

Cluster	Haze	Fog	Stratus	Convective Cloud
$w = 10^{-3}$	$10^{-2}$	$10^{-1}$	1	5 g/m <sup>3</sup>
$u = 17$	1.1	0.27	0.07	0.03 km

\*From Ulaby.

Attenuation of suspended particles is formulated as

$$\alpha_n = bw\theta^v \tag{9.7}$$

As before,  $w$  is the liquid water concentration, and  $b$  and  $v$  are parameters. Attenuation resulting from water vapor is estimated by using

$$\alpha_v = c\left(\frac{P}{101}\right)v\theta^v \approx c'\left(\frac{P}{101}\right)RH\theta^{-1.7} \tag{9.8}$$

All parameters are as previously defined with  $c'$  a frequency-dependent constant. For dry air,

$$\alpha_D = dp\theta^3 \tag{9.9}$$

where  $D$  is a frequency-dependent constant.

Table 9.5 contains the constants for the computation of attenuation in four frequency bands. Figure 9.7 shows some examples and frequency-dependent behavior of several environments.

For modeling purposes, the total attenuation along a propagation path containing the environments considered above is

$$\alpha_T L_T = \alpha_R L_R + \alpha_w L_w + \alpha_v L_v + \alpha_D L_D \tag{9.10}$$

where the path lengths  $L$  pertain to the paths through the environment of concern. Height-dependent meteorological data are needed for path-dependent attenuation

**Table 9.5**  
Coefficients and Exponents for Calculating Specific Attenuation in Four Frequency Bands\*\*

EHF Window	Frequency (GHz)	Rain (Low) R≤50		Rain (High) R = 25–200		Snow		Haze, Fog, Cloud		Water Vapor		Dry Air d
		a	x	a	x	a <sub>s</sub>	x <sub>s</sub>	b	y	c	c'	
		× 10 <sup>−2</sup> × 10 <sup>−2</sup>										
W1	25	0.11	1.08	0.14	1.02	0.05 dry	1.7	0.30	7.0	0.017	0.44	0.022
	35	0.24	1.02	0.34	0.91	0.25 moist	0.9	0.59	6.4	0.010	0.27	0.035
	50	0.48	0.91	0.66	0.82	0.5 wet	0.6	1.17	5.9	0.017	0.44	0.270
W2	70	0.80	0.81	0.86	0.79	0.3 dry	1.5	2.20	4.8	0.032	0.83	0.336
	90	1.03	0.76	0.94	0.78	1.4 moist	1	3.45	3.6	0.049	1.27	0.054
	115	1.12	0.73	0.98	0.77	2.5 wet	0.7	5.17	2.2	0.082	2.11	0.230
W3	120	1.16	0.72	0.99	0.77	0.5 dry	1.3	5.53	1.9	0.087	2.22	0.800
	140	1.25	0.71	1.00	0.77	2.5 moist	1	6.95	0.9	0.116	2.98	0.029
	160	1.30	0.70	1.01	0.76	4.0 wet	0.9	8.36	−0.1	0.190	4.88	0.024
W4	200	1.48	0.66	1.06	0.76	0.7 dry	1	10.9	−1.6	0.280	7.14	0.024
	220	1.47	0.66	1.05	0.76	3.0 moist	1	12.1	−2.1	0.240	6.20	0.026
	250	1.47	0.66	1.03	0.76	5.2 wet	1	13.4	−2.8	0.300	7.63	0.029
AVERAGE OF REPORTED FIELD DATA												
		a		a <sub>s</sub> (Moist)		a <sub>s</sub> (Wet)		b		c		
W1	35			0.2		0.4(1)		0.4(1)		0.009(3)		
W2	90	0.9(1)*		1.8(5)		3.0(6)		4.5(5)		0.04(2)		
W3	140	1.1(3)		3.0(8)		5(1)		6(1)		0.13(5)		
W4	220	1.5(8)		3.5(10)		6(1)		10(2)		0.3(1)		

\*\*From Liebe.

\*Digits in parentheses give the standard deviation from the mean in terms of the final listed digits.

a (dB/km)/(mm/hr)

b, c (dB/km)/(g/m<sup>3</sup>)

c' (dB/km)/%

d (dB/km)/kPa

estimates. Otherwise, specific attenuation values are assumed, with total attenuation values being simply the product of the geometrical path length and the specific attenuations.

9.6 SUMMARY

This summary is intended to show the use of data sets from this and the previous two chapters. The example provided will establish environmental specifications for a 35- or 95-GHz radar operating within the atmosphere. The material provided in the example also serves as the basis for analysis, radar system simulation, or higher-order system simulation.

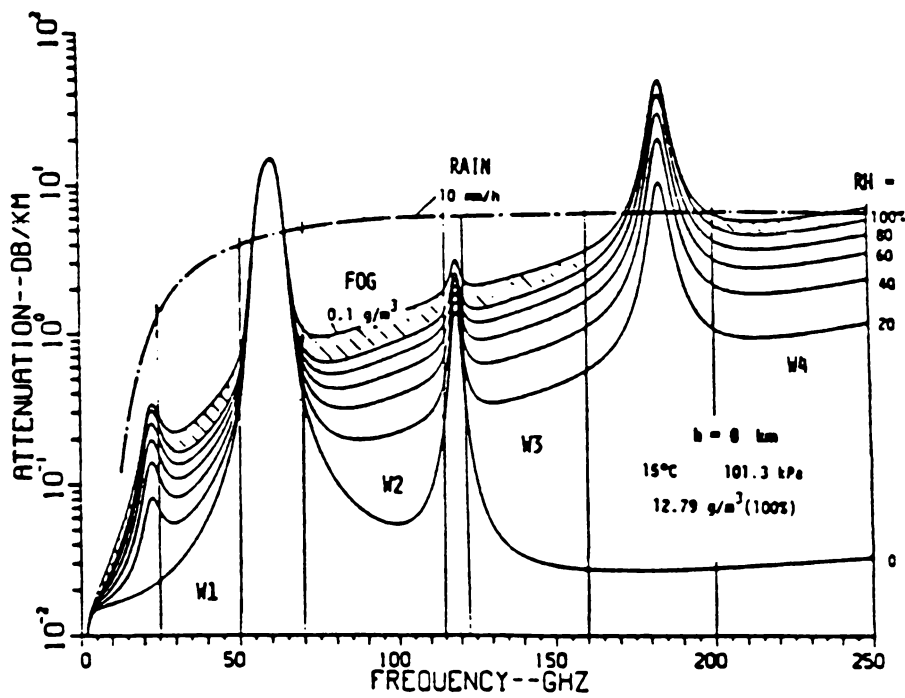


**Figure 9.7** Specific Attenuation at Sea Level for Various Relative Humidities and Including Fog and Rain. (From Liebe)

**EXAMPLE: ENVIRONMENTAL RADAR PARAMETER SPECIFICATIONS**

Clear air attenuation values are considered for varying frequencies, altitudes, and humidities. Simple formulas are given for estimating the altitude-dependent attenuation at 35 and 95 GHz. Uniform rain is assumed with an upper bound established at the zero-degree isotherm. Path dependence is applied to establish an upper bound on the attenuation. Cloud data include fog, haze, and stratus clouds with defined upper and lower bounds.

*Rain Occurrences.* The radar systems are assumed to be deployed within the continental United States. The systems are intended to be fully operational within rainstorms characterized by rain rates of 4 mm/hr or less. Rainfall rates of 4 mm/hr or less expected within the climatic regions are as follows:

- $B_1$  — 10.0 hr/yr
- $B_2$  — 17.5 hr/yr
- $D_1$  — 39.2 hr/yr
- $D_2(D)$  — 67.7 hr/yr

- $D_3$  — 109.5 hr/yr
- $E$  — 144.0 hr/yr
- $F$  — 13.7 hr/yr

*Clear Air.* Attenuation in clear air depends on frequency, altitude, and humidity. Figures 7.1 through 7.3 provide attenuation expressed as a function of frequency for several altitudes and relative humidities (at or referenced to sea level) at an assumed temperature of 15°. Adjustments may be necessary for high-humidity climates or regions.

Clear attenuation is plotted as a function of altitude in Figures 9.8 and 9.9. The attenuations are estimated from

$$a_c = A \exp(-Bh) \quad (\text{dB/km})$$

where  $a_c$  is the clear air attenuation,  $h$  is the altitude (km), and the constants  $A$ ,  $B$  are as given in Table 9.6. Clear air attenuations below 0.01 dB/km are assumed to be negligible.

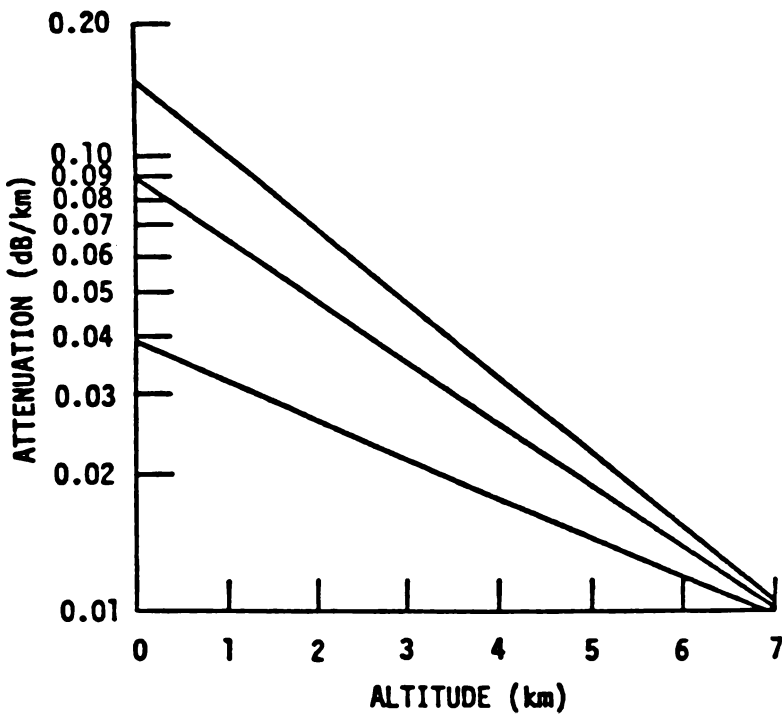


**Figure 9.8** Clear Air Attenuation at Altitudes of 0–7 km, 35 GHz



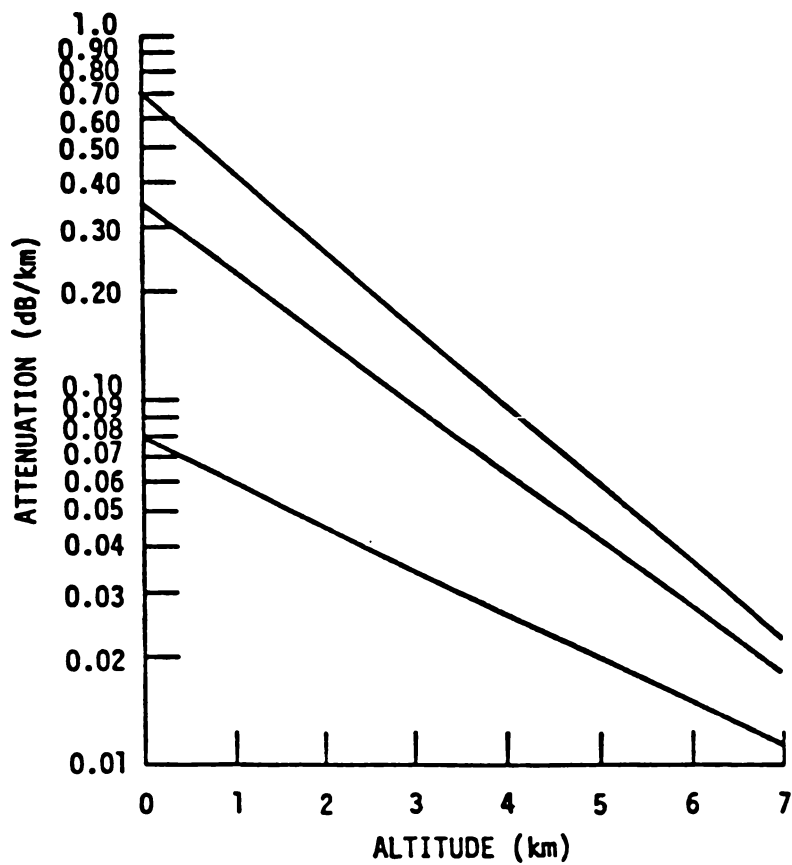


Figure 9.9 Clear Air Attenuation at Altitudes of 0–7 km, 95 GHz

Table 9.6  
Constants for Clear Air Attenuation Estimates

Frequency	Relative Humidity	A	B	Limits
35 GHz	100	0.15	0.3816	$0 \leq h \leq 7$ km $a_c = 0, h > 7$ km
	50	0.09	0.311	
	5	0.04	0.1984	
95 GHz	100	0.70	0.4846	$0 \leq h \leq 10$ km $a_c = 0, h > 10$ km
	50	0.36	0.4181	
	5	0.08	0.2677	

*Rain.* A point or specific rain rate not to exceed 4 mm/hr is specified. A spatially uniform rain is assumed, with an upper bound coinciding with the zero-degree isotherm level. To account for the cellular structure of rain, path length (multiplicative) factors are used, which will depend on the lengths of the propagation paths, and will increase the attenuation estimates for rain rates equal to or less than 4 mm/hr. Path length factors are provided for frequencies of 35 and 95 GHz.

The height of the zero-degree isotherm is estimated from

$$H_I = 2.8 - 1.9 \sin[2(\Lambda - 45)]$$

where  $\Lambda$  is the latitude expressed in degrees.  $H_I$  is plotted in Figure 9.10. Observable radar targets due to water or ice particulates that may occur above this designated altitude are ignored.

The attenuation ( $a$ ) due to rain is specified as follows:

$$a = \alpha R^\beta \quad (\text{dB/km})$$

where  $R$  is the rain rate in units of mm/hr, and  $\alpha$  and  $\beta$  are constants as follows:

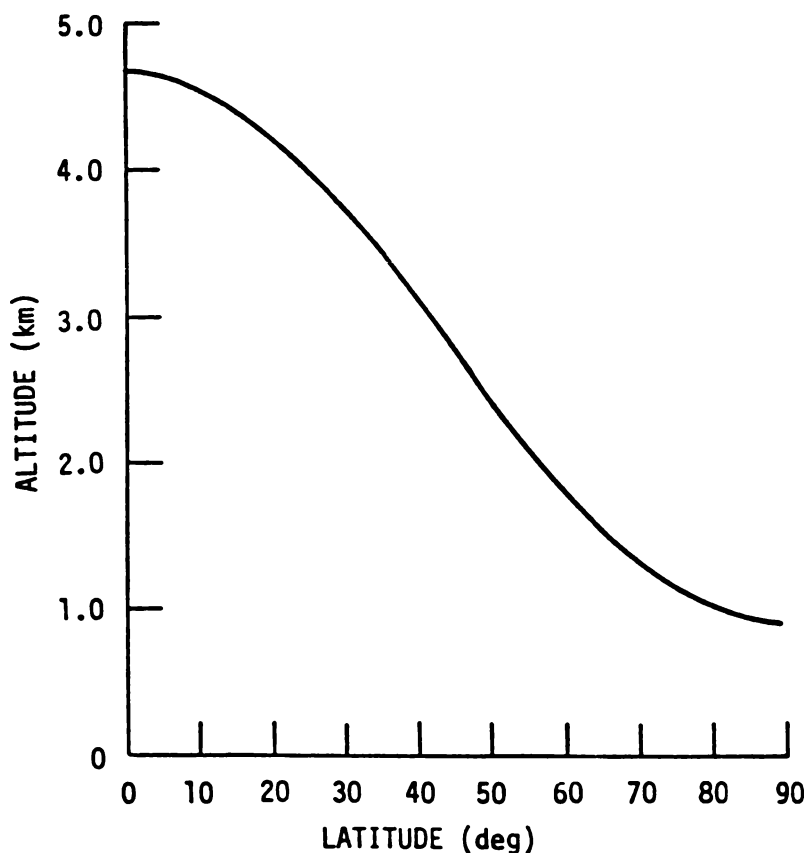


**Figure 9.10** Height of the Zero-Degree Isotherm

$$f = 35 \text{ GHz}, \alpha = 0.232, \quad \beta = 1.022$$

$$f = 95 \text{ GHz}, \alpha = 1.050, \quad \beta = 0.749$$

At a frequency of 35 GHz, with  $R = 4$  mm/hr, the specific attenuation is 0.957 or about 1 db/km. When  $\Lambda = 45^\circ$ , the total one-way attenuation along a zenith propagation path is  $3 \times 0.957$  or 2.871 dB.

The path-dependent attenuation ( $A$ ) is taken into account as follows:

$$A = \delta a(H_i - H_0)/\sin\theta$$

where

$A$  = one-way path-dependent attenuation

$a$  = specific attenuation

$H_i$  = height of the zero-degree-isotherm

$H_0$  = height of radar

$\theta$  = elevation angle

$\delta$  = path length factor

In this formulation  $\theta \leq 10^\circ$ . For elevation angles of less than  $10^\circ$ , slant paths are used directly. Path length factors are plotted in Figures 9.11 and 9.12 for rain rates of 1, 2, and 4 mm/hr for frequencies of 35 and 95 GHz. Path lengths are horizontal with

$$D = (H_i - H_0)/\tan \theta$$

The influence of the path length factor on the attenuation is negligible when zenith or short propagation paths are encountered. Otherwise, the resultant path-dependent attenuation estimates may serve as an upper bound.

Uniform backscatter cross sections along a propagation path are assumed. The volume backscatter,  $\sigma_v$ , expressed in square meters per cubic meter, is computed from

$$\sigma_v = (\pi^5 10^{-10} |K|^2 Z)/\lambda^4$$

where

$\lambda$  = wavelength

$|K|^2$  = temperature-dependent parameter set at 0.93

$Z$  = reflectivity factor

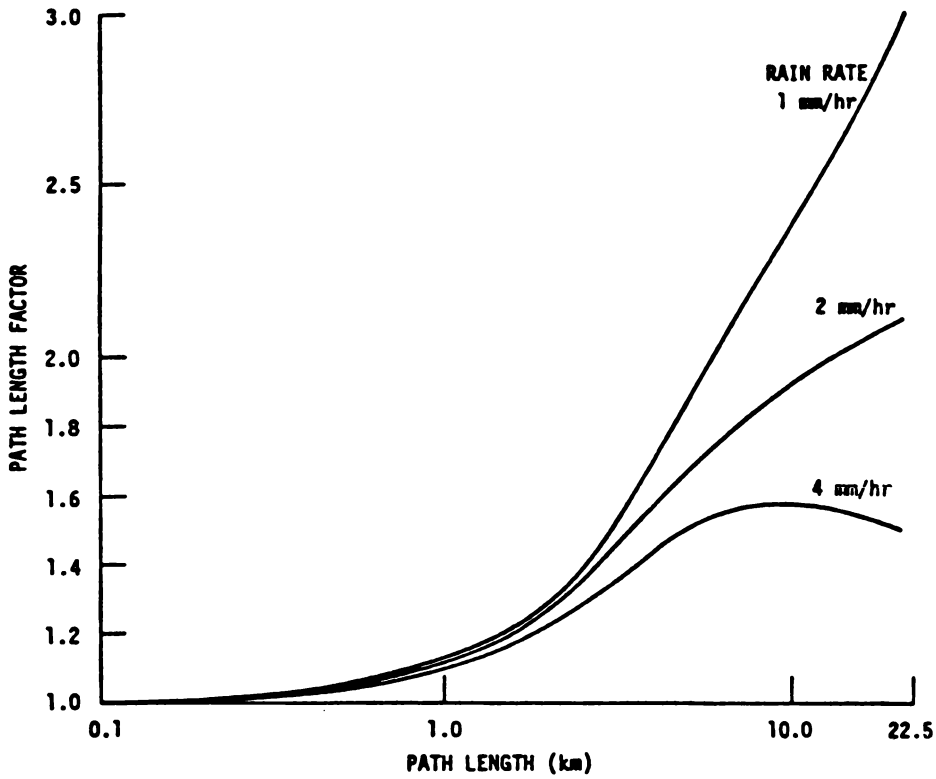


Figure 9.11 Path Length Factors for Light Rain of 1 to 4 mm/hr at a Frequency of 35 GHz

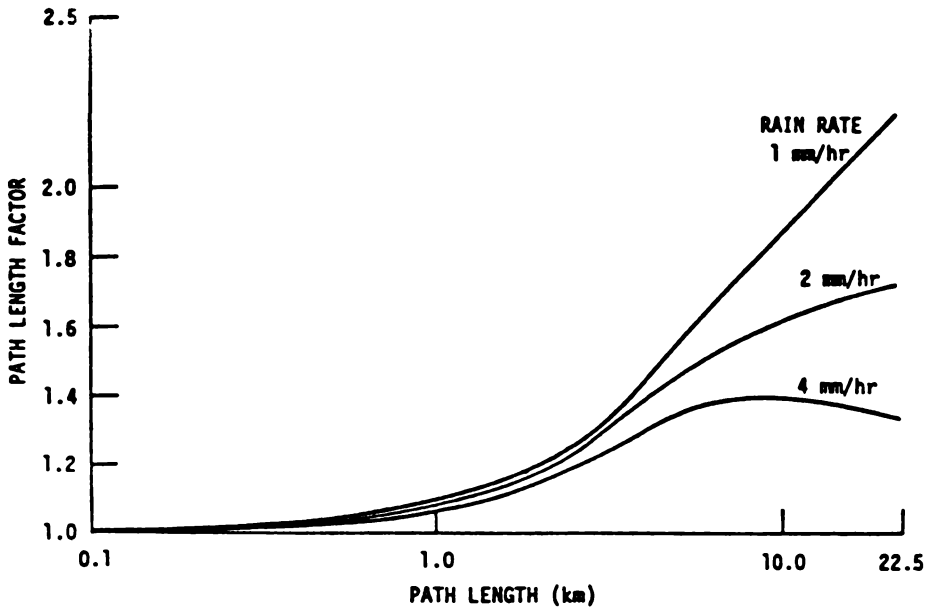


Figure 9.12 Path Length Factors for Light Rain of 1 to 4 mm/hr at a Frequency of 94 GHz

The reflectivity factor is

$$Z = pR^q$$

where  $R$  is the rain rate (mm/hr), and  $p$  and  $q$  are constants given as follows:

$f = 35 \text{ GHz}$

$p = 350, q = 1.32; R \leq 5$

(mm/hr)

$p = 450, q = 1.15; 5 < R \leq 20$

(mm/hr)

$p = 780, q = 0.95; 20 < R \leq 100$

(mm/hr)

$f = 95 \text{ GHz}$

$p = 1200, q = 0.60; R < 100$

(mm/hr)

*Clouds.* Let us consider fog, haze, and low stratus clouds, with characteristics given in Table 9.7. Attenuation estimates are obtained from

$$a_c = bw\theta^y \text{ (dB/km)}$$

where

- $a_c$  = cloud attenuation
- $b, y$  = frequency-dependent parameters
- $w$  = water content (gm/m<sup>3</sup>)
- $\theta$  = temperature-dependent value set at 1.024 (20°)

The parameters  $b, y$  are as follows:

$f = 35\text{GHz}$

$b = 0.59, y = 6.40$

$f = 95\text{GHz}$

$b = 3.79, y = 3.32$

Table 9.7  
Cloud Parameters

Type of Cloud	Composition	Cloud Base (km)	Thickness (km)	Water Content (gm/m <sup>3</sup> )
Fog	Water	0	0.05	10 <sup>1</sup>
Haze	Water	0	1.50	10 <sup>-2</sup>
Stratus	Water	0.1–0.7	0.20–0.80	1.0

For example, a stratus cloud with a thickness of 0.8 km and a zenith propagation path at a frequency of 35 GHz has a one-way attenuation of 0.549 dB, while at 95 GHz the comparable result is 3 dB.

*Abridgment.* Because of the upper altitude bound placed on the three environments, they may become negligible for some applications. However, ground-based radars can be expected to be adversely affected by the environments.



## *Appendix A*

### *Gaussian Antenna—Scaling Factors and Series Coefficients*

We now compile formulas for aperture, near, and far fields of large-aperture, rectangular, and circular antennas. We include diffraction integrals, Hermite-Gaussian field expansion formulas for rectangular apertures, and Laguerre-Gaussian field expansion formulas for circular apertures. Tables of optimal scale factors and series coefficients are provided for cosine, truncated-Gaussian, and Taylor aperture distributions for the rectangular antennas, and cosine and truncated-Gaussian aperture distributions for the circular ones.

#### **Diffraction Integrals**

In the approximate Gaussian theory of large-aperture antennas, orthogonal Hermite-Gaussian and Laguerre-Gaussian expansions replace the diffraction integrals. A number of formulas, including diffraction integrals, provided here formed the basis for the derivation of the field expansions. They are provided for reference purposes.

#### *The Rectangular Antenna*

For a rectangular antenna with sides  $(a, b)$  positioned in the  $(x, y)$  plane with beam directed along the  $z$ -axis, the formulas are as follows:

*Aperture Coordinates*  $(\xi, \eta)$

*Field Coordinates*  $(x, y, z), (r, \theta, \phi)$



*Position vectors*

$$r, r', r_0$$

$r$  to observation point

$r'$  to aperture point

$r_0$  aperture to observation point

*General Form*

$$E(r) = \frac{jk}{4\pi r} (1 + \cos\theta) \iint E(r') \exp(-jkr_0) dA$$

*General, Rectangular Field Coordinates*

$$r_0 = \sqrt{(x - \xi)^2 + (y - \eta)^2 + z^2}$$

*General, Spherical Field Coordinates*

$$r_0 = \sqrt{(r \sin\theta \cos\phi - \xi)^2 + (r \sin\theta \sin\phi - \eta)^2 + (r \cos\theta)^2}$$

*Far-field Limit ( $a \geq b$ )*

$$r \geq \frac{2a^2}{\lambda}$$

*Far-field Approximation*

$$r_0 \approx r - \sin\theta(\xi \cos\phi + \eta \sin\phi)$$

*Aperture Distribution*

$$f(\xi, \eta)$$

*Separable Aperture Distribution*

$$f(\xi)g(\eta)$$

*Far-field Diffraction Integral*

$$E(r, \theta, \phi) = \frac{jk}{4\pi r} \exp(-jkr) (1 + \cos\theta) \iint f(\xi, \eta) \exp[jk \sin\theta(\xi \cos\phi + \eta \sin\phi)] d\xi d\eta$$

*Far-field Antenna Pattern*

$$F(\theta, \phi) = \iint f(\xi, \eta) \exp[jk \sin\theta(\xi \cos\phi + \eta \sin\phi)] d\xi d\eta$$

*Far-field Variables*

$$u = k \sin\theta \cos\phi$$

$$v = k \sin\theta \sin\phi$$

*Fourier Transform Pair*

$$F(u) = \int_{-\infty}^{+\infty} f(\xi) \exp(-ju\xi) d\xi$$

$$f(\xi) = \frac{1}{2\pi} \int_{-\infty}^{+\infty} F(u) \exp(ju\xi) du$$

*Fourier Transform Pair*

$$f(\xi) \leftrightarrow F(u)$$

$$g(\eta) \leftrightarrow G(v)$$

*Near-field Approximation*

$$r_0 \approx \frac{1}{2} \left[ r + \frac{(x - \xi)^2 + (y - \eta)^2 + z^2}{r} \right]$$

*Near-field Diffraction Integral*

$$E(x, y, z) = \frac{jk}{4\pi r} \exp(-jkr)(1 + \cos\theta) \\ \times \iint f(\xi, \eta) \exp \left\{ -\frac{jk}{2r} [(x - \xi)^2 + (y - \eta)^2 - (x^2 + y^2)] \right\} d\xi d\eta$$

*Near-field Antenna Pattern*

$$E(x, y, z) = \iint f(\xi, \eta) \exp \left\{ \frac{jk}{2r} [(x - \xi)^2 + (y - \eta)^2 - (x^2 + y^2)] \right\} d\xi d\eta$$

*Near-field Diffraction Integral*

$$(r \approx z) \\ (\cos\theta \approx 1)$$

$$E(x, y, z) = jk \frac{\exp(-jkz)}{2\pi r} \iint f(\xi, \eta) \exp \left\{ \frac{jk}{2z} [(x - \xi)^2 + (y - \eta)^2] \right\} d\xi d\eta$$

*Fresnel Transform Pair*

$$F(x) = \frac{1}{\zeta\sqrt{2\pi}} \int_{-\infty}^{+\infty} f(\xi) \exp\left(\frac{j\xi^2}{2\zeta^2}\right) \exp(-jx\xi) d\xi$$

$$f(\xi) = \frac{\sigma}{\sqrt{2\pi}} \exp\left(-\frac{j\xi^2}{2\xi^2}\right) \int_{-\infty}^{+\infty} F(x) \exp(jx\xi) dx$$

*Transform Equivalence*

$$\frac{1}{\sigma\sqrt{2\pi}} \exp\left(\frac{j\xi^2}{2\zeta^2}\right) f(\xi) \leftrightarrow F(x)$$

*The Circular Antenna*

For a circular antenna with diameter  $d$ , similarly positioned, we have the formulas:

*Aperture Coordinates*

$$(\rho, \phi')$$

*Field Coordinates*

$$(r, \theta, \phi)$$

### General, Spherical Field Coordinates

$$r_0 = \sqrt{(r \sin\theta \cos\phi - \rho \cos\phi')^2 + (r \sin\theta \sin\phi - \rho \sin\phi')^2 + (r \cos\theta)^2}$$

### Far-field Limit

$$r \geq \frac{2d^2}{\lambda}$$

### Far-field Approximation

$$r_0 \approx r - \rho \sin\theta \cos(\phi - \phi')$$

### Aperture Distribution

$$f(\rho, \phi')$$

### Separable Aperture Distribution

$$f(\rho)g(\phi')$$

### Far-field Diffraction Integral

$$E(r, \theta, \phi) = \frac{jk}{4\pi r} \exp(-jkr) (1 + \cos\theta) \\ \times \iint f(\rho, \phi') \exp[jk\rho \sin\theta \cos(\phi - \phi')] \rho \, d\rho \, d\phi'$$

### Circularly Symmetric Antenna

$$g(\phi') = 1$$

### Far-field Variable

$$u = k \sin\theta$$

### Bessel Function Identity

$$J_0(u\rho) = \frac{1}{2\pi} \int_{-\pi}^{+\pi} \exp[ju\rho \cos(\phi - \phi')] \, d\phi$$

### Far-field Diffraction Integral (Circular Symmetry)

$$E(r, \theta, \phi) = \frac{jk}{2r} \exp(-jkr)(1 + \cos\theta) \int f(\rho) J_0(u\rho) \rho \, d\rho$$

### Far-field Antenna Pattern (Circular Symmetry)

$$E(\theta) = \int f(\rho) J_0(u\rho) \rho \, d\rho$$

### Hankel Transform Pair

$$F(u) = \int_0^\infty f(\rho) J_0(u\rho) \rho \, d\rho$$

$$f(\rho) = \int_0^\infty F(u) J_0(u\rho) u \, du$$

### Hankel Transform Pair

$$f(\rho) \overset{h}{\leftrightarrow} F(u)$$

*Near-field Approximation*

$$r_0 \approx r - \rho \sin \theta \cos(\phi - \phi') + \frac{\rho^2}{2r}$$

*Near-field Diffraction Integral*

$$E(r, \theta, \phi) = \frac{jk}{4\pi r} \exp(-jkr)(1 + \cos \theta) \times \\ \int f(\rho, \phi') \exp\left\{jk\left[\rho \sin \theta \cos(\phi - \phi') - \frac{\rho^2}{2r}\right]\right\}$$

*Near-field Diffraction Integral  
(Circular Symmetry)*

$$E(r, \theta, \phi) = \frac{jk}{2r} \exp(-jkr) (1 + \cos \theta) \int f(\rho) J_0(u\rho) \exp\left(\frac{\rho^2}{2r}\right) \rho \, d\rho$$

*Near-field Antenna Pattern  
(Circular Symmetry)*

$$E(r, \theta) = \int f(\rho) J_0(u\rho) \exp\left(-j\frac{\rho^2}{2r}\right) \rho \, d\rho \, d\theta$$

*Transform Equivalence*

$$f(\rho) \exp\left(-j\frac{\rho^2}{2r}\right) \xleftrightarrow{h} F(u)$$

## Orthogonal Functions

A review of orthogonal functions is now provided. The orthogonality relationships are demonstrated in the tabulation of Hermite-Gaussian and Laguerre-Gaussian functions that follow:

*Orthogonal Functions*

$$\Psi_m(x), \Psi_n(x)$$

*Region of Orthogonality*

$$(a, b)$$

*Condition of Orthogonality*

$$\int_a^b \Psi_m(x) \Psi_n(x) \, dx = 0, \quad n \neq m$$

*Weighting Function*

$$r(x)$$

*Condition of Orthogonality*

$$\int_a^b r(x) \Psi_m(x) \Psi_n(x) \, dx, \quad n \neq m$$

Series Expansion

$$f(x) = A_0\Psi_0(x) + A_1\Psi_1(x) + A_2\Psi_2(x) + \dots = \sum_0^{\infty} A_n\Psi_n(x)$$

$$r(x)f(x)\Psi_n(x) = \sum_0^{\infty} A_nr(x)\Psi_n(x)\Psi_k(x)$$

Series Integrations

$$\int_a^b r(x)f(x)\Psi_k(x) \, dx = \sum_0^{\infty} A_n \int_a^b r(x)\Psi_n(x)\Psi_k(x) \, dx$$

Series Coefficients

$$A_n = \frac{\int_a^b r(x)f(x)\Psi_n(x) \, dx}{\int_a^b r(x)[\Psi_n(x)]^2 \, dx}$$

Parameter Definition

$$\int_a^b r(x)[\Psi_n(x)]^2dx = h_n$$

Hermite Polynomial Examples

$f_n$	$H_n(x)$	$H_{e_n}(x)$
$a$	$-\infty$	$-\infty$
$b$	$+\infty$	$+\infty$
$r(x)$	$\exp(-x^2)$	$\exp(-x^2/2)$
$h_n$	$\sqrt{\pi} \, 2^n n!$	$\sqrt{2\pi n!}$

Hermite-Gaussian Field Expansions

Hermite-Gaussian field expansions apply to rectangular and square antennas. To avoid cumbersome notation, normalized aperture coordinates maintain previous designations. As a result, aperture dimension will appear in the field formulas.

Coordinates are as follows:

Normalized Aperture Coordinates

$$\xi \rightarrow \frac{\xi}{a}, \rightarrow \eta \rightarrow \frac{\eta}{b}, (\xi, \eta)$$

Field Coordinates

$$(x, y, z), (r, \theta, \phi)$$

## *Hermite Polynomials*

### *Rodrique's Formula*

$$H_n(\xi) = (-1)^n \exp(x^2) \frac{d^n}{dx^n} [\exp(-x^2)]$$

### *Hermite Polynomials*

$$H_0(\xi) = 1$$

$$H_1(\xi) = 2\xi$$

$$H_2(\xi) = 4\xi^2 - 2$$

$$H_3(\xi) = 8\xi^3 - 12\xi$$

$$\vdots$$

$$\vdots$$

$$\vdots$$

### *Recurrence Formulas*

$$H_n(\xi) = 2\xi H_{n-1}(\xi) - 2(n-1)H_{n-2}(\xi)$$

$$H'_n(\xi) = 2nH_{n-1}(\xi)$$

### *Orthogonality*

$$\int_{-\infty}^{\infty} H_m(\xi) H_n(\xi) \exp(-\xi^2) d\xi = 0 \quad m \neq n$$

$$\int_{-\infty}^{\infty} [H_n(\xi)]^2 \exp(-\xi^2) d\xi = 2^n n! \sqrt{\pi}$$

### *Orthogonal Series*

$$f(\xi) = C_0 H_0(\xi) + C_1 H_1(\xi) + C_2 H_2(\xi) + \dots$$

### *Coefficients*

$$C_n = \frac{1}{2^n n! \sqrt{\pi}} \int_{-\infty}^{+\infty} f(\xi) H_n(\xi) \exp(-\xi^2) d\xi$$

### *Orthogonal Series Coefficients*

$$F(\xi) = C_0 H_0(\xi) \exp(-x^2) + C_1 H_1(\xi) \exp(-\xi^2) + C_2 H_2(\xi) \exp(-\xi^2) + \dots$$

$$F(\xi) = f(\xi) \exp(-\xi^2)$$

$$C_n = \frac{1}{2^n n! \sqrt{\pi}} \int_{-\infty}^{+\infty} F(\xi) H_n(\xi) d\xi$$

### *Field Expansions*

*Hermite-Gaussian Function*

$$\psi_n(\xi) = H_n(\xi) \exp\left(-\frac{\xi^2}{2}\right)$$

*Scale Factors*

$$\alpha, \beta$$

*Aperture Field Expansion*

$$f(\xi) = \sum_0^{\infty} C_n \psi_n(\alpha \xi)$$

*Expansion Coefficients*

$$C_n = \frac{1}{2^n n! \sqrt{\pi}} \int_{-1/2}^{+1/2} f(\xi) \psi_n(\alpha \xi) d\xi$$

*Separable Aperture Distribution*

$$f(\xi, \eta) = f(\xi)g(\eta)$$

*Fourier Transforms*

$$f(\xi) \leftrightarrow F(u)$$

$$g(\eta) \leftrightarrow G(v)$$

*Far-field Variables*

$$u = k \sin\theta \cos\phi$$

$$v = k \sin\theta \sin\phi$$

*Far field*

$$E(r, u, v) = j \frac{abk}{4\pi r} \exp(-jkr)(1 + \cos\theta)F(u)G(v)$$

*Aperture Field Transform*

$$C_n \psi_n(\alpha \xi) \leftrightarrow \frac{\sqrt{2\pi}}{\alpha} j^n C_n \psi_n\left(\frac{au}{\alpha}\right)$$

*Far-Field Expansion*

$$E(r, u, v) = j \frac{abk}{2\alpha\beta r} \exp(-jkr)(1 + \cos\theta) \left[ \sum_0^{\infty} j^n C_n \psi_n\left(\frac{au}{\alpha}\right) \right] \left[ \sum_0^{\infty} j^n D_n \psi_n\left(\frac{bv}{\beta}\right) \right]$$

*Near Field*

$$E(x, y, z) = j \frac{\rho\gamma kab}{4\pi r\alpha\beta} \left(1 + \frac{z}{r}\right) \exp(-jkr) \exp\left[-j \frac{k(x^2 + y^2)}{2z}\right]$$

$$\times \sum_0^{\infty} C_n \int_{-\infty}^{+\infty} H_n(\rho\xi) \exp\left(-\frac{\xi^2}{2}\right) \exp(jav\xi) d\xi$$

$$\times \sum_0^{\infty} D_n \int_{-\infty}^{+\infty} H_n(\gamma\eta) \exp\left(-\frac{\eta^2}{2}\right) \exp(jbv\eta) d\eta$$

### Field Variables

$$v = \frac{k\rho x}{\alpha z}$$

$$v = \frac{kb\gamma y}{\beta z}$$

### Complex Scaling Factors

$$\rho = \sqrt{1 + j\frac{ka^2}{\alpha^2 z}}$$

$$\gamma = \sqrt{1 + j\frac{kb^2}{\beta^2 z}}$$

### Transform

$$H_n(\rho\xi) \exp\left(-\frac{\xi^2}{2}\right) \leftrightarrow \sqrt{2\pi} j^n H_n(\rho v) \exp\left(-\frac{v^2}{2}\right) + 0(\rho^{n-1} - \rho^n)$$

### Near-field Expansion

$$E(x, y, z) \approx j\frac{\rho\gamma kab}{2r\alpha\beta} \left(1 + \frac{z}{r}\right) \exp(-jkr) \exp\left[-j\frac{k(x^2 + y^2)}{2z}\right]$$

$$\times \sum_0^{\infty} C_n j^n H_n(\rho v) \exp\left(-\frac{v^2}{2}\right)$$

$$\times \sum_0^{\infty} D_m j^m H_m(\gamma v) \exp\left(-\frac{v^2}{2}\right)$$

### Gaussian Equivalent

$$|E(x, y, z)| = \left(\frac{1}{1 + \chi^2}\right)^{1/2} \exp\left[-\frac{\alpha^2}{2a^2} \left(\frac{1}{1 + \chi^2}\right) (x^2 + y^2)\right]$$

### Square Antenna

$$(\chi = \alpha^2 z / ka^2)$$



Tables

Tables I through XXI (from Bogush and Elkins), which follow, contain scaling factors and series coefficients for truncated Hermite-Gaussian series approximations of cosine, truncated-Gaussian, and Taylor aperture distributions. The scaling factors are optimized to radiated power, limiting the total radiated power to the maximum achievable by the antenna of concern.

The cosine aperture distributions of Tables 1 through V are expressed in powers of the cosine function:

$$\cos^n\left(\pi\frac{x}{a}\right), \quad n = 0, 1, 2, 3, 4$$

The uniform aperture is represented when  $n = 0$ . The truncated-Gaussian aperture distributions of Tables VI through IX are

$$\exp\left[-1.386 \cdot \left(\frac{a}{a_3}\right)^2\left(\frac{x}{a}\right)^2\right], \quad \left(\frac{a}{a_3}\right) = 1, 2, 3, 4$$

The Taylor distributions of Tables X through XXI are defined by

$$\text{Taylor}(x, \text{dB}, \bar{n}) = 1 + 2 \sum_{n=1}^{\bar{n}-1} F(n, \text{dB}, \bar{n}) \cos\left(\frac{n\pi x}{a}\right)$$

where  $x$  is the aperture coordinate, and  $-a \leq x \leq a$ , dB is the sidelobe level, and  $\bar{n}$  is the number of equal amplitude sidelobes to one side of the principal lobe. The coefficients  $F(n, \text{dB}, \bar{n})$  are given by

$$F(n, \text{dB}, \bar{n}) = \frac{[(\bar{n} - 1)!]^2 \prod_{m=1}^{\bar{n}-1} \left[1 - \left(\frac{n}{z_m}\right)^2\right]}{(\bar{n} - 1 + n)!(\bar{n} - 1 - n)!}$$

where  $z_m$  is the  $m$ th zero of the space factor given by

$$z_m = \bar{n} \left[ \frac{A^2 + \left(n - \frac{1}{2}\right)^2}{A^2 + \left(\bar{n} - \frac{1}{2}\right)^2} \right]$$

**Table I**  
Optimal Scale Factors and Expansion Coefficients for a Uniform Aperture Distribution

$$\cos^0\left(\pi\frac{x}{a}\right) \approx \sum_{n=0}^{2(N-1)} C_{2n}\psi_{2n}\left(\alpha\frac{x}{a}\right)$$

$$-.5 \leq \frac{x}{a} \leq .5$$

<i>N</i>	$\alpha$	$C_0$	$C_2$	$C_4$	$C_6$	$C_8$	$C_{10}$
1	2.79997	1.18579					
2	4.47571	1.37853	0.241408				
3	5.77578	1.40873	0.327004	0.265244			
4	6.87320	1.41338	0.348061	0.0389673	0.00201159		
5	7.83956	1.41408	0.352503	0.0428852	0.00311226	0.00011725	
6	8.71241	1.41420	0.353363	0.0438993	0.00351920	0.000187288	0.548924E-5

**Table II**  
Optimal Scale Factors and Expansion Coefficients for a Cosine Aperture Distribution

$$\cos\left(\pi\frac{x}{a}\right) \approx \sum_{n=0}^{2(N-1)} C_{2n}\psi_{2n}\left(\alpha\frac{x}{a}\right)$$

$$-.5 \leq \frac{x}{a} \leq .5$$

<i>N</i>	$\alpha$	$C_0$	$C_2$	$C_4$	$C_6$	$C_8$	$C_{10}$
1	4.02194	1.05947					
2	5.57175	1.20761	0.116507				
3	6.79731	1.27106	0.182818	0.00909733			
4	7.84367	1.30522	0.221716	0.0161629	0.000545233		
5	8.77192	1.32636	0.246540	0.0211159	0.00103428	0.264513E-4	
6	9.61462	1.34070	0.263605	0.0246446	0.00141455	0.522251E-4	0.107677E-5

**Table III**  
Optimal Scale Factors and Expansion Coefficients for a Cosine Squared Aperture Distribution

$$\cos^0\left(\pi\frac{x}{a}\right) \approx \sum_{n=0}^{2(N-1)} C_{2n}\psi_{2n}\left(\alpha\frac{x}{a}\right)$$

$$-.5 \leq \frac{x}{a} \leq .5$$

<i>N</i>	$\alpha$	$C_0$	$C_2$	$C_4$	$C_6$	$C_8$	$C_{10}$
1	5.04763	1.03187					
2	6.53293	1.15233	0.0818093				
3	7.71063	1.21444	0.135143	0.00512109			
4	8.72072	1.25257	0.171563	0.00986878	0.000259696		
5	9.62026	1.27840	0.197752	0.0138191	0.000542274	0.110155E-4	
6	10.4394	1.29706	0.217405	0.0170441	0.000805871	0.241259E-4	0.400646E-6

**Table IV**  
Optimal Scale Factors and Expansion Coefficients for a Cosine Cubed Aperture Distribution

$$\cos^3\left(\pi\frac{x}{a}\right) \approx \sum_{n=0}^{2(N-1)} C_{2n}\psi_{2n}\left(\alpha\frac{x}{a}\right)$$
$$-.5 \leq \frac{x}{a} \leq .5$$

N	α	C <sub>0</sub>	C <sub>2</sub>	C <sub>4</sub>	C <sub>6</sub>	C <sub>8</sub>	C <sub>10</sub>
1	5.04763	1.02133					
2	7.37349	1.12483	0.657059				
3	8.52000	1.18270	0.110990	0.00351627			
4	9.50445	1.22051	0.143952	0.00705828	0.000157212		
5	10.3828	1.24737	0.168987	0.0102447	0.000345679	0.600249E-5	
6	11.1834	1.26750	0.188621	0.0130200	0.000537363	0.139314E-4	0.199307E-6

**Table V**  
Optimal Scale Factors and Expansion Coefficients for a Cosine Fourth Aperture Distribution

$$\cos^4\left(\pi\frac{x}{a}\right) \approx \sum_{n=0}^{2(N-1)} C_{2n}\psi_{2n}\left(\alpha\frac{x}{a}\right)$$
$$-.5 \leq \frac{x}{a} \leq .5$$

N	α	C <sub>0</sub>	C <sub>2</sub>	C <sub>4</sub>	C <sub>6</sub>	C <sub>8</sub>	C <sub>10</sub>
1	6.69552	1.01596					
2	8.12203	1.10798	0.0562010				
3	9.24673	1.16187	0.0960443	0.00266707			
4	10.2122	1.19842	0.126073	0.00548252	0.000107848		
5	11.0746	1.22518	0.149627	0.00813305	0.000244820	0.377910E-5	
6	11.861	1.24572	0.168603	0.0105328	0.000391470	0.909817E-5	0.116314E-6

**Table VI**  
Optimal Scale Factors and Expansion Coefficients for a Truncated Gaussian Aperture Distribution,  
 $a/a_3 = 1$

$$\exp\left[-1.3868 \cdot \left(\frac{x}{a}\right)^2\right] \approx \sum_{n=0}^{2(N-1)} C_{2n}\psi_{2n}\left(\alpha\frac{x}{a}\right)$$
$$-.5 \leq \frac{x}{a} \leq .5$$

N	α	C <sub>0</sub>	C <sub>2</sub>	C <sub>4</sub>	C <sub>6</sub>	C <sub>8</sub>	C <sub>10</sub>
1	2.99323	1.12857					
2	4.57166	1.30888	0.191501				
3	5.84029	1.35675	0.273014	0.0201175			

**Table VI continued**

4	6.92218	1.37447	0.302745	0.0308473	0.00149611		
5	7.87925	1.38356	0.315666	0.0353340	0.00239510	0.858748E-4	
6	8.74588	1.38924	0.322884	0.0373620	0.00280547	0.000141663	0.401058E-5

**Table VII**

Optimal Scale Factors and Expansion Coefficients for a Truncated Gaussian Aperture Distribution,  
 $a/a_3 = 2$

$$\exp\left[-1.3868 \cdot (2)^2 \cdot \left(\frac{x}{a}\right)^2\right] \approx \sum_{n=0}^{2(N-1)} C_{2n} \psi_{2n}\left(\alpha \frac{x}{a}\right)$$

$$-.5 \leq \frac{x}{a} \leq .5$$

$N$	$\alpha$	$C_0$	$C_2$	$C_4$	$C_6$	$C_8$	$C_{10}$
1	3.68634	1.03569					
2	4.90224	1.16619	0.0596582				
3	6.05653	1.23850	0.162481	0.00873998			
4	7.08350	1.27967	0.203288	0.0154979	0.000612760		
5	8.00839	1.30576	0.229996	0.0200776	0.00109997	0.340580E-4	
6	8.85388	1.32364	0.248828	0.0233453	0.00143862	0.616036E-4	0.155878E-5

**Table VIII**

Optimal Scale Factors and Expansion Coefficients for a Truncated Gaussian Aperture Distribution,  
 $a/a_3 = 3$

$$\exp\left[-1.3868 \cdot (3)^2 \cdot \left(\frac{x}{a}\right)^2\right] \approx \sum_{n=0}^{2(N-1)} C_{2n} \psi_{2n}\left(\alpha \frac{x}{a}\right)$$

$$-.5 \leq \frac{x}{a} \leq .5$$

$N$	$\alpha$	$C_0$	$C_2$	$C_4$	$C_6$	$C_8$	$C_{10}$
1	5.02307	1.00228					
2	5.59534	1.05469	0.0289594				
3	6.49653	1.12098	0.0716819	0.00210406			
4	7.40331	1.17223	0.109581	0.00505684	0.000134767		
5	8.25942	1.21005	0.140415	0.00812849	0.000305776	0.714037E-5	
6	9.06065	1.23841	0.165221	0.0110168	0.000487233	0.155393E-4	0.317253E-6

**Table IX**

Optimal Scale Factors and Expansion Coefficients for a Truncated Gaussian Aperture Distribution,  
 $a/a_3 = 4$

$$\exp\left[-1.3868 \cdot (4)^2 \cdot \left(\frac{x}{a}\right)^2\right] \approx \sum_{n=0}^{2(N-1)} C_{2n} \psi_{2n}\left(\alpha \frac{x}{a}\right)$$

Table IX continued

$$-.5 \leq \frac{x}{a} \leq .5$$

$N$	$\alpha$	$C_0$	$C_2$	$C_4$	$C_6$	$C_8$	$C_{10}$
1	6.66203	1.00003					
2	6.78199	1.00891	0.00450340				
3	7.2773	1.04315	0.0229860	0.000247633			
4	7.9632	1.08471	0.0478860	0.00105482	0.281331E-4		
5	8.6913	1.122243	0.0729176	0.00236783	0.509216E-4	0.744799E-6	
6	9.4104	1.15427	0.0958999	0.00398366	0.000110211	0.225567E-5	0.322874E-7

Table X

Optimal Scale Factors and Expansion Coefficients for a 20 dB Taylor Aperture Distribution,  $\bar{n} = 3$

$$\text{Taylor (20 dB, } \bar{n} = 3) \approx \sum_{n=0}^{2(N-1)} C_{2n} \psi_{2n} \left( \alpha \frac{x}{a} \right)$$
$$-.5 \leq \frac{x}{a} \leq .5$$

$N$	$\alpha$	$C_0$	$C_2$	$C_4$	$C_6$	$C_8$	$C_{10}$
1	3.29619	1.37183					
2	4.54808	1.56021	0.152663				
3	5.80711	1.65702	0.251329	0.0174314			
4	6.89132	1.70626	0.299844	0.0278401	0.00134519		
5	7.85166	1.73647	0.328572	0.0330932	0.00217602	0.788015E-4	
6	8.72118	1.75707	0.348469	0.0362517	0.00258911	0.000129903	0.372725E-5

Table XI

Optimal Scale Factors and Expansion Coefficients for a 20 dB Taylor Aperture Distribution,  $\bar{n} = 4$

$$\text{Taylor (20 db, } \bar{n} = 4) \approx \sum_{n=0}^{2(N-1)} C_{2n} \psi_{2n} \left( \alpha \frac{x}{a} \right)$$
$$-.5 \leq \frac{x}{a} \leq .5$$

$N$	$\alpha$	$C_0$	$C_2$	$C_4$	$C_6$	$C_8$	$C_{10}$
1	3.24643	1.35186					
2	4.47792	1.53718	0.150634				
3	5.70416	1.63175	0.246777	0.0171687			
4	6.85188	1.68351	0.297581	0.0277011	0.00150252		
5	7.83014	1.71346	0.326768	0.0323605	0.00230793	0.888458E-4	
6	8.70728	1.73336	0.347368	0.0351692	0.00263883	0.000141231	0.419616E-5

**Table XII**

Optimal Scale Factors and Expansion Coefficients for a 20 dB Taylor Aperture Distribution,  $\bar{n} = 5$

$$\text{Taylor (20 dB, } \bar{n} = 5) \approx \sum_{n=0}^{2(N-1)} C_{2n} \psi_{2n} \left( \alpha \frac{x}{a} \right)$$

$$-.5 \leq \frac{x}{a} \leq .5$$

$N$	$\alpha$	$C_0$	$C_2$	$C_4$	$C_6$	$C_8$	$C_{10}$
1	3.20328	1.33436					
2	4.41749	1.51710	0.148812				
3	5.62642	1.61036	0.243454	0.0170551			
4	6.73988	1.66084	0.292746	0.0272527	0.00148214		
5	7.77625	1.69252	0.323538	0.0321304	0.00228508	0.997966E-4	
6	8.67515	1.71257	0.344231	0.0351068	0.00255485	0.000149593	0.480573E-5

**Table XIII**

Optimal Scale Factors and Expansion Coefficients for a 20 dB Taylor Aperture Distribution,  $\bar{n} = 6$

$$\text{Taylor (20 dB, } \bar{n} = 6) \approx \sum_{n=0}^{2(N-1)} C_{2n} \psi_{2n} \left( \alpha \frac{x}{a} \right)$$

$$-.5 \leq \frac{x}{a} \leq .5$$

$N$	$\alpha$	$C_0$	$C_2$	$C_4$	$C_6$	$C_8$	$C_{10}$
1	3.16950	1.32058					
2	4.37033	1.50132	0.147353				
3	5.56587	1.59355	0.240857	0.0169456			
4	6.66756	1.64356	0.289524	0.0269835	0.00148326		
5	7.67081	1.67440	0.319454	0.0316636	0.00225997	0.983400E-4	
6	8.61477	1.69546	0.341259	0.347634	0.00254042	0.000147588	0.531654E-5

**Table XIV**

Optimal Scale Factors and Expansion Coefficients for a 30 dB Taylor Aperture Distribution,  $\bar{n} = 4$

$$\text{Taylor (30 db, } \bar{n} = 4) \approx \sum_{n=0}^{2(N-1)} C_{2n} \psi_{2n} \left( \alpha \frac{x}{a} \right)$$

$$-.5 \leq \frac{x}{a} \leq .5$$

$N$	$\alpha$	$C_0$	$C_2$	$C_4$	$C_6$	$C_8$	$C_{10}$
1	3.89725	1.59898					
2	4.98032	1.77732	0.120435				



**Table XVII continued**

$N$	$\alpha$	$C_0$	$C_2$	$C_4$	$C_6$	$C_8$	$C_{10}$
1	3.85167	1.58063					
2	4.92247	1.75694	0.119165				
3	5.93053	1.86440	0.209080	0.00934999			
4	6.89738	1.93472	0.274287	0.0181001	0.000666218		
5	7.81005	1.98230	0.321436	0.0251086	0.00126338	0.399979E-4	
6	8.66439	2.01567	0.356151	0.0306838	0.00173583	0.727402E-4	0.199517E-4

**Table XVIII**

Optimal Scale Factors and Expansion Coefficients for a 40 dB Taylor Aperture Distribution,  $\bar{n} = 6$

$$\text{Taylor (40 dB, } \bar{n} = 6) \approx \sum_{n=0}^{2(N-1)} C_{2n} \psi_{2n} \left( \alpha \frac{x}{a} \right)$$

$$-.5 \leq \frac{x}{a} \leq .5$$

$N$	$\alpha$	$C_0$	$C_2$	$C_4$	$C_6$	$C_8$	$C_{10}$
1	4.42324	1.80130					
2	5.48114	1.98039	0.113639				
3	6.40466	2.09022	0.199133	0.00690727			
4	7.26822	2.16603	0.265248	0.0142486	0.000387537		
5	8.09110	2.22117	0.317026	0.0210627	0.000838004	0.196287E-4	
6	8.87798	2.26253	0.357924	0.0270692	0.00128680	0.421412E-4	0.882927E-6

**Table XIX**

Optimal Scale Factors and Expansion Coefficients for a 40 dB Taylor Aperture Distribution,  $\bar{n} = 7$

$$\text{Taylor (40 dB, } \bar{n} = 7) \approx \sum_{n=0}^{2(N-1)} C_{2n} \psi_{2n} \left( \alpha \frac{x}{a} \right)$$

$$-.5 \leq \frac{x}{a} \leq .5$$

$N$	$\alpha$	$C_0$	$C_2$	$C_4$	$C_6$	$C_8$	$C_{10}$
1	4.42114	1.80046					
2	5.47862	1.97948	0.113597				
3	6.40173	2.08924	0.199053	0.00690489			
4	7.26484	2.16502	0.265134	0.0142427	0.000387391		
5	8.09751	2.22014	0.316896	0.0210551	0.000837751	0.196308E-4	
6	8.87185	2.26137	0.357670	0.0270430	0.00128509	0.420704E-4	0.879622E-6

**Table XX**

Optimal Scale Factors and Expansion Coefficients for a 40 dB Taylor Aperture Distribution,  $\bar{n} = 8$

$$\text{Taylor (40 dB, } \bar{n} = 8) \approx \sum_{n=0}^{2(N-1)} C_{2n} \psi_{2n} \left( \alpha \frac{x}{a} \right)$$



Table XX continued

$$-.5 \leq \frac{x}{a} \leq .5$$

$N$	$\alpha$	$C_0$	$C_2$	$C_4$	$C_6$	$C_8$	$C_{10}$
1	4.41462	1.79462					
2	5.47078	1.97662	0.113462				
3	6.39261	2.08623	0.198799	0.00689723			
4	7.25437	2.16188	0.264773	0.0142242	0.000386945		
5	8.07561	2.21690	0.316445	0.0210251	0.000836536	0.196081E-4	
6	8.85991	2.25812	0.357211	0.0270126	0.00128386	0.420427E-4	0.453174E-5

Table XXI

Optimal Scale Factors and Expansion Coefficients for a 40 dB Taylor Aperture Distribution,  $\bar{n} = 9$

Taylor (40 dB,  $\bar{n} = 9$ )  $\approx \sum_{n=0}^{2(N-1)} C_{2n} \psi_{2n} \left( \alpha \frac{x}{a} \right)$

$$-.5 \leq \frac{x}{a} \leq .5$$

$N$	$\alpha$	$C_0$	$C_2$	$C_4$	$C_6$	$C_8$	$C_{10}$
1	4.40656	1.79459					
2	5.46106	1.97309	0.113291				
3	6.38130	2.08250	0.198479	0.00688741			
4	7.24141	2.15799	0.264324	0.0142011	0.000386380		
5	8.06099	2.21290	0.315890	0.0209886	0.000835078	0.195815E-4	
6	8.84352	2.25402	0.356565	0.0269630	0.00128139	0.419615E-4	0.879807E-6

Laguerre-Gaussian Field Expansions

Laguerre-Gaussian field expansions apply to circular antennas. As before, normalized coordinates are used, while maintaining previous notation. Circularly-symmetric antennas are considered, resulting in a one-dimensional, radially-dependent, aperture distribution.

Coordinates are as follows:

Normalized Aperture Coordinates

$$\rho \rightarrow \frac{\rho}{d}, (\rho, \phi') \rightarrow (\rho)$$

Field Coordinates

$$(r, \theta, \phi)$$

Laguerre Polynomials

*Rodrique's Formula*

$$L_n(\rho) = \exp(\rho) \frac{d^n}{d\rho^n} [\rho^n \exp(-\rho)]$$

*Laguerre Polynomials*

$$L_0(\rho) = 1$$

$$L_1(\rho) = -\rho + 1$$

*Recurrence Formulas*

$$L_2(\rho) = \rho^2 - 4\rho + 2$$

$$L_3(\rho) = -\rho^3 + 9\rho^2 - 18\rho + 6$$

.

.

.

$$L_{n+1}(\rho) = (2n + 1 - \rho)L_n(\rho) + n^2 L_{n-1}(\rho)$$

$$L'_n(\rho) = nL'_{n-1}(\rho) - nL_{n-1}(\rho)$$

$$\rho L'_n(\rho) = nL_n(\rho) - n^2 L_{n-1}(\rho)$$

*Orthogonality*

$$\int_0^\infty \exp(-\rho) L_m(\rho) L_n(\rho) d\rho = 0 \quad m \neq n$$

$$\int_0^\infty \exp(-\rho) [L_n(\rho)]^2 d\rho = (n!)^2$$

*Orthogonal Series*

$$f(\rho) = C_0 L_0(\rho) + C_1 L_1(\rho) + C_2 L_2(\rho) + \dots$$

*Coefficients*

$$C_n = \frac{1}{(n!)^2} \int_0^\infty \exp(-\rho) f(\rho) L_n(\rho) d\rho$$

*Orthogonal Series*

$$F(\rho) = C_0 L_0(\rho^2) \exp(\rho^2/2) + C_1 L_1(\rho^2) \exp(\rho^2/2) + C_2 L_2(\rho^2) \exp(\rho^2/2) + \dots$$

$$F(\rho) = f(\rho^2) \exp(\rho^2/2)$$

*Coefficients*

$$C_n = \frac{2}{(n!)^2} \int_0^\infty \rho F(\rho) \exp\left(-\frac{\rho^2}{2}\right) L_n(\rho^2) d\rho$$

*Field Expansions**Laguerre-Gaussian Function*

$$\psi(\rho) = L_n(\rho^2) \exp\left(-\frac{\rho^2}{2}\right)$$

*Scaling Factor*

$$\alpha$$

*Aperture Field Expansion*

$$f(\rho) = \sum_{n=0}^{\infty} C_n \psi(\alpha \rho)$$

*Expansion Coefficients*

$$C_n = \frac{2\alpha}{(n!)^2} \int_0^{1/2} \rho f(\rho) \exp\left(-\frac{\alpha^2 \rho^2}{2}\right) L_n(\alpha^2 \rho^2) d\rho$$

*Field Variable*

$$u = k \sin\theta$$

*Near-Field*

$$E(r, u) = j C_n \frac{k a^2 \exp(-j k r)}{2 r} (1 + \cos\theta) \times \int_0^\infty L_n(\alpha^2 \rho^2) \exp\left(-\frac{\alpha^2 \rho^2 \Omega^2}{2}\right) J_0(\rho u) \rho d\rho$$

*Field Parameter*

$$\Omega = \left(1 + j \frac{k d^2}{\alpha^2 r}\right)$$

*Hankel Transform*

$$L_n(\alpha^2 \rho^2) \exp\left(-\frac{\alpha^2 \rho^2 \Omega^2}{2}\right) \xleftrightarrow{h} \frac{(1 - 2\Omega^2)^n}{\alpha^2 \Omega^2} \times \exp\left(-\frac{u^2}{2\alpha^2 \Omega^2}\right) L_n\left[\frac{u^2}{\alpha^2 \Omega^2 (2 - \Omega^2)}\right]$$

*Near-field Expansion*

$$E(r, u) = j \frac{k}{2r} \left(\frac{d}{\alpha \Omega}\right)^2 (1 + \cos\theta) \exp(-j k r)$$

$$\times \sum_{n=0}^{\infty} C_n (1 - 2\Omega^{-2}) L_n \left[ \frac{u^2}{\alpha^2 \Omega^2 (2 - \Omega^2)} \right] \exp \left( -\frac{u^2}{2\alpha^2 \Omega^2} \right)$$

### Far-field Expansion

$$E(r, u) = j \frac{k}{2r} \left( \frac{d}{\alpha} \right)^2 (1 + \cos \theta) \exp(-jkr) \\ \times \sum_{n=0}^{\infty} (-1)^n C_n L_n \left( \frac{u^2}{\alpha^2} \right) \exp \left( -\frac{u^2}{2\alpha^2} \right)$$

### Gaussian Equivalent Circular Antenna ( $\chi = kd^2/\alpha^2 r$ )

$$E(r, u) = \frac{k}{r} \left( \frac{d}{\alpha} \right)^2 (1 + \chi^2)^{-1/2} \exp \left[ -\frac{u^2}{2\alpha^2 (1 + \chi^2)} \right]$$

### Tables

Tables XXII through XXVII (from Elkins, Bogush, and Jordan) contain optimal scaling factors and series coefficients for circular, truncated-Gaussian, and cosine aperture distributions. The truncated-Gaussian distributions of Tables XXII through XXIV are defined as

$$\exp \left[ -1.3868 \left( \frac{d}{d_3} \right)^2 \left( \frac{r}{d} \right)^2 \right], \quad \left( \frac{d}{d_3} \right) = 1, 2, 3.$$

Tables XXV, XXVI, and XXVII contain cosine aperture distributions:

$$\cos^n \left( \pi \frac{r}{d} \right), \quad n = 0, 1, 2$$

The uniform circular aperture is represented when  $n = 0$ .

**Table XXII**  
Optimal Scales and Laguerre-Gaussian Coefficients for Truncated Gaussian  
Distributed Antennas,  $d/d_3 = 1$

$N$	$\alpha$	$C_0$	$C_1$	$C_2$	$C_3$	$C_4$	$C_5$
1	3.3197	1.31295					
2	4.85114	1.72238	-0.966412				
3	6.08282	1.84765	-1.47062	0.833163			
4	7.13868	1.89449	-1.66959	1.34021	-0.753976		
5	8.07646	1.91806	-1.75531	1.56652	-1.25409	0.698876	

Table XXII continued

6	8.92816	1.93268	-1.80143	1.66881	-1.49595	1.10934	-0.657113
---	---------	---------	----------	---------	----------	---------	-----------

$\exp[-1.3868\ u(d/d_3)^2] \approx \sum_{n=0}^N C_n \psi_n(\alpha x) 0 \leq u \leq 0.5$

Table XXIII  
Optimal Scales and Laguerre-Gaussian Coefficients for Truncated Gaussian  
Distributed Antennas,  $d/d_3 = 2$

$N$	$\alpha$	$C_0$	$C_1$	$C_2$	$C_3$	$C_4$	$C_5$
1	3.87222	1.10540					
2	5.13618	1.39490	-0.483167				
3	6.27677	1.55773	-0.845231	0.364278			
4	7.28666	1.65380	-1.07494	0.662798	-0.310716		
5	8.19666	1.71646	-1.22829	0.848127	-0.571338	0.278698	
6	9.0297	1.76040	-1.33840	1.01474	-0.754827	0.515475	-0.256559

$\exp[-1.3868\ u(d/d_3)^2] \approx \sum_{n=0}^N C_n \phi_n(\alpha u) 0 \leq u \leq 0.5$

Table XXIV  
Optimal Scales and Laguerre-Gaussian Coefficients for Truncated Gaussian  
Distributed Antennas,  $d/d_3 = 3$

$N$	$\alpha$	$C_0$	$C_1$	$C_2$	$C_3$	$C_4$	$C_5$
1	5.05448	1.00977					
2	5.7449	1.13793	-0.151141				
3	6.67361	1.28145	-0.358565	0.899841			
4	7.58068	1.39428	-0.549136	0.212399	-0.0696124		
5	8.43051	1.48008	-0.710513	0.339901	-0.157382	0.0593339	
6	9.22414	1.54629	-0.844765	0.461228	-0.249962	0.129534	-0.0527475

$\exp[-1.3868\ u(d/d_3)^2] \approx \sum_{n=0}^N C_n \phi_n(\alpha u) 0 \leq u \leq 0.5$

Table XXV  
Optimal Scales and Laguerre-Gaussian Coefficients for  
Cosine Distributed Antennas,  $\cos^0$  (Uniform Distribution)

$N$	$\alpha$	$C_0$	$C_1$	$C_2$	$C_3$	$C_4$	$C_5$
1	3.1704	1.43067					
2	4.76879	1.88346	-1.22089				
3	6.02503	1.97861	-1.78437	1.09745			
4	7.09377	1.99631	-1.94956	1.70280	-1.01238		
5	8.03954	1.99940	-1.98941	1.91847	-1.63444	0.948691	
6	8.89669	1.99991	-1.99790	1.98015	-1.88724	1.57624	-0.898312

$\cos^0(\pi x) = \sum_{n=0}^N C_n \psi_n(\alpha x) 0 \leq u \leq 0.5$

**Table XXVI**  
Optimal Scales and Laguerre-Gaussian Coefficients for Cosine Distributed Antennas,  $\cos^1$

$N$	$\alpha$	$C_0$	$C_1$	$C_2$	$C_3$	$C_4$	$C_5$
1	4.27313	1.15071					
2	5.79129	1.47096	-0.556469				
3	6.99358	1.62305	-0.925454	0.362079			
4	8.02248	1.70858	-1.15613	1.668380	-0.266420		
5	8.9377	1.76281	-1.30801	0.892362	-0.520159	0.210157	
6	9.76981	1.80006	-1.41423	1.05537	-0.723616	0.424430	-0.172806

$$\cos^1(\pi x) = \sum_{n=0}^N C_n \psi_n(\alpha x) \quad 0 \leq u \leq 0.5$$

**Table XXVII**  
Optimal Scales and Laguerre-Gaussian Coefficients for Cosine Distributed Antennas,  $\cos^2$

$N$	$\alpha$	$C_0$	$C_1$	$C_2$	$C_3$	$C_4$	$C_5$
1	5.23761	1.08318					
2	6.70736	1.33906	-0.377392				
3	7.87153	1.48238	-0.657128	0.197663			
4	8.87072	1.57429	-0.860523	0.394261	-0.123506		
5	9.76132	1.63842	-1.01231	0.564481	-0.264493	0.0855266	
6	10.5729	1.68562	-1.12908	0.707062	-0.399896	0.190759	-0.0629528

$$\cos^2(\pi x) = \sum_{n=0}^N C_n \psi_n(\alpha x) \quad 0 \leq u \leq 0.5$$



## *Appendix B*

### *Statistical Data*

The theory of fractals involves statistical processes that possess *self-similar* characteristics. The probability distributions encountered are dominated by hyperbolic ones, where  $P(X > x) \propto 1/x^\alpha$ ;  $X$  is a random variable and  $x$  is its value, and the parameter  $\alpha$  is a positive exponent. We have recently found that many natural occurrences, such as clouds and rain cells, have temporal and spatial features that are realistically represented by fractal curves, which are, in turn, characterized by hyperbolically-distributed random variables. The primary intent of this appendix is to introduce the hyperbolic distribution in enough detail to support its use in the fractal model described in Chapter 8.

However, fractal formulations imply application of fractional mathematical procedures. In order to provide a basis for the use of the hyperbolic distribution, background for pursuance of fractal theory and derivations of several formulas used in a random number scheme (which will also be described), a brief review of fractional differentiation and integration is included. The fractional Riemann-Liouville integral, Weyl's derivatives, and Grunwald's formula are three prominent differentiation and integration formulas that appear in fractional and fractal formulations. Each formula will be derived from recognizable differentiation and integration formulas of integer order. Because the gamma function is prominent in the derivations, a review of its properties is provided. The discussions also include a delineation of the properties of differential operators.

A convenient method for generating sequences of hyperbolically distributed random variables needed in the fractal model is the *inverse method*. Given a hyperbolic probability density function of the form  $\alpha(x)^{-\alpha-1}$  and a distribution function of the form  $x^{-\alpha}$ , the sequence is formed from  $(1 - u)^{1/\alpha}$ , where  $u$  is a random sample taken from a uniform distribution over  $(0, 1)$ . But the defining sequence is also an integration of a function of identical form. We can appreciate that an integration of the function  $1/x^\alpha$ , with  $\alpha \neq 1$ , implies a fractional integration, but when  $\alpha = 1$ , the integration yields a logarithmic solution. In this inverse sense, random sequences with exponential, Rayleigh, and Gaussian distributions evolve,



and each distribution is prominent in the representation of certain radar target and clutter signals. Since the Weibull and log-normal distributions, also prominent in radar target analysis, are extensions of the exponential and Gaussian distributions, respectively, it follows that an integration of a function of this form can conveniently generate sequences with distributions that are hyperbolic, exponential, Gaussian, Weibull, or log-normal. Since integrations of integer order are special cases of fractional ones, the use of fractional integrations in the number-generating scheme yields sequences with distributions that are perturbations of the original ones. The resulting sequences may be of additional value in fractal models, as well as in the modeling of radar target and clutter returns. As a result, and for generality, the generation of a sequence of random numbers was formulated, based on the inverse method and a fractional integration of the function  $1/x^\alpha$ . We provide examples that demonstrate its usefulness in generating sequences of hyperbolic and other forms, for use in fractal and general radar applications.

## Fractional Differentiation and Integration

The material contained herein on fractal differentiation and integration was obtained from the reported work of Oldham and Spanier, Dold and Eckman, and Laudie, Osler, and Tremblay. The gamma function properties were assembled from a handbook of mathematical functions by Abramowitz and Stegun. We also make reference to Mandelbrot for specific examples of the use of fractional differentiations and integrations in fractal formulations.

### Differential Operators

Differential operators of integer order are recognizable as  $d/dx$ ,  $d^2/dx^2$ , *et cetera*. Since differentiation and integration are inverse operations, it follows that indefinite integration can be associated with  $d^{-1}/dx^{-1}$ ,  $d^{-2}/dx^{-2}$ , *et cetera*, where means must be provided for specifying the lower limit of integration. It also follows that non-integer or fractional operators become  $d^q/dx^q$ . Contrary to differentiation of integer order, it has been established by Laudie, *et al.*, that each fractional derivative also depends on a lower limit.

It is convenient to define a differential operator as  $D = d/dx$ . Specifying  $q$  as the order of fractional integration or differentiation, with  $x_0$  the lower limit,  $D$  is written as  $D_{x-x_0}^q$ . Given  $f(x)$ , the operation  $D_{x-x_0}^q f(x)$  yields:

1.  $f(x)$  when  $q = 0$ ;
2. an integration when  $q < 0$ ;
3. a differentiation when  $q > 0$ .

In formal treatments of fractional integration and differentiation, the parameter  $q$  is arbitrary and may be an irrational, fractional, or complex number. Of

particular interest here are real parameters and integrations.

### *The Gamma Function*

From Abramowitz and Stegun, the following Euler's formulas define:

#### 1. *Integral:*

$$\Gamma(z) = \int_0^{\infty} t^{z-1} e^{-t} dt \quad \Re(z) > 0 \quad (\text{B.1})$$

#### 2. *Euler's Formula:*

$$\Gamma(z) = \lim_{n \rightarrow \infty} \frac{n! n^z}{z(z+1) \dots (z+n)} \quad (z \neq 0, -1, -2, \dots) \quad (\text{B.2})$$

#### 3. *Infinite Product:*

$$\frac{1}{\Gamma(z)} = z e^{\gamma z} \prod_{n=1}^{\infty} \left[ \left(1 + \frac{z}{n}\right) e^{-z/n} \right] \quad (|z| < \infty) \quad (\text{B.3})$$

Generally,  $\Gamma(z)$  is an analytic function, except when  $z = 0, -1$ , or  $-2, \dots$ , where simple poles with residues  $(-1)/n!$  exist. The reciprocal  $1/\Gamma(z)$  is an entire function, having zeros at  $z = 0, -1, -2, \dots$ . The gamma function and its reciprocal are plotted in Figure B.1.

Some additional properties of the gamma function of value arise from their factorial representations. First,

$$\Gamma(z+1) = z! \quad (\text{B.4})$$

With  $n$  an integer, we have

$$\Gamma(n+1) = n! \quad (\text{B.5})$$

Two useful relationships are the recurrence formula:

$$\Gamma(z+1) = z\Gamma(z) = z! = z(z-1)! \quad (\text{B.6})$$

and the reflection formula:

$$\Gamma(z)\Gamma(1-z) = -z\Gamma(-z)\Gamma(z) = \pi \csc(\pi z) \quad (\text{B.7})$$

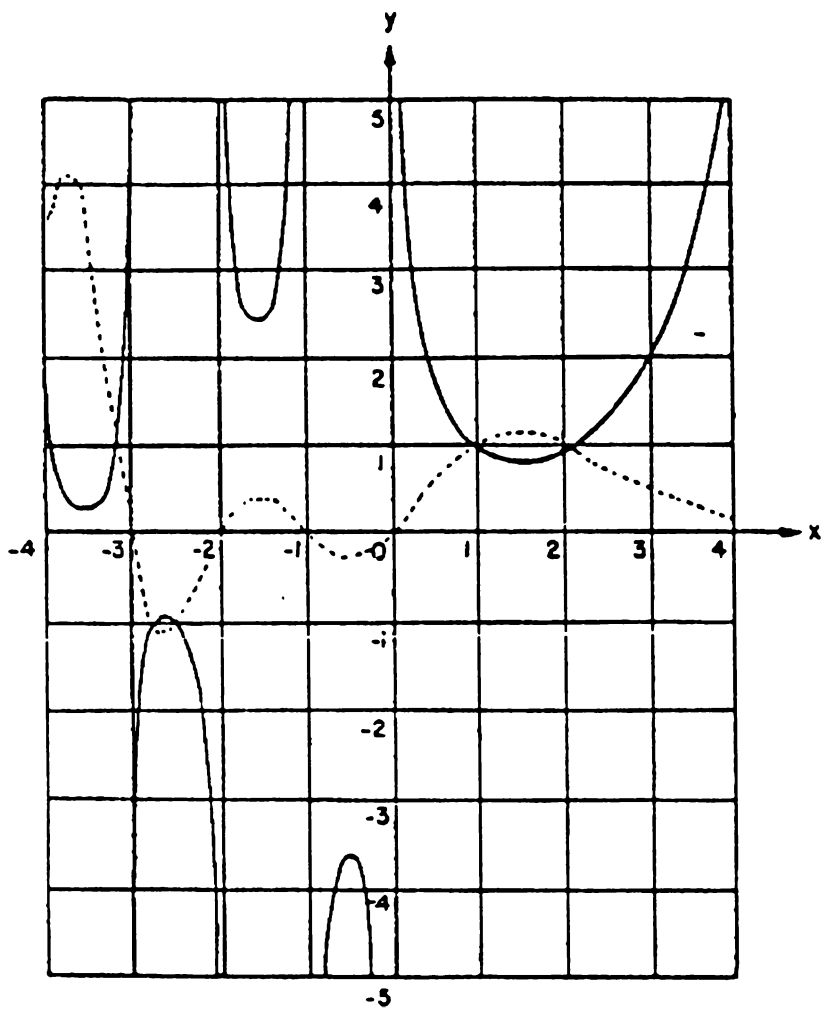


**Figure B.1** Properties of the Gamma Function and its Inverse. (From Abramwitz and Stegun)

Some useful numerical values of the gamma function are

$$\Gamma\left(\frac{1}{4}\right) = 3.6256 \tag{B.8}$$

$$\Gamma\left(\frac{1}{2}\right) = \sqrt{\pi} \tag{B.9}$$

$$\Gamma(1) = 1.0000 \tag{B.10}$$

and

$$\Gamma\left(\frac{3}{2}\right) = \sqrt{\pi/4} \quad (\text{B.11})$$

Equations (B.1) through (B.11) are formulas that will prove useful in the equation derivations that follow. Also, as we will appreciate later, fractional differentiations and integrations are not readily interpreted in a geometrical way. The properties of the gamma function given in Figure B.1 will help to remove some of the abstractness inherent in the derivations.

### *Riemann-Liouville and Weyl's Integrals*

As stated by Eckman, the introduction of the Riemann-Liouville fractional integration formula can be accomplished in a number of ways. The approach selected, although somewhat abstract, is readily understood, and involves both Leibniz's theorem for differentiating an integral and Cauchy's iterated integral, from which the Riemann-Liouville integral and Weyl fractional derivatives evolve. From Oldham and Spanier,

$$D_{x-x_0}^{-1} f = \int_{x_0}^x f(y) dy = \frac{1}{n!} \frac{d^n}{dx^n} \int_{x_0}^x [x - y]^n f(y) dy \quad (\text{B.12})$$

where  $n = 0, 1, 2, \dots$ . If we let  $n = 1$  and integrate once, we obtain

$$D_{x-x_0}^{-2} f = \int_{x_0}^x dx_1 \int_{x_0}^{x_1} f(x_0) dx_0 = \frac{1}{1!} \int_{x_0}^x [x - y] f(y) dy \quad (\text{B.13})$$

Now we let  $n = z$ , and integrate twice to obtain

$$D_{x-x_0}^{-3} f = \int_{x_0}^x dx_2 \int_{x_0}^{x_2} dx_1 \int_{x_0}^{x_1} f(x_0) dx_0 = \frac{1}{2!} \int_{x_0}^x [x - y]^2 f(y) dy \quad (\text{B.14})$$

Continuing this process  $(n - 1)$  times leads to

$$\begin{aligned} D_{x-x_0}^{-n} f &= \int_{x_0}^x dx_{n-1} \int_{x_0}^{x_{n-1}} dx_{n-2} \dots \int_{x_0}^{x_1} f(x_0) dx_0 \\ &= \frac{1}{(n-1)!} \int_{x_0}^x [x - y]^{n-1} f(y) dy \end{aligned} \quad (\text{B.15})$$

The expanded integral in Equation (B.15) is Cauchy's iterated integral. If, in the second integral,  $-n = q$  with the factorial  $(n - 1)!$  replaced by the gamma function, then

$$D_{x-x_0}^q = \frac{1}{\Gamma(-q)} \int_{x_0}^x (x-y)^{-q-1} f(y) dy \quad (\text{B.16})$$

which is the Riemann-Liouville fraction integral of order  $-q$ .

When  $x_0$  is  $\infty$  or  $-\infty$ , Equation (B. 16) becomes

$$D_{x-\infty}^q = \frac{(-1)^q}{\Gamma(-q)} \int_x^\infty (y-x)^{-q-1} f(y) dy \quad (\text{B.17})$$

and

$$D_{x+\infty}^q = \frac{1}{\Gamma(-q)} \int_{-\infty}^x (x-y)^{-q-1} f(y) dy \quad (\text{B.18})$$

which are Weyl's fractional integrals. Eckman points out and Mandelbrot demonstrates that care must be taken in their use because of restrictions on  $f(y)$ .

As an example, consider the function  $f(x) = x$ . Use of Equation (B.16) with  $x_0 = 0$  yields

$$D_x^q f = \frac{1}{\Gamma(-q)} \int_0^x \frac{y}{(x-y)^{q-1}} dy \quad (\text{B.19})$$

Changing variables,  $w = x - y$ , results in

$$D_x^q f = \frac{1}{\Gamma(-q)} \int_0^{x+y} \frac{(w-x)}{w^{q+1}} dw \quad (\text{B.20})$$

with the solution:

$$D_x^q f = \frac{x^{-q+1}}{\Gamma(2-q)} \quad (\text{B.21})$$

Note that when  $q = -n$  (a negative integer), Equation (B.21) becomes

$$D_x^{-n} f = \frac{x^{n+1}}{(n+1)!} \quad (\text{B.22})$$

the expected result. The behavior of the function  $f(x) = x$  when subjected to several fractional integrations is displayed in Figure B.2. The results show a well behaved transition of the fractional integrations between integer operations ( $q = 0, -1$ ) and the fractional ones. The fractional integration may be interpreted as

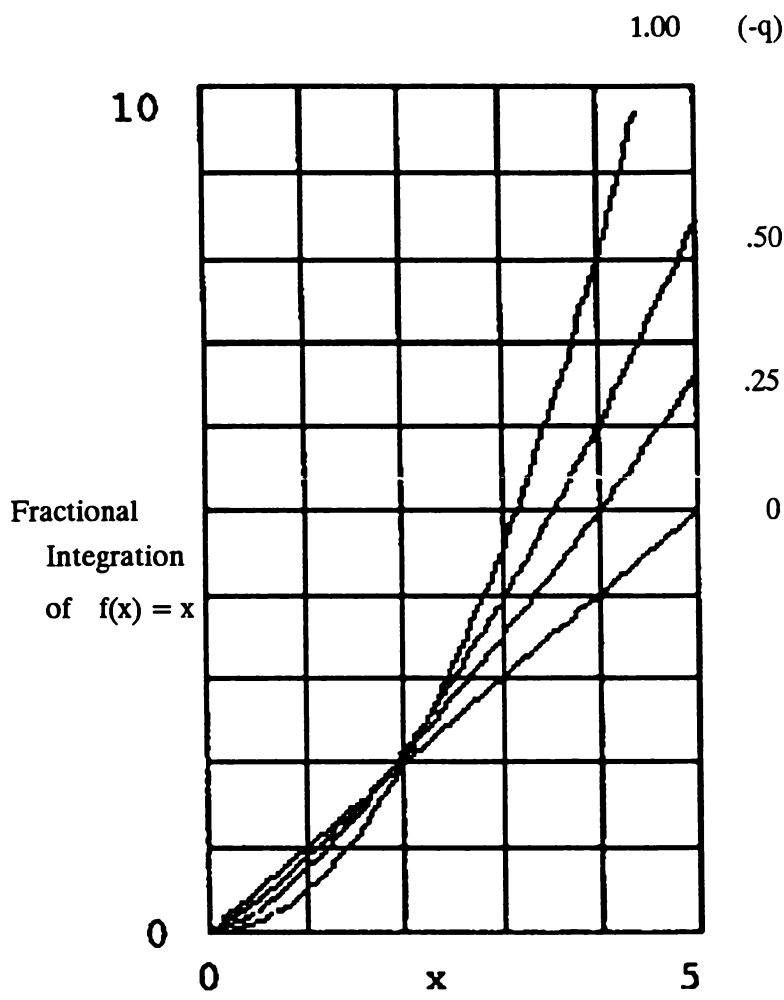


**Figure B.2** Fractional Integration of the Function  $f(x) = x$

a weighting of the single integer result by the inverse gamma function plotted in Figure B.1.

*Grunwald's Formula*

Fractional differentiation is introduced by a generalization of limits of difference quotients used to define derivatives of integer order. Fractional integration is introduced in a similar way by the generalization of the limits of a Riemann sum, which represents an indefinite integral of integer order. Both results are combined to obtain a unified, fractional differentiation and integration formula, which is credited to Grunwald. This result is especially important because it provides the basis for numerical procedures in general fractional calculus theory.

### Differentiation

If we let the starting point in the derivation of a fractional derivative be the recognized definition of a derivative of unity order, expressed as a special case of a fractional derivative of order  $q = 1$  and  $x_0 = 0$ . Then,

$$D_x^1 f = \lim_{\Delta x \rightarrow 0} \left[ \frac{f(x) - f(x - \Delta x)}{\Delta x} \right] \quad (\text{B.23})$$

Differentiating Equation (B.23) once yields

$$D_x^2 f = \lim_{\Delta x \rightarrow 0} \left[ \frac{f(x) - 2f(x - \Delta x) + f(x - 2\Delta x)}{\Delta x^2} \right] \quad (\text{B.24})$$

As we continue, repeated differentiation of Equation (B.23) leads to

$$D_x^n f = \lim_{\Delta x \rightarrow 0} (\Delta x)^{-n} \sum_{j=0}^n (-1)^j \binom{n}{j} f(x - j\Delta x) \quad (\text{B.25})$$

Now, using the identity:

$$(-1)^j \binom{n}{j} = \binom{j - n - 1}{j} \quad (\text{B.26})$$

where  $\Delta x = (x - x_0)/N$  yields the final differentiation result for derivatives of integer order, we have

$$D_{x-x_0}^n f = \lim_{\Delta x \rightarrow 0} \left( \frac{x - x_0}{N} \right)^N \sum_{j=0}^{N-1} \binom{j - n - 1}{j} f \left[ x - j \left( \frac{x - x_0}{N} \right) \right] \quad (\text{B.27})$$

because

$$\binom{j - n - 1}{j} = \frac{\Gamma(j - n)}{\Gamma(-n)\Gamma(j - 1)} \quad (\text{B.28})$$

Replacing  $n$  with  $q$  in Equation (B.27), and substituting (B.28) into (B.27), yields the final differentiation result for derivatives of fractional and integer order:

$$D_{x-x_0}^q f = \lim_{\Delta x \rightarrow 0} \left( \frac{x - x_0}{N} \right)^q \frac{1}{\Gamma(-q)} \sum_{j=0}^{N-1} \frac{\Gamma(j - q)}{\Gamma(j + 1)} \left[ f \left[ x - j \left( \frac{x - x_0}{N} \right) \right] \right] \quad (\text{B.29})$$

## INTEGRATION

Proceeding as before, consider the integration of unity order:

$$D_{x-x_0}^{-1} f = \int_{x_0}^x f(y) dy \quad (\text{B.30})$$

as a limit of a Riemann sum. Then,

$$D_{x-x_0}^{-1} f = \lim_{\Delta x \rightarrow 0} \left( \frac{x-x_0}{N} \right) \sum_{j=0}^{N-1} (j+1) f \left[ x - j \left( \frac{x-x_0}{N} \right) \right] \quad (\text{B.31})$$

The use of Cauchy's iterated integral, Equation (B.15), for higher orders of integration leads to

$$D_{x-x_0}^{-n} f = \lim_{N \rightarrow \infty} \left( \frac{x-x_0}{N} \right)^n \sum_{j=0}^{N-1} \binom{j+n-1}{j} f \left[ x - j \left( \frac{x-x_0}{N} \right) \right] \quad (\text{B.32})$$

Now we let  $n$  be replaced by  $-q$ . Substituting Equation (B.28) into (B.32) yields

$$D_{x-x_0}^q f = \lim_{N \rightarrow \infty} \left( \frac{x-x_0}{N} \right) \frac{1}{\Gamma(q)} \sum_{j=0}^{N-1} \frac{\Gamma(j+q)}{\Gamma(j+1)} f \left[ x - j \left( \frac{x-x_0}{N} \right) \right] \quad (\text{B.33})$$

which is equivalent to the fractional differentiation result when  $q$  is negative.

## GRUNWALD'S FORMULA

The result in Equation (B.33) is Grunwald's result, which yields a compact differentiation and integration formula. Grunwald's formula can be placed in a more useful form using a gamma function recursion relationship. For  $x_0 = 0$ , Equation (B.33) can be placed in the form:

$$D_x^q f = \frac{N^q}{x^q} \left[ \left[ \left[ \left[ \left[ f_{N-1} \binom{N-q-2}{N-1} + f_{N-2} \right] \left( \frac{N-q-3}{N-2} \right) + f_{N-3} \right] \left( \frac{1-q}{2} \right) + f_1 \right] \left( \frac{-q}{1} \right) + f_0 \right] \right] \quad (\text{B.34})$$

As we can see, the direct use of gamma functions is avoided, thus leading to a simplified result convenient for numerical analysis. It represents a good first



estimate of fractional differentiations and integrations in a single formula. Further discussion of its derivation and extension to other fractional numerical procedures are described by Oldham and Lavoie.

## OBSERVATIONS

We now make several observations:

1. Integrations and differentiations of integer order are special cases of fractional ones.
2. Fractional integrations and differentiations can be performed by using a single (Grunwald's) formula.
3. While factorials appear in the integer order operations, the gamma function appears in the more general fractional ones.

The Riemann-Liouville and Weyl's formulas appear in fractal derivations, and are fundamental to the theory of fractional calculus.

## The Hyperbolic Distribution

Several forms of the hyperbolic probability distribution are described. The discussions include some definitions.

### Definitions

It is convenient to define the following parameters:

- $X$  = random variable;
- $x$  = value of random variable;
- $F(x)$  = cumulative probability distribution function =  $P(X \leq x)$ ;
- $G(x)$  = probability distribution function =  $P(X > x)$ ;  
=  $1 - P(X \leq x)$ ;
- $f(x)$  = Probability density function;
- $u$  = Random sample taken from a uniform distribution over  $(0, 1)$ .

The following identities are also cited without specific reference:

$$\int x^n dx = \frac{x^{n+1}}{n+1} \quad (\text{B.35})$$

$$\int x^{-n} dx = \frac{x^{n+1}}{-n+1} \quad (n \neq 1) \quad (\text{B.36})$$

and

$$\int \frac{dx}{x} = \ln x \quad (n = 1) \quad (\text{B.37})$$

Additional definitions will be provided as needed.

### *The Hyperbolic Distribution*

The hyperbolic probability distribution appears in several forms. The form introduced by Pareto and described by Sussman will be adopted.

$$G(x) = \begin{cases} 1 & , \quad x < \delta \\ \left(\frac{\delta}{x}\right)^\alpha & , \quad x \geq \delta \end{cases} \quad (\text{B.38})$$

When plotted on log-log graph paper, a straight line results because,

$$\log\left(\frac{\delta}{x}\right)^\alpha = -\alpha \log x + \alpha \log \delta \quad (\text{B.39})$$

The parameter  $\alpha$  is the slope of the straight line. In other formulations,  $\alpha$  is defined as the order of the hyperbolic distributions. In fractal formulations,  $\alpha$  is related to a fractal dimension.

### ***EXAMPLE: ANOTHER FORM OF THE HYPERBOLIC PROBABILITY DISTRIBUTION***

Mertze expresses the hyperbolic distribution in the following way:

$$f(x) = \frac{nh^n}{(x + h)^{n+1}}, \quad \begin{cases} h > 0 \\ x \geq 0 \end{cases}$$

where it is readily verified that

$$\int_0^\infty f(x) dx = \int_0^\infty \frac{nh^n}{(x + h)^{n+1}} dx = \frac{nh^n}{nh^n} = 1$$

Then the mean is

$$\bar{x} = nh^n \int_0^\infty \frac{x}{(x+h)^{n+1}} dx = \frac{h}{(n-1)}$$

with variance:

$$\sigma^2 = \frac{2h^2}{(n-1)(n-2)}$$

and standard deviation:

$$\sigma = h \sqrt{\frac{2}{(n-1)(n-2)}}$$

Mertze points out that  $\bar{x}$  is finite when  $n > 1$  and  $\sigma$  is finite when  $n > 2$ . The probability density function is

$$f(x) = \alpha \left( \frac{\delta}{x} \right)^{\alpha+1}, \quad (x \geq 1) \quad (\text{B.40})$$

Note that

$$\int_0^\infty f(x) dx = \int_0^\infty \alpha \left( \frac{\delta}{x} \right) dx = 1.0 \quad (\text{B.41})$$

which is the required result. When  $\delta = 1$ , the probability distribution is

$$G(x) = \left( \frac{1}{x} \right)^\alpha \quad (\text{B.42})$$

for  $x \geq 1$  with  $G(x) = 1.0$  for  $x < 1$ . Plots of the hyperbolic distribution function are provided in Figure B.3.

### *Exponential-Hyperbolic Distribution*

The singularity of the function  $(1/x)^\alpha$  when  $x = 0$  can be removed by the introduction of an exponential function into the probability distribution in a way where a hyperbolic distribution is dominant for large  $x$  with the exponential function dominating when  $x$  is small. We suggest a probability distribution of the form:

$$\lim_{x \rightarrow \infty} G(X > x) = \frac{1}{x^\alpha} \quad (\text{B.43})$$

and

$$\lim_{x \rightarrow 0} G(X > x) = 1 \quad (\text{B.44})$$

Let us first consider the exponential  $\exp(-x^\alpha)$ , then let the following distribution function be introduced:

$$G(x) = P(X > x) = \frac{1 - \exp(-x^\alpha)}{x^\alpha} \quad (\text{B.45})$$

It is readily verified that Equation (B.45) satisfies the conditions of Equations (B.43) and (B.44). By expanding  $\exp(-x^\alpha)$  in Equation (B.45), then differentiating and rearranging terms, the probability density function  $f(x)$  is derived:

$$f(x) = \frac{\alpha}{x^{\alpha+1}} [(1 + x^\alpha) \exp(-x^\alpha) - 1] \quad (\text{B.46})$$

The term outside the bracket is recognized as the hyperbolic probability density function. The terms within the bracket are interpreted as an exponential weighting function. Then,

$$F(x) = \left(1 - \frac{1}{x^\alpha}\right) + \frac{\exp(-x^\alpha)}{x^\alpha} \quad (\text{B.47})$$

which is the cumulative hyperbolic probability distribution function perturbed by an exponential factor  $e^{-x^\alpha}/x^\alpha$ . The distribution function, Equation (B.44), is plotted in Figure B.4 for several values of the parameter  $\alpha$ . The exponential behavior for small  $x$  can be noted, as can the hyperbolic behavior evident for large  $x$ .

## A Random Number Generator

The algorithm we will describe serves its initial purpose for use in the fractal models. However, through the application of fractional integration, another parameter, in addition to those characterizing the probability distribution, is introduced. The distributions of interest are the hyperbolic, exponential, Rayleigh, Gaussian, Weibull, and the log-normal. The resulting sequences are generally applicable in the area of fractal modeling and the analysis of radar target and clutter returns.

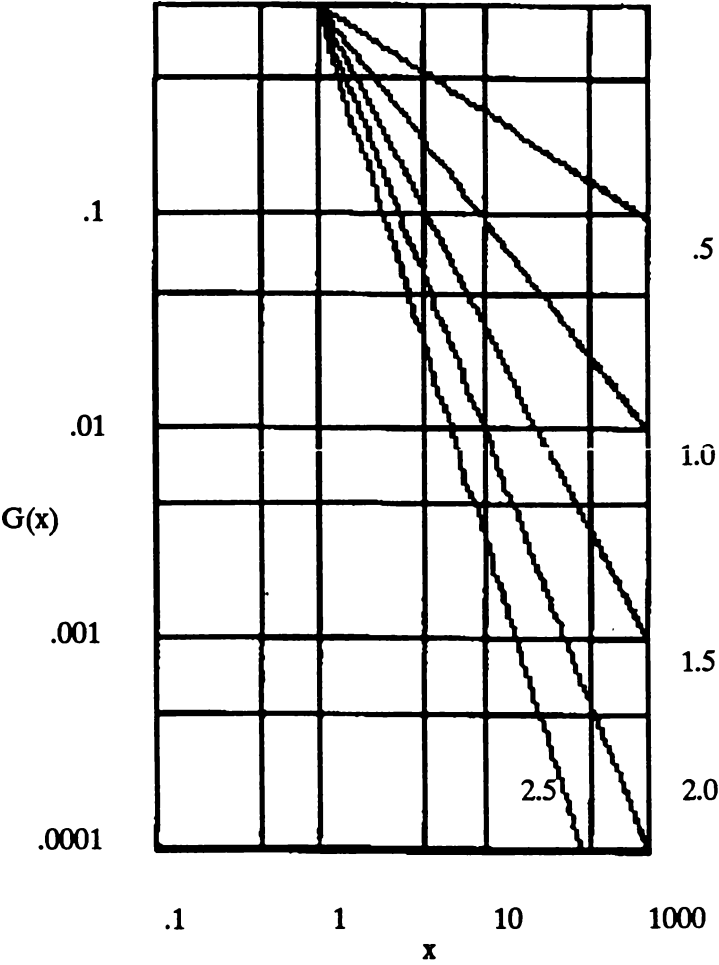


**Figure B.3** Hyperbolic Distribution of Order  $\alpha$

*Two Parameter Hyperbolic Distributions*

A random sequence with parameters  $\alpha$ , the order of the hyperbolic distribution, and additional parameter  $q$  are developed. Random samples  $X$ , with hyperbolically-distributed  $x$  are readily obtained using the inverse method. Reviewing briefly, we let  $u = F(x)$  for a given value of  $u$ , then write  $X$  as  $X = F^{-u}(u)$ . Then, from Equation (B.41) and considering definitions of  $F(x)$  and  $G(x)$ , we have:

$$X = \frac{1}{(1 - u)^{1/\alpha}} \tag{B.48}$$

where again,  $0 < u < 1$ ,  $0$ , a random sample taken from a uniform distribution. Equation (B.48) can be used directly for the generation of random sequences that

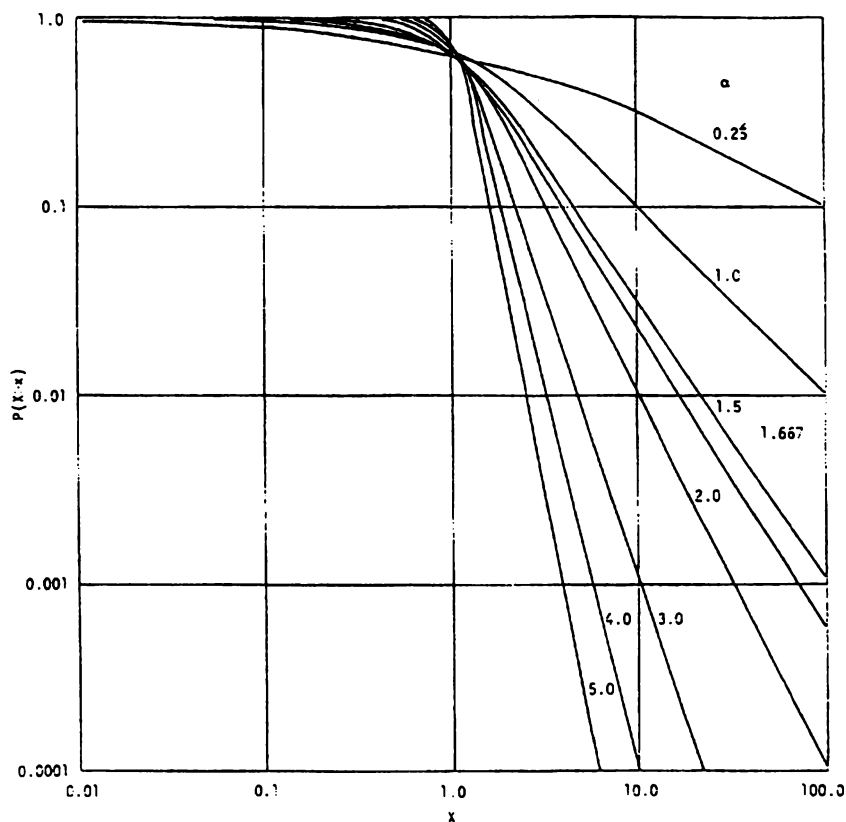


**Figure B.4** Exponential-Hyperbolic Distribution of Order  $\alpha$

are hyperbolically distributed. We now consider the result of Equation (B.48) first as the integral

$$X = \frac{1}{(1-u)^{1/\alpha}} = -\frac{1}{\alpha} \int_u^{\infty} \frac{d\zeta}{(1-\zeta)^{1/\alpha+1}} \quad (\text{B.49})$$

Then we introduce  $X$  in the form of a general Weyl integral:

$$X = \frac{1}{\alpha \Gamma(q)} \int_{1-u}^{\infty} \frac{(y-u)^{q-1}}{y^{1/\alpha+1}} dy \quad (\text{B.50})$$

The solution is

$$X = \frac{\Gamma(1/\alpha + 1 - q)}{\alpha \Gamma(1/\alpha + 1)} (1-u)^{q-1/\alpha-1} \quad 0 < q < 1/\alpha + 1 \quad (\text{B.51})$$

which is considered to be a generalization of Equation (B.48). By letting  $q = -1$  and using the recurrence relationship  $\Gamma(x + 1) = x \Gamma(x)$ , we obtain  $X = (1 - u)^{-1/\alpha}$ , which is equation (B.48)

*Exponential, Rayleigh, and Gaussian Distributions in Fractional Form*

Referring to Equation (B.49), because  $\alpha > 0$ ,  $(1/\alpha + 1) > 1$ , we consider the special case  $(1/\alpha + 1) \rightarrow 1$ . Since a logarithmic solution of the integral is expected, we consider:

$$-\ln(u) = \int_0^{1-u} \frac{dx}{1-x} \tag{B.52}$$

where the following can be noted:

1.  $X = -\ln(u)$  yields a random sequence that is exponentially distributed;
2.  $X = \sqrt{-\ln(y)}$  yields a random sequence that is Rayleigh distributed;
3. With  $\theta$  a random number, uniformly distributed between 0 and  $2\pi$ , two independent Gaussian random sequences can be obtained from  $x = \sqrt{-\ln u}(\cos\theta)$  and  $y = \sqrt{-\ln u}(\sin\theta)$ . The resulting Gaussian samples are of zero mean with a variance of 1/2.

Now we let the integral in Equation (B.48) be written in fractional form; then, applying the Riemann-Liouville integral yields

$$X = D_{1-u}^q \left( \frac{1}{1-y} \right) = \frac{1}{\Gamma(-q)} \int_0^{1-u} \frac{(1-u-y)^{-q-1}}{(1-y)} dy \tag{B.53}$$

The solution of Equation (B.50) can be obtained using Grunwald's formula.

Because  $\Gamma(1) = 1$ , Equation (B.53) reduces to Equation (B.52) when  $q = -1$ . When  $q \neq -1$  but  $q < 0$ , the resulting sequences, obtained following the procedure indicated below Equation (B.52), are referred to as fractional, exponential Rayleigh and Gaussian sequences. They are generated from a fractional integration of the function  $1/x$  and perturb the distribution about the integer value of  $q = -1$ .

Figures B.5 and B.6 contain plots of  $1/x$ ,  $\ln x$ ,  $1/(1-x)$ , and  $\ln(1-x)$ . Fractional integrations of  $(1/x)$  for  $-2.5 < q < 0$  are plotted in Figure B.5. In each instance, the fractional integration can be interpreted as a weighting function that yields solutions approaching  $1/x$  as  $q \rightarrow 0$ , and zero as  $q \rightarrow -\infty$  (except at  $x = 0$ ). In an inverse probabilistic sense, the plots in Figure B.5 indicate the difference in the character of the sequences expected when the variable  $x$  is replaced by  $u$ , (a random number from a uniform distribution). In particular, when  $q = -1$ , a sequence of exponentially-distributed numbers results. Deviations from the

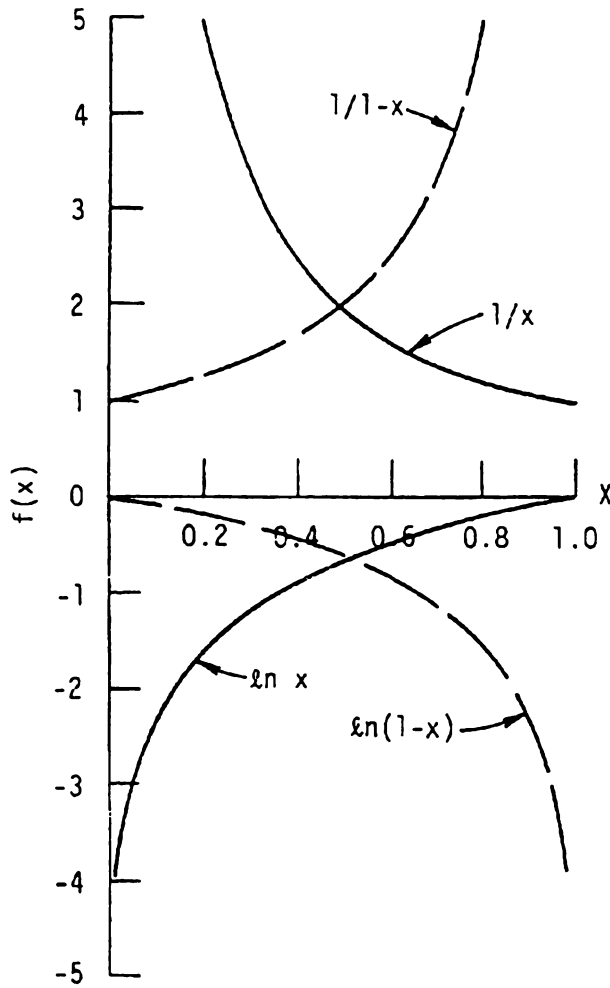


**Figure B.5** Plots of  $x$ ,  $1-x$ ,  $\ln x$ ,  $\ln(1-x)$ , for  $0 < x < 1$

expected exponential sequence can be inferred from the curves as the fractional order of integration  $q$  is varied above and below the nominal value of  $-1$ .

### *Weibull and Log-Normal Distributions*

Given a sequence of random numbers that are exponentially distributed and generated by the inverse function  $\ln(1/(1-u))$ , a Weibull sequence with parameter  $(K, a)$  results when  $\ln(1/(1-u))$  is replaced by  $K^a[\ln(1/(1-u))]^a$ . Similarly, given a Gaussian sequence, a log-normal sequence is formed when the random number  $g$  is replaced by  $\exp(g\sigma_L - C\sigma_L)$ , where  $(\sigma_L, C)$  are parameters of a log-normal distribution. The probability density functions for the Weibull and log-normal distributions are



$$f(x) = \frac{1}{\sqrt{2\pi} \sigma} \exp\left(-\frac{x^b}{\alpha}\right) \quad (\text{B.54})$$

and with  $\ln x$  a normal distribution, and  $r$  the standard deviation of  $\ln x$ ,

$$f(x) = \frac{1}{(2\pi r^2)^{1/2}} \exp\{-[\ln(x/\bar{x})]^2/2r^2\} \quad (\text{B.55})$$

respectively.

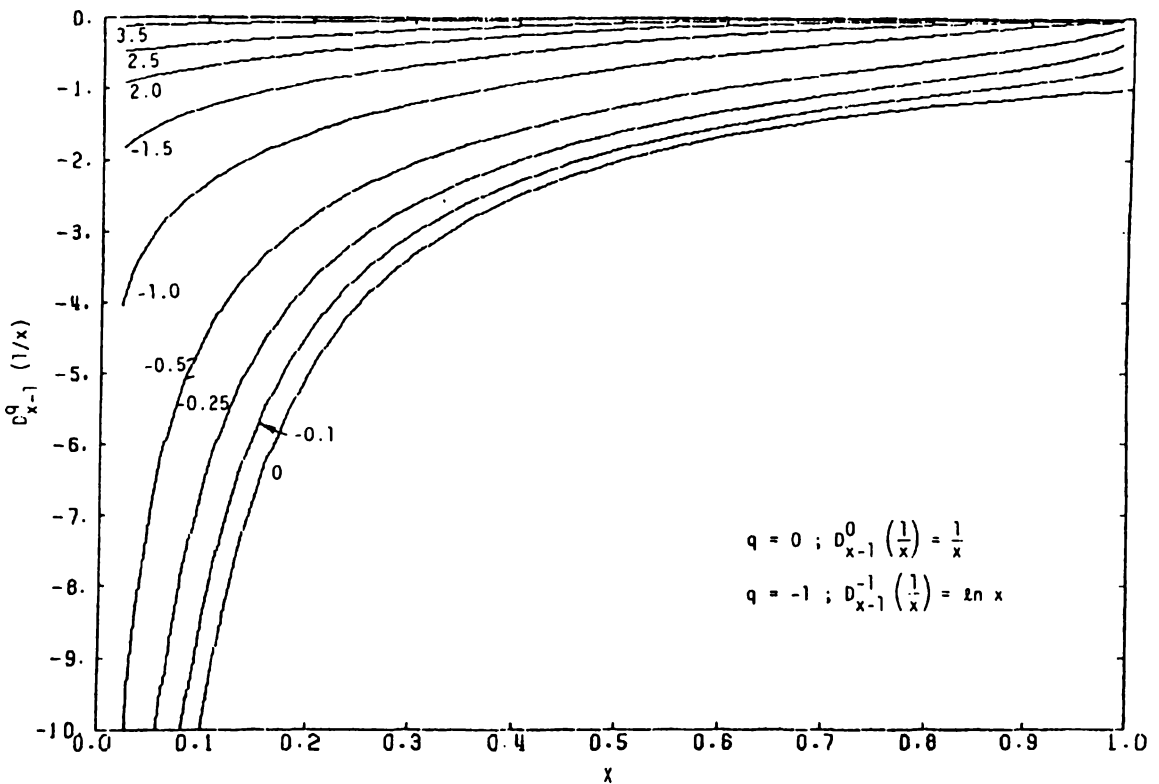


**Figure B.6** Fractional Integration of the Function  $1/x$

### Algorithm

A methodology for the generation of random sequences using the inverse method and fractional integrations is provided in Figure B.7. Sequences are generated by a fractional integration of  $1/x^\alpha$ . In this formulation, a random sequence with an exponential distribution is obtained by setting  $\alpha = 1$  and  $q = -1$ . Perturbations of this sequence occur when  $\alpha \neq 1$  and  $q \neq -1$ . The Riemann-Liouville integration of  $1/x$  yields  $\ln x$ , as expected. Similarly, the gamma function solution of the Weyl

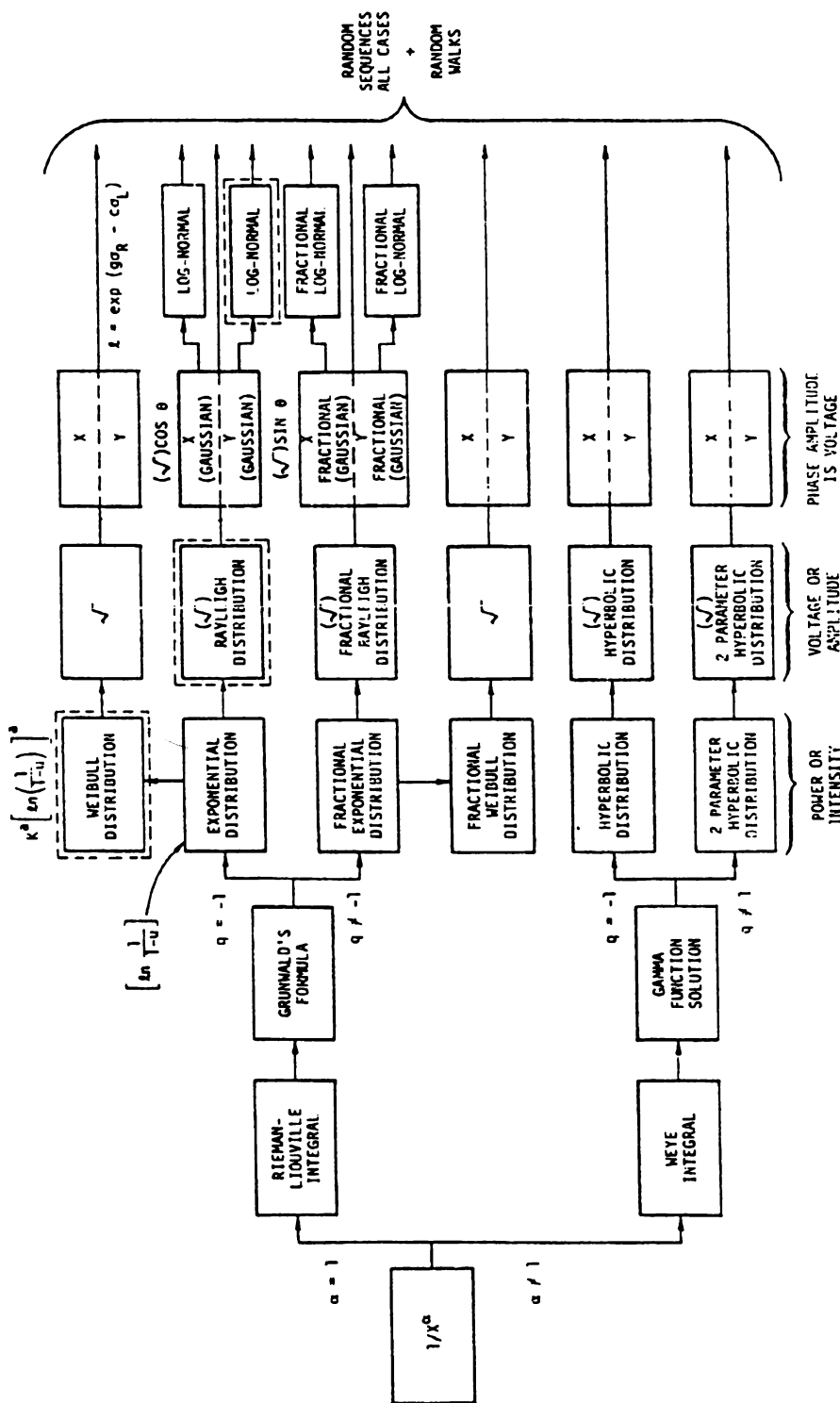


**Figure B.7** A Methodology for the Generation of Random Sequences from Fractional Integrations of  $1/x^\alpha$

integral yields  $1/1 - u^{1/\alpha}$ , which is the generating sequence for the hyperbolic distribution  $1/x^\alpha$ .

Perturbations of the hyperbolic distribution may be obtained by changes in the fractional order of integrations about  $q = -1$ . Considering the elementary function  $1/x$ , its integration in logarithmic form, and the representation of exponential functions in the distributions, extension to other distributions may be possible.

Figures B.8 through B.12 provide examples of perturbed Rayleigh sequences obtained from the Riemann-Liouville integrations; Probability density functions are also provided. Results of this type for Rayleigh and the other distributions included in this methodology should be of value in the general area of radar target and statistical clutter evaluations.

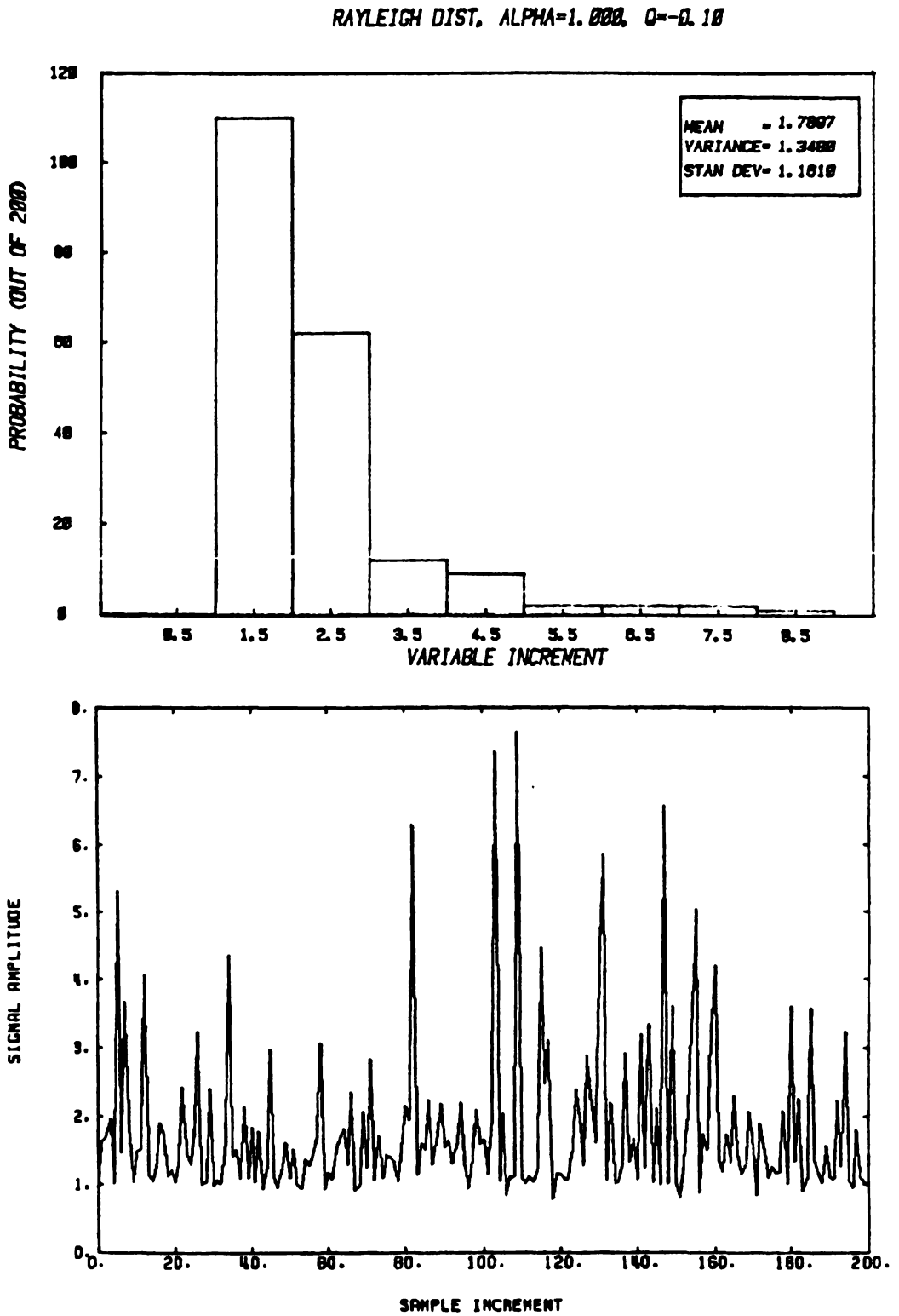


Figure B.8 Perturbed Rayleigh Distribution and Sequence,  $q = -0.10$

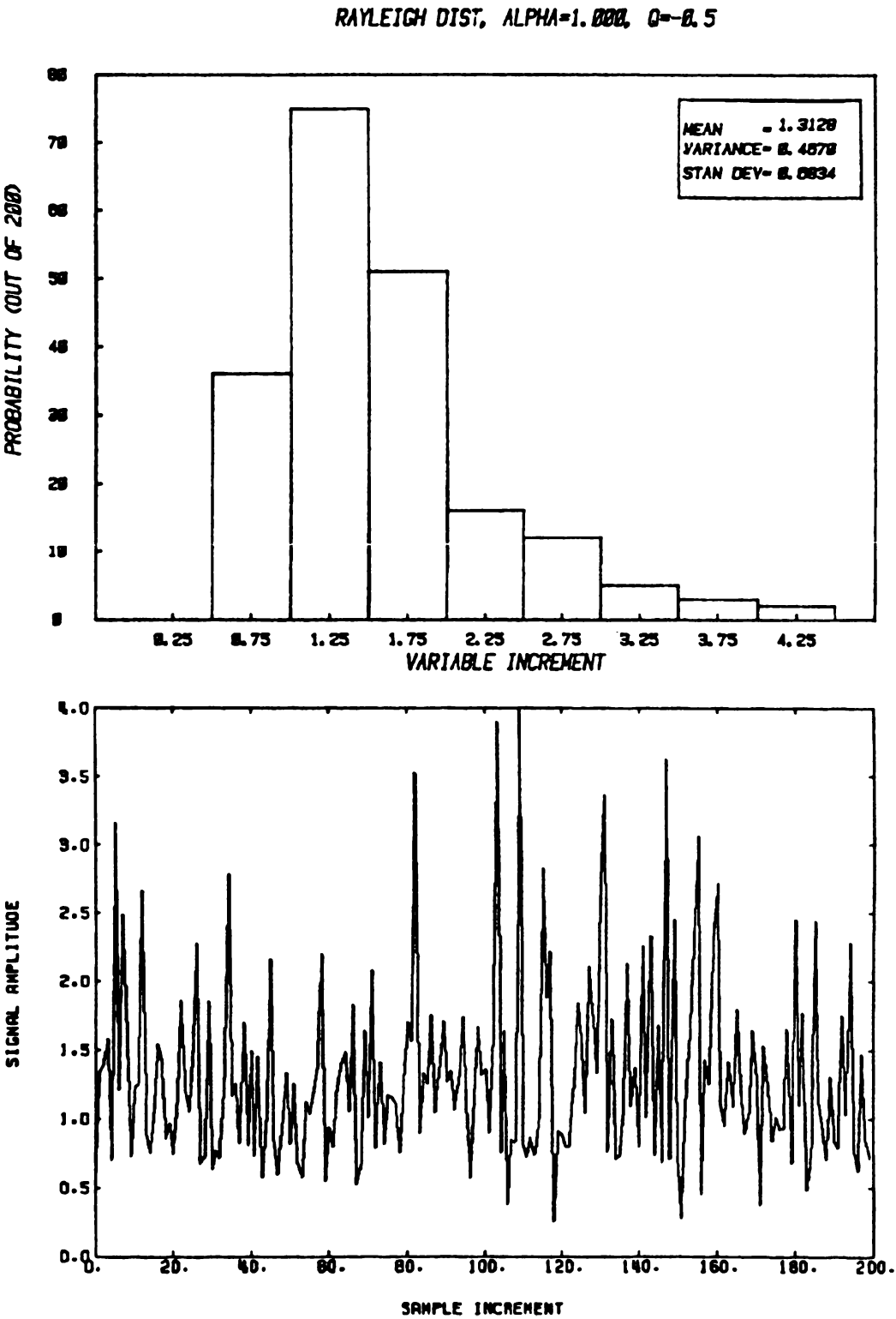


Figure B.9 Perturbed Rayleigh Distribution and Sequence,  $q = -0.50$

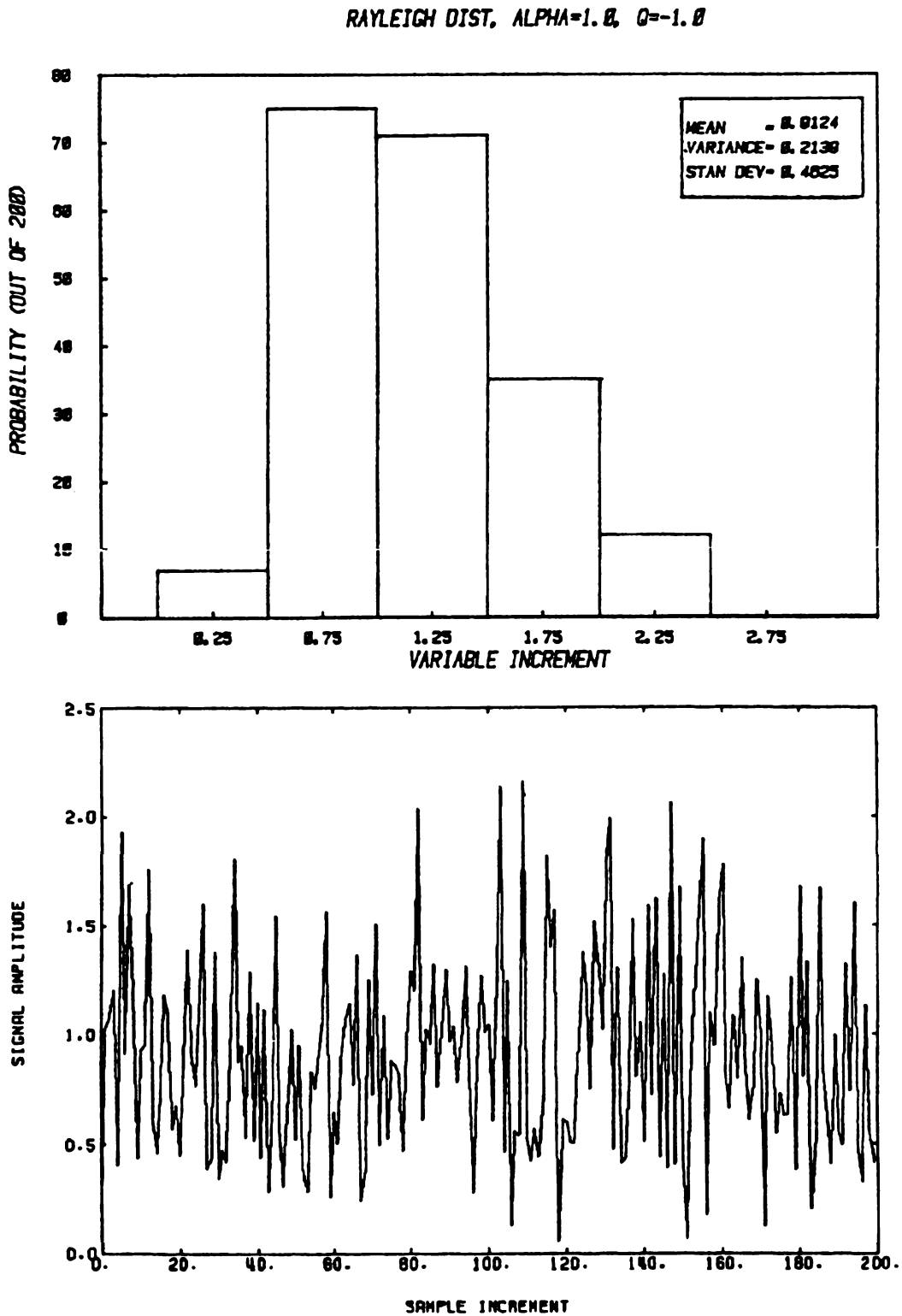


Figure B.10 Perturbed Rayleigh Distribution and Sequence,  $q = -1.00$

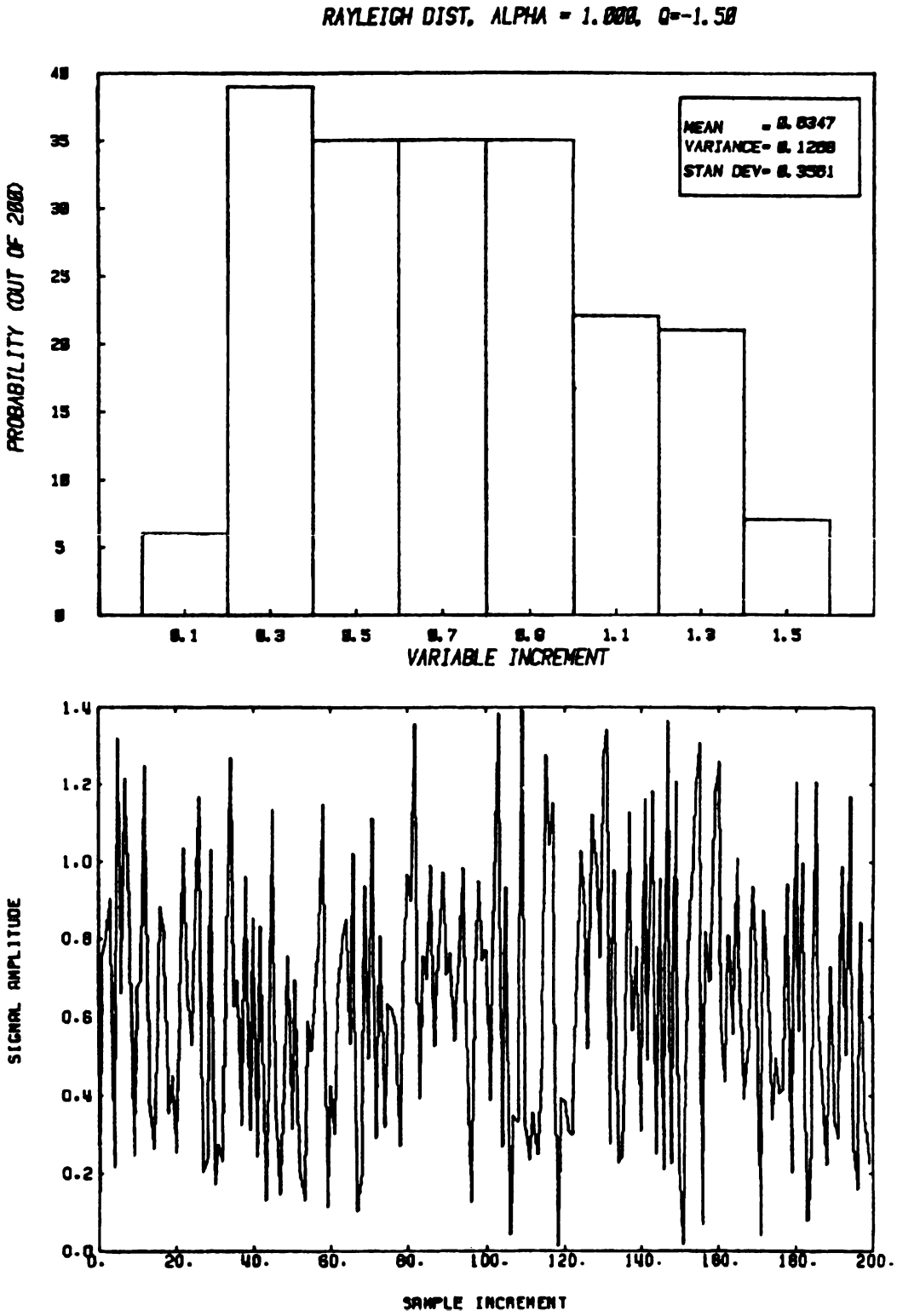


Figure B.11 Perturbed Rayleigh Distribution and Sequence,  $q = -1.50$

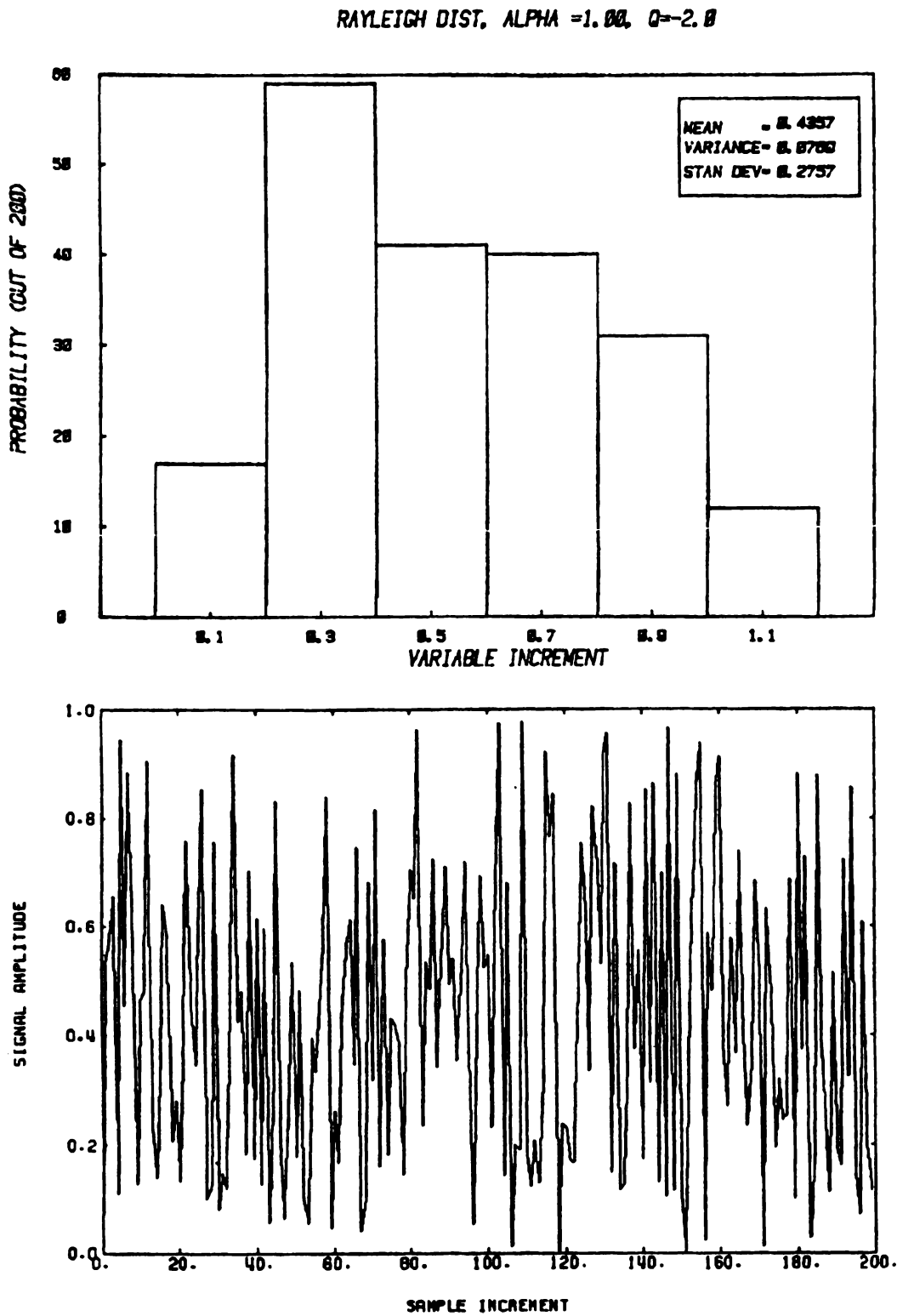


Figure B.12 Perturbed Rayleigh Distribution and Sequence,  $q = -2.00$



## REFERENCES

The bibliography contained herein was assembled to provide a collection of material adequate for an introduction to the formulations of fractals and fractional mathematical procedures. The list is not complete, but spans the theoretical to applications areas in a representative way. The references cited contain numerous additional references for specific needs or as additions to this initial collection.

The first two books cited are essential in an introduction to fractals. The first by Mandelbrot provides the fundamental formulations. The second, by Oldham and Spanier, is an excellent textbook on fractional calculus.

1. Mandelbrot, B.B. *The Fractal Geometry of Nature*, W.H. Freeman, New York, 1983.
2. Oldham, K.B. and J. Spanier, *The Fractional Calculus*, Academic Press, Orlando, Florida, 1974.
3. McBride, A.C. *Fractional Calculus and Integral Transforms of Generalized Functions*, Pitman Publishers, Belmont, California, 1979.
4. Dold, A. and B. Eckmann, *Fractional Calculus and Its Applications*, Springer-Verlag, New York, 1975.

A recent paper on fractal rain representations that also includes implications to other environments was written by Lovejoy and Mandelbrot. The importance of the hyperbolic distribution was pointed out. This paper plus other related work are as follows.

5. Lovejoy, S. and B.B. Mandelbrot, "Fractal Properties of Rain and a Fractal Model," *Tellus*, 37A, 1985, pp. 209–232.
6. Lovejoy, S., La geometrie fractale des nuages et des regions de pluie et les simulations aleatoires, *La Houille Blanche*, 1983.
7. Waymire, E., V.K. Gupta, and I.R. Iturbf, "Scale Considerations in the Modeling of Temporal Rainfall," *Water Resources Research*, Vol. 20, No.11, November 1984, pp. 1611–1619.
8. Waymire, E. and V.K. Gupta, "The Mathematical Structure of Rainfall Representations, A Review of Stochastic Rainfall Models," *Water Resources Research*, Vol. 17, No. 5, October 1981, pp. 1261–1272.
9. Waymire, E. and V.K. Gupta, "The Mathematical Structure of Rainfall Representations, A Review of the Theory of Point Processes," *Water Resources Research*, Vol. 17, No. 5, October 1981, pp. 1273–1285.
10. Waymire, E. and V.K. Gupta, "The Mathematical Structure of Rainfall Representations, Some Applications of the Point Process Theory to Rainfall Processes," *Water Resources Research*, Vol. 17, No. 5, October 1981, pp. 1287–1294.

A few specialized papers on diffractals (i.e., waves that have encountered fractals) are as follows:

11. Berry, M.V., "Diffractals," *J. Phys. A: Math Gen*, Vol. 12, 1979, pp. 781–797.
12. Berry, M.V., "Diffractal Echos," *J. Phys. A: Math Gen*, Vol. 14, 1981, pp. 3101–3110.
13. Jordan, D.L., R.C. Hollins, and E. Jokeman, "Experimental Measurements of Non-Gaussian Scattering by a Fractal Diffuser," *J. Applied Phys.*, B 31, 1983, pp. 179–186.

Papers of a general nature that include rigorous theoretical developments, applications, as well as qualitative discussion, constitute the remainder of the list of references.

14. Mandelbrot, B.B., "Intermittent Turbulence in Self-Similar Cascades: Divergence of High Moments and Dimension of Carrier," *J. Fluid Mech.*, Vol. 62, Part 2, 1974, pp. 331–358.
15. Lavoie, J.L., T.J. Osler, and R. Tremblay, "Fractal Derivatives and Special Functions," *SIAM Review*, Vol. 18, No. 2, April 1976, pp. 240–268.
16. Demko, S., L. Hodges, and B. Naylork, "Construction of Fractal Objects with Iterated Function Systems," *SIGGRAPH*, Vol. 19, No. 3, 1985, pp. 279–286.
17. Peachey, D.R., "Solid Texturing of Complex Surfaces," *SIGGRAPH*, Vol. 19, No. 3, 1985, pp. 279–286.
18. Perlin, K., "An Image Synthesizer," *SIGGRAPH*, Vol. 19, No. 3, 1985, pp. 287–296.
19. Bloomenthal, J., "Modeling the Mighty Maple," *SIGGRAPH*, Vol. 19, No. 3, 1985, pp. 305–311.
20. Reeves, W.T. and R. Blau, "Approximate and Probabilistic Algorithms for Shading and Rendering Structured Particle Systems," *SIGGRAPH*, Vol. 19, No. 3, 1985, pp. 313–322.
21. McDermott, J., "Geometrical Forms Known as Fractals Find Sensor in Chaos," *Smithsonian*, December 1983, pp. 110–117.
22. Pentrand, A.P., "Fractal-Based Description of Natural Scenes," *IEEE Trans on Pattern Analysis and Machine Intelligence*, Vol. PAMI-6, No. 6, November 1984, pp. 661–674.
23. Montroll, E.W. and M.F. Shlesinger, "Maximum Entropy Formalism, Fractals, Scaling Phenomena, and I/F Noise: A Tail of Tails," *Journal of Statistical Physics*, Vol. 32, No. 2, 1983, pp. 209–230.
24. Farmer, J.D., E. Ott, and J.A. Yorke, "The Dimension of Chaotic Attractors," *Los Alamos National Laboratory*, LA-UR-82-2856.
25. Grassberger, P. and I. Procaccia, "Characterization of Strange Attractors," *Physical Review Letters*, Vol. 50, No. 5, January 1983, pp. 346–349.
26. Termonia, Y. and Z. Alexandrowicz, "Fractal Dimensions of Strange Attractors from Radius Versus Size of Arbitrary Clusters," *Physical Review Letters*, Vol. 51, No. 14, October 1983, pp. 1265–1268.
27. Mandelbrot, B.B. and J.W. VanNess, "Fractional Brownian Motions, Fractional Noises and Applications," *SIAM Review*, Vol. 10, No. 4, October 1968, pp. 422–437.
28. Mandelbrot, B.B. and J.R. Wallis, "Computer Experiments with Fractional Gaussian Noises, Parts 1, 2, and 3," *Water Resources Research*, Vol. 5, No. 1, February 1969, pp. 228–267.
29. Mandelbrot, B.B., "A Fast Fractional Noise Generator," *Water Resources Research*, Vol. 7, No. 3, June 1971, pp. 543–553.
30. Mandelbrot, B.B., "Fonctions Aleatoires Pluri-Temporelles: Approximation Poissonienne de Cas Brownien et Generalisations," *Compte Rendus, Paris, Serie A*, t. 280, 28 April 1975, pp. 1075–1078.
31. West, B., "Fractal Phase Screens," *LJI-R-83-236*, Center for Studies of Nonlinear Dynamics, La Jolla, CA, June 1983.
32. Mandelbrot, B.B., "Some Long-Run Properties of Geophysical Records," *Water Resources Research*, Vol. 5, No. 2, April 1969, pp. 321–340.
33. Mandelbrot, B.B. and J.R. Wallis, "Noah, Josephy, and Operational Hydrology," *Water Resources Research*, Vol. 4, No. 5, October 1968, pp. 900–918.
34. Mandelbrot, B.B., "Fractals in Physics," *Journal of Statistical Physics*, Vol. 34, No. 5–6, 1984, pp. 895–930.



## ***Appendix C***

### ***Bibliography***

The bibliography is separated into two groups: The Radar Equation and The Atmospheric Environment and Data Compilations and Models. The required research into a variety of technical topics and disciplines included books, papers, and articles. When radar theory is emphasized, references including books, radar books, and papers and articles are listed separately. The background material for the atmospheric topics is a mixture of books and articles, which are combined here in one list. An additional bibliography, covering fractals, is contained in Appendix B, which is a mathematical supplement to the fractal models described in Chapter 8.

We have attempted to provide a comprehensive compilation of reference material which covers the topics we have discussed and conforms to our space limitations. Our choice of reference materials was influenced by the specifics of the subjects under investigation about which a vast amount of data is available. Therefore, the omission of some references pertaining to the topics discussed is probable, but this is not an indication of the quality, quantity or relative importance of the material used or omitted. The reader is encouraged to study these subjects further; our references provide merely a quantitative starting point.

#### **THE RADAR EQUATION**

Long-standing basic field theory references are listed here. A majority of the equation derivations applied followed the theoretical formulations of Schelkunoff, the applications and theory of work by Hu, and a recent description of field theory methods by Skitek. The Gaussian theory of large aperture antennas was described and placed in radar equation form. The summaries and expansions were the work of Bogush and Elkins. Data and references from publications by Barton provided additional material on a number of radar topics.

## Books

- Abramowitz, M., and I.A. Stegun, *Handbook of Mathematical Functions*, Washington, DC: NBS Applied Mathematics Series 55, 1965.
- Adler, R.B., L.J. Chu, and R.M. Fano, *Electromagnetic Energy Transmission and Radiation*, New York: John Wiley and Sons, 1965.
- Beyer, W.H., *CRC Standard Mathematical Tables*, Boca Raton, FL: CRC Press, 1980.
- Blake, L.V., *Antennas*, Dedham, MA: Artech House, 1984.
- Bohm, D., *Quantum Theory*, Englewood Cliffs, NJ: Prentice-Hall, 1951.
- Born, M., and E. Wolf, *Principles of Optics*, New York: Pergamon Press, 1983.
- Bowman, F., *Introduction to Bessel Functions*, New York: Dover Publications, 1958.
- Bracewell, R., *The Fourier Transform and its Applications*, New York: McGraw-Hill, 1965.
- Brigham, E.O., *The Fast Fourier Transform*, Englewood Cliffs, NJ: Prentice-Hall, 1974.
- Budden, K.G., *The Wave Guide Mode Theory of Wave Propagation*, Englewood Cliffs, NJ: Prentice-Hall, 1961.
- Churchill, R.V., *Fourier Series and Boundary Value Problems*, New York: Dover Publications, 1963.
- Collin, R.E., *Field Theory of Guided Waves*, New York: McGraw-Hill, 1960.
- Condon, E.U., and H. Odishaw, *Handbook of Physics*, New York: McGraw-Hill, 1958.
- Constant, F.W., *Theoretical Physics - Electromagnetism*, Reading, MA: Addison-Wesley, 1958.
- Duffieux, P.M., *The Fourier Transform and its Application to Optics*, New York: John Wiley and Sons, 1970.
- Dwight, H.B., *Tables of Integrals and Other Mathematical Data*, New York: Macmillan, 1957.
- Feller, W., *An Introduction to Probability Theory and its Applications*, Vol. I, New York: John Wiley and Sons, 1950.
- Feynman, R.P., R.B. Leighton, and M. Sands, *Lectures on Physics*, Vol. I, Reading, MA: Addison-Wesley, 1963.
- Feynman, R.P., R.B. Leighton and M. Sands, *Lectures on Physics*, Vol. II, Reading, MA: Addison-Wesley, 1963.
- Fonte, R.L., *Signal Analysis and Estimation — An Introduction*, New York: John Wiley and Sons, 1988.
- Franklin, P., *An Introduction to Fourier Methods and the Laplace Transformation*, New York: Dover Publications, 1949.
- Fujimoto, K., H. Henderson, K. Hirusawa, and J.R. James, *Small Antennas*, New York: John Wiley and Sons, 1987.
- Ghose, R.N., *Microwave Circuit Theory and Analysis*, New York: McGraw-Hill, 1963.
- Guillemin, E.A., *The Mathematics of Circuit Analysis*, New York: John Wiley and Sons, 1949.

- 
- Hall, A.D., *A Methodology for System Engineering*, New York: Van Nostrand Reinhold, 1962.
- Hall, G.L., ed., *The AARL Antenna Book*, Newington, CT: American Radio Relay League, 1984.
- Harvey, A.F., *Microwave Engineering*, New York: Academic Press, 1963.
- Hildebrand, F.B., *Advanced Calculus for Engineers*, Englewood Cliffs, NJ: Prentice-Hall, 1949.
- Jackson, J.D., *Classical Electrodynamics*, New York: John Wiley and Sons, 1962.
- Jahnke, E., and F. Emde, *Tables of Functions*, New York: Dover Publications, 1945.
- James, G.L., *Geometrical Theory of Diffraction for Electromagnetic Waves*, New York: IEEE, Peter Peregrinus, 1980.
- Jasik, H., ed., *Antenna Engineering Handbook*, New York: McGraw-Hill, 1961.
- Jay, F., ed., *IEEE Standard Dictionary of Electrical and Electronics Terms*, New York: IEEE, 1984.
- Jull, E.V., *Aperture Antennas and Diffraction Theory*, New York: IEEE, Peter Peregrinus, 1981.
- Jones, D.S., *The Theory of Electromagnetism*, New York: Macmillan, 1964.
- Klein, M.V., *Optics*, New York: John Wiley and Sons, 1970.
- Korn, G.A. and T.M. Korn, *Mathematical Handbook for Scientists and Engineers*, New York: McGraw-Hill, 1968.
- Kraus, J.D., *Antennas*, New York: McGraw-Hill, 1950.
- Kraus, J.D., *Electromagnetics*, New York: McGraw-Hill, 1953.
- Lee, Y.W., *Statistical Theory of Communication*, New York: John Wiley and Sons, 1967.
- Machol, R.E., ed., *System Engineering Handbook*, New York: McGraw-Hill, 1965.
- Margenau, H., and G.M. Murphy, *The Mathematics of Physics and Chemistry*, New York: D. Van Nostrand, 1956.
- Mason, M., and W. Weaver, *The Electromagnetic Field*, New York: Dover Publications, 1929.
- Maxwell, J.C., *A Treatise on Electricity and Magnetism*, Vol. I, New York: Dover Publications, 1954 (original, 1891).
- Maxwell, J.C., *A Treatise on Electricity and Magnetism*, Vol. II, New York: Dover Publications, 1954 (original, 1891).
- Mentzer, J.R., *Scattering and Diffraction of Radio Waves*, New York: Pergamon Press, 1955.
- Morse, P.M., and H. Feshbach, *Methods of Theoretical Physics*, Part I, New York: McGraw-Hill, 1953.
- Morse, P.M., and H. Feshbach, *Methods of Theoretical Physics*, Part II, New York: McGraw-Hill, 1953.
- Page, L., *Introduction to Theoretical Physics*, New York, D. Van Nostrand, 1959.
- Panofsky, W.K.H., and M. Phillips, *Classical Electricity and Magnetism*, Reading MA: Addison-Wesley, 1955.

- 
- Papoulis, A.P., *Probability, Random Variables, and Stochastic Processes*, New York: McGraw-Hill, 1965.
- Papoulis, A.P., *Systems and Transforms with Applications in Optics*, New York: McGraw-Hill, 1968.
- Papoulis, A.P., *The Fourier Integral and its Applications*, New York: McGraw-Hill, 1962.
- Parzen, E., *Modern Probability Theory and its Applications*, New York: John Wiley and Sons, 1960.
- Ramo, S., and J.R. Whinnery, *Fields and Waves in Modern Radar*, New York: John Wiley and Sons, 1953.
- Rhodes, D.R., *Synthesis of Planar Antenna Sources*, Oxford, England: Clarendon, 1974.
- Sammerfeld, A., *Electrodynamics*, New York: Academic Press, 1952.
- Sarbacher, R.I., and W.A. Edson, *Hyper and Ultrahigh Frequency Engineering*, New York: John Wiley and Sons, 1943.
- Schelkunoff, S.A., *Advanced Antenna Theory*, New York: John Wiley and Sons, 1952.
- Schelkunoff, S.A., *Applied Mathematics for Engineers and Scientists*, New York: D. Van Nostrand, 1965.
- Schelkunoff, S.A., *Electromagnetic Fields*, New York: Blaisdell Publishing, 1963.
- Schelkunoff, S.A., *Electromagnetic Waves*, New York: D. Van Nostrand, 1943.
- Schelkunoff, S.A., and H.T. Friis, *Antennas — Theory and Practice*, New York: John Wiley and Sons, 1952.
- Silver, S., *Microwave Antenna Theory and Design*, Vol. XII: MIT Radiation Laboratory Series, New York: McGraw-Hill, 1949.
- Skitek, G.G., and S.V. Marshall, *Electromagnetic Concepts and Applications*, Englewood Cliffs, NJ: Prentice-Hall, 1982.
- Slater, J.C., and N.H. Frank, *Electromagnetism*, New York: McGraw-Hill, 1947.
- Smith, D.B., "Government Research Contracts," *Handbook of Business Administration* in Maynard, H.B., ed., New York: McGraw-Hill, 1967, pp.5–103 to 5–119.
- Smythe, W.R., *Static and Dynamic Electricity*, New York: McGraw-Hill, 1950.
- Sokolnikoff, I.S., *Principles and Techniques of Applied Mathematics*, New York: John Wiley and Sons, 1956.
- Stratton, J.A., *Electromagnetic Theory*, New York: McGraw-Hill, 1941.
- Titchmarsh, E.C., *Introduction to the Theory of Fourier Integrals*, Oxford, England: Clarendon Press, 1948.
- Ulab, F.T., R.K. Moore and A.K. Fung, *Microwave Remote Sensing: Active and Passive, Vol. I - Microwave Remote Sensing Fundamentals and Radiometry*, Dedham, MA: Artech House, 1981.
- Ulab, F.T., R.K. Moore and A.K. Fung, *Microwave Remote Sensing: Active and Passive, Vol. II - Radar Remote Sensing and Surface Scattering and Emission Theory*, Dedham, MA: Artech House, 1982.

- Ulaby, F.T., R.K. Moore, and A.F. Fung, *Microwave Remote Sensing: Active and Passive, Vol. III - From Theory to Applications*, Dedham, MA: Artech House, 1986.
- Ware, L.A., and H.R. Reed, *Communication Circuits*, New York: John Wiley and Sons, 1959.
- Watkins, D.A., *Topics in Electromagnetic Theory*, New York: John Wiley and Sons, 1958.
- Weaver, J.H., *Applications of Discrete and Continuous Fourier Analysis*, New York: John Wiley and Sons, 1983.
- Wylie, C.R., Jr., *Advanced Engineering Mathematics*, New York: McGraw-Hill 1951.

## **Radar Books**

- Bachmam, C.G., *Radar Targets*, Lexington, MA: Lexington Books, 1982.
- Barton, D.K., and H.R. Ward, *Handbook of Radar Measurement*, Englewood Cliffs, NJ: Prentice-Hall, 1969.
- Barton, D.K., *Modern Radar System Analysis*, Norwood, MA: Artech House, 1988.
- Barton, D.K., *Radar System Analysis*, Englewood Cliffs, NJ: Prentice-Hall, 1964.
- Barton, D.K., ed., *Radars, Vol. I: Monopulse Radar*, Dedham, MA: Artech House, 1974.
- Barton, D.K., ed., *Radars, Vol. II: The Radar Equation*, Dedham, MA: Artech House, 1974.
- Barton, D.K., ed., *Radars, Vol. III: Pulse Compression*, Dedham, MA: Artech House, 1975.
- Barton, D.K., ed., *Radars, Vol. IV: Radar Resolution and Multipath Effects*, Dedham, MA: Artech House, 1975.
- Barton, D.K., ed., *Radars, Vol. V: Radar Clutter*, Dedham, MA: Artech House, 1975.
- Barton, D.K., ed., *Radars, Vol. VI: Frequency Agility and Diversity*, Dedham, MA: Artech House, 1977.
- Barton, D.K., ed., *Radars, Vol. VII: CW and Doppler Radar*, Dedham, MA: Artech House, 1978.
- Berkowitz, R.S., ed., *Modern Radar*, New York: John Wiley and Sons, 1965.
- Bhartia, P., and I.J. Bahl, *Millimeter Wave Engineering and Applications*, New York: John Wiley and Sons, 1984.
- Blake, L.V., *Radar Range Performance Analysis*, Dedham, MA: Artech House, 1986.
- Brookner, E., *Radar Technology*, Dedham, MA: Artech House, 1977.
- Constant, J.N., *Introduction to Defense Radar System Engineering*, New York: Macmillan, 1972.
- Crispin, J.W., Jr., and K.M. Siegal, *Methods of Radar Cross Section Analysis*, New York: Academic Press, 1968.
- Currie, N.C., and C.E. Brown, eds., *Principles and Applications of Millimeter-Wave Radar*, Norwood, MA: Artech House, 1987.
- Difranco, J.V., and W.L. Rubin, *Radar Detection*, Dedham, MA: Artech House, 1980.



- 
- Eaves, J.L., and E.K. Reedy, eds., *Principles of Modern Radar*, New York: D. Van Nostrand, 1987.
- Hirsch, H.L., and O.C. Grove, *Practical Simulation of Radar Antennas and Radomes*, Norwood, MA: Artech House, 1987.
- Hovanessian, S.A., *Introduction to Synthetic Array and Imaging Radars*, Dedham, MA: Artech house, 1980.
- Hovanessian, S.A., *Radar Detection and Tracking Systems*, Dedham, MA: Artech House, 1973.
- Hovanessian, S.A., *Radar System Design and Analysis*, Dedham, MA: Artech House, 1984.
- Kahrilas, P.J., *Electronic Scanning Radar Systems (ESRS) Design Handbook*, Dedham, MA: Artech House, 1975.
- Long, M.W., *Radar Reflectivity of Land and Sea*, Dedham, MA: Artech House, 1983.
- Oliner, A.A., and G.H. Knittel, *Phased Array Antennas*, Dedham, MA: Artech House, 1972.
- Ostroff, E.D., M. Borkowski, H. Thomas., and J. Curtis, *Solid-State Radar Transmitters*, Dedham, MA: Artech House, 1985.
- Ostrovityanov, R.V., and F.A. Basalov, *Statistical Theory of Extended Targets*, Dedham, MA: Artech House, 1985.
- Mensa, D.L., *High Resolution Radar Imaging*, Dedham, MA: Artech House, 1981.
- Meyer, D.P., and H.A. Mayer, *Radar Target Detection*, New York: Academic Press, 1973.
- Mitchell, R.L., *Radar Signal Simulation*, Dedham, MA: Artech House, 1976.
- Nathanson, F.E., *Radar Design Principles*, New York: McGraw-Hill, 1969.
- Rhodes, D.R., *Introduction to Monopulse*, New York: McGraw-Hill, 1959.
- Ridenour, L.N., *Radar System Engineering, Vol. I: MIT Radiation Laboratory Series*, New York: McGraw-Hill, 1949.
- Rihaczek, A.W., *Principles of High-Resolution Radar*, New York: McGraw-Hill, 1969.
- Ruck, G.T., ed., *Radar Cross Section Handbook*, Vol. I, New York: Plenum Press, 1970.
- Ruck, G.T., ed., *Radar Cross Section Handbook*, Vol. II, New York: Plenum Press, 1970.
- Skolnik, M.I., *Introduction to Radar Systems*, 2nd ed., New York: McGraw-Hill, 1980.
- Skolnik, M.I., ed., *Radar Handbook*, New York: McGraw-Hill, 1970.
- Stimson, G.W., *Introduction to Airborne Radar*, El Segundo, CA: Hughes Aircraft Company, 1983.
- Van Trees, H.L., *Detection, Estimation and Modulation Theory*, New York: John Wiley and Sons, 1968.
- Woodward, P.M., *Probability and Information Theory with Applications to Radar*, New York: Pergamon Press, 1953.

## Papers and Articles

- Blake, L.V., "A Guide to Basic Pulse-Radar Maximum-Range Calculation — Part I - Equations, Definitions, and Aids to Calculation," *NRL*, Washington, DC., December 1969.
- Bogert, V.P., ed., "Fast Fourier Transform and its Application to Digital Filtering and Spectral Analysis," Special Issue, *IEEE Trans. on Audio and Electroacoustics*, Vol. AU-15, No. 2, June 1967.
- Bogush, A.J., Jr., and R.E. Elkins, "Gaussian Field Expansions for Large Aperture Antennas," *IEEE Trans. on Antennas and Propagation*, Vol. AP-34, No. 2, February 1986, pp. 228–243.
- Bogush, A.J., Jr., and R.E. Elkins, "The Truncated Gaussian Antenna, Theory and Applications," *IEE Proc. 4th Int. Conf. Antennas*, April 1985.
- Bolle, D.M., and J. Jacobs, "The Radiation Pattern of Long Thin Antennas for Short Pulse Excitation," *IRE Trans. on Antennas and Propagation*, Vol. AP-10, No. 6, November 1962, pp. 787–788.
- Crispin, J.W., Jr., R.F. Goodrich, and U.M. Siegel, "A Theoretical Method for the Calculation of the Radar Cross Sections of Aircraft and Missiles," Univ. of Mich., Report No. 2591-1-H, July 1959.
- Elkins, R.E., A.J. Bogush Jr., and R.H. Jordan, "Optimal Scale Factors for Gaussian Field Expansions for a Circular Aperture," *IEEE Trans. on Antennas and Propagation*, Vol. AP-35, No. 12, December 1987.
- Fante, R.E., "Effect of Fresnel Zone Blockage on Very Low Sidelobe Antennas," *RADC*, Report 77-361, October 1977.
- Goodrich, R.F., et al., "Studies in Radar Cross Sections XLVII — Diffraction and Scattering by Regular Bodies — I: the Sphere," Univ. of Mich., Report No. 3648-1-T, December 1961.
- Hong, S., S.L. Borisom, and D.P. Ford, "Short Pulse Scattering by a Long Wire," *IEEE Trans. on Antennas and Propagation*, Vol. AP-16, No. 3, May 1968.
- Hu, M.K., "Study of Near-Zone Fields of Large Aperture Antennas, Part I," *SURI*, Report 574F1, Syracuse Univ., April 1957.
- Hu, M.K., "Study of Near-Zone Fields of Large Aperture Antennas, Part II," *SURI*, Report 574F2, Syracuse Univ., April 1957.
- Keller, J.B., "A Geometrical Theory of Diffraction, Calculus of Variations and its Application," *Proc. of Symposium in Applied Math*, McGraw-Hill, 1952, pp. 27–52.
- Kennaugh, E.M., "Research Studies on the Polarization Properties of Radar Targets," Vols. I and II, Ohio State Univ., July 1984.
- Kleinman, R.E., and T.B.A. Senior, "Studies in Radar Cross Sections XLVIII — Diffraction and Scattering by Regular Bodies — II: The Cone," Univ. of Mich., Report No. 3648-2-T, January 1963.

- Mailloux, R.J., "Phased Array Theory and Technology," *Proc. IEEE*, Vol. 70, No. 3, March 1982, pp. 246-292.
- Manneback, C., "Radiation from Transmission Lines," *AIEE Journal*, Vol. 42, February 1923, pp. 95-105.
- Pannell, J.H., J. Rheinstein, and A.F. Smith, "Radar Scattering from a Conducting Cone-Sphere," *MIT, Lincoln Lab. Report No. 349*, March 1964.
- Peters, L., Jr., "End-Fire Echo Area of Long Thin Bodies," *IRE Trans. on Antennas and Propagation*, Vol. AP-6, January 1958, pp. 133-139.
- Rheinstein, J., "Scattering of Short Pulses of Electromagnetic Waves," *IEEE Proceedings*, Vol. 53, No. 8, August 1965, pp. 1069-1070.
- Rice, S.O., "Mathematical Analysis of Random Noise," *BSTJ*, Vol. 23, No. 3, July 1944, pp. 282-332.
- Schelkunoff, S.A., "On Diffraction and Radiation of Electromagnetic Waves," *Physical Review*, Vol. 56, 1939, pp. 308-316.
- Schelkunoff, S.A., "Principle and Complementary Waves in Antennas," *IRE Proceedings*, Vol. 34, January 1946, pp. 23-32.
- Schelkunoff, S.A., "Some Equivalence Theorem of Electromagnetics and their Application to Radiation Problems," *BSTJ*, Vol 15, 1936, pp. 92-112.
- Schelkunoff, S.A., "Theory of Antennas of Arbitrary Size and Shape," *IRE Proceedings*, Vol. 29, September 1941, pp. 493-521.
- Stratton, J.A., and L.J. Chu, "Diffraction Theory of Electromagnetic Waves," *Physical Review*, Vol. 53, 1939, pp. 99-107.
- Ufimtsev, P. Ya., "Diffraction of Plane Electromagnetic Waves by a Thin Cylindrical Conductor," *Symposium on Wave Diffraction*, Odessa, October 1960.

## **THE ATMOSPHERIC ENVIRONMENT, DATA COMPILATIONS, AND MODELS**

- Battan, L.J., *Fundamentals of Meteorology*, Englewood Cliffs, NJ: Prentice-Hall, 1979.
- Battan, L.J., "Radar Attenuation by Melt Ice Spheres," *J. of Applied Meteorology*, 10, 1971, pp. 247-252.
- Battan, L.J., *Radar Observation of the Atmosphere*, Chicago, IL: Univ. of Chicago Press, 1973.
- Beckwith, W.B., "Hail Observations in the Denver Area," *United Air Lines Met. Cir.*, No. 40, 1956.
- Carrier, L.W., et al, "The Backscattering and Extinction of Visible and Infrared Radiation by Selected Major Cloud Models," *Appl. Opt.*, Vol 6, pp. 1209-1216.
- Changon, S.A., and G.E. Stout, "Crop-Hail Intensities in Central and Northwest United States," *Jur. Applied. Meteorology*. Vol. 6, 1967, pp. 542-548.
- Craig, R.A., *The Upper Atmosphere*, New York: Academic Press, 1965.

- 
- Crane, R.K., "A Global Model for Rain Attenuation Prediction," *EASCON 78 Record*, IEEE Pub. 78CH 1354-4 AES, Arlington, VA., September 1978.
- Crane, R.K., "A Two-Component Rain Model for the Prediction of Attenuation Statistics," *Radio Science*, Vol. 17, No. 6, November-December 1982, pp. 1371-1387.
- Crane, R.K., "Prediction of Attenuation by Rain," *IEEE Trans. on Communications*, Vol. Com-28, No. 9, September, 1980, pp. 1717 to 1733.
- Crane, R.K. and D.W. Blood, "Handbook for the Estimation of Microwave Propagation Effects — Link Calculations for Earth — Space Paths," *ERT*, Doc. No. P-7376-TRI, 1979.
- Davies, K., *Ionospheric Radio Propagation*, Washington, DC: NBS Monograph 80, 1965.
- Deirmendjian, D., "Electromagnetic Scattering on Spherical Polydispersions," *American Elsevier*, New York: 1969.
- Donn, W.L., *Meteorology*, New York: McGraw-Hill, 1965.
- Douglas, R.H., "Size Distribution of Alberta Hail Samples," *Science Report*, MW-36, 1963, pp. 55-71.
- Doviak, R.J., and D.S. Zrnić, *Doppler Radar and Weather Observations*, New York: Academic Press, 1984.
- Downs, W.R., "A Review of Atmospheric Information in the Optical and Microwave Spectral Regions," *BRL*, Report MR-2710, December 1976.
- Elkins, R.E., and A.J. Bogush Jr., "Fractal Simulation of Clouds," *Fourth Tri-Service Clouds Modeling Workshop*, AF Geophysics Laboratory, June, 1986.
- Elterman, L., "UV, Visible, and IR Attenuation for Altitudes to 50 km," *AFCRL*, Report-68-0153, Bedford, MA, 1968.
- Encyclopedia Britannica*, Chicago: William Benton, 1969.
- Encyclopedia of Science and Technology*, New York: McGraw-Hill, 1982.
- Fairbridge, R.W., *Encyclopedia of Atmospheric Sciences and Astrogeology*, New York: Reinhold, 1967.
- Gardner, G.Y., "Visual Simulation of Clouds," *SIGGRAPH '85, Computer Graphics*, Vol. 19, No. 3, p. 297.
- Gunn, K.L.S. and T.W.R. East, "The Microwave Properties of Precipitation Particles," *Quart. J. Roy. Meteor. Soc.*, 80: pp. 522-45.
- Goldhirsch, J., "Path Attenuation Statistics Influenced by Orientation of Rain Cells," *IEEE Trans. on Antennas and Propagation*, Vol. AP-24, No. 6, 1976, pp. 792-799.
- Holford, I., *Guinness Book of Weather*, London: Guinness Superlatives Limited, 1977. Contains tabulated data of cloud genus and basic characteristics.
- Ippolito, L.J., "Radio Propagation for Communications," *IEEE Proc.*, Vol. 69, No. 6, June 1981, pp. 697-727.
- Ippolito, L.J., R. D. Kaul, and R.G. Wallace, "Propagation Effects Handbook for Satellite Systems Design," *NASA*, Ref. Pub. 1082(03), June 1983.

- 
- Kimball, J.H., *Cloud and Weather Atlas*, New York: Coward-McCann, 1944.
- Khrgian, A.K., *Cloud Physics*, Jerusalem, 19XX.
- Kobayashi, H.K., "Atmospheric Effects on Millimeter Radio Waves," *Atmospheric Science Lab.*, NM, ASL-TR-0049, January 1980.
- Kobayashi, H.K., "Effect of Hail, Snow and Melting Hydrometeors on Millimeter Radio Waves," *Atmospheric Science Lab.*, NM., TR-0092, July 1981.
- Lai-Ian, Lo, B.M. Fammin and A.W. Straiton, "Attenuation of 8.7 and 3.2 mm Radio Waves by Clouds," *IEEE Trans. on Antennas and Propagation*, Vol. AP-23, No. 6, pp. 782-786, November 1975.
- Laws, J.O. and D.A. Parsons, "The Relation of Raindrop Size to Intensity," *Trans. Am. Geophys. Union*, Vol. 24, 1943. pp. 452-460.
- Liebe, H.J., "Atmospheric EHF Window Transparencies Near 35, 90, 140, and 220 GHz," *IEEE Trans. on Antennas and Propagation*, Vol. AP-31, No. 1, January. 1983, pp. 127-135.
- Liebe, H.J., *Atmosphere Water Vapor: A Nemesis for Millimeter Wave Propagation*, New York: Academic Press, April 1980.
- Liebe, H.J. "Modeling Attenuation and Phase of Radio Waves in Air at Frequencies below 1000 GHz," *Radio Science*, Vol. 16, No. 6, November-December, 1981, pp. 1183-1199.
- Lovejoy, S., "Statistical Characterization of Rain Areas in Terms of Fractals," *20th Conf. on Radar Meteorology*, American Meteorological Society, 1981.
- Lovejoy, S., and B.B. Mandelbrot, "Fractal Properties of Rain, and a Fractal Model," *Tellus*, Vol. 37A, No. 3, 1985, p.209.
- Lovejoy, S., and D. Schertzer, "Generalization Scale Invariance in the Atmosphere and Fractal Models of Rain," *Water Resources Research*, Vol. 21, No. 8, August 1985, pp. 1233-1250.
- Ludlam, F.H., *Clouds and Storms*, University Park, PA: Pennsylvania State University Press, 1980.
- Mandelbrot, B.B., *The Fractal Geometry of Nature*, New York: W.H. Freeman and Co., 1983.
- Marshall, J.S., and W.M. Palmer, "The Distribution of Raindrops with Size," *Jour. Meteorology*, Vol. 5, 1948, pp. 165-166.
- Mason, B.J., *The Physics of Clouds*, Oxford, England: Clarendon Press, 1971.
- Meijer, D.H.E., R.D. Mountain, and R.J. Soulen, Jr., eds., "Sixth International Conference on Noise in Physical Systems," *NBS*, SP 614, 1981.
- McCartney, E.J., *Optics of the Atmosphere Scattering by Molecules and Particles*, New York: John Wiley and Sons, 1976.
- Montroll, E.W., and M.F. Shlesinger, "Maximum Entropy Formalism, Fractals, Scaling Phenomena, and 1/f Noise: A Tale of Tails," *Jur. of Statistical Physics*, Vol. 32, No. 2, 1983.
- Nakaya, U., and T. Terada., "Simultaneous Observations of the Mass, Falling Velocity, and Form of Individual Snow Crystals," *Jour. Fac. Sci.*, Hokkaido Univ., Ser II, 1, 191, 1935, pp. 237-240, 340.
- Nemarich, J., et al, "Characteristics of Near-Millimeter Wave Propagation in Snow," *SPIE*, Vol. 305, 1981.

- Olsen, R.L., D.V. Rodgers, and D.B. Hodge, "The  $aR^b$  Relation in the Calculation of Rain Attenuation," *IEEE Trans. on Antennas and Propagation*, AP-26, 1978, pp. 318–329.
- Palmer, E. and C. Newton, *Atmospheric Circulation Systems*, New York: Academic Press, 1969.
- Peitgen, H.O., and P.H. Richter, *The Beauty of Fractals*, New York: Springer-Verlag, 1986.
- Peitgen, H.O., and D. Saupe, *The Science of Fractal Images*, New York; Springer-Verlag, 1988.
- Pentland, A., "Fractal-Based Description of Natural Scenes," *IEEE Trans. on Pattern Analysis and Machine Intelligence*, Vol. PAMI-6, No. 6, November 1984, p. 661.
- Perrie, D. W., *Cloud Physics*, New York: John Wiley and Sons, 19XX.
- Pietronero, L., And E. Tosatti, eds. *Fractals in Physics*, Elsevier Science, Amsterdam, 1986.
- Richard, V.W., J.E. Kammerer, and R.G. Reitz, "140-GHz Attenuation and Optical Visibility Measurements of Fog, Rain, and Snow," *ARBRL-MR-2800*, December 1977.
- Scorer, R., and H. Wexler, *A Colour Guide to Clouds*, New York: Macmillan, 1963.
- Seagraves, M.A., "Optical Characteristics of Wind Blown Dust," *Proc. of the Inter. Soc. of Optical Engineering*, Vol. 305, 1981.
- Sekhon, R.S., and R.C. Srivastava, "Snow Size Spectra and Radar Reflectivity," *J. Atmos. Sci.*, 27: 299–307, 1970.
- Setzer, D.E. "Computed Transmission Through Rain at Microwave and Visible Frequencies," *BSTJ*, October, 1970. pp. 1873–1892.
- "Snow Symposium IV," *U.S. Army CE*, CRREL Special Report 84–35, August 1984.
- Straiton, A.W., et al, "Atmospheric Limitations on the Use of Radio Waves with Frequencies of 15, 35, and 95 GHz," *AFAL-TR-72–264*, September 1972.
- Thompson, J.H., "Dust Clouds - Models and Propagation Effects," *Proc. of the Workshop on Millimeter and Submillimeter Atmospheric Propagation Applicable to Radar and Missile Systems*, TR-RR-80–3, February 1980.
- Tverskoi, P.N., *Physics of the Atmosphere*, Jerusalem, 1965.
- Ulaby, F.T., R.K. Moore, and A.K. Fung, *Microwave Remote Sensing*, Vol. I, Dedham, MA: Artech House, 1981.
- U.S. Standard Atmosphere*, 1962, Washington, DC: U.S. Government Printing Office, 1962.
- U.S. Standard Atmosphere*, 1976, Washington, DC: U.S. Government Printing Office, 1976.
- Valley, S.L., *Handbook of Geophysics and Space Environments*, New York: McGraw-Hill, 19XX.
- Van deHulst,., *Light Scattering by Small Particles*, New York: John Wiley and Sons, 1954.
- Wallace, H.B., "Millimeter Wave Propagation Measurements at the Ballistic Research Laboratory," *SPIE*, Vol. 305, 1981.
- Wexler, R., and D. Atlas, "Radar Reflectivity and Attenuation of Rain," *Jour. of Applied Meteorology*, Vol. 2, 1963, pp. 276–280.
- Wilcox, F.P., "Weather Performance Projection," *IEEE International Radar Conference*, April 1980.



# *INDEX*

- Absorption, 8
- Aerosol, 9, 254
- Airborne radar obstruction, 238–239
- Ambiguity function, 192
- Ampere, 74–75
- Ampere's circuital law, 74
- Antenna, 46, 50, 120–177
  - array, 169–177
  - circular, 158–162, 216–225, 241, 387–389
  - dipole, 126–130
  - infinite Guassian, 162–164
  - line source, 132
  - rectangular, 139–140, 149–158, 385–387
  - slot, 130–131
  - square, 206–216, 241
  - thin wire traveling wave, 132–137
  - truncated Guassian, 164–168
  - two-term expansion, 168–169
- Antenna directivity, 102
- Antenna gain, 43, 51, 57, 99, 205, 209–213
- Antenna patterns, 120–121, 142
  - parameters of, 123–124
- Aperture blockage, 237, 239
- Aperture field expansions, 149
- Atmosphere,
  - effects on radar, 8–9
  - models of, 10–11
- Atmospheric data (for radar applications), 11–12
- Attenuation, 27–28, 311, 374–375
  - clear air, 277–284, 377–278
  - effects of altitude on, 280–284
  - effects of humidity on, 280–284
  - path-averaged, 316–318
  - path-dependent, 380
  - zenith, 284–286
- Backscatter, 311–312, 318–320
- Beam steering unit, *see* Servo system
- Beamwidth, 204–205
- Boundary conditions, 78–80
- Brewster angle, 117
- Brownian motion, 343, 349–350
- CGS system, 72
- Cauchy's iterated integral, 413
- Climate regions, 266–268
- Cloud cover, 258–260
- Clouds, 254–260, 367–371, 382–383
  - families of, 254–256
  - formation of, 254
- Crane, R.K., 11, 309–310
- Debris, 321–325, 360
- Differential operators, 410–411
- Drop size distribution, 301–309
  - Laws and Parsons (L-P), 302–303, 304–309, 311, 325
  - Marshall and Palmer (M-P), 31, 302, 313
- Duality, 131
- Duplexer, 46
- Dust, 371–372
- Dynamo region, 252
- Effective radiated power (ERP), 26
- Electric current density, 84–86
- Electric flux density, 75–77
- Equivalence theorem, 90
- Euler's formula, 411
- Exceedance probability, 265–266
- Exosphere, 251
- Faraday's law, 72–73
- Fog, 260–263, 365–367



- 
- Fog occurrences, 268–270
  - Fourier transform, 122, 138–145, 146–147
  - Fractals
    - formulations of, 341
    - in rain models, 360–362
    - versus* Euclidean geometry, 342
  - Fractal models, 346–358
    - fractal sheet, 354
    - fractional Brownian motion, 343, 348–349, 351
    - fractional Brownian sheets, 349–354
    - hyperbolic fractal sheet, 354–358
  - Fractal sum-of-pulse algorithm, 358, 360
  - Fractional sum-of-pulse (FSP) model, 358, 360
  - Fraunhofer fields, 90, 94
  - Fresnel fields, 90, 94, 155
  - Friis' transmission formula, 18, 24–25, 98, 99, 100–101, 102–103
  - Gamma function, 411–413
  - Geometric optics, 70, 180, 185–186
  - Giorgi system of units, *see* MKS system of units
  - Global rain distributions, 266, 309–310, 360
  - Green's function, 87–89
  - Ground-based radar systems, 52
  - Grundwald's formula, 354, 415–418
  - Gaussian law, 75–77
  - Gaussian equivalents, 148, 208–209, 218–219, 242
  - Gaussian field expansions, 24, 32, 147–169, 158–162, 199–200, 216–218
    - two-term, 239–240, 243
  - Gaussian radar equation, 7, 213–216, 218–220, 242–243
    - meteorological form, 220–225, 243
  - Hail, 258, 325, 336–340
  - Hankel transform methods, 145–147
  - Haze, 365
  - Hermite Gaussian
    - field expansion, 390–402
    - function, 149–152
  - Huygen's principle, 173
  - Hyperbolic probability distribution, 409, 418–421
    - two parameter, 422–424
  - Interference susceptibility, 232–233
  - International Civil Aviation Organization (ICAO), 252
  - International Commission for Aerial Navigation (ICAN), 252
  - International Radio Consultative Committee (CCOR), 266
  - International System of Units (*Système Internationale*), 72
  - Inverse method, 409
  - Ionosphere, 251, 252
  - Kirchhoff's theory, 7, 2, 121–122
  - Kirchhoff's diffraction formula, 90–96, 104–106
  - Laguerre Gaussian
    - field expansion, 390–402
    - function, 158–159
  - Lapse rate, 247
  - Laws and Parsons (L-P) drop size distribution, *see* Drop size distribution
  - Linearly frequency modulated (LFM) pulse, 45, 49
  - Log-normal distribution, 410, 425–426
  - Lorentz gauge, 85–86
  - Loss budget, 58
  - Lossless dielectrics, *see* Perfect dielectrics
  - Lossy dielectrics, 114–115
  - MKS (Giorgi) system of units, 72
  - Magnetic current density, 84, 86
  - Magnetic flux density, 77, 84
  - Marshall and Palmer (M-P) drop size distribution. *see* Drop size distribution
  - Mass extinction coefficient, 370
  - Matched filter, 191
  - Maxwell's equations, 5, 70–82
    - differential forms, 77–78, 107
    - free space form, 81
    - integral forms, 72–77
    - phasor form, 80
    - static form, 81–82
    - steady current form, 81–82
  - Mesosphere, 250–251
  - Meteorological radar equation, 28–32, 220–225, 243
  - Mie scattering theory, 8, 10, 312, 313
  - National Advisory Committee for Aeronautics (NACA), 252
  - Near fields, 90, 144–145
  - Ohm's law (Ohm's law at a point), 71

- 
- One-way transmission equation, 24, 102–103.  
*See also* Friis' transmission formula
- Orthogonal functions, 389–390
- Ozone layer, 250
- Path-averaged attenuation, *see* Attenuation
- Path length factors, 27, 318, 319, 380
- Path loss, 26–28
- Pattern degradation, 235–239
- Perfect dielectrics, 110–114, 115–117
- Phase delay, 284–285, 293–294
- Physical optics, 70, 104, 180, 182–184
- Pileus, 254
- Plane-wave spectrum field representation, 122
- Plane waves, 106–119
- Point rain rate (PRR), 265
- Power densities, 201–203, 226–234
- Power reciprocity theorem, *see* Reciprocity
- Power transfer, 203–204
- Poynting's theorem, 96–97
- Precipitation, 256–258
- Principle (spherical) waves, 134
- Propagation constant, 286–288
- Pulse repetition frequency (PRF), 43, 46, 49
- Radar acquisition, 33–34
- Radar controller, 46
- Radar cross section, 7, 45, 54, 70, 106, 177–186  
 of rain, 311–314
- Radar equation, 3–4, 5–7, 17–18, 196–197  
 bistatic, 22  
 classical form, 5, 17, 18–21  
 definition of, 17  
 formal description, 5–7  
 Gaussian form of, *see* Gaussian radar equation  
 Meteorological form of, *see* Meteorological radar equation  
 Search form, 22–24
- Radar parameters, 38–53  
 performance parameters, 44–46  
 subsystem parameters, 46–53
- Radar performance analysis, 60–67
- Radar requirements, 33–38
- Radar siting, 233, 238
- Radar signal, 188–195
- Radar tubes, 48–49
- Radar waveforms, 192–195
- Radiated field, 90, 120–121
- Radiated power density, *see* Power density
- Radio frequency (RF), 44
- Radome analysis, 233–234
- Radome nose tips, 238
- Rain, 258, 378–382  
 drop size, *see* Drop size distribution  
 types of, 298–299  
 vertical profile of, 300–301
- Rain models  
 backscatter formulation, 318–320  
 path dependent, 316–325  
 two-component dependence, 320–325  
 uniform, 311–316
- Rayleigh scattering, 8, 70, 180, 184–185
- Receiver, 47
- Reciprocity, 97–100
- Reflectivity constant, 31–32
- Refraction, 8–9
- Reimann-Liouville integral, 413–415
- Resonant scattering, 70
- Robustness, 9–10
- Scattering centers, 40, 177–180
- Schelkunoff's mode theory of antennas, 134, 137
- Sensitivity time control (STC) circuit, 53
- Servo system, 46, 52
- Signal bandwidth, 57
- Silver's formulation, 235, 239
- Smoke, 372
- Snell's law of refraction, 117, 290
- Snow, 258, 325, 332–336
- Spherical waves, *see* Principle waves
- Stoke's law, 77
- Storms, 298. *See also* Rain
- Stratopause, 250
- Stratosphere, 248–250
- Stratton-Chu diffraction formulas, 91–92
- Swerling model, *see* Target model
- System Internationale* (SI), *see* International system of units
- System losses, 57–58
- System noise temperature, 57
- Target models, 41, 187–188  
 log-normal Weibull distribution, 188  
 Swerling model, 41, 54, 187
- Thermosphere, 251–252
- Time delay, 294–295
- Transmitted power, 57

Transmitter, 46, 48  
Transverse electromagnetic wave (TEM), 111  
Tropopause, 248  
  
U.S. Standard Atmosphere, 56, 252–254  
  
Vector potentials, 82–90  
Vertical profiles, 300–301  
Voltage Standing Wave Ratio (VSWR), 58  
Volume cell, 320, 321–325, 360  
Von Koch curve, 344–345  
  
Waveforms, 192–195  
Weibull distribution, 425–426  
Weyl's integral, 413–415  
  
Yearly average rainfall, 309  
  
Z-R relationships, 313, 314  
Zenith attenuation, *see* Attenuation